

Utah State University

DigitalCommons@USU

All Graduate Theses and Dissertations

Graduate Studies

12-2019

Reducing Thermal Bridging and Understanding Second-Order Effects in Concrete Sandwich Wall Panels

Taylor J. Sorensen
Utah State University

Follow this and additional works at: <https://digitalcommons.usu.edu/etd>



Part of the [Civil and Environmental Engineering Commons](#)

Recommended Citation

Sorensen, Taylor J., "Reducing Thermal Bridging and Understanding Second-Order Effects in Concrete Sandwich Wall Panels" (2019). *All Graduate Theses and Dissertations*. 7642.
<https://digitalcommons.usu.edu/etd/7642>

This Dissertation is brought to you for free and open access by the Graduate Studies at DigitalCommons@USU. It has been accepted for inclusion in All Graduate Theses and Dissertations by an authorized administrator of DigitalCommons@USU. For more information, please contact digitalcommons@usu.edu.



REDUCING THERMAL BRIDGING AND UNDERSTANDING
SECOND-ORDER EFFECTS IN CONCRETE
SANDWICH WALL PANELS

by

Taylor J. Sorensen

A dissertation submitted in partial fulfillment
of the requirements for the degree

of

DOCTOR OF PHILOSOPHY

in

Civil Engineering

(Structural Engineering)

Approved:

Marc Maguire, Ph.D.
Major Professor

Nick Roberts, Ph.D.
Committee Member

Marv Halling, Ph.D.
Committee Member

Andrew Sorensen, Ph.D.
Committee Member

Paul Barr, Ph.D.
Committee Member

Richard S. Inouye, Ph.D.
Vice Provost for Graduate Studies

UTAH STATE UNIVERSITY
Logan, Utah

2019

Copyright © Taylor Sorensen 2019

All Rights Reserved

ABSTRACT

Reducing Thermal Bridging and Understanding Second-Order Effects in Concrete Sandwich Wall Panels

by

Taylor J. Sorensen, Doctor of Philosophy

Utah State University, 2019

Major Professor: Dr. Marc Maguire
Department: Civil and Environmental Engineering

Recent advances in concrete sandwich wall panels (SWP) have sought to optimize structural efficiency by reducing wythe thickness. This is possible by utilizing increased composite action between wythes from improved SWP connectors. Partially-composite SWPs often achieve optimal structural efficiency, but at the expense of thermal efficiency. Conversely, some people strongly advocate non-composite SWP structures since these typically have higher thermal efficiency than partially-composite SWP structures, but do so at the expense of structural efficiency. This project sought to help allow SWPs to achieve optimal structural and thermal efficiency without sacrificing one or the other by increasing thermal efficiency of concrete SWP structures by identifying common locations of thermal bridging and developing alternate designs to eradicate (as much as possible) the use of solid sections in concrete sandwich wall panel design.

This study performed infrared thermographic inspections of 79 SWP structures across the United States of America and analyzed heat transfer in SWP connections to identify details that can decrease thermal bridging in future SWP construction. Because corbel connections can be particularly difficult locations to avoid thermal bridging for partially-composite SWPs, 12 corbel connections were designed, created, and structurally tested to maintain a continuous thermal break and thereby eliminate thermal bridging. Nine successful alternative thermally efficient corbel connections were created, with GFRP grating providing the most promising results for application in SWP corbel construction. Use of SWP connectors to transfer loads between wythes locally at corbel connections was also found to be a feasible option.

Corbel specimens were modeled using the Beam-Spring Method with good agreement with experimental results, with a predicted-to-measured ratio of 1.014 and a standard deviation of 0.286. Such validation led to completion of a parametric study to evaluate performance of the PCI Second-Order Analysis method, to quantify 2nd order effects in SWPs, and to investigate effects of length, panel stiffness, and wythe configuration on SWP behavior under combined axial and flexural loading.

Findings of this dissertation will help reduce energy use and thermal bridging, increase sustainability, lessen environmental impact, and increase the safety of concrete sandwich wall panel structures.

(472 pages)

PUBLIC ABSTRACT

Reducing Thermal Bridging and Understanding

Second-Order Effects in Concrete

Sandwich Wall Panels

Taylor J. Sorensen

Structural engineers have traditionally detailed structures with structural and fabrication efficiency in mind, but often based on a limited understanding of thermal efficiency. Some connection designs can create significant thermal bridging, leading to unnecessary heat transfer and even premature degradation through condensation. Thermal bridging occurs when heat transfer is given a path through a more conductive material like concrete or steel rather than insulation. Concrete sandwich wall panels (SWP) tend to be highly efficient at preventing heat transfer in the middle of panels, with greatest heat transfer occurring at connections. This project identified thermally efficient details for future SWP construction to reduce heat transfer, lessen environmental impact, and increase sustainability of SWP structures. It can be particularly difficult to avoid thermal bridging at corbel connections, so 12 corbel specimens were created and tested to provide alternative corbel design options for engineers. Nine details were successfully created and are presented. Corbel specimens were modeled using the Beam-Spring Method with good agreement. After validating the Beam-Spring Model, a parametric study investigated effectiveness of the PCI Second Order Analysis and the effect of length, panel stiffness, and wythe configuration on SWP behavior under axial and flexural loads.

ACKNOWLEDGMENTS

I would like to express my deep appreciation to the Portland Cement Association Education Foundation for their continued support, guidance, sponsorship, and interest in this project. Appreciation should also be extended to the Precast/Prestressed Concrete Institute and the Tilt-Up Concrete Association for their willingness to help to identify and recommend precasters and contractors to assist me in identifying SWP buildings in cities across the United States to include in this study. These many precasters, contractors, and engineers also deserve recognition and thanks for their participation in this study in identifying SWP structures for us to visit to help us promote SWP structures as a whole in the industry. I am very grateful to the gracious owners of these structures that allowed us to visit and photograph their beautiful structures. Special thanks to Parker Syndergaard and Sattar Dorafshan for their help in taking many of the thermal images.

Appreciation should also be extended to the various donors who contributed to the making of the concrete sandwich wall panels, including HK Composites for donating all HK SWP connectors used in this project, IconX LLC for donating the GFRP and CFRP IconX connectors, Owens Corning Infrastructure Solutions for the donation of the GFRP bars, and Fibergrate Composite Structures for donating the FRP grating used in this project. Special thanks to those graduate and undergraduate workers who assisted in preparing, casting, and testing the corbel specimens including Zachary Benson, Colby Bench, Tyler Daniels, Quinn Lythgoe, Ethan Schow, Reese Mikesell, Zack Hulsey, Nick Langford, and Jared McRory. I would also like to express my gratitude for Fray Pozo for

his assistance in helping me create an API that allowed me to perform so many Beam-Spring Models in a most efficient manner.

I am humbly grateful for all of the spectacular professors, teachers, and mentors I have had through my educational experience, both through my childhood and in my higher education, and would like to thank them all for the way they have touched my life through their teachings, friendship, and examples.

I would like to express special thanks for my advisor, Dr. Marc Maguire, who has been a phenomenal mentor and friend. His continual guidance, supervision, constructive advice, and wise counsel has helped me arrive where I am now. I would not have pursued such a course of action if it were not for his intervention and his ability to see in me what I had not thought to imagine. Thank you for your influence, encouragement, and guidance.

Finally, I wish to express the deepest and most profound love and gratitude to my family, and most particularly my wife. No one has been so supportive as she. Thank you for being patient and for sticking with me through the thick and thin. I wouldn't have been able to do it without you!

Taylor J. Sorensen

CONTENTS

ABSTRACT	iii
PUBLIC ABSTRACT	v
ACKNOWLEDGMENTS	vi
LIST OF FIGURES	x
LIST OF TABLES	xix
LIST OF SYMBOLS AND NOTATION.....	xx
LIST OF ABBREVIATIONS.....	xxiii
INTRODUCTION	1
Background.....	1
Objective.....	2
Dissertation Outline	3
LITERATURE REVIEW AND BACKGROUND	5
History of SWP Efficiency	5
Heat Transfer in Buildings	11
SWP Corbel Connections	17
Dissertation Significance and Contributions to Literature	25
THERMAL DETAILING.....	27
Common Thermal Bridging Locations.....	27
Thermal Analyses	78
THERMALLY EFFICIENT CORBEL CONNECTIONS	108
Preliminary Analysis	108
Experimental Design	108
Experimental Program.....	122
Test Results	139
ANALYSIS AND PARAMETRIC STUDY OF CONCRETE SANDWICH WALL	
PANELS UNDER AXIAL LOADS	160
Previous Research	160
Model Verification	165
Parametric Study	180
CONCLUSIONS.....	195

REFERENCES	201
APPENDICES	211
Appendix A. THERMAL ANALYSIS EXAMPLES.....	212
Appendix B. CORBEL DESIGN CALCULATIONS	281
Appendix C. CORBEL FABRICATION DRAWINGS.....	422
Appendix D. BEAM-SPRING MODEL SPRING STIFFNESSES	435
Appendix E. PCI SECOND-ORDER ANALYSIS EXAMPLE	437
CURRICULUM VITAE.....	444

LIST OF FIGURES

Figure	Page
2-1 Thermal resistance (R-values) comparison of insulation types.....	8
2-2 Stress distribution comparisons for differing levels of composite action	11
2-3 Frozen condensation visible on exterior of a building	13
2-4 Heat transfer through thermal bridge at base of wall	14
2-5 Heat transfer through thermal bridge at base of wall	15
2-6 Residential Energy End-Use in 2009	16
2-7 Commercial Energy End-Use in 2012.....	17
2-8 Thermal bridging at corbel connections in SWP structure.....	18
3-1 SWP structure with marginal thermal bridging.....	29
3-2 SWP structure with minimal thermal bridging around windows	29
3-3 SWP structure with minimal thermal bridging at corners	30
3-4 SWP structure with no thermal bridging at roof termination	30
3-5 Well-detailed SWP structure	31
3-6 SWP structure with thermal bridging around windows	32
3-7 SWP structure with thermal bridging around doors	32
3-8 SWP with thermal bridging at reinforcement of door corner.....	33
3-9 Sample of structurally sound details resulting in thermal bridging.....	34
3-10 Sample of improved details that prevent moderate thermal bridging	35
3-11 Sample details that minimize heat transfer around windows and doors	35
3-12 SWP with thermal bridging at solid sections around loading dock	36

Figure	Page
3-13 SWP with thermal bridging at solid sections around door	37
3-14 SWP with thermal bridging at penetration through insulation.....	38
3-15 SWP with thermal bridging at thru-fastened awning connections	39
3-16 SWP with thermal bridging where awning beams penetrate insulation.....	39
3-17 SWP with thermal bridging where basketball standard was attached	40
3-18 Sample details of structural penetrations of insulation	41
3-19 Sample penetration detail with solid section for external canopy	41
3-20 SWP structure with thermal bridging at side lifting anchors	42
3-21 Close-up view of thermal bridging in SWP lifting anchors	43
3-22 SWP structure with severe thermal bridging from lifting points	43
3-23 Profile view of common design for omitting insulation at lifting anchors	44
3-24 Profile view of common design approach for lifting anchors	44
3-25 Plan view of common lifting anchor detail	45
3-26 Example lifting anchor detail that does not puncture insulation	45
3-27 SWP structure with thermal bridging at corbel locations.....	46
3-28 SWP structure with severe thermal bridging at corbel locations	47
3-29 Sample of corbel details	48
3-30 Sample corbel details showing less insulation displaced	48
3-31 Sample of corbel details with continuous but reduced insulation	49
3-32 Sample of corbel details that prevent thermal bridging	49
3-33 SWP structure with partial thermal bridging at roof termination.....	50
3-34 SWP structure with thermal bridging at roof termination.....	51

Figure	Page
3-35 SWP structure with thermal bridging at roof and joist embedment	51
3-36 Sample roof termination details with common thermal bridging.....	52
3-37 Sample roof termination details	53
3-38 Sample roof termination details	54
3-39 Sample of ideal roof termination details	54
3-40 SWP structure with thermal bridging at floor termination.....	55
3-41 SWP structure with heavy thermal bridging where 2 nd floor terminates	55
3-42 Sample floor termination details	56
3-43 Sample floor termination details with reduced but continuous insulation	57
3-44 Sample floor termination details with insulation continuity	57
3-45 SWP structure with thermal bridging at foundation connection	59
3-46 SWP structure with thermal bridging at foundation connections.....	59
3-47 Sample foundation connection details.....	60
3-48 Sample foundation details	61
3-49 Sample foundation details	61
3-50 Sample foundation details	62
3-51 Visual definition of corner types	63
3-52 Heat transfer comparison for reentrant and salient corners.....	64
3-53 SWP structure with thermal bridging at a reentrant corner.....	65
3-54 SWP structure with thermal bridging at a reentrant corner.....	65
3-55 SWP structure with thermal bridging at salient corner butt joint.....	66
3-56 SWP structure with thermal bridging along butt joint of salient corner	66

Figure	Page
3-57 Four corner joint detail options	67
3-58 Common butt joint connections with much thermal bridging, plan views	68
3-59 Sample corner details blocking insulation out and replacing after	69
3-60 Sample salient corner details with minimal thermal bridging.....	69
3-61 Sample reentrant corner details with minimal thermal bridging	69
3-62 SWP structure with severe thermal bridging around panel edges.....	70
3-63 SWP with significant thermal bridging at panel-to-panel connections	70
3-64 Common panel-to-panel connections resulting in significant heat transfer	71
3-65 Front view of similar details to the Figure 3-64.....	72
3-66 Examples of ideal panel-to-panel details.....	72
3-67 SWP with thermal bridging from joints/space between insulation	73
3-68 SWP structure with thermal bridging at insulation joints	74
3-69 SWP structure with thermal bridging due to insulation joints	74
3-70 Insulation joint details	75
3-71 SWP structure with thermal bridging due to use of steel truss connectors	77
3-72 Parallel-path method electric circuit analogy	79
3-73 Isothermal-planes method electric circuit analogy.....	82
3-74 Zone method electric circuit analogy	83
3-75 Characteristic section method electric circuit analogy.....	85
3-76 SWP used in analyses of this dissertation	88
3-77 Panel layout of SWP example comparing inclusion/exclusion of steel	89
3-78 Panel layout of SWP analyzed with solid section around window	91

Figure	Page
3-79	Percent loss in thermal efficiency vs. square window width 91
3-80	Panel layout of SWP example analyzed with penetrations 93
3-81	Percent loss in thermal efficiency vs. number of penetrations 93
3-82	Panel layout of SWP example analyzed with 4 steel lifting anchors 94
3-83	Percent loss in thermal efficiency vs. number of pick points..... 95
3-84	Panel layout of SWP example analyzed with solid section at corbel..... 96
3-85	Percent loss in thermal efficiency vs. required solid area for a corbel..... 96
3-86	Panel layout of SWP example analyzed with solid sections at roof 98
3-87	Percent loss in thermal efficiency vs number of roof connections..... 98
3-88	Panel layout of SWP example analyzed with solid sections at floor 99
3-89	Percent loss in thermal efficiency vs number of floor connections 99
3-90	SWP layout of example analyzed with solid sections at foundation..... 101
3-91	Percent loss in thermal efficiency vs insulation block out width 101
3-92	Panel layout of SWP analyzed with 3 panel-to-panel connectors..... 104
3-93	Percent loss in thermal efficiency vs number of connections 104
3-94	Panel layout of SWP example analyzed with insulation 105
3-95	Percent thermal efficiency loss vs net cumulative insulation joint width 105
3-96	SWP layout of example analyzed with a) steel pins and b) steel truss 107
4-1	Profile view of specimen designs 110
4-2	Strut-and-tie model created for solid section 113
4-3	Comparison of strut-and-tie models for SWP corbel connections 115
4-4	Corbel designs from Set 1: SolidWall, SolidSec, GFRP2, and GFRP3 124

Figure	Page
4-5 Corbel designs from Set 2: HKVer, HKHor, IconG, and IconC	125
4-6 Corbel designs from Set 3: RedIns, IconCHat, GridVer, and GridHor	126
4-7 Concrete specimen formwork and rebar for Set 1	127
4-8 Concrete specimen formwork and rebar for Set 2	127
4-9 Concrete specimen formwork and rebar for Set 3	128
4-10 Cutting holes for FRP penetration and HDPE prism placement	129
4-11 Placing foam and connectors in SWP specimens	129
4-12 Removing air voids in concrete wythes using pencil vibrator	130
4-13 Front view of initial test setup for corbel testing	131
4-14 Profile view of initial test setup for corbel testing	132
4-15 Photo of initial test setup for Set 1	133
4-16 Front view of modified test setup for corbel testing	135
4-17 Profile view of modified test setup for corbel testing	136
4-18 Photo of revised test setup used for Set 2 and 3	137
4-19 Comparison of load vs. tip deflection for all corbel specimens	141
4-20 SolidWall specimen immediately after failure	143
4-21 Cracking in corbel of SolidWall specimen after failure	144
4-22 Cracking in SolidSec specimen immediately prior to failure	145
4-23 Cracking in corbel of SolidSec specimen after failure	146
4-24 Crack developed on backside of GFRP3 specimen during testing	147
4-25 GFRP3 (left) and GFRP2 (right) specimens following corbel failure	148
4-26 Ruptured GFRP bars from GFRP3 specimen	149

Figure	Page
4-27 HKHor specimen SWP (left) and corbel (right) after failure	150
4-28 HKVer specimen after failure	151
4-29 Crack failure surface in SWP connector panel designs.....	151
4-30 IconG corbel secured only by framing bar after failure	153
4-31 IconCHat corbel after failure secured by corbel reinforcement	154
4-32 RedIns specimen after failure.....	155
4-33 Failure of the GridVer specimen	157
4-34 Failure of the GridHor specimen.....	157
5-1 Beam-Spring Models for SWP specimens	167
5-2 Average GFRP modulus of elasticity vs. clear span	174
5-3 Applied load vs. slip results for corbel specimens	178
5-4 Percent of applied load shared by outside wythe	181
5-5 Connector force distribution for varying eccentricities.....	182
5-6 Maximum connector shear force vs. concentrated corbel stiffness.....	183
5-7 Maximum connector axial force vs. concentrated corbel stiffness	183
5-8 Ratio of 2 nd Order to 1 st Order Moment vs. Length for a 3-3-3 SWP.....	186
5-9 Logistic relationship between DCA and panel stiffness	189
5-10 BSM and PCI predictions for stress and deflection in a 3-2-3 SWP.....	190
5-11 BSM and PCI predictions for stress and deflection in a 3-3-3 SWP.....	191
5-12 BSM and PCI predictions for stress and deflection in a 3-4-3 SWP.....	192
A-1 Panel layout and cross-section with electrical circuit analogy.....	215
A-2 Window example panel layout and cross-section	220

Figure	Page
A-3 Solid section example panel layout and cross-section	224
A-4 Penetration without replacing blocked out material example	227
A-5 Penetration with concrete fill example	230
A-6 Penetration with insulation fill example	233
A-7 Lifting anchor example panel layout and cross-section	237
A-8 Corbel example panel layout and cross-section	240
A-9 Roof example panel layout and cross-section	243
A-10 Floor with omitted insulation example	246
A-11 Floor with reduced insulation example	250
A-12 Foundation example panel layout and cross-section	253
A-13 Panel connection example panel layout and cross-section	256
A-14 Insulation Joint example panel layout	259
A-15 Steel pin connector example panel layout and cross-section	266
A-16 Steel truss connector example panel layout and cross-section	274
A-17 Determination of HK connector spacing	347
A-18 Determination of IconX connector spacing	363
A-19 Determination of IconX connector spacing	379
C-1 SolidWall specimen details	423
C-2 SolidSec specimen details	424
C-3 GFRP3 specimen details	425
C-4 GFRP2 specimen details	426
C-5 HKHor specimen details	427

Figure	Page
C-6 HKVer specimen details.....	428
C-7 IconG specimen details	429
C-8 IconC specimen details.....	430
C-9 IconCHat specimen details.....	431
C-10 RedIns specimen details	432
C-11 GridVer specimen details	433
C-12 GridHor specimen details.....	434

LIST OF TABLES

Table		Page
4-1	Test specimens	109
4-2	Test matrix for SWP corbel specimens.....	123
4-3	Material testing results	140
4-4	Test results for corbel specimen testing	142
5-1	Properties used in SWP Beam-Spring Models	168
5-2	Ratios of predicted-to-measured elastic slope for applied load vs. slip.....	179
A-1	Material conductivities used in this study.....	213
A-2	Surface air film resistances	214
D-1	Boundary condition spring input values (in kips/in).....	436

LIST OF SYMBOLS AND NOTATION

The following symbols are used in this paper.

A_{cs}	cross-sectional area at the end of strut
A_f	area of flexural reinforcement
A_h	total area of shear reinforcement parallel to primary tension reinforcement
A_i	area of section i
A_n	area of tensile reinforcement to resist direct tensile force, N_u
A_{nz}	area of each face of nodal zone
A_{ps}	area of prestressing reinforcement
A_s	area of steel reinforcement
A'_s	area of compression reinforcement along length of strut
A_{sc}	area of primary tension reinforcement
A_{vf}	area of shear-friction reinforcement to resist direct shear, V_u
a_i	fractional surface-weighted area percentage
a_v	shear span (face of column to applied corbel load)
b	member width
b_c	corbel width
d	effective depth to centroid of tension reinforcement
E_c	modulus of elasticity of concrete
E_s	modulus of elasticity of mild reinforcement
E_z	affected width dimension for characteristic section method

F_{nn}	nominal compressive strength of nodal zones
F_{ns}	nominal compressive strength of strut
F_{nt}	nominal strength of nodal ties
f'_c	concrete compressive strength
f_{ce}	effective concrete compressive strength in strut
Δf_p	increase in stress in prestressed reinforcement due to factored loads
f_{py}	yield stress of prestressed reinforcement
f_r	rupture stress of concrete
f'_s	stress in compression reinforcement along length of strut
f_{se}	stress in prestressed reinforcement
f_y	yield stress of mild steel reinforcement
H/V	ratio of horizontal and vertical applied loads
i	section of interest
k_i	thermal conductivity of material i
L	length
m	connector diameter used in zone method and modified zone method
N_u	applied horizontal force on corbel
p	reinforcement ratio = $\frac{A_s}{bd}$
R_i	thermal resistance of element i
U	thermal transmittance
V_{sus}	sustained load
V_u	ultimate strength

W	affected width dimension for zone method
W_n	affected width dimension for modified zone method
α	empirical value used in characteristic section method
β	empirical value used in characteristic section method
β_n	nodal zone coefficient
β_s	strut coefficient

LIST OF ABBREVIATIONS

ACI	American Concrete Institute
ACMA	American Composites Manufacturers Association
APA	Engineered Wood Association
ASHRAE	American Society of Heating, Refrigerating, and Air-Conditioning
ASTM	American Society for Testing and Materials
BDI-STs	Bridge Diagnostics Inc. Structural Testing System
BSM	Beam-Spring Model
CBECS	Commercial Buildings Energy Consumption Survey
CFRP	carbon fiber reinforced polymer
EIS	U.S. Energy Information Administration
EPS	expanded polystyrene
FDOT	Florida Department of Transportation
FEM	finite element model
FRP	fiber reinforced polymer
GFRP	glass fiber reinforced polymer
HDO	high-density overlay plywood
HDPE	high-density polyethylene
IECC	International Energy Conservation Code
ISO	polyisocyanurate
LVDT	linear variable differential transformer
MDO	medium-density overlay plywood

PCI	Precast/Prestressed Concrete Institute
R-value	thermal resistance (in English units)
RECS	Residential Energy Consumption Survey
SMASH Lab	Systems, Materials, and Structural Health Laboratory
SWP	sandwich wall panel
TCA	Tilt-Up Concrete Association
USU	Utah State University
XPS	extruded polystyrene

CHAPTER 1

INTRODUCTION

Background

Concrete sandwich wall panels (SWPs) are a popular form of construction for buildings today due to their high thermal efficiency, competitive cost, and quick construction. They have become increasingly popular due to increasing stringency of energy codes and recent changes requiring structures to maintain a continuous insulative building envelope (International Code Council, Inc., 2017).

Concrete sandwich wall panels consist of a layer of insulation sandwiched between two layers (or wythes) of concrete, which are then connected through the insulation by SWP connectors. This type of construction offers a number of additional benefits including superior fire resistance, protection of insulation from damage or deterioration, and excellent moisture protection, contributing to its growing popularity.

Although SWPs are generally very thermally efficient by nature, many panels tend to have localized heat loss at similar locations from structure to structure, namely at the connections. This localized heat transfer, also called thermal bridging, can be a result of either shortcomings to detailing or construction. Certain connection details can create significant thermal bridging, limiting thermal efficiency and even causing premature degradation through condensation at times. The probability of thermal bridging occurring in these structures can be decreased by providing good structural details.

A common location of thermal bridging in partially-composite SWPs today is at corbel locations. Thermal bridging often occurs at these connections due to frequent

inclusion of solid concrete sections for the purpose of transferring structural loads from the corbel to both wythes equally. This type of heat transfer can be avoided by reducing the use of solid sections in SWP structures.

Objective

This project aimed to improve thermal efficiency of partially-composite SWPs by performing infrared thermographic inspections of concrete SWP structures to identify common locations of heat loss. This study investigated thermal bridging in concrete SWP structures for the purpose of identifying thermally efficient details that can be used in the industry to improve sustainability, reduce energy use and heat transfer, and reduce environmental impact of concrete SWP buildings.

While this dissertation does not present any new analysis techniques, it provides visual evidence of several types of common and necessary details that affect thermal performance and provides several analyses to quantify these effects. Several details that can provide improved building envelope are also presented for use. Armed with this knowledge, engineers and architects can make more informed decisions and strive to maintain the very effective building envelope a SWP provides. This project intended to document the improvements to the SWP system over the years, which, across the United States, provides an excellent combination of structure and envelope.

This project also focused on improving thermal efficiency by creating alternative designs for SWP corbel connections that are structurally sufficient and thermally superior to currently popular details. This study did so by creating, building, and testing alternative designs to prove structural adequacy and reduce thermal bridging at corbel

connections. The results of this study will help optimize thermal performance of concrete SWP structures by helping maintain a continuous insulative building envelope so that heat transfer is minimized.

The final objective of this project was to validate use of the Beam-Spring Method for predicting SWP behavior under combined flexural and axial loading. This method had shown promise for such application, and was therefore used to model the corbel specimens created herein. Results show that the BSM provides good agreement with the experimental data. A parametric study was also performed to quantify second-order effects in SWPs and to investigate effects of length, panel stiffness, and wythe configuration on SWP behavior under combined axial and flexural loading.

The findings of this project will ultimately decrease environmental impact of SWP structures by reducing the building material required for their construction, improving sustainability, reducing energy use and heat transfer, and increase the safety of concrete SWP structures.

Dissertation Outline

Chapter 2 presents a literature review, including a brief history and explanation of the benefits of using concrete SWP construction, heat transfer and thermal efficiency of structures, and SWP corbel connections. Chapter 3 discusses detailing of concrete SWPs and sample thermal analyses of such details. Chapter 4 explains an experimental program to test existing and proposed corbel connections to improve SWP thermal efficiency, including specimen design and construction, test setup, and test results. Chapter 5 presents analysis and a parametric study of SWP specimens under combined axial and

flexural loading using the Beam-Spring Model. Chapter 6 contains the important conclusions of this study.

CHAPTER 2

LITERATURE REVIEW AND BACKGROUND

History of SWP Efficiency

Concrete sandwich wall panels (SWP) are walls consisting of two layers of concrete separated by a layer of insulation and connected by a series of SWP connectors. This type of structure provides a number of advantages over other systems including excellent durability, quick construction, fire resistance, large vertical space between supports, versatile design, protection for insulation against deterioration and moisture, and superior energy performance. In addition, it also has very good thermal mass.

Each layer of concrete or insulation in a SWP is commonly called a wythe, and the naming convention for SWPs follows the wythe thicknesses. For example, a 2-3-6 SWP would indicate a 2-in thick exterior concrete wythe, a 3-in thick insulation wythe, and a 6-in thick interior structural wythe. Likewise, a 3-3-3 SWP would mean a panel where all concrete and insulation wythes are 3 inches thick (PCI, 2011).

Concrete sandwich wall panels have been used in industry in the United States since the early 20th century, with one of the earliest documented constructions being in 1906 (Collins, 1954). Since 1906, the interest in thermal efficiency has increased dramatically. The thermal benefits of this type of construction were noted from the beginning, but various historical events have helped to spur greater interest in this aspect of the panels, most notably the world energy crises. According to the U.S. Energy Information Administration (EIA), renewable energy sources only accounted for 10% of the USA's energy consumption in 2016, indicating that 90% of energy in the USA relied

on non-renewable sources (U.S. Energy Information Administration, 2017). The most recent United States energy crisis occurred in the 2000s, demonstrating the need for energy conservation. The combination of energy shortages and the ever increasing awareness of the finite reserve of our energy sources resulted in a significant movement towards finding affordable, alternative sources of renewable energy, and in improving energy efficiency.

An example of this can be seen in the development and evolution of building energy codes over time. There are two principle energy codes in the United States, namely the International Energy Conservation Code (IECC) (2017) and the American Society of Heating, Refrigerating, and Air-conditioning (ASHRAE) Standard 90.1 (2016). These codes have been developed to reduce energy consumption, reduce costs associated with energy generation, and reduce carbon dioxide emissions. The IECC establishes insulation requirements for different portions of the United States of America by dividing the USA into eight Climate Zones. The IECC required zones 5-8 to have continuous insulation as well as insulation in the stud cavity. This requirement was extended to zones 3-4 in the 2009 IECC (2009), and has steadily increased until 2015. It is clear from these recent changes and the requirement of edge-to-edge insulation that maintaining continuity in the building envelope is important to creating a sustainable and thermally efficient structure.

The objective of an edge-to-edge insulation requirement is to reduce thermal bridging in structures. Thermal bridging is when an element of a structure has a significantly higher thermal conductivity than surrounding elements, allowing a

significant amount of heat to escape (Figure 2-8). This thermal bridging can be costly for building owners, especially over the lifetime of a structure. Luckily, the majority of thermal bridging in SWP structures is avoidable (Sorensen & Maguire, 2017).

As thermal efficiency has increasingly become a priority to the public, advancements in industry have helped to significantly reduce thermal bridging in concrete SWP structures. In the 1906 SWP structure, the two concrete wythes were separated by a thermal barrier of air (Collins, 1954). Although air is not the most thermally insulative material, its resistance to heat transfer was far better than having concrete fill that layer. Today, rigid foam insulation is used instead of air to improve thermal isolation of buildings. Currently there are three principle types of rigid insulation used with sandwich wall panels: expanded polystyrene (EPS), extruded polystyrene (XPS), and polyisocyanurate (ISO). Each has inherent benefits and disadvantages. EPS insulation is made by heating solid beads of polystyrene, which expands the beads with air. It is typically semi-permeable and has a thermal resistance ranging from $R = 3.6$ to 4.2 per inch of thickness depending on the density of the foam (Holladay, 2016a). XPS insulation, alternatively, begins with solid crystals of polystyrene but is mixed and melted with a blowing agent and additives in an extruder until it becomes a liquid. It is then forced through a die and is shaped as a foam. XPS is known for having high compressive strength and resistance to water, having a thermal resistance per inch of approximately $R = 5$. The current blowing agents used for XPS (hydrochlorofluorocarbons, HCFCs) are quite controversial currently due to their potential to harm the ozone, but are anticipated to be replaced with another agent by 2020 (Holladay, 2016a). ISO uses pentane as a

blowing agent, which is not harmful to the environment, but this insulation is quite absorbent of moisture, one reason it often has laminated faces. It has the highest thermal resistance rating ($R = 5.7$ to 6.5 per inch) but the thermal resistance steadily decreases with temperature below 15°C (60°F) whereas XPS and EPS increase in thermal resistance as temperature decreases. ISO and XPS insulations are also subject to thermal drift, which means the thermal resistance naturally decreases over time. This is due to the blowing agent slowly being replaced by regular air inside the insulation (Holladay, 2016b). Each insulation has advantages and disadvantages, but selection of the best insulation will depend heavily on the conditions and needs of any given project. The average thermal resistance values are summarized in Figure 2-1.

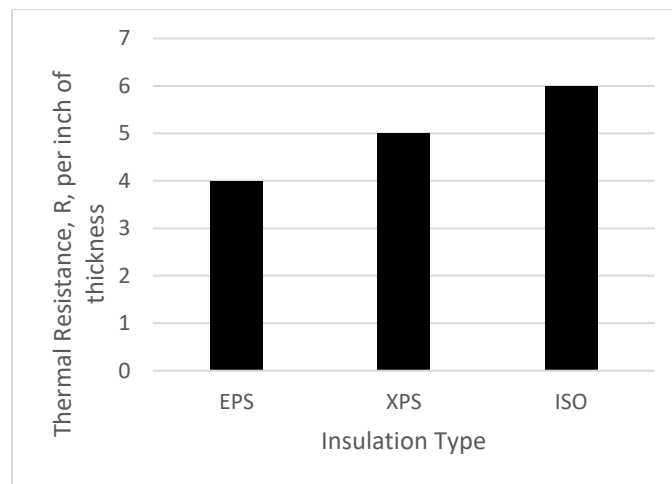


Figure 2-1 Thermal resistance (R-values) comparison of insulation types (data retrieved from (Holladay, 2016a))

Historically, steel connectors (truss connectors, pins, etc.) were a common way to connect concrete wythes. By the 1990s, it had become apparent that these steel

connectors were decreasing the thermal advantage that SWPs had over other types of construction due to heat transfer at these connections because of the high thermal conductivity of the steel. To improve the thermal efficiency of SWPs, the industry began investigating different types of connectors made of fiber-reinforced polymer [plastic] (FRP) to replace the conventional steel ties. For example, Einea et al. (1994) proposed four different shapes, with only one (in the shape of a bent bar) successfully passing through the first stages of consideration in their study. The geometry of the bar allowed the axial capacity of the connectors to determine the shear capacity of the panels. This study concluded that FRP connectors were structurally sufficient and far superior thermally to alternative steel connectors. Today there are a variety of FRP connectors available on the market.

In addition to such advances, concrete SWPs also naturally benefit from thermal mass. Thermal mass is the ability of a material to absorb and store energy, and is calculated by multiplying the density of the material, the thickness of the material, and the specific heat of the material together. Al-Homoud (2005) explained how this benefits structures by stating that thermal mass “reduces heat gain in the structure by delaying entry of heat into the building (until the sun has set).” Because concrete is very dense, it can absorb and store significant energy during the day to be used in the evening and night time when there is greatest need to heat a structure. This shift of the peak energy load reduces peak heating and cooling loads. The energy codes also make provisions where the required thermal resistance of a structure can be lowered if sufficient thermal mass is

present since thermal mass helps to offset and reduce the amount of heating and cooling necessary for a given structure. Concrete structures almost always have sufficient thermal mass to benefit from these code provisions. Concrete SWPs are in a unique position to benefit from both the excellent insulative capabilities inherent to this form of construction, as well as the benefits of thermal mass.

Advancements have also increased structural efficiency, allowing SWPs to become much more slender as designers take advantage of composite action in design. Sandwich wall panels are generally classified into two groups, according to the amount of composite action they are designed to have. Sandwich wall panels designed to have 0% composite action are known as non-composite panels, where panels designed to count on any degree of composite action greater than 0% are known as partially-composite panels. The strain distribution in SWPs will vary depending on this percentage (Holladay, 2016a). As percentage of composite action increases, so does the structural efficiency of the wall panel since this allows much more slender panels to withstand greater structural capacities. Along with the narrowing of wall thickness, however, comes a set of challenges, many relating to the thermal efficiency of the structure.

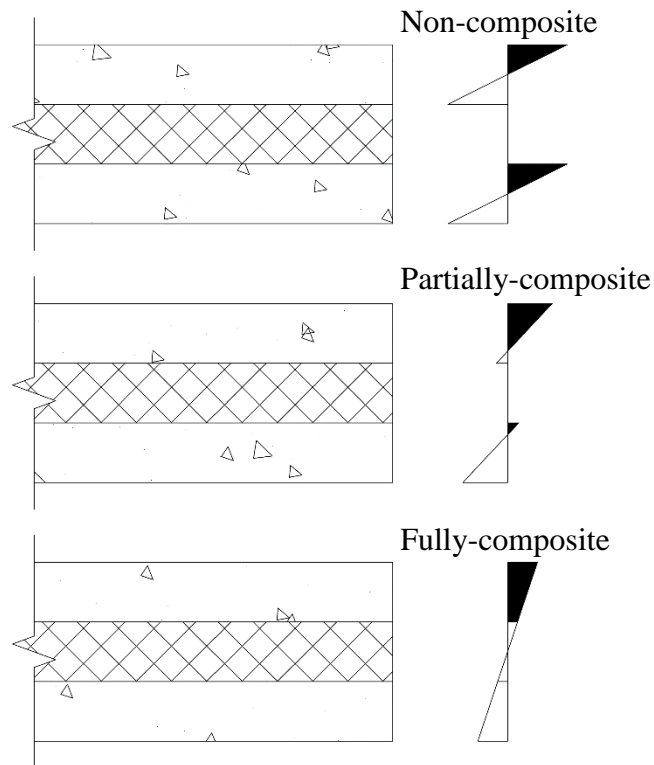


Figure 2-2 Stress distribution comparisons for differing levels of composite action

Heat Transfer in Buildings

The introduction of FRP connectors in SWP construction has gained considerable traction among owners, architects and engineers since their introduction, solving the most glaring issue with sandwich panel efficiency. However, there are several other areas of concern, including thermal bridging in connections, thermal bowing, and condensation that need to be addressed.

All buildings experience heat transfer. Even the most well-designed, meticulously-detailed, carefully-constructed structure will experience heat transfer because there is no material that exists that is a perfect insulator. Proper design, detailing,

and construction can reduce the amount of heat transferred, however, by eliminating short-cuts for the heat to escape (also known as thermal bridging) and thereby reducing condensation formation in structures. Thermal imaging is one way to identify locations of thermal bridging so that thermal resistance of a structure can be determined.

Thermal Bridging

Thermal bridging occurs when a component of a building has significantly higher heat transfer than surrounding components. This allows significant heat to escape. Thermal bridging can be thought of as a thermal short circuit for heat. To illustrate, think of a building like a bucket of water. If there are holes through the bucket, water will leak out; likewise, penetrations of highly conductive material through the insulation of the building are like holes in the bucket where heat will leak out. Thermal bridging at various locations within a structure can make those areas much hotter or colder than other parts of the building, causing uncomfortable occupants in certain rooms in addition to overall reduction in thermal efficiency. Examples of thermal bridging can include steel connectors that puncture the insulation, solid concrete sections used in design, or corbels that require concrete to displace insulation to attain the required capacity. Ideally, the concrete wythes of the SWP would be completely separated by the insulation, with no penetrations of any kind. This unfortunately cannot happen in most cases due to many different structural, lifting, and fabrication requirements. However, one purpose of this report is to compile past and present best-practices in order to allow for continued improvement of SWPs.

Condensation

If heat is entering or leaving the building through thermal bridges, it can create localized patches of warmer or colder concrete on the inside or outside of the concrete. If the temperature of the concrete reaches the dew point, condensation will occur at the localized thermal bridges. An example of this in a sandwich panel structure is shown in Figure 2-3, where there are solid corbel sections holding the roofing components. These thermal bridges have condensed and even frozen in this case. This phenomenon was also demonstrated by Seshappa and Dixon (2013). This condensation can cause unwanted water freezing and thawing, concrete moisture that could initiate corrosion, and water damage to interior and exterior components (drywall, insulation, exterior paint, etc.). Deterioration of insulation due to moisture can also lead to a further increase in heat transfer.



Figure 2-3 Frozen condensation visible on exterior of a building

Thermal Imaging

Thermal cameras can be used to photograph structures to identify areas of greater or lesser temperatures on the exterior of a building. If ambient outside temperature is significantly different than the inside temperature of a structure, locations of greater temperature difference identified in thermal images can reasonably be assumed to be locations of thermal bridging in structures. Figure 2-4 and Figure 2-5 demonstrate how thermal images can be used to identify locations of thermal bridging. Figure 2-4 shows a thermal image from outside a wall from which two lighter spots may be seen near the floor. Lighter areas are areas of warmer temperature, so heat is apparently escaping through these locations. Figure 2-5 is a thermal image of the same wall but taken from the inside of the building. Note that there are again two spots near the floor, but they are darker spots, indicating colder surface temperatures at these locations.

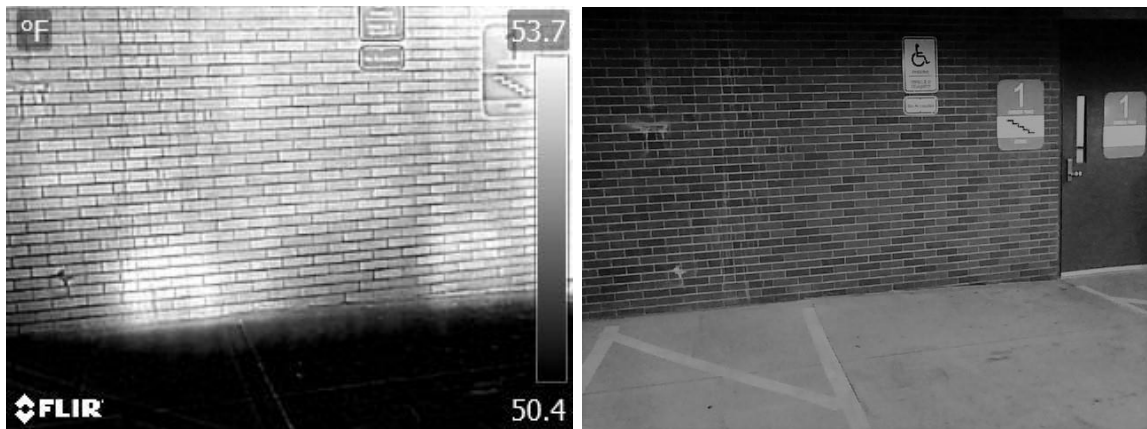


Figure 2-4 Heat transfer through thermal bridge at base of wall (exterior of stairwell)

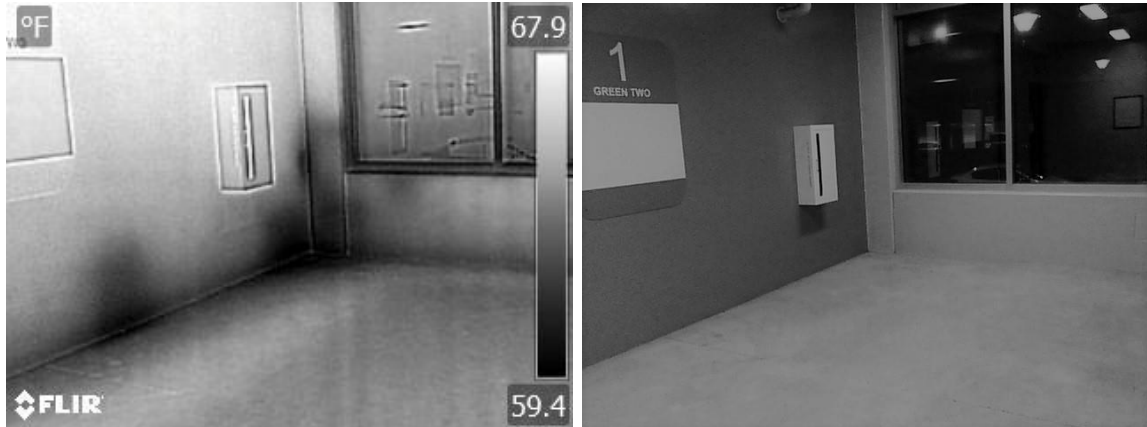


Figure 2-5 Heat transfer through thermal bridge at base of wall (interior of Figure 2-4 stairwell)

Radiant heating from the sun can cause the surface of a building to be higher than it would be due to heat transfer alone. This can distort the results and make it difficult to identify what portion of temperature is due to solar radiation and which is thermal bridging, or even mask thermal bridging altogether. Ideal conditions for thermal imaging structures would be in the coldest part of winter during the middle of the night since this would be the time that the temperature difference between inside and outside would be greatest, and because the effects of the sun would have been minimized. For summer conditions (particularly when analyzing a freezer or cold-storage facility), similar conditions would be desired, but on the hottest day of the year. The results for summer measurements would likely not be as good as winter results since the temperature at nighttime typically drops and a highest possible temperature would be preferred, but the effects of solar radiation should be avoided if identification of thermal bridging in buildings is sought for, which is why the thermal images need to ideally be taken at night.

Furthermore, winter conditions are typically more relevant when compared to summer conditions because the greatest energy concern in the United States of America is for heating structures. According to the U.S. Energy Information Administration (EIA) in the most recent Residential Energy Consumption Survey (RECS) released to the public (U.S. Energy Information Administration, 2009), heating accounted for 41.5% of residential energy use in 2009, whereas air conditioning only accounted for about 6.2% (see Figure 2-6). The EIA's most recent Commercial Buildings Energy Consumption Survey (CBECS) released to the public (U.S. Energy Information Administration, 2012) related that 25.2% of energy use in 2012 was used for heating structures and about 9.4% was used for cooling (see Figure 2-7). Although it is obviously desirable to prevent thermal bridging in any season of the year, the easiest, most applicable, and ideal time of the year to take the thermal images in the USA is in winter for most buildings.

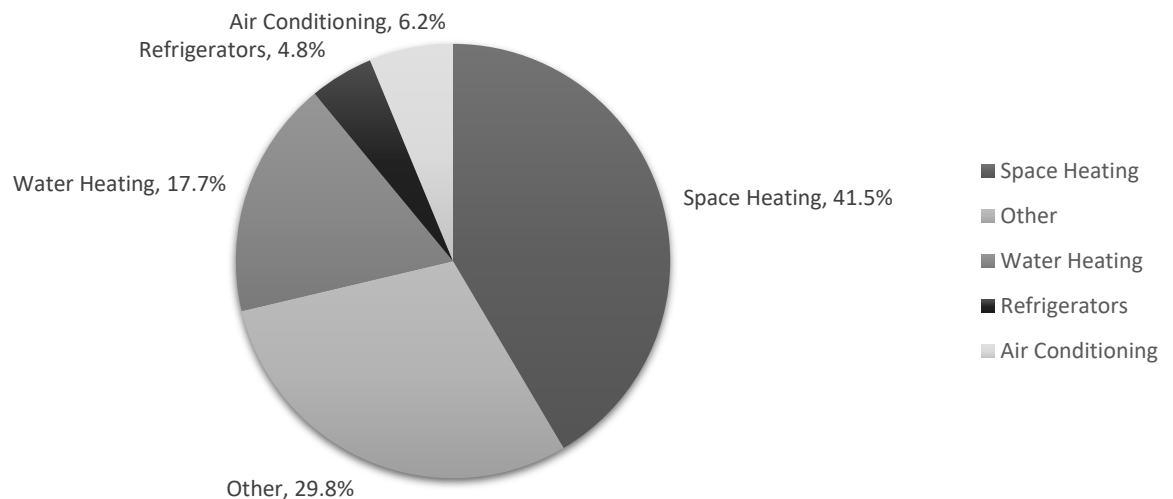


Figure 2-6 Residential Energy End-Use in 2009 (data retrieved from (U.S. Energy Information Administration, 2009))

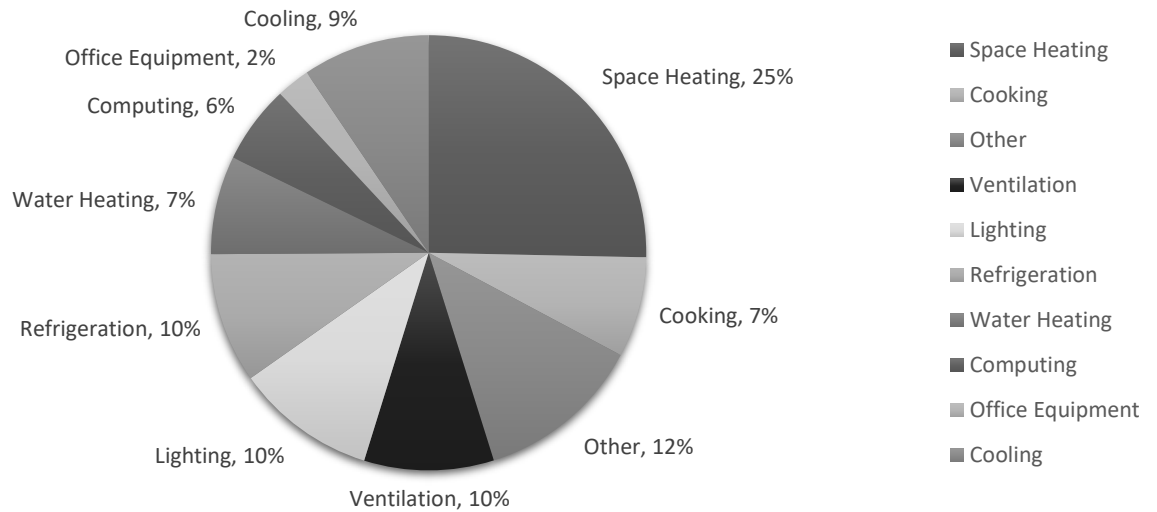


Figure 2-7 Commercial Energy End-Use in 2012 (data retrieved from (U.S. Energy Information Administration, 2012))

SWP Corbel Connections

As industry continues to push the boundaries by making wall panels more slender and more structurally efficient, the solutions for transferring loads at connections can often do so at the expense of thermal efficiency. One such connection is at corbel locations (Figure 2-8), a particular concern because such connections often serve as a junction for high load transfer, and due to the typically regular spacing of such connections (Sorensen & Maguire, 2017). Previous research has demonstrated, however, that thermal bridging for corbels can be avoided through careful detailing and by using innovative design.

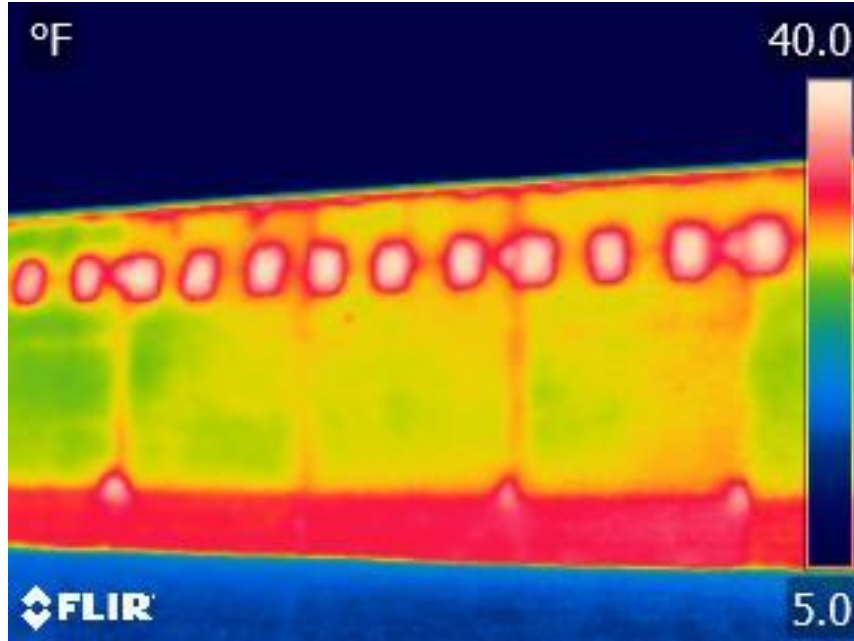


Figure 2-8 Thermal bridging at corbel connections in SWP structure

Corbel Design Research

There have been several researchers in the past that have sought to improve our ability to understand and design safe corbel connections. Kriz and Rath (1965) sought to create a design criteria for corbel connections, creating an experimental program to create and test 195 corbels. Of these 195 corbels, 124 were subjected to vertical loading only while the other 71 were loaded both vertically and laterally. The tests considered a wide range of variables, including ratio of the horizontal applied load to the vertical applied load, size and shape of the corbel, amount and distribution of stirrup reinforcement, ratio of shear span to effective depth, concrete strength, and reinforcement ratio. From this study, Kriz and Rath developed an empirical equation to predict ultimate strength for a

corbel with vertical loading only (Eq (2-1)) and with combined vertical and lateral loading (Eq (2-2)) as follows:

$$V_u = \Phi [6.5bd\sqrt{f'_c}(1 - 0.5^{d/a})(1000p)^{1/3}] \quad (2-1)$$

$$V_u = \Phi \left[6.5bd\sqrt{f'_c}(1 - 0.5^{d/a}) \left(\frac{(1000p)^{(1/3+0.4H/V)}}{10^{0.8H/V}} \right) \right] \quad (2-2)$$

Where: V_u = ultimate strength, *lbs*

b = corbel width, *in*

d = effective depth to centroid of tension reinforcement, *in*

f'_c = concrete compressive strength, *psi*

a = shear span (face of column to applied corbel load), *in*

p = reinforcement ratio = $\frac{A_s}{bd} \leq 0.013$

A_s = area of steel, *in*²

H/V = ratio of horizontal and vertical applied loads

Mattock, Chen, and Soongswang (1976) built upon the research of Kriz and Rathes by testing 28 corbel specimens to create a design methodology for the design of horizontal stirrup reinforcement. They argued that a minimum amount of horizontal stirrup reinforcement greater than or equal to half of the main tension reinforcement required to resist moment or one-third of the yield strength of the reinforcement required to resist shear should be required to avoid premature diagonal tension failure.

With respect to the creation of thermally insulative corbel connections in SWPs, little research has been completed in the literature other than one study performed by Elkady (2013). In his study, he presented two alternative connections to avoid thermal bridging and validated the designs by testing 7 specimens experimentally. One detail utilized #3 GFRP bars and the other used the proprietary NU-Tie connector with positive results. Elkady's findings confirmed that creating corbel connections in SWPs without thermal bridging is feasible.

Current Practice

In practice currently, there are three common details used for corbel connections. The most common of them in partially-composite SWPs involves creating a solid section at the corbel location. This ensures 100% composite action at the corbel and ensures adequate load transfer such that both wythes will share the load equally. Unfortunately, however, concrete is a poor insulator. This means that such solid sections allow a significant amount of heat to be lost. Sorensen & Maguire (2017) showed that 1 sq ft solid concrete sections spaced every 6 ft o.c. in a 12'x30' panel will yield an approximate drop in thermal efficiency of about 10%.

For those concerned with the thermal performance of the structure and conscious of thermal bridging, a popular approach is to avoid the problem by designing the panels to be non-composite. This typically bypasses the problem because non-composite panels rely entirely on the interior wythe to withstand all structural loads. This means that the interior wythe is usually thick enough that there is no need to reduce, remove, or penetrate insulation for a corbel connection. Although this selection can be a good option

for thermal efficiency, it is made at the partial expense of structural efficiency as non-composite walls are thicker than non-composite walls and require more material.

An alternative approach some use in industry is to create an internal pilaster within a partially-composite SWP. This is done by local thickening of the wythe at the corbel location by reducing the insulation thickness to attain sufficient structural capacity for the inside wythe to withstand the entire load by itself. This approach is a sort of hybrid between non-composite and composite panel design by allowing wythes to work compositely, but also allowing the interior wythe to withstand the immediate local stresses and loads induced on the corbel. This type of design can be more labor-intensive than the previous two approaches though, and often requires the insulation to be cut from a thickness of 4 or 3 inches down to only an inch at corbel locations. Each of these design approaches has benefits, but each also carries its own set of challenges.

The four failure modes for corbels according to ACI 318-14 (2014) and Elzanaty, Nilson, & Slate (1986) include shearing at the corbel/wall interface, crushing/splitting in the compression strut, yielding of the tension tie, or local bearing or shear failure under the loading plate. There are two codified methods for designing corbels in ACI 318-14 (2014): the Deep Beam Method and the Strut-and-Tie Method. The following sections give a brief synopsis about each.

Deep Beam Method

The Deep Beam Method (also known as the Cantilever Beam Method), as its name denotes, treats the corbel as it would a deep cantilever beam. The Deep Beam method is found in ACI 318-14 §16.5 (2014) as well as in the PCI Design Handbook (2010). For a

beam to be designed by the provisions of this method, the span-to-depth ratio, $\frac{a_v}{d}$, must be less than or equal to 1.0 and must have a factored horizontal tensile force, N_{uc} , less than or equal to the factored shear force. This method also requires that the corbel face height be at least $0.5d$ to avoid premature failure due to crack propagation from the sloping face.

According to this method, the nominal concrete capacity for use of normalweight concrete is determined by §16.5.2.4 as:

$$\Phi V_n = \Phi \min \left(\begin{array}{c} 0.2f'_c b_w d \\ (480 + 0.08f'_c) b_w d \\ 1600b_w d \end{array} \right) \geq V_u \quad (2-3)$$

It is important to note also that this method requires the corbel to be designed for a horizontal force of at least $0.2V_u$ unless tensile forces are somehow prevented from being applied to the corbel.

Aside from checking nominal shear, tensile, and moment capacity of the corbel, there are also reinforcement limits according to ACI 318-14 §16.5.5.1, which mandate that the primary tension reinforcement be

$$A_{sc} \geq \max \left(\begin{array}{c} A_f + A_n \\ \left(\frac{2}{3}\right) A_{vf} + A_n \\ 0.04 \left(\frac{f'_c}{f_y}\right) (b_w d) \end{array} \right) \geq V_u \quad (2-4)$$

Where: A_{sc} = area of primary tension reinforcement

A_f = area of flexural reinforcement

A_n = area of tensile reinforcement to resist direct tensile force, N_u

A_{vf} = area of shear-friction reinforcement to resist direct shear, V_u

And the total area of closed stirrups parallel to A_{sc} be

$$A_h = 0.5(A_{sc} - A_n) \quad (2-5)$$

spaced such that A_h is uniformly distributed within $\frac{2}{3}d$ from the primary tension reinforcement.

Finally, anchorage of the primary tension reinforcement is paramount at the front of the corbel or bracket, which explains the requirement of the code to ensure anchorage by either welding a transverse bar of at least equal size that is designed to develop the yield stress of the primary tension reinforcement, bending the primary tension reinforcement back to form a horizontal loop, or using some others means to ensure that yield stress is developed in the primary tension reinforcement.

Strut-and-Tie Method

The other method allowed for in the code is the Strut-and-Tie Method. It is found in Chapter 23 of ACI 318-14 (2014). This method essentially reduces the complex stresses in the corbel to a simplified truss model. After determining the forces within each component of the truss, only the stresses of these elements must be compared to the permissible stresses (Brown, et al., 2005). The compressive elements of this fictitious truss are called struts, and the tensile elements are called ties.

There are two distinct regions considered in the strut-and-tie model: beam regions (B-regions) and discontinuous regions (D-regions). B-regions are those where the assumption that “plane sections remain plane” and other basic principles of strain distribution apply. D-regions are regions with some sort of discontinuity, whether it be

geometric or with regards to loading/reactions They encompass the discontinuity itself, plus a distance equal to the depth of the member, h , away from the discontinuity. The code allows D-regions to be designed using strut-and-tie modeling. Because corbels are a geometric discontinuity, they qualify for such a design.

D-regions are designed to transfer all factored loads to an adjacent B-region or support. The code requires the angle between the axes of any strut and any tie entering a single node to be at least 25° . The strength of struts is calculated as

$$F_{ns} = f_{ce}A_{cs} + f'_sA'_s \quad (2-6)$$

Where F_{ns} = nominal compressive strength of strut

f_{ce} = effective concrete compressive strength in strut = $0.85\beta_s f'_c$

β_s = strut coefficient (0.4 – 1.0)- see ACI 318-14 Table 23.4.3

A_{cs} = cross-sectional area at the end of the strut under consideration

f'_s = stress in compression reinforcement along length of strut

A'_s = area of compression reinforcement along length of strut

The strength of ties is calculated as

$$F_{nt} = A_s f_y + A_{ps}(f_{se} + \Delta f_p) \quad (2-7)$$

Where $(f_{se} + \Delta f_p) \leq f_{py}$

$A_{tp} = 0$ if member is nonprestressed

The code allows Δf_p to be taken as 60,000 psi for bonded prestressed reinforcement and 10,000 psi for unbonded prestressed reinforcement.

The strength of nodal zones is calculated as:

$$F_{nn} = f_{ce} A_{nz} \quad (2-8)$$

Where $f_{ce} = 0.85\beta_n f'_c$

β_n = nodal zone coefficient (0.6 – 1.0)- see ACI 318-14 Table 23.4.3

A_{nz} = area of each face of a nodal zone

Dissertation Significance and Contributions to Literature

The expected results for these objectives provide additional tools for engineers, architects, contractors, and others to enable the creation of structures that capitalize on both the thermal benefits of a continuous insulative building envelope (which non-composite SWP structures can most easily achieve currently) and the structural benefits of composite SWP design. Current practice consists of choosing one at the expense of the other. The results of this project presented herein help composite panels to perform competitively with the popular non-composite systems, improving the sustainability of SWP structures by decreasing the material required for construction, and decreasing thermal bridging in structures. The increase in thermal efficiency of structures will help to save money for owners by decreasing energy costs associated with heating and cooling the structure, which also will decrease costs for communities as well by decreasing the energy production demand. As a result, improved thermal efficiency in buildings consequently will help decrease CO₂ emissions. Therefore an inadvertent benefit of this

research is improved air quality. The findings of this project also provide validation for the Beam-Spring Model in its use for panels subjected to combined axial and flexural loading. This means engineers have an additional tool to help them confidently and accurately account for $P-\delta$ effects in SWP design, granting greater peace of mind for the designer and greater safety for the structure.

CHAPTER 3

THERMAL DETAILING

Engineers, designers, and contractors typically spend most of their attention on creating a safe and stable structure, which is clearly the most important goal. Once the objective of safety is reached, however, the issues of thermal efficiency should be addressed. Minor changes in detailing and design can significantly increase thermal efficiency, with little to no additional time required in design and construction. Though it is true that thermal bridging may still result from fabrication shortcomings, this is difficult to predict. Making minor changes can save property owners thousands of dollars in heating costs per year, improve the occupant's comfort and decrease life cycle costs. All of which improve client satisfaction and further promotes both the individual companies and firms involved in construction, as well as the industry as a whole.

Common Thermal Bridging Locations

Thermal bridging tends to occur in common locations among SWP structures (Sorensen, Dorafshan, & Maguire, 2017). To help improve and optimize thermal efficiency of SWP structures, historical connection details are identified and discussed in the following sections, including windows and doors, solid sections, wall penetrations, lifting points, corbels, roof termination, floor termination, connections to the foundation, corners, panel-to-panel connections, insulation joints, and metal SWP connectors. Lighter areas of the thermal images indicate locations of higher temperature, while darker areas indicate lower temperatures. Most of the images presented are from older structures.

Identifying information is withheld to protect those involved. Permission to be onsite was obtained from all appropriate building managers/owners in all cases. All thermal images were taken with a FLIR E8 thermal camera with 320x240 spatial resolution and $\pm 0.2^{\circ}\text{C}$ sensitivity, between 9:00 pm and sunrise, between January and early March to maximize the thermal differences. Utilizing the details suggested in this section will help SWP structures continue to achieve their potential as the most thermally efficient building system currently on the market.

Thermally Efficient Buildings

State-of-the-art SWP buildings are in all cases exceptionally thermally efficient. When properly detailed and constructed, it is difficult to find an alternative mode of construction that will yield better results. Figure 3-1 shows a multi-story SWP structure where the entire face of the building is essentially the same color, indicating that heat is being lost equally across all parts of the wall (no severe thermal bridging). At first glance there seems to be some thermal bridging between floors, but these lighter locations are most likely due to differing reflectivity for the architectural rustication bands that appear at these locations



Figure 3-1 SWP structure with marginal thermal bridging

An example of good detailing around windows is shown in Figure 3-2 where the color of the wall appears mostly homogeneous. Notice that there is no significant rise in temperature adjacent to the windows. Again, there are lines discernable where rustication bands are located which are due to reflectivity of the surface. Figure 3-3 shows a building with corners that have been well-detailed to avoid unnecessary heat transfer.

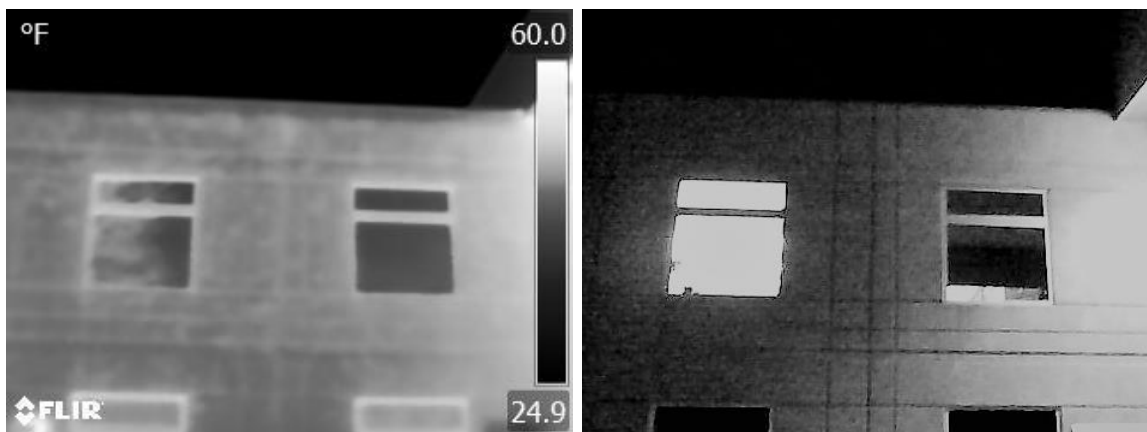


Figure 3-2 SWP structure with minimal thermal bridging around windows

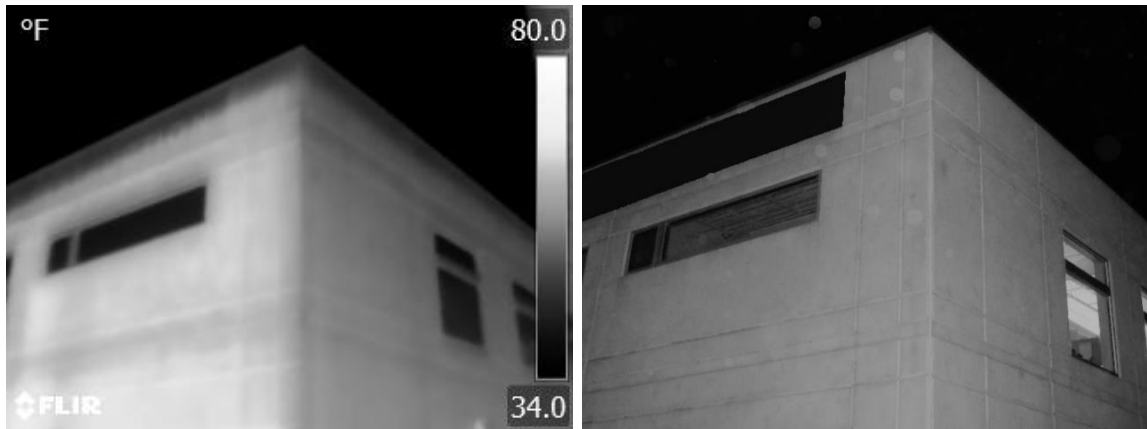


Figure 3-3 SWP structure with minimal thermal bridging at corners

Figure 3-4 shows a SWP building with good roof termination since no concentration of heat transfer occurs there as well. Good detailing can lead to outstanding thermal performance and the elimination of unnecessary thermal bridging. Figure 3-5 shows another such example of a SWP structure that was well-detailed.

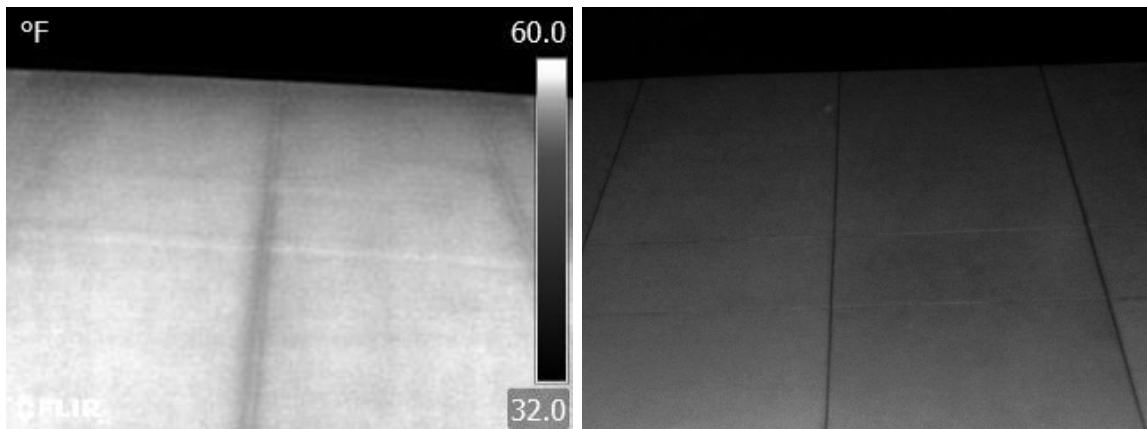


Figure 3-4 SWP structure with no thermal bridging at roof termination

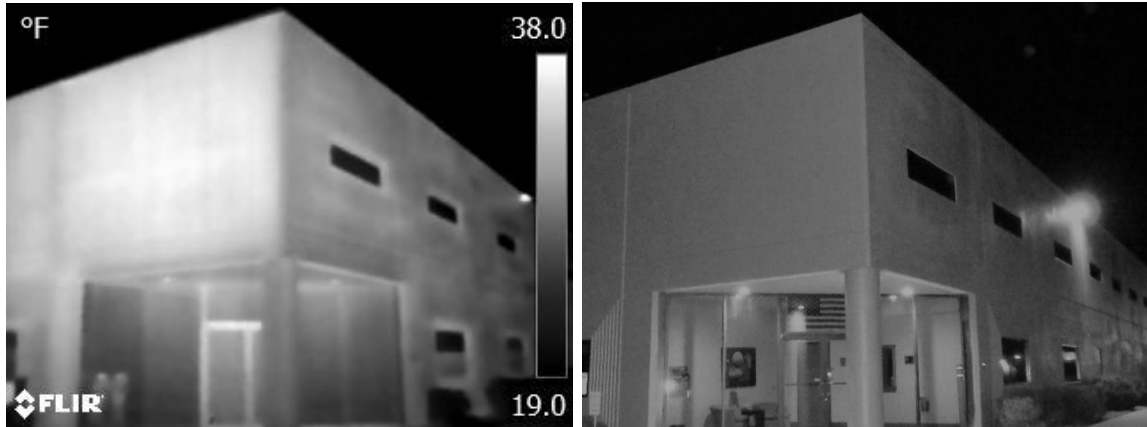


Figure 3-5 Well-detailed SWP structure

Windows and Doors

Thermal Imaging Results

Windows and Doors can complicate thermal design because of stress concentrations around the edges of these openings. Designing these locations as solid sections is one way engineers opt to deal with this structural issue, but this approach typically decreases the energy efficiency by creating a substantial thermal bridge (Sorensen, Dorafshan, & Maguire, 2017). Figure 3-6 and Figure 3-7 show how significant heat can be lost when this is done.

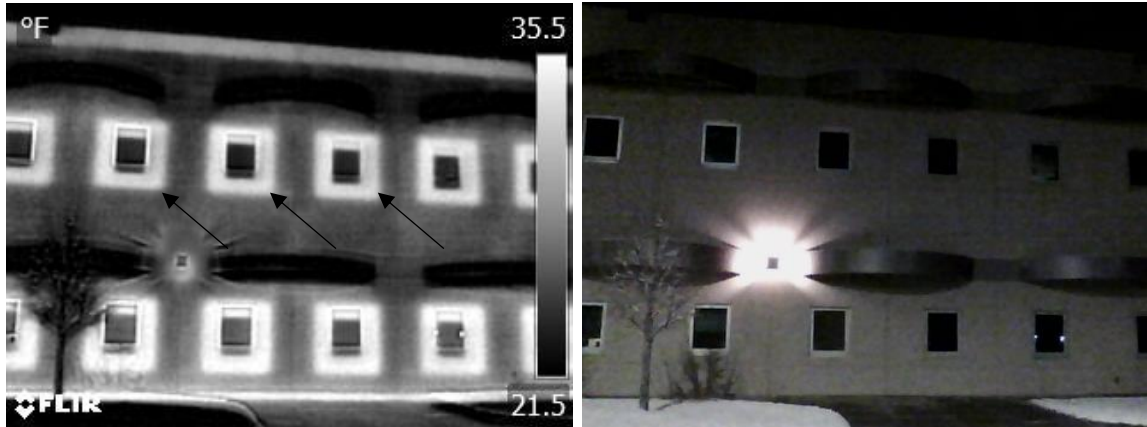


Figure 3-6 SWP structure with thermal bridging around windows: thermal image (left) and visual image (right)

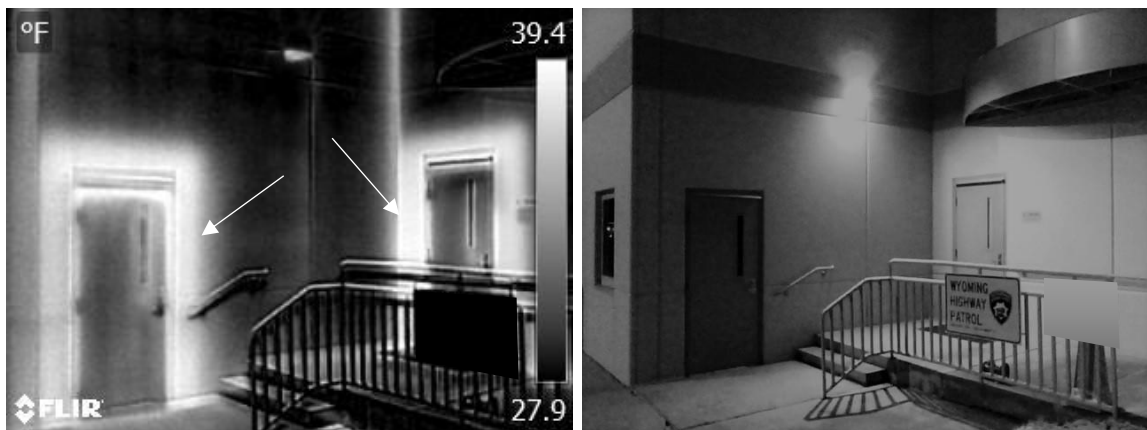


Figure 3-7 SWP structure with thermal bridging around doors: thermal image (left) and visual image (right)

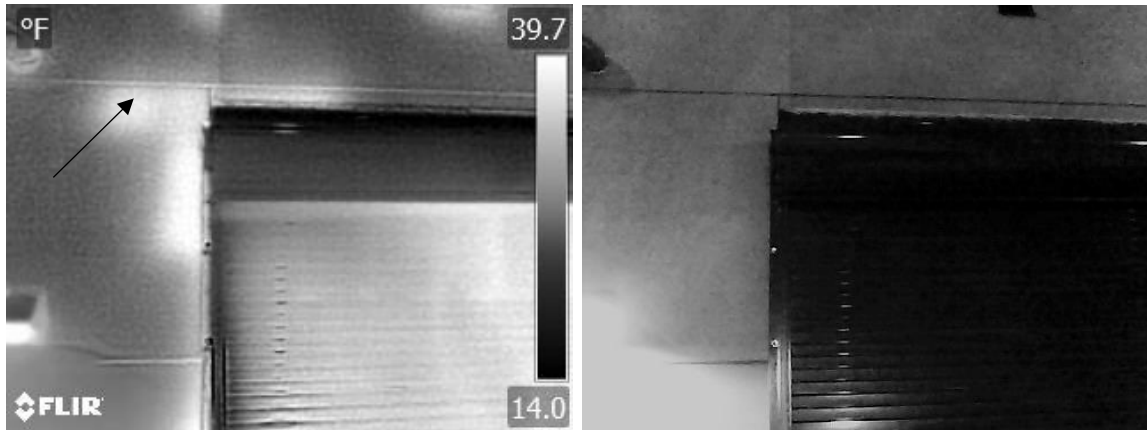


Figure 3-8 SWP with thermal bridging at reinforcement of door corner: thermal image (left) and visual image (right)

Detail Discussion and Recommendations

It is intuitive that if insulation is displaced, heat transfer will occur. Doors and windows are no exception to this logic. Figure 3-9 shows some examples of common details used for windows and doors that are structurally sound, but that can result in a significant amount of thermal bridging. In many cases, structures that are designed with thermal bridging were designed as such for structural or durability purposes and cannot be avoided without some form of technological advancement.

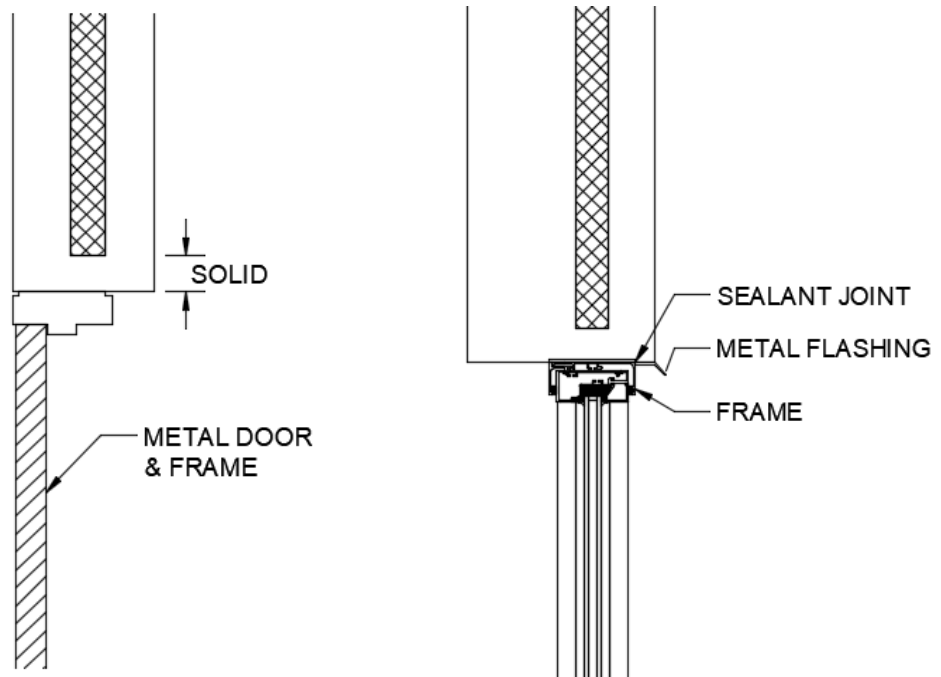


Figure 3-9 Sample of structurally sound details resulting in thermal bridging around windows and doors

The reason these details tend to result in significant thermal bridging is due to the solid concrete section directly bordering the windows. Figure 3-10 shows details that have attempted to eliminate these solid sections by extending some insulation to the window/door edges, which is what should happen. These details require a reduced amount of insulation though, probably to account for the stresses near the window and door frames. Ideally, to decrease thermal bridging, the insulation should not need to be reduced at all around windows and doors as shown in Figure 3-11. However, this may not be possible due to fenestration requirements and loading demands.

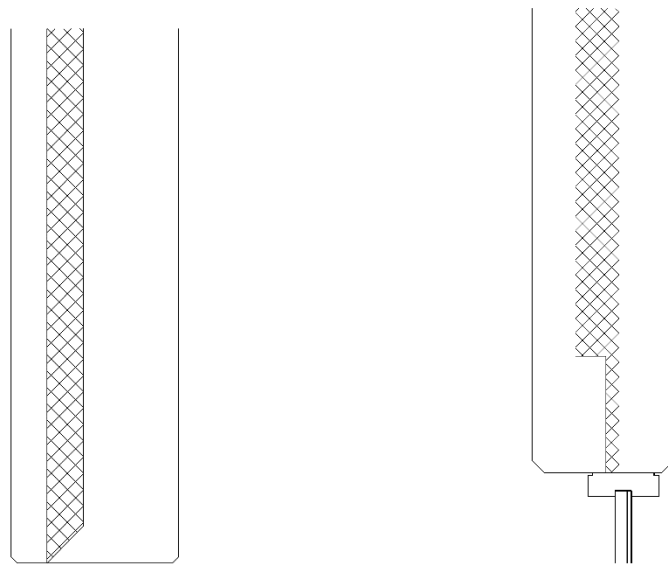


Figure 3-10 Sample of improved details that prevent moderate thermal bridging around windows and doors

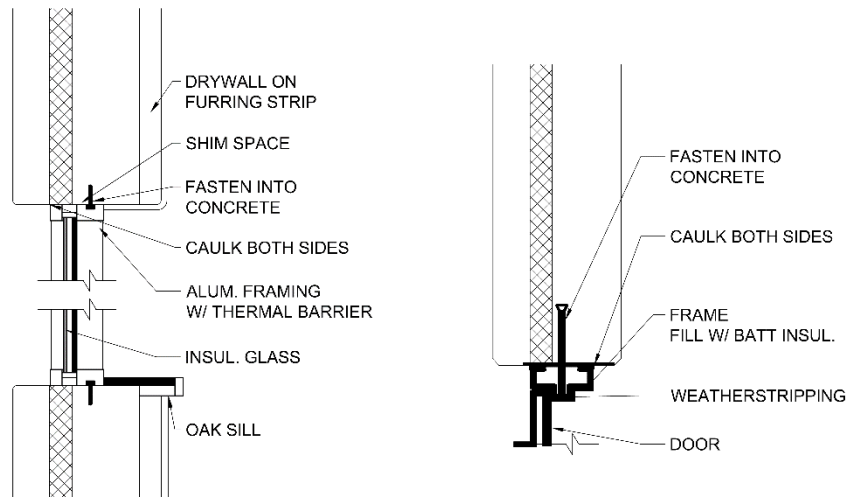


Figure 3-11 Sample details that minimize heat transfer around windows and doors by maintaining continuous insulative envelope

Solid Sections

Thermal Imaging Results

Solid sections are an easy way to ensure that the strength required can be obtained for any particular part of a building, but can cause thermal bridges since concrete is a relatively good conductor of heat, when compared to the insulation. Significant heat can be transferred in these sections as is shown in Figure 3-12 and Figure 3-13. It might be noted that some of the most common locations for solid sections to occur tend to be around doors and windows, panel edges, and foundations. It should be noted that there are many solid sections in contemporary buildings that have been unavoidable in the past due to structural considerations. The purpose of the section is to draw attention to solid sections, in order for future solutions to be developed.

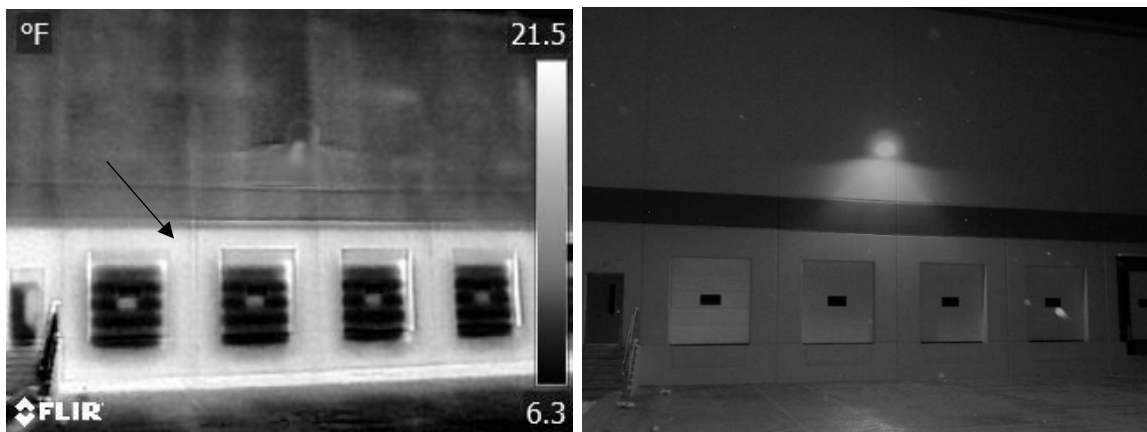


Figure 3-12 SWP with thermal bridging at solid sections around loading dock: thermal image (left) and visual image (right)

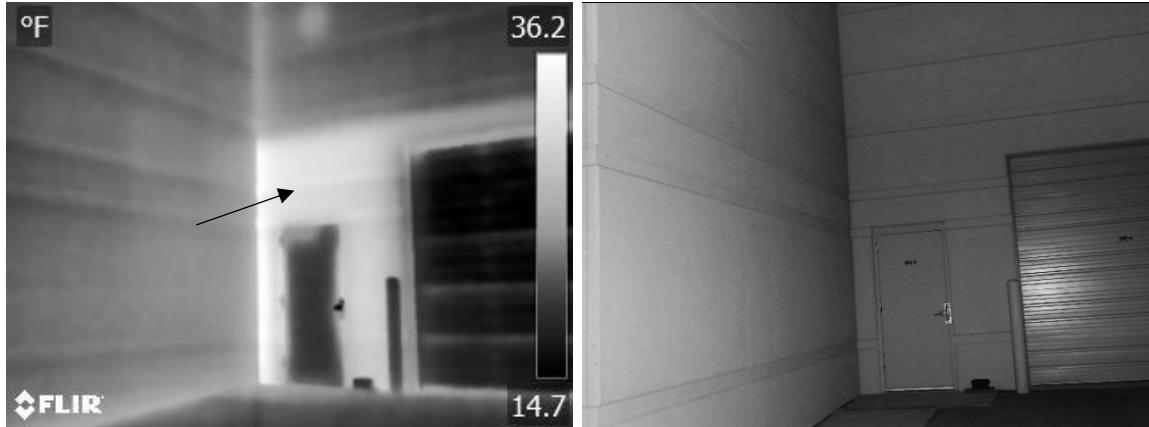


Figure 3-13 SWP with thermal bridging at solid sections around door: thermal image (left) and visual image (right)

Detail Discussion and Recommendations

Solid sections need to be designed and detailed, but there is no simple way to avoid thermal bridging at these locations due to the extreme difficulty in maintaining continuity in the building envelope. Therefore, they are often avoided as much as possible since they clearly create large voids in the thermal resistance of a structure. There are no recommended details to use for this because the recommendation is to avoid solid sections when possible. Alternative methods of construction have been developed that in most instances can replace the need for solid sections, such as partially or fully-composite concrete sandwich wall sections (Olsen et al. 2017, Al-Rubaye et al. 2017).

Wall Penetrations

Thermal Imaging Results

There are times when SWP buildings require some penetrations through the insulation, but to increase thermal effectiveness, they should be avoided when possible. One common penetration required among SWP structures is for plumbing and electrical wiring (Figure 3-14). Although it might be necessary for a pipe or conduit to cross through the insulation, the temptation to run the wiring or plumbing between the concrete wythes should be avoided as this requires that insulation be displaced. This can be aesthetically pleasing but significantly decreases thermal performance of the structure. This is often a necessity of building operations and is an issue in all building types.

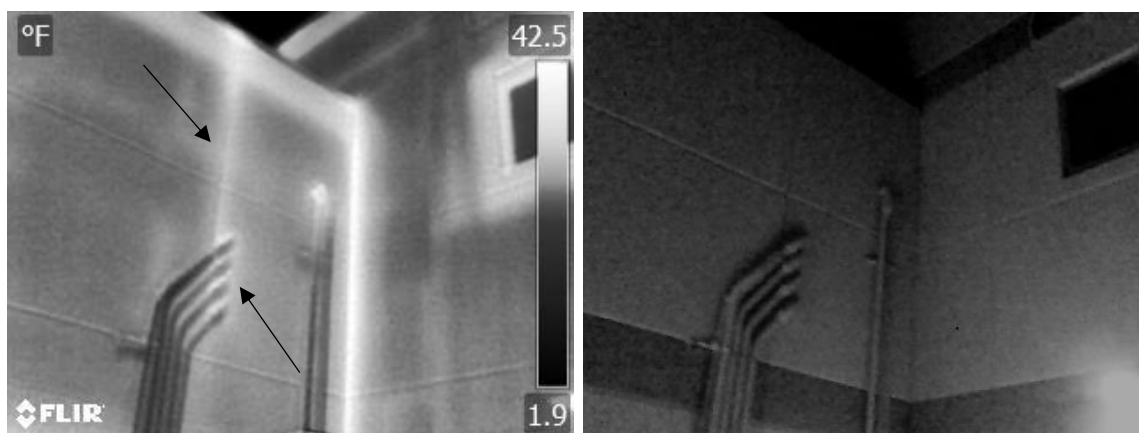


Figure 3-14 SWP with thermal bridging at penetration through insulation: thermal image (left) and visual image (right)

Another common penetration is due to the attachment of external awnings to SWPs. Since non-composite systems require all structural, load-bearing elements to tie

into the structural wythe, which is typically located on the inside of the building, this is a particular issue for non-composite panels as the connection must bypass both the outer layer of concrete and the insulation. It can be a problem for partially-composite SWPs as well if capacity cannot be obtained by tying into the outside wythe alone. Figure 3-15 and Figure 3-16 show that this type of penetration can result in substantial heat transfer.

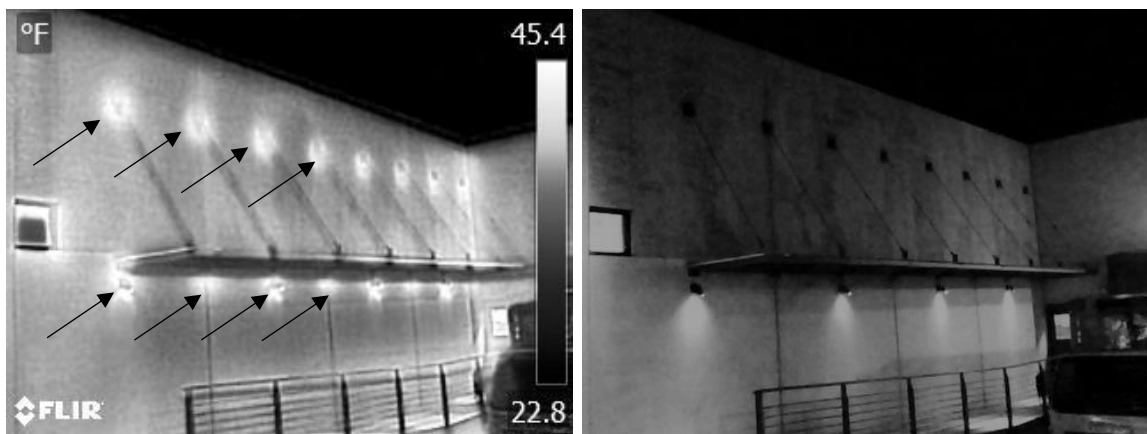


Figure 3-15 SWP with thermal bridging at thru-fastened awning connections: thermal image (left) and visual image (right)

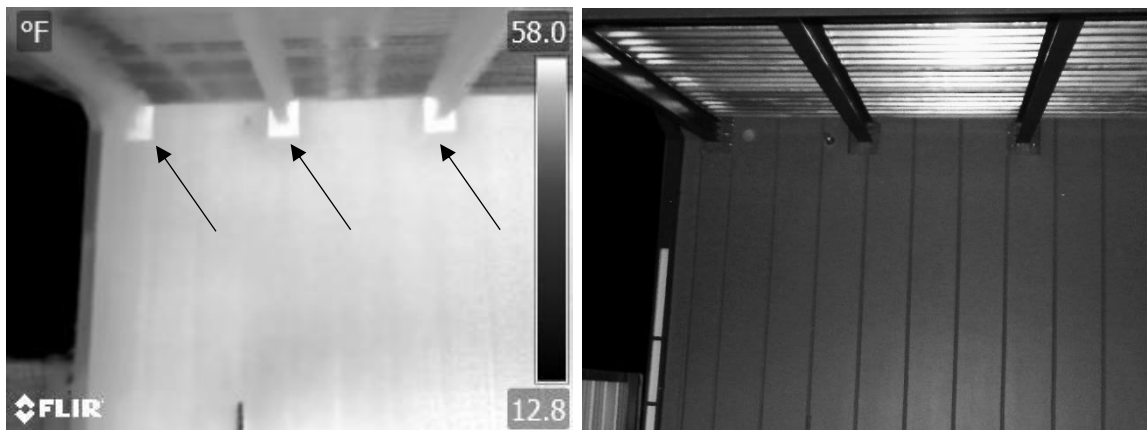


Figure 3-16 SWP with thermal bridging where awning beams penetrate insulation: thermal image (left) and visual image (right)

Similar to awnings, other common wall penetrations are typically due to the need to secure some sort of item (whether structural or otherwise) to the building. Figure 3-17 shows an example of this where a penetration was required to secure a basketball hoop to the wall.

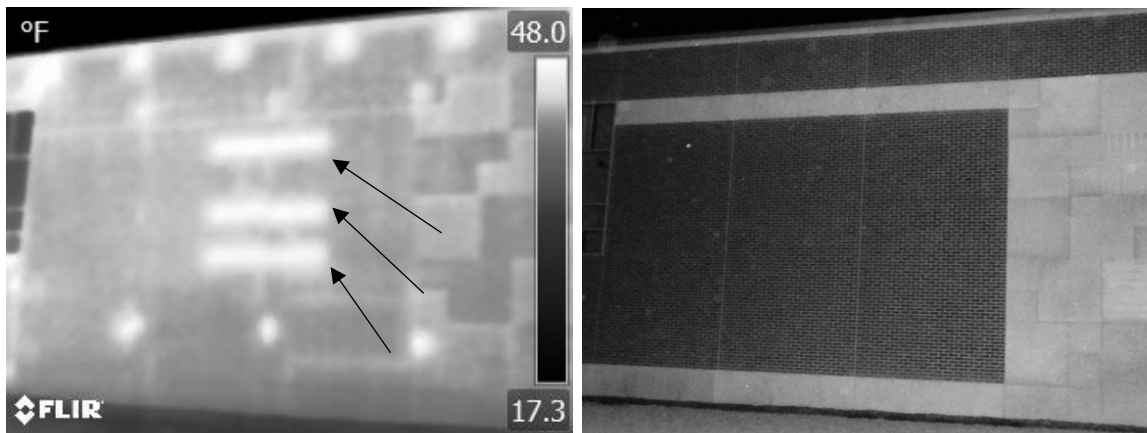


Figure 3-17 SWP with thermal bridging where basketball standard was attached: thermal image (left) and visual image (right)

Detail Discussion and Recommendations

As previously noted, penetrations should typically be avoided if possible. Figure 3-18 shows two details of insulation penetrations that are structurally very sound, but that result in significant thermal bridging even if the insulation were to be replaced around the penetrating element. If a penetration is unavoidable, it is best to use materials with low conductivity if possible (such as FRP).

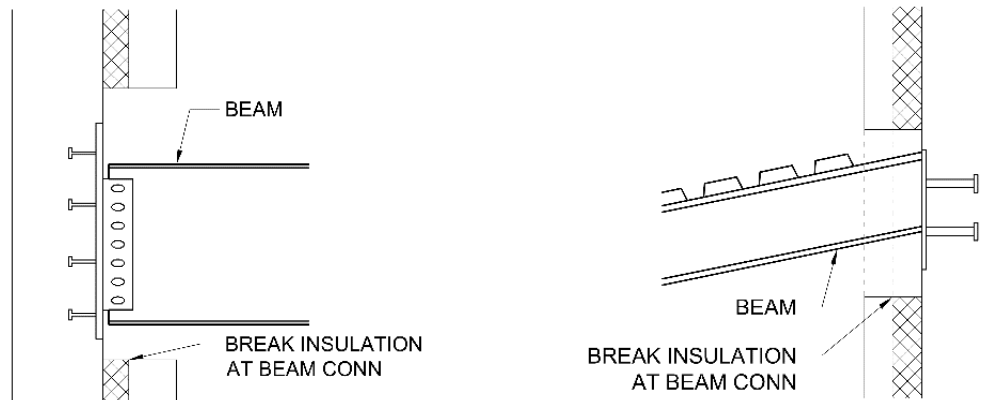


Figure 3-18 Sample details of structural penetrations of insulation resulting in significant thermal bridging- insulation is often replaced around the structural element, but thermal bridging still typically occurs through the element itself

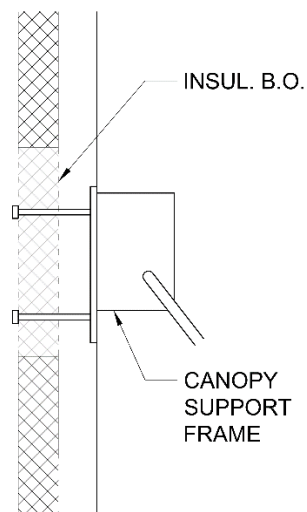


Figure 3-19 Sample penetration detail with solid section for external canopy support

Lifting Anchors

Thermal Imaging Results

Lifting anchors (also known as lifting points or pick points) are required for all SWPs to allow the panels to be lifted into place during the erection stage of construction. Due to available technological and strength limitations of the anchors themselves, these anchors often require puncturing, reducing, or removing insulation to attain the required capacity, which results in thermal bridging. After the wall is lifted into place, the lifting anchors are never used again however, which means excessive heat transfer unnecessarily occurs here for the duration of the lifetime of the structure. This heat transfer can accumulate into considerable cost for owners over time. Thermal images showing thermal bridging from lifting anchors are shown in Figure 3-20, Figure 3-21, and Figure 3-22.

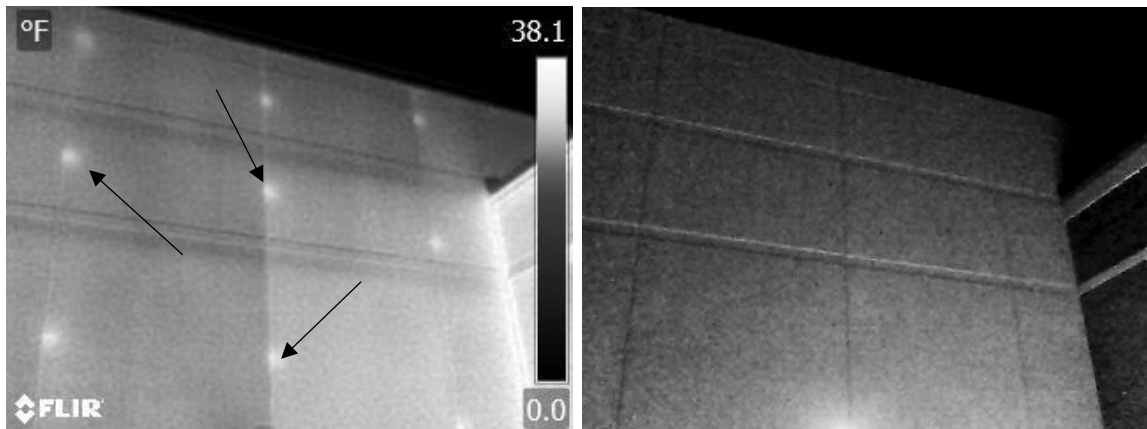


Figure 3-20 SWP structure with thermal bridging at side lifting anchors: thermal image (left) and visual image (right)

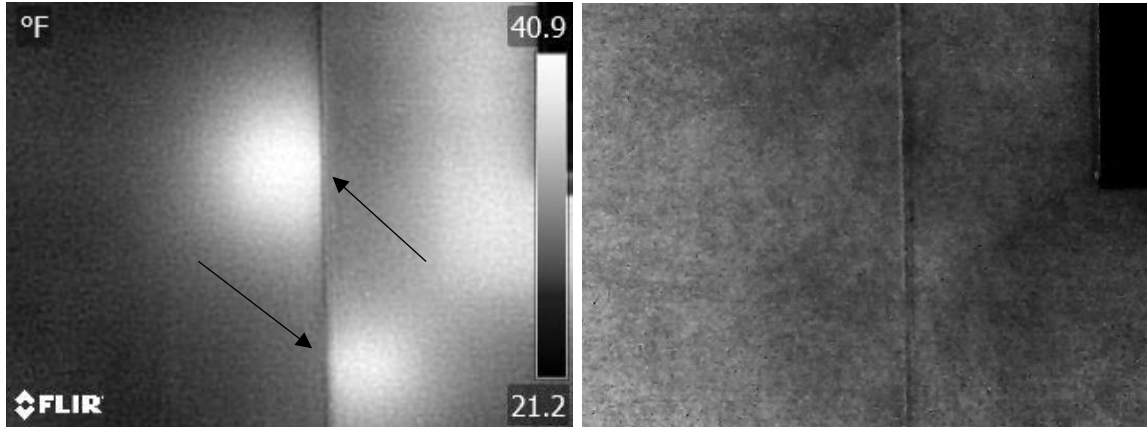


Figure 3-21 Close-up view of thermal bridging in SWP lifting anchors: thermal image (left) and visual image (right)

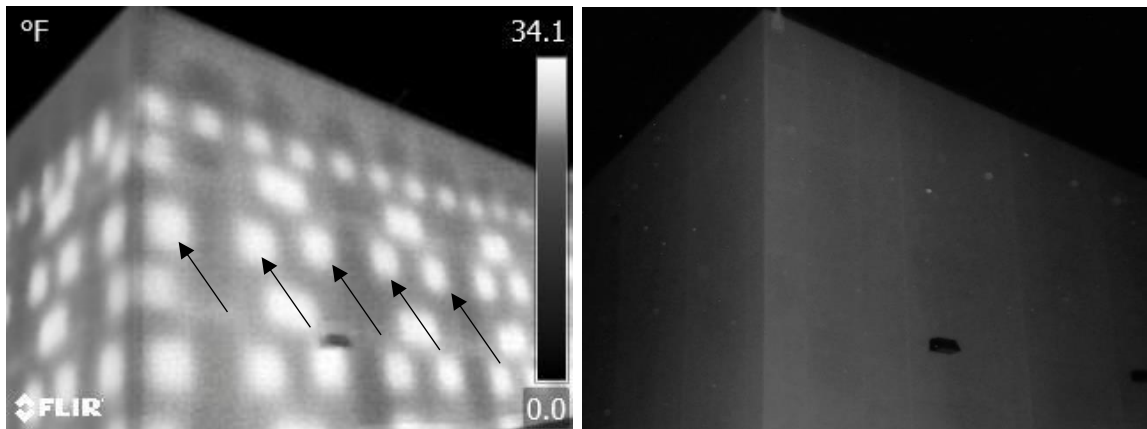


Figure 3-22 SWP structure with severe thermal bridging from lifting points (among other losses): thermal image (left) and visual image (right)

Detail Discussion and Recommendations

Although lifting anchors are necessary, thermal bridging at these locations can be avoided or mitigated in many situations. Figure 3-23 shows a common example of a

detail where insulation is omitted entirely to attain the required capacity to lift the panel into place. This is a safe detail, but thermally detrimental.

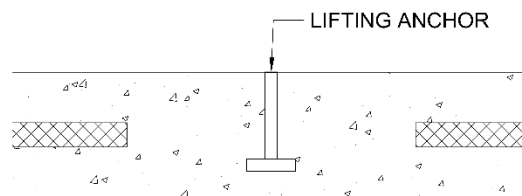


Figure 3-23 Profile view of common design for omitting insulation at lifting anchors

A better solution when thicker concrete area is required to attain lifting anchor capacity/embedment is shown in Figure 3-24 where there is only partial thinning of the insulation, allowing sufficient capacity to be attained. These details perform significantly better thermally than details that require omitting insulation altogether. Rebar is often laid with the anchor to help reach the desired capacity (Figure 3-25).

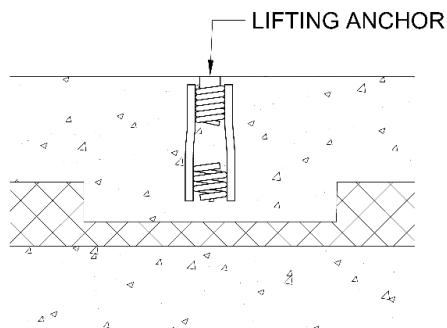


Figure 3-24 Profile view of common design approach for lifting anchors: decreasing insulation at lifting anchor locations to attain required capacity

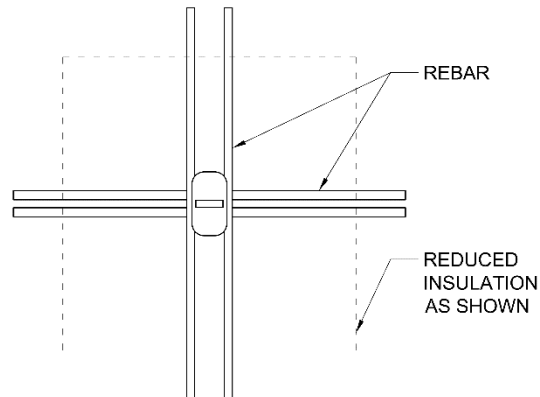


Figure 3-25 Plan view of common lifting anchor detail showing decreased insulation around lifting anchor

Ideally, no penetration will be made in the insulation. This is common in non-composite SWP structures. Figure 3-26 is a good example of such a detail.

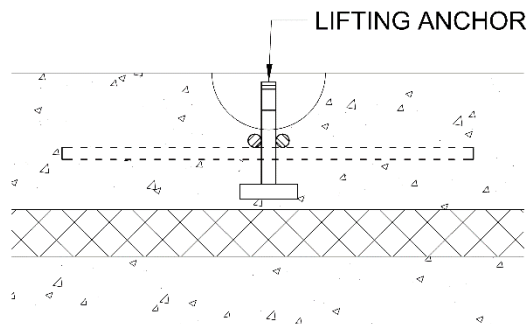


Figure 3-26 Example lifting anchor detail that does not puncture insulation

Corbels

Thermal Imaging Results

Thermal bridging at corbel locations can be difficult or impossible to avoid, especially with partially-composite panels where the wythes are typically very slender and because corbels are typically a junction for high load transfer to occur. Non-composite panels do not typically have this issue since only the inside wythe is designed to withstand the structural loads. The structural wythe of a non-composite SWP is typically thick enough so that corbels can tie directly into it without puncturing the insulation. Composite SWP systems require both wythes to withstand gravity loads though. Figure 3-27 and Figure 3-28 display thermal bridging at corbel locations.

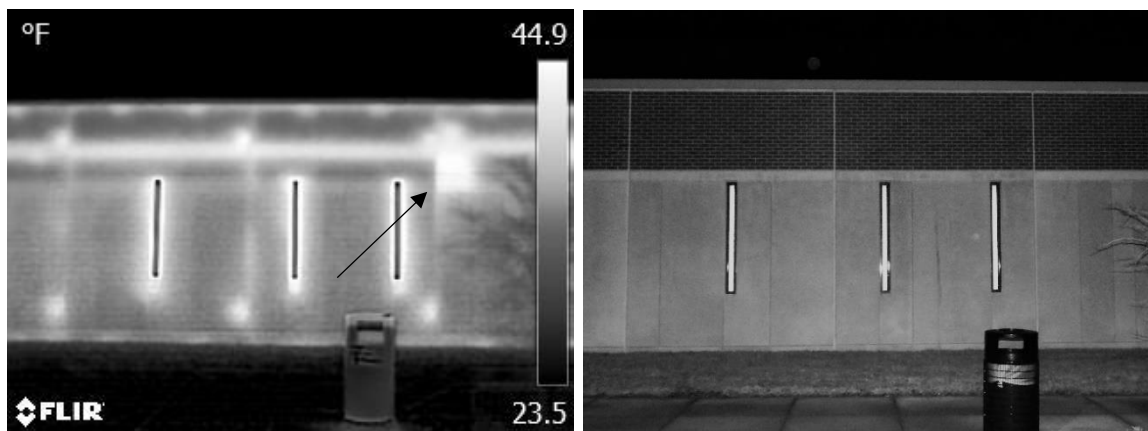


Figure 3-27 SWP structure with thermal bridging at corbel locations: thermal image (left) and visual image (right)



Figure 3-28 SWP structure with severe thermal bridging at corbel locations: thermal image (left) and visual image (right)

Detail Discussion and Recommendations

To simplify the issue of providing structural integrity at corbel locations in SWPs, insulation is often omitted at these connections as is shown in Figure 3-29 and Figure 3-30. It is obvious that the thermally ideal situation displaces as little insulation as possible. Figure 3-31 displays sample details where continuity of the insulation is maintained by reducing insulation at corbel locations as opposed to omitting it entirely to attain the required capacity. If possible, this approach is preferable to omitting the insulation and creating a thermal bridge. Some designs can reach capacity without the need of reducing or omitting insulation at all (Figure 3-32), but this is not always possible from one project to another. Improved corbel detailing is currently a major need for the improvement of thermal and structural efficiency in the industry. One research study was performed to create thermally insulative corbel details that reduce thermal bridging at corbel locations, but the connection was proprietary in nature (Elkady et al 2015). The next chapter herein

presents alternative corbel details and methodology that can be used to eliminate thermal bridging at corbel connections in industry.

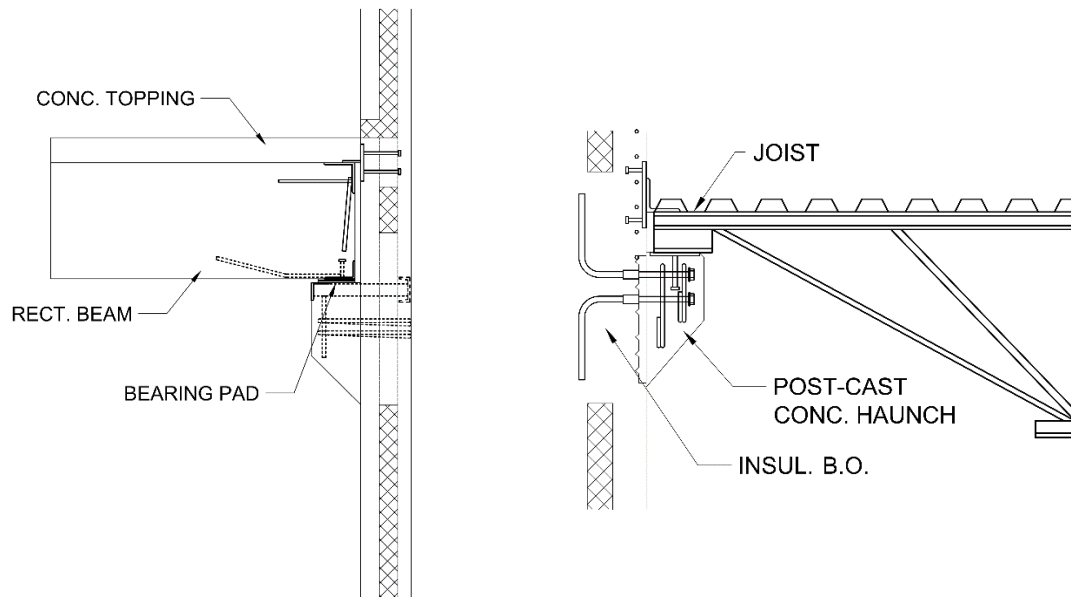


Figure 3-29 Sample of corbel details that are structurally secure but thermally ineffective

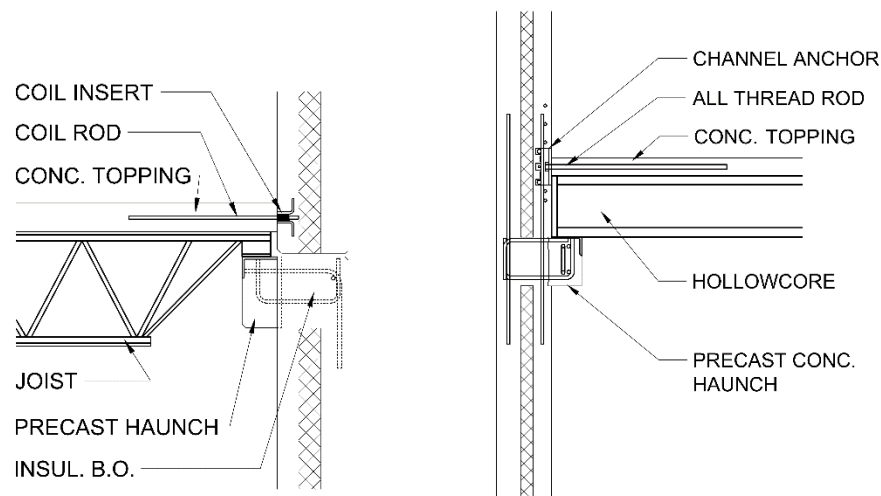


Figure 3-30 Sample corbel details showing less insulation displaced, but still resulting in substantial thermal bridging

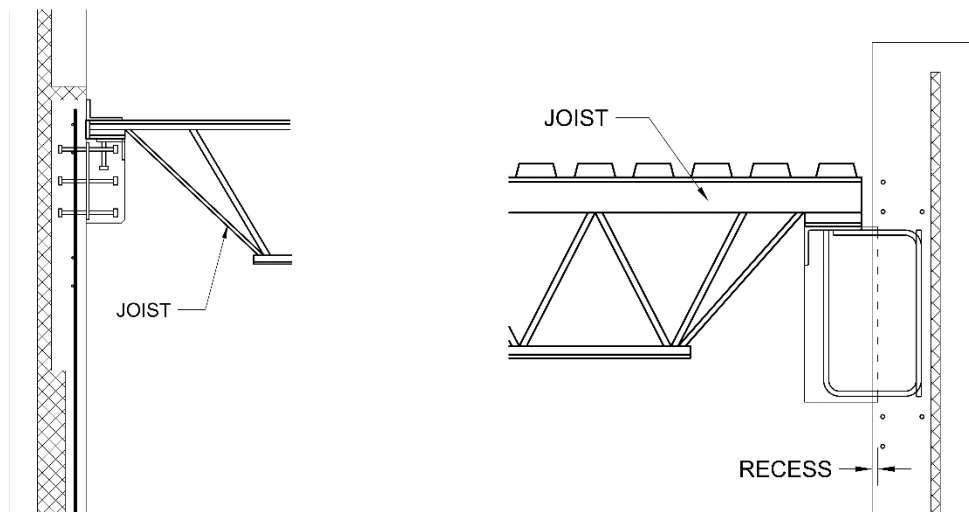


Figure 3-31 Sample of corbel details with continuous but reduced insulation

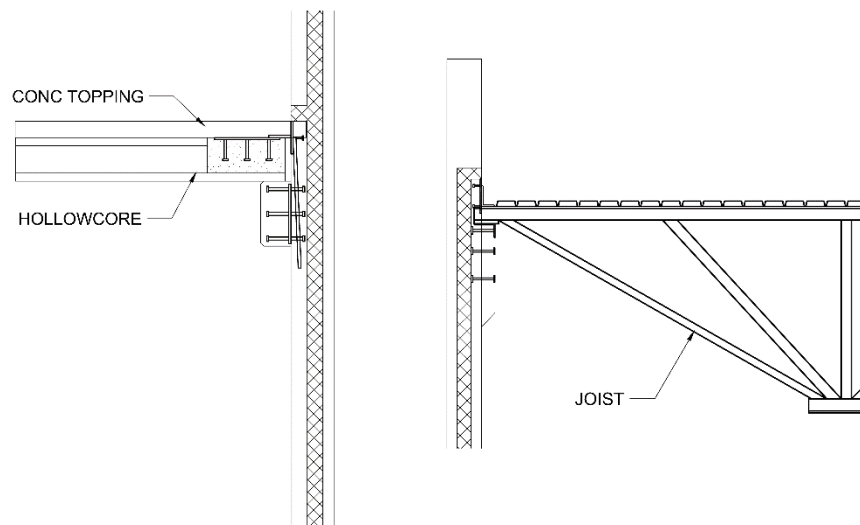


Figure 3-32 Sample of corbel details that prevent thermal bridging by reducing insulation displacement

Roof Termination

Thermal Imaging Results

Roof termination is another common location of thermal bridging. Roof termination may even be the location with the greatest potential heat transfer due to the fact that heat rises, meaning greater heat concentration and temperatures would be expected near the roof of the structure than near the floor. During winter especially, this could create the greatest differential between outside and inside air temperature. Thermal bridging occurs when there are discontinuities in the insulative building envelope from roof to wall. This is commonly due to the difficulty and durability of the details. Figure 3-33, Figure 3-34, and Figure 3-35 show examples of buildings with thermal bridging occurring at roof termination locations. Note that in Figure 3-33 there is only thermal bridging in a portion of the roof termination, indicating that thermal bridging can be prevented by proper panel detailing.

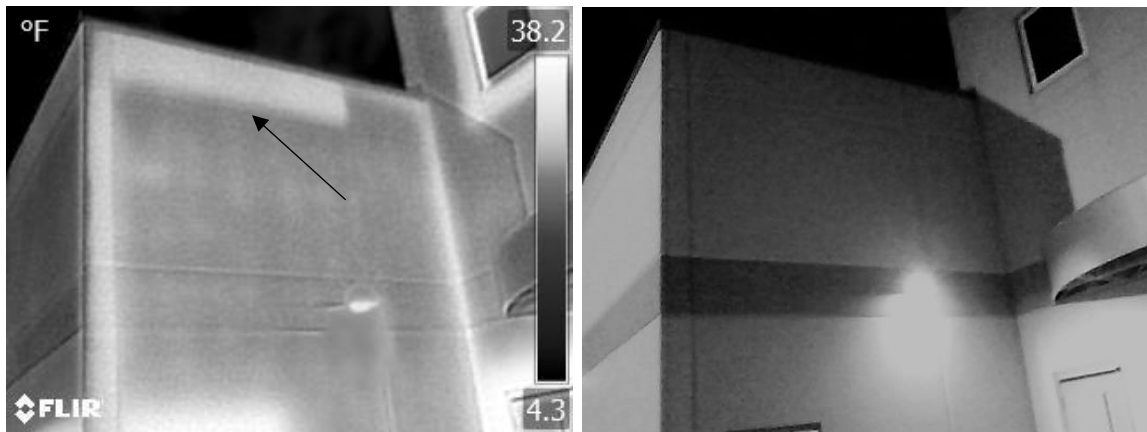


Figure 3-33 SWP structure with partial thermal bridging at roof termination: thermal image (left) and visual image (right)

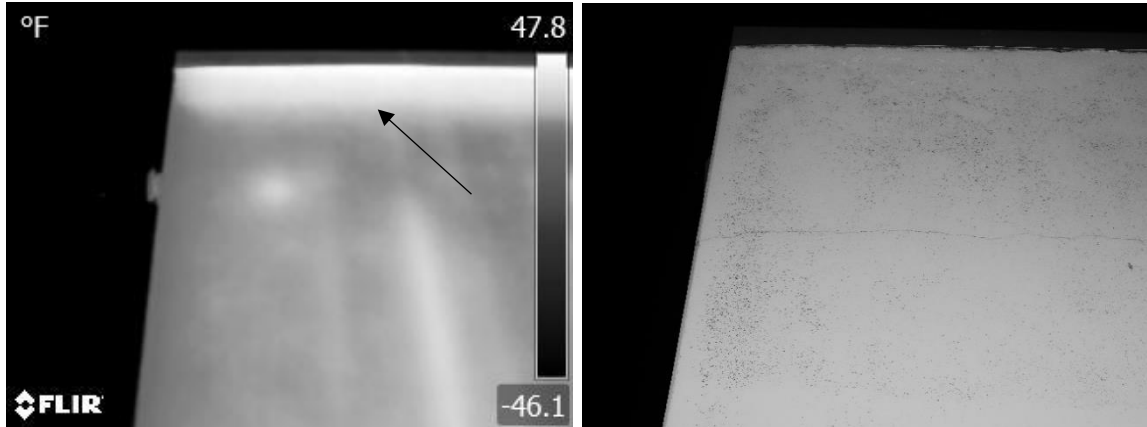


Figure 3-34 SWP structure with thermal bridging at roof termination: thermal image (left) and visual image (right)

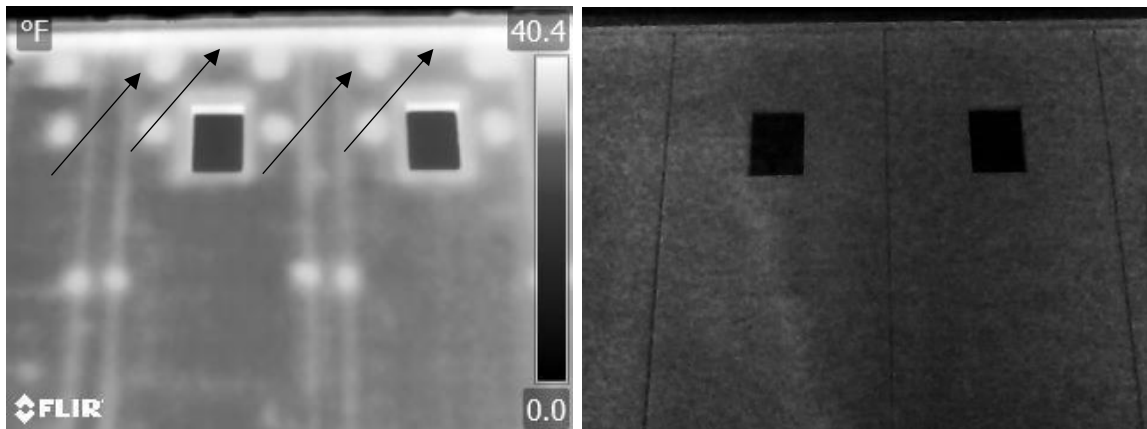


Figure 3-35 SWP structure with thermal bridging at roof and joist embedment: thermal image (left) and visual image (right)

Detail Discussion and Recommendations

Roof termination connections for SWPs are typically done by way of an embedment plate or by embedding the member itself directly into the SWP. Corbels can also be used in conjunction with these connections, but for the purposes of this report

corbels have been addressed as a separate discussion. Regardless of the connection, continuity of the insulative building envelope is what is important in reducing thermal bridging. Figure 3-36 shows sample details where insulation is blocked out for capacity to be attained for the roof connection. By omitting insulation, thermal bridging occurs at these locations.

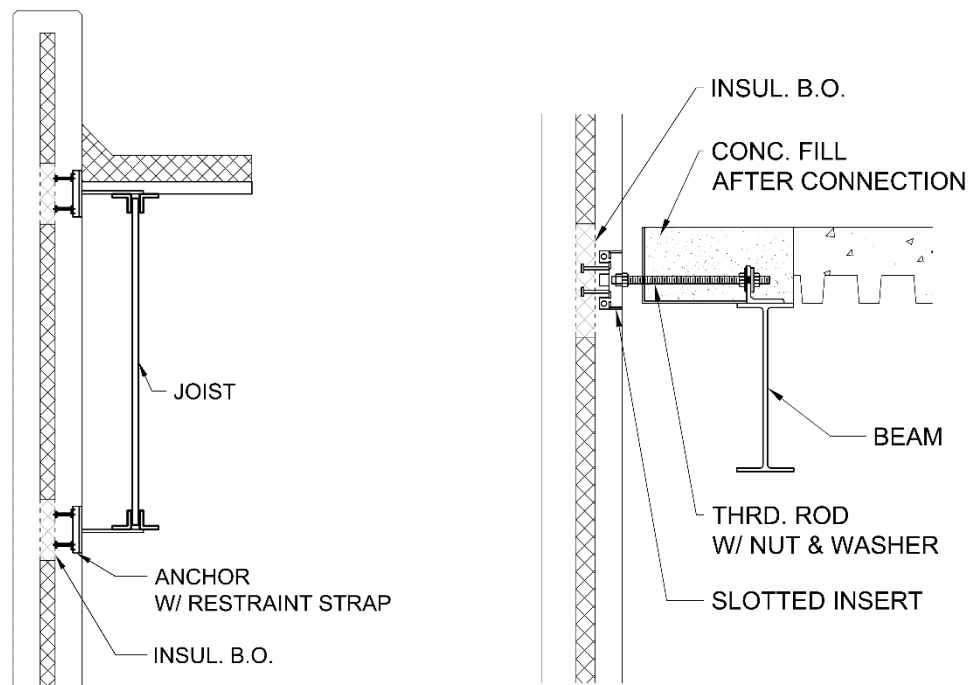


Figure 3-36 Sample roof termination details with common thermal bridging

Figure 3-37 and Figure 3-38 include details that are more thermally efficient because they make no such breach in the insulation. One might note in these details, however, that no indication is made of how the roof insulation is to connect to the wall panel insulation. Occasionally no provision is made to maintain continuity between the

insulation of the roof and the insulation of the wall panel, so that even though no additional breach is made in the insulation of the wall panel, there is a large breach in the overall system resulting in significant thermal bridging between the panel and the roof. This thermal bridging is not always readily apparent using thermal images from the sides of the structure since this thermal bridging may occur behind the parapet and in a location that can only be seen from the roof. Because there was no roof access in this project, no thermal images were included of possible heat transfer at this boundary. Figure 3-39, and several details presented in the above corbel section, show samples of details for maintaining continuity in the insulation between the roof and the wall.

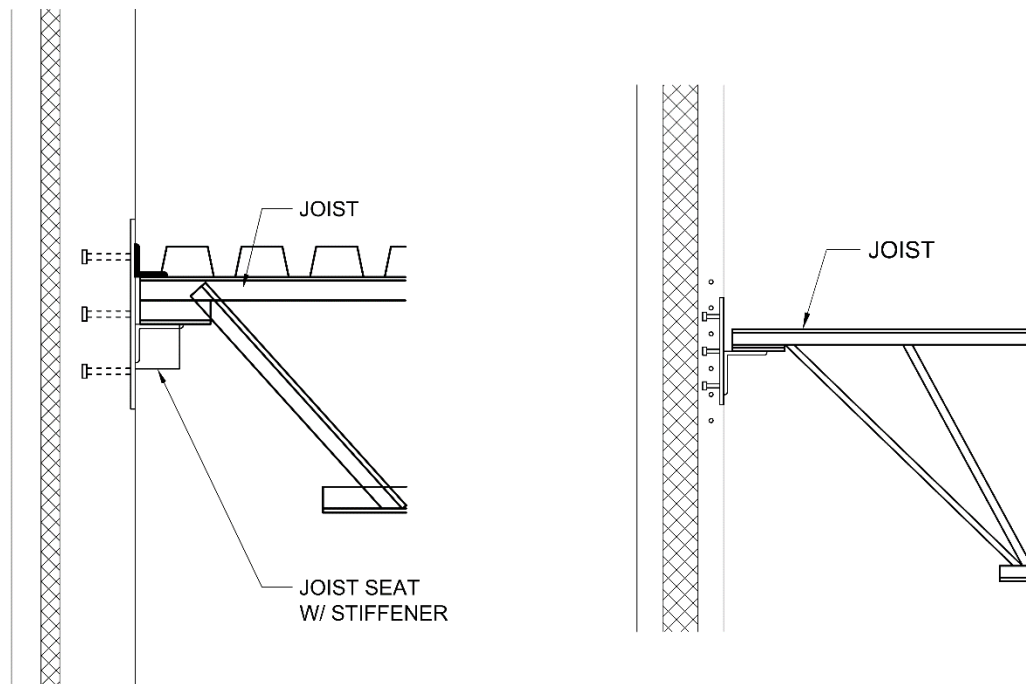


Figure 3-37 Sample roof termination details where embedment plate does not puncture or reduce insulation

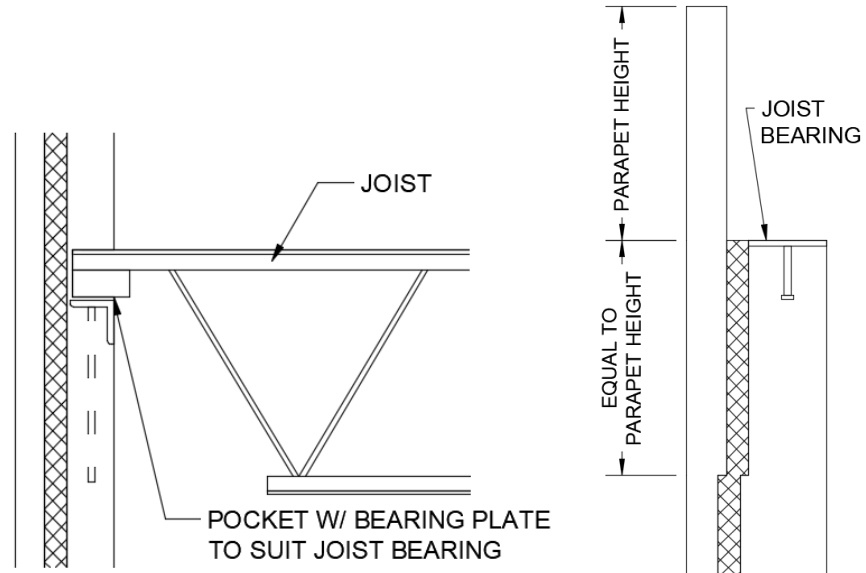


Figure 3-38 Sample roof termination details where roof joist embedded in wall panel does not puncture or reduce insulation

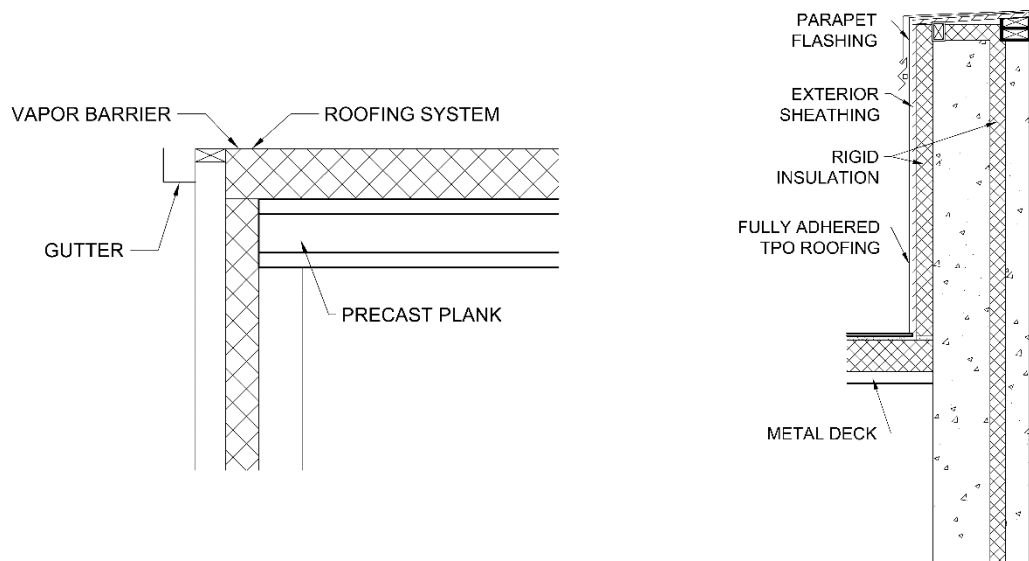


Figure 3-39 Sample of ideal roof termination details where wall and roof insulation tie together

Floor Termination

Thermal Imaging Results

Similar to roof termination and corbels, floor termination connections can be a problem when they require penetrating, reducing, or omitting the insulation. Thermal bridging at these location makes it easy to see the second floor in Figure 3-40 and Figure 3-41.

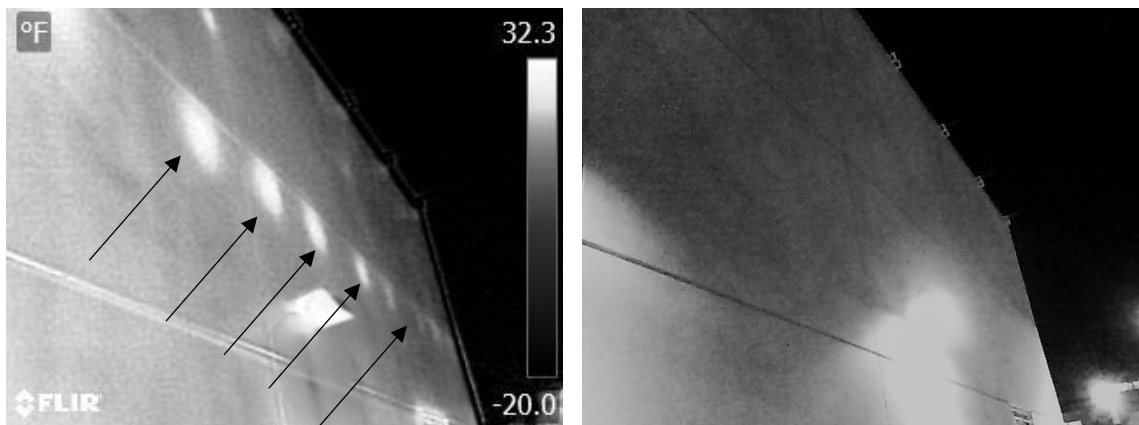


Figure 3-40 SWP structure with thermal bridging at floor termination: thermal image (left) and visual image (right)

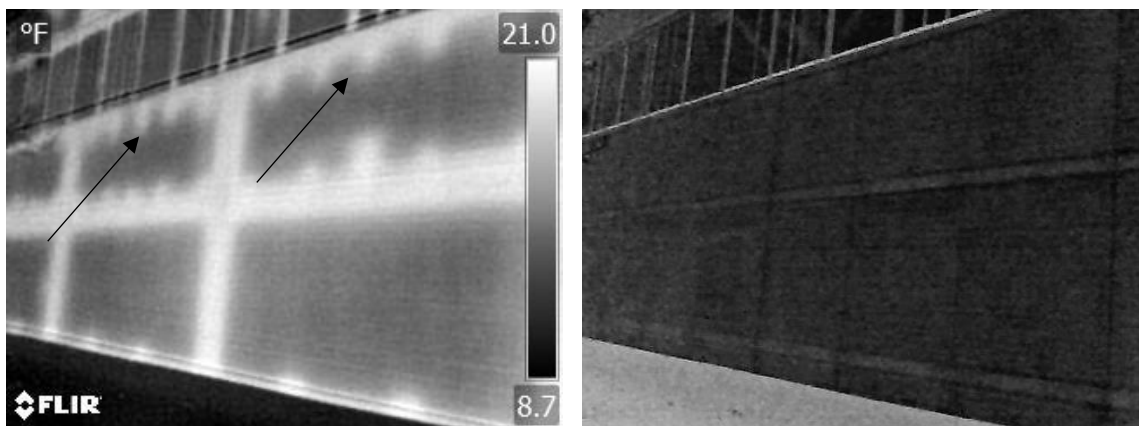


Figure 3-41 SWP structure with heavy thermal bridging where 2nd floor terminates (note arrows): thermal image (left) and visual image (right)

Detail Discussion and Recommendations

As has been previously discussed with respect to other types of connections, the key to thermal efficiency in floor termination lies in maintaining continuity in the insulation. Figure 3-42 displays examples of common floor termination details where breaches in the insulation are made to attain capacity. Figure 3-43 shows improved details with reduced insulation, but that still maintain continuity. Figure 3-44 contains examples of details that permit no such breach in the insulation and maintain continuity necessary to reduce heat transfer. Like corbel design and detailing, alternative designs and details should be further investigated to reduce the thermal bridging at these locations.

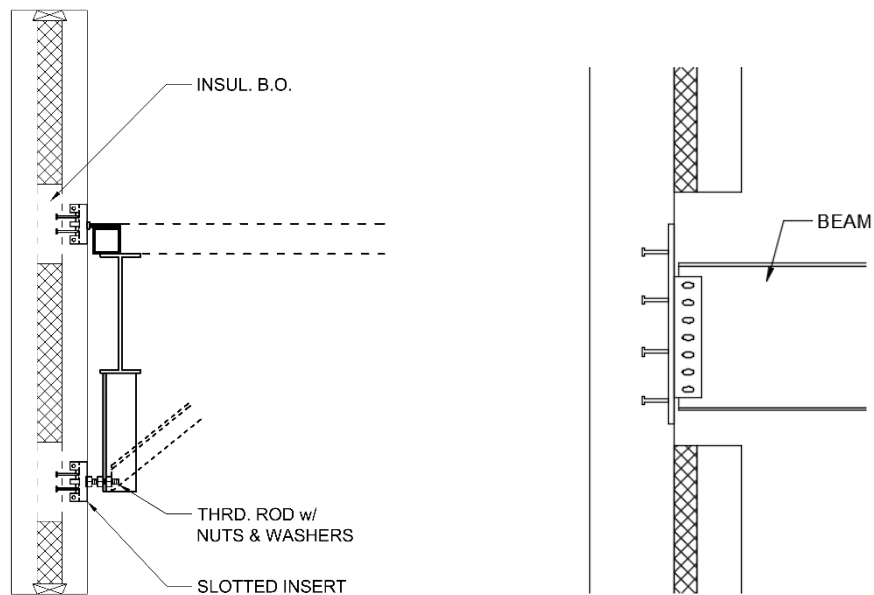


Figure 3-42 Sample floor termination details that create a thermal breach in the insulation

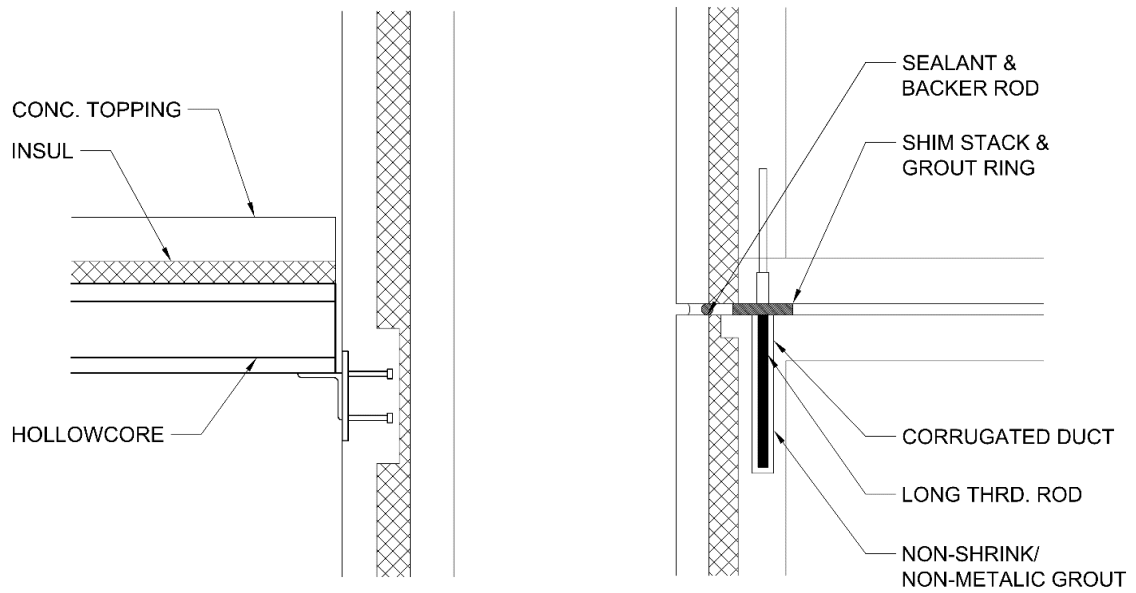


Figure 3-43 Sample floor termination details with reduced but continuous insulation

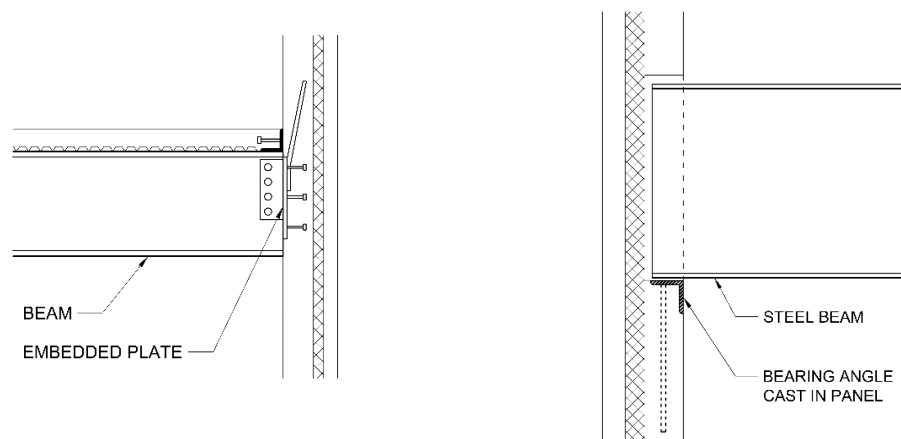


Figure 3-44 Sample floor termination details with insulation continuity

Foundation

Thermal Imaging Results

Foundations are commonly solid concrete sections, which is why connections between the base of SWPs to the foundation are prime locations for thermal bridging to occur. Even when foundations are insulated, connections between these foundations and SWPs can result in thermal bridging if care is not taken to make the insulative building envelope as continuous as possible. An example of this is shown in Figure 3-45 where both bottom panels were detailed the same, but thermal bridging is more severe in the left panel than in the right at the foundation. This may indicate that the detail might have been good, but that construction was not carefully completed. Figure 3-46 shows a foundation where connections to the SWP obviously required blocking out insulation. This type of detailing may make connections easier during construction, but they cost the owner a significant amount of money over time and should be avoided to increase the sustainability of designs.

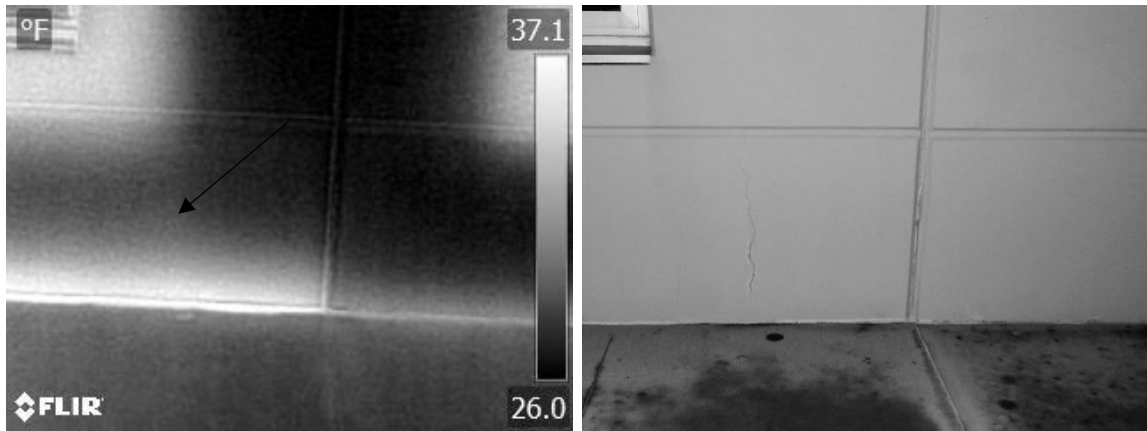


Figure 3-45 SWP structure with thermal bridging at foundation connection: thermal image (left) and visual image (right)

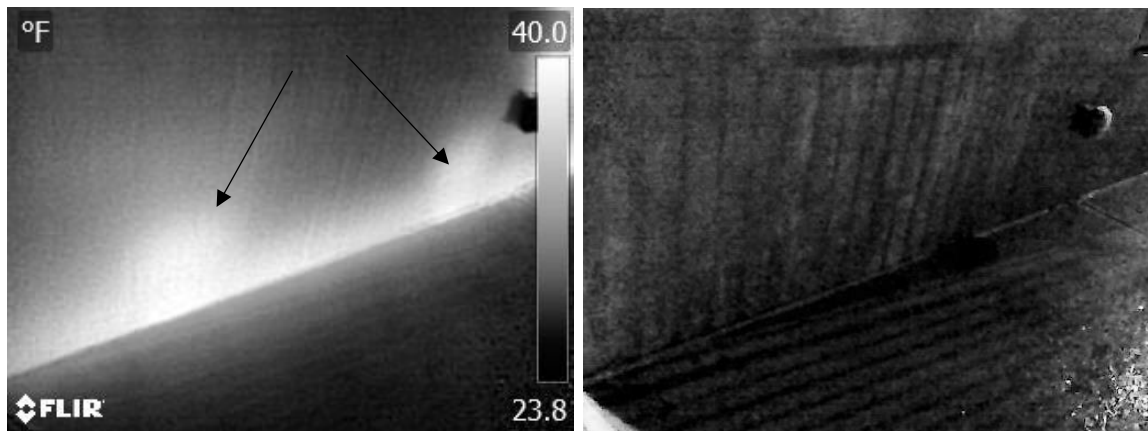


Figure 3-46 SWP structure with thermal bridging at foundation connections: thermal image (left) and visual image (right)

Detail Discussion and Recommendations

Foundation connections are typically critical connections since all loads must eventually be transferred to the foundation. Figure 3-47 shows details using a common

approach for creating these connections that block out a portion of the insulation at the location of the connection, and then fill it in with concrete after the connection has been made. This creates a thermal bridge, as demonstrated in the structure shown in Figure 3-46. Figure 3-48 shows details with insulation extending to the ground, an improvement over blocking out insulation for connections. Figure 3-49 show further improved details that extend the insulation well below the ground level, and Figure 3-50 shows details that not only extend insulation deeper in the ground, but also provide some degree of insulation around the interior of the foundation. This leaves only a very slender area where heat might bridge out of the structure laterally.

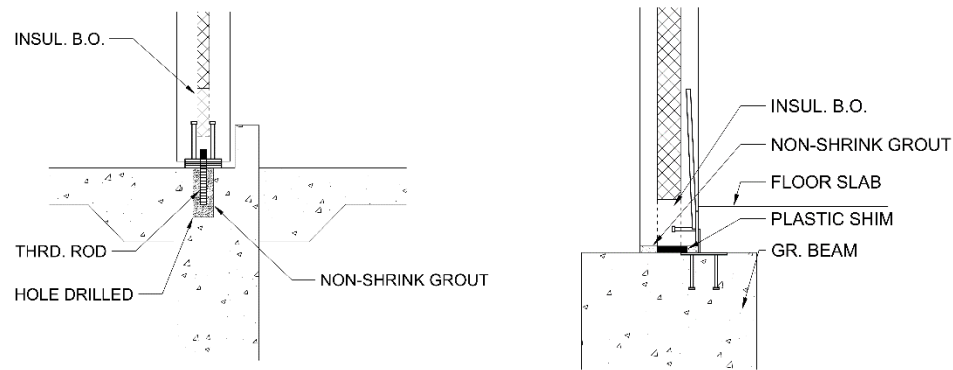


Figure 3-47 Sample foundation connection details where insulation blocked out at connection and filled with concrete

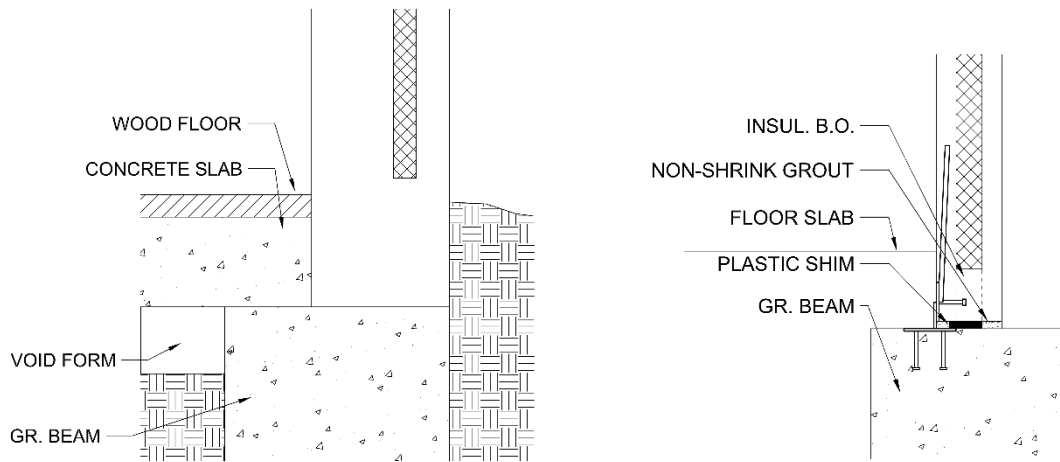


Figure 3-48 Sample foundation details with insulation almost or barely reaching ground surface

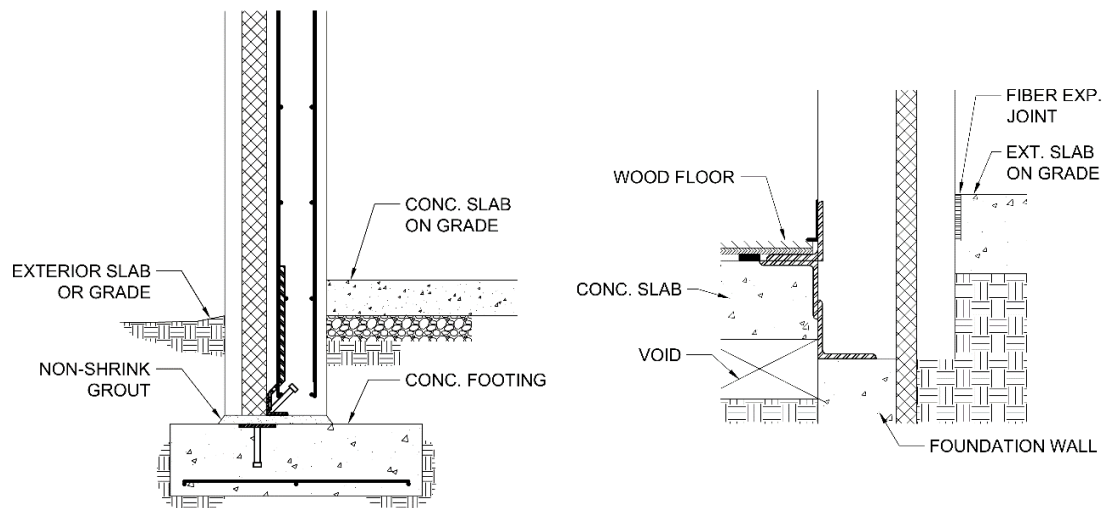


Figure 3-49 Sample foundation details where insulation extends well below ground surface

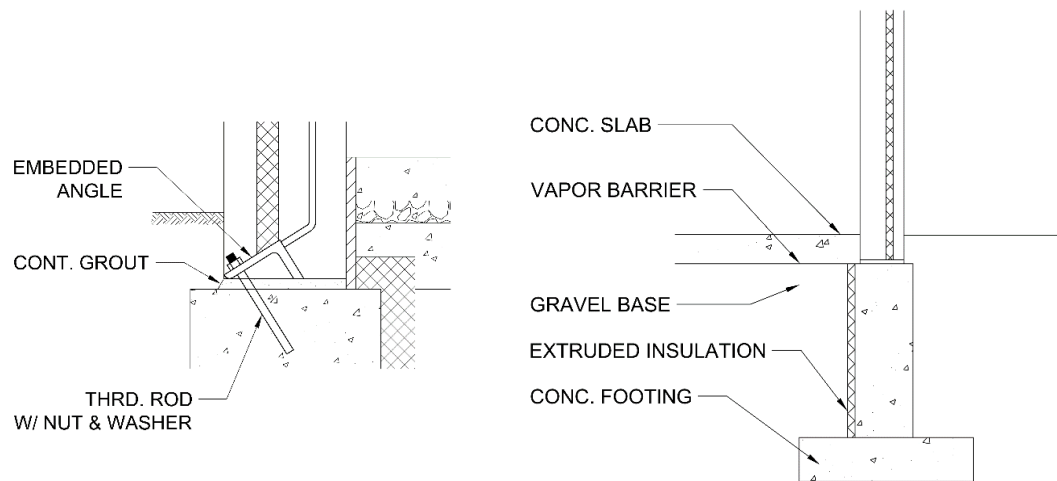


Figure 3-50 Sample foundation details where insulation is also placed around foundation

Corners

Corners are a common location for thermal bridging to occur. The two types of corners that exist are called reentrant corners and salient corners. Reentrant corners are corners facing into a building (angle inside greater than 180°). Salient corners, consequently, are corners facing out away from a building (angle inside less than 180°). Figure 3-51 shows a visual definition and example of both reentrant and salient corners.

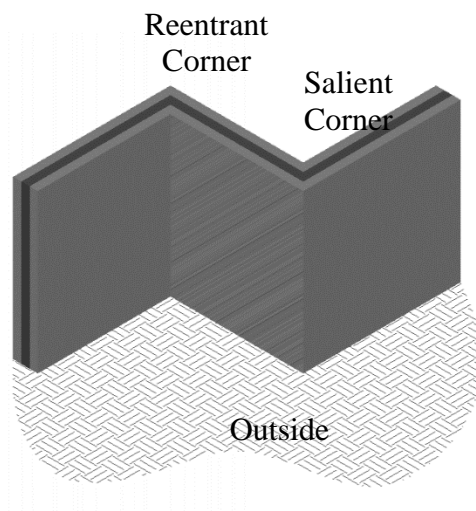


Figure 3-51 Visual definition of corner types viewing from the outside of a building: Reentrant corner (left, facing into building) and Salient corner (right, facing outward from building)

Thermal bridging can (and does) occur commonly at both types of corners, but reentrant corners naturally tend to be of greater concern thermally. Consider the reentrant corner found in Figure 3-51. This corner has an angle inside the building of 270° , whereas the salient corner has only an angle of 90° inside the building. The joint at the reentrant corner, therefore, is exposed to heat from 270° , whereas the salient corner is exposed to much less heat (only 90° , or likely 33% of the heat exposure at the reentrant corner). This is justified by the fact that heat transfer is proportional to surface area and temperature difference. Another way to think of it, then, is that the reentrant corner has a larger area experiencing a difference in temperature than a salient corner. Since heat will flow from high temperatures to low temperatures, there is more potential heat trying to escape from a reentrant corner than a salient one. This is demonstrated by the internal temperature gradient shown in Figure 3-52 which models heat flow through the wall from

Figure 3-51 with a constant inside temperature of 75° F and an exterior air temperature of 32° F. Although thermal bridging can still occur at the salient corner location, it is likely to be less severe than at the reentrant corner.

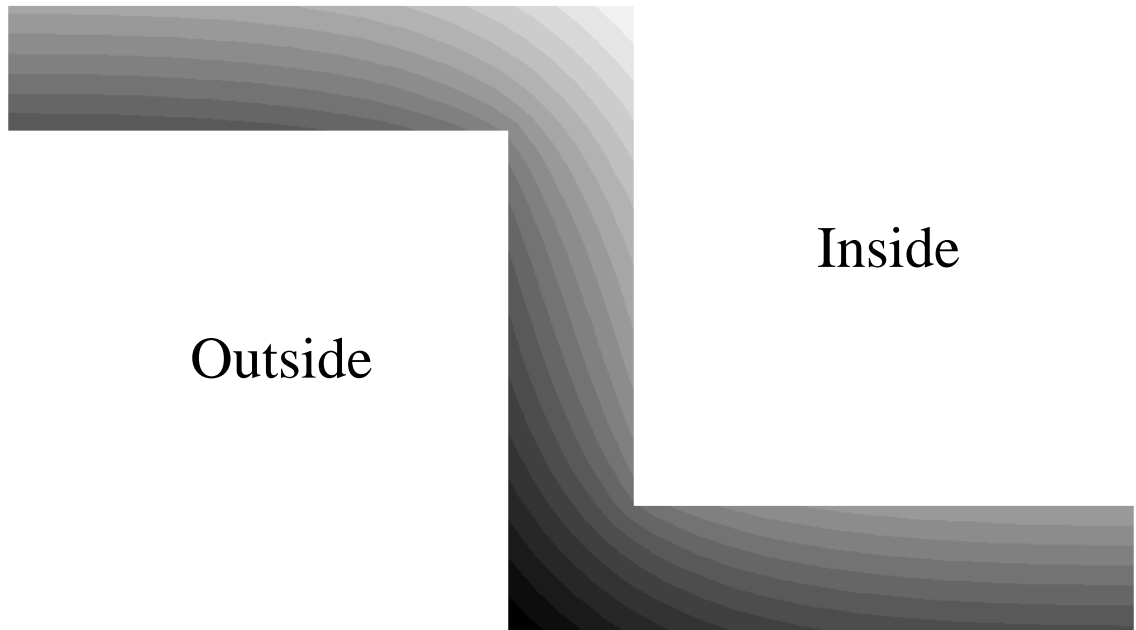


Figure 3-52 Heat transfer comparison for reentrant and salient corners

Thermal Imaging Results

Thermal bridging is a common problem at both types of corners. Examples of thermal bridging in reentrant corners may be seen in Figure 3-53 and Figure 3-54. Figure 3-55 and Figure 3-56 show thermal bridging at salient corners. The detailing and joint type are apparent influences on the thermal bridging in a corner connection.

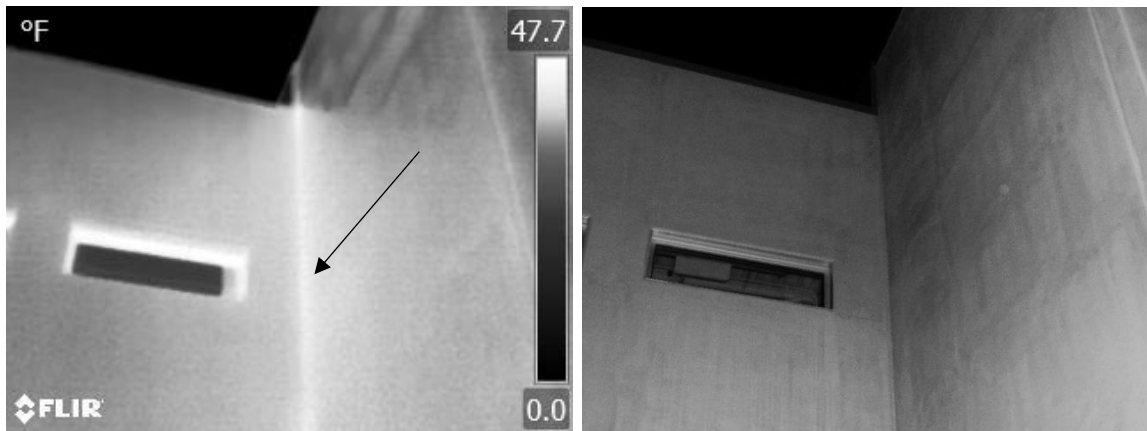


Figure 3-53 SWP structure with thermal bridging at a reentrant corner: thermal image (left) and visual image (right)

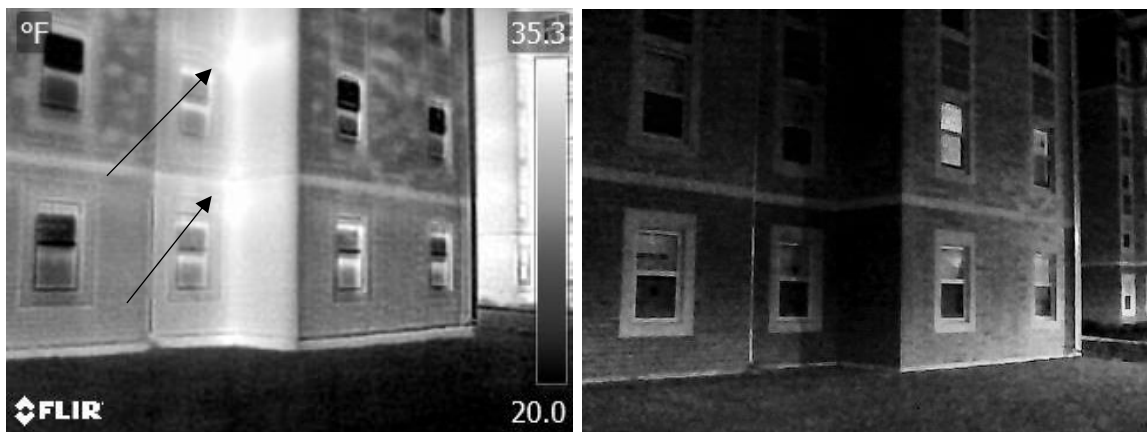


Figure 3-54 SWP structure with thermal bridging at a reentrant corner: thermal image (left) and visual image (right)

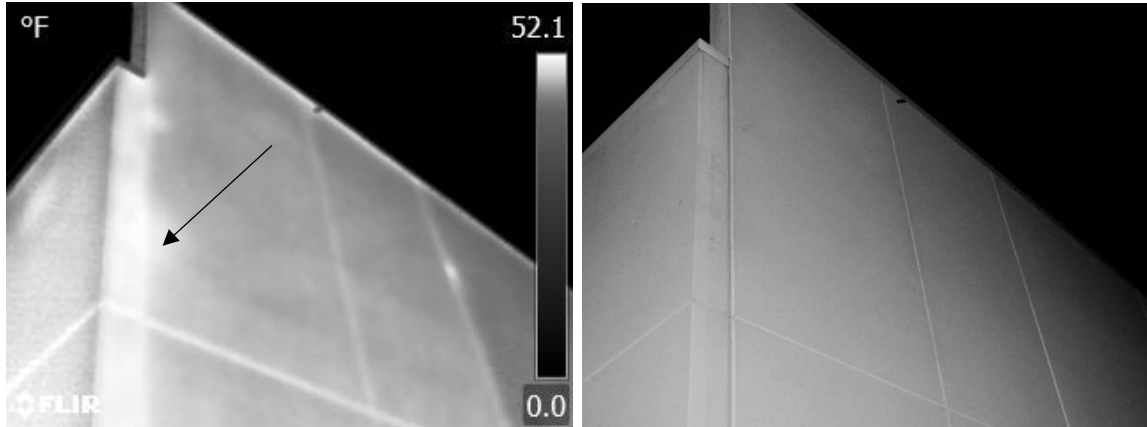


Figure 3-55 SWP structure with thermal bridging at salient corner butt joint: thermal image (left) and visual image (right)



Figure 3-56 SWP structure with thermal bridging along butt joint of salient corner: thermal image (left) and visual image (right)

Detail Discussion and Recommendations

Corners can be detailed in a many ways. Each detail can have an advantageous or detrimental effect on thermal performance, but details for corners are often selected based on fabrication concerns (Seshappa and Dixon 2013). Figure 3-57 shows a variety of joint

types. A butt joint, the most common of corner joints, can provide excellent structural performance and easy installation, but its thermal efficiency is poor due to discontinuity in the insulating wythe. Figure 3-58 shows sample details of a common butt joint connections used where insulation is omitted or penetrated, and a thermal bridge results.

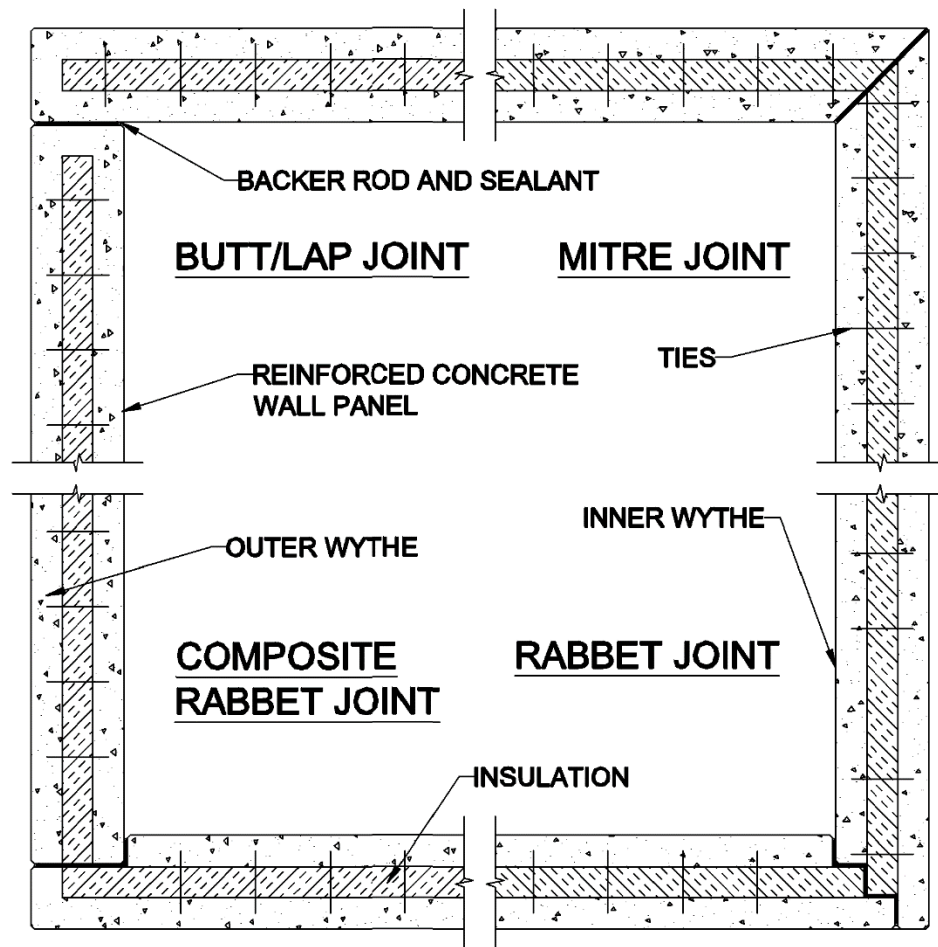


Figure 3-57 Four corner joint detail options, clockwise from top-left: butt, mitre, rabbet, and composite rabbet joint

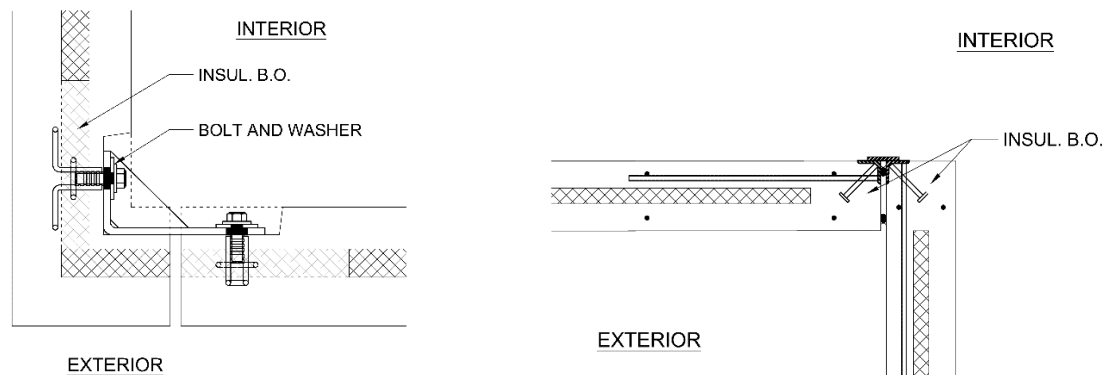


Figure 3-58 Common butt joint connections with much thermal bridging, plan views

Other types of corner joints exist as well, and can often offer better thermal resistance than butt joints. A mitred or rabbeted corner joint allows direct connection of the insulating wythe through the corner, providing greatly improved thermal efficiency. Judicious use of caulking and spray foam insulation at corner connections can further improve thermal efficiency. Since it is sometimes desirable to conceal corner connections within the wall for aesthetics, Figure 3-59 introduces example details of removing insulation to make the corner connection, followed by replacing the insulation after the connection is completed. This is an improvement over filling the void with concrete as insulation better helps resist the heat flow. Example details that do not require puncturing or omitting insulation for both salient and reentrant corners are shown in Figure 3-60 and Figure 3-61 respectively.

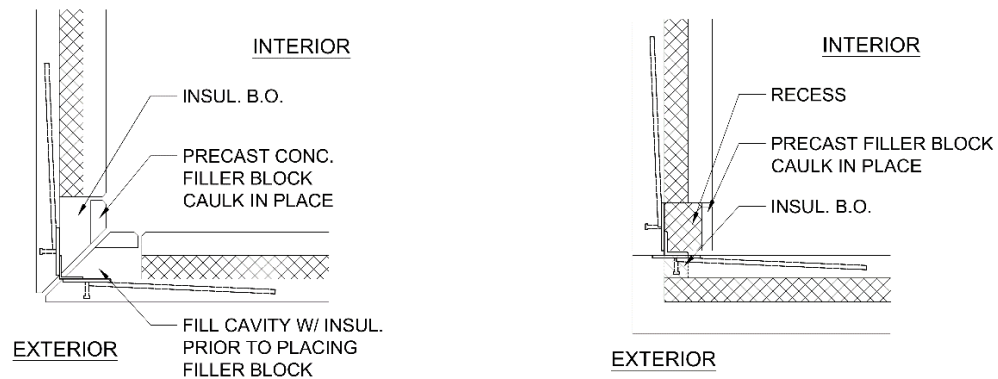


Figure 3-59 Sample corner details blocking insulation out and replacing after construction

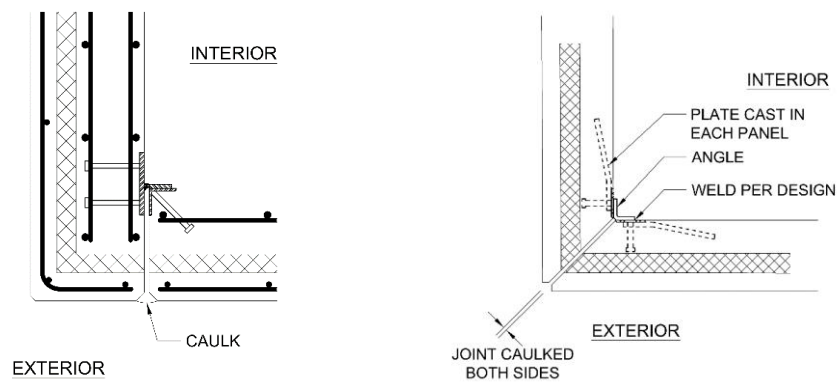


Figure 3-60 Sample salient corner details with minimal thermal bridging

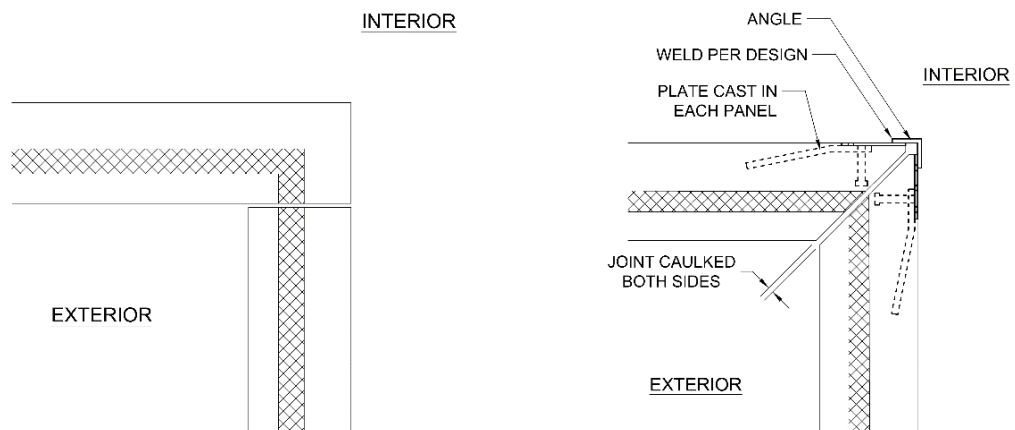


Figure 3-61 Sample reentrant corner details with minimal thermal bridging

Panel-to-Panel Connections

Thermal Imaging Results

Panel-to-panel connections are frequently and arguably the most abundant connection in SWP structures, which is why attention should be paid to the thermal performance of these connections. Figure 3-62 and Figure 3-63 show examples of thermal bridging at panel-to-panel connections.

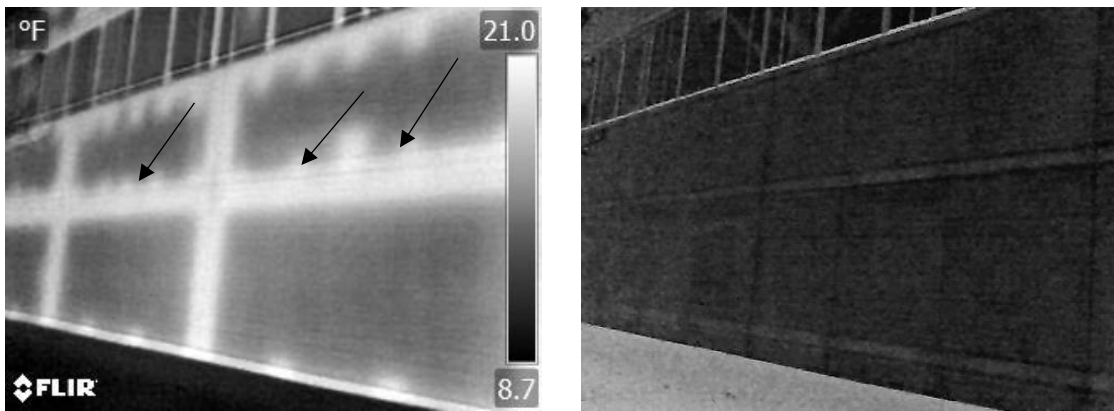


Figure 3-62 SWP structure with severe thermal bridging around panel edges: thermal image (left) and visual image (right)

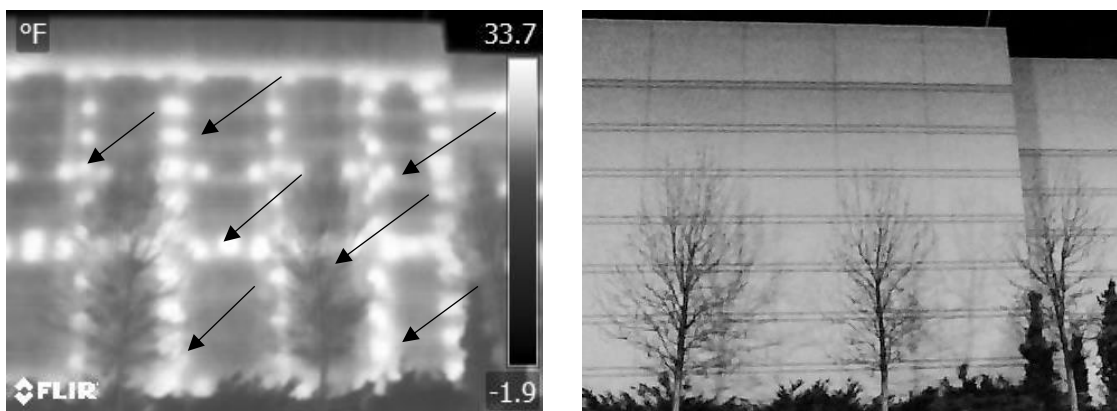


Figure 3-63 SWP with significant thermal bridging at panel-to-panel connections: thermal image (left) and visual image (right)

Detail Discussion and Recommendations

In many cases, the panel-to-panel connections are structural, as they may help transfer horizontal loads between panels and tie the structure together. Any penetrations, omissions, or reductions in insulation will result in decreased thermal resistance. Figure 3-64 shows example panel-to-panel details where insulation is required to be displaced to achieve proper connectivity. Figure 3-65 shows a front view of connections similar to those found in Figure 3-64. Ideally panel-to-panel connections will not displace or puncture the insulation as shown in the sample details in Figure 3-66. If it is not possible to avoid puncturing or displacing insulation to achieve required capacity, it is preferable to use a thermally resistant material so as not to create a thermal bridge in the structure.

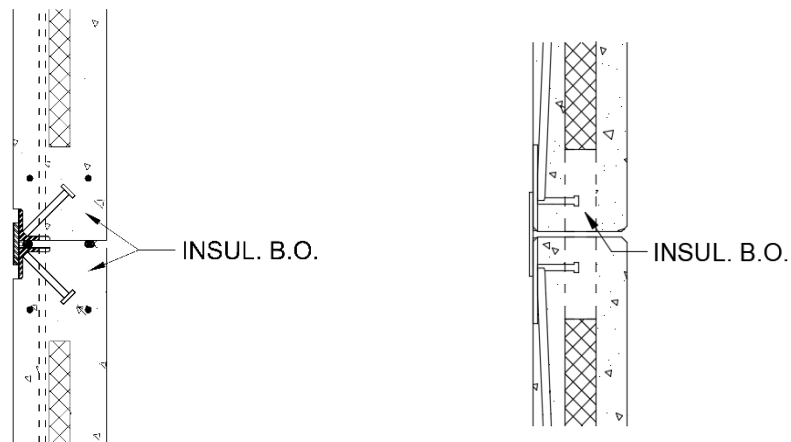


Figure 3-64 Common panel-to-panel connections resulting in significant heat transfer

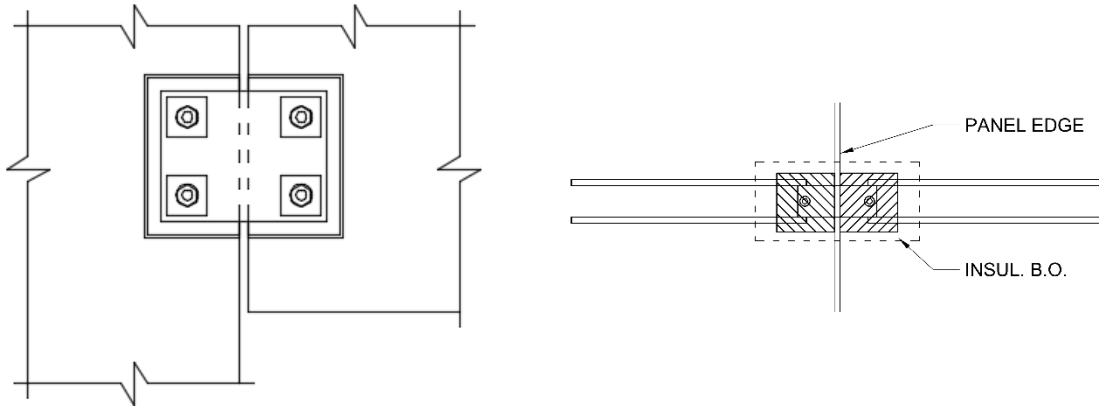


Figure 3-65 Front view of similar details to the Figure 3-64

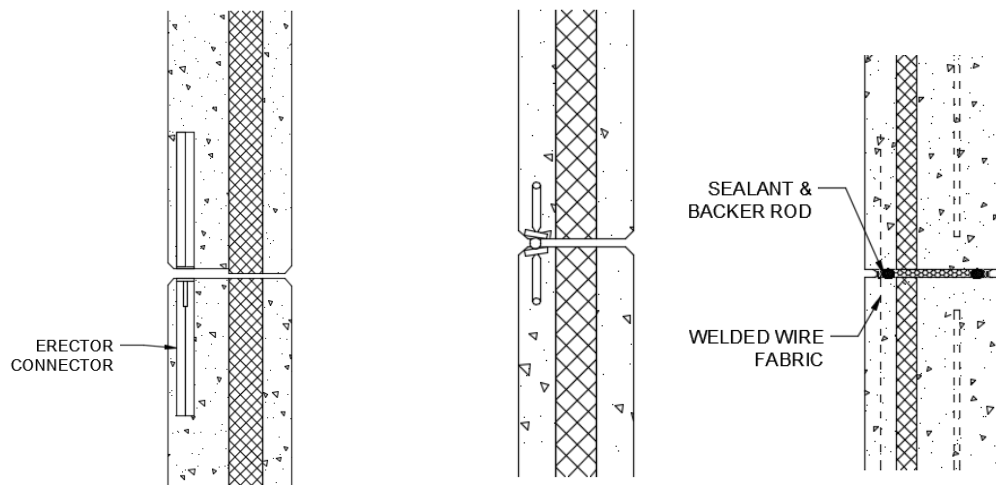


Figure 3-66 Examples of ideal panel-to-panel details

Insulation Joints

Thermal Imaging Results

Concrete sandwich wall panels are typically created by first pouring one layer of concrete and then placing the insulation down and allowing the concrete to cure before pouring the final wythe of concrete. The panel size often differs from the size the insulation sheets come in though, meaning that sheets almost always have to be cut to fit the size of the panels. If insulation is not carefully cut to fit exactly in the form work, concrete can seep through the gaps or joints in the insulation, creating thermal bridging. Figure 3-67, Figure 3-68, and Figure 3-69 show examples of this occurring in buildings across the United States.

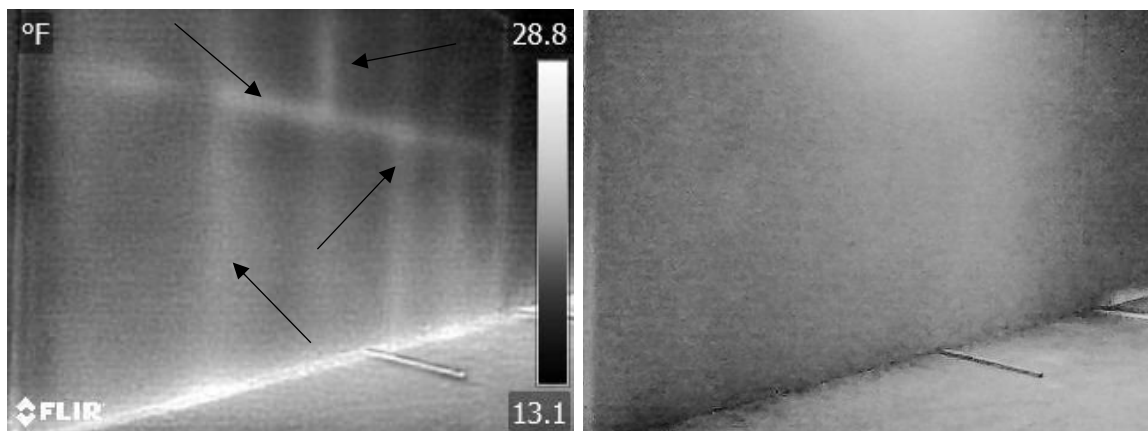


Figure 3-67 SWP with thermal bridging from joints/space between insulation: thermal image (left) and visual image (right)

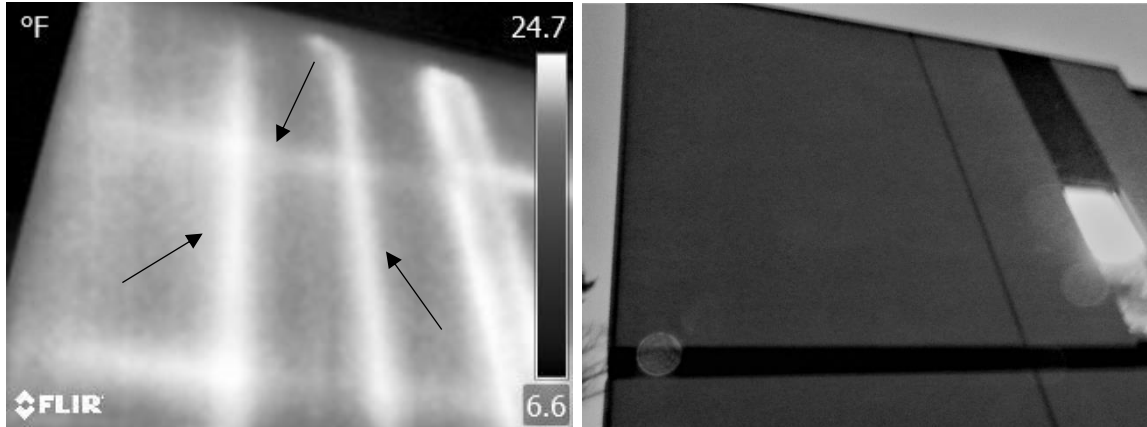


Figure 3-68 SWP structure with thermal bridging at insulation joints: thermal image (left) and visual image (right)

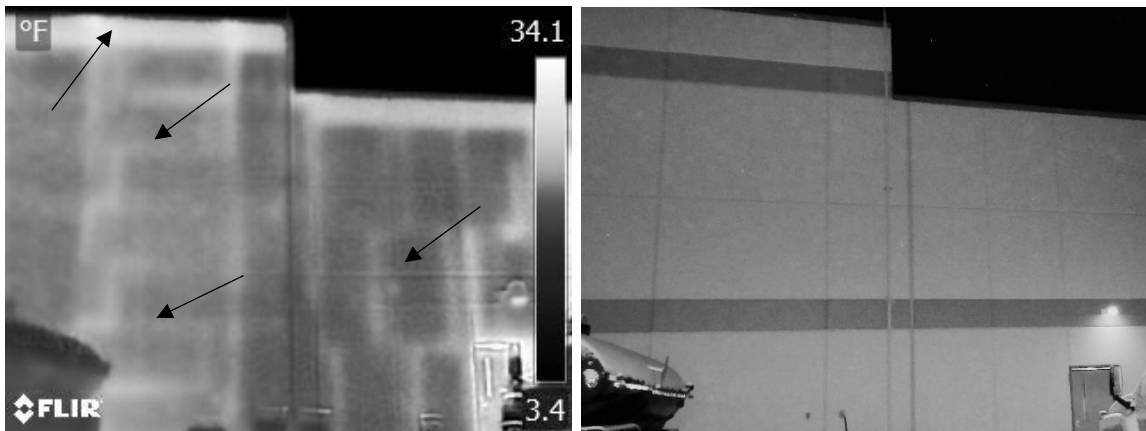


Figure 3-69 SWP structure with thermal bridging due to insulation joints: thermal image (left) and visual image (right)

Detail Discussion and Recommendations

Since thermal bridging is most prone to occur at joints and connections in SWPs, it is intuitive that the fewer joints that exist in a panel, the better. This includes insulation joints, or joints between pieces of insulation where concrete could possibly leak through.

As alluded to in the previous section, the most common type of joint for insulation is a butt joint (Figure 3-70), where insulation panels are cut with a straight edge and placed edge-to-edge against each other. The use of different types of joints with the insulation may be beneficial to prevent fresh concrete breaching through the insulation.

Einea et al. (1991) proposed various details to help minimize these issues (Figure 3-70). The most common joint in practice is the butt joint (see Figure 3-70a). Figure 3-70b shows a variation of the butt joint where two layers of insulation are used and the butt joint is staggered, making it highly unlikely that concrete will leak through.

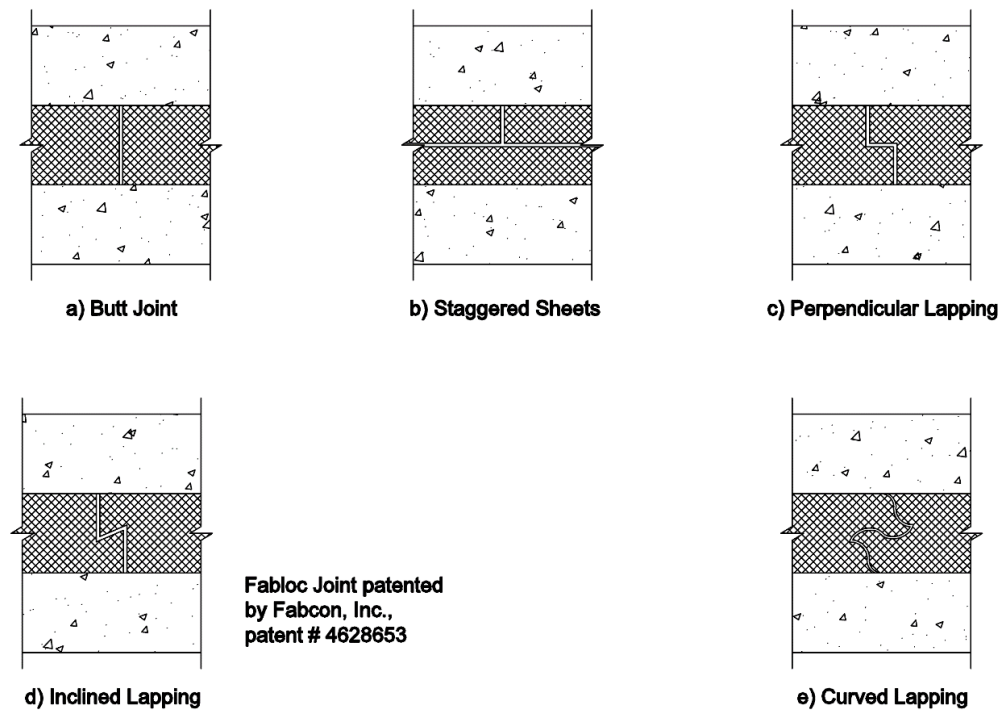


Figure 3-70 Insulation joint details- a) butt joint, b) staggered sheets, c) perpendicular lapping, d) inclined lapping, e) and curved lapping (adapted from Einea et al. 1991)

Another idea using is perpendicular lapping, which uses one thicker sheet of insulation instead of two thinner sheets and cuts the end to stagger the joint as one unit. An example of perpendicular lapping can be seen in Figure 3-70c. Taking perpendicular lapping one step further, inclined lapping has a slight rise in the joint so that any possible concrete that leaks into the joint will be trapped and not allowed to pass to the other side (Figure 3-70d).

The final detail proposed by Einea et al. (1991) is curved lapping, which cuts the insulation with curves to create a longer joint (and consequently a longer conduit or pathway) so that it is even more unlikely to have concrete breach from one concrete layer to another. An example of curved lapping may be seen in Figure 3-70e.

Thermal bridging at insulation joints could occur with even the best of details. By providing good detailing for insulation joints, however, the probability of thermal bridging occurring due to construction can significantly decrease.

SWP Connectors

Thermal Imaging Results

As mentioned in Chapter 2, steel connectors were used to connect the inner and outer wythes of concrete SWPs for many years because there were no other options and they provided a low cost way to obtain composite behavior between wythes. Over time as improved energy efficiency was desired, thermally resistant connectors made of fiber-reinforced polymer (FRP) were developed and have gained considerable popularity since (Einea et al. 1994, Olsen and Maguire 2016, Al-Rubaye et al. 2017, Olsen et al. 2017). Steel ties (often in the form of wire trusses) are no longer popular, but, according to their

manufacturers, are still being purchased and many older structures use them. Figure 3-71 shows that considerable thermal bridging results from using steel wythe connectors.

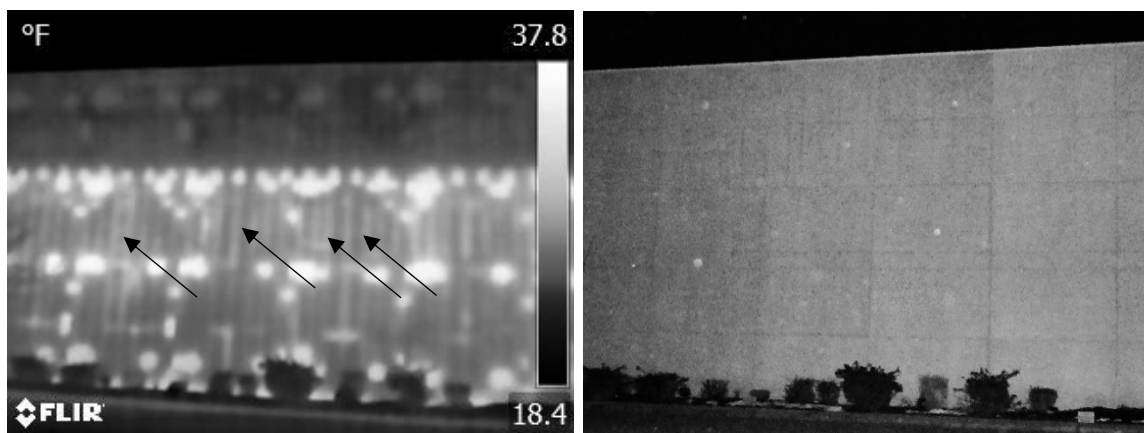


Figure 3-71 SWP structure with thermal bridging due to use of steel truss connectors (frequent vertical lines in left image): thermal image (left) and visual image (right)

Detail Discussion and Recommendations

Even using considerably thicker insulation, steel SWP connectors act as thermal bridges, allowing a significant amount of heat transfer to occur. Details are not provided for their use because the best recommendation for the thermal performance of a concrete SWP is to use an alternative connector made of a material with lower thermal conductivity such as FRP connectors. These FRP connectors are often proprietary and it is not the intent of this report to endorse a particular proprietary solution. However, using thermally insulative connectors will save building owners thousands of dollars by decreasing costs to heat and cool their structure.

Thermal Analyses

Thermal analysis is a necessary step in the optimization of thermal efficiency among structures and should be utilized by engineers and designers to ensure designs and details are sustainable as well as durable and meet strength and serviceability requirements. As such, considerable effort has been made to develop methods of determining thermal resistance in buildings as a way of comparing this performance from one structure to another. The following sections summarize the principle methods used to evaluate R-value for SWP structures and provide some examples of thermal analyses.

Determination of Thermal Resistance (R-Value)

There are several options available to measure the thermal resistance of SWPs, namely the parallel-path method, the isothermal-planes method, the zone and modified zone methods, and the characteristic section method. Other methods exist such as finite element modeling and experimental testing, though these options tend to be expensive, time-intensive, and complicated.

Parallel-Path Method

The parallel-path method uses an electric circuit analogy to calculate thermal resistance. This method assumes that heat transfer occurs in only one dimension at steady-state conditions and travels through different parallel-paths through the wall with no lateral heat transfer. This means that sections of a SWP with different thermal conductivities as shown in Figure 3-72, for example, would be modeled as separate and parallel-paths. This method specifically assumes there is no heat transfer laterally through

layers that are homogenous (such as the foam insulation or the concrete wythes). The thermal resistance is calculated for each heat path first by summing the consecutive thermal resistances for the layers in each pathway, and the overall R-value can be calculated as the reciprocal of the sum of the surface-weighted thermal transmittance values (U-factor) for each path (ASHRAE, 2013). This may be expressed as:

$$U = a_a U_a + a_b U_b + \cdots + a_n U_n \quad (3-1)$$

where U_i = thermal transmittance through path a, b, \dots, n

a_i = surface-weighted path percentages for area of each transmittance

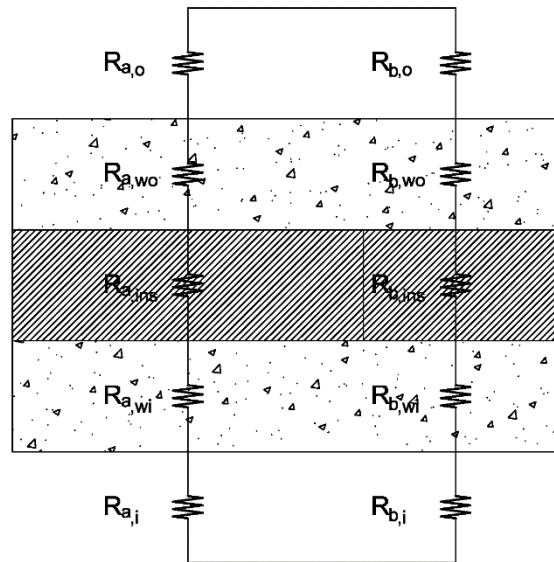


Figure 3-72 Parallel-path method electric circuit analogy

In the example in Figure 3-72, there are two principle paths for heat. Substituting the relationship between thermal conductance and thermal resistance yields:

$$\frac{1}{R} = \frac{a_a}{R_a} + \frac{a_b}{R_b} \quad (3-2)$$

where R_a = total thermal resistance of heat path a

R_b = total thermal resistance of heat path b

The thermal resistances of each heat path are in series, so the total thermal resistance of each heat path is the sum of the thermal resistances in series, yielding:

$$\frac{1}{R} = \frac{a_a}{\sum R_{ai}} + \frac{a_b}{\sum R_{bi}} \quad (3-3)$$

where R_{ai} = thermal resistance of element i in heat path a

R_{bi} = thermal resistance of element i in heat path b

The 2013 ASHRAE Handbook-Fundamentals recommends using the parallel-path method when thermal conductivity of the different materials in the layer are somewhat close together (within same order of magnitude).

Isothermal-Planes Method

The isothermal-planes method utilizes the same electric circuit analogy to calculate thermal resistance for a panel, but assumes that some lateral heat transfer does occur. Just like electricity, heat tends to follow the path of least resistance. Modeling the different elements of a wall system like a circuit with resistors in series and in parallel according to the actual wall assembly, the overall thermal resistance of the wall can be

calculated. For paths where heat must travel through various layers in series, the overall path resistance is the sum of the individual layer resistances. For paths where heat travels through parallel elements, thermal resistance can be calculated using the parallel-path method. An overall R-value can then be determined by combining these systems in parallel and in series together. The resultant thermal resistance for the system shown in Figure 3-73 would therefore be:

$$R = R_o + R_{wo} + \frac{1}{\frac{a_a}{R_{a,ins}} + \frac{a_b}{R_{b,ins}}} + R_{wi} + R_i \quad (3-4)$$

where R_o = thermal resistance outside air on outside wythe

R_{wo} = thermal resistance of outside wythe

$R_{a,ins}$ = thermal resistance of insulation wythe of material a

$R_{b,ins}$ = thermal resistance of insulation wythe of material b

R_{wi} = thermal resistance of inside wythe

R_i = thermal resistance of inside air on inside wythe

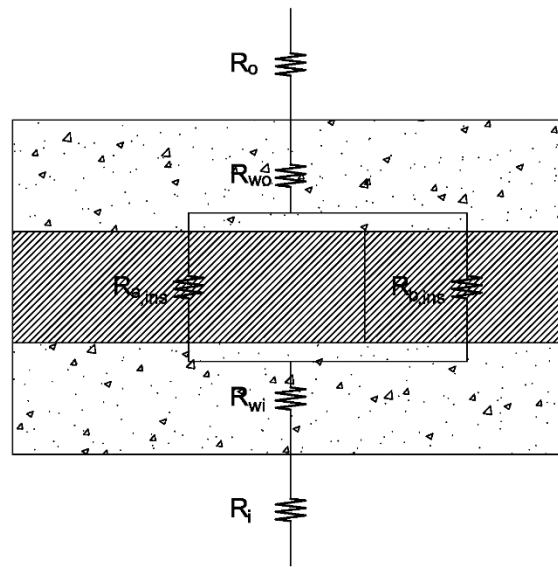


Figure 3-73 Isothermal-planes method electric circuit analogy

Zone and Modified Zone Methods

The zone method and modified zone method are similar to the parallel-path and isothermal-planes methods but are used when there are widely spaced, highly conductive elements in a structure. For SWPs, this essentially means steel connectors. The zone method separates the panel into zone A (containing the conductive element) and zone B (the remaining portion of the panel). The resistances are calculated for each zone and then are combined using the parallel-path method, where area resistances are added together for elements in series and where area conductances are added together for elements in parallel (Figure 3-74). The only difference between the zone method and the modified zone method is in how the widths of the zones are calculated. The zone method calculates the width, W , as

$$W = m + 2d \quad (3-5)$$

where m = width or diameter of the connector or thermal bridging element

d = distance from panel surface to connector ($d \geq 0.5$ in)

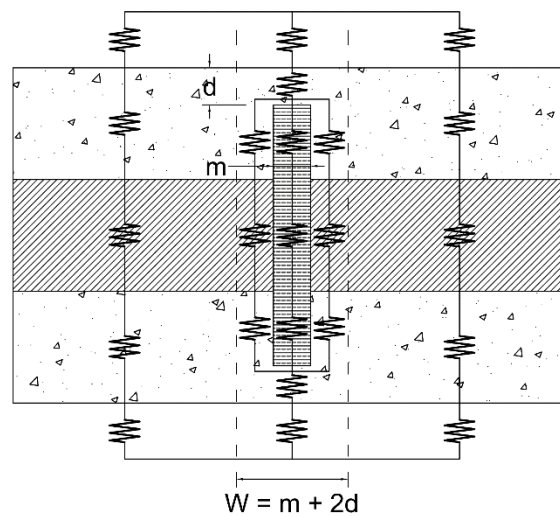


Figure 3-74 Zone method electric circuit analogy

Because SWP structures differ somewhat from the metal-frame structures for which the zone method was developed, Lee and Pessiki (2008) developed a new way to determine the width of this zone that could be used with the zone method to yield accurate results. This modified zone method calculates width of zone A as:

$$W_n = (0.174k_{conc} - k_{ins} + 0.0026k_{ct} + 2.24)m + 0.02k_{conc} - 0.6k_{ins} + 0.0024k_{ct} + 2.35 - 0.15d \quad (3-6)$$

where k_{conc} = concrete thermal conductivity

k_{ins} = insulation thermal conductivity

k_{ct} = metal wythe connector thermal conductivity

m = width or diameter of connector

d = depth from panel surface to connector ($d \geq 0.5$ in)

The R-value can then be determined by using the same procedure as the zone method using this value for the width of zone A.

Characteristic Section Method

Pessiki and Lee (2003) also developed a method similar to the zone method for determining thermal resistance for SWPs that have consistent solid sections. The panel is again divided into two zones where the section with the solid portion is assumed to have no insulation and the other section is assumed to be perfectly insulated (no thermal bridging) as shown in Figure 3-75 (PCI, 2010). Total thermal resistance is calculated by combining the two zones together using the parallel-path method.

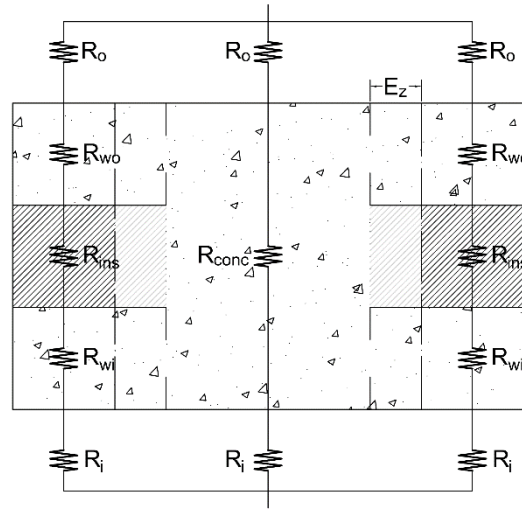


Figure 3-75 Characteristic section method electric circuit analogy

The zone to be modeled as entirely uninsulated will actually be larger than the actual solid section itself. This additional affected zone dimension, E_z , is (in inches):

$$E_z = 1.4 - 0.1\alpha t_{ins} + \beta[0.4t_{co} + 0.1(t_{ci} - t_{co})] \quad (3-7)$$

where t_{ins} = insulation thickness (inches)

t_{co} = outside concrete wythe thickness (inches)

t_{ci} = inside concrete wythe thickness (inches).

Since this equation is empirical, all units must be in inches or $\frac{\text{Btu}\cdot\text{in}}{\text{hr}\cdot\text{ft}^2\cdot^\circ\text{F}}$ for the result to be accurate. The α and β values are factors that account for the thermal conductivity of the insulation and the concrete, and are calculated as follows:

$$\alpha = 1 + 2.25 * \left(\frac{k_{ins} - 0.26}{0.26} \right) \quad (3-8)$$

$$\beta = 1 + 1.458 * \left(\frac{k_{conc} - 12.05}{12.05} \right) \quad (3-9)$$

where k_{ins} = insulation thermal conductivity (Btu·in/[hr·ft²·°F])

k_{conc} = concrete thermal conductivity (Btu·in/[hr·ft²·°F])

The affected zone dimension is intuitively the amount of area surrounding the solid section that is affected by the thermal bridging. Once E_z is calculated, it should be added to each side to determine the area of the affected area. One could use equation (3-5) above to calculate the resulting width in each dimension, substituting the width of the solid section in either direction for m , and E_z for d .

After determining the affected area, the R-value is determined for both zones separately and then combined using the parallel-path method. The R-value for the affected zone, again, is calculated by assuming the entire zone is a solid section. The R-value for the remaining zone is calculated as if it is perfectly insulated with no further thermal bridging.

Other Methods

There are other methods for determining R-value of concrete SWPs that may be more accurate than the methods herein described, but they are often expensive, time consuming, and quite complicated. One alternative is finite element modeling, though the software is often costly and requires qualified personnel to perform the thermal models.

Another alternative that is likely the most accurate is actual physical testing using the guarded hot box method (ASTM C236) (ASTM C1363). This method involves placing a panel inside a hot box apparatus that is designed to maintain steady-state conditions with cold air on one side of the panel and hot air on the other. This method is very accurate since the surface temperatures and areas can be measured directly, but is very expensive and time-intensive, and is typically not practical for use in the field. Although it would be ideal to perform finite element modeling or actual experimental testing for each project, it is impractical to do so. The methods presented in the previous sections have been shown to be sufficiently accurate for the purposes of design and are recommended for use in performing preliminary thermal analyses for structures.

Thermal Analysis Examples

Thermal analyses were performed for each type of detail discussed in this study. Each example was based off of real details in conjunction with an assumed 12 ft \times 30 ft SWP with a 3-3-3 configuration (meaning that concrete wythes and the insulation wythe each were 3 inches thick for a total of 9 inches). This SWP is displayed in Figure 3-76. All examples in this report used the same material conductivities. These values are expressed in Table A-1 in Appendix A and were obtained from the *ASHRAE Handbook 2013- Fundamentals* (2013) and *Fundamentals of Heat and Mass Transfer* (Incropera & DeWitt, 2002). Examples were selected to show a good spread of scenarios. The heat transfer in a structure for any given detail could be more or less than the examples shown here, based upon many variables that have previously been discussed. Each section briefly discusses the results of the calculations. The actual calculations themselves are

included in Appendix A at the end of the report. Air film resistance differs slightly for summer and winter according to *ASHRAE Handbook 2013- Fundamentals* (2013). Because greatest heat transfer tends to occur in winter, the winter air film resistance values were used in the examples in this report. See Appendix A for comparison of summer vs. winter values.

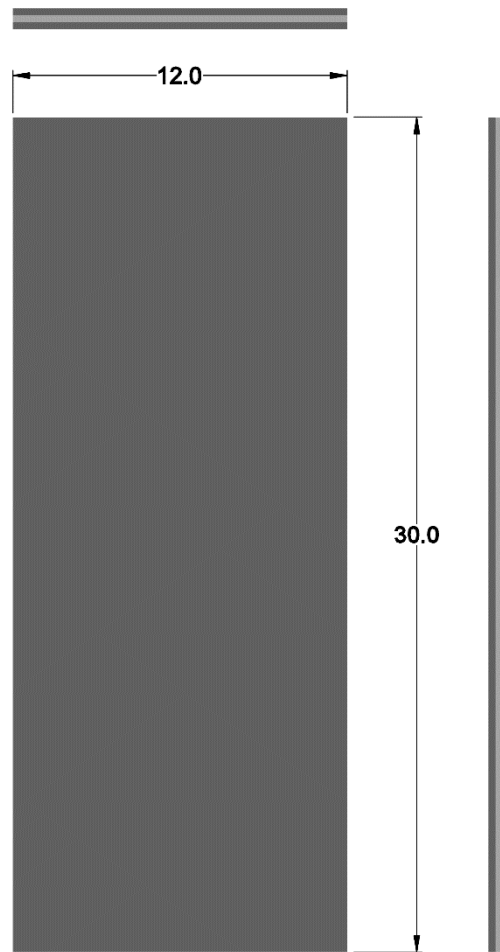


Figure 3-76 SWP used in analyses of this dissertation

When solid sections are created around a steel connection that does not penetrate the entire thickness of the panel, the inclusion of the steel property becomes negligible to

the heat transfer that occurs through this section. An example of this may be steel welding plates inserted into panels to which joists and beams can be welded for floor or roof members. For this reason the steel component is often ignored in the following examples to simplify calculations. To demonstrate the insignificance of this exclusion, a floor connection was analyzed to compare the effects of including the steel element in the calculations. A steel connection in the middle of a $1\text{ ft} \times 1\text{ ft}$ solid concrete section placed every 6 ft on center (o.c.) was modeled with and without the steel using the isothermal-planes method to compare the effects of including the steel element (Figure 3-77). The results showed a difference of about 0.0023% between the inclusion and exclusion of the steel element when enshrouded in a concrete section (Appendix A). They are essentially the same.

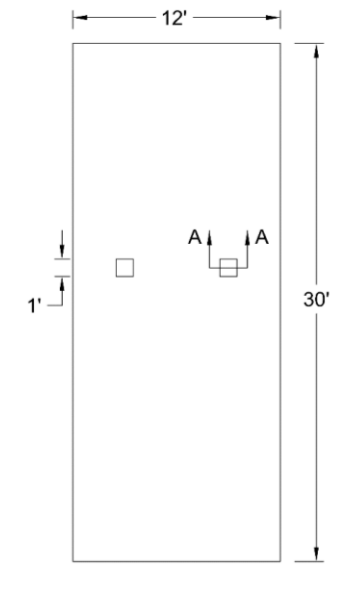


Figure 3-77 Panel layout of SWP example comparing inclusion/exclusion of steel element

Windows and Doors

Windows and doors designed with a solid section immediately surrounding the structural element can be detrimental to thermal performance of the building. To demonstrate the effect of such a design, consider a 12 ft \times 30 ft panel with one 4 ft \times 4 ft window in the middle with 2 inches of solid concrete penetrating the insulation around the window edges (Figure 3-78). Since this analysis is for a solid concrete section, the characteristic section method is the most appropriate method to use for a most accurate prediction of panel R-value. A SWP with these dimensions and a 3-3-3 configuration would result in about a 17.7% decrease in R-value as opposed to a panel with no thermal breaches whatsoever. The calculations are included in Appendix A. This is significant, especially if there are many windows in the structure, if the windows are larger, or if the solid section around the windows is designed to be thicker. Figure 3-79 shows how increasing window size affects the thermal resistance. Solutions to this issue can likely be found by working with the fenestration supplier.

Solid Walls

It should be apparent that solid concrete panels will perform exceedingly worse than insulated sandwich wall panels. The difference in thermal performance between the two is remarkably different. Comparing the thermal bridging for the same 12 ft \times 30 ft panel considered previously to a solid 12 ft \times 30 ft panel with the same thickness will yield a decrease in R-value of 91.5%. The calculations can be seen in Appendix A. It is likely that insulation will be applied to the interior of the building at the solid panel location to mitigate this effect, however, this requires additional cost and time.

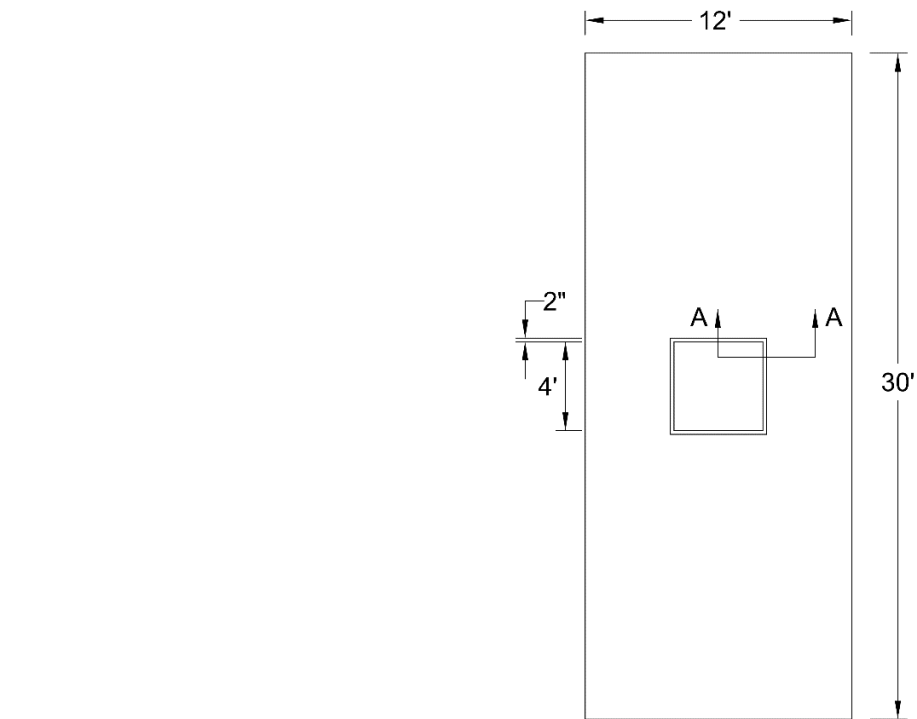


Figure 3-78 Panel layout of SWP analyzed with solid section around window

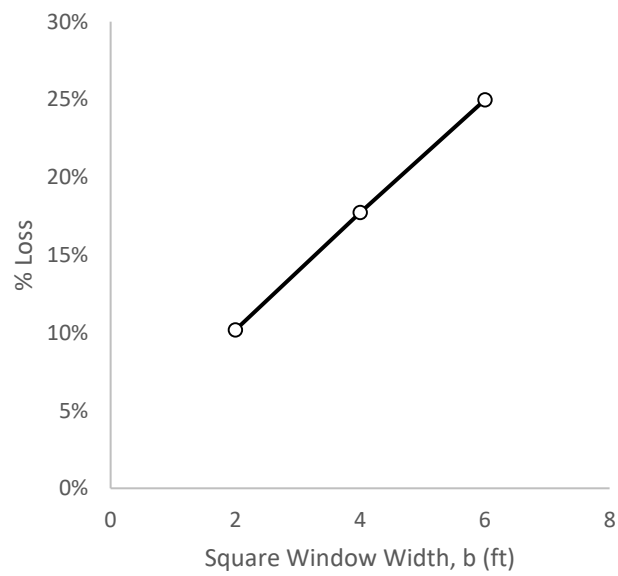


Figure 3-79 Percent loss in thermal efficiency vs. square window width

Wall Penetrations

Although necessary at times, wall penetrations ought to be avoided when possible. A structure with an external, low-roof attachment where steel roof beams puncture the insulation to attach to the interior structural wythe was analyzed for comparison of the effects of such a penetration. The beams were assumed to be W6×13 members spaced every 6 ft o.c., with a 1 ft × 1 ft section of insulation blocked out for each penetration (Figure 3-80). The following three examples were considered for the penetration: a 1 ft × 1 ft section of insulation and outer wythe removed and not replaced around the beam, a 1 ft × 1 ft section of insulation and outer wythe removed with concrete filled in around the penetrating member after construction, and a 1 ft × 1 ft section of insulation and outer wythe removed where insulation was filled in around the penetrating member. As expected, the greatest decrease in R-value results when there is no fill after the penetrating member is installed. The decrease in R-value for this panel when the void was not filled would be about 13%. When concrete filled the void, the R-value decreased by 10%, and filling the void with insulation resulted in an 8% decrease. There will still be a decrease even filling insulation in around the penetrating member because the penetration itself is a large thermal bridge. The larger the member or deeper the penetration, the greater the heat transfer that will occur. If a penetration is absolutely unavoidable, it is intuitive that it is best to fill insulation in around the penetration to minimize the thermal bridging. See Appendix A for more details. Figure 3-81 shows how the percent loss in R-value increases as the number of penetrations in a panel increases using values from the case where the insulation and concrete are not replaced.

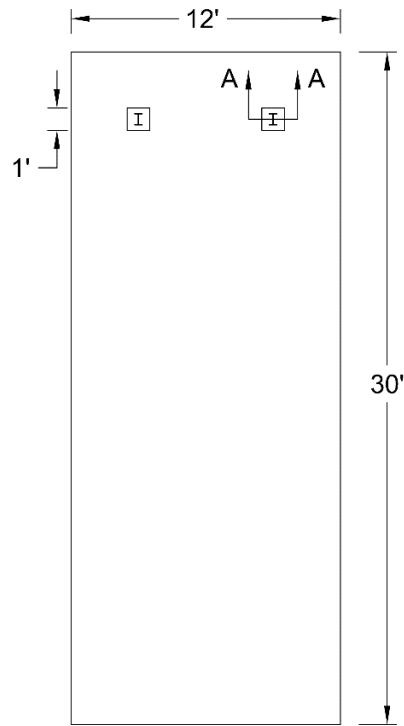


Figure 3-80 Panel layout of SWP example analyzed with penetrations

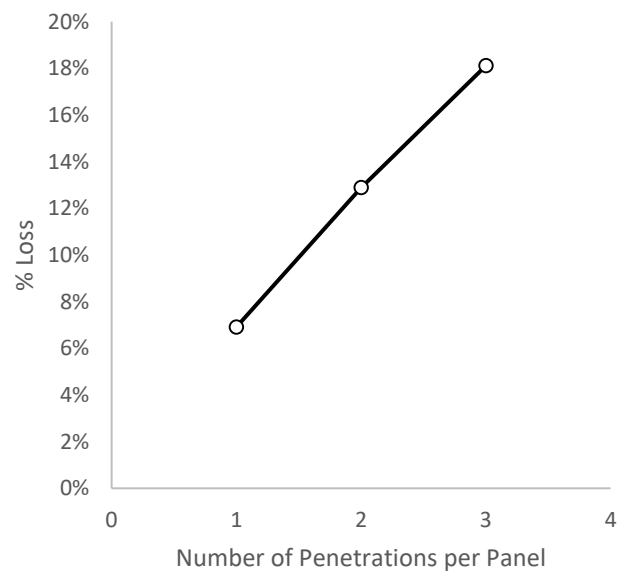


Figure 3-81 Percent loss in thermal efficiency vs. number of penetrations

Lifting Anchors

All panels require some way to lift them into place during erection. The most common solution to this problem is by using lifting anchors. Unfortunately many lifting anchors require reducing or omitting the insulation to achieve capacity. This is becoming ever more common as industry continues to push the limits of slenderness to use less material and create more sustainable design for structures. R-value for a SWP with 4 steel lifting anchors was calculated (Figure 3-82). To simplify modeling, the lifting anchors were simulated as cylinders that penetrated the depth of the SWP. Using 4 steel lifting anchors resulted in a decrease of about 9.8% in R-value. Calculations and results are shown in Appendix A. Using more lifting anchors results in a greater decrease (see Figure 3-83).

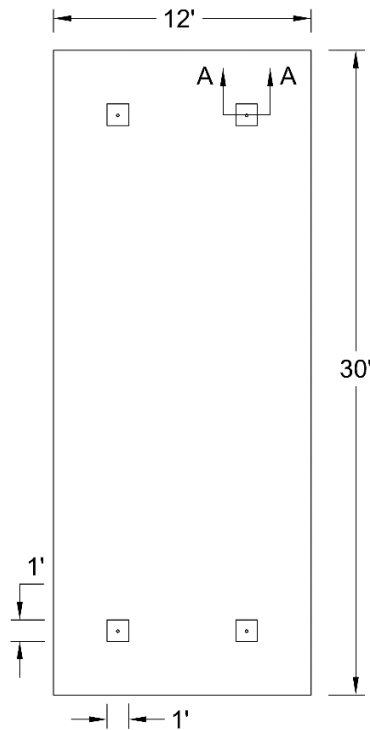


Figure 3-82 Panel layout of SWP example analyzed with 4 steel lifting anchors

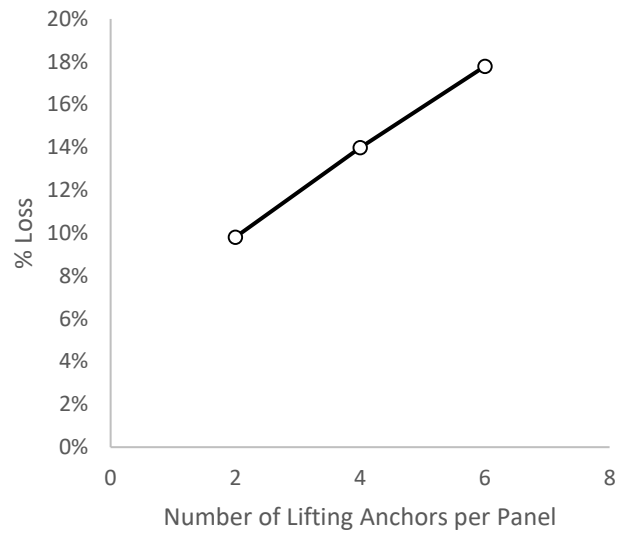


Figure 3-83 Percent loss in thermal efficiency vs. number of pick points

Corbels

Corbels are often a necessary detail for many load bearing panels, so they cannot be eliminated. To ensure safety, insulation is frequently reduced or omitted, creating large thermal breaches. A single corbel requiring a solid section of 20 inches by 28 inches per panel would result in an approximate drop in R-value of about 10.9% (see Figure 3-84 and Appendix A). Depending on the frequency or additional size, the R-value could be lower (Figure 3-85). As stated above, research is currently ongoing to eliminate this issue, and is discussed further in the next chapter.

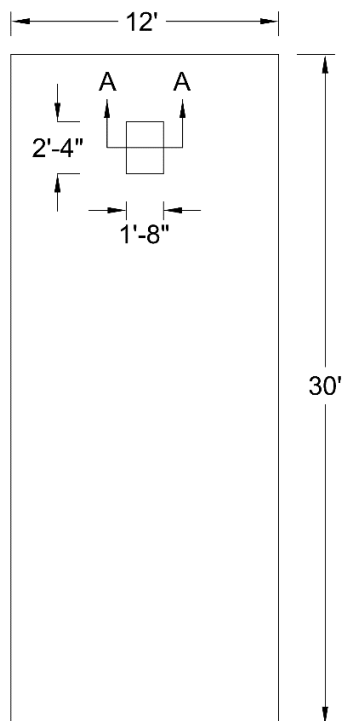


Figure 3-84 Panel layout of SWP example analyzed with solid section at corbel

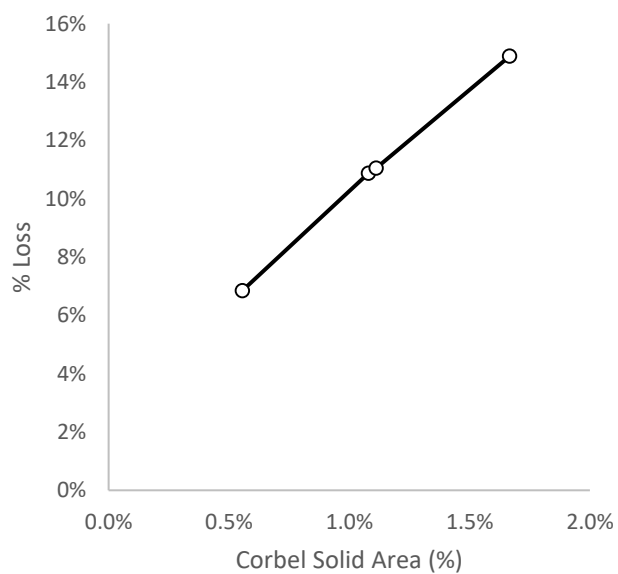


Figure 3-85 Percent loss in thermal efficiency vs. required solid area for a corbel

Roof Termination

Proper roof termination can greatly improve thermal efficiency. Embedment plates often used for roof joists can displace further insulation and cause additional thermal bridging to occur. A roof joist embedment plate that displaces a square foot of insulation every 6 ft from a 12 ft \times 30 ft panel will result in about a 10.7% reduction in thermal resistance in the summer, and 11.2% in the winter (see Figure 3-86 and Appendix A). Increased number of these connections results in greater thermal bridging (Figure 3-87). Further heat transfer is expected to occur between the wall and the roof if continuity of the insulation is not maintained, though the amount that is lost is difficult to determine from simplistic methods used here. For determination of this heat transfer, a finite element model would be required.

Floor Termination

Floor termination also commonly uses embedment plates to connect beams and girders to the SWP system. Some larger joists require two embedment plates (one for the top chord and one for the bottom chord). A similar example was used to calculate potential thermal bridging from such a design. Joists were assumed to be spaced 6 ft. o.c. with two square foot blocks of insulation removed for joist attachment (Figure 3-88). This resulted in a 20.1% decrease in thermal resistance. Calculations are shown in Appendix A. Figure 3-89 displays how the number of these connections influences the decrease in thermal efficiency attained in a SWP.

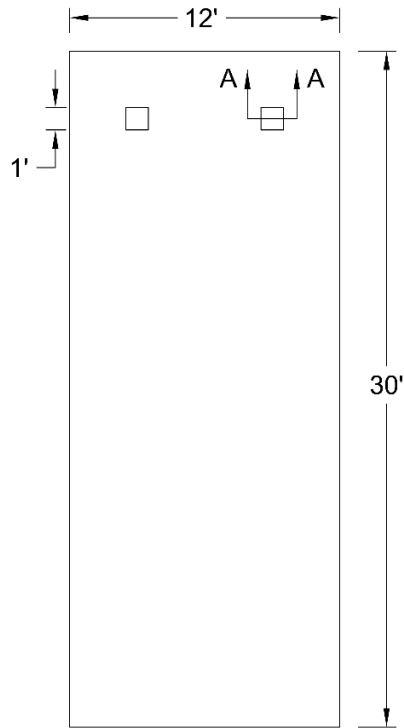


Figure 3-86 Panel layout of SWP example analyzed with solid sections at roof connections

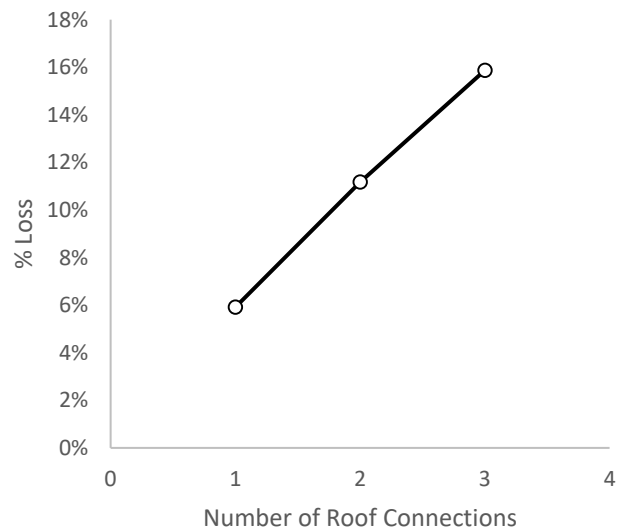


Figure 3-87 Percent loss in thermal efficiency vs number of roof connections

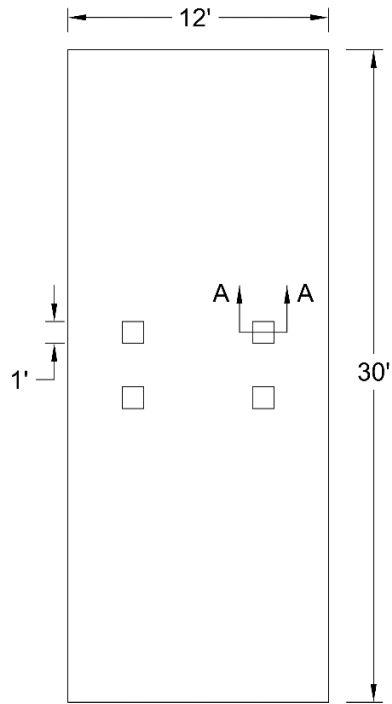


Figure 3-88 Panel layout of SWP example analyzed with solid sections at floor connections

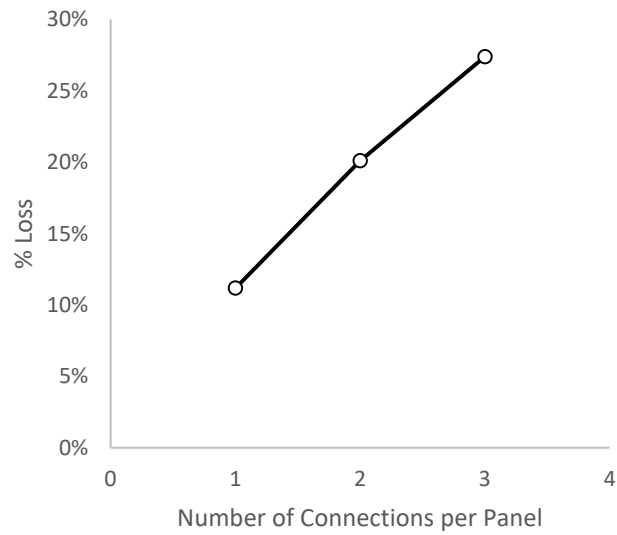


Figure 3-89 Percent loss in thermal efficiency vs number of floor connections

Insulation is not always omitted from the details, however. To compare the difference it makes to reduce insulation instead of removing it altogether, this example was performed again but assuming that insulation was reduced from 3 inches to only 1 inch for a 2 ft \times 2 ft space every 6 ft. o.c. with significant results. By using such an approach, only a 6.5% decrease in R-value would be noted as opposed to 20%. Though reducing insulation is not ideal, it is clearly better than omitting insulation entirely.

Foundation

The foundation is another location that can be complex to calculate heat transfer since this typically occurs in 3 dimensions along the base of the wall, and even directly through the slab into the ground. This means FE modeling is typically ideal if heat transfer at the foundation is a concern. Some basic modeling can be performed for connections from the foundation to the SWP though since these connections often require that insulation be removed so that embedment plates in the wall can be welded to the foundation. This type of example was performed assuming an 8" \times 8" segment of insulation was blocked out every 6 ft. o.c. (Figure 3-90). Results demonstrated a simple 8" \times 8" section of insulation at this spacing could result in a 6.9% decrease in R-value (Appendix A). As the solid section width for these connections increases, there is greater loss in R-value (Figure 3-91).

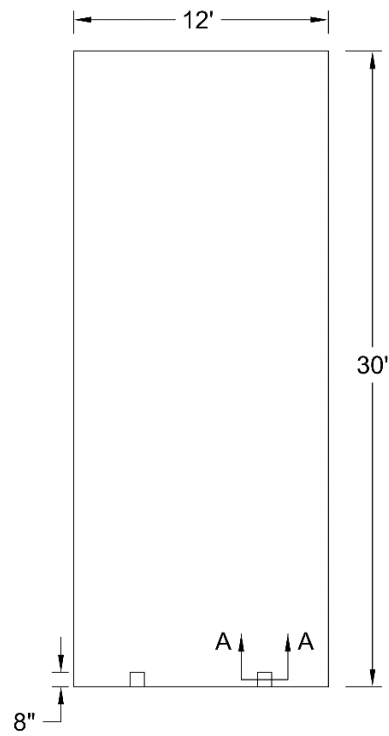


Figure 3-90 SWP layout of example analyzed with solid sections at foundation connections

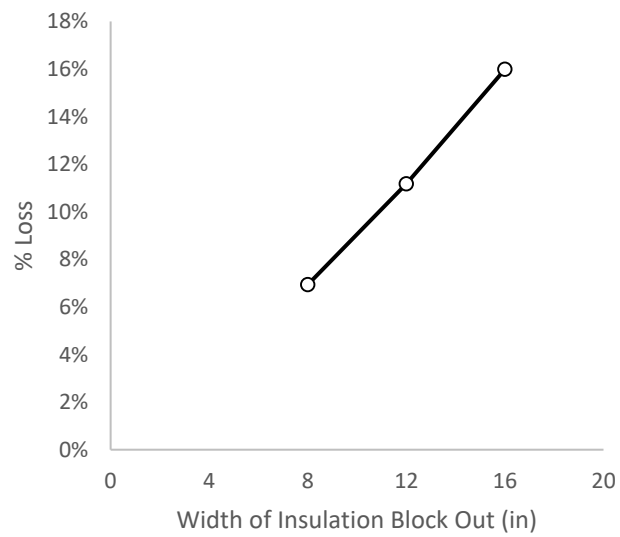


Figure 3-91 Percent loss in thermal efficiency vs insulation block out width

Corners

Corners are a very common location for thermal bridging, but are a 3-dimensional element with at least 2-dimensions of heat transfer occurring, making it very difficult to model this heat transfer with the 1-dimensional methods herein described. Finite element modeling would be required for corners, so no example is included in this report.

Panel-to-Panel Connections

Panel-to-panel connections can be significant sources of thermal bridging as well due to the high number of them in structure. A 12 ft \times 30 ft SWP with 3 connections to each neighboring panel where each connection requires blocking out a 1 ft \times 1 ft section of insulation (shown in Figure 3-92) can result in an approximate 15.9% decrease in R-value (Appendix A). That is particularly significant when you consider how many panels are in a structure. Minimizing the number of connections required between panels will help to decrease loss in efficiency (Figure 3-93). Particular attention should be given to the detailing of these connections.

Insulation Joints

Insulation joints can be an unanticipated way for thermal bridging to happen because designers do not typically plan on such thermal bridging to occur. This thermal bridging happens as a result of the construction process. To quantify thermal bridging from insulation joints, the characteristic section method was first used, assuming that all gaps between insulation segments added up to a total of $\frac{1}{4}$ inch along the entire length and also along the width (Figure 3-94). This $\frac{1}{4}$ inch was lumped together and used as the

affected area in the characteristic section method. Larger gaps in insulation can clearly create significant thermal bridges. This resulted in a 37.1% decrease from the ideal panel using the characteristic section method. The characteristic section method is an empirical equation used to provide an additional width to be considered as part of the solid region for improved accuracy. Use of the characteristic section method is a simplified method that may not accurately analyze this situation due to the narrowness of the concrete solid section, considering that this method ultimately estimated 5% of the concrete was “affected” (and therefore considered as solid section) compared to the 0.25% actual solid area. This sheds considerable doubt on the accuracy of these results. Because the width of the breach is so small, it is possible that the affected area may be much smaller, though it is unknown how much smaller. For comparison this example was repeated but instead of using the affected zone width calculated by the characteristic method equation, it was assumed that the affected width (E_z) was equal to the width itself ($\frac{1}{4}$ inch). This was a significantly smaller affected area than the characteristic section method predicted, but still resulted in a decrease of thermal resistance of approximately 7.3%. It is very plausible that the actual affected zone could exceed this width, so 7% can be assumed to be a minimum loss for an overall total gap of this size. See Appendix A for more details. Thicker net cumulative solid insulation joint width intuitively results in more thermal bridging (Figure 3-95).

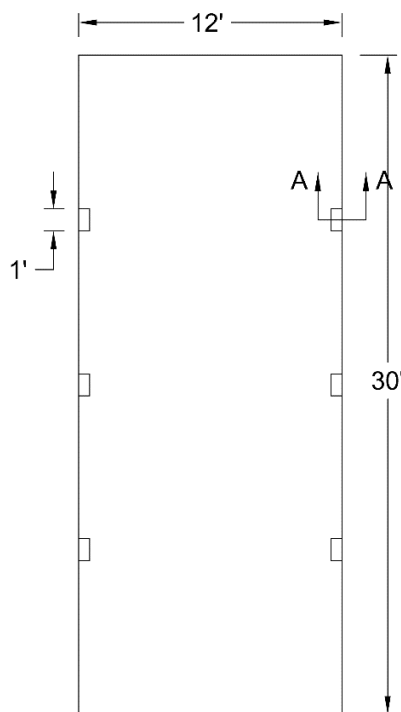


Figure 3-92 Panel layout of SWP analyzed with 3 panel-to-panel connectors per panel

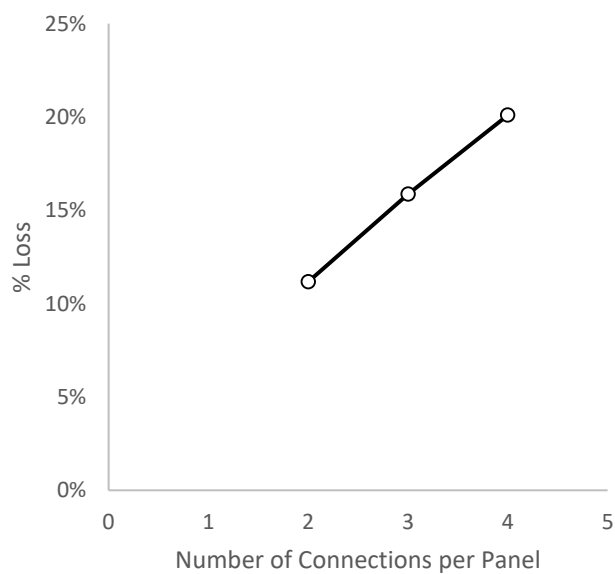


Figure 3-93 Percent loss in thermal efficiency vs number of connections

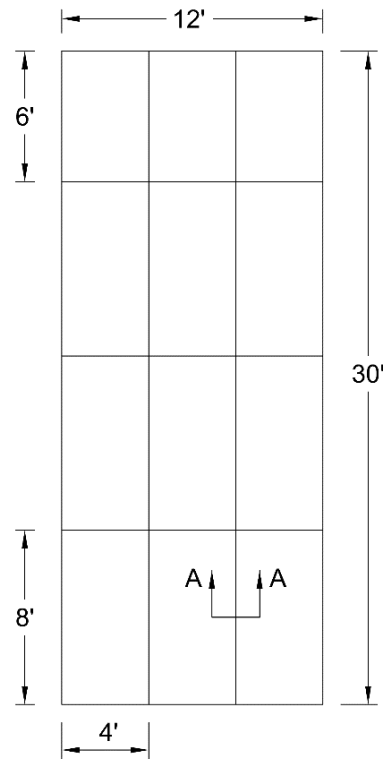


Figure 3-94 Panel layout of SWP example analyzed with insulation joints

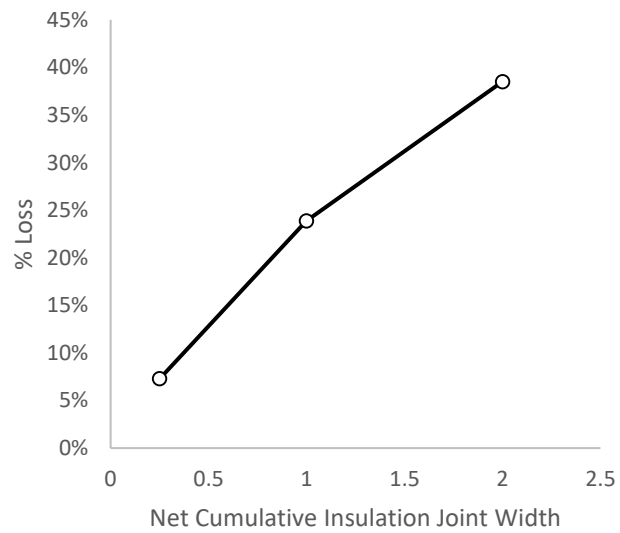


Figure 3-95 Percent thermal efficiency loss vs net cumulative insulation joint width

SWP Connectors

Steel SWP connectors are not nearly as popular today as they have been in the past due to the advent of new connectors with improved thermal resistance, but they are still used occasionally in the field. A 12 ft × 30 ft panel was analyzed having steel connector pins spaced every 18" × 24" o.c with a diameter of ¼ inch (Figure 3-96). The geometry of these pins was such that each pin crossed through the insulation twice per location. A simple thermal analysis using the zone method revealed that using pins similar to these would result in approximately an 8.5% decrease in R-value (see Appendix A). This configuration was selected as it seemed the most unobtrusive of the available steel SWP connectors. Repeating the analysis using steel truss connectors (also shown in Figure 3-94) resulted in a decrease in R-value of 25%. Using larger connectors or steel truss connectors clearly results in more significant heat transfer, and should be avoided in the interest of improving sustainability and thermal efficiency of SWP structures.

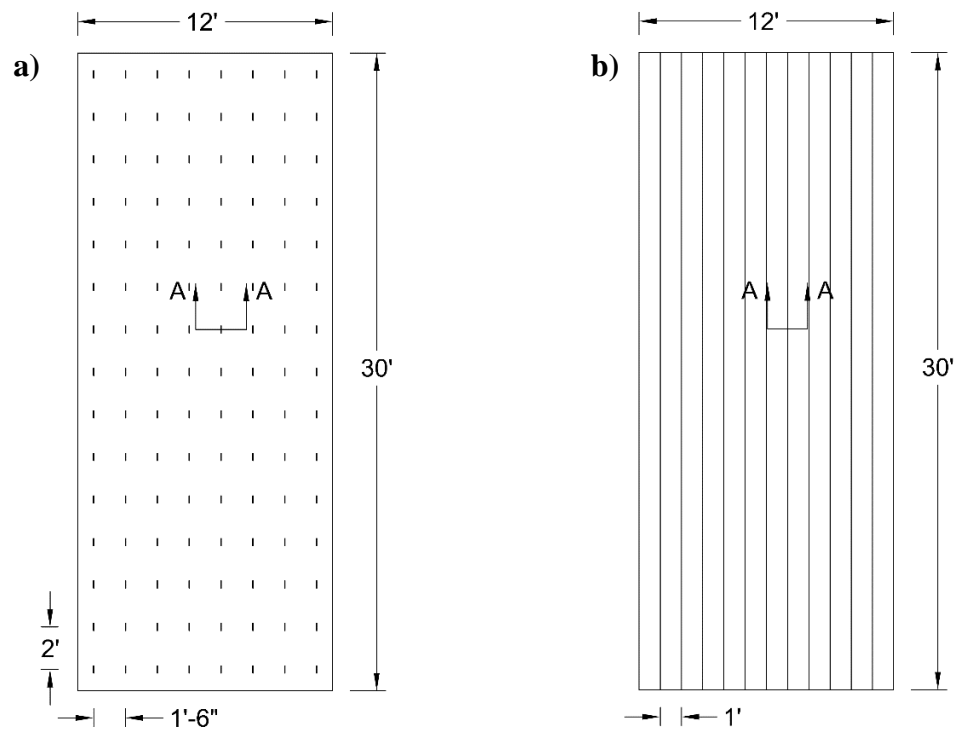


Figure 3-96 SWP layout of example analyzed with a) steel pins and b) steel truss connectors

Summary

As shown in this chapter, thermal analysis of details is a good way to predict thermal performance of structural designs to optimize thermal efficiency and decrease thermal bridging. Some of the examples shown resulted in significant thermal bridging, but it should be noted that thermal bridging can occur in a building at multiple locations, meaning that the results could compound upon one another to decrease thermal efficiency further. Careful attention to detail will help prevent unnecessary heat transfer from occurring in SWP structures. Using the techniques in this chapter, engineers and architects can evaluate the details prior to inclusion in the final structure.

CHAPTER 4

THERMALLY EFFICIENT CORBEL CONNECTIONS

The research included in this chapter focused on creating alternative corbel connection designs in partially-composite concrete sandwich wall panels to reduce heat transfer by eliminating thermal bridging. This chapter contains information regarding the design and creation of such details and their respective testing specimens.

Preliminary Analysis

To ensure that designs were structurally adequate, this project aimed to emulate stresses found in practice within SWP corbel connections. Preliminary analyses were performed prior to specimen creation using finite element modeling (FEM) to determine if stresses surrounding the corbel would simulate those of a full-scale panel. Results demonstrated that utilization of a 6 ft \times 8 ft 3-3-3 SWP achieved comparable local stresses as a 12 ft \times 30 ft panel commonly used in the field, reducing the required volume of specimens by 86.7% to achieve the same purpose. Thus 6 ft \times 8 ft panel width and height respectively were shown to be adequate.

Experimental Design

For designs to be efficacious, the following criteria were considered:

- Continuation of thermal break
- Nominal capacity
- Sustained loading

Designs were created to emulate local stresses of composite SWP corbels in the field and to emulate behavior of full-scale panels. This resulted in a six foot wide by eight foot tall 3-3-3 SWP where the corbel was 8-in deep and 10-in wide with a face height of 10-in and a height of 14-in at the corbel-wall interface. After testing the first set of 4 corbel specimens, panel sizes were modified slightly to 68" \times 102" to better accommodate the test setup. This will be discussed in a later section.

The majority of designs utilized strut-and-tie modeling, though the deep beam method was used as well. Twelve designs were created (shown in Table 4-1), consisting of three control designs common in industry and nine proposed alternative designs.

Figure 4-2 shows a profile view of all specimen designs. The following sections discuss determination of design load and methodology behind each design creation of the control and proposed specimens.

Table 4-1 Test specimens

Name	Primary Tension Element	Name	Primary Tension Element
SolidWall	Rebar	GridHor	GFRP Grating
SolidSec	Rebar	GridVer	GFRP Grating
RedIns	Rebar	GFRP3	#3 GFRP U-bars
HatIcon	IconX CFRP SWP Connectors	GFRP2	#2 GFRP U-bars
IconXG	IconX GFRP SWP Connectors	HKVer	HK SWP Connectors
IconXC	IconX CFRP SWP Connectors	HKHor	HK SWP Connectors

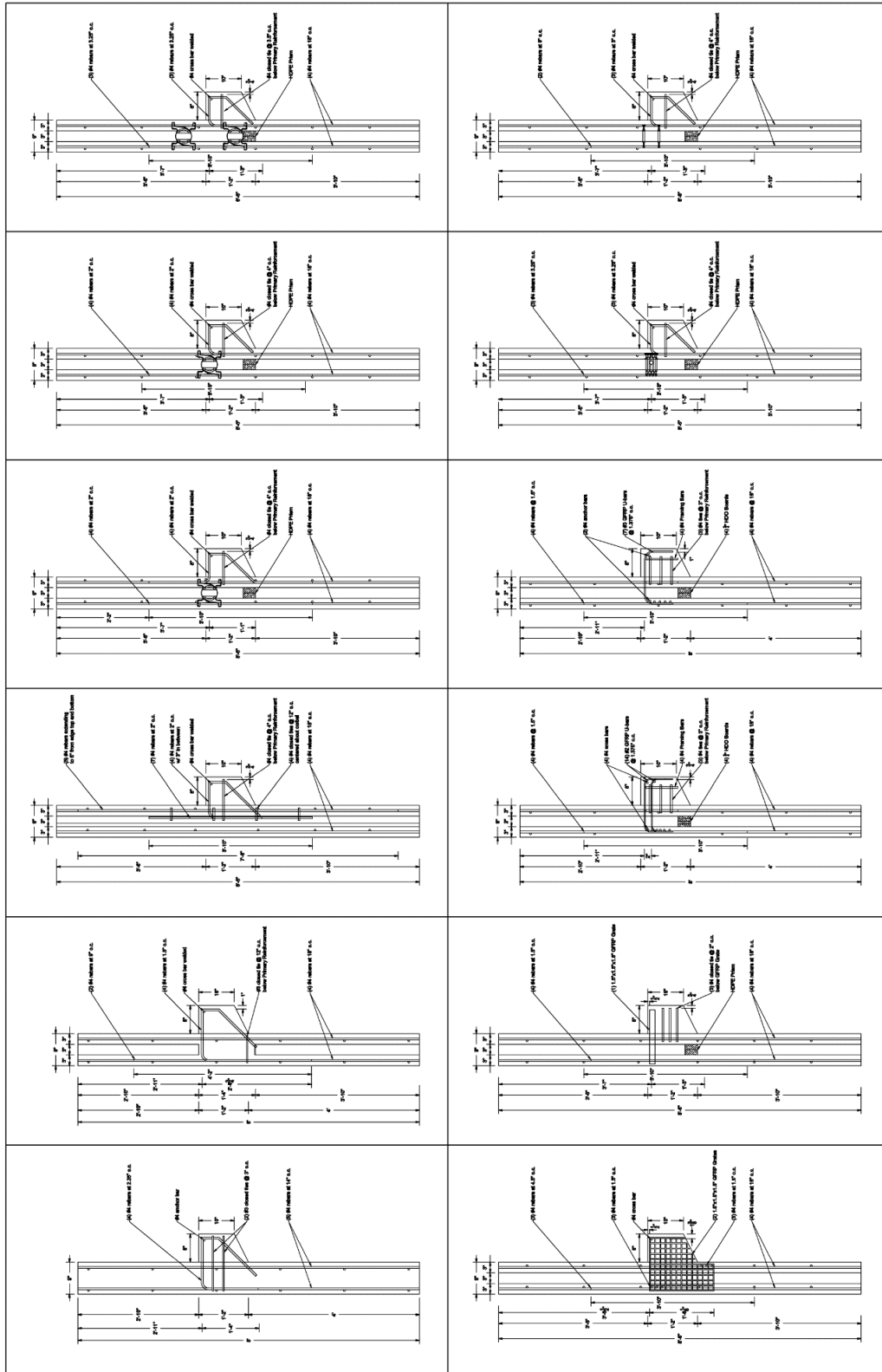


Figure 4-1 Profile view of specimen designs, top left to bottom right: a) SolidWall, b) SolidSec, c) RedIns, d) IconXCHat, e) IconXC, f) IconXG, g) GridVer, h) GridHor, i) GFRP2, j) GFRP3, k) HKVer, and l) HKHor

Load Determination

Careful consideration was made to emulate typical loads used in industry. Corbels are typically used to support beams or slabs used in flooring systems. The most common types of beams to be supported include steel joists or double-tee beams. Because double-tee beams provide greater self-weight than steel joists, it is logical that design for such would be more conservative than for steel joists. For this reason, design assumed that the corbels would support a 12DT28+2 double-tee beam with a span of 50 ft, having a self-weight of 81 psf (PCI, 2010) in an attempt to use a member that might be common for a large part of the industry. Aside from the applied vertical load, ACI 318-14 also requires that corbels be designed to include a horizontal force greater than or equal to 20% of the vertical force, which was incorporated into design (2014).

In seeking alternative materials to use in design that satisfy the requirements of being thermally insulative and adequately strong, it became quickly apparent that many of the most viable options currently are fiber reinforced polymer (FRP) materials. These materials are almost always susceptible to significant creep when subjected to a constant load over time, however, and can suddenly fail without warning. This is called creep rupture. The time that FRP bar can sustain a load prior to creep rupture is called endurance time. Endurance time is inversely related to the ratio of sustained load to ultimate load. Creep rupture is not a factor for steel under normal circumstances and subjected to normal temperatures, but, because FRP materials were used in many of the designs, had to be held into consideration.

Assuming a superimposed dead load and live load of 15 psf and 55 psf, respectively, the following design loads were used for this study:

- Factored load, $V_u = 30.5 \text{ kip}$
- Sustained load, $V_{sus} = 16.5 \text{ kip}$.

Control Specimens

As previously mentioned, there are two common designs currently used in industry for corbels in partially-composite SWPs. The first is the most common, utilizing solid sections to withstand structural loads (Kerkstra Precast, 2014) (Kerkstra Precast, 2016). The second creates a locally thickened wythe by reducing the insulation at the corbel location. This second option is also sometimes referred to as an “internal pilaster” (Frankl B. A., Lucier, Hassan, & Rizkalla, 2011) (Frankl B. , Lucier, Rizkalla, Blaszk, & Harmon, 2008) (Altus Group, Inc., 2018) (Altus Group, Inc., 2012). One specimen following each of these designs was created, as well as one solid concrete wall (no insulation) to serve as control specimens to demonstrate how the performance of the new designs compare to those commonly found in industry at the moment. It may be noted that the use of a shelf angle is also quite common, typically requiring a solid section to attain adequate embedment in partially-composite SWPs. Such a specimen was omitted from this study as the focus was specifically on corbel creation, however.

The solid concrete wall and the reduced insulation walls were created using the deep beam method included in ACI 318-14 §16.5. Because wythe thickness was only 3 inches, many of the SWP designs were limited to the use of a maximum size of #4 rebar

to accommodate for the minimum bend radius allowed by ACI 318 (2014). To maintain consistency, the solid wall was also limited to using #4 rebar.

The internal pilaster design increased the wythe thickness from 3 inches to 5 inches at the corbel location for the length of the SWP (top to bottom) by reducing the insulation from 3 inches to 1 inch. This was required so that the internal wythe could withstand the entire transfer of load from the corbel without failure. Because the wythe was still relatively slender, this design required quite a bit of steel reinforcement to ensure that premature failure of the wythe did not occur.

The solid section specimen was designed using a strut-and-tie model shown in Figure 4-2. The solid section was created by removing a 12" \times 16" piece of insulation at the location of the corbel. This approach ensures that full-composite action is achieved at the location of the corbel. Unfortunately, it also creates a large thermal bridge in the wall panel.

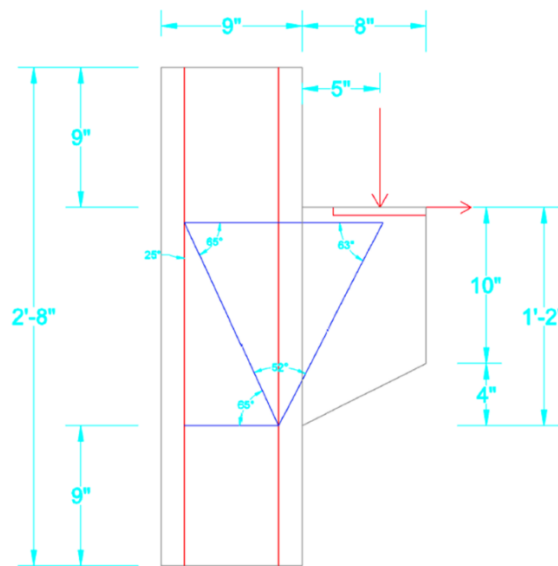


Figure 4-2 Strut-and-tie model created for solid section

Because of the discontinuity of the geometry of the panel at the corbel location and construction limitations, the SWP and the corbel had to be placed during separate pours. This meant that design provisions had to account for a cold joint at the corbel-wall interface. To account for this, special care had to be taken to ensure that adequate shear reinforcement crossed this boundary. This requirements was typically fulfilled by use of stirrups. Details for the control specimens can be found in Appendix A.

Proposed Connections

Maintaining consistent panel thickness and corbel size between specimens allowed the design of proposed connections to use the same strut-and-tie model for each. Common strut-and-tie models used to design corbels in solid concrete walls often have a diagonal compressive strut that will develop within the wall itself as shown in Figure 4-2, allowing for more even distribution of stresses and better resolution of the fictitious truss. For SWPs however, the presence of the insulation does not allow for such a strut to develop because the compressive strength of the insulation is significantly smaller than that of concrete. For this reason, the strut-and-tie model for the SWPs without solid concrete sections was a slightly different than for a solid wall. Figure 4-3 shows a comparison of the strut and tie models used in the solid wall specimen and the SWP specimens.

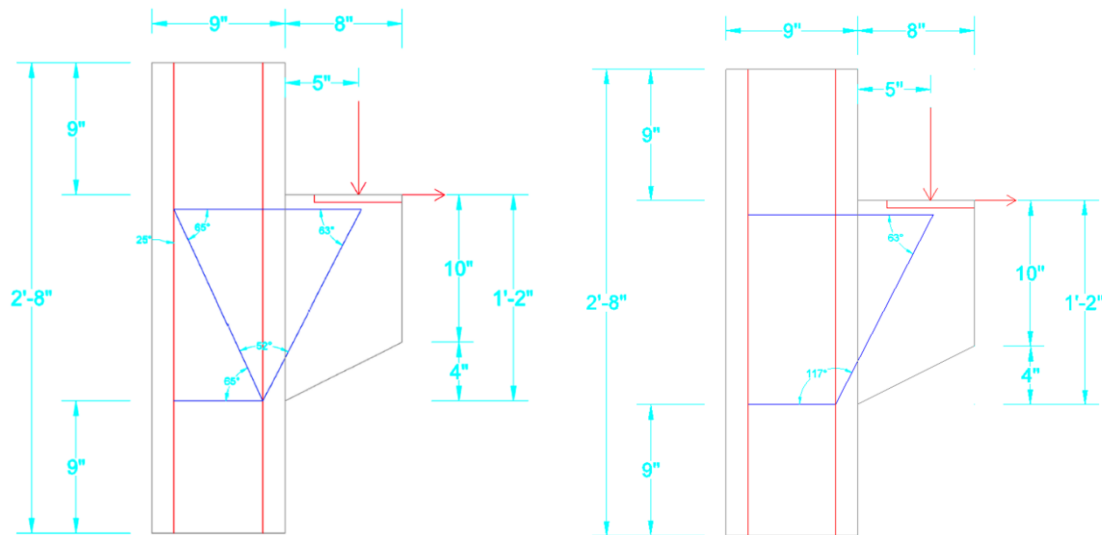


Figure 4-3 Comparison of strut-and-tie models for SWP corbel connections with (left) and without (right) solid sections

Because the tension element of the connection is typically known to be the governing component of design (Elkady, 2013), designs were based around selecting a material for this component that was thermally insulative, sufficiently strong, readily available, and practical to fabricate. The most viable option currently to achieve the required thermal resistance and strength appeared to be fiber reinforced polymer (FRP) products, such as glass fiber reinforced polymer (GFRP) and carbon fiber reinforced polymer (CFRP), although other materials were also considered. The greatest challenges to using the majority of such products were attaining adequate development or embedment since the thickness of the wythe was quite slender, and avoiding creep failure. Many possibilities were explored for the tension component, including:

- GFRP U-bar
- Headed GFRP bar
- Threaded GFRP rod with nut
- Carbon fiber rod
- GFRP or CFRP plates
- GFRP Grid
- Plywood
- Liquid crystal polymer synthetic fiber rope
- Multiple types of SWP connectors

Of these materials, 9 designs were created as proposed alternative connections to those used in practice currently, as presented previously in Table 4-1 and Figure 4-1. Two specimens were created using different size GFRP U-bars because such bars could rely on the bend of the bar to obtain adequate development of bar capacity, and are also reasonably available in the field (ACI 440.1R-15, 2015). Due to the limitations on bend radius imposed by the outer wythe thickness, only #2 and #3 GFRP bars were used. For the ultimate strength limit state, the corbels only required five #2 bars or three #3 GFRP bars to resist the loads. The consideration of creep failure, however, required fourteen #2 bars or seven #3 bars be used. The use of so many #2 GFRP bars required that reinforcement be placed in two rows to fit within the 10-in width of the corbel used in this testing.

A downside to using U-bar is that the specific size, length, and shape must be specifically ordered because it cannot be bent in the field (FDOT, 2016), so changes to

design later in the construction phase can be particularly costly. In seeking a corbel design that would utilize materials commonly found on a job site, an attractive option was the use of SWP connectors which are already on hand for construction of sandwich wall panels.

Five specimens were created utilizing SWP connectors to transfer the force of the tensile tie between the inside and outside wythes. This was done because such connectors were created to obtain adequate embedment for the purpose of attaining some degree of composite action within wall panels. The proposed connection designs aimed to utilize the pull-out capacity of these connectors to transfer the tensile load. Two connector types were selected for such experimentation: HK composite ties and IconX connectors. For many SWP connectors, it was clear that the orientation of the connectors could significantly affect behavior by contributing to the shear capacity of the panel. HK connectors, for example, are very stiff in one direction but relatively flexible in another. For this reason, two specimens were created utilizing the same number of HK connectors but orienting them in opposite directions orthogonally. Due to the limit state of creep failure, 8 IconX GFRP connectors were required to withstand the resultant force in the tension tie of the corbel. Because IconX connectors are available in both GFRP material and CFRP material, an additional specimen was created using IconX CFRP connectors since this would only require 3 connectors to transfer the load under sustained loading conditions. During testing, an unexpected crack developed along the bend in the rebar of the IconX CFRP specimen leading to premature failure. For this reason, a fifth specimen was created where the long leg of the rebar reinforcement within the corbel was bent

upward into the wythe as opposed to downward. This rebar shape will be referred to herein as a “hat bar” for convenience. The use of a hat bar with the specimens ensured that when such a crack develops, it is crossed by steel to increase corbel capacity.

The final two specimens were created utilizing GFRP grating. Such grating is often used in corrosive environments to avoid increased maintenance costs and to increase the life of grating (ACMA, 2014). One of these designs oriented the grid horizontally in the panel with the sole purpose of withstanding the tensile tie developed in the top of the corbel, and then relied upon stirrups to withstand the shear at the face of the corbel. The second GFRP grid specimen oriented the grids vertically, allowing it to resist the tension tie at the top of the corbel, the compressive strut at the base of the corbel, as well as the shear at the corbel-wall interface. This last design was created with simplicity in mind, hoping to substantially reduce preparation time and labor cost. Although the grid is continuous with evenly spaced bars from top to bottom for the vertical specimen, only the top three and bottom three bars were considered to resist the tensile and compressive forces, respectively. It was considered conservative to ignore the additional capacity provided by the intermediate bars.

The compression strut formed at the base of the corbel through the SWP normal to the panel face was much easier to address than the tensile tie at the top of the corbel as there are multiple materials with low thermal conductivities that also have higher compressive strengths. Most of the designs relied on a high-density polyethylene (HDPE) prisms to transfer this load at the corbel base due to its high compressive strength and thermal resistance. Another material considered for this purpose was wood as it has a

strength contrary to the grain, relatively low thermal conductivity (especially as compared to concrete), high availability, and very low cost. The embedment of wood into concrete is typically avoided currently due to concerns regarding the wood's tendency to absorb water and swell, which can lead to cracking in the concrete member (Batie, 2012). To see if wood could be a practical and cheap alternative for this application, two specimens used high density overlay plywood (HDO) boards of the same size and dimensions as the HDPE prisms to transfer the lower compression strut loads. The HDO boards were cut to size and glued together using an epoxy. Although there is no published data regarding the absorptivity of HDO board, it is logical that HDO would tend to have a lower absorption due to the percentage of epoxy in their material composition and due to the significantly smaller vapor permeance of the material (APA, 2011). To further reduce possible effects of moisture within the concrete however, the HDO prisms were then sealed using 3 coats of latex paint to ensure that expansion of the prisms was not an issue.

Materials

Concrete SWPs are typically designed using concrete strength ranging from 5000 psi to 8000 psi (Elkady, 2013). The SWP specimens in this study were designed for 8000 psi concrete. Concrete was supplied by Staker & Parson Companies. Due to concerns regarding congestion of reinforcement in some specimens (particularly that which utilized #2 GFRP bars), the concrete specified for all specimens limited the aggregate size to 3/8" to lessen the likelihood of having voids at the corbel location.

Compressive tests were performed on concrete cylinders to determine concrete compressive strength at the time of testing for each specimen. Cylinders were cast using

concrete midway through each concrete pour and field cured with the specimen according to ASTM C31 (2017). All cylinders had a diameter of 4 inches and a height of 8 inches (4" × 8"). Cylinders were tested according to ASTM C39 (2017).

Aside from compressive tests, elastic modulus and split tension tests were also performed on concrete cylinders to determine the modulus of elasticity and the tensile capacity of the concrete for each specimen. Elastic modulus was determined according to ASTM C469 (2014), and split tension testing was performed according to ASTM C496 (2017).

Sandwich wall panels are often prestressed to mitigate problems with premature cracking during stripping and handling, transportation, and construction loading, and under service loads. Mild reinforcement does not carry the same benefit of prestressed reinforcement in this regard, making such panels more susceptible to cracking than their prestressed counterparts. For this reason, it was considered conservative to use mild reinforcement for all panels in this study.

As mentioned previously, SWP designs herein were limited to a maximum rebar size of 0.5-inch diameter (#4 rebar) to accommodate the minimum bend radius allowed by ACI 318-14 due to the wythe thickness being only 3 inches. In all cases where rebar was used, deformed bar was utilized with a minimum yield strength of 60 ksi. Rebar used within each pour came from the same heat of steel. The rebar used in Pour 3 was from the same heat as Pour 2.

To maintain consistency between panel specimens, each SWP utilized the same type of evenly distributed SWP connector. HK composite connectors are mold injected

GFRP ties that have randomly aligned glass fibers in a thermoplastic matrix. They have an overall length of 6.5 inches with a minimum embedment in either wythe of 1.5 inches, and a width and thickness of 3 inches and 0.5 inches respectively. The HK connectors were spaced at the maximum recommended spacing of 16-inches on center longitudinally and transversely for all specimens. HK composite ties were selected due to their low cost and high availability. It is quickly noted that some specimens utilized other SWP connectors to resist the tension tie in the top of the corbel. Although it would be unlikely for engineers or contractors to use a mix of propriety connectors from different companies, HK connectors were still used in these panels as well to simplify comparison of panel performance by reducing the difference in stiffness and degree of composite action that would be present by using only IconX connectors in place of the HK connectors. Thus, all panels used HK connectors to connect the outer and inner wythes, and any other connectors were used for the sole purpose of transferring the tensile load created by the corbel.

The high density polyethylene (HDPE) prisms were created using 2" × 4" plastic lumber. Each 2" × 4" was cut to the right length and then glued using a fast-drying epoxy to avoid thermal bridging that would be present due to the use of metal screws. All HDPE boards were supplied by Engineered Plastic Systems, LLC under the name of Bear Board.

The foam used in the study for all specimens consisted of extruded polystyrene (XPS) rigid foam insulation produced by Dow. According to the specifications provided by the manufacturer (Dow, n.d.), a compressive strength of 25 psi was determined for the

foam using ASTM D1621 (2016) and a thermal resistance of $15.0 \left[\frac{\text{ft}^2 \cdot \text{hr} \cdot ^\circ\text{F}}{\text{Btu}} \right]$ for a thickness of 3 inches was determined using ASTM C518 (2017). Since thermal conductivity is the inverse of thermal resistance per inch of thickness, the thermal conductivity can be shown to be $0.2 \left[\frac{\text{Btu} \cdot \text{in}}{\text{ft}^2 \cdot \text{hr} \cdot ^\circ\text{F}} \right]$.

Experimental Program

Test Specimens and Test Matrix

A test matrix was created for the testing of 12 designs created to improve the thermal performance of structures by decreasing thermal bridging at corbel connections (Table 4-1). The specimens included a solid concrete wall for a control specimen, two designs commonly used in industry currently, and nine proposed alternative designs. Corbels specimens were poured in sets of four, as shown in Table 4-2.

After testing the first set, minor changes were made to facilitate testing of future specimens. Specimens in the first set were exactly 6 ft (72 inches) wide and 8 ft (96 inches) tall, but since the test setup utilized a strong wall with holes spaced 3 ft on center in both directions, the first set required that square pieces be cut from the corners to allow the tieback to fit around the specimen properly. This was not the only dimensional issue with the panels, however; the top edge of the panel was centered in the middle of the tieback. Because deflection at the top of the panel was expected to be quite small during the peak of testing, the tests were able to be carried out without issue, but some modifications were made to set 2 and 3 to make testing easier and safer. To allow the tieback rods to fit on either side of the panel, the panel width was reduced from 72 inches

Table 4-2 Test matrix for SWP corbel specimens

Set	Name	Primary Tension Element	Primary Compression Element
1	*SolidWall	Rebar	Concrete
	*SolidSec	Rebar	Concrete
	GFRP2	#2 GFRP U-bars	HDO Prism
	GFRP3	#3 GFRP U-bars	HDO Prism
2	IconG	IconX GFRP Connectors	HDPE Prism
	IconC	IconX CFRP Connectors	HDPE Prism
	HKVer	HK SWP Connectors	HDPE Prism
	HKHor	HK SWP Connectors	HDPE Prism
3	*RedIns	Rebar	Concrete
	IconCHat	IconX CFRP Connectors	HDPE Prism
	GridHor	GFRP Grid	HDPE Prism
	GridVer	GFRP Grid	GFRP Grid
* control specimens			

to 68 inches. Similarly, to ensure that the top of the panel extended well above the tie back, the panel height was lengthened from 96 inches to 102 inches.

The reinforcement details of each specimen are shown below by pour in Figure 4-4, Figure 4-5, and Figure 4-6. Complete fabrication drawings are included in Appendix A. The following sections discuss the test setup and instrumentation used in testing.

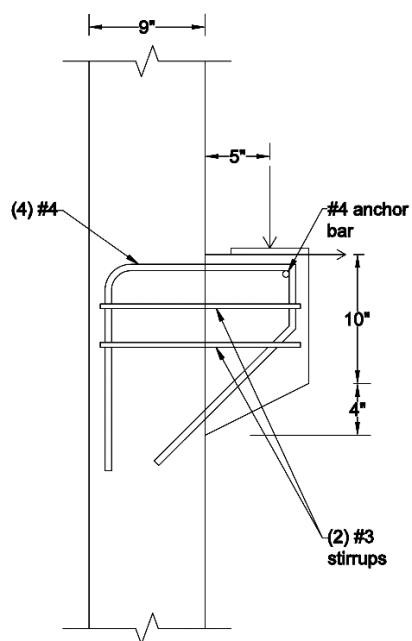
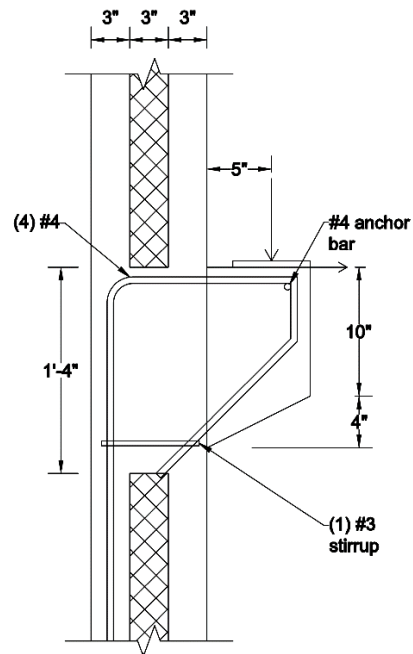
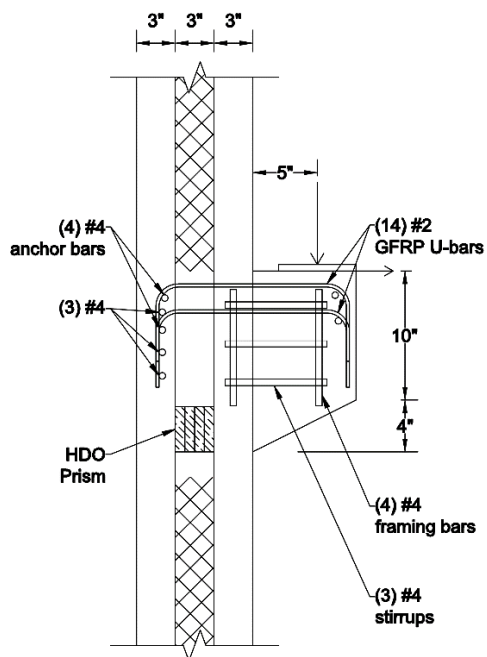
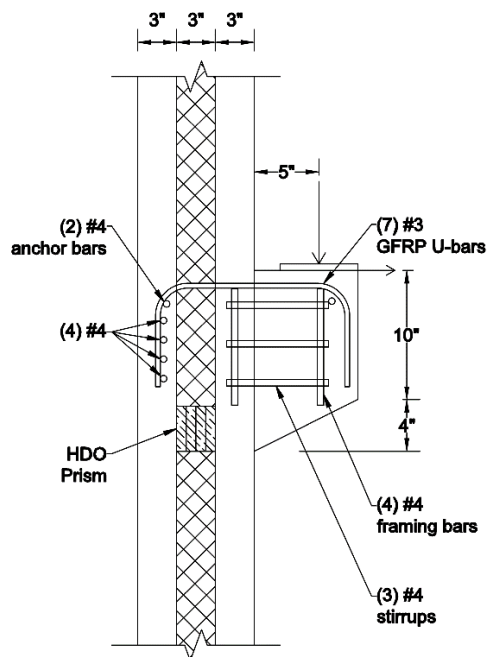
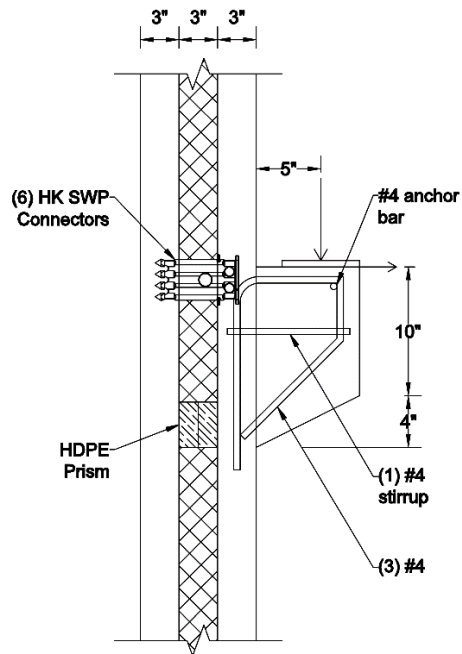
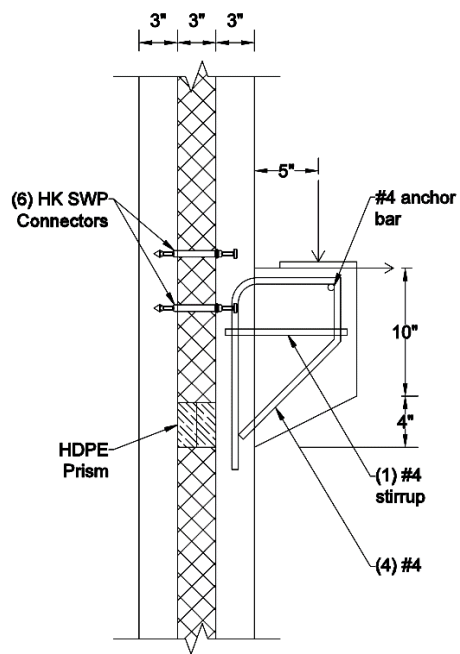
**SolidWall****SolidSec****GFRP2****GFRP3**

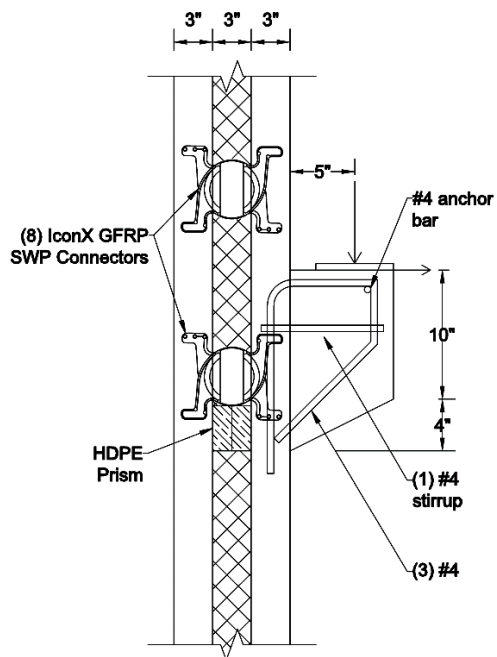
Figure 4-4 Corbel designs from Set 1: SolidWall, SolidSec, GFRP2, and GFRP3



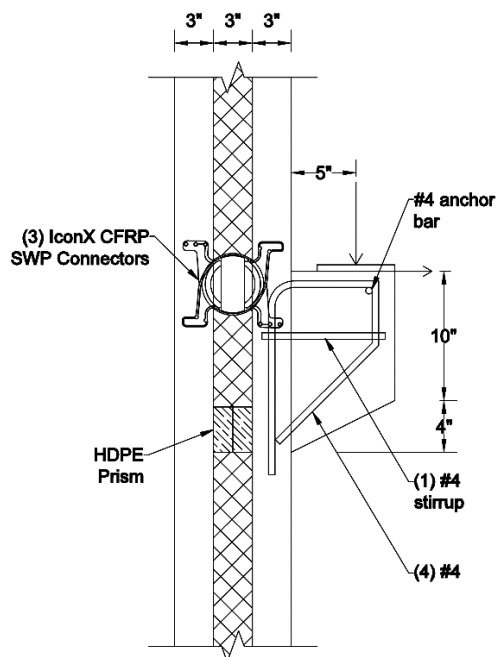
HKVer



HKHor

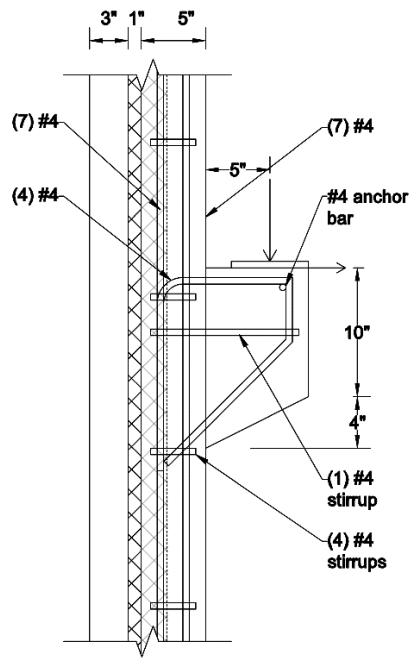


IconG

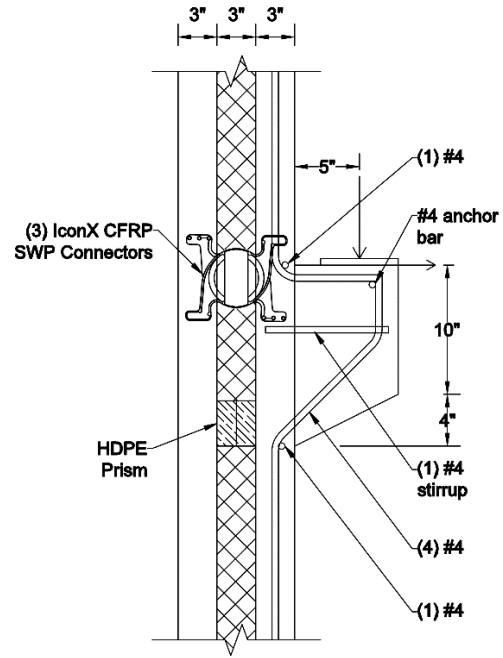


IconC

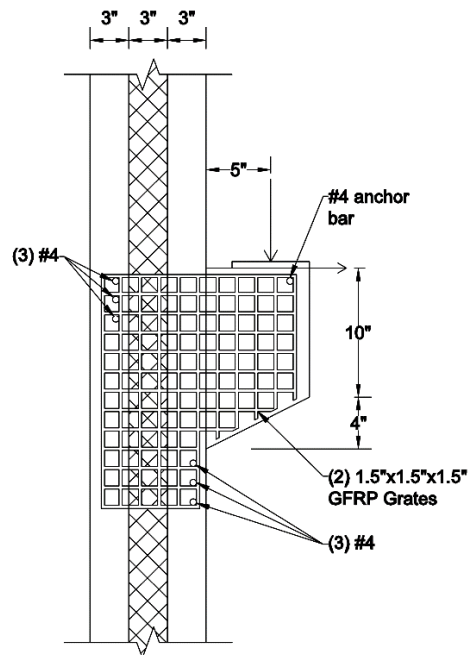
Figure 4-5 Corbel designs from Set 2: HKVer, HKHor, IconG, and IconC



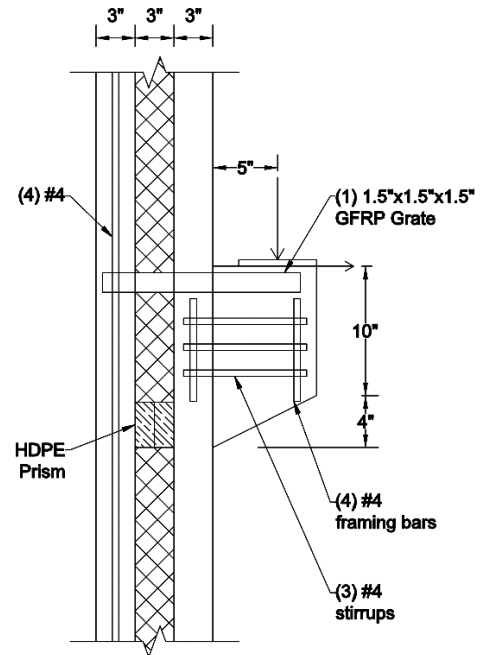
RedIns



IconCHat



GridVer



GridHor

Figure 4-6 Corbel designs from Set 3: RedIns, IconCHat, GridVer, and GridHor

Specimen Construction

Specimens were cast in a single pour horizontally, layer by layer. Due to space restrictions, only four specimens were cast per pour (see Figure 4-7, Figure 4-8, and Figure 4-9).



Figure 4-7 Concrete specimen formwork and rebar for Set 1

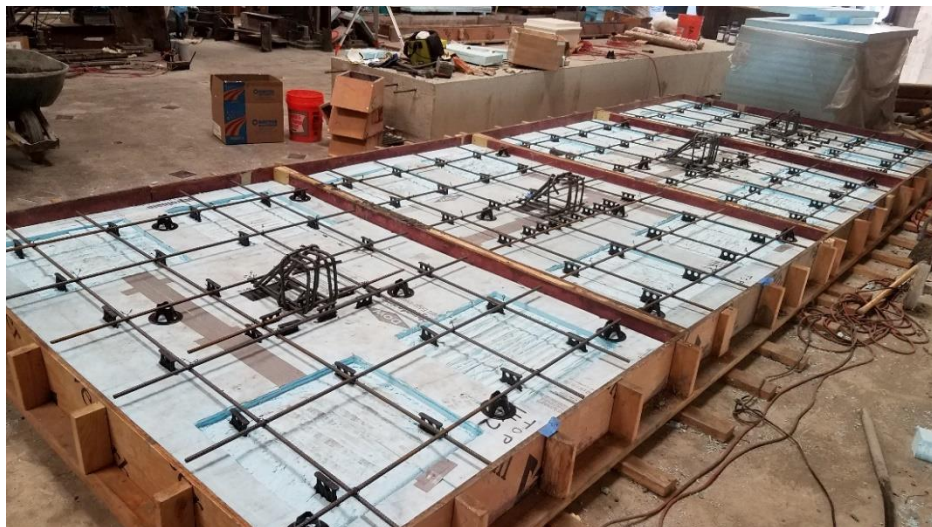


Figure 4-8 Concrete specimen formwork and rebar for Set 2

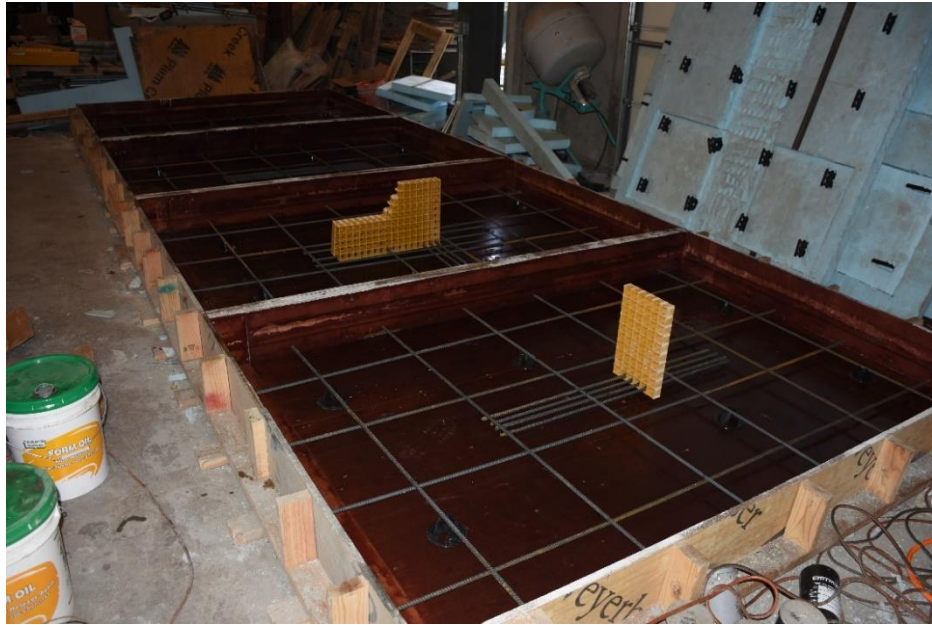


Figure 4-9 Concrete specimen formwork and rebar for Set 3

Forms were built using HDO boards to provide a smooth, durable, and reusable formwork made to last for the duration of the project. Prior to each pour, reinforcement was tied in mats, foam was cut, connectors were staged, and forms were cleaned, marked, and prepared with form oil. Because each of the proposed design connections required a material to cross the insulation, preparation also required that holes be cut where the connecting materials would penetrate the insulation. Holes were also cut where the HDPE or HDO prisms were placed when utilized in design (Figure 4-10).

After preparations were completed, concrete was delivered and poured into the formwork. After the outside wythe of each specimen was poured, the foam and connectors were placed before pouring the inside wythe of each panel (Figure 4-11). Care was taken to ensure that connectors remained perpendicular to the foam.



Figure 4-10 Cutting holes for FRP penetration and HDPE prism placement



Figure 4-11 Placing foam and connectors in SWP specimens

As concrete was poured for each wythe, a pencil vibrator was used to help the concrete fill all voids and level the amount of concrete in the form (Figure 4-12). Each connector and all corbel reinforcement was vibrated to ensure that concrete adequately bonded around the reinforcement and to avoid voids at these particularly important locations.



Figure 4-12 Removing air voids in concrete wythes using pencil vibrator

After concrete was placed, panels were screeded and finished with a trowel, lifting anchors were inserted in the appropriate locations, and the panels were covered with moistened burlap and plastic to cure. After the bottom wythe was poured and prior to pouring the top wythe, a sample of concrete was taken to perform a slump test and pour 4" × 8" cylinders for compression testing. The slump test was performed and cylinders were cured in accordance with ASTM C31 (2017).

Test Setup

The corbel specimens were loaded using a 3-ft thick strong wall and strong floor located in the Utah State University Systems, Materials, and Structural Health (SMASH) Laboratory. Drawings of the initial test setup are shown in Figure 4-13 and Figure 4-14, and Figure 4-15 shows a photo of the actual setup.

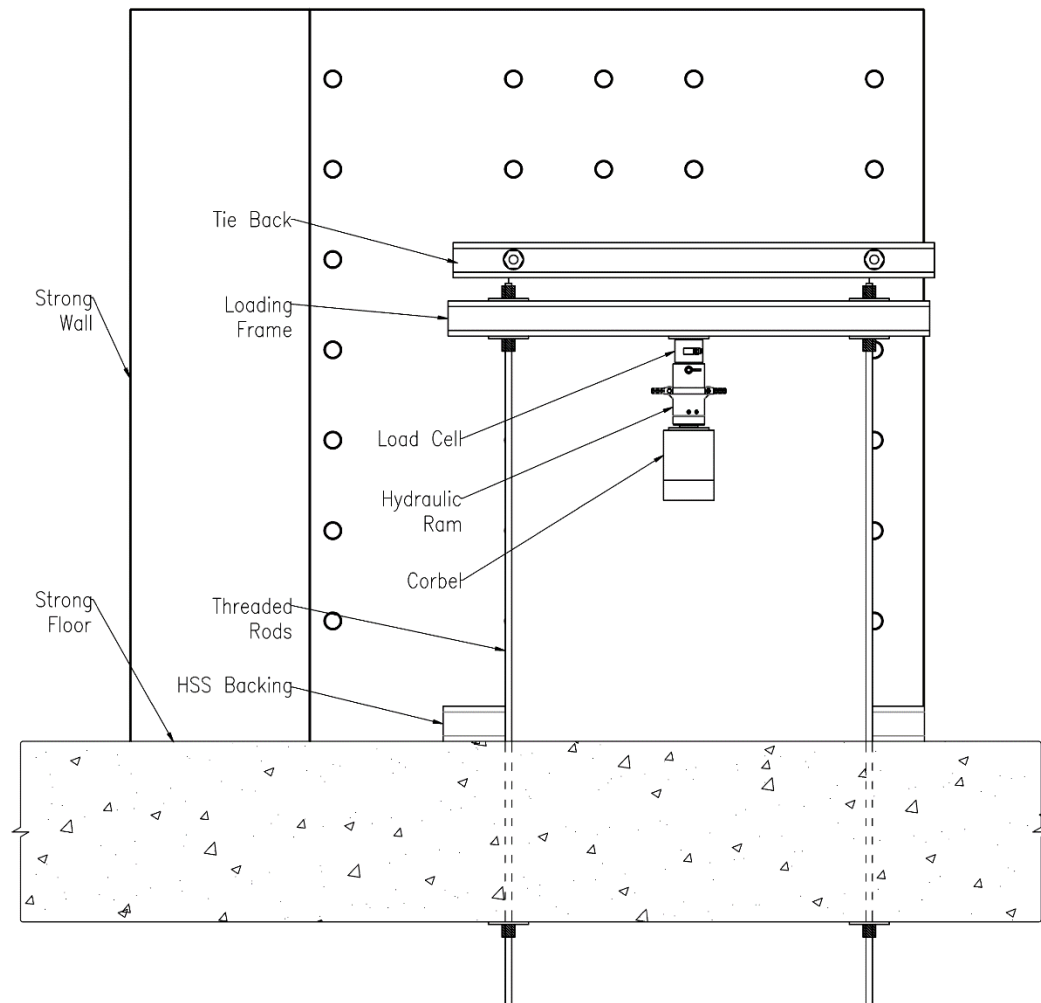


Figure 4-13 Front view of initial test setup for corbel testing

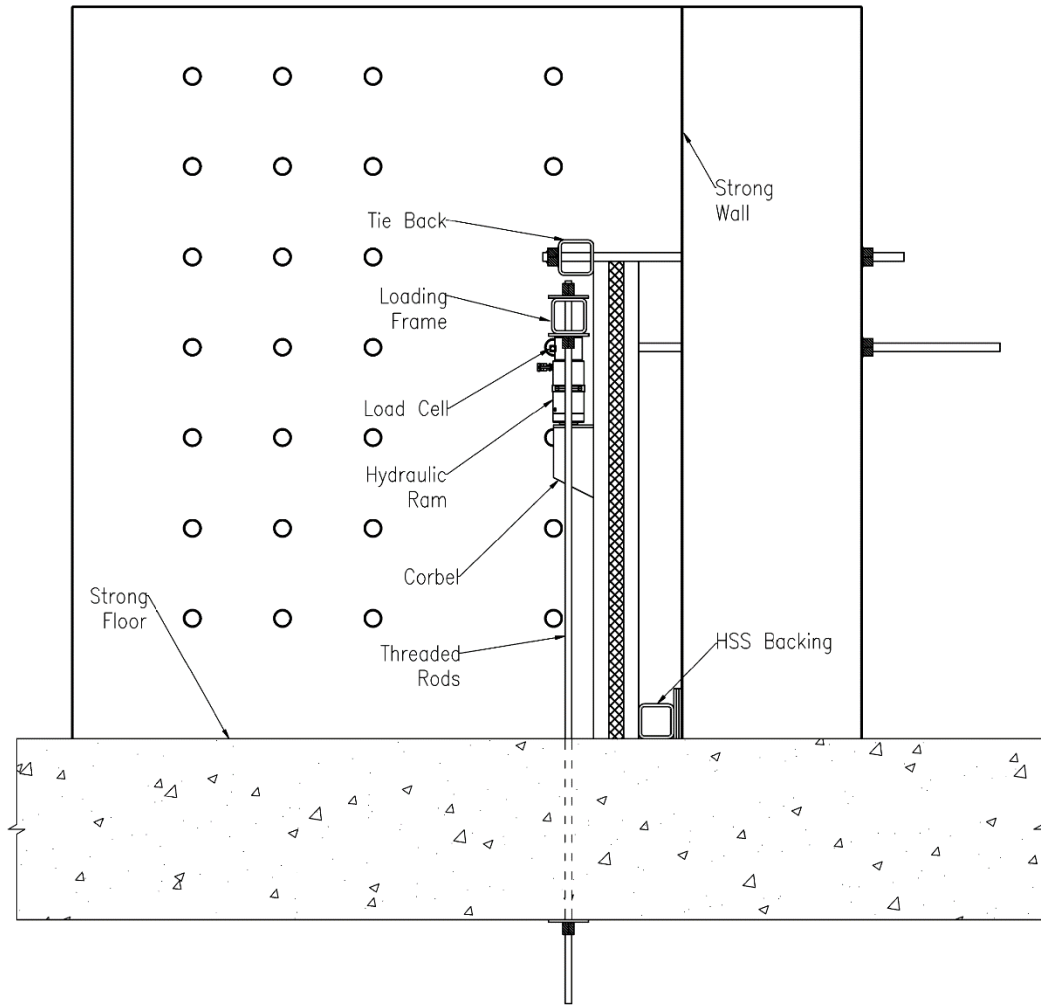


Figure 4-14 Profile view of initial test setup for corbel testing

As in any structural design, it was essential to establish a continuous load path from the structure to the ground for safe testing of the specimens. In the first test setup, the load was applied to specimens using a single 120-kip hydraulic ram, which transferred the load to the load cell and then to a loading frame centered above the corbel. The frame was connected to the strong floor using threaded rods, thus the load applied to the corbel was transferred through the rods directly to the floor itself.



Figure 4-15 Photo of initial test setup for Set 1

This first setup had the ram bear directly on a plate placed on the corbel bearing surface. This was problematic, however, since the corbel had a tendency to rotate as the applied load increased. Excessive rotation would cause the load cell to be propelled

forward from the pressure, creating a big safety concern. The rotation also caused the ram to bear unevenly on the plate, which was not a direct concern for testing since the plate would evenly distribute the load to the corbel, though it would permanently deform plates during testing which was not ideal. Finally, the greatest issue with the original test setup was that the capacity of the panels exceeded the frame. The panels were designed assuming a concrete strength of 8 ksi concrete. Due to technical issues with the pump used to control the hydraulic ram, testing was delayed by 6 months however, and the concrete strength at the time of testing was around 12 ksi. This unanticipated delay and consequential increase in capacity caused the GFRP specimens to surpass the HSS crosshead strength of the loading frame, causing yielding to occur prior to panel failure. Fortunately, strain hardening of the cross head allowed the testing to be completed for the first set of specimens, but a new crosshead was fabricated for the second and third sets to double the capacity of the loading frame.

The new testing setup made a few simple changes to enhance loading assembly, as shown in Figure 4-16, Figure 4-17, and Figure 4-18. First, the new crosshead was fabricated to have twice the capacity of the original crosshead, using a $16'' \times 8'' \times 1/2''$ HSS section. The increased crosshead depth created an issue of clearance between the crosshead and the tieback as clearance was limited prior to the change. To compensate for this conflict, the hydraulic ram was moved beneath the strong floor and an additional ram was attached to the other rod so that load was applied using two hydraulic rams controlled by the same pump. This also doubled the potential capacity for applied load. A

rotating bearing was also inserted between the load cell and corbel to ensure loading remained normal to the loading face of the corbel.

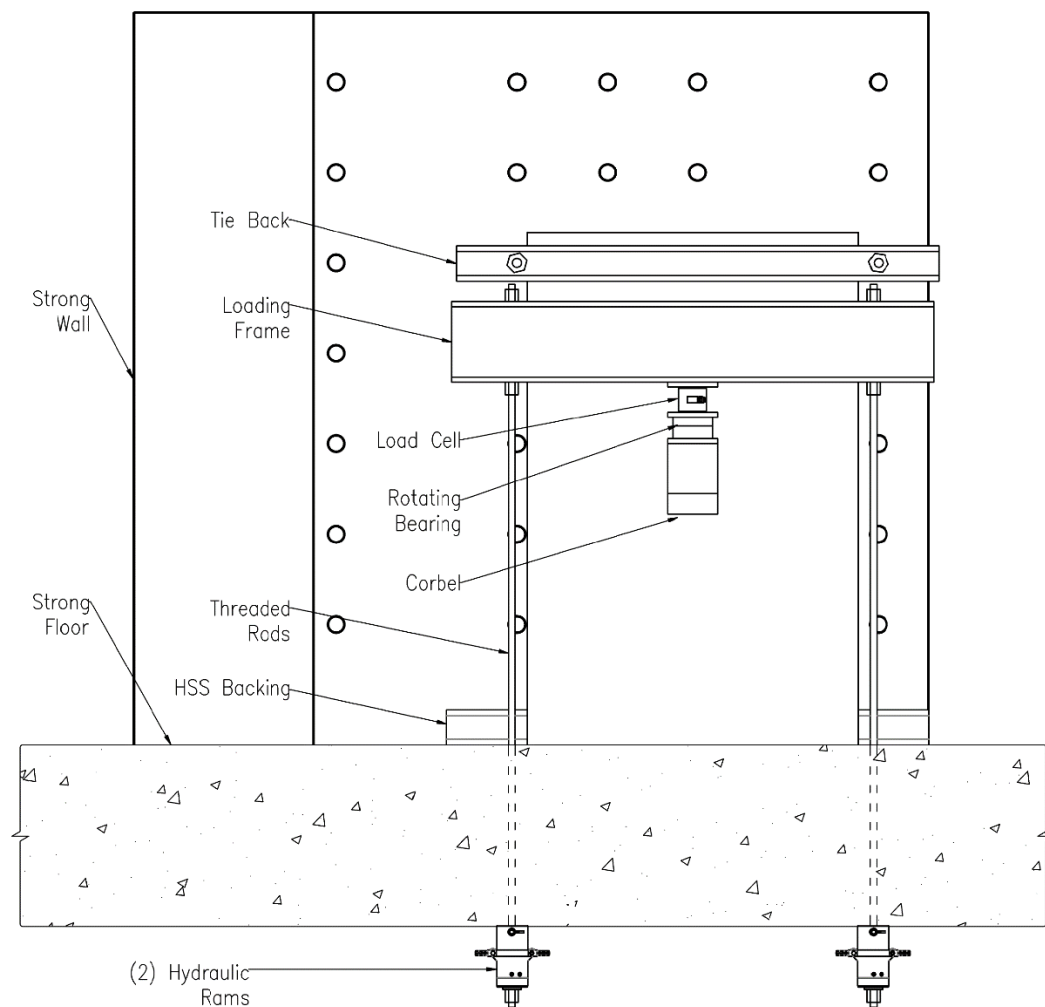


Figure 4-16 Front view of modified test setup for corbel testing

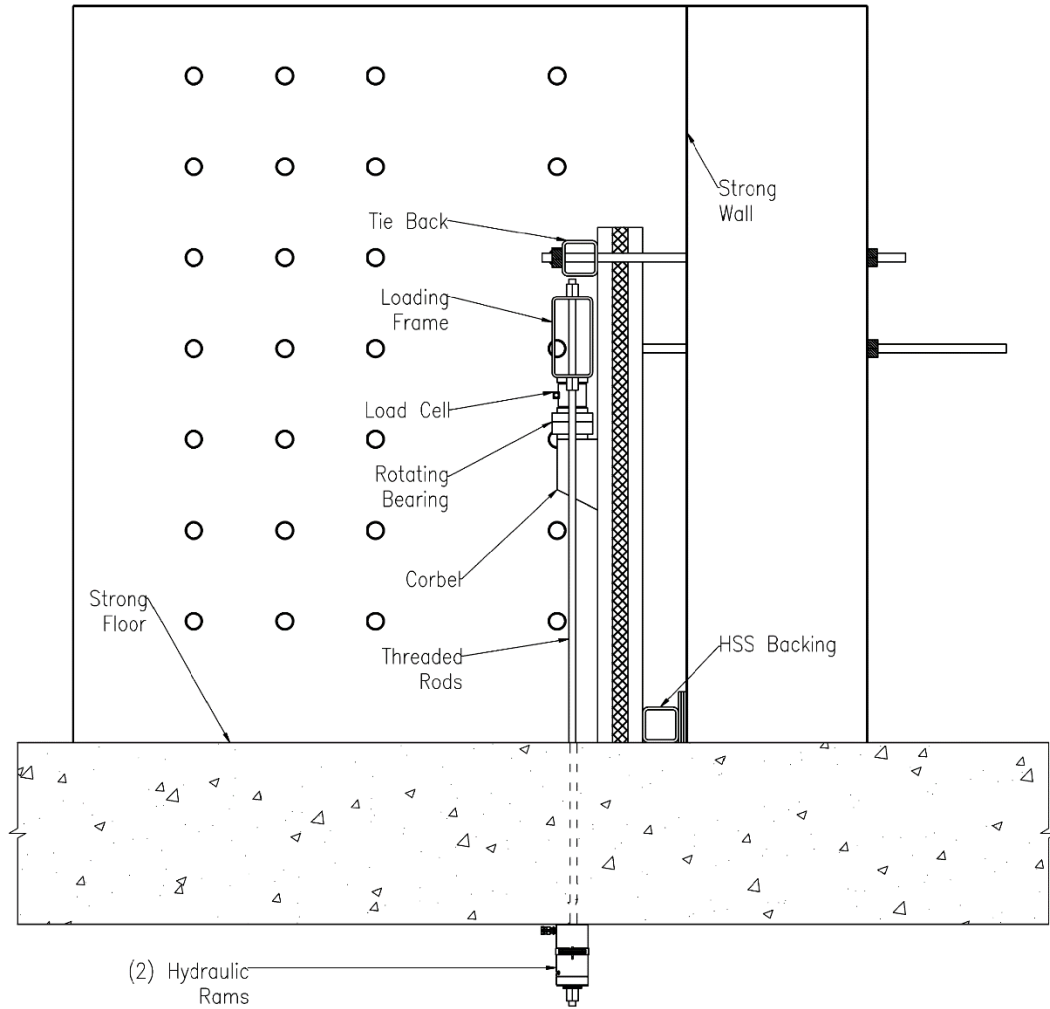


Figure 4-17 Profile view of modified test setup for corbel testing



Figure 4-18 Photo of revised test setup used for Set 2 and 3

Because the load applied to a corbel connection is an eccentric load on the wall panel, there is a consequential force couple created so that the bottom of the panel will tend to rotate out from the building and the top of the panel will tend to rotate into the building. It was necessary to create a system to resist the lateral rotation and resultant horizontal force for each couple component. For the wall panel specimens, a tie back was used to resist the horizontal rotation away from the strong wall at the top of the panel, and an additional HSS section was used to resist the rotation towards the strong wall at the base of the panel. All HSS components used during the initial test setup consisted of $7'' \times 7'' \times 5/8''$ square HSS sections.

Instrumentation

The equipment used to collect the test data was a Bridge Diagnostics Inc.- Structural Testing System (BDI-STs). Load was measured for each test using a Geokon load cell. Linear variable differential transformers (LVDT) were used to measure slip between wythes at the top, third, and bottom connector lines. Since the solid wall specimen did not have two wythes to measure slip between, on this specimen the LVDTs were used to measure the deflection of the corbel tip from the face of the panel. A UniMeasure LX-PA string potentiometer (string pot) was used to measure vertical deflection of the corbel tip during testing.

The LVDTs were all mounted on the same wythe with a wood mount placed on the other from which displacement could be measured. The LVDTs were mounted over connector lines to measure slip at connector locations. Five LVDTs were attached along the lateral edges of each panels in Sets 2 and 3. Although it would be ideal to have the

sixth LVDT to measure displacement at the top of the panel, the test setup did not allow space for the sixth LVDT to be used. LVDTs were mounted facing the top of the panel where possible. Unfortunately space limitations required that the bottom LVDTs face down towards the ground. The string pot was placed centered with the corbel and directly beneath the tip to measure vertical deflection of the tip during loading.

Test Results

In this study, 12 SWP corbel specimens were created and tested to identify alternative designs to be used in industry that are structural sufficient and thermally superior to currently popular details. This section presents the results of this testing. The principle difference between details was in the selection of the material to resist the primary resultant tensile tie located at the top of the corbel during loading. Due to material costs and time constraints, only one specimen of each design could be constructed and tested. The previous sections explain the design and fabrication of the testing results presented herein.

Material Testing

Concrete testing was performed for all specimens tested. For each specimen, three concrete cylinders were tested in compression according to ASTM C39. Three additional cylinders were tested according to ASTM C469 to determine the modulus of elasticity before being tested in split tension according to ASTM C496 to approximate the tensile capacity of the concrete. The average results are displayed in Table 4-3. It may be noted that although the specified concrete strength in design was 8 ksi, the strength was far exceeded in Sets 1 and 2. This may be attributed to delays in testing due to technical

Test Results

The ultimate capacity, tip deflection at ultimate, and the cause of failure for each specimen are summarized in Table 4-4. For the SolidWall and SolidSec specimens, the shear cracks that formed due to the tension in the bottle-shaped strut in the corbel led to failure. For the GFRP specimens, rupture of the GFRP bars led to failure. For the SWP connector specimens in Set 2 (HK and IconX specimens), failure occurred due to concrete shear breakout of the corbel. There was not sufficient data to determine quality of performance of the HDO prisms compared to the HDPE prisms, though it is clear that the HDO prisms were structurally adequate for this connection. Figure 4-19 displays a plot comparing the applied load vs. tip deflection during testing for all corbel specimens.

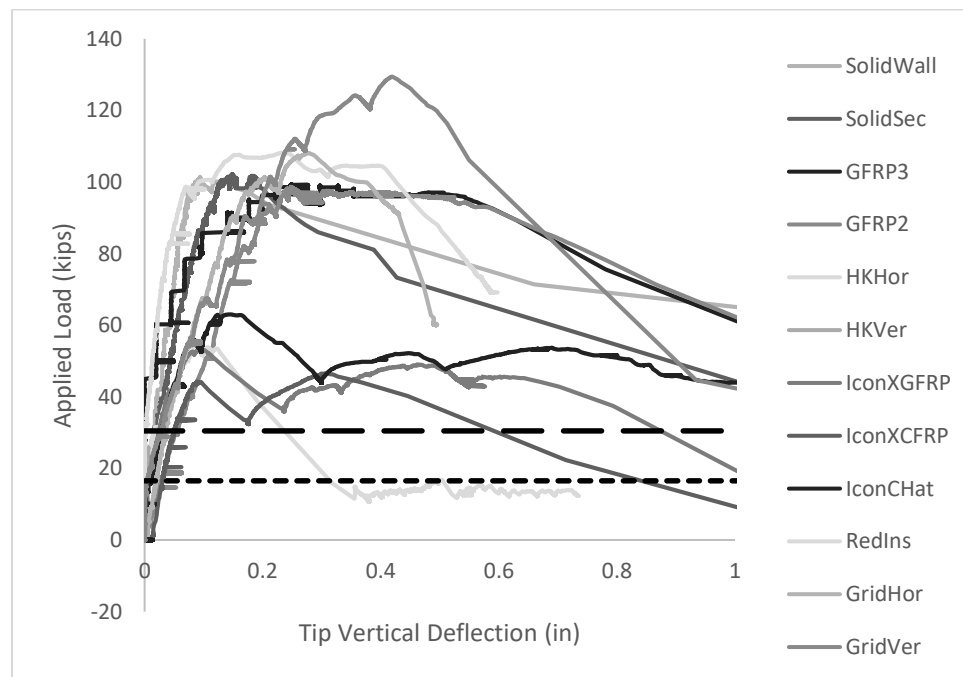


Figure 4-19 Comparison of load vs. tip deflection for all corbel specimens, where design load is indicated by the dashed line and sustained load is indicated by the dotted line

Table 4-4 Test results for corbel specimen testing

Specimen	Ultimate Capacity (kip)	Tip Deflection at Ultimate (in)	Cause of Failure
SolidWall	101.4	0.094	shear cracks in corbel strut
SolidSec	102.1	0.147	shear cracks in corbel strut
GFRP3	99.3	0.249	GFRP rupture
GFRP2	98.6	0.248	GFRP rupture
HKHor	53.9	0.107	concrete shear breakout
HKVer	25.9	0.006	concrete shear breakout
IconG	53.5	0.093	concrete shear breakout
IconC	46.6	0.306	concrete shear breakout
IconCHat	63.0	0.144	corbel breakout
RedIns	108.2	0.231	corbel breakout and shear cracks in corbel
GridHor	108.2	0.276	concrete breakout above corbel
GridVer	129.4	0.419	GFRP rupture/shear

Specimen Failure and Behavior

SolidWall Specimen

Due to delays in testing as mentioned previously, the SolidWall specimen was not tested until day 186, at which point the concrete strength had increased to 11.5 ksi. No visible cracking occurred until an applied load of 84 kips. Such cracking occurred from the top right corner of the corbel heading 30° towards the top right corner of the wall panel, and continuing to left at the same angle downwards from the top left corner as can be seen in Figure 4-20.



Figure 4-20 SolidWall specimen immediately after failure

The failure for the SolidWall specimen was very abrupt at a failure load of 101.4 kips. Although the ultimate load for the SolidWall specimen was very high, the tip deflection prior to failure was very low, being only 0.094 inches, not providing much warning prior to failure. Upon inspection following the failure, it is apparent that the failure occurred within the corbel itself. The cracking in the corbel revealed that the failure was likely due to tensile stresses formed from bottlenecking in the diagonal compressive strut in the corbel.



Figure 4-21 Cracking in corbel of SolidWall specimen after failure

SolidSec Specimen

The age of the SolidSec specimen at testing was 206 days. This specimen surprisingly failed at a load slightly exceeding that of the solid wall at 102.1 kips. The deflection at failure was 0.147-in. Visible cracking did not occur until approaching failure (at 101 kips). Such cracking can be seen in Figure 4-22: one from the top left corbel corner laterally to the edge of the SWP, another from the top right corner at 45° towards the bottom right of the panel, another from the bottom right of the corbel also heading 45° towards the bottom right of the panel, and a fourth from the bottom center of the corbel heading directly down to the bottom of the panel.



Figure 4-22 Cracking in SolidSec specimen immediately prior to failure

The failure for the SolidSec specimen was very abrupt like the SolidWall specimen. The failure mechanism of this specimen was also similar to the SolidWall. The failure occurred within the corbel itself, and the failure appeared to be likely due to tensile stresses formed from bottlenecking in the diagonal compressive strut in the corbel according to the corbel cracks (see Figure 4-23).



Figure 4-23 Cracking in corbel of SolidSec specimen after failure

GFRP2 and GFRP 3 Specimens

The GFRP3 and GFRP2 specimens were tested 5 days apart at 256 days and 261 days, respectively. The concrete strength at the time was 12.11 ksi. Visible cracking occurred at an applied load of 99 kips, again commencing from the top corners of the corbel and heading laterally to the edges of the SWP. An additional crack developed laterally across the backside of the wall panel approximately 3 ft from the floor as shown in Figure 4-24.



Figure 4-24 Crack developed on backside of GFRP3 specimen during testing

The failure for the GFRP specimens were much more ductile than the SolidWall or SolidSec specimens, having 0.249 in and 0.248 in of deflection, respectively. Despite their superior ductility, they still maintained comparable capacities to those of the SolidWall and SolidSec specimens with the GFRP3 failing at 99.3 kips and the GFRP2 specimen failing at 98.6 kips.

The failure behavior was extremely intriguing in these specimens (see Figure 4-25). The failure occurred due to rupture of the GFRP bars, which is what was expected in the designs. Figure 4-26 shows the ruptured GFRP bars from the GFRP3 specimen. Because the GFRP bars ruptured, the corbel was relatively easy to remove after unloading the corbel. Upon closer inspection after removing the corbel, GFRP2 specimen showed indications of local bearing failure at the base of the corbel in the outside wythe. This seems to indicate that the GFRP2 design was able to transfer the applied corbel load so effectively to the outside wythe that the entire corbel section from corbel tip to the corresponding area in the outside wythe acted as one solid, composite connection. This failure was extremely fascinating and successful.

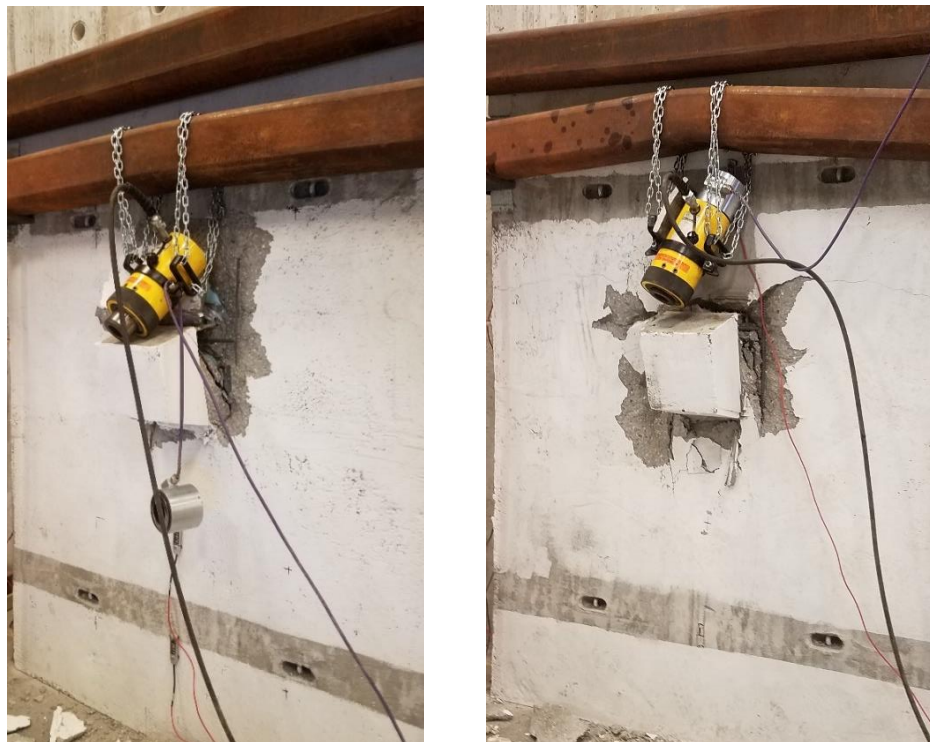


Figure 4-25 GFRP3 (left) and GFRP2 (right) specimens following corbel failure



Figure 4-26 Ruptured GFRP bars from GFRP3 specimen

HKHor and HKVer Specimens

The age of the HKHor specimen on the day of testing was 139 days, whereas the HKVer specimen was 146 days when tested, having a concrete compressive strength of 10.73 ksi. The design approach for Set 2 panels was to try to use one of the most common materials on a SWP construction site to transfer the tensile force in the top of the corbel through the insulation: SWP connectors. This was a promising approach because SWP connectors are made for the purpose of attaining adequate anchorage with minimal embedment, and are thermally insulative. Designs were therefore created using SWP connectors to transfer the load from the corbel wythe to the outside wythe.

The ultimate load for the HKHor specimen was 53.9 kips, which was acceptable considering that the ultimate factored design load was 30.5 kips. The HKVer specimen

failed at only 25.9 kips, however, which is below the expected design load. After removing the HKVer corbel, it became apparent why this occurred (see Figure 4-27 and Figure 4-28). The strut-and-tie model used required that reinforcement be provided in the top of the corbel to resist 23.1 kips in the top tie. The original SWP designs in Set 2 used bent rebar to resist this load in the corbel wythe, and then a collection of SWP connectors to transfer this load to the outside wythe. An unfortunate oversight of this 2-dimensional model was in how the load was to be transferred from the rebar to the SWP connector. Because this consideration was not taken into account, the design essentially relied only upon the surrounding concrete to transfer this tensile load, allowing a crack to form around the shape of the bent corbel rebar resulting in premature failure (Figure 4-29). It is also interesting to note that only one of the 6 HK connectors was within this region in the horizontal specimen. Instead of the connector failing by concrete breakout, the connector failed in shear as seen in Figure 4-27.



Figure 4-27 HKHor specimen SWP (left) and corbel (right) after failure



Figure 4-28 HKVer specimen after failure

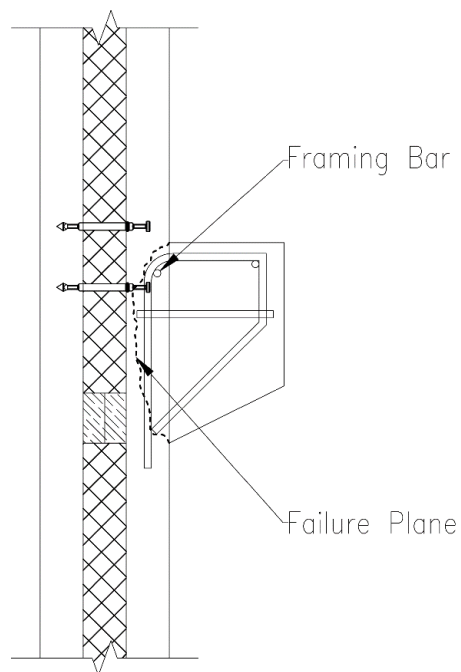


Figure 4-29 Crack failure surface in SWP connector panel designs

To help tie the corbel reinforcement into the wall panel rebar mat for the concrete pour, a framing bar was used at the top bend of the rebar for each SWP connector specimen (see Figure 4-29). This framing bar was the means to providing adequate corbel capacity for 3 of the 4 panels in Set 2.

Because the ultimate capacity was lower for these panels, the deflection was also lower as expected. For the HKHor specimen, the deflection at failure was 0.107 in. For the HKVer specimen, the string pot broke during testing and deflection was not recorded. This was replaced for future tests.

IconG and IconC Specimens

The IconX specimens also suffered the same design flaw as those using the HK connectors, but both had framing bars of adequate length to provide capacity to exceed the factored design loads (see Figure 4-30). The age of the IconG specimen on the day of testing was 160 days and the age of the IconC specimen was 165 days when tested, with a concrete strength of 10.61 ksi. The IconG specimen failed at 53.5 kips with a tip deflection of 0.093 in, and the IconC specimen failed at 46.6 kips with a tip deflection of 0.306 in.



Figure 4-30 IconG corbel secured only by framing bar after failure

There was no cracking in these panels other than the concrete shear breakout surface surrounding the corbel.

IconCHat Specimen

In an attempt to overcome the issue of the crack experienced with the IconX and HK connector specimens, hat bars were used to provide reinforcement across concrete crack locations. The age of the IconCHat specimen on the day of testing was 38 days and the age, with a concrete strength of 9.82 ksi. The IconCHat specimen failed at 63.0 kips with a tip deflection of 0.144 in, providing twice the capacity required by the design loads.

The same crack that had failed the IconC and IconG specimens appeared in the IconCHat specimen as well (Figure 4-31), though the provided reinforcement crossing this boundary allowed the capacity to increase by 35%, from 46.6 kips to 63.0 kips. The amount of steel used in both the IconC and IconCHat designs was equivalent with the only difference between the two designs being the detailing of the corbel reinforcement. Therefore, it is clear that proper detailing can significantly influence design capacity of a corbel.



Figure 4-31 IconCHat corbel after failure secured by corbel reinforcement

RedIns Specimen

The age of the RedIns specimen at testing was 38 days. This specimen failed at a load exceeding that of the solid wall and solid section specimens at 108.2 kips. The deflection at failure was 0.231 in. Visible cracking was identified at 98 kips. The failure for the RedIns specimen was semi-abrupt, but was able to carry substantial load following the principal failure. The specimen exhibited ductile behavior after the initial brittle failure. The initial failure mechanism of this specimen was similar to the Icon and HK specimens with concrete breakout immediately surrounding the corbel. Further loading caused the corbel itself to fail with shear cracking in the corbel strut parallel to the diagonal rebar reinforcement (see Figure 4-32).



Figure 4-32 RedIns specimen after failure

GridHor and GridVer Specimens

The FRP Grid specimens were tested at 34 days of age. The concrete strength at the time was 9.82 ksi. Although the concrete strength was the weakest among specimens, these panels both proved to have the greatest capacity of all specimens tested. The GridHor specimen held 108.2 kips (over 3 times the factored design loads) and the GridVer specimen held 129.4 kips (over 4 times the required nominal capacity).

Aside from having the greatest capacities, the failures of the Grid specimens proved to be 2 of the 3 most ductile failures in this study as well. With 0.42 inches of tip deflection at failure, the GridVer specimen exhibited the most ductile failure of all. The GridHor specimen had 0.276 inches of deflection at ultimate, falling short of the 0.31 inches exhibited by the IconCHat specimen. The capacities of these corbels far exceeded the design loads as well as the capacities of all control specimens.

The failure behavior was extremely intriguing in these specimens. The failure in the GridVer specimen (Figure 4-33) initially appeared to be a combination of shear failure of the GFRP and pull-out of the GFRP glass strands from the longitudinal bars. Upon closer observation however, it was determined that failure was actually due to rupture of the GFRP bars in the grid. In the GridHor specimen, the grid reinforcement appeared to be completely intact with concrete failure occurring in the surrounding concrete and in the corbel (Figure 4-34). Both grid designs proved to be exceptionally successful.



Figure 4-33 Failure of the GridVer specimen



Figure 4-34 Failure of the GridHor specimen

Summary and Discussion

The proposed connections presented herein attempt to identify ways to transfer structural load from corbel connections to composite SWPs without creating thermal bridges. These connections use various materials such as GFRP U-bars, SWP connectors, and GFRP grating to achieve such a purpose.

The GFRP2 and GFRP3 specimens had very similar strength to the control specimens commonly used in design currently, but had significantly more ductility. Challenges to their use include that they require quite a bit more labor than other connections due to the need for tying several bars to existing rebar mats whereas some other connections require little additional preparation or labor. They also provide the less flexibility as their geometry cannot be altered in the field, so they must be preordered to the proper lengths.

The greatest benefit of the SWP connector designs is that they use materials that are already on hand on the job site, and the designs could be easily altered by adding or removing SWP connectors where needed. The obvious difficulty with these designs is ensuring that an adequate amount of steel crosses all potential crack boundaries. A great way around this would be to use the hat bar as in the IconCHat specimen. By simply bending the longest leg of the corbel rebar up into the wythe instead of back down (thus creating the hat bar), this forces any crack that would develop to cross steel, reinforcing the corbel block and allowing the SWP connectors to achieve their breakout or tensile capacity. This study seems to prove that detailing can provide a significant amount of additional capacity (up to 33% in this particular study). Utilization of this approach

requires that care be taken to ensure that all connectors required to transfer the tensile load in the top of the corbel should be embedded in the corbel concrete block. The IconCHat specimen proves the feasibility of these designs, and allows engineers to use SWP connectors to create economically convenient designs to avoid unnecessary heat transfer in SWP structures.

The final and arguably most successful approach utilized GFRP grating to transfer the corbel loads between wythes. The greatest challenge with implementation of this material is that constructability is a concern, since most contractors and precasters will precast the corbels to save on erection time and reduce the number of pours required to create panels. This could be overcome without too much difficulty, but is likely the greatest challenge regarding the use of FRP grating as a primary reinforcement for corbel connections in concrete SWPs at the moment. Further research on this area could make FRP grating the most feasible and viable option to overcome thermal bridging in corbel connections.

CHAPTER 5

ANALYSIS AND PARAMETRIC STUDY OF CONCRETE SANDWICH WALL PANELS UNDER AXIAL LOADS

P- δ effects can result from uneven thermal expansion between wythes, uneven creep or shrinkage between wythes, camber that has been introduced (whether purposely or otherwise) during construction, out-of-plane loads and vertical loading. These are current concerns in industry because P- δ effects can amplify the moment on SWPs, which are typically considered slender elements (where slenderness is determined according to ACI 318-14 §6.2.5). Questions relating to P- δ include how P- δ should be handled in sandwich panel design and how P- δ load effects are distributed through the panel. Composite action in contemporary SWPs is only beginning to be understood, and recent research has only focused on composite action due to flexure in SWPs. This chapter presents analyses of the specimens presented in the previous chapter and a parametric study investigating SWP behavior due to variation of panel length, wythe configuration, and connector stiffness when subjected to an applied axial force and eccentricity.

Previous Research

Although P- δ effects can be a problem for non-composite SWPs as well, they are of particular concern for partially-composite SWPs due to the high shear transfer between wythes as a result of uneven wythe expansion (such as from thermal expansion). Composite action can be a result of FRP connectors (Al-Rubaye, Sorensen, Olsen, &

Maguire, 2018), FRP grids (Hassan & Rizkalla, 2010), FRP or steel trusses (Salmon, Einea, Tadros, & Culp, 1997), or even solid concrete sections (Lee & Pessiki, 2008) (Olsen, Al-Rubaye, Sorensen, & Maguire, 2017). Where flexible shear connectors or FRP pins are used, low degrees of composite action are typically exhibited (Pessiki & Mlynarczyk, 2003) (Tomlinson, 2015).

There have been multiple studies to date that have analyzed the flexural response of SWPs, but few have considered the axial response of such systems. In 1969, Allen published equations regarding sandwich theory including analysis and design of insulated panels under axial loads and in flexure. Although Allen mentions that such theory may be applicable in the building industry, the emphasis of the study was for aerospace applications (Allen, 1969). As such, he cautioned that the thicker faces and weaker cores often used in buildings may invalidate the assumption made in the design that faces are thin (such as in the metal skin of aircrafts).

Salmon and Einea (1995) presented a continuum model to evaluate deflections due to volume change between wythes with particular application to thermal expansion for SWPs with steel or FRP truss connectors. The equation the model was based off of for computing deflections had been presented in a number of equivalent derivations prior to this study (Allen, 1969) (Holmberg & Plem, 1965) (Gordaninejad & Bert, 1989) (Frostig & Baruch, 1990) (Paydar & Park, 1990) (Ha, 1992). They compared their results to finite element models for validation with good agreement, also noting that as length of the wall panels increased, the amount of thermal bowing became increasingly insensitive to connector stiffness.

Benayoune et al. (2006) (2007) performed experimental testing of SWPs with solid concrete sections under axial loads to compare experimental results to the current design predictions of the time provided by the American Concrete Institute (ACI). The study proposed a formula that was semi-empirical in nature to better fit the experimental results.

Frankl et al. (2011) conducted experiments on SWPs under combined axial and flexural loads to evaluate the performance of a new connector type consisting of a CFRP shear grid. Although axial load was included during testing, the objective and conclusions of the study focused on flexural response.

Tomlinson (2015) presented theoretical models to predict flexural and axial response of a panel for the purpose of accounting for partial composite behavior and to determine longitudinal shear force transferred between wythes. These models were validated by experimental results, where various predetermined axial loads were applied to panels before they were tested to failure in flexure. A parametric study demonstrated that as slenderness of axially loaded panels increases, the composite action also increases. This conclusion agreed with the findings of Salmon and Einea (1995).

There is currently no codified guidance for how second-order ($P-\delta$) effects should be handled in SWP structures, leading many people to rely on using a modified version of the Second-Order Analysis method which is prescribed by the PCI Handbook (2010) to predict such effects in solid wall panels. It is currently unknown if this is actually conservative or unconservative for use with SWPs as this method has not been validated for such application, which can be disconcerting for some. This procedure first calculates

the midspan deflection due to first-order effects as the sum of the deflection due to applied eccentric axial loads, the deflection due to flexural/lateral load, and deflection due to initial bowing. The method then calculates the midspan deflection as the sum of the deflection due to first-order effects plus the deflection due to second-order effects. The PCI Second-Order Analysis then uses a basic equation of mechanics to calculate a prediction of deflection due to second-order effects. The midspan deflection is then recalculated again as the sum of this new deflection due to second-order effects plus the original deflection due to first-order effects and a new second-order deflection is calculated. This iterative process is repeated until increased midspan deflection is negligible (i.e. the deflection converges), or can be bypassed by calculating such deflection directly using a geometric series. If convergence does not occur, instability of the wall is assumed and the section must be redesigned. Once convergence occurs, the predicted midspan deflection can be used to predict the moment and stress. An excellent example of this type of analysis can be found in the PCI Design Handbook.

The concern regarding use of this method with SWPs is that this procedure relies heavily on an accurate estimate of the stiffness of the panel prior to cracking ($E \times I$) and recommends use of the moment magnification method. This can pose a particularly difficult challenge for SWPs as EI is highly dependent on the amount of composite action attained in the wall panel, and this percent composite action is not only little understood and typically unknown, but is continually changing depending on the loading state of the panel (Olsen, Al-Rubaye, Sorensen, & Maguire, 2017). Recommendations of the percentage of composite action from the manufacturer can be (and currently are) used in

such cases to predict an effective moment of inertia and effective section modulus, though they are assumed to be very conservative estimates. An important contribution to the literature would be validation of the current PCI Second-Order Analysis for use with SWPs.

Although there have been several successful attempts from previous researchers to model the axial response of a SWP, each was established with specific limitations and for specific connectors, situations, or sets of circumstances. Olsen et al. (2017) presented a generalized model capable of accommodating panels of any thickness or length with any connector types, distributions, or stiffnesses called the Beam-Spring Model.

Although the model was proposed for flexural loads, the authors mentioned its application could also extend to panels with unsymmetrical wythes, irregular connector patterns, and axial forces including $P-\Delta$ and $P-\delta$.

The Beam-Spring Model is very straightforward, simple, and versatile, making it a very useful tool for SWP design and analysis. Beam-Spring Models consist of beam and spring elements only. Beam elements are assigned appropriate wythe and material properties, and are placed at a distance equal to the actual distance between the centroids of the wythes. Springs are likewise assigned stiffnesses based on the cumulative stiffness provided in each connector line (allowing any assortment of connectors to be used). Boundary conditions are selected to emulate as closely as possible existing conditions. This simple procedure has been shown to produce very reliable predictions of SWP performance effects (Al-Rubaye, Sorensen, Dorafshan, & Maguire, 2018).

This chapter presents a parametric study modeling SWPs of varying heights, connector stiffnesses, and connector distributions using the Beam-Spring Model to identify load-deflection response of partially-composite SWPs due to the addition of axial force to the system. The results were compared with predicted values using the PCI Second-Order Analysis and are presented herein.

Model Verification

Beam-Spring Models (BSM) were created for the 12 corbel specimens presented in the previous chapter. The BSM Results were first compared with the experimental results for model validation. The Beam-Spring Model is very straightforward, simple, and versatile, making it a very useful tool for SWP design and analysis. Beam-Spring Models consisted of beam and spring elements only. Beam elements were assigned appropriate wythe and material properties, and were placed at a distance equal to the actual distance between the centroids of the wythes. Springs were likewise assigned stiffnesses based on the cumulative stiffness provided in each connector line (allowing any assortment of connectors to be used). Boundary conditions were selected to emulate as closely as possible those of the testing conditions. The following sections discuss model creation and the results.

Model Descriptions

The models for each panel were created using the finite element software SAP2000 and were based on the geometry of the panel as shown in Figure 5-1. Each model was assigned appropriate material properties as well corresponding to the actual panel. Table 5-1 displays the properties and dimensions used for each model.

The HK composite connector has a stiffness of 94.8 kip/in (Olsen & Maguire, 2016). All panels were modeled for their respective height with links placed every 16 inches on center, equivalent to the spacing of the HK SWP connector lines placed in the actual SWP specimens. Each of these links was assigned the cumulative connector stiffness for that particular line. As an example, the majority of connector lines only had the uniformly spaced HK ties at 16" o.c. in both directions. Since this yielded 4 HK connectors per line, the stiffness for the links at these locations was

$$k = 4(k_{HK}) = 4\left(94.8 \frac{k}{in}\right) = 379.2 \text{ k/in} \quad (5-1)$$

In some specimens of Set 2 and 3, the reinforcement used to transfer the tensile load created at the top of the corbel by the applied load coincided with the connector line, so the stiffness at this connector location included the stiffness of the four HK connectors in addition to any stiffness provided by the given tensile reinforcement. Although it has been demonstrated that insulation can, at times, provide a substantial contribution to stiffness between SWP wythes (Olsen, Al-Rubaye, Sorensen, & Maguire, 2017) (Al-Rubaye, Sorensen, & Maguire, 2017) (Tomlinson, 2015), such contribution was conservatively ignored in the Beam-Spring Models herein because there were no means established to quantify or eliminate such effects.

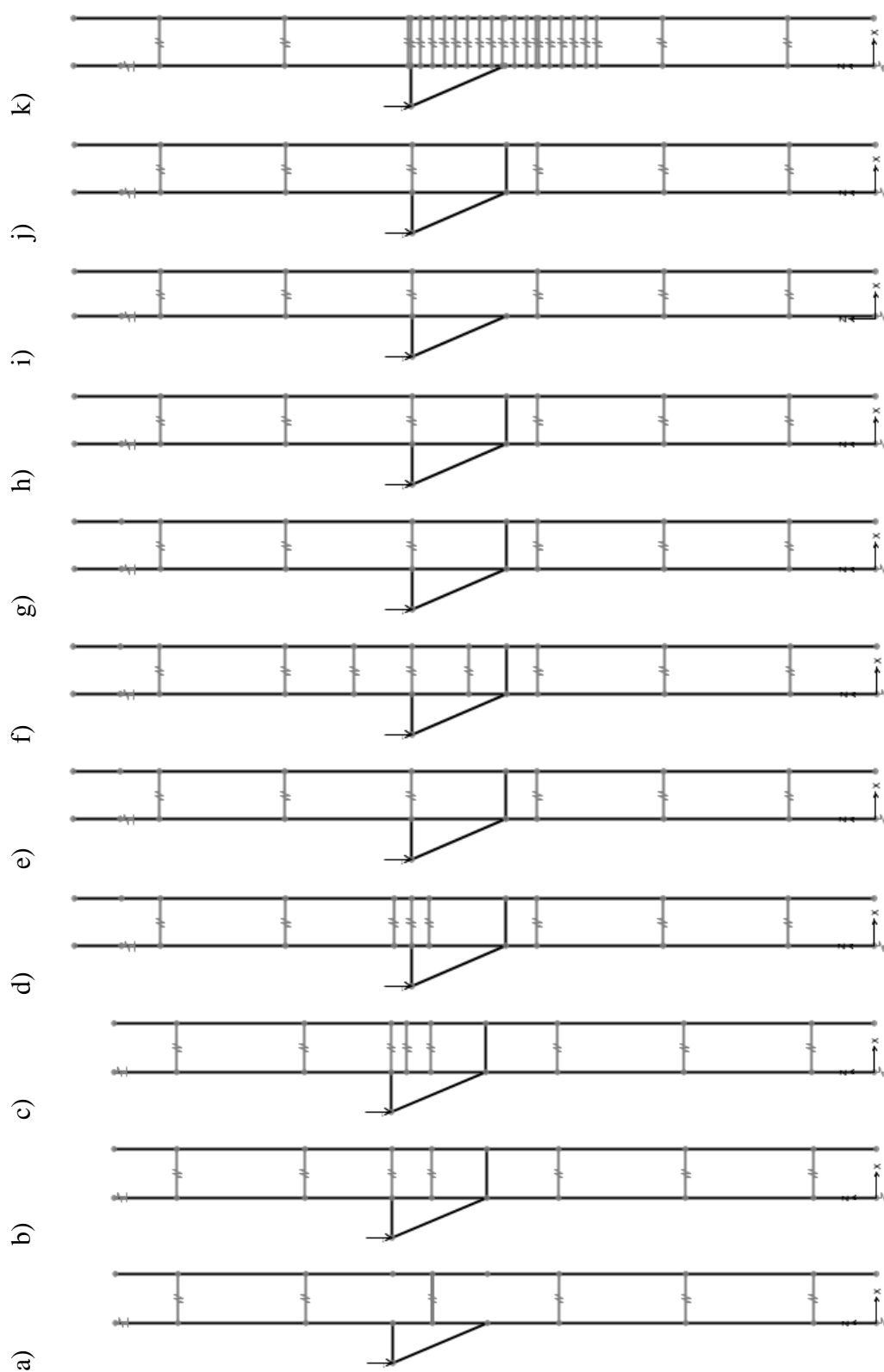


Figure 5-1 Beam-Spring Models for SWP specimens: a) SolidSec, b) GFRP3, c) GFRP2, d) HKHor, e) HKVer, f) IconG, g) IconC, h) IconCHat, i) RedIns, j) GridHor, k) GridVer

Table 5-1 Properties used in SWP Beam-Spring Models

	h	b	f'_c	E_c	$K_{rein,f,x}$	$K_{rein,f,y}$
SolidSec	96	72	11.87	6321	-	-
GFRP3	96	72	12.11	6618	634.0	10
GFRP2	96	72	12.11	6618	282.4	10
HKHor	102	68	10.73	6549	284.4	60
HKVer	102	68	10.73	6549	568.8	568.8
IconG	102	68	10.61	7014	600.72	600.72
IconC	102	68	10.61	7014	1043.04	1043.04
IconCHat	102	68	9.82	5528	1043.04	1043.04
RedIns	102	68	9.82	5528	-	-
GridHor	102	68	9.82	5528	1714.8	409.2
GridVer	102	68	9.82	5528	490.0	10

Beam elements for wythes were assigned their respective geometrical and material properties as found in Table 5-1. The corbel was also modeled with beam elements, having nodes placed so as to emulate the strut and tie model used for design. Thus, a triangle was used to model the corbel in place of a quadrilateral. The corbel beam elements were assigned the same material properties as the wythes, but were assigned a depth of only 10 inches instead of the depth equal to the width of the SWP since the corbel was only 10 inches wide in reality. These beam elements had fixed connections to

the inside wythe elements. Because the overall dimensions and layouts of panels were very similar, only minor geometrical changes were necessary between panels.

As mentioned, the primary tension reinforcement was represented by a spring with associated stiffnesses. To model the compression reinforcement where the strut forms at the base of the corbel, an additional beam element was used with pinned connections to each wythe. The material used for these specimens was either HDO prisms (for set 1) or HDPE prisms (for set 2 and 3). The modulus of elasticity assigned to this beam element for HDO and HDPE was 520 ksi and 116 ksi, respectively (APA, 2011) (Engineering ToolBox, 2003). There is little data regarding the compressive strength of HDO board perpendicular to the face, therefore the axial compression modulus of elasticity and compressive strength were used (APA D510C, 2012).

Idealized boundary conditions were considered for use in the Beam-Spring Model for the SWP corbel specimens, but it was discovered that the test setup provided a significant amount of fixity at the top and bottom of the panels. To adequately emulate testing conditions, three springs were used in the models for boundary conditions at the top and bottom of the inside wythe, providing stiffness vertically, transversely, and rotationally. The stiffnesses used for the models were extremely similar, validating their reflection of actual conditions. The stiffnesses used in the model are displayed in Table D-1 in Appendix D.

The model for specimen with the solid concrete section at the corbel location resembled the other specimens of Set 1 except for the obvious difference of inclusion of an additional beam element at the corbel location representing the solid concrete

connection. This beam element was assigned a height of 16 inches and a depth of 12 inches to emulate the size of the actual solid section and had fixed conditions where it attached to each wythe. The slip in this specimen was measured on the connector line immediately below the corbel and on the second connector line from the top because the solid section occurred where slip was being measured at the corbel location in the other panels. No LVDT was used on the top connector line here.

The axial stiffness of the GFRP #2 and #3 bar used was calculated by rearranging Hooke's law:

$$\delta = \frac{PL}{AE} \rightarrow K_x = \frac{P}{\delta} = \frac{AE}{L} \quad (5-2)$$

Where: K_x = axial stiffness of GFRP bar

A = area of the bar

E = modulus of elasticity of the bar

L = original unsupported length of the bar (= insulation thickness)

With the modulus of elasticity of the GFRP bar being 2470 ksi and with 7 GFRP bars in the connector line, the axial stiffness of the GFRP was calculated to be 634 kip/in. The shear stiffness of the GFRP bar was unknown, and shear stiffness of GFRP is known to be highly variable (Mottram, 2004). It was apparent, however, that there would be significantly less shear stiffness than axial stiffness due to the slenderness of the bar, so an assumed stiffness of 10 k/in was used in the model and was assumed to be conservative.

A similar approach to the GFRP3 specimen was used for the GFRP2 specimen as well, but with the addition of a separate connector link below the primary tension

reinforcement in the corbel. This was because the GFRP2 specimen was required to place reinforcement into 2 rows for it all to fit inside the corbel limitations. This additional link can be seen by comparing Figure 5-1 b) and c). Although the GFRP3 and GFRP2 bars were made of the same material, the axial stiffness for the GFRP2 specimen differed as well because of the difference in areas of the bars (see Eq. (5-2)), resulting in a stiffness of 282.4 kip/in.

The HKHor specimen was the first panel of set 2, meaning that the HDO prism was then replaced by the HDPE prism. This panel also required the separate inclusion of links to represent the six horizontal HK connectors used to transfer the tensile force at the top of the corbel (three per spring). This can be seen in Figure 5-1 d). Because the geometry of the HK connectors is such that the unbraced portion is approximately equal to its width, the axial and transverse stiffness was assumed to be the same. The axial stiffness was therefore calculated to be 284.4 kips/in. The stiffness of the connectors in out-of-plane bending is unknown, therefore a transverse stiffness was assumed to be equal to 20% of the shear stiffness, resulting in roughly 60 kips/in.

The HKVer specimen was very simple in that it required no alteration from the typical model since the primary tension reinforcement lined up precisely with the regular line of HK connectors. The stiffness of this connector line was therefore increased from only 4 HK connectors to include 6 additional connectors, and increase of 568.8 kips/in.

The reinforcement for the IconG panel consisted of 8 IconX GFRP connectors placed in two lines of 4 connectors each, thus the model (Figure 5-1 f) added two additional springs to represent these connector lines. It was very important to include the

stiffness effects of these connectors as IconX connectors are currently the stiffest connectors in the market with 150.2 kips/in for the GFRP connectors and 347.7 kips/in for the CFRP connectors. Since the shape of these connectors is bisymmetrical, the axial stiffness was assumed to be equal to the shear stiffness as well. With four connectors per line, this meant each representative spring was assigned a shear and axial stiffness of 600.72 kips/in.

The geometrical layout of the Beam-Spring Model for the IconC and IconCHat specimens was exactly identical to the model of the HKVer specimen, with only concrete properties varying and the stiffness of the connector line at the corbel location. The IconC and IconCHat specimens both used three IconX CFRP specimens with a total stiffness of 1043.04 kips/in in addition to the four HK ties in the connector line.

The RedIns specimen was unique because it required no additional ties between wythes, but instead required a modification of wythe properties to accommodate the thickened wythe section at the corbel location. This was completed by calculating the centroid location and moment of inertia for the interior wythe (accounting for the thickened section), and then modifying the distance between the beam elements to emulate the actual distance between the new centroids. The thickened section shortened the centroid distance between wythes from 6 inches to 5.66 inches, so the wythes in this model were also reduced to 5.66 inches. Because the Beam-Spring Model modeled the panel in 2-D, modeling the geometric discontinuity of the thickened section presented a challenge. To keep the model simple, an equivalent wythe thickness was calculated using

the new modulus of elasticity (336.55 in^4) and the existing SWP width (68 in), resulting in an equivalent wythe thickness of 3.90 inches.

The GridHor specimen model was also identical to the HKVer, IconC, and IconCHat models, varying only the stiffness of the connector line at the corbel. Because GFRP grating has not historically been used in such an application where the grid is stressed axially, the axial stiffness of the GFRP grid was calculated in the same manner as the GFRP rebar specimens by using Eq (5-2). The modulus of elasticity of the grid was calculated using the equation for calculating the deflection of a beam in bending, in conjunction with the load-deflection tables provided by the manufacturer:

$$\delta = \frac{PL^3}{48EI} \rightarrow E = \frac{PL^3}{48\delta I} \quad (5-3)$$

Because the load deflection data provided by the manufacturer included various clear spans ranging from 18 inches to 58 inches and under loads varying from 50 lbs to 2000 lbs, the modulus of elasticity was calculated for each combination of load and deflection, then averaged. The averages had a linear relationship where the modulus of elasticity increased with unbraced length Figure 5-2. Because the “clear span” in the case of this corbel specimen was equal to the distance between wythes (3 inches), the modulus of elasticity was estimated using the linear line of best fit created using the averages for modulus of elasticity vs. clear span. This resulted in a modulus of elasticity of 2063 ksi.

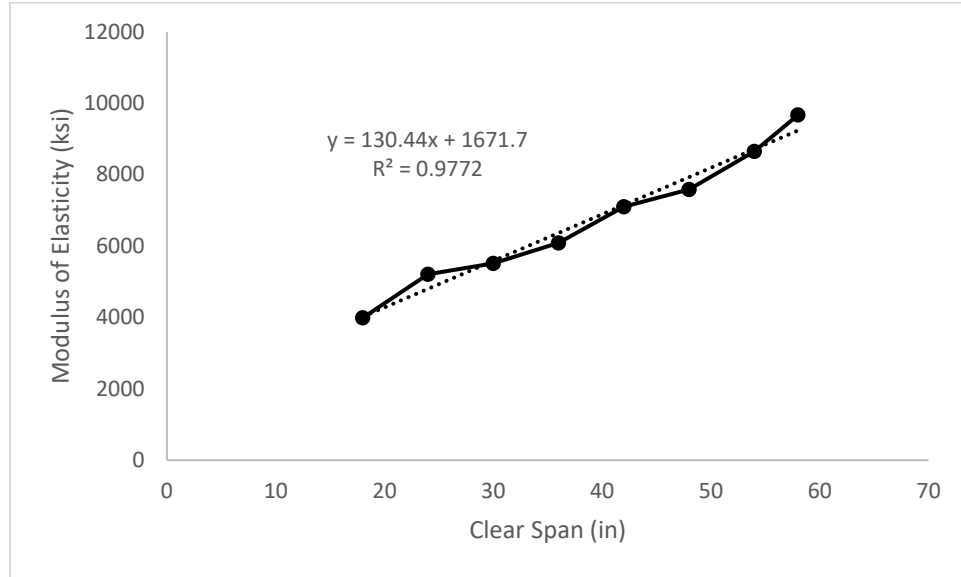


Figure 5-2 Average GFRP modulus of elasticity vs. clear span

With the modulus of elasticity for the GFRP grid, the axial stiffness was calculated using Eq (5-2) as 1714.8 kip/in. The transverse stiffness was calculated using the relationship between load and deflection for a beam fixed at one end and free to deflect vertically but not rotate at the other with a concentrated load at the deflected end. This scenario reflects the conditions of loading on a dowel-styled SWP connector. The equation for deflection under such boundary conditions (AISC, 2011) can be rearranged to solve for stiffness as:

$$\delta = \frac{PL^3}{12EI} \rightarrow K = \frac{P}{\delta} = \frac{12EI}{L^3} \quad (5-4)$$

Since the moment of inertia of the grid is provided by the manufacturer as 0.51 in⁴/ft, the resulting transverse stiffness calculated is equal to 409.2 kip/in. These values

were therefore included with the stiffness values of the HK connectors to model panel behavior.

The final specimen, the GridVer, was unique in that it provided all necessary load transfer within the corbel (i.e. no compression prism was necessary at the bottom of the corbel). The geometrical model of the specimen included links to represent each transverse component of the grid that crossed the insulation between wythes (Figure 5-1k). Because the area that each link represented differed from that of the GridHor specimen, the axial stiffness also differed according to the relationship found in Eq (5-2). This resulted in an axial stiffness of 489.96 kip/in. Determining the transverse stiffness was somewhat more ambiguous. Because of the orientation of the grid, the moment of inertia was quite a bit different with bending about the weak axes of the grid elements. This naturally decreased the moment of inertia substantially, which was to be expected (0.0017 in^4 per individual bar within the grate as opposed to 0.064 in^4). Using Eq (5-4) with this value, however, underpredicted panel performance because it ignored the contribution of the vertical bracing from the lateral grating connections. These lateral grating bars provide bracing that helps distribute the load to adjacent bars and resist bending due to the fixed connection of the material at bracing locations. Doing so clearly provides additional stiffness unaccounted for in the assumptions of the basic equations of mechanics used when oriented in such a way. On the other hand, calculating the moment of inertia of just two grating bars with the assumption that they act perfectly composite yields a moment of inertia of 0.4 in^4 (or a stiffness of 370.5 kip/in), greatly overestimating the panel performance. By investigation, the transverse stiffness that

provided predictions closest to the actual values was around 10 kip/in, a conservative and plausible result falling in the range between 1.5 kip/in and 370.5 kip/in.

Model Results

As mentioned, all Beam-Spring Models were created using SAP2000. Each corbel specimen was modeled with a 1-kip applied unit load to determine the resultant forces within links at locations where LVDTs had measured slip during testing (top link, bottom link, and link representing the nearest HK line at or above the corbel location). This load could then be used to calculate the slip of the panel at that connector location by using the stiffness relationship of force divided by slip, which has served as the basis for estimation of stiffness for Eq (5-2) and (5-4) as well:

$$K = \frac{P}{\delta} \quad (5-5)$$

By rearranging Eq (5-5) so as to divide the resultant link force by the assigned stiffness of the connector line assigned in the model, the slip could be attained. This estimated slip was a result of a unit load. Because this analysis considers only the elastic range of the panel, the applied load vs. slip relationship is linear, allowing the model result to be multiplied by the load at failure for comparison of measured to predicted load values.

The predictions of the Beam-Spring Models were extremely favorable with good agreement with the experimental results. Figure 5-3 displays the experimental and Beam-Spring Model results for comparison. To quantify such a comparison, a ratio of the

measured-to-predicted slopes was created, where the measured slope was obtained by fitting a best-fit line to the data with an intercept through zero. The average of these ratios for the corbel specimens was excellent at 1.01, but the standard deviation of 0.286 was a little higher than expected. This can be attributed to the test setup itself. The initial scope of the project involved testing only of the corbel itself. Only after testing was completed was it realized that testing of SWPs under axial and eccentric loads with corbel connections such as these does not currently exist in the literature. As such, boundary conditions for testing had not been idealized as a pin and roller. Furthermore, the foam would ideally be debonded to eradicate effects of concrete bond to insulation. Both of these factors contributed to the variability in the data demonstrated by the standard deviation. Were these tests to be duplicated, the idealization of boundary conditions and debonding of insulation should be performed to provide cleaner results. The individual resultant ratios comparing predicted-to-measured results are displayed in Table 5-2.

As has been shown, these results validate that the Beam-Spring Model can effectively be used for predictions of elastic performance in axial applications. These tests were used for such validation because they were convenient, however they were not specifically setup for this method (as indicated by the necessity of use of springs at boundary conditions). A simpler analysis with similar results could be achieved if testing were repeated with idealized boundary conditions for further validation. It may also be beneficial for testing to be performed with a true axial load applied to the inside wythe only, thereby reducing additional eccentricity that is naturally introduced by the corbel. Thus the inside wythe would have a pure axial load and the effects of such a load would

be more clearly visible. This is a suggestion for future research. The results shown herein are, however, adequate to validate use of such a model for axial load applications.

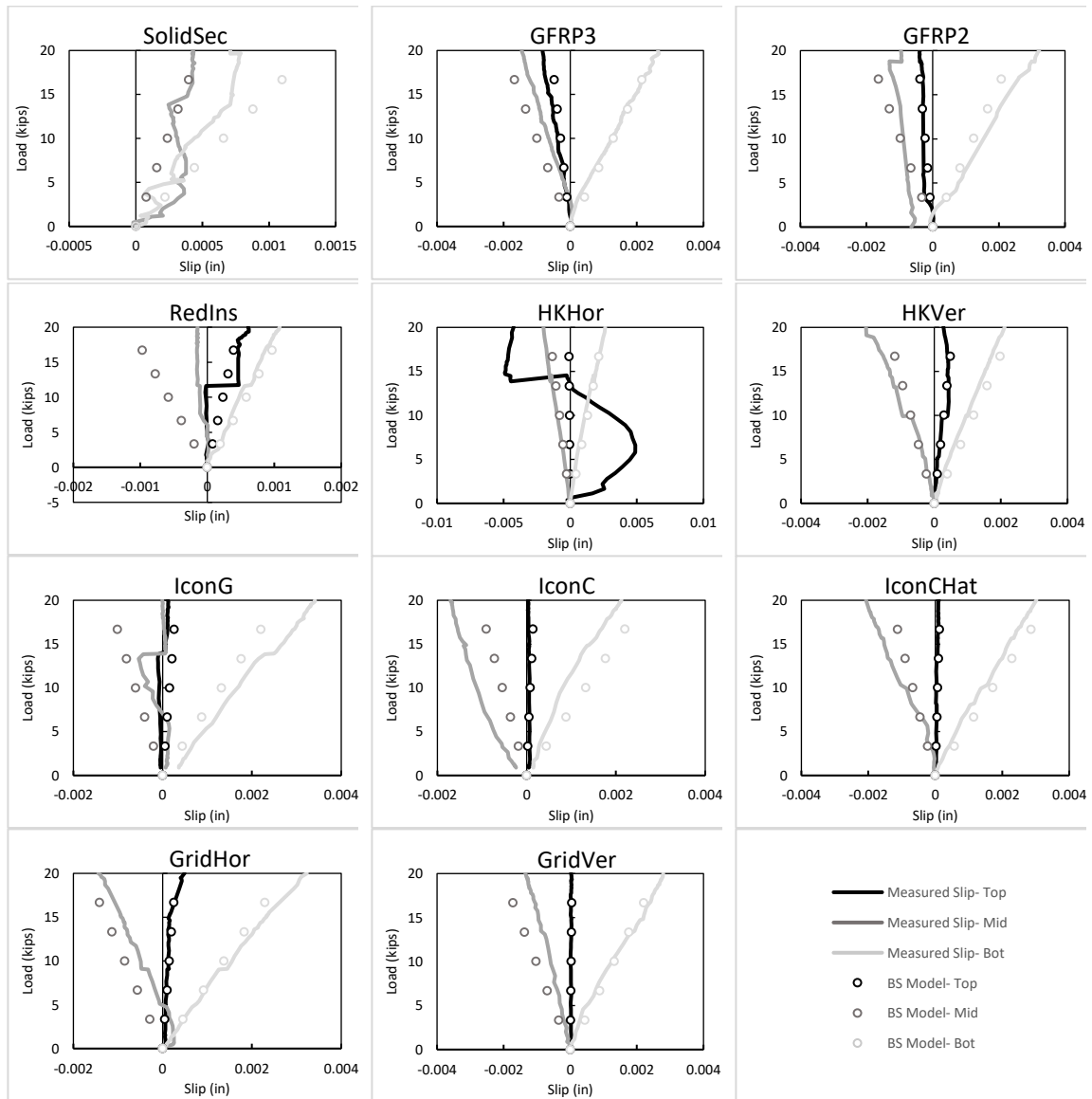


Figure 5-3 Applied load vs. slip results for corbel specimens

Table 5-2 Ratios of predicted-to-measured elastic slope for applied load vs. slip

	Top	Mid	Bot	Avg
SolidWall	_*	_*	_*	_*
SolidSec	_*	1.203	0.662	0.933
GFRP3	1.420	0.701	0.999	1.040
GFRP2	0.982	0.747	1.285	1.005
HKHor	-†	1.293	0.974	1.133
HKVer	0.925	1.299	0.857	1.027
IconG	0.829	0.991	1.315	1.072
IconC	0.674	1.734	0.761	1.056
IconCHat	0.683	1.517	0.864	1.021
RedIns	1.264	-†	0.910	0.775
GridHor	1.197	0.767	1.134	1.033
GridVer	0.752	0.630	1.061	0.815
Avg	0.970	1.099	0.984	1.014
StDev	0.269	0.400	0.205	0.286

* Value not measured

† LVDT malfunction

Parametric Study

A parametric study was performed to explore the proportion of axial force shared between SWP wythes, and to demonstrate the effects of several variables on the load-deflection response of partially-composite SWPs due to the addition of axial force to the system. The study was completed utilizing the Beam-Spring Method.

Axial Force Sharing Between Wythes

In the literature currently, there is no data regarding how applied axial load is shared between wythes. This often leads engineers to assume that the wythe where the load is applied (typically the inside wythe) will carry 100% of the axial portion of the load. To explore what proportion of axial force is actually shared between wythes, a parametric study was performed for panels ranging from 12 to 60 ft in 6-ft increments for connector-line stiffnesses of 10, 100, 1000, and 10000 kips/in. Beam-Spring Models were created with an applied unit load of 1 kip concentric with the centroid of the interior wythe and no flexural load. The results are shown in Figure 5-4.

As can be seen in the plot of percentage of applied load vs. panel stiffness, greater axial load is shared between the wythes as stiffness and length increases. Even with the greatest stiffness and length modeled however (10000 kip/in/ft² and 60 ft, respectively), the outside wythe only carried about 3.8% of the axial load. This can likely be attributed to the fact that quite a bit of deflection must occur before the SWP connectors are fully engaged. Because concrete is a very stiff material, the axial deflection due to an applied

load is much smaller than the deflection required to engage the connectors, resulting in minimal load sharing between wythes for pure axial load applied to a single wythe.

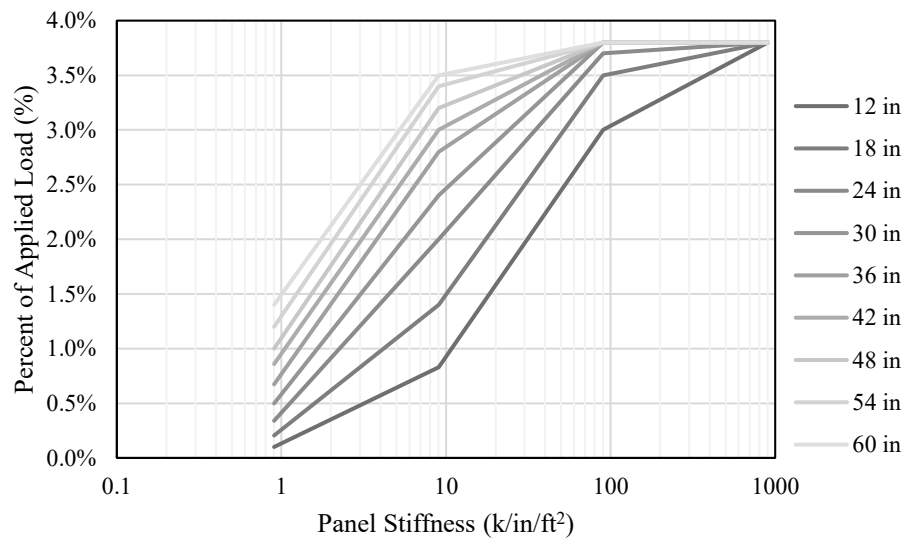


Figure 5-4 Percent of applied load shared by outside wythe

Effects of Load Eccentricity on Connector Force Distribution

Although some connections are designed to apply gravity loads concentrically with the interior wythe, frequently loads are applied with an eccentricity (such as at corbel connections). To explore the effects of this load eccentricity on connector force, Beam-Spring Models were created for a 30-ft SWP with uniformly distributed connectors with a stiffness of 1000 kips/in. Eccentricities for an applied unit load included 0, 2, 4, 6, and 8 inches from the centroid of the inside wythe. The eccentricity was accounted for in the model by applying an equivalent moment at the location of the top connector-line, simulating a corbel connection. The connector force distribution is shown in Figure 5-5.

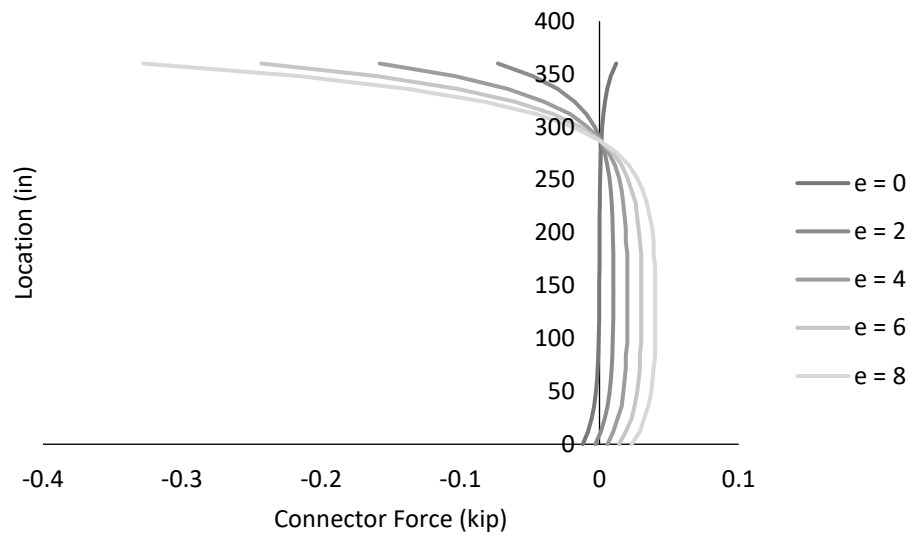


Figure 5-5 Connector force distribution for varying eccentricities

When there is no eccentricity, the connector force distribution shows equal and opposite forces between the top and bottom of the panel. As even a little eccentricity is introduced, however, the top connectors begin to experience significantly greater shear force. The flexural effects of eccentricity seem to dominate the behavior of the panel as compared to those from axial load (as shown previously in Figure 5-4). Since many of the alternative corbel designs created in the previous chapter attempted to transfer local corbel loads by concentrating SWP connectors at the corbel connection, the models were replicated again by modifying the top connector-line stiffness to be 1000, 2000, 3000, 4000, and 5000 kips/in. Results of maximum shear and axial connector force vs. concentrated connector-line stiffness at the top of the panel are displayed in Figure 5-6 and Figure 5-7, respectively.

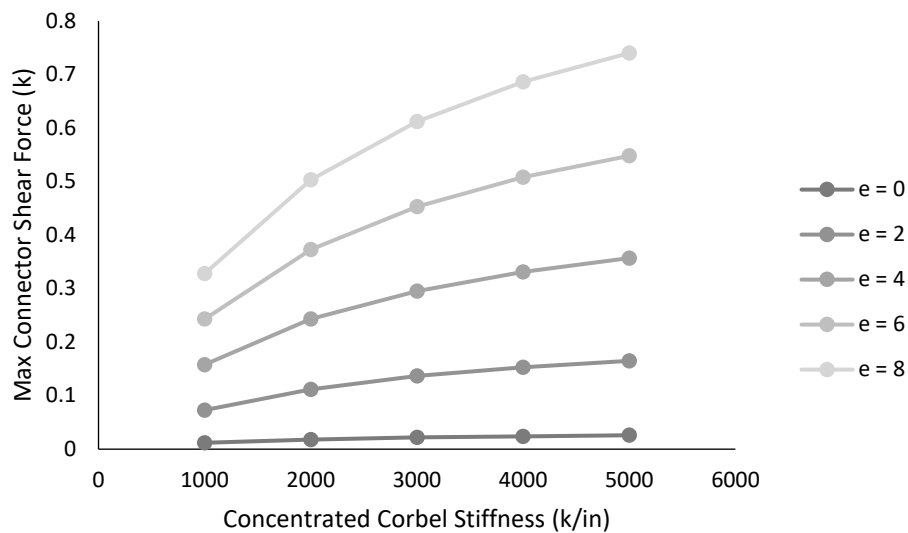


Figure 5-6 Maximum connector shear force vs. concentrated corbel stiffness

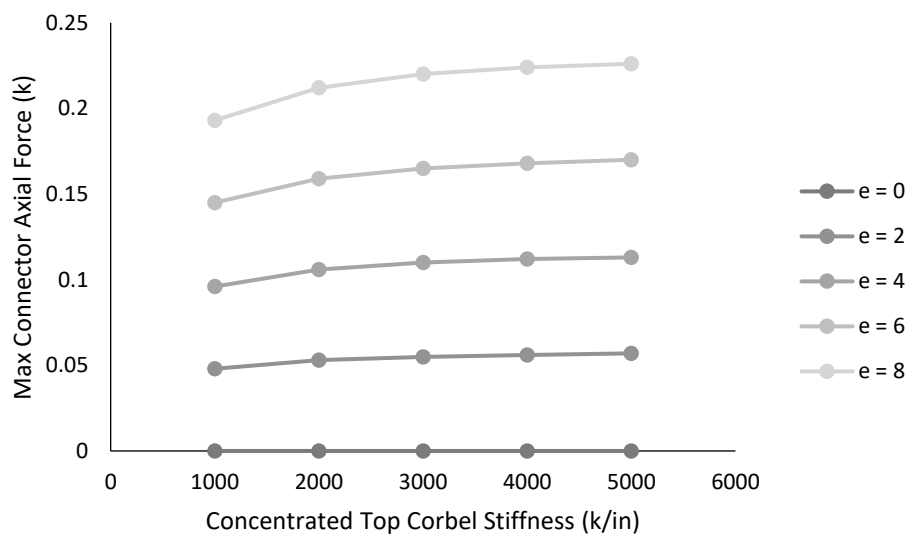


Figure 5-7 Maximum connector axial force vs. concentrated corbel stiffness

The maximum shear and axial forces experienced in the panel both increase as the concentrated connector-line stiffness at the top of the panel increases. It is also notable that eccentricity causes greater variance in shear force than in max axial connector force.

Since SWP connectors often consist of fiber-reinforced polymer (FRP), special consideration should be given to the max forces experienced to ensure that creep failure does not occur. This could be especially concerning when the effects of lateral loads are taken into consideration as well, such as wind.

Factors of Load-Deflection Response

To demonstrate the effects of different variables on the load-deflection response of partially-composite SWPs due to the addition of axial force to the system, an additional parametric study was performed. The study was completed using a Beam-Spring Model for a SWP with 8 ksi concrete.

Models included beam elements representing the concrete wythes connected by spring elements every 12 inches on center. Panels were simply supported with a pin at the bottom of the inside wythe (fixed translation longitudinally and laterally with free rotation) and a vertical roller at the top of the inside wythe (fixed translation laterally with free longitudinal translation and free rotation).

Panel response was modeled by varying panel length, wythe configuration, and connector stiffness. Lengths varied from 12 ft to 60 ft in 6-ft increments for a total of 9 length variations. Three wythe thickness combinations were considered: 3-2-3, 3-3-3, and 3-4-3. Connector stiffness was discovered to have a logistic behavior as opposed to the commonly linear assumption made currently in industry (Al-Rubaye, Sorensen, & Maguire, 2017). For this reason, the following 10 connector line stiffnesses were tested to obtain adequate points to establish the logistic relationship between degree composite action and stiffness in units of kips/inch: 10^{-4} , 10^{-1} , 10^0 , 10^1 , 10^2 , 10^3 , 10^4 , 10^5 , 10^6 , and

10⁸. All connector distributions were uniform. The panel was assumed to carry a dead load of 30 kips and a live load of 12 kips placed at an eccentricity of 7.5 inches from the face of the wall. A wind load of 35 psf was applied to the model in conjunction with the oft governing load combination of $1.2D + 0.5L_R + 1.0W$. With these variables in place, 270 BSM models were created.

Necessity of P- δ Effect Consideration in SWPs

As mentioned previously, there is currently no codified guidance for the treatment of second-order effects in SWPs. The PCI Handbook (2010) provides provisions and recommendations for calculating P- δ effects for solid wall panels (the Second-Order Analysis), however, which are often used by industry professionals for application to SWPs in the absence of specific relevant guidance. Although there are situations where the effects of P- δ can be trivial (i.e. negligible axial force or minute eccentricity), these effects are often so great that to ignore such forces or to make incorrect and unconservative assumptions would be not only foolish, but catastrophic. Figure 5-8 shows the ratio of the BSM results for moment due to the second-order elastic analysis to those of the first order linear elastic analysis for different stiffnesses (in units of kips/in/ft²).

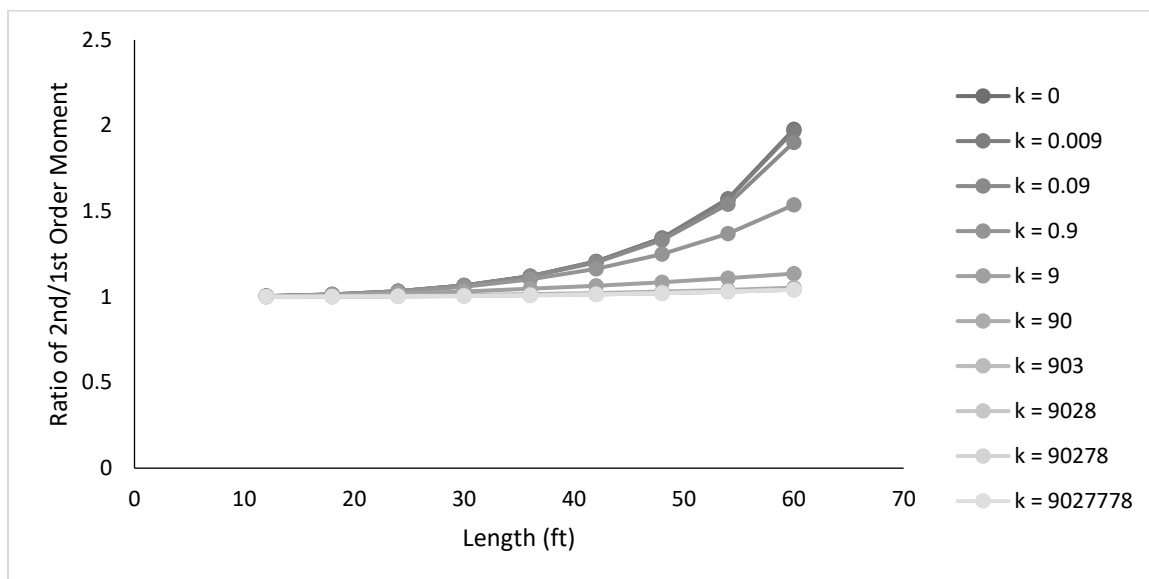


Figure 5-8 Ratio of 2nd Order to 1st Order Moment vs. Length for a 3-3-3 SWP (where k is in units of $k/in/ft^2$)

As can be seen from the figure, the moment predicted can be up to 2 times greater when the effects of secondary moment are included. It is also evident from Figure 5-8 that $P-\delta$ effects are increasingly concerning as length increases or stiffness decreases. For composite SWP connectors today, connector stiffnesses usually fall between 50-500 $kip/in/ft^2$, yielding a predicted moment magnification of between 4-13% for a length of 60 ft. Therefore, secondary moments in SWPs should be considered for safe design. Effects of $P-\delta$ should not be ignored.

Comparison of BSM Results and Current Industry Predictions

Results of stress and midspan deflection for all Beam-Spring Models (BSM) were compared to predictions made using the PCI Second-Order Analysis. An example of calculations for determining predictions of stress and midspan deflection by applying the

PCI method to SWPs can be found in Appendix E. As mentioned previously, this procedure relies heavily on an accurate estimate of the stiffness of the panel prior to cracking ($E \times I$), which can be difficult as EI is highly dependent on the amount of composite action attained in the wall panel, and this percent composite action is typically unknown. Those in industry will typically rely on manufacturer recommendations for a percent composite action for use in this method, but because an arbitrary connector line stiffness was used for the models, there were no manufacturer recommendations available. Instead, a separate BSM was created for each panel where only a uniformly distributed flexural load was applied to attain the degree composite action to use for estimation of EI , since this is a common approach connector manufacturers use currently for such determination (Olsen, Al-Rubaye, Sorensen, & Maguire, 2017). The resultant deflection was used to determine the degree composite action used for calculation of the effective moment of inertia in conjunction with non-composite and fully-composite moments of inertia. This degree of composite action was calculated using Eq. (5-6).

$$K_d = \frac{I_{BSM} - I_{NC}}{I_{FC} - I_{NC}} \quad (5-6)$$

Where I_{BSM} = moment of inertia of SWP predicted by BSM

I_{NC} = theoretical non-composite moment of inertia of SWP

I_{FC} = theoretical fully-composite moment of inertia of SWP

To determine the effective section modulus, a separate degree of composite action must be calculated based off of the moments. This could be done using a similar equation to Eq (5-6):

$$K_{Mn} = \frac{M_{n,BSM} - M_{n,NC}}{M_{n,FC} - M_{n,NC}} \quad (5-7)$$

Where $M_{n,BSM}$ = maximum moment of SWP predicted by BSM

$M_{n,NC}$ = theoretical maximum moment of non-composite SWP

$M_{n,FC}$ = theoretical maximum moment of fully-composite SWP

Effective section modulus can also be calculated from the BSM using the relationship between moment and stress obtained from the model:

$$S = \frac{M}{\sigma} \quad (5-8)$$

A linear interpolation is commonly used for degree composite action (as demonstrated by its calculation above). The degree of composite action actually demonstrates a logistic relationship according to panel length, connector stiffness, and connector configuration. Figure 5-9 shows this relationship between DCA and panel stiffness for a 3-3-3 SWP of varying lengths (in feet). Because the realistic practical range for SWP stiffnesses is between 50 k/in/ft² and 500 k/in/ft², an approximately linear interpolation is reasonable. Therefore linear interpolation is used currently in practice.

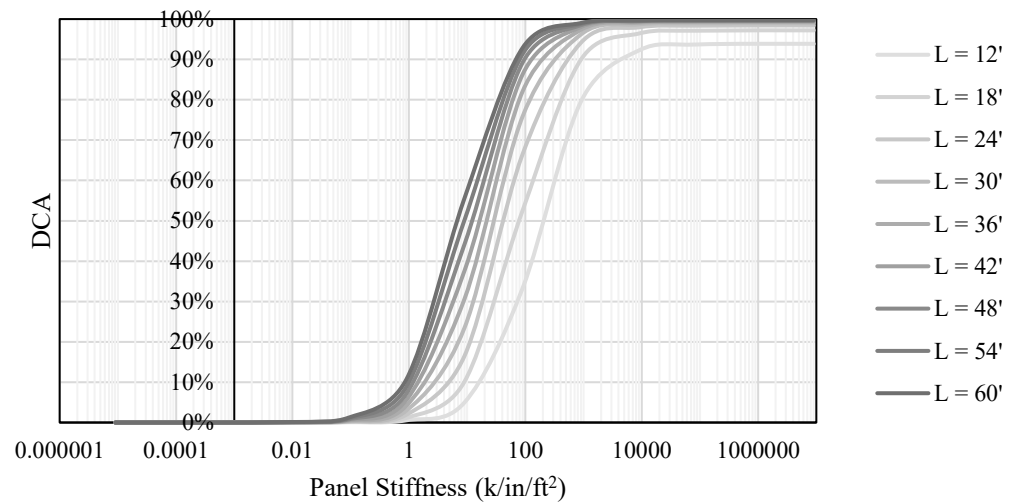


Figure 5-9 Logistic relationship between DCA and panel stiffness

Beam-Spring Model results for deflection and stress were taken from the midspan of the outside wythe. These values were used for comparison with those predicted by the PCI Second-Order Analysis method. The results of the 3-2-3 models can be seen in Figure 5-10. Figure 5-10 (a) and (c) display the individual deflection predictions from the BSM and PCI methods respectively, with the ratio of the two plotted in Figure 5-10 (e). Likewise, Figure 5-10 (b) and (d) display the individual deflection predictions for the BSM and PCI methods respectively, with the ratio of the two plotted in Figure 5-10 (f). Similarly, the results of the 3-3-3 and 3-4-3 models are displayed in Figure 5-11 and Figure 5-12.

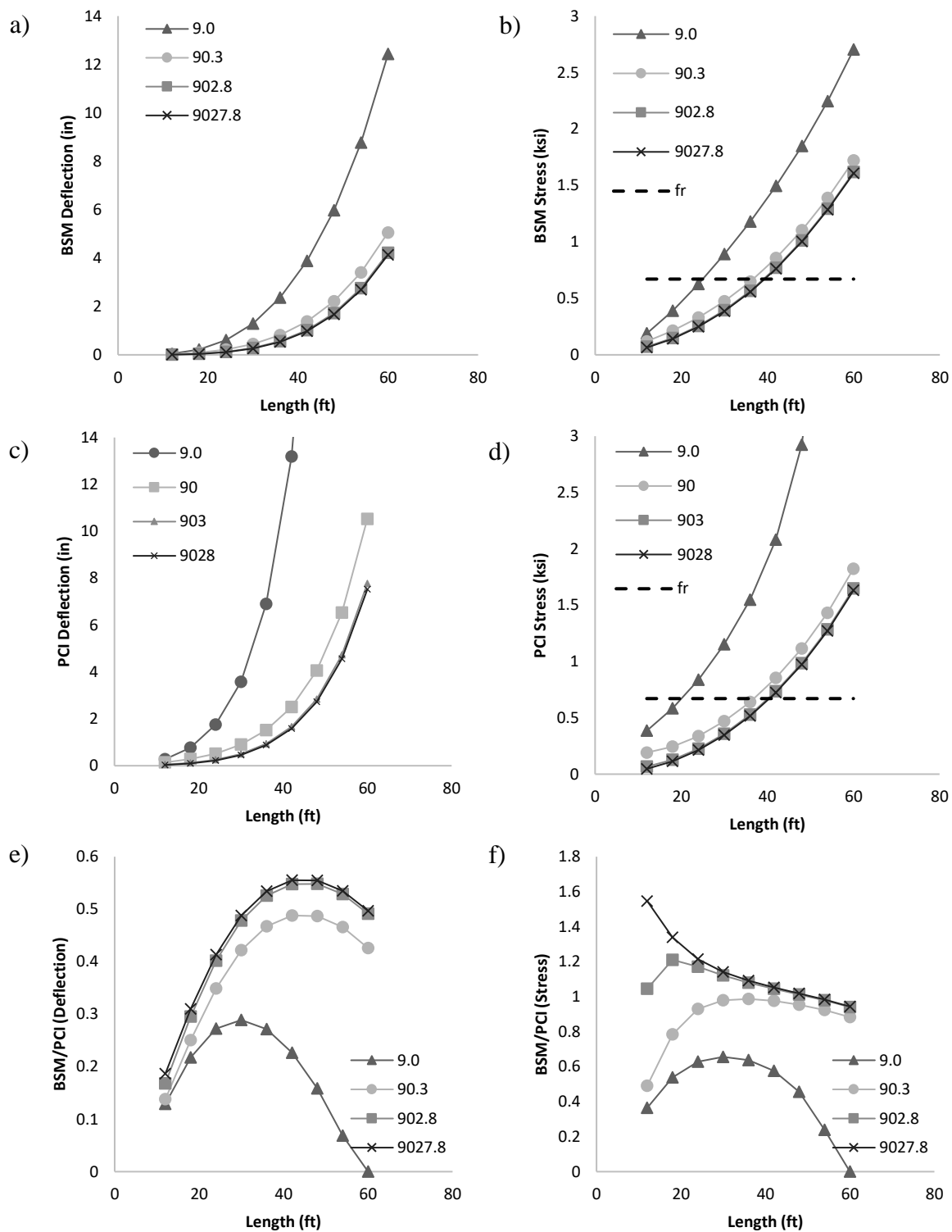


Figure 5-10 BSM and PCI predictions for stress and deflection in a 3-2-3 SWP: a) BSM deflection, b) BSM stress, c) PCI deflection, d) PCI stress, e) ratio of BSM/PCI deflection, and f) ratio of BSM/PCI stress

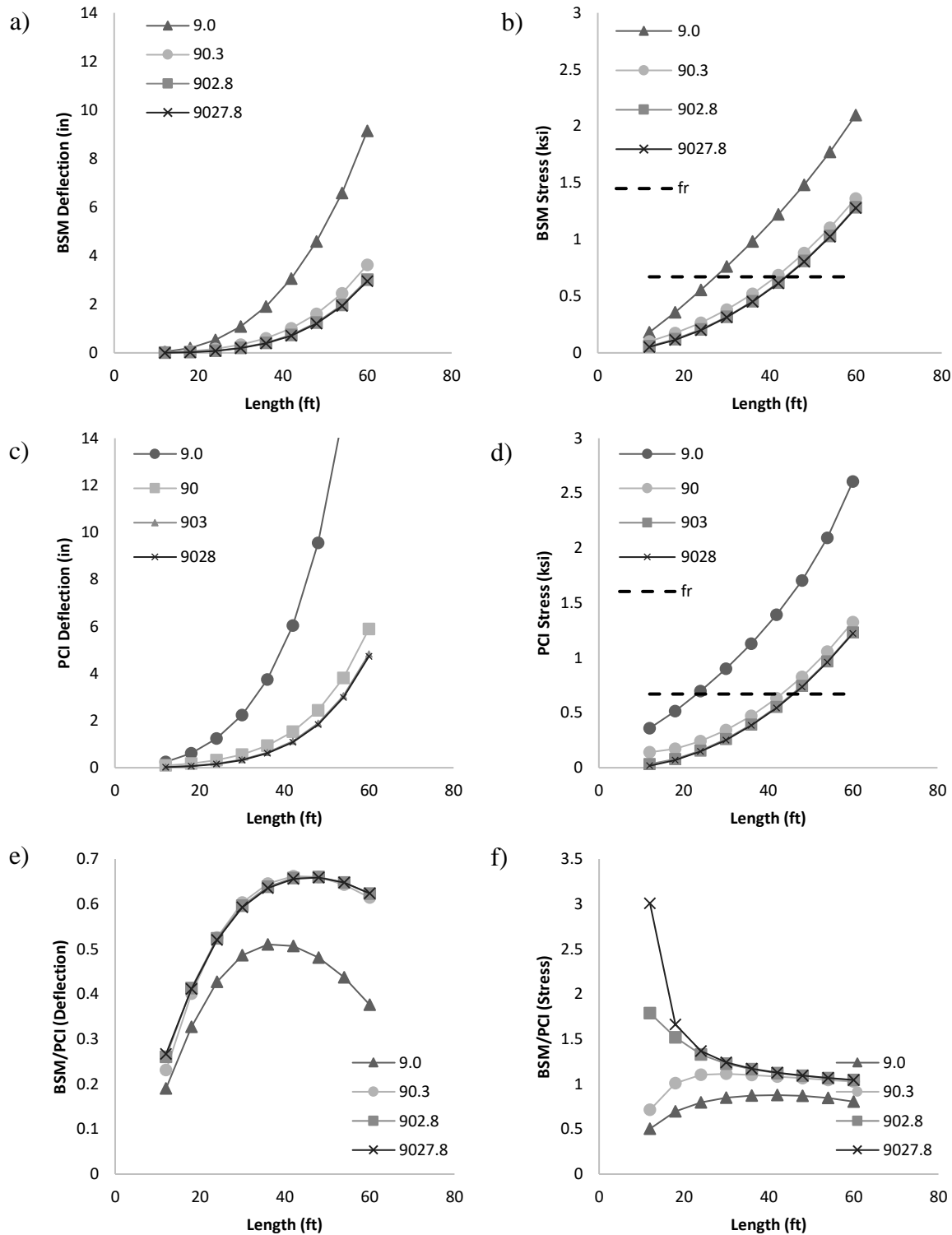


Figure 5-11 BSM and PCI predictions for stress and deflection in a 3-3-3 SWP: a) BSM deflection, b) BSM stress, c) PCI deflection, d) PCI stress, e) ratio of BSM/PCI deflection, and f) ratio of BSM/PCI stress

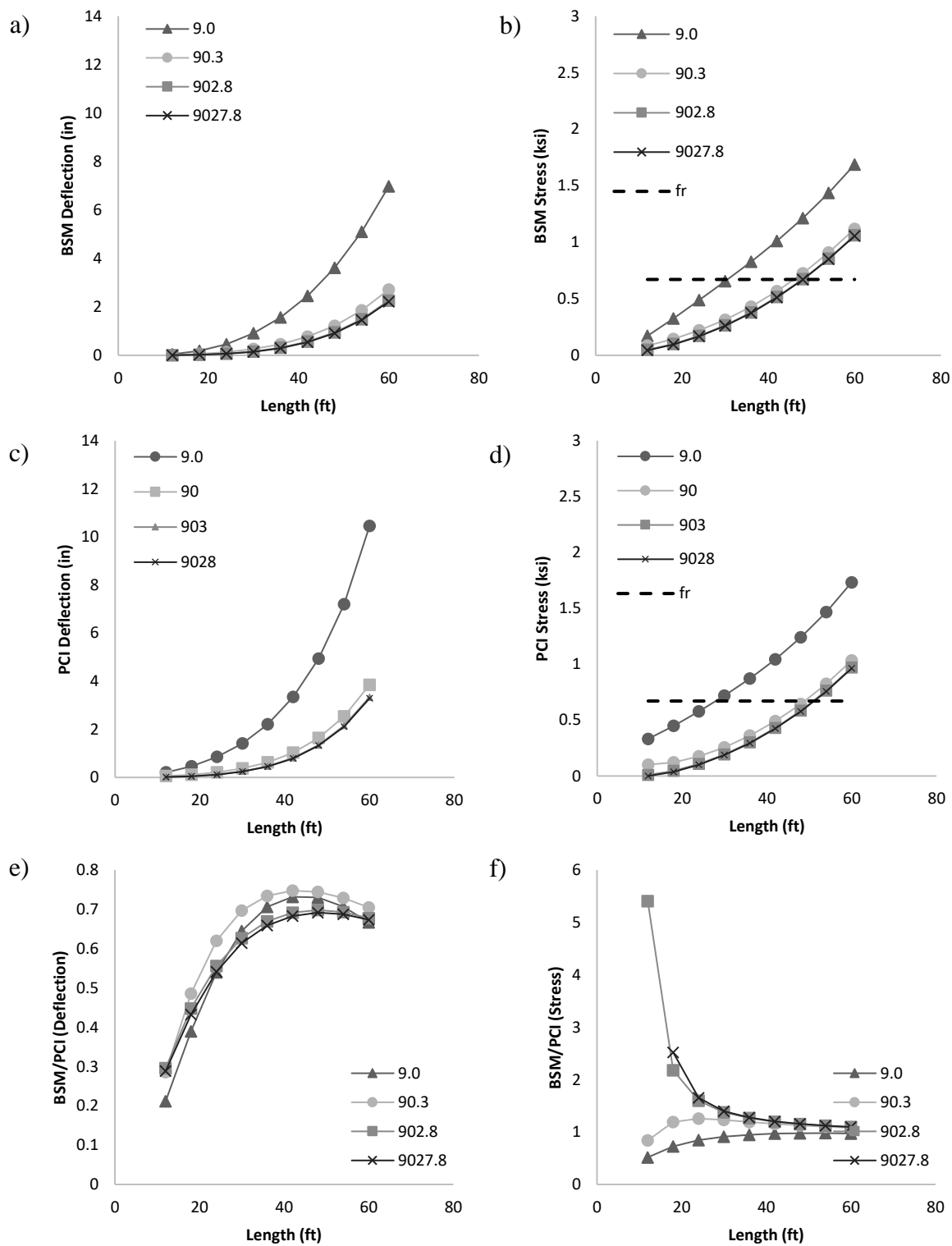


Figure 5-12 BSM and PCI predictions for stress and deflection in a 3-4-3 SWP: a) BSM deflection, b) BSM stress, c) PCI deflection, d) PCI stress, e) ratio of BSM/PCI deflection, and f) ratio of BSM/PCI stress

As expected, deflection and stress at the midheight increase with panel height. By observation, the relationship between stress or deflection and length appears to be quadratic or exponential in nature. By looking at the individual predictions of the BSM and PCI methods, it is also immediately apparent that stiffness greatly effects the behavior of the panel. Although the general shape of the relationship of deflection or stress vs. length is similar, it appears that there is a certain threshold where, when passed, an increase in stiffness has minimal effect on behavior (compare lines for stiffness values equal to 903 and 9028 k/in/ft² among all plots). This is because the stiffness has begun to approach the upper plateau of the logistical relationship between stiffness and degree composite action (see Figure 5-9).

As stated, plots (e) and (f) in Figure 5-10 thru Figure 5-12 display the ratios of BSM predicted values to those predicted by the PCI Second Order analysis. At first glance the plots of the stress ratios is concerning, showing that the BSM predicts some stresses up to 5 times greater than the PCI predictions. Upon closer examination, however, it is quickly noted that this large ratio is due to the fact that the stresses predicted by the PCI method for shorter lengths and higher stiffness are very small (near zero). It is intuitive that this would be the case, that deflections would be minimal for shorter, stiffer panels. Having a number near zero in the denominator of a ratio means that it is much more likely for the ratio to be large. Therefore the ratios presented are useful and interesting, but have their limitations. The ratios show that the current practice of using the PCI Second Order analysis is conservative for deflection prediction as ratios tend to fall at or below 1 in every instance, peaking around 0.748 when using a 3-4-3

configuration with minimal panel stiffness. This means that the PCI method is conservative for deflection calculation.

Ratios of stress predictions were much closer to 1 for stiffnesses around 100 kips/in/ft² or less. As insulation thickness increased, the ratio of predictions between the BSM and PCI methods also increased. This indicates that PCI approximations are closer to BSM approximations as insulation thickness is reduced. Because greater insulation and panel thicknesses yielded values exceeding 1.0, it is recommended that testing be performed to assess accuracy of PCI method predictions to ensure that predictions are not unconservative for thicker SWP insulation configurations. It should be remembered that the PCI calculations rely on an accurate estimate of the moment of inertia and section moduli, which are inherently difficult to predict for panel behavior. This may explain the deviance in predictions from using the PCI method and the BSM method.

Finally, a comparison of the values for different wythe configurations shows that greater insulation thickness also tends to lead decreased deflection and decreased stress. It is also interesting to note in comparing plots (e), that as insulation thickness increases, the ratio of BSM/PCI predictions becomes very consistent for different panel stiffnesses. This can be seen by the spread between lines in Figure 5-10(e) compared with the dense overlay of lines in Figure 5-12 (e). This seems to indicate that the relationship between the BSM and PCI methods becomes more consistent as wythe thickness increases, or the disparity between the two becomes more predictable and stiffness becomes a less influential variable. More simulations should be run to validate this hypothesis, though it seems plausible based on the results presented for the 3-in concrete wythe SWPs.

CHAPTER 6

CONCLUSIONS

Concrete sandwich wall panels are one of the most thermally efficient building envelopes today, and are increasing in popularity due to the combination of their natural resistance to heat transfer and their superior thermal mass as compared to other systems. Although they are inherently thermally superior to other building envelope systems, one of the keys to maximizing the thermal benefits of this system is proper detailing of the SWP connections.

One of the primary foci of this study was understanding thermal performance of SWP structures through conscientious detailing and through the development of alternative designs for the purpose of reducing or eliminating thermal bridging. When heat transfer occurs in SWP structures, it tends to occur in similar locations from building to building. This study involved the thermal imaging of 79 SWP structures across the United State of America to identify good and poor details commonly used in industry. Building details were then obtained and analyzed to compile examples of good details and better details for use in future construction to optimize the thermal potential for efficiency of SWP structures. Thermal analyses were performed identifying common locations of thermal bridging, including windows and doors, solid sections, wall penetrations, lifting points, corbels, roof termination, floor termination, connections to the foundation, corners, panel-to-panel connections, insulation joints, and metal SWP connectors. This dissertation discussed these details and provided recommendations for future construction. Examples of thermal analyses were also presented in this report and

illustrated the impact on thermal efficiency of various details. It is recommended that architects, engineers, and designers utilize thermal analyses of structural details prior to construction so that optimal thermal efficiency is achieved. By implementing the suggestions set forth in this report, energy use will be decreased, more sustainable designs will be created to more effectively compete against other modes of construction in the industry, and significant money will be saved for clients by lowering heating and cooling costs. The majority of thermal bridging in SWP buildings can be avoided by consciously designing to avoid it.

It is important to note that all buildings experience heat transfer, and while this dissertation has presented many ways to improve detailing to minimize thermal bridging, the vast majority of contemporary panels perform very well and meet owner expectations.

A very common location of thermal bridging in SWP structures was at corbel locations. For this reason, this study also undertook an experimental program in which corbel specimens were designed, created, and tested in an attempt to provide alternative corbel details for use in industry that better capitalize upon the potential for structural and thermal efficiency that exists in partially-composite concrete SWP structures. A total of 12 corbel specimens were created and tested at the Utah State University SMASH Lab to demonstrate structural adequacy of the designs. The most important conclusion of the results was that thermal bridging at corbel connections is avoidable and, therefore, unnecessary. Of specimens tested, those using GFRP grating achieved the greatest composite action and consequently the highest ultimate capacities. Another significant

finding was that SWP connectors can be used to transfer the primary tension force in corbel connections, providing a convenient and affordable way to transfer local corbel loads between partially-composite wythes.

The final portion of this study focused on predicting SWP behavior when subjected to axial and flexural loads. The corbel specimens tested herein were modeled using the Beam-Spring Method with great success. Ratios of predicted-to-measured elastic slope for applied load vs. slip were calculated with an average ratio of 1.014 and a standard deviation of 0.286, showing good agreement between predicted and measured results. The Beam-Spring Method was validated for use with SWPs subjected to axial loads. A parametric study was performed with the Beam-Spring Method, investigating the influence of length, connector stiffness, and wythe configurations on SWP behavior. Models were created for 270 different panels with lengths varying from 12 to 60 ft in 6 ft increments, stiffnesses varying from 0.0001 to 10,000,000 kips/in by powers of 10, and with wythe configurations of 3-2-3, 3-3-3, and 3-4-3 being considered. Predictions of the BSM were compared to the PCI Second-Order Analysis for application to SWPs, demonstrating that the BSM yielded comparable predictions to the PCI method. It was noted that PCI Second-Order Analysis predictions, as applied to SWP analysis, were generally conservative for deflection predictions and often conservative for stress predictions. Further research should be performed to assess how conservative the PCI predictions are for stress prediction for thicker insulation wythe configurations when utilizing very stiff connectors. Degree of composite action was shown to exhibit a logistic relationship with panel stiffness. This parametric study could potentially be expanded to

create design tables as an additional resource for engineers designing SWPs under axial and flexural loads. Such tables would need to account for various SWP connector configurations, lengths, and additional stiffnesses, but could ultimately be used similar to those included in the AISC Steel Construction Manual.

In summary, the following conclusions can be made from this study:

- Regarding SWP thermal efficiency:
 - Concrete SWP construction can provide a very thermally efficient building envelope.
 - Thermal bridging tends to occur at similar locations among SWP structures.
 - Thermal bridging can be avoided in SWP structures by proper detailing and careful attention.
 - Use of steel SWP connectors is extremely detrimental to thermal performance of SWP structures and should be avoided.
- Regarding SWP corbel connections:
 - Thermal bridging at corbel connections is avoidable.
 - Specimens using GFRP grating achieved the greatest composite action and consequently the highest ultimate capacities.
 - FRP grating can be used in corbels to improve thermal performance and structural efficiency.
 - SWP connectors can be used in corbel connections to transfer the applied loads between wythes without creating thermal bridging.

- HDO prisms embedded in concrete can provide adequate compressive strength for corbel connections, although further research is required regarding absorption and potential for HDO expansion in concrete.
- Regarding prediction of SWP behavior under axial and flexural loads:
 - The Beam-Spring Model accurately predicted SWP performance of panels under axial loads with an average ratio of predicted-to-measured elastic slope for applied load vs. slip of 1.014 and a standard deviation of 0.286.
 - Moment magnification was quantified to be between 5-15% for SWPs modeled and presented herein.
 - The PCI Second-Order Analysis generally provides conservative predictions for deflection due to second-order effects.
 - The PCI Second-Order Analysis often provides conservative predictions for stress due to second-order effects, particularly for smaller insulation thicknesses.
 - The BSM yields comparable predictions to the PCI method.
 - Degree of composite action exhibits a logistic relationship with panel stiffness

Possible areas for future work recommended from this project include:

- Comparison of SWP thermal performance to that of other building envelope types

- Additional testing of corbel specimens to validate the findings herein
- Quantifying the capacity provided by transverse bars embedded in thin concrete sections under concrete break out conditions.
- Validating quantification of shallow plate embedment in SWPs
- Expansion of parametric study to investigate effects of connector distributions, eccentricity magnitude, connector configurations, and additional wythe thicknesses on SWP behavior under combined loading
- Development of design tables for SWP design under axial and flexural loads

REFERENCES

- ACI 318-14. (2014). *Building Code Requirements for Structural Concrete*. Farmington Hills, MI: American Concrete Institute.
- ACI 440.1R-15. (2015). *Guide for the Design and Construction of Structural Concrete Reinforced with Fiber-Reinforced Polymer (FRP) Bars*. Farmington Hills, MI: American Concrete Institute.
- ACMA. (2014). *FRP Composites Grating Manual: For Pultruded and Molded Grating and Stair Treads* (1st ed.). Arlington, VA: American Composites Manufacturers Association. Retrieved from http://www.acmaeducationhub.org/Files/Org/9b2c8431fc504376b7ffb965213316fe/LearningProduct/1-10Pages_from_FRP_Composites_Grating_Manual_v8a.pdf
- AISC. (2011). *Steel Construction Manual* (14th ed.). Chicago, IL: American Institute of Steel Construction.
- Al-Homoud, M. S. (2005, March). Performance Characteristics and Practical Applications of Common Building Thermal Insulation Materials. *Building and Environment*, 40(3), 353-366.
- Allen, H. (1969). *Analysis and Design of Structural Sandwich Panels*. Oxford, London: Pergamon Press.
- Al-Rubaye, S., Sorensen, T., & Maguire, M. (2017). Investigating Composite Action at Ultimate for Commercial Sandwich Wall Panel Composite Connectors. *PCI/NBC*. Cleveland, OH.

Al-Rubaye, S., Sorensen, T., Dorafshan, S., & Maguire, M. (2018). Matrix Model

Accuracy of Partially Composite Concrete Sandwich Panels. *PCI/NBC*.

Cleveland, OH.

Al-Rubaye, S., Sorensen, T., Olsen, J., & Maguire, M. (2018). Evaluating Elastic

Behavior for Partially Composite Precast Concrete Sandwich Wall Panels. *PCI*

Journal, 71-88.

Altus Group, Inc. (2012). *CarbonCast High Performance Insulated Wall Panels with C-*

Grid carbon fiber epoxy grid shear connections. Bethlehem, PA: Altus Group,

Inc. Retrieved from <https://altusprecast.com/wp-content/uploads/carboncast->

[insulated-wall-panel-tech-brief_092012.pdf](https://altusprecast.com/wp-content/uploads/carboncast-insulated-wall-panel-tech-brief_092012.pdf)

Altus Group, Inc. (2018). High-Performance Insulated Sandwich Walls Using Composite

Design. Greenville, SC, USA. Retrieved from

<https://www.aecdaily.com/course/797160/html5/index.html>

ANSI/ASHRAE/IES Standard 90.1-2016 . (2016). *Energy Standard for Buildings Except*

Low-Rise Residential Buidlings. Atlanta, GA: ASHRAE.

APA. (2011). *HDO/MDO Plywood Product Guide*. Tacoma, WA: APA- The Engineered

Wood Association. Retrieved from

https://murphyplywood.com/pdfs/softwood/HDO_MDO_Product_Guides.pdf

APA D510C. (2012). *Panel Design Specification*. Tacoma, WA: The Engineered Wood

Association.

ASHRAE. (2013). *ASHRAE Handbook 2013- Fundamentals*. Atlanta, GA: ASHRAE.

- ASTM C1363. (2011). *Standard Test Method for Thermal Performance of Building Materials and Envelope Assemblies by Means of a Hot Box Apparatus*. West Conshohocken, PA: ASTM International. doi:10.1520/C1363-11
- ASTM C236. (1993). *Standard Test Method for Steady-State Thermal Performance of Building Assemblies by Means of a Guarded Hot Box (Withdrawn 2001)*. West Conshohocken, PA: ASTM International. doi:10.1520/C0236-89R93E01
- ASTM C31/C31M-17. (2017). *Standard Practice for Making and Curing Concrete Test Specimens in the Field*. West Conshohocken, PA: ASTM International. doi:10.1520/C0031_C0031M-17
- ASTM C39/C39M-17a. (2017). *Standard Test Method for Compressive Strength of Cylindrical Concrete Specimens*. West Conshohocken, PA: ASTM International. doi:10.1520/C0039_C0039M-17A
- ASTM C469/C469M-14. (2014). *Standard Test Method for Static Modulus of Elasticity and Poisson's Ratio of Concrete in Compression*. West Conshohocken, PA: ASTM International. doi:10.1520/C0469_C0469M-14
- ASTM C496/C496-17. (2017). *Standard Test Method for Splitting Tensile Strength of Cylindrical Concrete Specimens*. West Conshohocken, PA: ASTM International. doi:10.1520/C0496_C0496M-17
- ASTM C518-17. (2017). *Standard Test Method for Steady-State Thermal Transmission Properties by Means of the Heat Flow Meter Apparatus*. West Conshohocken, PA: ASTM International. doi:10.1520/C0518-17

ASTM D1621-16. (2016). *Standard Test Method for Compressive Properties of Rigid Cellular Plastics*. West Conshohocken, PA: ASTM International.

doi:10.1520/D1621-16

Batie, S. (2012, May 12). Column: Wooden posts in concrete is a recipe for disaster.

Herald & Review. Retrieved from https://herald-review.com/news/opinion/editorial/columnists/houseworks/column-wooden-posts-in-concrete-is-a-recipe-for-disaster/article_640f7b74-9b78-11e1-ac9d-0019bb2963f4.html

Benayoune, A., Samad, A., Abang Ali, A., & Trikha, D. (2007). Response of Pre-cast Reinforced Composite Sandwich Panels to Axial Loading. *Construction and Building Materials*, 21(3), 677-685.

Benayoune, A., Samad, A., Trikha, D., Abang Ali, A., & Ashrabov, A. (2006). Structural Behavior of Eccentrically Loaded Precast Sandwich Panels. *Construction and Building Materials*, 20(9), 713-724.

Brown, M. D., Sankovich, C. L., Bayrak, O., Jirsa, J. O., Breen, J. E., & Wood, S. L. (2005). *Design for Shear in Reinforced Concrete Using Strut-and-Tie Models*. Austin, TX: The University of Texas at Austin. Retrieved from http://ctr.utexas.edu/wp-content/uploads/pubs/0_4371_2.pdf

Collins, F. T. (1954). Precast Concrete Sandwich Panels for Tilt-up Construction. *Journal of the American Concrete Institute*, 26(2), 149-164.

Dow. (n.d.). *STYROFOAM Brand Scoreboard Extruded Polystyrene Foam Insulation*. Retrieved from

http://msdssearch.dow.com/PublishedLiteratureDOWCOM/dh_09a0/0901b80380

[9a0341.pdf?filepath=styrofoam/pdfs/noreg/179-04435.pdf&fromPage=GetDoc](http://msdssearch.dow.com/PublishedLiteratureDOWCOM/dh_09a0/0901b803809a0341.pdf?filepath=styrofoam/pdfs/noreg/179-04435.pdf&fromPage=GetDoc)

Einea, A., Salmon, D., Fogarasi, G., Culp, T., & Tadros, M. (1991). State-of-of-the-Art of Precast Concrete Sandwich Panels. *PCI Journal*, 36(6), 78-98.

Einea, A., Salmon, D., Tadros, M., & Culp, T. (1994). A New Structurally and Thermally Efficient Precast Sandwich Panel System. *Concrete International*, 39(4), 90-101.

Elkady, M. (2013). *Precast Concrete Insulated Wall Panel Corbels Without Thermal Bridging*. Lincoln, NE: University of Nebraska.

Elzanaty, A. H., Nilson, A. H., & Slate, F. O. (1986). Shear Capacity of Reinforced Concrete Beams Using High Strength Concrete. *ACI Journal Proceedings*, 83(2), 290-296.

Engineering ToolBox. (2003). *Young's Modulus- Tensile and Yield Strength for Common Materials*. Retrieved 04 16, 2019, from

https://www.engineeringtoolbox.com/young-modulus-d_417.html

FDOT. (2016). *Index D21310 Fiber Reinforced Polymer (FRP) Bar Bending Details*.

Florida Department of Transportation. Retrieved from

https://fdotwww.blob.core.windows.net/sitefinity/docs/default-source/content2/roadway/ds/dev/idds/idds-d21310.pdf?sfvrsn=9dd0b073_0

Frankl, B. A., Lucier, G. W., Hassan, T. K., & Rizkalla, S. H. (2011). Behavior of Precast, Prestressed Concrete Sandwich Wall Panels Reinforced with CFRP Shear Grid. *PCI Journal*, 56(2), 42-54. doi:10.15554/pcij.03012011.42.54

- Frankl, B., Lucier, G., Rizkalla, S., Blaszak, G., & Harmon, T. (2008). Structural Behavior of Insulated Prestressed Concrete Sandwich Panels Reinforced with FRP Grid. *Fourth International Conference on FRP Composites in Civil Engineering (CICE2008)*. Zurich, Switzerland: International Institute for FRP in Construction. Retrieved from http://www.iifc.org/proceedings/CICE_2008/papers/2.C.2.pdf
- Frostig, Y., & Baruch, M. (1990). Bending of Sandwich Beams with Transversely Flexible Core. *AIAA Journal*, 28(3), 523-531.
- Gordaninejad, F., & Bert, C. (1989). A New Theory for Bending of Thick Sandwich Beams. *International Journal of Mechanical Sciences*, 31(11-12), 925-934. doi:10.1016/0020-7403(89)90033-7
- Ha, K. (1992). Exact Analysis of Bendign and Overall Buckling of Sandwich Beam Systems. *Computers & Structures*, 45(1), 31-40. doi:10.1016/0045-7949(92)90342-W
- Hassan, T. K., & Rizkalla, S. H. (2010). Analysis and Design Guidelines of Precast, Prestressed Concrete, Composite Load-Bearing Sandwich Wall Panels Reinforced With GFRP Grid. *PCI Journal*, 1-16.
- Holladay, M. (2016a). *Choosing Rigid Foam*. (The Taunton Press, Inc.) Retrieved from Green Building Advisor: <http://www.greenbuildingadvisor.com/articles/dept/musings/choosing-rigid-foam>
- Holladay, M. (2016b). *Thermal Drift of Polyiso and XPS*. (The Taunton Press, Inc.) Retrieved from Green Building Advisor:

<http://www.greenbuildingadvisor.com/articles/dept/musings/thermal-drift-polyiso-and-xps>

Holmberg, A., & Plem, E. (1965). *Behavior of Load Bearing Sandwich-Type Structures*. Byggforskningen.

Incropera, F., & DeWitt, D. (2002). *Fundamentals of Heat and Mass Transfer* (5th ed.). New York, NY: John Wiley & Sons.

International Code Council, Inc. (2009). *2009 International Energy Conservation Code*. Country Club Hills, IL: International Code Council, Inc.

International Code Council, Inc. (2017). *2018 International Energy Conservation Code*. Country Club Hills, IL: International Code Council, Inc.

Kerkstra Precast. (2014, 09 16). *Wall Panel- Spot Corbel (12" Wide)*. Retrieved from https://www.kerkstra.com/uploads/9/9/2/4/99244278/3220-_wall_panel_-_spot_corbel_12_inches_wide.pdf

Kerkstra Precast. (2016, 01 23). *Wall Panel Hollowcore/Solid Slab Corbel*. Retrieved from https://www.kerkstra.com/uploads/9/9/2/4/99244278/3221-_wall_panel_hollowcore-_solid_slab_corbel.pdf

Kriz, L. B., & Raths, C. H. (1965, February). Connections in Precast Concrete Structures- Strength of Corbels. *PCI Journal*, 16-61.

Lee, B., & Pessiki, S. (2008). Revised Zone Method R-value Calculation for Precast Concrete Sandwich Panels Containing Metal Wythe Connectors. *PCI Journal*, 53(5), 86-100.

- Mattock, A. H., Chen, K. C., & Soongswang, K. (1976). The Behavior of Reinforced Concrete Corbels. *PCI Journal*, 52-77.
- Mottram, J. (2004). Shear Modulus of Standard Pultruded Fiber Reinforced Plastic Material. *Journal of Composites for Construction*, 8(2).
doi:10.1061/(ASCE)1090-0268(2004)8:2(141)
- Olsen, J., & Maguire, M. (2016). Shear Testing of Precast Concrete Sandwich Wall Panel Composite Shear Connectors. *PCI/NBC*. Nashville, TN.
- Olsen, J., Al-Rubaye, S., Sorensen, T., & Maguire, M. (2017). *Developing a General Methodology for Evaluating Composite Action in Insulated Sandwich Wall Panels*. Chicago, IL: Report Submitted to the PCI.
- Paydar, N., & Park, G. (1990). Optimal Design of Sandwich Beams. *Computers & Structures*, 34(4), 523-526.
- PCI. (2010). *PCI Design Handbook: MNL-120-10* (7th ed.). Chicago, IL: Precast/Prestressed Concrete Institute.
- PCI. (2011). State of the Art of Precast/Prestressed Concrete Sandwich Wall Panels. *PCI Journal*, 56(2), 131-176.
- Pessiki, S., & Lee, B. (2003). *Development of the Characteristic Section Method to Estimate Thermal R-Values for Precast Concrete Sandwich Wall Panels: Paper 27*. ATLSS Reports. Retrieved from <http://preserve.lehigh.edu/engr-civil-environmental-atlss-reports/27>
- Pessiki, S., & Mlynarczyk, A. (2003). Experimental Evaluation of the Composite Behavior of Precast Concrete Sandwich Wall Panels. *PCI Journal*, 54-71.

Salmon, D., & Einea, A. (1995). Partially Composite Sandwich Panel Deflections.

Journal of Structural Engineering, 121(4), 778-783.

Salmon, D., Einea, A., Tadros, M., & Culp, T. (1997). Full Scale Testing of Precast

Concrete Sandwich Panels. *ACI Structural Journal*, 354-362.

Seshappa, V., & Dixon, D. (2013). Best Practices in Precast Insulated Wall Panel Design

and Detailing. *PCI/NBC*. Grapevine, TX.

Sorensen, T., & Maguire, M. (2017). *Phase 1: Identification of Energy-Efficient*

Detailing for Concrete Sandwich Wall Panels. Logan, UT: Utah State University.

Sorensen, T., Dorafshan, S., & Maguire, M. (2017). Thermal Evaluation of Common

Locations of Heat Loss in Sandwich Wall Panels. *ASCE Congress on Technical*

Advancement. Duluth, MN.

Tomlinson, D. (2015). *Behaviour of Partially Composite Precast Concrete Sandwich*

Panels Under Flexural and Axial Loads. Kingston, Ontario, Canada: Queen's

University.

U.S. Energy Information Administration. (2012). *Major Fuel Consumption (Btu) by End*

Use, 2012: Table E1. In Forms EIA-871A, C, D, E, and F of the 2012

Commercial Buildings Energy Consumption Survey. Office of Energy

Consumption and Efficiency Statistics. Retrieved from

<https://www.eia.gov/consumption/commercial/data/2012/index.php?view=consumption#e1-e11>

U.S. Energy Information Administration. (2017). *Monthly Energy Review: Table 1.3.*

Office of Energy Consumption and Efficiency Statistics. Retrieved from

<https://www.eia.gov/totalenergy/data/monthly/pdf/mer.pdf>

U.S. Energy Information Administration. (2009). *Summary Household Site Consumption*

and Expenditures in the U.S.: Table CE1.1. In Forms EIA-457 A and C-G of the

2009 Residential Energy Consumption Survey. Office of Energy Consumption

and Efficiency Statistics. Retrieved from

<https://www.eia.gov/consumption/residential/data/2009/index.php?view=consumption>

APPENDICES

APPENDIX A. THERMAL ANALYSIS EXAMPLES

Material Properties

All examples in this report used the same material conductivities. These values are expressed in Table A-1 and were obtained from the *ASHRAE Handbook 2013-Fundamentals* and *Fundamentals of Heat and Mass Transfer* (Incropera & DeWitt, 2002).

Table A-1 Material conductivities used in this study

Material	Conductivity, k	
	<i>(BTU·in/hr·ft²·°F)</i>	<i>(W/m·K)</i>
Concrete	13.33	1.923
Insulation (XPS)	0.18	0.026
Carbon Steel	443	63.9

The surface air film resistances were assumed to be the same for all panels, and are summarized in Table A-2. These values were also obtained from the *ASHRAE Handbook 2013-Fundamentals* in Table 10 of Chapter 26 (ASHRAE, 2013).

Table A-2 Surface air film resistances

Variable	Resistance, R	
	$(hr \cdot ft^2 \cdot ^\circ F / BTU)$	$(m^2 \cdot K / W)$
R_i	0.68	0.120
R_o (summer)	0.25	0.044
R_o (winter)	0.17	0.030

Exclusion of Steel

As expressed earlier, the inclusion of the steel property becomes negligible to the heat transfer that occurs through the section when solid sections are created around a steel connection that does not penetrate the entire thickness of the panel. To demonstrate the insignificance of this exclusion, a floor connection was analyzed to compare the effects of including the steel element in the calculations. First, the inclusion of the steel component was calculated. A steel connection in the middle of a 1 ft \times 1 ft solid concrete section placed every 6 ft on center (o.c.) was modeled with and without the steel using the isothermal-planes method to compare the effects of including the steel element (Figure A-). The isothermal-planes method was selected because the zone method is only valid when the steel is present, so to maintain equal grounds for comparison, the isothermal-planes method was used for both.

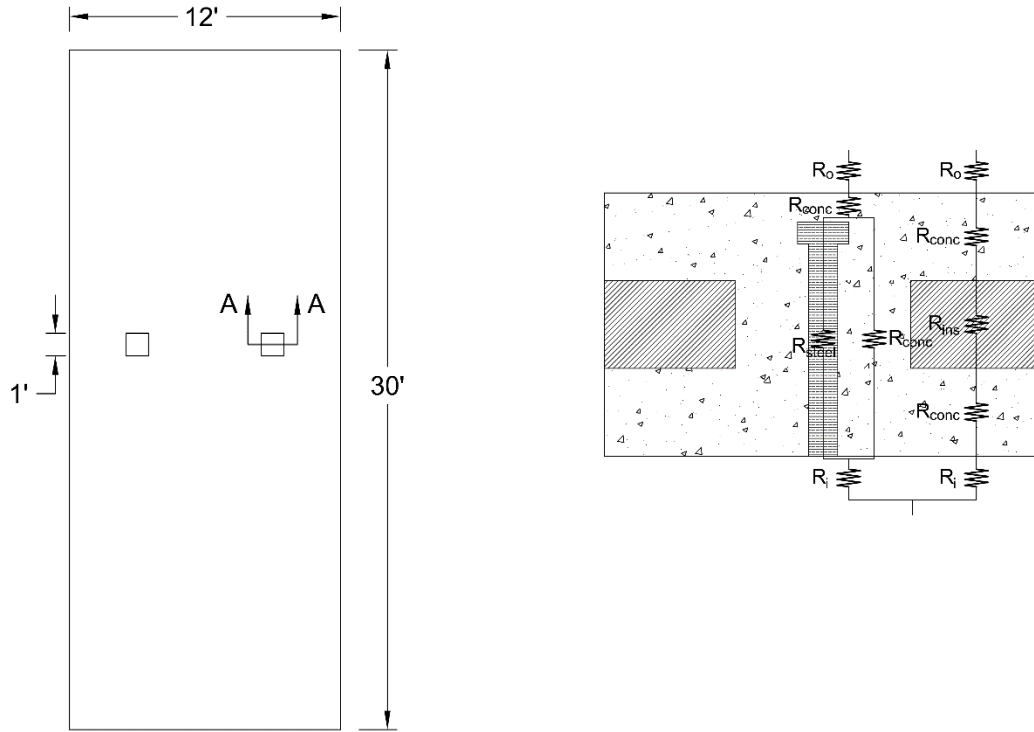


Figure A-1 Panel layout and cross-section with electrical circuit analogy

The metal plate was assumed to have an embedment rod diameter of 1 inch and an embedment depth of 8 inches. The thermal analysis is easier to follow using the S.I. system since the unit conversions are simpler than the English system, so calculations are shown here in metrics. Area proportions must be calculated to weight the influence of each thermal resistance appropriately. The fractional areas for the concrete and steel in the solid section are

$$a_{steel} = \frac{A_{steel}}{A_{conc}} = \frac{5.07 * 10^{-4} m^2}{0.09 m^2} = 0.00003$$

$$a_{conc} = 1 - a_{steel} = 0.99997.$$

The fractional area of solid section vs the observed area are

$$a_{solid} = \frac{A_{solid}}{A_{obs}} = \frac{0.09 \text{ m}^2}{16.72 \text{ m}^2} = 0.006$$

$$a_{ins} = 1 - a_{solid} = 0.994$$

where A_{obs} = observed area (total area divided by no. of connectors per panel).

The two paths in series shall be calculated separately and then combined using parallel-path method [see Equation (3-4)] as follows:

$$R = \frac{1}{\frac{a_{solid}}{R_o + R_{cover} + \frac{1}{\frac{a_{steel}}{R_{steel}} + \frac{a_{conc}}{R_{conc}}}} + R_i} + \frac{a_{ins}}{R_o + R_{wo} + R_{ins} + R_{wi} + R_i}.$$

where R_o = thermal resistance of outdoor air film

R_i = thermal resistance of outdoor air film

R can be calculated as

$$R = \frac{t}{k}$$

where t = thickness of the layer in the direction of heat flow

k = thermal conductivity.

The R-values for each component using this equation are shown in the following table.

Element	Thickness, t (m)	Conductivity, k (W/m·K)	Thermal Resistance (m ² ·K/W)
Outdoor air film (summer)	n.a.	n.a.	$R_o = 0.044$
Outdoor air film (winter)	n.a.	n.a.	$R_o = 0.030$
Concrete cover over embed	0.025	1.923	$R_{cover} = 0.013$
Steel	0.203	63.9	$R_{steel} = 0.003$
Solid concrete parallel to steel	0.203	1.923	$R_{conc} = 0.106$
Regular concrete wythes	0.076	1.923	$R_{wo} = R_{wi} = 0.040$
Insulation wythe	0.076	0.026	$R_{ins} = 2.935$
Indoor air film	n.a.	n.a.	$R_i = 0.120$

For winter,

$$R = \frac{1}{\frac{0.006}{0.044 + 0.013 + \frac{1}{\frac{0.00003}{0.003} + \frac{0.99997}{0.106}}} + 0.12} + \frac{0.994}{0.044 + 2 * 0.040 + 2.935 + 0.12}$$

$$= 2.98527 \frac{m^2 \cdot K}{W}.$$

For summer,

$$R = \frac{1}{\frac{0.006}{0.030 + 0.013 + \frac{1}{\frac{0.00003}{0.003} + \frac{0.99997}{0.106}}} + 0.12} + \frac{0.994}{0.030 + 2 * 0.040 + 2.935 + 0.12}$$

$$= 3.00704 \frac{m^2 \cdot K}{W}.$$

These calculations were then repeated using conductivity of concrete in place of steel (the same as modeling a solid concrete section) with the following results.

For winter,

$$R = \frac{1}{\frac{0.006}{0.044 + 0.013 + \frac{1}{\frac{0.00003}{0.106} + \frac{0.99997}{0.106}}} + 0.12} + \frac{0.994}{0.044 + 2 * 0.040 + 2.935 + 0.12}$$

$$= 2.98534 \frac{m^2 \cdot K}{W}.$$

For summer,

$$R = \frac{1}{\frac{0.006}{0.030 + 0.013 + \frac{1}{\frac{0.00003}{0.106} + \frac{0.99997}{0.106}}} + 0.12} + \frac{0.994}{0.030 + 2 * 0.040 + 2.935 + 0.12}$$

$$= 3.00710 \frac{m^2 \cdot K}{W}.$$

These results are summarized in the following table.

Season	Including Steel, R_{inc}	Excluding Steel, R_{exc}	Difference, $(R_{inc} - R_{exc})/R_{inc}$
Summer	2.98527	2.98534	0.00237%
Winter	3.00704	3.00710	0.00216%

Note that the difference between the values is about two thousandths of a percent.

This is likely due to the fact that concrete is already significantly more conductive than the insulation (74 times more conductive using the values in this example). Although steel is even more conductive than concrete (a little less than 5 times as conductive as concrete), the difference in conductivity is not nearly as drastic as the difference between the conductivity of the concrete and the insulation. Also, the area is small and this steel is

not penetrating the entire thickness of the concrete, so the heat still must travel through the concrete to exit the panel. Due to the insignificant contribution of the steel to the R-value, inclusion of the steel is unnecessary and is excluded from many of the following examples.

Window Example

Consider a 12 ft \times 30 ft panel with one 4 ft \times 4 ft window in the middle with 2 inches (0.05 m) of solid concrete penetrating the insulation around the window edges. The characteristic section method is the most appropriate method to use for a most accurate prediction of panel R-value since we are dealing with a solid concrete section.

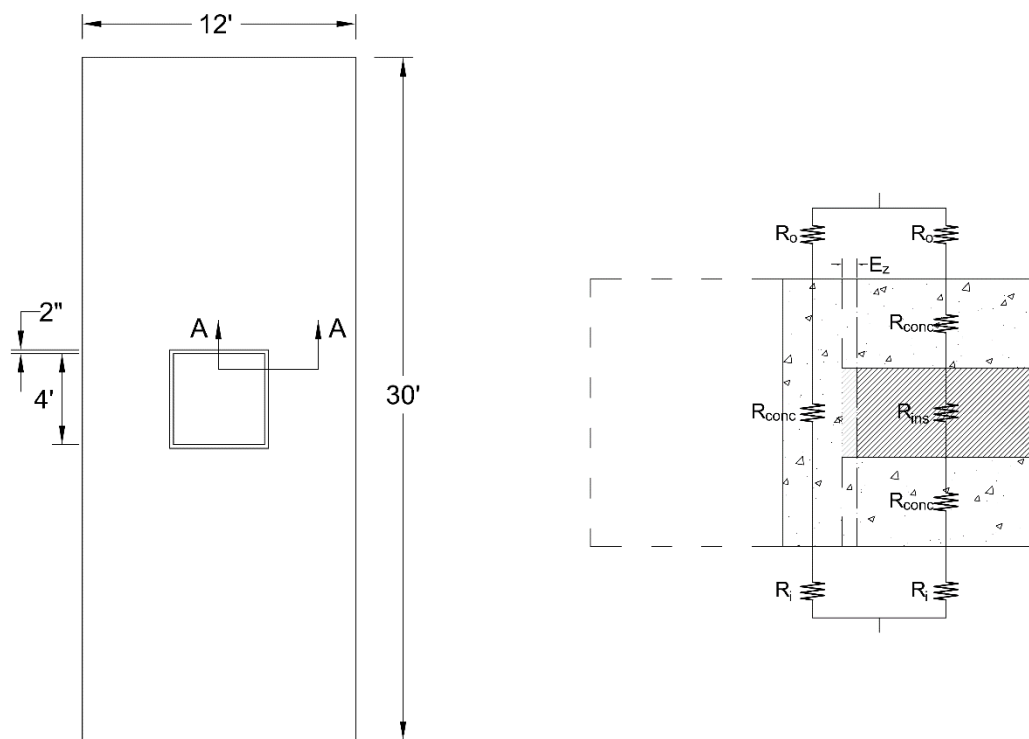


Figure A-2 Window example panel layout and cross-section with electrical circuit analogy

First calculate the affected zone dimensions. Remember that these empirical equations require that units be input as inches and BTU·in/[hr·ft²·°F] to work.

$$E_z = 1.4 - 0.1\alpha t_{ins} + \beta[0.4t_{wo} + 0.1(t_{wi} - t_{wo})]$$

$$\alpha = 1 + 2.25 * \left(\frac{0.026 - 0.26}{0.26} \right) = 0.308$$

$$\beta = 1 + 1.458 * \left(\frac{1.923 - 12.05}{12.05} \right) = 1.155$$

$$\begin{aligned} E_z &= 1.4 - 0.1(0.308)(3 \text{ inches}) \\ &\quad + 1.155[0.4(3 \text{ inches}) + 0.1(3 \text{ inches} - 3 \text{ inches})] \\ &= 2.694 \text{ in} = \mathbf{0.068 \text{ m}} \end{aligned}$$

Next calculate the fractional area percentages. This will be done by calculating the total panel area without the window and then the area of the affected section.

$$A_{total} = 3.66 \text{ m} * 9.14 \text{ m} - (1.22 \text{ m})^2 = 31.959 \text{ m}^2$$

$$\begin{aligned} b_{aff} &= b_{win} + b_{solid} + 2 * E_z = 1.22 \text{ m} + 0.05 \text{ m} + 2 * 0.068 \text{ m} \\ &= 1.458 \text{ m} \end{aligned}$$

$$\begin{aligned} h_{aff} &= h_{win} + h_{solid} + 2 * E_z = 1.22 \text{ m} + 0.05 \text{ m} + 2 * 0.068 \text{ m} \\ &= 1.458 \text{ m} \end{aligned}$$

$$A_{aff} = b_{aff} * h_{aff} - A_{win} = 1.458 \text{ m} * 1.458 \text{ m} - (1.22 \text{ m})^2 = 0.638 \text{ m}^2$$

$$a_{aff} = \frac{A_{aff}}{A_{total}} = \frac{0.638 \text{ m}^2}{31.959 \text{ m}^2} = 2.00\%$$

$$a_{insulated} = 1 - a_{aff} = 98.00\%$$

R-value can then be calculated based off of the electrical circuit analogy in Figure A-2 as:

$$R = \frac{1}{\frac{a_{aff}}{R_o + R_{conc} + R_i} + \frac{a_{insulated}}{R_o + R_{wo} + R_{ins} + R_{wi} + R_i}}$$

where R_o = thermal resistance of outdoor air film

R_i = thermal resistance of outdoor air film

R is calculated as

$$R = \frac{t}{k}$$

where t = thickness of the layer in the direction of heat flow

k = thermal conductivity.

The R-values for each component using this equation are shown in the following table.

Element	Thickness, t (m)	Conductivity, k (W/m·K)	Thermal Resistance (m ² ·K/W)
Outdoor air film (summer)	n.a.	n.a.	$R_o = 0.044$
Outdoor air film (winter)	n.a.	n.a.	$R_o = 0.030$
Solid concrete section	0.229	1.923	$R_{conc} = 0.119$
Outside concrete wythe	0.076	1.923	$R_{wo} = 0.040$
Insulation wythe	0.076	0.026	$R_{ins} = 2.935$
Inside concrete wythe	0.076	1.923	$R_{wi} = 0.040$
Indoor air film	n.a.	n.a.	$R_i = 0.120$

For winter,

$$R = \frac{1}{\frac{0.02}{0.030 + 0.119 + 0.120} + \frac{0.98}{0.030 + 0.040 + 2.935 + 0.040 + 0.120}}$$

$$= 2.604 \frac{m^2 \cdot K}{W} = \mathbf{14.784} \frac{ft^2 \cdot ^\circ F \cdot hr}{Btu}.$$

For summer,

$$\begin{aligned}
 R &= \frac{1}{\frac{0.02}{0.044 + 0.119 + 0.120} + \frac{0.98}{0.044 + 0.040 + 2.935 + 0.040 + 0.120}} \\
 &= 2.638 \frac{m^2 \cdot K}{W} = \mathbf{14.982} \frac{ft^2 \cdot ^\circ F \cdot hr}{Btu}.
 \end{aligned}$$

Solid Section Example

Consider a 12 ft × 30 ft solid concrete panel. It involves a system in series as shown in the figure below.

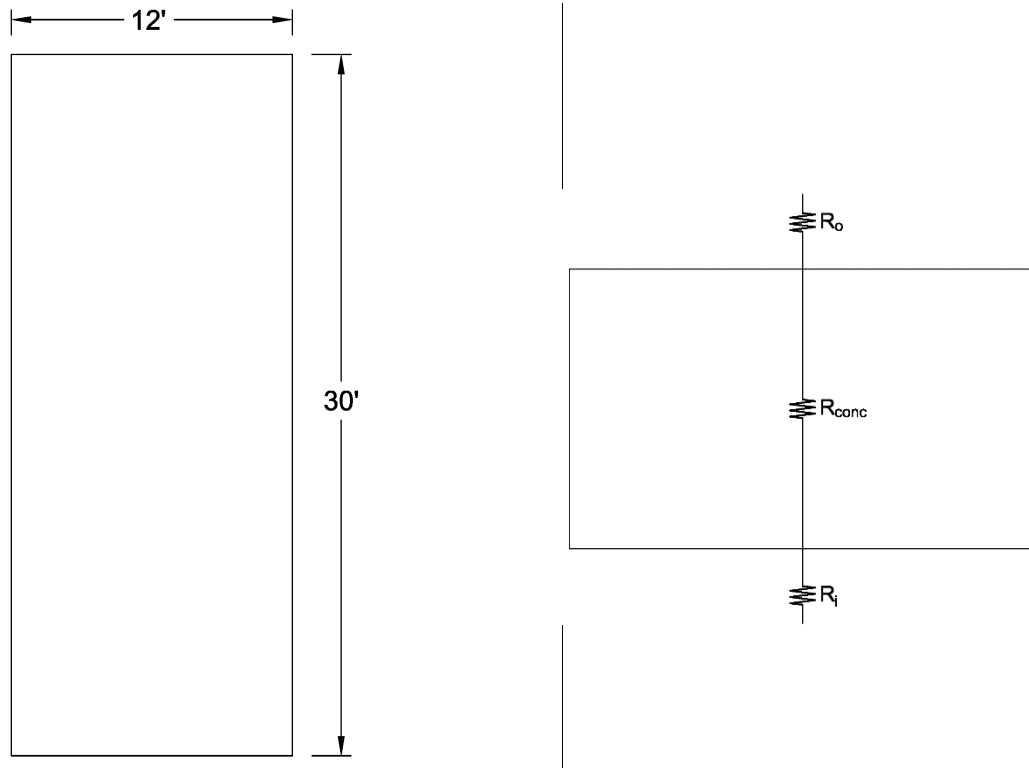


Figure A-3 Solid section example panel layout and cross-section with electrical circuit analogy

Since it is a system in series, the R-value is calculated by summing the R-values together. R is calculated as

$$R = \frac{t}{k}$$

where t = thickness of the layer in the direction of heat flow

k = thermal conductivity.

The R-values for each component using this equation are shown in the following table. Note that thickness of the solid section in this example incorporated the additional thickness of the corbel.

Element	Thickness, t (m)	Conductivity, k (W/m·K)	Thermal Resistance (m ² ·K/W)
Outdoor air film (summer)	n.a.	n.a.	$R_o = 0.044$
Outdoor air film (winter)	n.a.	n.a.	$R_o = 0.030$
Solid concrete section	0.229	1.923	$R_{conc} = 0.119$
Indoor air film	n.a.	n.a.	$R_i = 0.120$

For winter,

$$\begin{aligned}
 R &= R_o + R_{conc} + R_i = 0.044 + 0.119 + 0.120 = 0.269 \frac{m^2 \cdot K}{W} \\
 &= 1.525 \frac{ft^2 \cdot ^\circ F \cdot hr}{Btu}.
 \end{aligned}$$

For summer,

$$\begin{aligned}
 R &= R_o + R_{conc} + R_i = 0.030 + 0.119 + 0.120 = 0.283 \frac{m^2 \cdot K}{W} \\
 &= 1.605 \frac{ft^2 \cdot ^\circ F \cdot hr}{Btu}.
 \end{aligned}$$

Comparing this to the R-value of a perfectly insulated 12 ft × 30 ft panel, a 91.5% decrease is observed in R-value for winter and a 91.1% decrease in summer.

Wall Penetration Example

Consider a 12 ft \times 30 ft non-composite panel (3-3-8) with an external, low-roof attachment where the steel roof beams puncture the insulation to attach to the interior structural wythe. The beams are W6x13 members spaced every 6 ft o.c., and require that a 1 ft \times 1 ft section of insulation are blocked out for each penetration. Three scenarios will be analyzed. The first example will examine this configuration where the blocked out concrete and insulation are not replaced, the second example will explore filling in the blocked out area surrounding the penetrating element with concrete, and the third example will do the same but with insulation. The parallel-path method will be utilized in all three examples.

Not Replaced

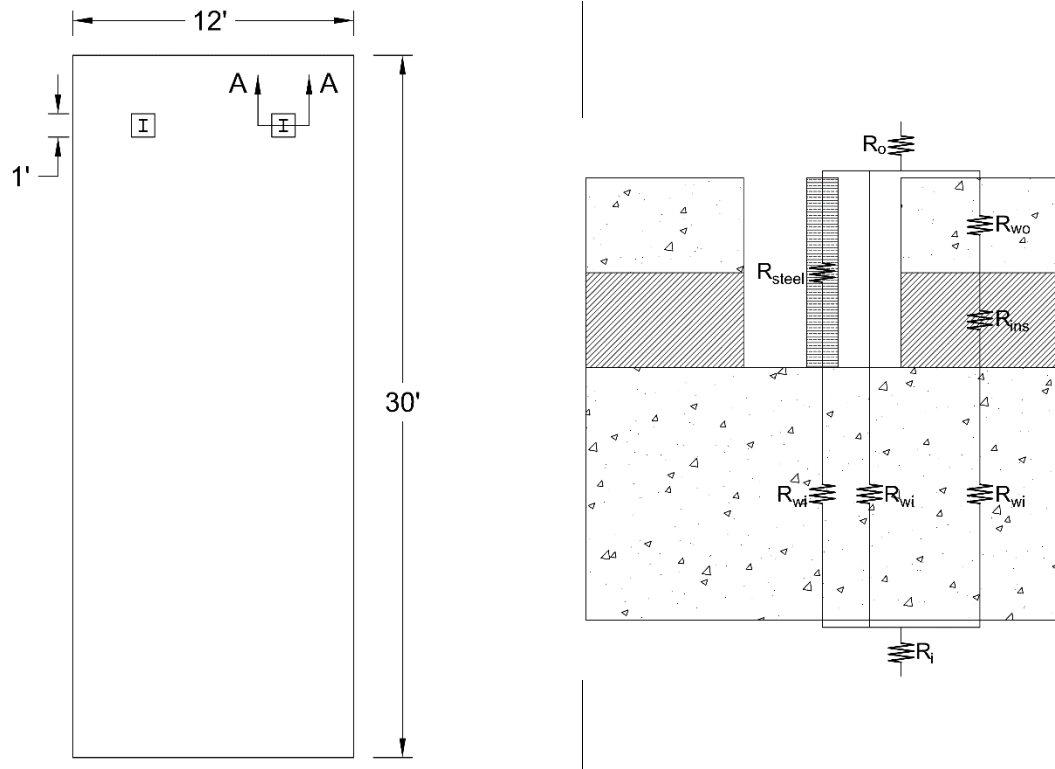


Figure A-4 Penetration without replacing blocked out material example panel layout and cross-section with electrical circuit analogy

First calculate the fractional area percentages. The penetration areas will be multiplied by 2 since there are two connections per panel.

$$A_{total} = 3.66 \text{ m} * 9.14 \text{ m} = 33.445 \text{ m}^2$$

$$A_{steel} = 2 * 4.740 \text{ in}^2 = 2 * 0.003 \text{ m}^2 = 0.006 \text{ m}^2$$

$$A_{square} = 2 * 1 \text{ ft}^2 = 2 * 0.093 \text{ m}^2 = 0.186 \text{ m}^2$$

$$A_{blockout} = A_{square} - A_{steel} = 0.186 \text{ m}^2 - 0.006 \text{ m}^2 = 0.180 \text{ m}^2$$

$$a_{steel} = \frac{A_{steel}}{A_{total}} = \frac{0.006 \text{ m}^2}{33.445 \text{ m}^2} = 0.018\%$$

$$a_{blockout} = \frac{A_{blockout}}{A_{total}} = \frac{0.180 \text{ m}^2}{33.445 \text{ m}^2} = 0.537\%$$

$$a_{insulated} = 1 - a_{steel} - a_{blockout} = 99.444\%$$

R-value can then be calculated based off of the electrical circuit analogy in Figure A-4 as:

$$R = R_o + \frac{1}{\frac{a_{steel}}{R_{steel} + R_{wi}} + \frac{a_{blockout}}{R_{wi}} + \frac{a_{insulated}}{R_{wo} + R_{ins} + R_{wi}}} + R_i$$

where R_o = thermal resistance of outdoor air film

R_i = thermal resistance of indoor air film

R is calculated as

$$R = \frac{t}{k}$$

where t = thickness of the layer in the direction of heat flow

k = thermal conductivity.

The R-values for each component using this equation are shown in the following table. Note that thickness of the solid section in this example incorporated the additional thickness of the corbel.

Element	Thickness, t (m)	Conductivity, k (W/m·K)	Thermal Resistance (m ² ·K/W)	
Outdoor air film (summer)	n.a.	n.a.	$R_o =$	0.044
Outdoor air film (winter)	n.a.	n.a.	$R_o =$	0.030
Steel	0.152	63.9	$R_{\text{steel}} =$	0.002
Outside concrete wythe	0.076	1.923	$R_{\text{wo}} =$	0.040
Insulation wythe	0.076	0.026	$R_{\text{ins}} =$	2.935
Inside concrete wythe	0.203	1.923	$R_{\text{wi}} =$	0.106
Indoor air film	n.a.	n.a.	$R_i =$	0.120

For winter,

$$\begin{aligned}
 R &= 0.030 + \frac{1}{\frac{0.00018}{0.002 + 0.106} + \frac{0.00537}{0.106} + \frac{0.99444}{0.040 + 2.935 + 0.106}} + 0.120 \\
 &= 2.814 \frac{m^2 \cdot K}{W} = \mathbf{15.978} \frac{ft^2 \cdot ^\circ F \cdot hr}{Btu}.
 \end{aligned}$$

For summer,

$$\begin{aligned}
 R &= 0.044 + \frac{1}{\frac{0.00018}{0.002 + 0.106} + \frac{0.00537}{0.106} + \frac{0.99444}{0.040 + 2.935 + 0.106}} + 0.120 \\
 &= 2.828 \frac{m^2 \cdot K}{W} = \mathbf{16.058} \frac{ft^2 \cdot ^\circ F \cdot hr}{Btu}.
 \end{aligned}$$

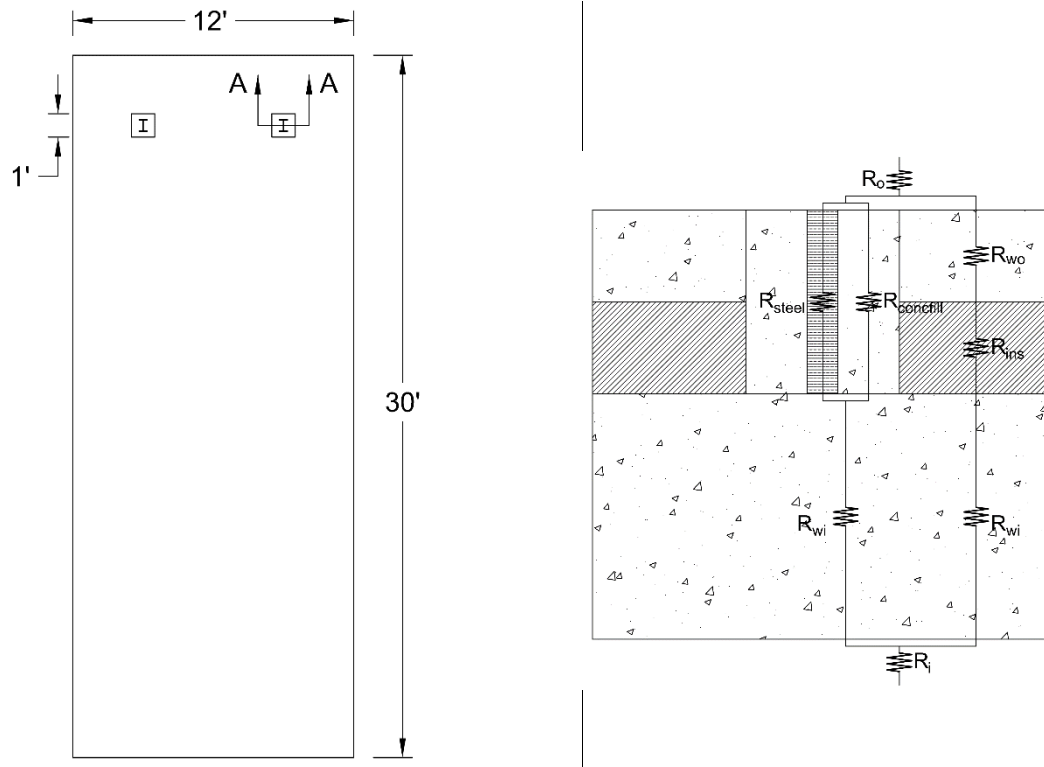
Concrete Fill

Figure A-5 Penetration with concrete fill example panel layout and cross-section with electrical circuit analogy

First calculate the fractional area percentages. The penetration areas will be multiplied by 2 since there are two connections per panel.

$$A_{total} = 3.66 \text{ m} * 9.14 \text{ m} = 33.445 \text{ m}^2$$

$$A_{steel} = 2 * 4.740 \text{ in}^2 = 2 * 0.003 \text{ m}^2 = 0.006 \text{ m}^2$$

$$A_{square} = 2 * 1 \text{ ft}^2 = 2 * 0.093 \text{ m}^2 = 0.186 \text{ m}^2$$

$$A_{blockout} = A_{square} - A_{steel} = 0.186 \text{ m}^2 - 0.006 \text{ m}^2 = 0.180 \text{ m}^2$$

$$a_{steel} = \frac{A_{steel}}{A_{square}} = \frac{0.006 \text{ m}^2}{0.186 \text{ m}^2} = 3.292\%$$

$$a_{blockout} = \frac{A_{blockout}}{A_{square}} = \frac{0.180 \text{ m}^2}{0.186 \text{ m}^2} = 96.708\%$$

$$a_{square} = \frac{A_{square}}{A_{total}} = \frac{0.186 \text{ m}^2}{33.445 \text{ m}^2} = 0.556\%$$

$$a_{insulated} = 1 - a_{steel} - a_{square} = 99.444\%$$

R-value can then be calculated based off of the electrical circuit analogy in Figure A-5 as:

$$R = R_o + \frac{1}{\frac{a_{square}}{1} + \frac{a_{insulated}}{R_{wo} + R_{ins} + R_{wi}}} + R_i$$

$$\left(\frac{a_{steel}}{R_{steel}} + \frac{a_{blockout}}{R_{concfill}} \right) + R_{wi}$$

where R_o = thermal resistance of outdoor air film

R_i = thermal resistance of outdoor air film

R is calculated as

$$R = \frac{t}{k}$$

where t = thickness of the layer in the direction of heat flow

k = thermal conductivity.

The R-values for each component using this equation are shown in the following table.

Element	Thickness, t (m)	Conductivity, k (W/m·K)	Thermal Resistance (m ² ·K/W)	
Outdoor air film (summer)	n.a.	n.a.	R _o =	0.044
Outdoor air film (winter)	n.a.	n.a.	R _o =	0.030
Steel	0.152	63.9	R _{steel} =	0.002
Concrete fill	0.152	1.923	R _{concfill} =	0.079
Outside concrete wythe	0.076	1.923	R _{wo} =	0.040
Insulation wythe	0.076	0.026	R _{ins} =	2.935
Inside concrete wythe	0.203	1.923	R _{wi} =	0.106
Indoor air film	n.a.	n.a.	R _i =	0.120

For winter,

$$\begin{aligned}
 R &= 0.030 + \frac{1}{\frac{0.00556}{\frac{1}{\left(\frac{0.03292}{0.002} + \frac{0.96708}{0.079}\right)} + 0.106} + \frac{0.99444}{0.040 + 2.935 + 0.106}} + 0.120 \\
 &= 2.917 \frac{m^2 \cdot K}{W} = \mathbf{16.564} \frac{ft^2 \cdot ^\circ F \cdot hr}{Btu}.
 \end{aligned}$$

For summer,

$$\begin{aligned}
 R &= 0.030 + \frac{1}{\frac{0.00556}{\frac{1}{\left(\frac{0.03292}{0.002} + \frac{0.96708}{0.079}\right)} + 0.106} + \frac{0.99444}{0.040 + 2.935 + 0.106}} + 0.120 \\
 &= 2.931 \frac{m^2 \cdot K}{W} = \mathbf{16.644} \frac{ft^2 \cdot ^\circ F \cdot hr}{Btu}.
 \end{aligned}$$

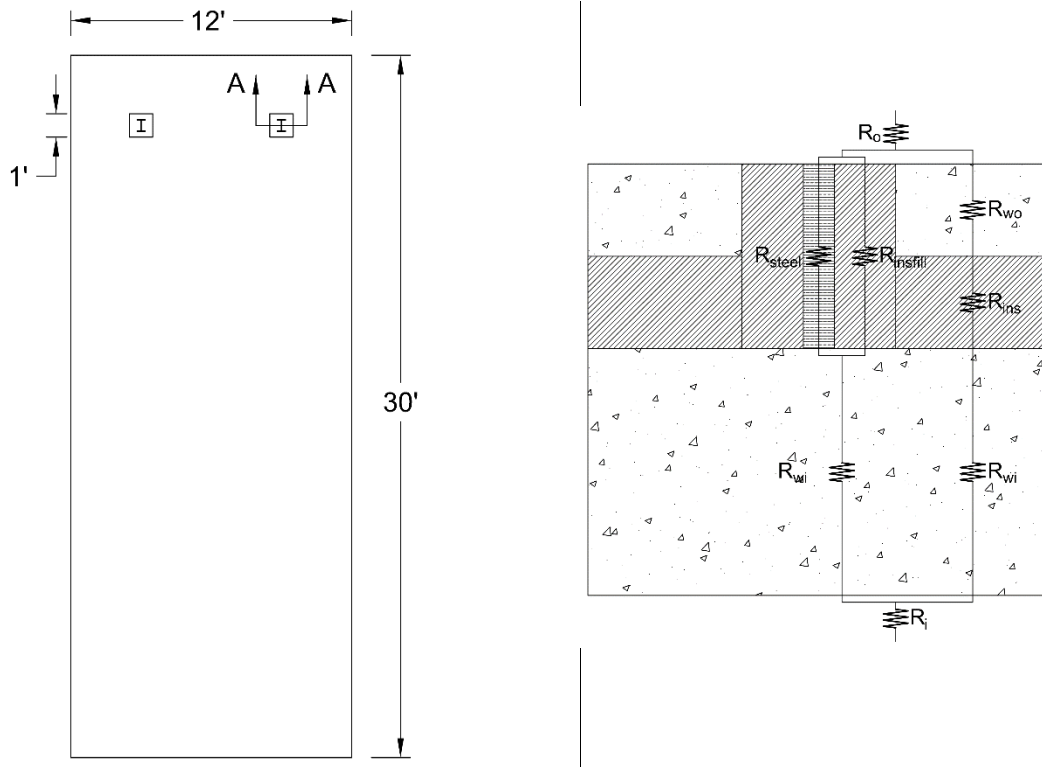
Insulation Fill

Figure A-6 Penetration with insulation fill example panel layout and cross-section with electrical circuit analogy

First calculate the fractional area percentages. The penetration areas will be multiplied by 2 since there are two connections per panel.

$$A_{total} = 3.66 \text{ m} * 9.14 \text{ m} = 33.445 \text{ m}^2$$

$$A_{steel} = 2 * 4.740 \text{ in}^2 = 2 * 0.003 \text{ m}^2 = 0.006 \text{ m}^2$$

$$A_{square} = 2 * 1 \text{ ft}^2 = 2 * 0.093 \text{ m}^2 = 0.186 \text{ m}^2$$

$$A_{blockout} = A_{square} - A_{steel} = 0.186 \text{ m}^2 - 0.006 \text{ m}^2 = 0.180 \text{ m}^2$$

$$a_{steel} = \frac{A_{steel}}{A_{square}} = \frac{0.006 \text{ m}^2}{0.186 \text{ m}^2} = 3.292\%$$

$$a_{blockout} = \frac{A_{blockout}}{A_{square}} = \frac{0.180 \text{ m}^2}{0.186 \text{ m}^2} = 96.708\%$$

$$a_{square} = \frac{A_{square}}{A_{total}} = \frac{0.186 \text{ m}^2}{33.445 \text{ m}^2} = 0.556\%$$

$$a_{insulated} = 1 - a_{steel} - a_{square} = 99.444\%$$

R-value can then be calculated based off of the electrical circuit analogy in Figure A-6 as:

$$R = R_o + \frac{1}{\frac{a_{square}}{1} + \frac{a_{insulated}}{R_{wo} + R_{ins} + R_{wi}}} + R_i$$

$$\left(\frac{a_{steel}}{R_{steel}} + \frac{a_{blockout}}{R_{insfill}} \right) + R_{wi}$$

where R_o = thermal resistance of outdoor air film

R_i = thermal resistance of indoor air film

R is calculated as

$$R = \frac{t}{k}$$

where t = thickness of the layer in the direction of heat flow

k = thermal conductivity.

The R-values for each component using this equation are shown in the following table.

Element	Thickness, t (m)	Conductivity, k (W/m·K)	Thermal Resistance (m ² ·K/W)
Outdoor air film (summer)	n.a.	n.a.	$R_o = 0.044$
Outdoor air film (winter)	n.a.	n.a.	$R_o = 0.030$
Steel	0.152	63.9	$R_{steel} = 0.002$
Insulation fill	0.152	1.923	$R_{insfill} = 5.870$
Outside concrete wythe	0.076	1.923	$R_{wo} = 0.040$
Insulation wythe	0.076	0.026	$R_{ins} = 2.935$
Inside concrete wythe	0.203	1.923	$R_{wi} = 0.106$
Indoor air film	n.a.	n.a.	$R_i = 0.120$

For winter,

$$\begin{aligned}
 R &= 0.030 + \frac{1}{\frac{0.00556}{\frac{1}{\left(\frac{0.03292}{0.002} + \frac{0.96708}{5.870}\right)} + 0.106} + \frac{0.99444}{0.040 + 2.935 + 0.106}} + 0.120 \\
 &= 2.973 \frac{m^2 \cdot K}{W} = \mathbf{16.883} \frac{ft^2 \cdot ^\circ F \cdot hr}{Btu}.
 \end{aligned}$$

For summer,

$$\begin{aligned}
 R &= 0.030 + \frac{1}{\frac{0.00556}{\frac{1}{\left(\frac{0.03292}{0.002} + \frac{0.96708}{5.870}\right)} + 0.106} + \frac{0.99444}{0.040 + 2.935 + 0.106}} + 0.120 \\
 &= 2.987 \frac{m^2 \cdot K}{W} = \mathbf{16.963} \frac{ft^2 \cdot ^\circ F \cdot hr}{Btu}.
 \end{aligned}$$

The results of these three examples are displayed in the following table.

Season	No Fill	Concrete Fill	Insulation Fill	Perfectly Insulated
Summer	2.828	2.931	2.987	3.164
Winter	2.814	2.917	2.973	3.178
Percent Efficiency	87%	90%	92%	100%

As would be expected, the greatest decrease in R-value results when there is no fill after the penetrating member is installed. The decrease in R-value for this panel when the void was not filled would be about 13%. When concrete filled the void, the R-value decreased by 10%, and filling the void with insulation resulted in an 8% decrease. There will still be a decrease even filling insulation in around the penetrating member because the penetration itself is a large thermal bridge. The larger the member or deeper the penetration, the greater the heat transfer that will occur. If a penetration is absolutely unavoidable, it is intuitive that it is best to fill insulation in around the penetration to minimize the thermal bridging.

Lifting Anchors Example

Consider a 12 ft × 30 ft panel with four steel lifting anchors that displace a square foot of insulation each. To simplify modeling, the lifting anchors were simulated as cylinders that penetrated the depth of the SWP with a diameter of 1.5 inches. This example will utilize the isothermal-planes method.

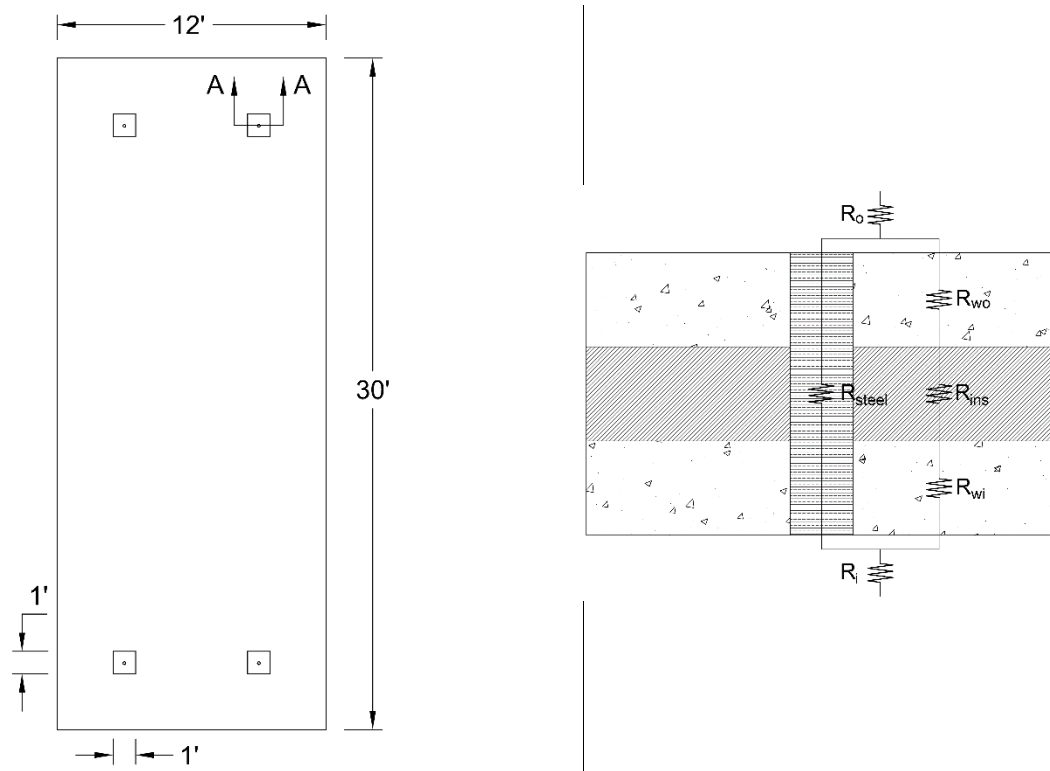


Figure A-7 Lifting anchor example panel layout and cross-section with electrical circuit analogy

First calculate the fractional area percentages. The solid area is multiplied by 4 since there are four lifting anchors per panel.

$$A_{total} = 3.66 \text{ m} * 9.14 \text{ m} = 33.445 \text{ m}^2$$

$$A_{steel} = 4 * \frac{\pi}{4} D_{steel}^2 = \pi * 0.038^2 = 0.00454 \text{ m}^2$$

$$a_{steel} = \frac{A_{steel}}{A_{total}} = \frac{0.00454 \text{ m}^2}{33.445 \text{ m}^2} = 0.014\%$$

$$a_{insulated} = 1 - a_{steel} = 99.986\%$$

R-value can then be calculated based off of the electrical circuit analogy in Figure A-7 as:

$$R = \frac{1}{\frac{a_{steel}}{R_{steel}} + \frac{a_{insulated}}{R_o + R_{wo} + R_{ins} + R_{wi} + R_i}}$$

where R_o = thermal resistance of outdoor air film

R_i = thermal resistance of indoor air film

R is calculated as

$$R = \frac{t}{k}$$

where t = thickness of the layer in the direction of heat flow

k = thermal conductivity.

The R-values for each component using this equation are shown in the following table. Note that thickness of the solid section in this example incorporated the additional thickness of the corbel.

Element	Thickness, t (m)	Conductivity, k (W/m·K)	Thermal Resistance (m ² ·K/W)	
Outdoor air film (summer)	n.a.	n.a.	$R_o =$	0.044
Outdoor air film (winter)	n.a.	n.a.	$R_o =$	0.030
Steel	0.229	63.9	$R_{conc} =$	0.0036
Outside concrete wythe	0.076	1.923	$R_{wo} =$	0.040
Insulation wythe	0.076	0.026	$R_{ins} =$	2.935
Inside concrete wythe	0.076	1.923	$R_{wi} =$	0.040
Indoor air film	n.a.	n.a.	$R_i =$	0.120

For winter,

$$\begin{aligned}
 R &= 0.030 + \frac{1}{\frac{0.00014}{0.0036} + \frac{0.99986}{0.040 + 2.935 + 0.040}} + 0.120 \\
 &= 2.854 \frac{m^2 \cdot K}{W} = \mathbf{16.205} \frac{ft^2 \cdot ^\circ F \cdot hr}{Btu}.
 \end{aligned}$$

For summer,

$$\begin{aligned}
 R &= 0.044 + \frac{1}{\frac{0.00014}{0.0036} + \frac{0.99986}{0.040 + 2.935 + 0.040}} + 0.120 \\
 &= 2.868 \frac{m^2 \cdot K}{W} = \mathbf{16.285} \frac{ft^2 \cdot ^\circ F \cdot hr}{Btu}.
 \end{aligned}$$

Corbel Example

Consider a 12 ft \times 30 ft panel with an 8 inch thick corbel placed in the middle requiring a 20" \times 28" solid section of concrete penetrating the insulation. The characteristic section method is the most appropriate method to use for a most accurate prediction of panel R-value since we are dealing with a solid concrete section.

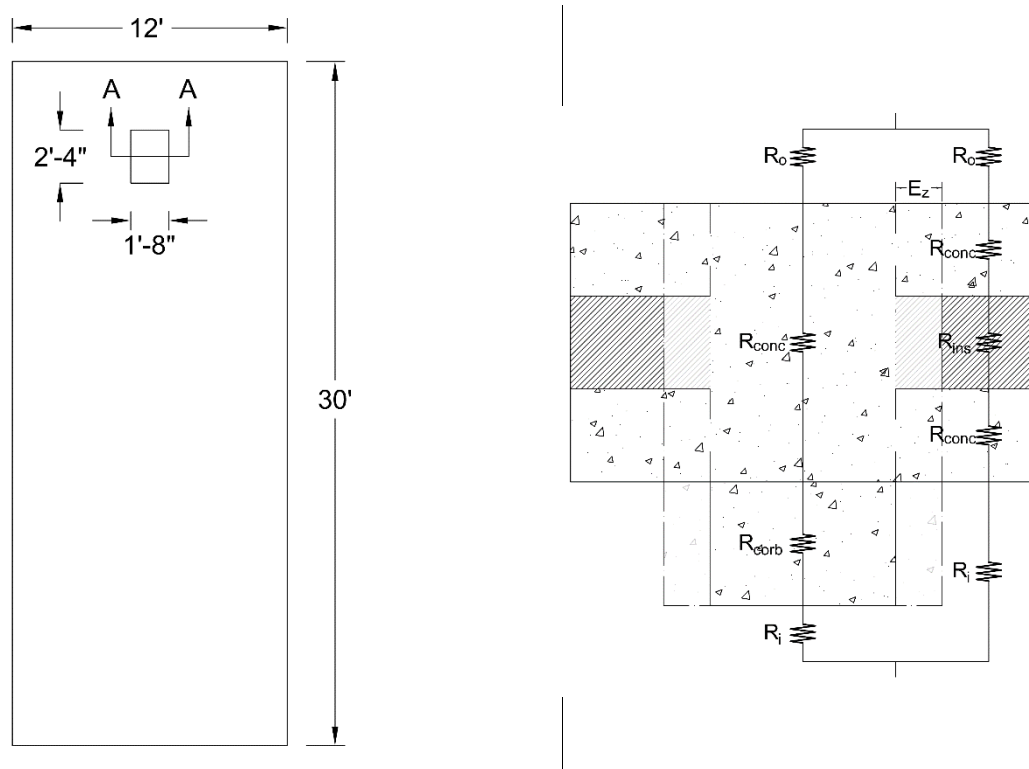


Figure A-8 Corbel example panel layout and cross-section with electrical circuit analogy

First calculate the affected zone dimensions. Remember that these empirical equations require that units be input as inches and $\text{BTU}\cdot\text{in}/[\text{hr}\cdot\text{ft}^2\cdot^\circ\text{F}]$ to work.

$$E_z = 1.4 - 0.1\alpha t_{ins} + \beta[0.4t_{wo} + 0.1(t_{wi} - t_{wo})]$$

$$\alpha = 1 + 2.25 * \left(\frac{0.026 - 0.26}{0.26} \right) = 0.308$$

$$\beta = 1 + 1.458 * \left(\frac{1.923 - 12.05}{12.05} \right) = 1.155$$

$$\begin{aligned} E_z &= 1.4 - 0.1(0.308)(3 \text{ inches}) \\ &\quad + 1.155[0.4(3 \text{ inches}) + 0.1(3 \text{ inches} - 3 \text{ inches})] \\ &= 2.694 \text{ in} = \mathbf{0.068 \text{ m}} \end{aligned}$$

Next calculate the fractional area percentages.

$$A_{total} = 3.66 \text{ m} * 9.14 \text{ m} = 33.445 \text{ m}^2$$

$$b_{aff} = b_{solid} + 2 * E_z = 0.508 \text{ m} + 2 * 0.068 \text{ m} = 0.645 \text{ m}$$

$$h_{aff} = b_{solid} + 2 * E_z = 0.711 \text{ m} + 2 * 0.068 \text{ m} = 0.848 \text{ m}$$

$$A_{aff} = b_{aff} * h_{aff} = 0.645 \text{ m} * 0.848 \text{ m} = 0.547 \text{ m}^2$$

$$a_{aff} = \frac{A_{aff}}{A_{total}} = \frac{0.547 \text{ m}^2}{33.445 \text{ m}^2} = 1.635\%$$

$$a_{insulated} = 1 - a_{solid} = 98.365\%$$

R-value can then be calculated based off of the electrical circuit analogy in Figure A-8 as:

$$R = \frac{1}{\frac{a_{aff}}{R_o + R_{conc} + R_{corb} + R_i} + \frac{a_{insulated}}{R_o + R_{wo} + R_{ins} + R_{wi} + R_i}}$$

where R_o = thermal resistance of outdoor air film

R_i = thermal resistance of outdoor air film

R is calculated as

$$R = \frac{t}{k}$$

where t = thickness of the layer in the direction of heat flow

k = thermal conductivity.

The R -values for each component using this equation are shown in the following table. Note that thickness of the solid section in this example incorporated the additional thickness of the corbel.

Element	Thickness, t (m)	Conductivity, k (W/m·K)	Thermal Resistance (m ² ·K/W)
Outdoor air film (summer)	n.a.	n.a.	$R_o = 0.044$
Outdoor air film (winter)	n.a.	n.a.	$R_o = 0.030$
Solid concrete section	0.432	1.923	$R_{conc} + R_{corb} = 0.225$
Outside concrete wythe	0.076	1.923	$R_{wo} = 0.040$
Insulation wythe	0.076	0.026	$R_{ins} = 2.935$
Inside concrete wythe	0.076	1.923	$R_{wi} = 0.040$
Indoor air film	n.a.	n.a.	$R_i = 0.120$

For winter,

$$\begin{aligned}
 R &= \frac{1}{\frac{0.02}{0.030 + 0.225 + 0.120} + \frac{0.98}{0.030 + 0.040 + 2.935 + 0.040 + 0.120}} \\
 &= 2.820 \frac{m^2 \cdot K}{W} = 16.015 \frac{ft^2 \cdot ^\circ F \cdot hr}{Btu}
 \end{aligned}$$

For summer,

$$\begin{aligned}
 R &= \frac{1}{\frac{0.02}{0.044 + 0.225 + 0.120} + \frac{0.98}{0.044 + 0.040 + 2.935 + 0.040 + 0.120}} \\
 &= 2.844 \frac{m^2 \cdot K}{W} = 16.150 \frac{ft^2 \cdot ^\circ F \cdot hr}{Btu}
 \end{aligned}$$

Roof Example

Consider a 12 ft \times 30 ft panel with a roof joist embedment plate that displaces a square foot of insulation every 6 ft o.c. As demonstrated in the example at the beginning of this Appendix, since the steel penetration of these plates is completely surrounded by concrete, the steel portion may be ignored to simplify calculations. The characteristic section method is the most appropriate method to use for a most accurate prediction of panel R-value since we are dealing with a solid concrete section then.

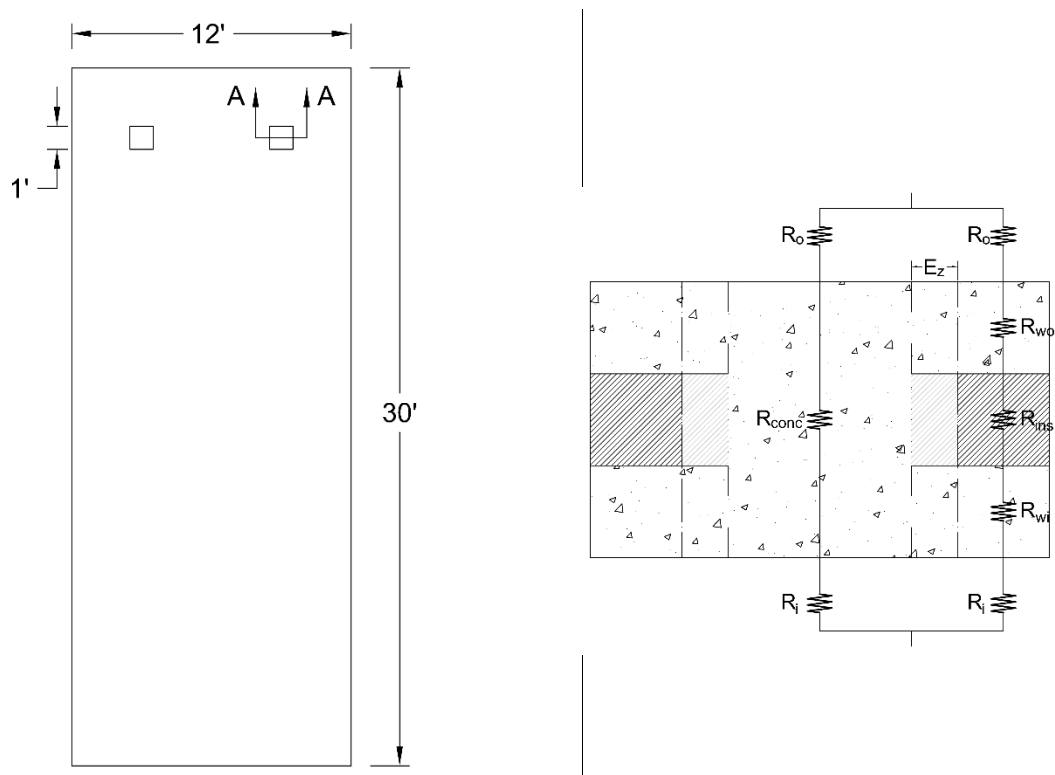


Figure A-9 Roof example panel layout and cross-section with electrical circuit analogy

First calculate the affected zone dimensions. Remember that these empirical equations require that units be input as inches and $\text{BTU}\cdot\text{in}/[\text{hr}\cdot\text{ft}^2\cdot^\circ\text{F}]$ to work.

$$E_z = 1.4 - 0.1\alpha t_{ins} + \beta[0.4t_{wo} + 0.1(t_{wi} - t_{wo})]$$

$$\alpha = 1 + 2.25 * \left(\frac{0.026 - 0.26}{0.26} \right) = 0.308$$

$$\beta = 1 + 1.458 * \left(\frac{1.923 - 12.05}{12.05} \right) = 1.155$$

$$\begin{aligned} E_z &= 1.4 - 0.1(0.308)(3 \text{ inches}) \\ &\quad + 1.155[0.4(3 \text{ inches}) + 0.1(3 \text{ inches} - 3 \text{ inches})] \\ &= 2.694 \text{ in} = 0.068 \text{ m} \end{aligned}$$

Next calculate the fractional area percentages. The affected area is multiplied by 2 since there are two connections per panel.

$$A_{total} = 3.66 \text{ m} * 9.14 \text{ m} = 33.445 \text{ m}^2$$

$$b_{aff} = b_{solid} + 2 * E_z = 0.305 \text{ m} + 2 * 0.068 \text{ m} = 0.442 \text{ m}$$

$$h_{aff} = b_{solid} + 2 * E_z = 0.305 \text{ m} + 2 * 0.068 \text{ m} = 0.442 \text{ m}$$

$$A_{aff} = 2 * b_{aff} * h_{aff} = 2 * 0.442 \text{ m} * 0.442 \text{ m} = 0.390 \text{ m}^2$$

$$a_{aff} = \frac{A_{aff}}{A_{total}} = \frac{0.390 \text{ m}^2}{33.445 \text{ m}^2} = 1.166\%$$

$$a_{insulated} = 1 - a_{solid} = 98.834\%$$

R-value can then be calculated based off of the electrical circuit analogy in Figure A-9 as:

$$R = \frac{1}{\frac{a_{aff}}{R_o + R_{conc} + R_i} + \frac{a_{insulated}}{R_o + R_{wo} + R_{ins} + R_{wi} + R_i}}$$

where R_o = thermal resistance of outdoor air film

R_i = thermal resistance of outdoor air film

R is calculated as

$$R = \frac{t}{k}$$

where t = thickness of the layer in the direction of heat flow

k = thermal conductivity.

The R -values for each component using this equation are shown in the following table. Note that thickness of the solid section in this example incorporated the additional thickness of the corbel.

Element	Thickness, t (m)	Conductivity, k (W/m·K)	Thermal Resistance (m ² ·K/W)
Outdoor air film (summer)	n.a.	n.a.	$R_o = 0.044$
Outdoor air film (winter)	n.a.	n.a.	$R_o = 0.030$
Solid concrete section	0.229	1.923	$R_{conc} = 0.119$
Outside concrete wythe	0.076	1.923	$R_{wo} = 0.040$
Insulation wythe	0.076	0.026	$R_{ins} = 2.935$
Inside concrete wythe	0.076	1.923	$R_{wi} = 0.040$
Indoor air film	n.a.	n.a.	$R_i = 0.120$

For winter,

$$\begin{aligned}
 R &= \frac{1}{\frac{0.01166}{0.030 + 0.119 + 0.120} + \frac{0.98834}{0.030 + 0.040 + 2.935 + 0.040 + 0.120}} \\
 &= 2.811 \frac{m^2 \cdot K}{W} = \mathbf{15.960} \frac{ft^2 \cdot ^\circ F \cdot hr}{Btu}.
 \end{aligned}$$

For summer,

$$\begin{aligned}
 R &= \frac{1}{\frac{0.01166}{0.044 + 0.119 + 0.120} + \frac{0.98834}{0.044 + 0.040 + 2.935 + 0.040 + 0.120}} \\
 &= 2.839 \frac{m^2 \cdot K}{W} = \mathbf{16.121} \frac{ft^2 \cdot ^\circ F \cdot hr}{Btu}.
 \end{aligned}$$

Floor Example

Consider a 12 ft \times 30 ft panel with floor beams that require two embedment plates spaced every 6 ft o.c. (one for the top wythe and one for the bottom wythe). The first example will examine such a configuration with solid 1 ft \times 1 ft sections at these locations. The second example will examine the same panel but with 1 inch of continuous insulation in place of a solid section.

Insulation Omitted (Solid Sections)

For this scenario, the characteristic section method is the most appropriate method to use for a most accurate prediction of panel R-value since we are dealing with a solid concrete section.

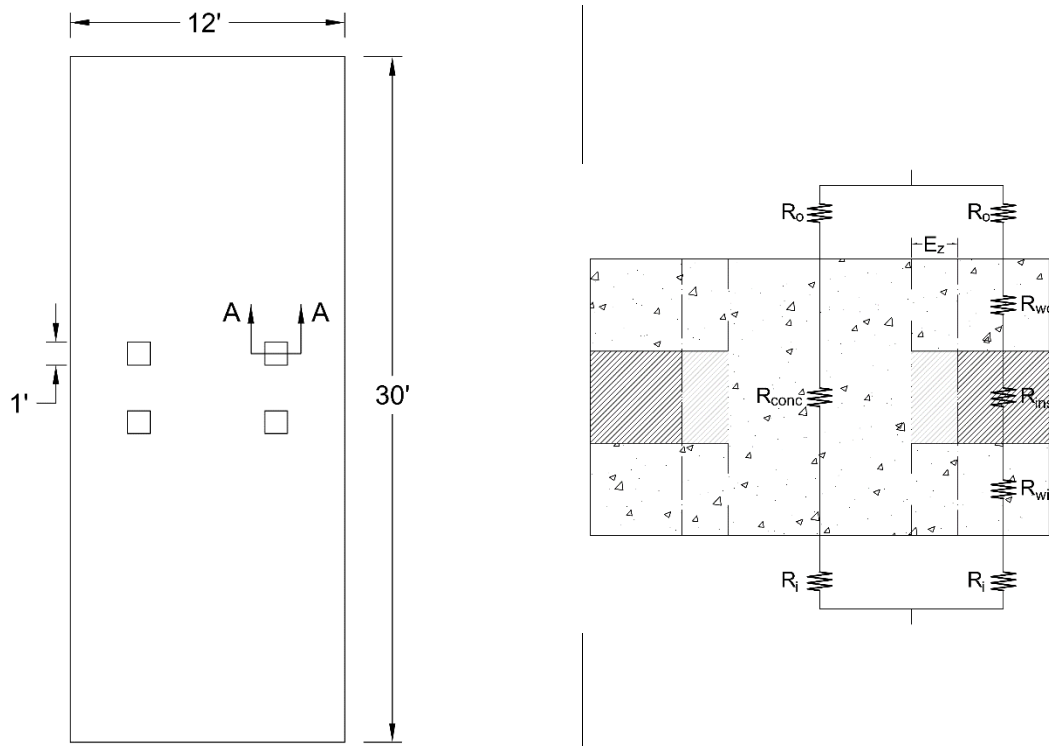


Figure A-10 Floor with omitted insulation example panel layout and cross-section with electrical circuit analogy

First calculate the affected zone dimensions. Remember that these empirical equations require that units be input as inches and BTU·in/[hr·ft²·°F] to work.

$$E_z = 1.4 - 0.1\alpha t_{ins} + \beta[0.4t_{wo} + 0.1(t_{wi} - t_{wo})]$$

$$\alpha = 1 + 2.25 * \left(\frac{0.026 - 0.26}{0.26} \right) = 0.308$$

$$\beta = 1 + 1.458 * \left(\frac{1.923 - 12.05}{12.05} \right) = 1.155$$

$$\begin{aligned} E_z &= 1.4 - 0.1(0.308)(3 \text{ inches}) \\ &\quad + 1.155[0.4(3 \text{ inches}) + 0.1(3 \text{ inches} - 3 \text{ inches})] \\ &= 2.694 \text{ in} = \mathbf{0.068 \text{ m}} \end{aligned}$$

Next calculate the fractional area percentages. The affected area is multiplied by 4 since there are two plates per floor beam, and two beam connections per panel.

$$A_{total} = 3.66 \text{ m} * 9.14 \text{ m} = 33.445 \text{ m}^2$$

$$b_{aff} = b_{solid} + 2 * E_z = 0.305 \text{ m} + 2 * 0.068 \text{ m} = 0.442 \text{ m}$$

$$h_{aff} = b_{solid} + 2 * E_z = 0.305 \text{ m} + 2 * 0.068 \text{ m} = 0.442 \text{ m}$$

$$A_{aff} = 4 * b_{aff} * h_{aff} = 4 * 0.442 \text{ m} * 0.442 \text{ m} = 0.780 \text{ m}^2$$

$$a_{aff} = \frac{A_{aff}}{A_{total}} = \frac{0.780 \text{ m}^2}{33.445 \text{ m}^2} = 2.333\%$$

$$a_{insulated} = 1 - a_{solid} = 97.667\%$$

R-value can then be calculated based off of the electrical circuit analogy in Figure A-10

as:

$$R = \frac{1}{\frac{a_{aff}}{R_o + R_{conc} + R_i} + \frac{a_{insulated}}{R_o + R_{wo} + R_{ins} + R_{wi} + R_i}}$$

where R_o = thermal resistance of outdoor air film

R_i = thermal resistance of outdoor air film

R is calculated as

$$R = \frac{t}{k}$$

where t = thickness of the layer in the direction of heat flow

k = thermal conductivity.

The R-values for each component using this equation are shown in the following table. Note that thickness of the solid section in this example incorporated the additional thickness of the corbel.

Element	Thickness, t (m)	Conductivity, k (W/m·K)	Thermal Resistance (m ² ·K/W)
Outdoor air film (summer)	n.a.	n.a.	$R_o = 0.044$
Outdoor air film (winter)	n.a.	n.a.	$R_o = 0.030$
Solid concrete section	0.229	1.923	$R_{conc} = 0.119$
Outside concrete wythe	0.076	1.923	$R_{wo} = 0.040$
Insulation wythe	0.076	0.026	$R_{ins} = 2.935$
Inside concrete wythe	0.076	1.923	$R_{wi} = 0.040$
Indoor air film	n.a.	n.a.	$R_i = 0.120$

For winter,

$$R = \frac{1}{\frac{0.02333}{0.030 + 0.119 + 0.120} + \frac{0.97667}{0.030 + 0.040 + 2.935 + 0.040 + 0.120}}$$

$$= 2.528 \frac{m^2 \cdot K}{W} = \mathbf{14.357} \frac{ft^2 \cdot ^\circ F \cdot hr}{Btu}.$$

For summer,

$$R = \frac{1}{\frac{0.01166}{0.044 + 0.119 + 0.120} + \frac{0.98834}{0.044 + 0.040 + 2.935 + 0.040 + 0.120}}$$

$$= 2.565 \frac{m^2 \cdot K}{W} = \mathbf{14.566} \frac{ft^2 \cdot ^\circ F \cdot hr}{Btu}.$$

Insulation Reduced (but Continuous)

For this scenario, the characteristic section method cannot be used since there are no longer solid sections in the panel. Instead, the parallel-path method is a good approach to use since there are two similar but separate paths heat might take. To show how significant the difference in R-value can be maintained by keeping some insulation continuity, it was determined to allot a larger area of reduced insulation (2 square feet instead of 1 square foot per connection) to have a conservative comparison of the benefit of doing this.

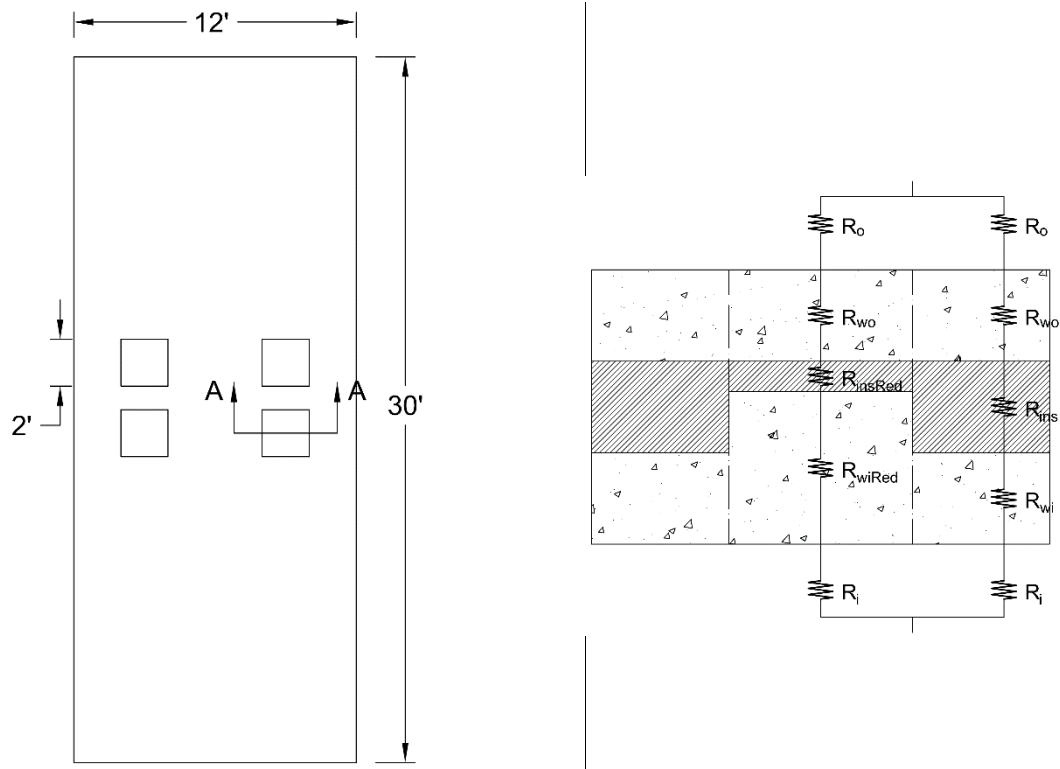


Figure A-11 Floor with reduced insulation example panel layout and cross-section with electrical circuit analogy

First calculate the fractional area percentages. The solid area is multiplied by 4 as in the previous example since there are two plates per floor beam, and two beam connections per panel.

$$A_{total} = 3.66 \text{ m} * 9.14 \text{ m} = 33.445 \text{ m}^2$$

$$A_{red} = 4 * b_{red} * h_{red} = 4 * 0.610 \text{ m} * 0.610 \text{ m} = 1.486 \text{ m}^2$$

$$a_{red} = \frac{A_{red}}{A_{total}} = \frac{1.486 \text{ m}^2}{33.445 \text{ m}^2} = 4.444\%$$

$$a_{insulated} = 1 - a_{solid} = 95.556\%$$

R-value can then be calculated based off of the electrical circuit analogy in Figure A-11

as:

$$R = \frac{1}{\frac{a_{red}}{R_o + R_{wo} + R_{insRed} + R_{wiRed} + R_i} + \frac{a_{insulated}}{R_o + R_{wo} + R_{ins} + R_{wi} + R_i}}$$

where R_o = thermal resistance of outdoor air film

R_i = thermal resistance of outdoor air film

R is calculated as

$$R = \frac{t}{k}$$

where t = thickness of the layer in the direction of heat flow

k = thermal conductivity.

The R-values for each component using this equation are shown in the following table.

Element	Thickness, t (m)	Conductivity, k (W/m·K)	Thermal Resistance (m ² ·K/W)
Outdoor air film (summer)	n.a.	n.a.	$R_o = 0.044$
Outdoor air film (winter)	n.a.	n.a.	$R_o = 0.030$
Outside concrete wythe	0.076	1.923	$R_{wo} = 0.040$
Insulation wythe	0.076	0.026	$R_{ins} = 2.935$
Reduced insulation wythe	0.025	0.026	$R_{insRed} = 0.978$
Inside concrete wythe	0.076	1.923	$R_{wi} = 0.040$
Reduced inside concrete wythe	0.127	1.923	$R_{wiRed} = 0.066$
Indoor air film	n.a.	n.a.	$R_i = 0.120$

For winter,

$$R = \frac{1}{\frac{0.04444}{0.030 + 0.040 + 0.978 + 0.066 + 0.12} + \frac{0.95556}{0.030 + 0.040 + 2.935 + 0.040 + 0.12}}$$

$$= 2.958 \frac{m^2 \cdot K}{W} = \mathbf{16.799} \frac{ft^2 \cdot ^\circ F \cdot hr}{Btu}.$$

For summer,

$$R = \frac{1}{\frac{0.04444}{0.044 + 0.040 + 0.978 + 0.066 + 0.12} + \frac{0.95556}{0.044 + 0.040 + 2.935 + 0.040 + 0.12}}$$

$$= 2.974 \frac{m^2 \cdot K}{W} = \mathbf{16.886} \frac{ft^2 \cdot ^\circ F \cdot hr}{Btu}.$$

The following table shows a comparison of the results when reducing insulation and when omitting the insulation. Keeping even a small portion of insulation continuous results in a 16-17 % increase in R-value in this case. Clearly a strong effort should be made to maintain continuity in the insulative building envelope.

Season	Omitted Ins, R_{omit}	Reduced Ins, R_{red}	Perfectly Insulated, R_{ideal}	Difference, $(R_{red} - R_{omit})/R_{omit}$
Summer	2.565	2.974	3.164	15.95%
Winter	2.528	2.958	3.178	17.01%

Foundation Example

Consider a 12 ft \times 30 ft panel with an 8" \times 8" segment of insulation blocked out every 6 ft. o.c. for connections to the foundation. The characteristic section method is again the most appropriate method to use in this case for a most accurate prediction of panel R-value since we are dealing with a solid concrete section.

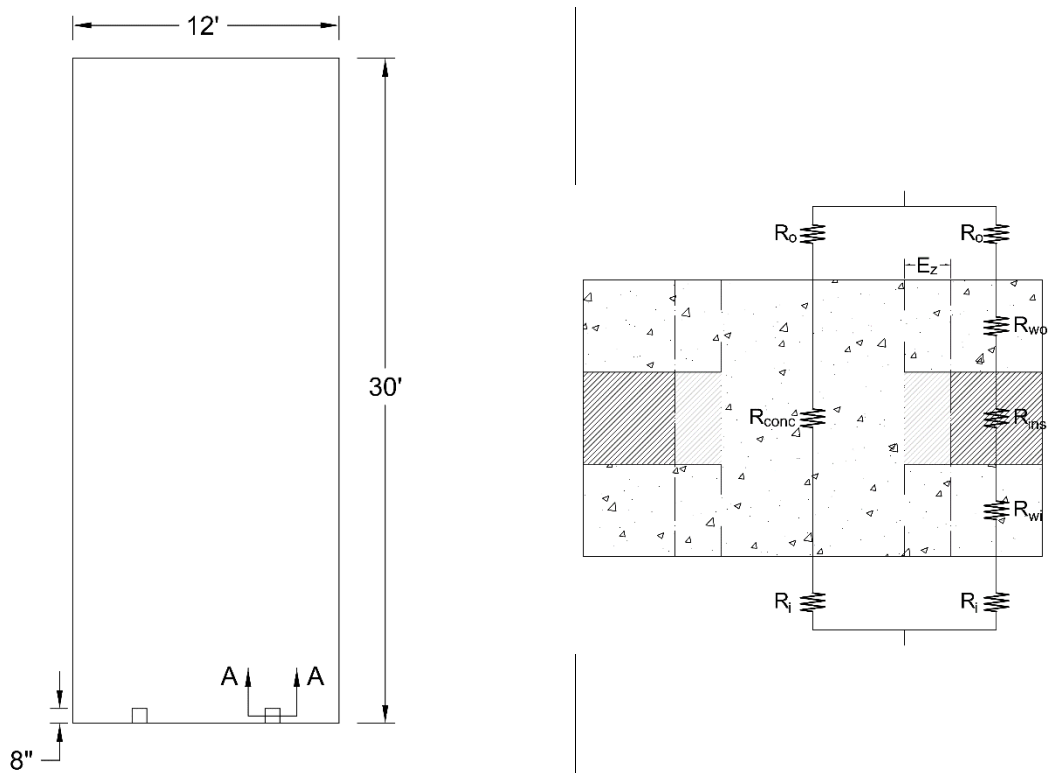


Figure A-12 Foundation example panel layout and cross-section with electrical circuit analogy

First calculate the affected zone dimensions. Remember that these empirical equations require that units be input as inches and $\text{BTU}\cdot\text{in}/[\text{hr}\cdot\text{ft}^2\cdot^\circ\text{F}]$ to work.

$$E_z = 1.4 - 0.1\alpha t_{ins} + \beta[0.4t_{wo} + 0.1(t_{wi} - t_{wo})]$$

$$\alpha = 1 + 2.25 * \left(\frac{0.026 - 0.26}{0.26} \right) = 0.308$$

$$\beta = 1 + 1.458 * \left(\frac{1.923 - 12.05}{12.05} \right) = 1.155$$

$$\begin{aligned} E_z &= 1.4 - 0.1(0.308)(3 \text{ inches}) \\ &\quad + 1.155[0.4(3 \text{ inches}) + 0.1(3 \text{ inches} - 3 \text{ inches})] \\ &= 2.694 \text{ in} = \mathbf{0.068 \text{ m}} \end{aligned}$$

Next calculate the fractional area percentages. The affected area is multiplied by 2 since there are two connections per panel.

$$A_{total} = 3.66 \text{ m} * 9.14 \text{ m} = 33.445 \text{ m}^2$$

$$b_{aff} = b_{solid} + 2 * E_z = 0.203 \text{ m} + 2 * 0.068 \text{ m} = 0.340 \text{ m}$$

$$h_{aff} = b_{solid} + 2 * E_z = 0.203 \text{ m} + 2 * 0.068 \text{ m} = 0.340 \text{ m}$$

$$A_{aff} = 2 * b_{aff} * h_{aff} = 2 * 0.340 \text{ m} * 0.340 \text{ m} = 0.231 \text{ m}^2$$

$$a_{aff} = \frac{A_{aff}}{A_{total}} = \frac{0.231 \text{ m}^2}{33.445 \text{ m}^2} = 0.691\%$$

$$a_{insulated} = 1 - a_{solid} = 99.309\%$$

R-value can then be calculated based off of the electrical circuit analogy in Figure A-12

as:

$$R = \frac{1}{\frac{a_{aff}}{R_o + R_{conc} + R_i} + \frac{a_{insulated}}{R_o + R_{wo} + R_{ins} + R_{wi} + R_i}}$$

where R_o = thermal resistance of outdoor air film

R_i = thermal resistance of outdoor air film

R is calculated as

$$R = \frac{t}{k}$$

where t = thickness of the layer in the direction of heat flow

k = thermal conductivity.

The R -values for each component using this equation are shown in the following table. Note that thickness of the solid section in this example incorporated the additional thickness of the corbel.

Element	Thickness, t (m)	Conductivity, k (W/m·K)	Thermal Resistance (m ² ·K/W)
Outdoor air film (summer)	n.a.	n.a.	$R_o = 0.044$
Outdoor air film (winter)	n.a.	n.a.	$R_o = 0.030$
Solid concrete section	0.229	1.923	$R_{conc} = 0.119$
Outside concrete wythe	0.076	1.923	$R_{wo} = 0.040$
Insulation wythe	0.076	0.026	$R_{ins} = 2.935$
Inside concrete wythe	0.076	1.923	$R_{wi} = 0.040$
Indoor air film	n.a.	n.a.	$R_i = 0.120$

For winter,

$$\begin{aligned}
 R &= \frac{1}{\frac{0.00691}{0.030 + 0.119 + 0.120} + \frac{0.99309}{0.030 + 0.040 + 2.935 + 0.040 + 0.120}} \\
 &= 2.945 \frac{m^2 \cdot K}{W} = \mathbf{16.721} \frac{ft^2 \cdot ^\circ F \cdot hr}{Btu}.
 \end{aligned}$$

For summer,

$$\begin{aligned}
 R &= \frac{1}{\frac{0.00691}{0.044 + 0.119 + 0.120} + \frac{0.99309}{0.044 + 0.040 + 2.935 + 0.040 + 0.120}} \\
 &= 2.968 \frac{m^2 \cdot K}{W} = \mathbf{16.853} \frac{ft^2 \cdot ^\circ F \cdot hr}{Btu}.
 \end{aligned}$$

Panel-to-Panel Example

Consider a 12 ft \times 30 ft panel with 3 connections to each neighboring panel where each connection requires blocking out a total of 1 ft \times 1 ft section of insulation (6 inches into the panel on each side of the joint as shown in the following figure). The characteristic section method is the most appropriate method to use in this case for a most accurate prediction of panel R-value dealing with solid concrete sections.

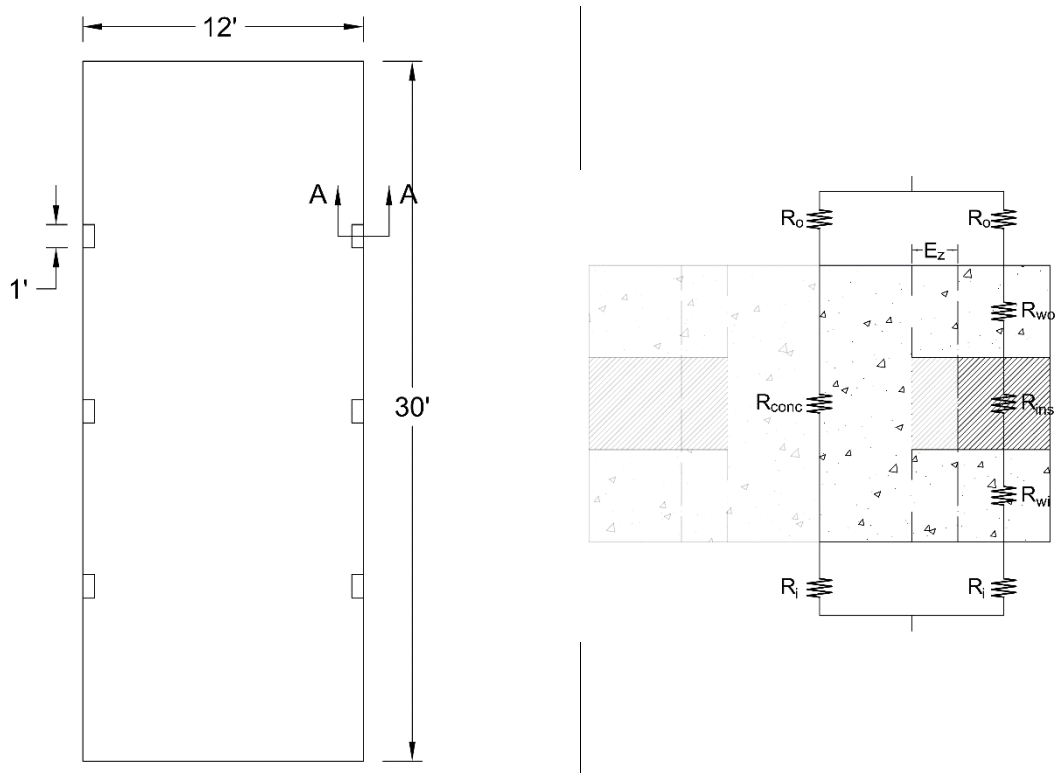


Figure A-13 Panel connection example panel layout and cross-section with electrical circuit analogy

First calculate the affected zone dimensions. Remember that these empirical equations require that units be input as inches and BTU·in/[hr·ft²·°F] to work.

$$E_z = 1.4 - 0.1\alpha t_{ins} + \beta[0.4t_{wo} + 0.1(t_{wi} - t_{wo})]$$

$$\alpha = 1 + 2.25 * \left(\frac{0.026 - 0.26}{0.26} \right) = 0.308$$

$$\beta = 1 + 1.458 * \left(\frac{1.923 - 12.05}{12.05} \right) = 1.155$$

$$\begin{aligned} E_z &= 1.4 - 0.1(0.308)(3 \text{ inches}) \\ &\quad + 1.155[0.4(3 \text{ inches}) + 0.1(3 \text{ inches} - 3 \text{ inches})] \\ &= 2.694 \text{ in} = 0.068 \text{ m} \end{aligned}$$

Next calculate the fractional area percentages. Because there are 6 half sections blocked out in each panel, the affected area is multiplied by $6/2 = 3$ since there are three collective connections (or three connection equivalents) per panel.

$$A_{total} = 3.66 \text{ m} * 9.14 \text{ m} = 33.445 \text{ m}^2$$

$$b_{aff} = b_{solid} + 2 * E_z = 0.203 \text{ m} + 2 * 0.068 \text{ m} = 0.442 \text{ m}$$

$$h_{aff} = b_{solid} + 2 * E_z = 0.203 \text{ m} + 2 * 0.068 \text{ m} = 0.442 \text{ m}$$

$$A_{aff} = 2 * b_{aff} * h_{aff} = 3 * 0.442 \text{ m} * 0.442 \text{ m} = 0.585 \text{ m}^2$$

$$a_{aff} = \frac{A_{aff}}{A_{total}} = \frac{0.585 \text{ m}^2}{33.445 \text{ m}^2} = 1.749\%$$

$$a_{insulated} = 1 - a_{solid} = 98.251\%$$

R-value can be calculated based off of the electrical circuit analogy in Figure A-13 as:

$$R = \frac{1}{\frac{a_{aff}}{R_o + R_{conc} + R_i} + \frac{a_{insulated}}{R_o + R_{wo} + R_{ins} + R_{wi} + R_i}}$$

where R_o = thermal resistance of outdoor air film

R_i = thermal resistance of outdoor air film

R is calculated as

$$R = \frac{t}{k}$$

where t = thickness of the layer in the direction of heat flow

k = thermal conductivity.

The R -values for each component using this equation are shown in the following table. Note that thickness of the solid section in this example incorporated the additional thickness of the corbel.

Element	Thickness, t (m)	Conductivity, k (W/m·K)	Thermal Resistance (m ² ·K/W)
Outdoor air film (summer)	n.a.	n.a.	$R_o = 0.044$
Outdoor air film (winter)	n.a.	n.a.	$R_o = 0.030$
Solid concrete section	0.229	1.923	$R_{conc} = 0.119$
Outside concrete wythe	0.076	1.923	$R_{wo} = 0.040$
Insulation wythe	0.076	0.026	$R_{ins} = 2.935$
Inside concrete wythe	0.076	1.923	$R_{wi} = 0.040$
Indoor air film	n.a.	n.a.	$R_i = 0.120$

For winter,

$$\begin{aligned}
 R &= \frac{1}{\frac{0.01749}{0.030 + 0.119 + 0.120} + \frac{0.98251}{0.030 + 0.040 + 2.935 + 0.040 + 0.120}} \\
 &= 2.662 \frac{m^2 \cdot K}{W} = \mathbf{15.116} \frac{ft^2 \cdot ^\circ F \cdot hr}{Btu}.
 \end{aligned}$$

For summer,

$$\begin{aligned}
 R &= \frac{1}{\frac{0.01749}{0.044 + 0.119 + 0.120} + \frac{0.98251}{0.044 + 0.040 + 2.935 + 0.040 + 0.120}} \\
 &= 2.695 \frac{m^2 \cdot K}{W} = \mathbf{15.304} \frac{ft^2 \cdot ^\circ F \cdot hr}{Btu}.
 \end{aligned}$$

Insulation Joints Example

Consider a 12 ft \times 30 ft panel assuming that all gaps between insulation segments add up to a total of $\frac{1}{4}$ inch along the entire length and also along the width as shown in the figure. The characteristic section method will be used to calculate the R-value.

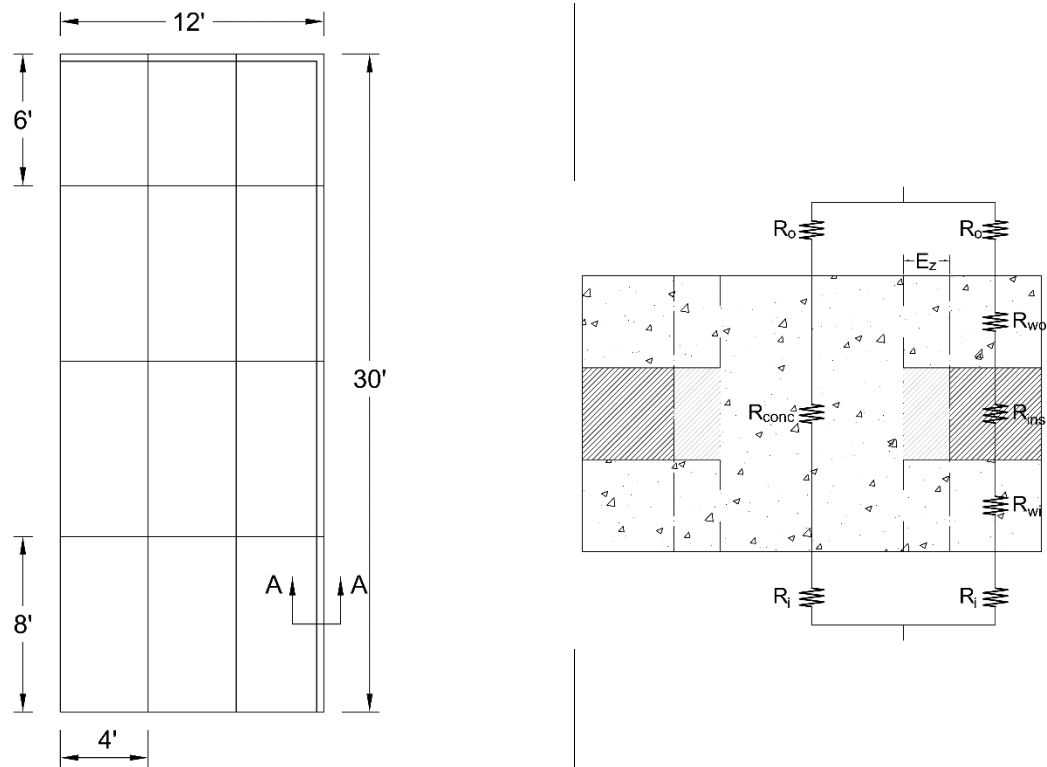


Figure A-14 Insulation Joint example panel layout, cross-section, and electrical circuit analogy

Using E_z

First calculate the affected zone dimensions. Remember that these empirical equations require that units be input as inches and BTU \cdot in/[hr \cdot ft $^2\cdot$ °F] to work.

$$E_z = 1.4 - 0.1\alpha t_{ins} + \beta[0.4t_{wo} + 0.1(t_{wi} - t_{wo})]$$

$$\alpha = 1 + 2.25 * \left(\frac{0.026 - 0.26}{0.26} \right) = 0.308$$

$$\beta = 1 + 1.458 * \left(\frac{1.923 - 12.05}{12.05} \right) = 1.155$$

$$\begin{aligned} E_z &= 1.4 - 0.1(0.308)(3 \text{ inches}) \\ &\quad + 1.155[0.4(3 \text{ inches}) + 0.1(3 \text{ inches} - 3 \text{ inches})] \\ &= 2.694 \text{ in} = \mathbf{0.068 \text{ m}} \end{aligned}$$

Next calculate the fractional area percentages. Since it is assumed that there is a consistent $\frac{1}{4}$ total solid concrete along the length and height of the panel, the area will be calculated with length being the constant 0.25 inches and the height being the sum of the length and height of the panel minus the overlap area. It would be senseless to add an “affected area” to the height value since this is limited to the actual height and length of the panel in this instance, therefore the affected area extension shall only be imposed upon the overall thickness value of the solid section.

$$A_{total} = 3.66 \text{ m} * 9.14 \text{ m} = 33.445 \text{ m}^2$$

$$b_{aff} = b_{solid} + 2 * E_z = 0.00635 \text{ m} + 2 * 0.068 \text{ m} = 0.143 \text{ m}$$

$$\begin{aligned} h_{aff} &= b_{total} + h_{total} - b_{solid} = 3.658 \text{ m} + 9.144 \text{ m} - 0.00635 \text{ m} \\ &= 12.795 \text{ m} \end{aligned}$$

$$A_{aff} = b_{aff} * h_{aff} = 0.143 \text{ m} * 12.795 \text{ m} = 1.832 \text{ m}^2$$

$$a_{aff} = \frac{A_{aff}}{A_{total}} = \frac{1.832 \text{ m}^2}{33.445 \text{ m}^2} = 5.478\%$$

$$a_{insulated} = 1 - a_{solid} = 94.522\%$$

R-value can then be calculated based off of the electrical circuit analogy in Figure A-14

as:

$$R = \frac{1}{\frac{a_{aff}}{R_o + R_{conc} + R_i} + \frac{a_{insulated}}{R_o + R_{wo} + R_{ins} + R_{wi} + R_i}}$$

where R_o = thermal resistance of outdoor air film

R_i = thermal resistance of outdoor air film

R is calculated as

$$R = \frac{t}{k}$$

where t = thickness of the layer in the direction of heat flow

k = thermal conductivity.

The R-values for each component using this equation are shown in the following table. Note that thickness of the solid section in this example incorporated the additional thickness of the corbel.

Element	Thickness, t (m)	Conductivity, k (W/m·K)	Thermal Resistance (m ² ·K/W)
Outdoor air film (summer)	n.a.	n.a.	$R_o = 0.044$
Outdoor air film (winter)	n.a.	n.a.	$R_o = 0.030$
Solid concrete section	0.229	1.923	$R_{conc} = 0.119$
Outside concrete wythe	0.076	1.923	$R_{wo} = 0.040$
Insulation wythe	0.076	0.026	$R_{ins} = 2.935$
Inside concrete wythe	0.076	1.923	$R_{wi} = 0.040$
Indoor air film	n.a.	n.a.	$R_i = 0.120$

For winter,

$$R = \frac{1}{\frac{0.05478}{0.030 + 0.119 + 0.120} + \frac{0.94522}{0.030 + 0.040 + 2.935 + 0.040 + 0.120}}$$

$$= 1.989 \frac{m^2 \cdot K}{W} = \mathbf{11.296} \frac{ft^2 \cdot ^\circ F \cdot hr}{Btu}.$$

For summer,

$$R = \frac{1}{\frac{0.05478}{0.044 + 0.119 + 0.120} + \frac{0.94522}{0.044 + 0.040 + 2.935 + 0.040 + 0.120}}$$

$$= 2.036 \frac{m^2 \cdot K}{W} = \mathbf{11.560} \frac{ft^2 \cdot ^\circ F \cdot hr}{Btu}.$$

This results in a 37% decrease from the ideal panel using the characteristic section method. The characteristic section method is an empirical equation used to provide an additional width to be considered as part of the solid region for improved accuracy. Use of the characteristic section method is a simplified method that may not accurately analyze this situation due to the narrowness of the concrete solid section, considering that this method ultimately estimated 15% of the concrete was “affected” (and therefore considered as solid section) compared to the less than 1% actual solid area.

Minimum Affected Area

Because the width of the breach is so small, it is possible that the affected area may be much smaller, though it is unknown how much smaller. This example shall now be repeated assuming that the affected width (E_z) is equal to the width itself (¼ inch) in

place of using the equation provided by the characteristic method equation to calculate this value. All other steps of the characteristic method shall be followed with this one exception.

First it is assumed that

$$E_z = 0.25 \text{ inches} = 0.00635 \text{ m}$$

Next calculate the fractional area percentages as before.

$$A_{total} = 3.66 \text{ m} * 9.14 \text{ m} = 33.445 \text{ m}^2$$

$$b_{aff} = b_{solid} + 2 * E_z = 0.00635 \text{ m} + 2 * 0.00635 \text{ m} = 0.019 \text{ m}$$

$$\begin{aligned} h_{aff} &= b_{total} + h_{total} - b_{solid} = 3.658 \text{ m} + 9.144 \text{ m} - 0.00635 \text{ m} \\ &= 12.795 \text{ m} \end{aligned}$$

$$A_{aff} = b_{aff} * h_{aff} = 0.019 \text{ m} * 12.795 \text{ m} = 0.244 \text{ m}^2$$

$$a_{aff} = \frac{A_{aff}}{A_{total}} = \frac{0.244 \text{ m}^2}{33.445 \text{ m}^2} = 0.729\%$$

$$a_{insulated} = 1 - a_{solid} = 99.271\%$$

R-value can then be calculated based off of the electrical circuit analogy in Figure A-14 as:

$$R = \frac{1}{\frac{a_{aff}}{R_o + R_{conc} + R_i} + \frac{a_{insulated}}{R_o + R_{wo} + R_{ins} + R_{wi} + R_i}}$$

where R_o = thermal resistance of outdoor air film

R_i = thermal resistance of outdoor air film

R is calculated as

$$R = \frac{t}{k}$$

where t = thickness of the layer in the direction of heat flow

k = thermal conductivity.

The R -values for each component using this equation are shown in the following table. Note that thickness of the solid section in this example incorporated the additional thickness of the corbel.

Element	Thickness, t (m)	Conductivity, k (W/m·K)	Thermal Resistance (m ² ·K/W)
Outdoor air film (summer)	n.a.	n.a.	$R_o = 0.044$
Outdoor air film (winter)	n.a.	n.a.	$R_o = 0.030$
Solid concrete section	0.229	1.923	$R_{conc} = 0.119$
Outside concrete wythe	0.076	1.923	$R_{wo} = 0.040$
Insulation wythe	0.076	0.026	$R_{ins} = 2.935$
Inside concrete wythe	0.076	1.923	$R_{wi} = 0.040$
Indoor air film	n.a.	n.a.	$R_i = 0.120$

For winter,

$$\begin{aligned}
 R &= \frac{1}{\frac{0.00729}{0.030 + 0.119 + 0.120} + \frac{0.99271}{0.030 + 0.040 + 2.935 + 0.040 + 0.120}} \\
 &= 2.934 \frac{m^2 \cdot K}{W} = \mathbf{16.658} \frac{ft^2 \cdot ^\circ F \cdot hr}{Btu}.
 \end{aligned}$$

For summer,

$$\begin{aligned}
 R &= \frac{1}{\frac{0.00729}{0.044 + 0.119 + 0.120} + \frac{0.99271}{0.044 + 0.040 + 2.935 + 0.040 + 0.120}} \\
 &= 2.957 \frac{m^2 \cdot K}{W} = \mathbf{16.793} \frac{ft^2 \cdot ^\circ F \cdot hr}{Btu}.
 \end{aligned}$$

This assumed a significantly smaller affected area than the characteristic section method, but still resulted in a decrease of thermal resistance of approximately 7.3%. It is very plausible that the actual affected zone could exceed this width, so 7% can be assumed to be a minimum for an overall total gap of this size.

SWP Connectors Example

Consider a 12 ft \times 30 ft panel with steel connectors. Two situations will be displayed in this example. The first involves steel pin connectors and the second steel truss connectors. The zone and modified zone methods will both be used and compared.

Steel Pins

The first example is an analysis of a panel with steel pins spaced every 18" \times 24" o.c with a diameter of $\frac{1}{4}$ inch and a 1 inch cover on both ends of the connector. The geometry of these pins is such that each pin crosses through the insulation twice per location.

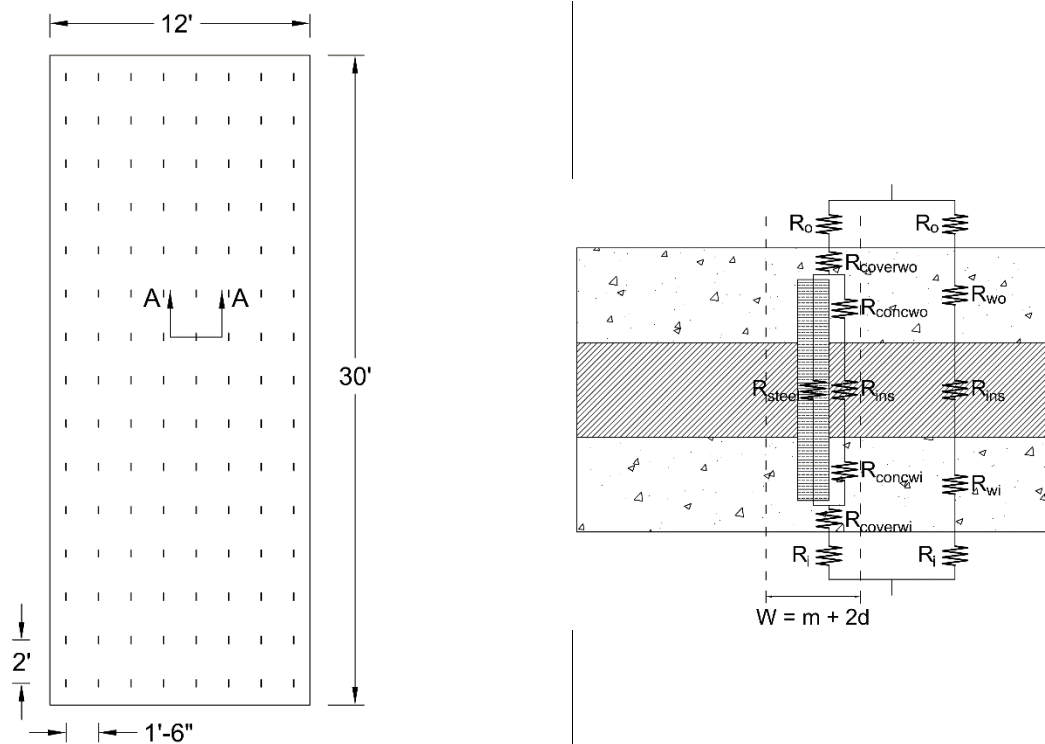


Figure A-15 Steel pin connector example panel layout and cross-section with electrical circuit analogy

First calculate the effective diameter and widths according to both the zone and modified zone methods. The zone method effective width (W) is listed first, followed by the modified zone method effective width (W_n). Values input into the modified zone method are in units of inches and $\text{BTU}\cdot\text{in}/\text{hr}\cdot\text{ft}^2\cdot^\circ\text{F}$.

$$m = \sqrt{4 * \frac{(A_{conn} * 2)}{\pi}} = \sqrt{4 * \frac{(6.334 * 10^{-5} m^2) * 2}{\pi}} = 0.00898 m$$

where A_{conn} = area of one segment of connector

$$W = m + 2d = 0.00898 m + 2 * 0.025 m = \mathbf{0.057 m}$$

$$\begin{aligned} W_n &= (0.174k_{conc} - k_{ins} + 0.0026k_{ct} + 2.24)m + 0.02k_{conc} - 0.6k_{ins} \\ &\quad + 0.0024k_{ct} + 2.35 - 0.15d \\ &= (0.174 * 13.333 - 0.18 + 0.0026 * 443 + 2.24) * 0.00898 + 0.02 \\ &\quad * 13.333 - 0.6 * 0.18 + 0.0024 * 443 + 2.35 - 0.15 * 1 \\ &= 4.586 in = \mathbf{0.116 m} \end{aligned}$$

Next calculate the fractional area percentages. The observed area will be the total area divided by the total number of connectors.

$$A_{total} = \frac{3.66 m * 9.14 m}{120} = 0.2787 m^2$$

$$A_{zoneA} = W^2 = (0.057 m)^2 = 0.0026 m^2$$

$$A_{zoneB} = A_{total} - A_{zoneA} = 0.2787 - 0.0026 = 0.2761 m^2$$

$$A_{modZA} = W_n^2 = (0.116 m)^2 = 0.0107 m^2$$

$$A_{modZB} = A_{total} - A_{modZA} = 0.2787 - 0.0107 = 0.2681 m^2$$

$$a_{zoneA} = \frac{A_{zoneA}}{A_{total}} = \frac{0.0026 \text{ m}^2}{0.2787 \text{ m}^2} = 0.920\%$$

$$a_{steelZ} = \frac{A_{steelZ}}{A_{zoneA}} = \frac{0.0000633 \text{ m}^2}{0.0026 \text{ m}^2} = 2.469\%$$

$$a_{restZ} = 1 - a_{steelZ} = 1 - 0.02469 = 97.531\%$$

$$a_{zoneB} = 1 - a_{zoneA} = 1 - 0.00920 = 99.080\%$$

$$a_{modZA} = \frac{A_{modZA}}{A_{total}} = \frac{0.0107 \text{ m}^2}{0.2787 \text{ m}^2} = 3.823\%$$

$$a_{steelM} = \frac{A_{steelM}}{A_{modZA}} = \frac{0.0000633 \text{ m}^2}{0.0107 \text{ m}^2} = 0.594\%$$

$$a_{restM} = 1 - a_{steelM} = 1 - 0.00694 = 99.406\%$$

$$a_{modZB} = 1 - a_{modZA} = 1 - 0.03276 = 96.117\%$$

R-value can then be calculated for both zone and modified zone method based off of the electrical circuit analogy in Figure A-15 as:

$$\frac{1}{R} = \frac{a_A}{R_A} + \frac{a_B}{R_B}$$

where

$$R_A = R_o + R_{coverwo} + \frac{1}{\frac{a_{steel}}{R_{steel}} + \frac{a_{rest}}{R_{concwo} + R_{ins} + R_{concwi}}} + R_{coverwi} + R_i$$

$$R_B = R_o + R_{wo} + R_{ins} + R_{wi} + R_i$$

where R_o = thermal resistance of outdoor air film

$R_{coverwo}$ = concrete cover on outside wythe side of connector

R_{steel} = thermal resistance of steel

R_{concwo} = concrete parallel to steel connector in outside wythe

R_{ins} = thermal resistance of insulation

R_{conzwi} = concrete parallel to steel connector in inside wythe

$R_{coverwi}$ = concrete cover on inside wythe side of connector

R_{wo} = thermal resistance of outside concrete wythe

R_{wi} = thermal resistance of inside concrete wythe

R_i = thermal resistance of indoor air film

R is calculated as

$$R = \frac{t}{k}$$

where t = thickness of the layer in the direction of heat flow

k = thermal conductivity.

The R-values for each component using this equation are shown in the following table. These elemental R-values are the same for both methods. The two methods only differ in the calculations of the fractional area percentages.

Element	Thickness, t (m)	Conductivity, k (W/m·K)	Thermal Resistance (m ² ·K/W)
Outdoor air film (summer)	n.a.	n.a.	$R_o = 0.044$
Outdoor air film (winter)	n.a.	n.a.	$R_o = 0.030$
Steel	0.178	63.9	$R_{steel} = 0.003$
Concrete cover (outer wythe)	0.025	1.923	$R_{coverwo} = 0.013$
Concrete parallel to connector (out)	0.051	1.923	$R_{concwo} = 0.026$
Concrete parallel to connector (in)	0.051	1.923	$R_{conzwi} = 0.026$
Concrete cover (inner wythe)	0.025	1.923	$R_{coverwi} = 0.013$
Outside concrete wythe	0.076	1.923	$R_{wo} = 0.040$
Insulation wythe	0.076	0.026	$R_{ins} = 2.935$
Inside concrete wythe	0.076	1.923	$R_{wi} = 0.040$
Indoor air film	n.a.	n.a.	$R_i = 0.120$

Zone Method

For winter,

$$\begin{aligned}
 R_{zoneA} &= R_o + R_{coverwo} + \frac{1}{\frac{a_{steelZ}}{R_{steel}} + \frac{a_{restZ}}{R_{concwo} + R_{ins} + R_{conzwi}}} + R_{coverwi} + R_i \\
 &= 0.030 + 0.013 + \frac{1}{\frac{0.02469}{0.003} + \frac{0.97531}{0.026 + 2.935 + 0.026}} + 0.013 + 0.120 \\
 &= 0.285 \frac{m^2 \cdot K}{W}.
 \end{aligned}$$

$$\begin{aligned}
 R_{zoneB} &= R_o + R_{wo} + R_{ins} + R_{wi} + R_i \\
 &= 0.030 + 0.040 + 2.935 + 0.040 + 0.120 \\
 &= 3.164 \frac{m^2 \cdot K}{W}.
 \end{aligned}$$

$$\begin{aligned}
 R &= \frac{1}{\frac{a_{zoneA}}{R_{zoneA}} + \frac{a_{zoneB}}{R_{zoneB}}} = \frac{1}{\frac{0.00920}{0.285} + \frac{0.99080}{3.164}} \\
 &= 2.895 \frac{m^2 \cdot K}{W} = \mathbf{16.437 \frac{ft^2 \cdot ^\circ F \cdot hr}{Btu}}.
 \end{aligned}$$

For summer,

$$\begin{aligned}
 R_{zoneA} &= R_o + R_{coverwo} + \frac{1}{\frac{a_{steel}}{R_{steel}} + \frac{a_{rest}}{R_{concwo} + R_{ins} + R_{concwi}}} + R_{coverwi} + R_i \\
 &= 0.044 + 0.013 + \frac{1}{\frac{0.02469}{0.003} + \frac{0.97531}{0.026 + 2.935 + 0.026}} + 0.013 + 0.120 \\
 &= 0.299 \frac{m^2 \cdot K}{W}
 \end{aligned}$$

$$\begin{aligned}
 R_{zoneB} &= R_o + R_{wo} + R_{ins} + R_{wi} + R_i \\
 &= 0.044 + 0.040 + 2.935 + 0.040 + 0.120 \\
 &= 3.178 \frac{m^2 \cdot K}{W}.
 \end{aligned}$$

$$\begin{aligned}
 R &= \frac{1}{\frac{a_{zoneA}}{R_{zoneA}} + \frac{a_{zoneB}}{R_{zoneB}}} = \frac{1}{\frac{0.00920}{0.299} + \frac{0.99080}{3.178}} \\
 &= 2.919 \frac{m^2 \cdot K}{W} = \mathbf{16.577 \frac{ft^2 \cdot ^\circ F \cdot hr}{Btu}}.
 \end{aligned}$$

Modified Zone Method

For winter,

$$\begin{aligned}
 R_{modZA} &= R_o + R_{coverwo} + \frac{1}{\frac{a_{steelM}}{R_{steel}} + \frac{a_{restM}}{R_{concwo} + R_{ins} + R_{concwi}}} + R_{coverwi} + R_i \\
 &= 0.030 + 0.013 + \frac{1}{\frac{0.00594}{0.003} + \frac{0.99406}{0.026 + 2.935 + 0.026}} + 0.013 + 0.120 \\
 &= 0.581 \frac{m^2 \cdot K}{W}
 \end{aligned}$$

$$\begin{aligned}
 R_{modZB} &= R_o + R_{wo} + R_{ins} + R_{wi} + R_i \\
 &= 0.030 + 0.040 + 2.935 + 0.040 + 0.120 \\
 &= 3.164 \frac{m^2 \cdot K}{W}.
 \end{aligned}$$

$$\begin{aligned}
 R &= \frac{1}{\frac{a_{modZA}}{R_{modZA}} + \frac{a_{modZB}}{R_{modZB}}} = \frac{1}{\frac{0.03823}{0.581} + \frac{0.96177}{3.164}} \\
 &= 2.705 \frac{m^2 \cdot K}{W} = 15.357 \frac{ft^2 \cdot ^\circ F \cdot hr}{Btu}.
 \end{aligned}$$

For summer,

$$\begin{aligned}
 R_{modZA} &= R_o + R_{coverwo} + \frac{1}{\frac{a_{steelM}}{R_{steel}} + \frac{a_{restM}}{R_{concwo} + R_{ins} + R_{concwi}}} + R_{coverwi} + R_i \\
 &= 0.044 + 0.013 + \frac{1}{\frac{0.00594}{0.003} + \frac{0.99406}{0.026 + 2.935 + 0.026}} + 0.013 + 0.120 \\
 &= 0.595 \frac{m^2 \cdot K}{W}
 \end{aligned}$$

$$\begin{aligned}
 R_{modZB} &= R_o + R_{wo} + R_{ins} + R_{wi} + R_i \\
 &= 0.044 + 0.040 + 2.935 + 0.040 + 0.120 \\
 &= 3.178 \frac{m^2 \cdot K}{W}.
 \end{aligned}$$

$$\begin{aligned}
 R &= \frac{1}{\frac{a_{modZA}}{R_{modZA}} + \frac{a_{modZB}}{R_{modZB}}} = \frac{1}{\frac{0.03823}{0.595} + \frac{0.96177}{3.178}} \\
 &= 2.726 \frac{m^2 \cdot K}{W} = \mathbf{15.479} \frac{ft^2 \cdot ^\circ F \cdot hr}{Btu}.
 \end{aligned}$$

Season	Zone	Modified	Perfectly Insulated
Summer	16.577	15.479	18.047
Winter	16.437	15.357	17.967

Steel Truss

The second example is an analysis of a panel with steel truss connectors spaced every 12 inches. The web members have a diameter of 0.225 inches and a 1 inch cover on both ends of the truss. Assume there are 91 web members per truss for this panel.

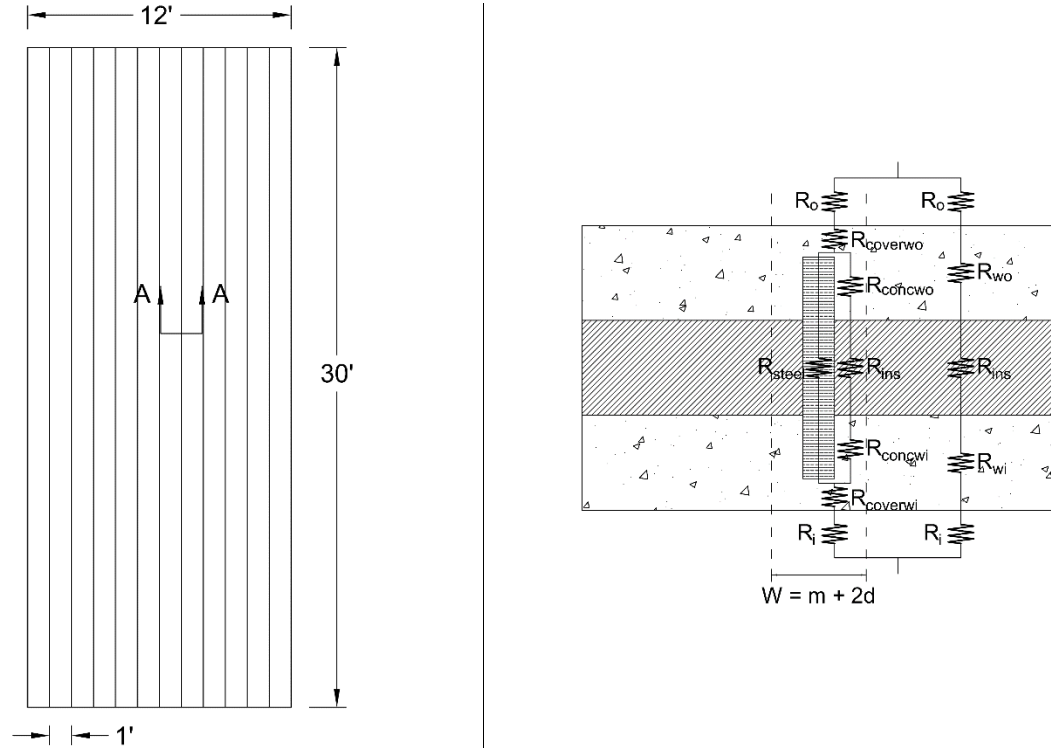


Figure A-16 Steel truss connector example panel layout and cross-section with electrical circuit analogy

First calculate the effective widths according to both the zone and modified zone methods. The zone method effective width (W) is listed first, followed by the modified zone method effective width (W_n). Values input into the modified zone method are in units of inches and $\text{BTU} \cdot \text{in} / \text{hr} \cdot \text{ft}^2 \cdot ^\circ\text{F}$.

$$W = m + 2d = 0.0057 \text{ m} + 2 * 0.0254 \text{ m} = \mathbf{0.057 \text{ m}}$$

$$W_n = (0.174k_{conc} - k_{ins} + 0.0026k_{ct} + 2.24)m + 0.02k_{conc} - 0.6k_{ins}$$

$$+ 0.0024k_{ct} + 2.35 - 0.15d$$

$$= (0.174 * 13.333 - 0.18 + 0.0026 * 443 + 2.24) * 0.0057 + 0.02$$

$$* 13.333 - 0.6 * 0.18 + 0.0024 * 443 + 2.35 - 0.15 * 1$$

$$= 4.162 \text{ in} = \mathbf{0.106 \text{ m}}$$

Next calculate the fractional area percentages. The observed area will be the total area divided by the total number of connectors.

$$A_{total} = \frac{3.66 \text{ m} * 9.14 \text{ m}}{6} = 5.574 \text{ m}^2$$

$$A_{steel} = \frac{\pi}{4} m^2 * 91 = \frac{\pi}{4} (0.0057 \text{ m})^2 * 91 = 0.00233 \text{ m}^2$$

$$A_{zoneA} = W * h = 0.057 \text{ m} * 9.14 \text{ m} = 0.517 \text{ m}^2$$

$$A_{zoneB} = A_{total} - A_{zoneA} = 5.574 - 0.517 = 5.057 \text{ m}^2$$

$$A_{modZA} = W_n * h = 0.106 \text{ m} * 9.14 \text{ m} = 0.967 \text{ m}^2$$

$$A_{modZB} = A_{total} - A_{modZA} = 5.574 - 0.967 = 4.607 \text{ m}^2$$

$$a_{zoneA} = \frac{A_{zoneA}}{A_{total}} = \frac{0.517 \text{ m}^2}{5.574 \text{ m}^2} = 9.271\%$$

$$a_{steelZ} = \frac{A_{steel}}{A_{zoneA}} = \frac{0.00233 \text{ m}^2}{0.517 \text{ m}^2} = 0.452\%$$

$$a_{restZ} = 1 - a_{steelZ} = 1 - 0.02469 = 99.548\%$$

$$a_{zoneB} = 1 - a_{zoneA} = 1 - 0.09271 = 99.729\%$$

$$a_{modZA} = \frac{A_{modZA}}{A_{total}} = \frac{0.967 \text{ m}^2}{5.574 \text{ m}^2} = 17.344\%$$

$$a_{steelM} = \frac{A_{steel}}{A_{modZA}} = \frac{0.0000633 \text{ m}^2}{0.967 \text{ m}^2} = 0.241\%$$

$$a_{restM} = 1 - a_{steelM} = 1 - 0.00241 = 99.759\%$$

$$a_{modZB} = 1 - a_{modZA} = 1 - 0.17344 = 82.656\%$$

R-value can then be calculated for both zone and modified zone method based off of the electrical circuit analogy in Figure A-16 as:

$$\frac{1}{R} = \frac{a_A}{R_A} + \frac{a_B}{R_B}$$

where

$$R_A = R_o + R_{coverwo} + \frac{1}{\frac{a_{steel}}{R_{steel}} + \frac{a_{rest}}{R_{concwo} + R_{ins} + R_{concwi}}} + R_{coverwi} + R_i$$

$$R_B = R_o + R_{wo} + R_{ins} + R_{wi} + R_i$$

where R_o = thermal resistance of outdoor air film

$R_{coverwo}$ = concrete cover on outside wythe side of connector

R_{steel} = thermal resistance of steel

R_{concwo} = concrete parallel to steel connector in outside wythe

R_{ins} = thermal resistance of insulation

R_{conzwi} = concrete parallel to steel connector in inside wythe

$R_{coverwi}$ = concrete cover on inside wythe side of connector

R_{wo} = thermal resistance of outside concrete wythe

R_{wi} = thermal resistance of inside concrete wythe

R_i = thermal resistance of indoor air film

R is calculated as

$$R = \frac{t}{k}$$

where t = thickness of the layer in the direction of heat flow

k = thermal conductivity.

The R-values for each component using this equation are shown in the following table. These elemental R-values are the same for both methods. The two methods only differ in the calculations of the fractional area percentages.

Element	Thickness, t (m)	Conductivity, k (W/m·K)	Thermal Resistance (m ² ·K/W)
Outdoor air film (summer)	n.a.	n.a.	$R_o = 0.044$
Outdoor air film (winter)	n.a.	n.a.	$R_o = 0.030$
Steel	0.178	63.9	$R_{steel} = 0.003$
Concrete cover (outer wythe)	0.025	1.923	$R_{coverwo} = 0.013$
Concrete parallel to connector (out)	0.051	1.923	$R_{concwo} = 0.026$
Concrete parallel to connector (in)	0.051	1.923	$R_{conzwi} = 0.026$
Concrete cover (inner wythe)	0.025	1.923	$R_{coverwi} = 0.013$
Outside concrete wythe	0.076	1.923	$R_{wo} = 0.040$
Insulation wythe	0.076	0.026	$R_{ins} = 2.935$
Inside concrete wythe	0.076	1.923	$R_{wi} = 0.040$
Indoor air film	n.a.	n.a.	$R_i = 0.120$

Zone Method

For winter,

$$\begin{aligned}
 R_{zoneA} &= R_o + R_{coverwo} + \frac{1}{\frac{a_{steelZ}}{R_{steel}} + \frac{a_{restZ}}{R_{concwo} + R_{ins} + R_{conzwi}}} + R_{coverwi} + R_i \\
 &= 0.030 + 0.013 + \frac{1}{\frac{0.00452}{0.003} + \frac{0.99548}{0.026 + 2.935 + 0.026}} + 0.013 + 0.120 \\
 &= 0.687 \frac{m^2 \cdot K}{W}
 \end{aligned}$$

$$\begin{aligned}
R_{zoneB} &= R_o + R_{wo} + R_{ins} + R_{wi} + R_i \\
&= 0.030 + 0.040 + 2.935 + 0.040 + 0.120 \\
&= 3.164 \frac{m^2 \cdot K}{W}.
\end{aligned}$$

$$\begin{aligned}
R &= \frac{1}{\frac{a_{zoneA}}{R_{zoneA}} + \frac{a_{zoneB}}{R_{zoneB}}} = \frac{1}{\frac{0.09271}{0.687} + \frac{0.90729}{3.164}} \\
&= 2.372 \frac{m^2 \cdot K}{W} = \mathbf{13.467 \frac{ft^2 \cdot ^\circ F \cdot hr}{Btu}}.
\end{aligned}$$

For summer,

$$\begin{aligned}
R_{zoneA} &= R_o + R_{coverwo} + \frac{1}{\frac{a_{steel}}{R_{steel}} + \frac{a_{rest}}{R_{concwo} + R_{ins} + R_{concwi}}} + R_{coverwi} + R_i \\
&= 0.044 + 0.013 + \frac{1}{\frac{0.00452}{0.003} + \frac{0.99548}{0.026 + 2.935 + 0.026}} + 0.013 + 0.120 \\
&= 0.701 \frac{m^2 \cdot K}{W}
\end{aligned}$$

$$\begin{aligned}
R_{zoneB} &= R_o + R_{wo} + R_{ins} + R_{wi} + R_i \\
&= 0.044 + 0.040 + 2.935 + 0.040 + 0.120 \\
&= 3.178 \frac{m^2 \cdot K}{W}.
\end{aligned}$$

$$\begin{aligned}
R &= \frac{1}{\frac{a_{zoneA}}{R_{zoneA}} + \frac{a_{zoneB}}{R_{zoneB}}} = \frac{1}{\frac{0.00920}{0.7001} + \frac{0.99080}{3.178}} \\
&= 2.394 \frac{m^2 \cdot K}{W} = \mathbf{13.595 \frac{ft^2 \cdot ^\circ F \cdot hr}{Btu}}.
\end{aligned}$$

Modified Zone Method

For winter,

$$\begin{aligned}
 R_{modZA} &= R_o + R_{coverwo} + \frac{1}{\frac{a_{steelM}}{R_{steel}} + \frac{a_{restM}}{R_{concwo} + R_{ins} + R_{concwi}}} + R_{coverwi} + R_i \\
 &= 0.030 + 0.013 + \frac{1}{\frac{0.00241}{0.003} + \frac{0.99759}{0.026 + 2.935 + 0.026}} + 0.013 + 0.120 \\
 &= 1.008 \frac{m^2 \cdot K}{W}
 \end{aligned}$$

$$\begin{aligned}
 R_{modZB} &= R_o + R_{wo} + R_{ins} + R_{wi} + R_i \\
 &= 0.030 + 0.040 + 2.935 + 0.040 + 0.120 \\
 &= 3.164 \frac{m^2 \cdot K}{W}.
 \end{aligned}$$

$$\begin{aligned}
 R &= \frac{1}{\frac{a_{modZA}}{R_{modZA}} + \frac{a_{modZB}}{R_{modZB}}} = \frac{1}{\frac{0.17344}{1.008} + \frac{0.82656}{3.164}} \\
 &= 2.308 \frac{m^2 \cdot K}{W} = \mathbf{13.107 \frac{ft^2 \cdot ^\circ F \cdot hr}{Btu}}.
 \end{aligned}$$

For summer,

$$\begin{aligned}
 R_{modZA} &= R_o + R_{coverwo} + \frac{1}{\frac{a_{steelM}}{R_{steel}} + \frac{a_{restM}}{R_{concwo} + R_{ins} + R_{concwi}}} + R_{coverwi} + R_i \\
 &= 0.044 + 0.013 + \frac{1}{\frac{0.00241}{0.003} + \frac{0.99759}{0.026 + 2.935 + 0.026}} + 0.013 + 0.120 \\
 &= 1.022 \frac{m^2 \cdot K}{W}
 \end{aligned}$$

$$\begin{aligned}
 R_{modZB} &= R_o + R_{wo} + R_{ins} + R_{wi} + R_i \\
 &= 0.044 + 0.040 + 2.935 + 0.040 + 0.120 \\
 &= 3.178 \frac{m^2 \cdot K}{W}.
 \end{aligned}$$

$$\begin{aligned}
 R &= \frac{1}{\frac{a_{modZA}}{R_{modZA}} + \frac{a_{modZB}}{R_{modZB}}} = \frac{1}{\frac{0.17344}{1.022} + \frac{0.82656}{3.178}} \\
 &= 2.327 \frac{m^2 \cdot K}{W} = \mathbf{13.214} \frac{ft^2 \cdot ^\circ F \cdot hr}{Btu}.
 \end{aligned}$$

Season	Zone	Modified	Perfectly Insulated
Summer	13.595	13.214	18.047
Winter	13.467	13.107	17.967

APPENDIX B. CORBEL DESIGN CALCULATIONS

Material Properties

This appendix contains the design calculations for each of the 12 specimens created and tested in this report. Each of the designs used either the Deep Beam method or the Strut-and-Tie method. Because the same loads were used for each specimen, the load determination calculations are included in a first separate section, followed by the calculations for each individual SWP.

Loads

Loading assumed that panels would support a 12DT28+2 double-tee beam with a span of 50 ft, having a self-weight of 81 psf in an attempt to use a member that might be common for a large part of the industry. Design also included a horizontal force equal to 20% of the vertical force as well. Loads for all SWP corbel specimens was as follows:

Double-tee length, $L_{DT} = 50 \text{ ft}$

Double-tee width, $b_{DT} = 12 \text{ ft}$

Double-tee self-weight, $p_{DT} = 81 \text{ psf}$

Floor super imposed dead load, $p_{SIDL} = 15 \text{ psf}$

Floor live load, $p_{LL} = 55 \text{ psf}$

Floor sustained load, $p_{LLsust} = 0.25 p_{LL} = 13.75 \text{ psf}$

Dead load, $w_{DL} = (p_{DT} + p_{SIDL})b_{DT} = (81 \text{ psf} + 15 \text{ psf})(12 \text{ ft}) = 1152 \text{ lbf/ft}$

Live load, $w_{LL} = p_{LL}b_{DT} = (55 \text{ psf})(12 \text{ ft}) = 660 \text{ lbf/ft}$

Sustained load, $w_{sust} = p_{LLsust} b_{DT} = (13.75 \text{ psf})(12 \text{ ft}) = 165 \text{ lb/ft}$

$$\begin{aligned}
 V_u &= \max \left[\begin{array}{c} 1.4 \left(\frac{w_{DL} * L_{DT}}{n_R} \right) \\ 1.2 \left(\frac{w_{DL} * L_{DT}}{n_R} \right) + 1.6 \left(\frac{w_{LL} * L_{DT}}{n_R} \right) \end{array} \right] \\
 &= \max \left[\begin{array}{c} 1.4 \left(\frac{1152 \text{ psf} * 50 \text{ ft}}{4} \right) \\ 1.2 \left(\frac{1152 \text{ psf} * 50 \text{ ft}}{4} \right) + 1.6 \left(\frac{660 \text{ psf} * 50 \text{ ft}}{4} \right) \end{array} \right] \\
 &= \max \left[\begin{array}{c} 20.16 \text{ kip} \\ 30.48 \text{ kip} \end{array} \right] = 30.5 \text{ kip} \\
 V_{serv} &= \left(\frac{w_{DL} * L_{DT}}{n_R} \right) + \left(\frac{w_{LL} * L_{DT}}{n_R} \right) = \left(\frac{1152 \text{ psf} * 50 \text{ ft}}{4} \right) + \left(\frac{660 \text{ psf} * 50 \text{ ft}}{4} \right) \\
 &= 22.65 \text{ kip} \\
 V_{sust} &= \left(\frac{w_{DL} * L_{DT}}{n_R} \right) + \left(\frac{w_{sust} * L_{DT}}{n_R} \right) = \left(\frac{1152 \text{ psf} * 50 \text{ ft}}{4} \right) + \left(\frac{165 \text{ psf} * 50 \text{ ft}}{4} \right) \\
 &= 16.46 \text{ kip}
 \end{aligned}$$

$$N_{uc} = 0.2 V_u = 0.2(30.5 \text{ kip}) = 6.10 \text{ kip}$$

$$R_u = \sqrt{V_u^2 + N_{uc}^2} = \sqrt{(30.5 \text{ kip})^2 + (6.1 \text{ kip})^2} = 31.08 \text{ kip}$$

$$\theta_R = \text{atan} \left(\frac{N_{uc}}{V_u} \right) = \text{atan} \left(\frac{6.1 \text{ kip}}{30.5 \text{ kip}} \right) = 11.31^\circ = 0.1974 \text{ rad}$$

SolidWall Calculations

The SolidWall specimen used the Deep Beam method for design.

Material Properties

Concrete

$$f'_c = 8.0 \text{ ksi}$$

$$f_r = 7.5\sqrt{f'_c} = 0.671 \text{ ksi}$$

$$w_c = 150 \text{ lbf/ft}$$

$$E_c = 33w_c^{1.5}\sqrt{f'_c} = 5422 \text{ ksi}$$

$$n = \frac{E_s}{E_c} = 5.348$$

Steel

$$f_y = 60 \text{ ksi}$$

$$E_s = 29000 \text{ ksi}$$

Geometrical Dimensions

SWP

$$t = 9 \text{ in}$$

$$b = 6 \text{ ft}$$

$$h = 8 \text{ ft}$$

$$d_{hout} = 7.5 \text{ in}$$

$$d_{hin} = 1.5 \text{ in}$$

$$I_g = \frac{bt^3}{12} = \frac{72 \text{ in}(9 \text{ in})^3}{12} = 4374 \text{ in}^4$$

Corbel

$$h_c = 14 \text{ in}$$

$$d = 12 \text{ in}$$

$$b_c = 10 \text{ in}$$

$$l_p = 8 \text{ in}$$

$$h_{cf} = 10 \text{ in}$$

$$c_c = 1.5 \text{ in}$$

$$I_{gc} = \frac{b_c h_c^3}{12} = \frac{10 \text{ in}(14 \text{ in})^3}{12} = 2287 \text{ in}^4$$

Plate Size

$$V_u = \Phi P_{nb} = \Phi 0.85 f'_c A_1$$

(ACI 318-14 §22.8.3.2)

$$\Phi_{\text{bear}} = 0.65 \quad (\text{ACI 318-14 §21.2.1})$$

$$A_1 = \frac{V_u}{\Phi_{\text{bear}} 0.85 f'_c} = \frac{30.5 \text{ kip}}{0.65(0.85)(8 \text{ ksi})} = 6.9 \text{ in}^2$$

$$L_{\text{bear}, \min} = \frac{A_1}{b_c} = 0.69 \text{ in}$$

Therefore use at least 1 in \times 10 in plate.

Shear Span, a_v

Assume $a_v = 5 \text{ in}$.

Determine Corbel Depth by Limiting Shear Transfer Strength, V_n

$$V_{n\max} = \min \left[\begin{array}{c} 0.2 f'_c b_c d \\ (480 + 0.8 f'_c) b_c d \\ 1600 b_c d \end{array} \right] \quad (\text{ACI 318-14 §11.8.3.2.1})$$

$$= \min \left[\begin{array}{c} 0.2(8 \text{ ksi})(10 \text{ in})(12 \text{ in}) \\ (0.48 + 0.8(8 \text{ ksi}))(10 \text{ in})(12 \text{ in}) \\ 1600(10 \text{ in})(12 \text{ in}) \end{array} \right]$$

$$= \min \left[\begin{array}{c} 192 \text{ kip} \\ 134.4 \text{ kip} \\ 192 \text{ kip} \end{array} \right]$$

$$= 134.4 \text{ kip} \geq V_u = 30.5 \text{ kip} \therefore \text{OK}$$

$$d_{\min} = \frac{V_u}{\left(\frac{\Phi V_{n\max}}{d} \right)} = \frac{30.5 \text{ kip}}{\left(\frac{0.75(134.4 \text{ kip})}{12 \text{ in}} \right)}$$

$$= 3.63 \text{ in} \leq 12 \text{ in} \therefore \text{OK, current } h \text{ will suffice}$$

$$\frac{a_v}{d} = \frac{5 \text{ in}}{12 \text{ in}} = 0.42 < 1 \therefore \text{OK} \quad (\text{ACI 318-14 §11.8.1a})$$

Determine Shear-Friction Reinforcement, A_{vf}

$$\mu = 1 \quad (\text{ACI 318-14 §11.6.4.3})$$

$$A_{vf,min} = \frac{V_u}{\Phi f_y \mu} = \frac{30.5 \text{ kip}}{0.75(60 \text{ ksi})(1)} = 0.68 \text{ in}^2 \quad \begin{array}{l} \text{(ACI 318-14 §11.8.3.2)} \\ \text{(ACI 318-14 §11.6.4.1)} \end{array}$$

Determine Direct Tension Reinforcement, A_n

$$A_{n,min} = \frac{N_{uc}}{\Phi f_y} = \frac{6.1 \text{ kip}}{0.75(60 \text{ ksi})} = 0.14 \text{ in}^2 \quad \text{(ACI 318-14 §11.8.3.4)}$$

Determine Flexural Reinforcement, A_f

$$\begin{aligned} M_u &= V_u a_v + N_{uc}(h_c - d) \\ &= (30.5 \text{ kip})(5 \text{ in}) + (6.1 \text{ kip})(14 \text{ in} - 12 \text{ in}) \\ &= 164.6 \text{ kip} \cdot \text{in} \end{aligned}$$

$$A_{f,min} = \frac{M_u}{\Phi f_y d} = \frac{164.6 \text{ kip} \cdot \text{in}}{0.75(60 \text{ ksi})(12 \text{ in})} = 0.31 \text{ in}^2 \quad \text{(ACI 318-14 §11.8.3.3)}$$

Determine Primary Tension Reinforcement, A_{sc}

$$A_{sc,min} = \max \left[\begin{array}{l} \frac{2}{3} A_{vf,min} + A_{n,min} \\ A_{f,min} + A_{n,min} \\ 0.04 \frac{f'_c}{f_y} b_c d \end{array} \right] \quad \text{(ACI 318-14 §11.8.3.4)}$$

$$= \max \left[\begin{array}{l} \frac{2}{3} (0.68 \text{ in}^2) + (0.14 \text{ in}^2) \\ (0.31 \text{ in}^2) + (0.14 \text{ in}^2) \\ 0.04 \left(\frac{8 \text{ ksi}}{60 \text{ ksi}} \right) (10 \text{ in})(12 \text{ in}) \end{array} \right]$$

$$= \max \left[\begin{array}{l} 0.59 \text{ in}^2 \\ 0.44 \text{ in}^2 \\ 0.64 \text{ in}^2 \end{array} \right] = 0.64 \text{ in}^2$$

Try (4) #4 bars, $A_{sc} = 0.8 \text{ in}^2$

$$s_{sc,max} = \frac{10 \text{ in} - 2(0.75 \text{ in})}{4 - 1} = 2.83 \text{ in}$$

Therefore use (4) #4 bars at 2.25" o.c.

Anchorage Requirements

$$l_{dh} = \left(\frac{f_y \psi_e \psi_c \psi_r}{50 \lambda \sqrt{f'_c}} \right) d_b \quad (\text{ACI 318-14 §25.4.3.1})$$

$$\psi_e = 1 \quad (\text{because using uncoated, regular rebar})$$

$$\psi_c = 1 \quad (\text{because cover not } \geq 2.5 \text{ in})$$

$$\psi_r = 1 \quad (\text{because not enclosed})$$

$$\lambda = 1 \quad (\text{because normalweight concrete})$$

$$d_b = 0.5 \text{ in}$$

$$l_{dh} = \left(\frac{(1)(1)(1)(60 \text{ ksi})}{50(1)\sqrt{8000 \text{ psi}} \left(\frac{1 \text{ ksi}}{1000 \text{ psi}} \right)} \right) d_b = 6.71 \text{ in}$$

$$l_{dh} = \max \left[\frac{l_{dh}}{8d_{b4}} \right] = \max \left[\frac{6.71 \text{ in}}{4 \text{ in}} \right] = 6.71 \text{ in} \quad (\text{ACI 318-11 §12.5.1})$$

Therefore need 7 inches of rebar beyond bend for principle reinforcement:

$$l_{out} = l_{dh} + (3d_b + d_b) = 8.71 \text{ in} \quad (\text{ACI 318-11 §12.5.1})$$

Principle reinforcement shall extend 12 inches from top of the bend.

Determine Shear Reinforcement, A_h

$$A_{h,min} = 0.5(A_{sc,min} - A_{n,min}) \quad (\text{ACI 318-14 §11.8.4})$$

$$= 0.5(0.64 \text{ in}^2 - 0.14 \text{ in}^2) = 0.25 \text{ in}^2$$

Therefore use (2) #3 stirrups, $A_h = 0.44 \text{ in}^2$, which must be distributed in two-thirds of effective corbel depth adjacent to A_{sc} . Therefore, place the bars 3" o.c. below A_{sc} .

Vertical/Longitudinal Reinforcement, A_{sl}

$$\Phi_{flex} = 0.9$$

$$\begin{aligned} M_u &= V_u \left(a_v + \frac{t}{2} \right) + N_{uc}(h_c - d) \\ &= 30.5 \text{ kip} \left(5 \text{ in} + \frac{9 \text{ in}}{2} \right) + 6.1 \text{ kip}(14 \text{ in} - 12 \text{ in}) \\ &= 301.8 \text{ kip} \cdot \text{in} \end{aligned}$$

$$A_{sl} = \frac{M_u}{\Phi f_y d_{reinf}} = \frac{301.8 \text{ kip} \cdot \text{in}}{0.9(60 \text{ ksi})(6 \text{ in})} = 0.93 \text{ in}^2$$

$$\rho = \frac{A_{sl,min}}{A_{gc}} = 0.0012 \quad (\text{ACI 381-14 §14.3.2})$$

$$A_{gcl} = b * t = 72 \text{ in} * 9 \text{ in} = 648 \text{ in}^2$$

$$A_{sl,min} = \rho A_{gcl} = 0.0012(648 \text{ in}^2) = 0.78 \text{ in}^2 < A_{sl} \quad \text{Therefore OK}$$

Design is restricted to using #4 bars because of limitations on bend radius, therefore

$$N_l = \frac{A_{sl}}{A_{\#4}} = \frac{0.93 \text{ in}^2}{0.2 \text{ in}^2} = 4.66 \quad \therefore \text{use (5) \#4 bars}$$

$$s = \frac{b - 2(0.75 \text{ in})}{N_l} = \frac{72 \text{ in} - 1.5 \text{ in}}{5} = 14.1 \text{ in}$$

$$s_{max} = \min \left(\frac{3t}{18 \text{ in}} \right) = \max \left(\frac{27 \text{ in}}{18 \text{ in}} \right) = 18 \text{ in} > s \quad \text{Therefore OK}$$

Therefore use (5) #4 bars spaced 14" o.c. to resist flexure. Place second layer of rebar on compression side for any reversed loading.

Horizontal/Transverse Reinforcement, A_{st}

$$\rho = \frac{A_{st,min}}{A_{gc}} = 0.0020 \quad (\text{ACI 381-14 §14.3.3})$$

$$A_{gct} = h * t = 96 \text{ in} * 9 \text{ in} = 864 \text{ in}^2$$

$$A_{st,min} = \rho A_{gcl} = 0.002(864 \text{ in}^2) = 1.73 \text{ in}^2$$

$$N_t = \frac{A_{st,min}}{A_{\#4}} = \frac{1.73 \text{ in}^2}{0.31 \text{ in}^2} = 6 \quad \therefore \text{use (6) \#5 bars}$$

$$s = \frac{h - 2(0.75 \text{ in})}{N_t} = \frac{96 \text{ in} - 1.5 \text{ in}}{5} = 15.75 \text{ in}$$

$$s_{max} = \min \left(\frac{3t}{18 \text{ in}} \right) = \max \left(\frac{27 \text{ in}}{18 \text{ in}} \right) = 18 \text{ in} > s \quad \text{Therefore OK}$$

Therefore use (6) #5 bars spaced 15" o.c. per code minimum requirements. Place second layer of rebar on opposite side for symmetry.

Lifting

$$x_{lift} = 18 \text{ in} = 1.5 \text{ ft} \quad (\text{anchor to edge distance})$$

$$x_{midL} = h - 2x_{anchor} = 8 \text{ ft} - 3 \text{ ft} = 5 \text{ ft}$$

$$x_{midR} = b - 2x_{anchor} = 6 \text{ ft} - 3 \text{ ft} = 3 \text{ ft}$$

Longitudinal Direction

$$w_{sw} = w_c b t = (150 \text{ pcf})(6 \text{ ft})(0.75 \text{ ft}) = 675 \frac{\text{lb}}{\text{ft}}$$

$$R_A = \frac{w_{sw} h}{2} = \frac{\left(0.675 \frac{\text{kip}}{\text{ft}}\right)(8 \text{ ft})}{2} = 2.7 \text{ kip}$$

$$V_{lift,left} = w_{sw} x_{lift} = \left(0.675 \frac{\text{kip}}{\text{ft}}\right)(1.5 \text{ ft})$$

$$= -1.0125 \text{ kip}$$

$$V_{lift,right} = w_{sw} x_{lift} + R_A = -1.01 \text{ kip} + 2.7 \text{ kip}$$

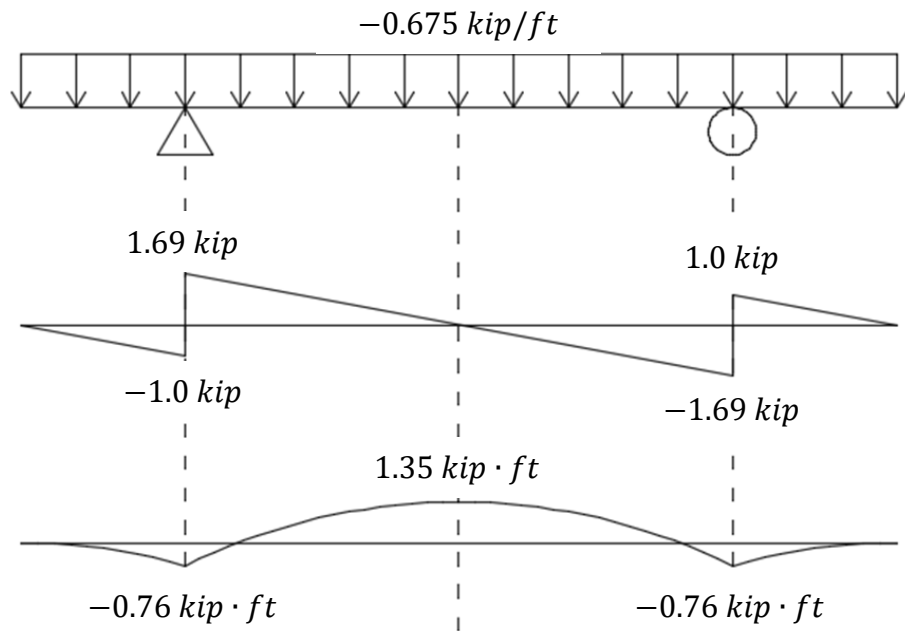
$$= 1.6875 \text{ kip}$$

$$M_{lift} = \frac{V_{lift,left} x_{lift}}{2} = \frac{(-1.01 \text{ kip})(1.5 \text{ ft})}{2}$$

$$= -0.7594 \text{ kip} \cdot \text{ft}$$

$$M_{mid} = M_{lift} + \frac{V_{lift,right}(0.5x_{midL})}{2}$$

$$= -0.76 \text{ kip} \cdot \text{ft} + \frac{1.69 \text{ kip}(0.5 \cdot 5 \text{ ft})}{2} = 1.35 \text{ kip} \cdot \text{ft}$$



Cracking moment is equal to

$$M_{cr} = \frac{7.5\sqrt{f'_c}I_g}{0.5t}$$

$$f'_{c,req} = \left(\frac{0.5tM_{mid}}{7.5I_g}\right)^2$$

$$= \left(\frac{0.5(9\text{ in})\left(1.35\text{ kip} \cdot \text{ft} * \frac{12\text{ in}}{\text{ft}}\right)}{7.5(4374\text{ in}^4)}\right)^2 = 0.0049\text{ ksi}$$

Therefore we need to attain at least 0.0049 ksi before lifting.

Transverse Direction

$$w_{sw} = w_c h t = (150\text{ pcf})(8\text{ ft})(0.75\text{ ft}) = 900 \frac{\text{lb}}{\text{ft}}$$

$$R_A = \frac{w_{sw}b}{2} = \frac{\left(0.9 \frac{\text{kip}}{\text{ft}}\right)(6\text{ ft})}{2} = 2.7\text{ kip}$$

$$V_{lift,left} = w_{sw}x_{lift} = \left(0.9 \frac{\text{kip}}{\text{ft}}\right)(1.5\text{ ft})$$

$$= -1.35\text{ kip}$$

$$V_{lift,right} = w_{sw}x_{lift} + R_A = -1.35\text{ kip} + 2.7\text{ kip}$$

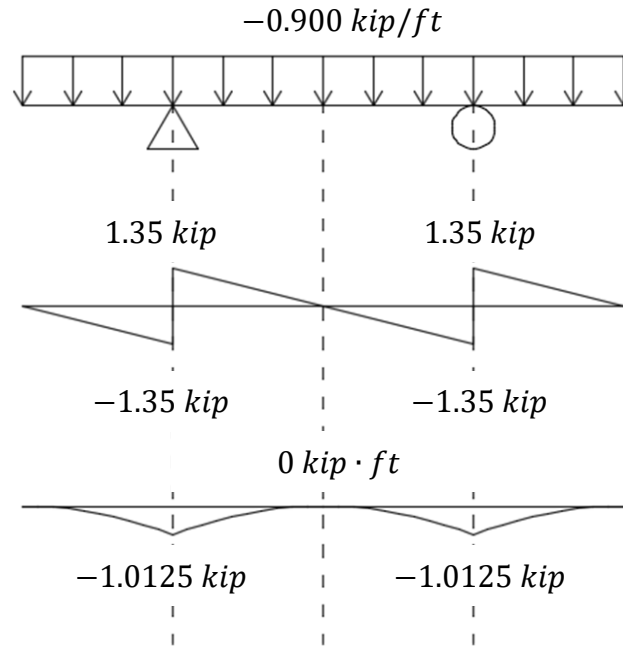
$$= 1.35\text{ kip}$$

$$M_{lift} = \frac{V_{lift,left}x_{lift}}{2} = \frac{(-1.35\text{ kip})(1.5\text{ ft})}{2}$$

$$= -1.0125\text{ kip} \cdot \text{ft}$$

$$M_{mid} = M_{lift} + \frac{V_{lift,right}(0.5x_{midT})}{2}$$

$$= -1.01\text{ kip} \cdot \text{ft} + \frac{1.35\text{ kip}(0.5*3\text{ ft})}{2} = 0\text{ kip} \cdot \text{ft}$$



Cracking moment is equal to

$$M_{cr} = \frac{7.5\sqrt{f'_c}I_g}{0.5t}$$

$$f'_{c,req} = \left(\frac{0.5tM_{lift}}{7.5I_g} \right)^2$$

$$= \left(\frac{0.5(9 \text{ in}) \left(1.02 \text{ kip} \cdot \text{ft} * \frac{12 \text{ in}}{\text{ft}} \right)}{7.5(4374 \text{ in}^4)} \right)^2 = 0.0028 \text{ ksi}$$

Therefore we need to attain at least 0.0028 ksi before lifting to avoid cracking the panel.

Since the concrete lifting anchor strengths are based on a concrete strength of 3.5 ksi,

however, the panels may not be lifted until $f'_c = 3.5 \text{ ksi}$.

$$f'_{c,req} = \max \begin{pmatrix} f'_{c,reqL} \\ f'_{c,reqT} \\ f'_{c,reqA} \end{pmatrix} = \max \begin{pmatrix} 0.0049 \text{ ksi} \\ 0.0028 \text{ ksi} \\ 3.5 \text{ ksi} \end{pmatrix} = 3.5 \text{ ksi}$$

SolidSec Calculations

The SolidSec specimen used the Strut-and-Tie method for design.

Material Properties

Concrete

$$f'_c = 8.0 \text{ ksi}$$

$$f_r = 7.5\sqrt{f'_c} = 0.671 \text{ ksi}$$

$$w_c = 150 \text{ lbf/ft}$$

$$E_c = 33w_c^{1.5}\sqrt{f'_c} = 5422 \text{ ksi}$$

$$n = \frac{E_s}{E_c} = 5.348$$

Steel

$$f_y = 60 \text{ ksi}$$

$$E_s = 29000 \text{ ksi}$$

Geometrical Dimensions

SWP

$$t_{wy0} = t_{wyi} = t_{ins} = 3 \text{ in}$$

$$t_{SWP} = t_{wy0} + t_{wyi} + t_{ins} = 9 \text{ in}$$

$$b = 6 \text{ ft}$$

$$h = 8 \text{ ft}$$

$$d_{hout} = 7.5 \text{ in}$$

$$d_{hin} = 1.5 \text{ in}$$

$$I_{gSWP} = \frac{bt_{SWP}^3}{12} - \frac{bt_{ins}^3}{12}$$

$$= \frac{72 \text{ in}(9 \text{ in})^3}{12} - \frac{72 \text{ in}(3 \text{ in})^3}{12} = 4212 \text{ in}^4$$

Corbel

$$h_c = 14 \text{ in}$$

$$d = 12 \text{ in}$$

$$b_c = 10 \text{ in}$$

$$l_p = 8 \text{ in}$$

$$h_{cf} = 10 \text{ in}$$

$$c_c = 1.5 \text{ in}$$

$$I_{gc} = \frac{b_c h_c^3}{12} = \frac{10 \text{ in}(14 \text{ in})^3}{12} = 2287 \text{ in}^4$$

Plate Size

$$V_u = \Phi P_{nb} = \Phi 0.85 f'_c A_1 \quad (\text{ACI 318-14 §22.8.3.2})$$

$$\Phi_{\text{bear}} = 0.65 \quad (\text{ACI 318-14 §21.2.1})$$

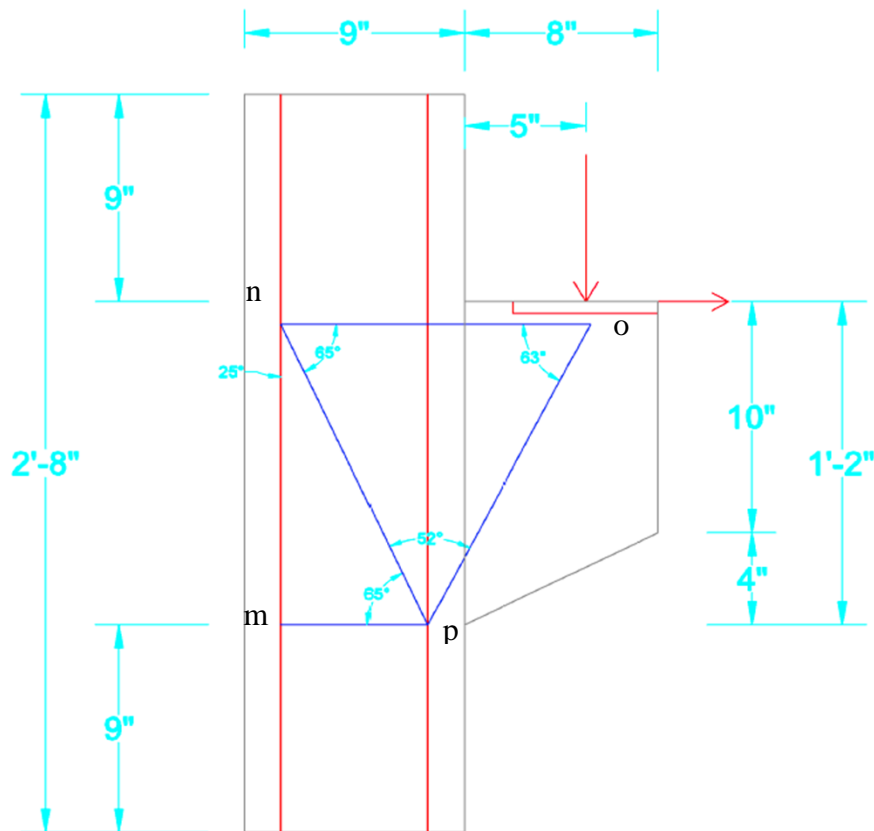
$$A_1 = \frac{V_u}{\Phi_{\text{bear}} 0.85 f'_c} = \frac{30.5 \text{ kip}}{0.65(0.85)(8 \text{ ksi})} = 6.9 \text{ in}^2$$

$$L_{\text{bear}, \text{min}} = \frac{A_1}{b_c} = 0.69 \text{ in}$$

Therefore use at least 1 in \times 10 in plate.

Shear Span, a_v

Assume $a_v = 5 \text{ in.}$

Determine Truss Geometry

$$\begin{aligned}
 l_{no} &= d_{hout} + a_v + (1 \text{ in}) \tan \theta_R \\
 &= 7.5 \text{ in} + 5 \text{ in} + (1 \text{ in}) \tan(11.31^\circ) = 12.7 \text{ in}
 \end{aligned}$$

$$\begin{aligned}
 \theta_{nop} &= \text{atan}\left(\frac{d}{l_{no} - (d_{hout} - d_{hin})}\right) \\
 &= \text{atan}\left(\frac{12 \text{ in}}{12.7 \text{ in} - (7.5 \text{ in} - 1.5 \text{ in})}\right) = 60.82^\circ
 \end{aligned}$$

$$l_{mn} = d = 12 \text{ in}$$

$$l_{mp} = d_{hout} - d_{hin} = 7.5 \text{ in} - 1.5 \text{ in} = 6 \text{ in}$$

$$\theta_{pno} = \text{atan}\left(\frac{d}{l_{mp}}\right) = \text{atan}\left(\frac{12}{6}\right) = 63.44^\circ$$

$$\begin{aligned}
 \theta_{npo} &= 180^\circ - \theta_{pno} - \theta_{nop} \\
 &= 180^\circ - 63.44^\circ - 60.82^\circ \\
 &= 55.74^\circ
 \end{aligned}$$

$$\theta_{mpn} = \theta_{pno} = 63.44^\circ$$

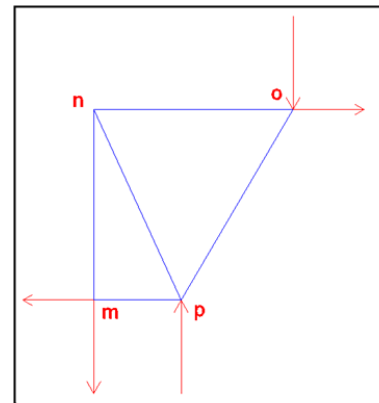
Determine Forces in Truss Components

$$\Sigma M_m = V_u l_{no} + N_{uc} l_{mn} - R_{py} l_{mp} = 0$$

$$\begin{aligned}
 R_{py} &= \frac{V_u l_{no} + N_{uc} l_{mn}}{l_{mp}} \\
 &= \frac{(30.5 \text{ kip})(12.7 \text{ in}) + (6.1 \text{ kip})(12 \text{ in})}{6 \text{ in}} \\
 &= 76.7 \text{ kip (C)}
 \end{aligned}$$

$$\Sigma F_y = 0$$

$$R_{my} = R_{py} - V_u = 46.2 \text{ kip (T)}$$



$$\Sigma F_x = 0$$

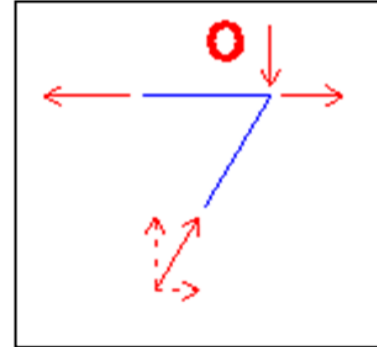
$$R_{mx} = N_{uc} = 6.1 \text{ kip (T)}$$

$$N_{opy} = V_u = 30.5 \text{ kip}$$

$$N_{opx} = \frac{N_{opy}}{\tan(\theta_{nop})} = \frac{30.5 \text{ kip}}{\tan(60.82^\circ)} = 17.0 \text{ kip}$$

$$\begin{aligned} N_{op} &= \sqrt{N_{opx}^2 + N_{opy}^2} \\ &= \sqrt{(17.0 \text{ kip})^2 + (30.5 \text{ kip})^2} \\ &= 34.9 \text{ kip (C)} \end{aligned}$$

$$\begin{aligned} N_{no} &= N_{opx} + N_{uc} = 17.0 \text{ kip} + 6.1 \text{ kip} \\ &= 23.1 \text{ kip (T)} \end{aligned}$$



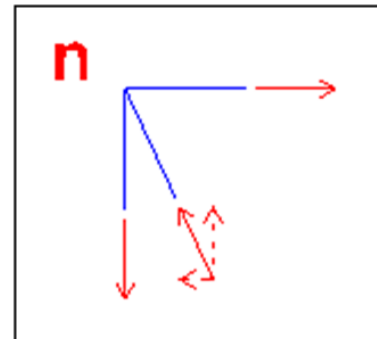
$$N_{np x} = N_{no} = 23.1 \text{ kip}$$

$$\begin{aligned} N_{np y} &= N_{np x} \tan(\theta_{pno}) \\ &= (23.1 \text{ kip}) \tan(63.44^\circ) = 46.2 \text{ kip} \end{aligned}$$

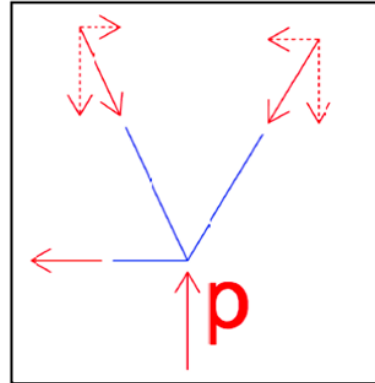
$$\begin{aligned} N_{np} &= \sqrt{N_{np x}^2 + N_{np y}^2} \\ &= \sqrt{(23.1 \text{ kip})^2 + (46.2 \text{ kip})^2} = \end{aligned}$$

$$51.7 \text{ kip (C)}$$

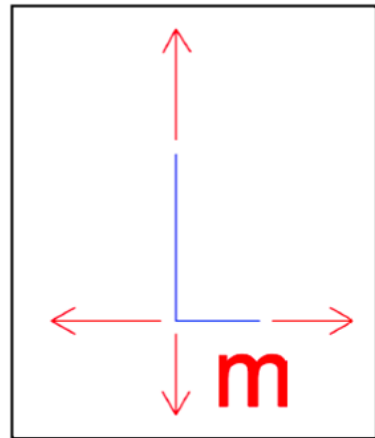
$$N_{mn} = N_{np y} = 46.2 \text{ kip (T)}$$

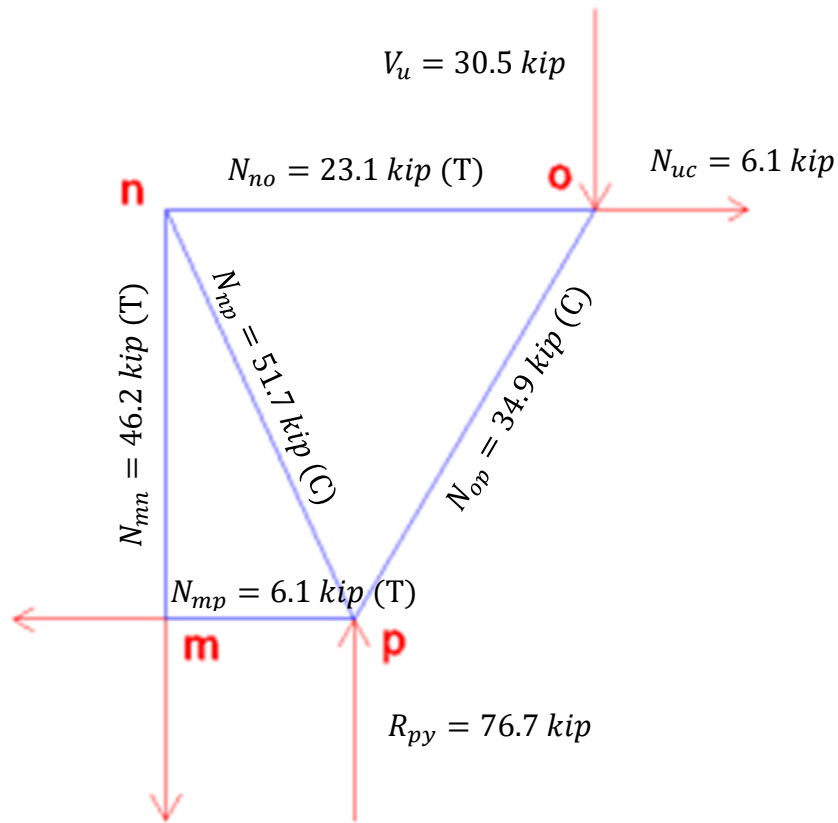


$$N_{mp} = N_{np\bar{x}} - N_{op\bar{x}} = 6.1 \text{ kip (T)}$$



$$N_{mn} - R_{my} = 46.2 \text{ kip} - 46.2 \text{ kip} = 0 \therefore OK$$





Select Strut, Tie, and Nodal Zone Dimensions

The most conservative β value for any relevant component will govern.

Nodes		Struts	
$\beta_{Nm} = 0.60$	(C-T-T)	$\beta_{s_{py}} = 1.0$	A bottle-shaped strut could develop in the concrete, so 0.75 will be used if reinforced properly. Otherwise, 0.6 must be used. Will assume inadequate reinforcement ($\beta=0.6$).
$\beta_{Nm} = 0.60$	(C-T-T)	$\beta_{s_{np}} = 0.6$	
$\beta_{Nm} = 0.80$	(C-C-T)	$\beta_{s_{op}} = 0.6$	
$\beta_{Nm} = 0.80$	(C-C-T)		

Because all components are affected by an element with a limiting value of 0.6, design must use $\beta = 0.6$ for all members.

$$\beta_s = 0.6$$

$$f_{ce} = 0.85\beta_s f'_c = 0.85(0.6)(8.0 \text{ ksi}) = 4.08 \text{ ksi}$$

$$\Phi f_{ce} = 0.75(4.08 \text{ ksi}) = 3.06 \text{ ksi}$$

Design Tension Ties

Member *mn*

$$w_{mn} = \frac{N_{mn}}{\Phi f_{ce} b_c} = \frac{46.2 \text{ kip}}{0.75(3.06 \text{ ksi})(10 \text{ in})} = 1.5 \text{ in} < \text{wythe thickness, } \therefore \text{OK}$$

$$A_{sreq,mn} = \frac{N_{mn}}{\Phi f_y} = \frac{46.2 \text{ kip}}{0.75(60 \text{ ksi})} = 1.03 \text{ in}^2 \quad \text{Therefore use (6) \#4 at 1.5" o.c.}$$

$$A_{smn} = 6(0.2 \text{ in}^2) = 1.2 \text{ in}^2$$

$$N_{nmn} = \Phi A_{smn} f_y = 0.75(1.2 \text{ in}^2)(60 \text{ ksi}) = 54 \text{ kip} \geq N_{mn} = 46.2 \text{ kip} \therefore \text{OK}$$

Anchorage Requirements

$$l_{dmp} = \left(\frac{3}{40} * \frac{f_y}{\lambda \sqrt{f'_c}} * \frac{\Psi_t \Psi_e \Psi_s}{\frac{(c_b + K_{tr})}{d_b}} \right) d_b \quad \begin{array}{l} \text{(ACI 318-14} \\ \text{\S 25.4.2.3)} \end{array}$$

If clear cover of $1.0d_b$ and a minimum clear spacing of $2d_b$ exists, the simplified version may be used:

$$l_{dmp} = \left(\frac{f_y \Psi_t \Psi_e}{25 \lambda \sqrt{f'_c}} \right) d_b \quad \begin{array}{l} \text{(ACI 318-14} \\ \text{\S 25.4.2.2)} \end{array}$$

$$\Psi_t = 1 \quad (\text{because not horizontal reinforcement})$$

$$\Psi_e = 1 \quad (\text{because using uncoated, regular rebar})$$

$$\lambda = 1 \quad (\text{because normalweight concrete})$$

$$d_b = 0.625 \text{ in}$$

$$l_{dmp} = \left(\frac{(60 \text{ ksi})(1)(1)}{25(1)\sqrt{8000 \text{ psi}} \left(1 \frac{\text{ksi}}{1000 \text{ psi}}\right)} \right) (0.625 \text{ in})$$

$$= 16.8 \text{ in}$$

Therefore need 18 inches of rebar extended on each side of the corbel for a total of 50 inches.

Member no

$$w_{no} = \frac{N_{no}}{\Phi f_{ce} b_c} = \frac{23.1 \text{ kip}}{0.75(3.06 \text{ ksi})(10 \text{ in})} = 0.76 \text{ in}$$

$$A_{sreq,no} = \frac{N_{no}}{\Phi f_y} = \frac{23.1 \text{ kip}}{0.75(60 \text{ ksi})} = 0.52 \text{ in}^2 \quad \text{Therefore use (4) \#4 at 1.5" o.c.}$$

$$A_{sno} = 4(0.2 \text{ in}^2) = 0.8 \text{ in}^2$$

$$N_{nno} = \Phi A_{sno} f_y = 0.75(0.8 \text{ in}^2)(60 \text{ ksi}) = 36 \text{ kip} \geq N_{mn} = 23.1 \text{ kip} \therefore OK$$

Anchorage Requirements

$$l_{dmp} = \left(\frac{f_y \Psi_e \Psi_c \Psi_r}{50 \lambda \sqrt{f'_c}} \right) d_b \quad (\text{ACI 318-14 §25.4.3.1})$$

$$\Psi_e = 1 \quad (\text{because using uncoated, regular rebar})$$

$$\psi_c = 1 \quad (\text{because cover not } \geq 2.5 \text{ in})$$

$$\psi_r = 1 \quad (\text{because not enclosed})$$

$$\lambda = 1 \quad (\text{because normalweight concrete})$$

$$d_b = 0.625 \text{ in}$$

$$l_{dh} = \left(\frac{1(1)(1)(60 \text{ ksi})}{50\lambda\sqrt{8000 \text{ psi}} \left(1 \frac{\text{ksi}}{1000\text{psi}}\right)} \right) \left(\frac{5}{8} \text{ in} \right)$$

$$= 8.4 \text{ in}$$

$$l_{dh} = \max \left(\frac{l_{dh}}{8d_b}, \frac{l_{dh}}{6 \text{ in}} \right) = 8.4 \text{ in}$$

Therefore need 8.5 inches of rebar beyond bend for principle reinforcement:

$$l_{out} = l_{dh} + (3d_b + d_b) = 10.9 \text{ in} \quad (\text{ACI 318-11 §12.5.1})$$

Principle reinforcement shall extend 12 inches from top of the bend. Since reinforcement is to be used also for member mn, the development length required for mn will be used here to ensure full development for all needs.

Anchor bar shall be welded to the end of the principle reinforcement to attain development on corbel tip.

Member mp

$$w_{no} = \frac{N_{mp}}{\Phi f_{ce} b_c} = \frac{6.1 \text{ kip}}{0.75(3.06 \text{ ksi})(10 \text{ in})} = 0.20 \text{ in}$$

$$A_{sreq,mp} = \frac{N_{mp}}{\Phi f_{ce}} = \frac{6.1 \text{ kip}}{0.75(3.06 \text{ ksi})} = 0.14 \text{ in}^2 \quad \text{Therefore use (1) \#3}$$

$$A_{smp} = 2(0.11 \text{ in}^2) = 0.22 \text{ in}^2$$

$$\Phi N_{nmp} = \Phi A_{smp} f_y = 0.75(0.22 \text{ in}^2)(60 \text{ ksi}) = 9.9 \text{ kip} \geq N_{mp} = 6.1 \text{ kip} \therefore OK$$

Design Compression Struts*Member op*

$$w_{op} = \frac{N_{op}}{\Phi f_{ce} b_c} = \frac{34.9 \text{ kip}}{0.75(3.06 \text{ ksi})(10 \text{ in})} = 1.14 \text{ in}$$

Member np

$$w_{np} = \frac{N_{np}}{\Phi f_{ce} b_c} = \frac{51.7 \text{ kip}}{0.75(3.06 \text{ ksi})(10 \text{ in})} = 1.7 \text{ in}$$

Member Rp

$$w_{py} = \frac{R_{py}}{\Phi f_{ce} b_c} = \frac{76.7 \text{ kip}}{0.75(3.06 \text{ ksi})(10 \text{ in})} = 2.5 \text{ in} < \text{wythe thickness therefore OK}$$

Vertical/Longitudinal Reinforcement, A_{sl}

Because reinforcement for the max moment at section mn of our truss has already been determined, the actual required reinforcement area will be determined using the moment at 18 inches from the max moment location.

$$\Phi_{flex} = 0.9$$

$$\begin{aligned} M_u &= V_u \left(a_v + \frac{t_{SWP}}{2} \right) + N_{uc}(h_c - d) \\ &= 30.5 \text{ kip} \left(5 \text{ in} + \frac{9 \text{ in}}{2} \right) + 6.1 \text{ kip}(14 \text{ in} - \\ &12 \text{ in}) \end{aligned}$$

$$= 301.8 \text{ kip} \cdot \text{in}$$

$$A_{sl} = \frac{\left(M_u - \left(\frac{18 \text{ in}}{48 \text{ in}} \right) M_u \right)}{\Phi f_y (d_{hout} - d_{hin})}$$

$$= \frac{301.8 \text{ kip} \cdot \text{in} \left(1 - \frac{3}{8}\right)}{0.9(60 \text{ ksi})(6 \text{ in})} = 0.58 \text{ in}^2$$

$$\rho = \frac{A_{sl,min}}{A_{gc}} = 0.0012 \quad (\text{ACI 381-14 §14.3.2})$$

$$A_{gcl} = b * (t_{wyo} + t_{wyi}) = 72 \text{ in} * 6 \text{ in} = 432 \text{ in}^2$$

$$A_{sl,min} = \rho A_{gcl} = 0.0012(432 \text{ in}^2) = 0.52 \text{ in}^2$$

Therefore OK

$$< A_{sl}$$

Design is restricted to using #4 bars because of cover limitations, therefore:

$$N_l = \frac{A_{sl}}{A_{\#4}} = \frac{0.52 \text{ in}^2}{0.2 \text{ in}^2} = 2.6 \quad \therefore \text{use (3) \#4 bars}$$

$$s = \frac{b - 2(0.75 \text{ in})}{N_l - 1} = \frac{72 \text{ in} - 1.5 \text{ in}}{2} = 35.25 \text{ in}$$

$$s_{max} = \min \left(\frac{3t}{18 \text{ in}} \right) = \max \left(\frac{27 \text{ in}}{18 \text{ in}} \right) = 18 \text{ in} < s \quad \text{Therefore } s = 18 \text{ in}$$

Therefore use (4) #4 bars spaced 18" o.c. to resist flexure. Place second layer of rebar on compression side for any reversed loading.

Horizontal/Transverse Reinforcement, A_{st}

$$\rho = \frac{A_{st,min}}{A_{gc}} = 0.0020 \quad (\text{ACI 381-14 §14.3.3})$$

$$A_{gct} = h * (t_{wyo} + t_{wyi}) = 96 \text{ in} * 6 \text{ in} = 576 \text{ in}^2$$

$$A_{st,min} = \rho A_{gcl} = 0.002(576 \text{ in}^2) = 1.15 \text{ in}^2$$

$$N_t = \frac{A_{st,min}}{A_{\#4}} = \frac{1.15 \text{ in}^2}{0.2 \text{ in}^2} = 6 \quad \therefore \text{use (6) \#4 bars}$$

$$s = \frac{h - 2(0.75 \text{ in})}{N_t - 1} = \frac{96 \text{ in} - 1.5 \text{ in}}{5} = 18.9 \text{ in}$$

$$s_{max} = \min \left(\frac{3t}{18 \text{ in}} \right) = \max \left(\frac{27 \text{ in}}{18 \text{ in}} \right) = 18 \text{ in} < s \quad \text{Therefore } s = 18 \text{ in}$$

Therefore use (6) #4 bars spaced 18" o.c. per code minimum requirements. Place second layer of rebar on opposite side for symmetry.

Lifting

$$x_{lift} = 18 \text{ in} = 1.5 \text{ ft} \quad (\text{anchor to edge distance})$$

$$x_{midL} = h - 2x_{anchor} = 8 \text{ ft} - 3 \text{ ft} = 5 \text{ ft}$$

$$x_{midT} = b - 2x_{anchor} = 6 \text{ ft} - 3 \text{ ft} = 3 \text{ ft}$$

Longitudinal Direction

$$w_{sw} = w_c b t = (150 \text{ pcf})(6 \text{ ft})(0.5 \text{ ft}) = 450 \frac{\text{lb}}{\text{ft}}$$

$$R_A = \frac{w_{sw} h}{2} = \frac{\left(0.45 \frac{\text{kip}}{\text{ft}}\right)(8 \text{ ft})}{2} = 1.8 \text{ kip}$$

$$V_{lift, left} = w_{sw} x_{lift} = \left(0.45 \frac{\text{kip}}{\text{ft}}\right)(1.5 \text{ ft})$$

$$= -0.675 \text{ kip}$$

$$V_{lift, right} = w_{sw} x_{lift} + R_A = -0.675 \text{ kip} + 1.8 \text{ kip}$$

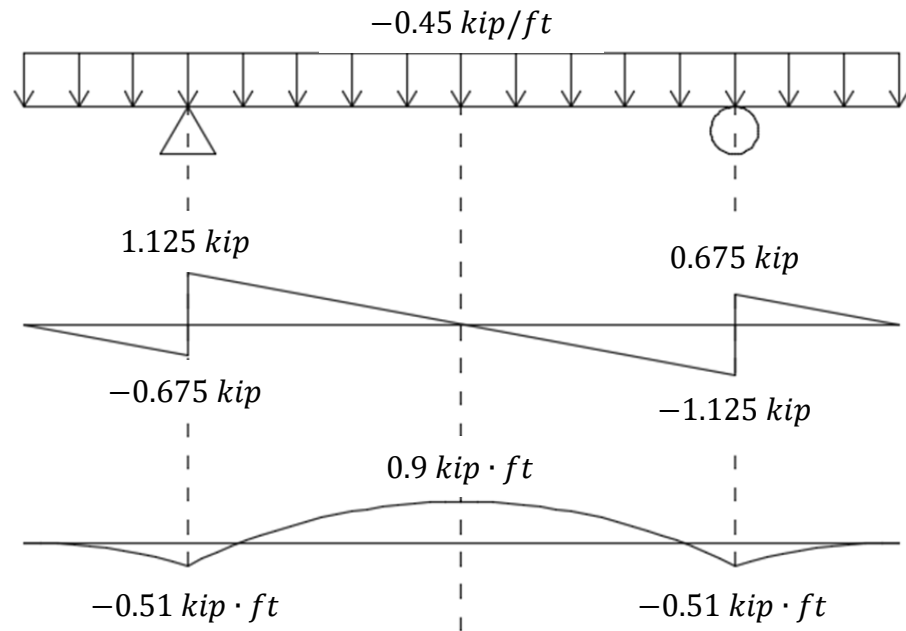
$$= 1.125 \text{ kip}$$

$$M_{lift} = \frac{V_{lift, left} x_{lift}}{2} = \frac{(-0.675 \text{ kip})(1.5 \text{ ft})}{2}$$

$$= -0.506 \text{ kip} \cdot \text{ft}$$

$$M_{mid} = M_{lift} + \frac{V_{lift,right}(0.5x_{midL})}{2}$$

$$= -0.51 \text{ kip} \cdot \text{ft} + \frac{0.675 \text{ kip}(0.5 \cdot 5 \text{ ft})}{2} = 0.9 \text{ kip} \cdot \text{ft}$$



Cracking moment is equal to

$$M_{cr} = \frac{7.5\sqrt{f'_c}I_g}{0.5t}$$

$$f'_{c,req} = \left(\frac{0.5(t_{wy0} + t_{wyi})M_{mid}}{7.5I_g} \right)^2$$

$$= \left(\frac{0.5(6 \text{ in}) \left(0.9 \text{ kip} \cdot \text{ft} \cdot \frac{12 \text{ in}}{\text{ft}} \right)}{7.5(4212 \text{ in}^4)} \right)^2 = 0.0024 \text{ ksi}$$

Therefore we need to attain at least 0.0024 ksi before lifting.

Transverse Direction

$$w_{sw} = w_c h t = (150 \text{ pcf})(8 \text{ ft})(0.5 \text{ ft}) = 600 \frac{\text{lb}}{\text{ft}}$$

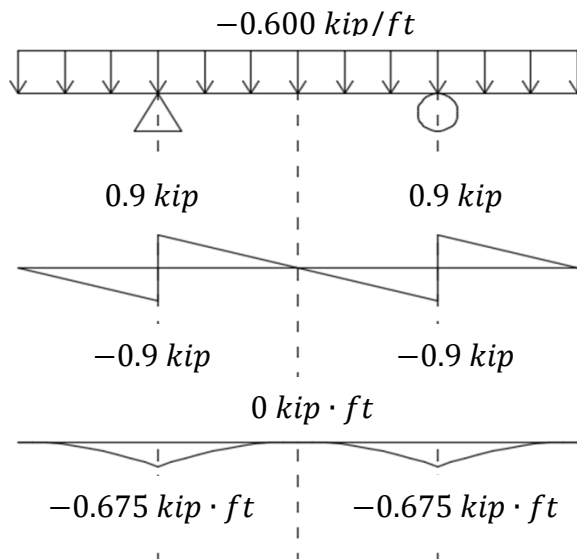
$$R_A = \frac{w_{sw} b}{2} = \frac{\left(0.6 \frac{\text{kip}}{\text{ft}}\right)(6 \text{ ft})}{2} = 1.8 \text{ kip}$$

$$\begin{aligned} V_{\text{lift, left}} &= w_{sw} x_{\text{lift}} = \left(0.6 \frac{\text{kip}}{\text{ft}}\right)(1.5 \text{ ft}) \\ &= -0.9 \text{ kip} \end{aligned}$$

$$\begin{aligned} V_{\text{lift, right}} &= w_{sw} x_{\text{lift}} + R_A = -0.9 \text{ kip} + 1.8 \text{ kip} \\ &= 0.9 \text{ kip} \end{aligned}$$

$$\begin{aligned} M_{\text{lift}} &= \frac{V_{\text{lift, left}} x_{\text{lift}}}{2} = \frac{(-0.9 \text{ kip})(1.5 \text{ ft})}{2} \\ &= -0.675 \text{ kip} \cdot \text{ft} \end{aligned}$$

$$\begin{aligned} M_{\text{mid}} &= M_{\text{lift}} + \frac{V_{\text{lift, right}}(0.5 x_{\text{midR}})}{2} \\ &= -0.675 \text{ kip} \cdot \text{ft} + \frac{0.9 \text{ kip}(0.5 \cdot 3 \text{ ft})}{2} = 0 \text{ kip} \cdot \text{ft} \end{aligned}$$



Cracking moment is equal to

$$\begin{aligned}
 M_{cr} &= \frac{7.5\sqrt{f'_c}I_g}{0.5t} \\
 f'_{c,req} &= \left(\frac{0.5(t_{wy0} + t_{wyi})M_{lift}}{7.5I_{gSWP}} \right)^2 \\
 &= \left(\frac{0.5(6 \text{ in}) \left(0.675 \text{ kip} \cdot \text{ft} * \frac{12 \text{ in}}{\text{ft}} \right)}{7.5(4212 \text{ in}^4)} \right)^2 \\
 &= 0.0013 \text{ ksi}
 \end{aligned}$$

Therefore we need to attain at least 0.0013 ksi before lifting to avoid cracking the panel.

Since the concrete lifting anchor strengths are based on a concrete strength of 3.5 ksi,

however, the panels may not be lifted until $f'_c = 3.5 \text{ ksi}$.

$$f'_{c,req} = \max \begin{pmatrix} f'_{c,reqL} \\ f'_{c,reqT} \\ f'_{c,reqA} \end{pmatrix} = \max \begin{pmatrix} 0.0024 \text{ ksi} \\ 0.0013 \text{ ksi} \\ 3.5 \text{ ksi} \end{pmatrix} = 3.5 \text{ ksi}$$

GFRP3 Calculations

The GFRP3 specimen used the Strut-and-Tie method for design.

Material Properties

<u>Concrete</u>	<u>Steel</u>	<u>FRP</u>
$f'_c = 8.0 \text{ ksi}$	$f_y = 60 \text{ ksi}$	$f_{yFRP3} = 120 \text{ ksi}$
$f_r = 7.5\sqrt{f'_c} = 0.671 \text{ ksi}$	$f_u = 75 \text{ ksi}$	$f_{FRP3SUS} = 0.2f_{yFRP3}$
$w_c = 150 \text{ lb}/\text{ft}$	$E_s = 29000 \text{ ksi}$	$= 0.2(120 \text{ ksi}) = 24 \text{ ksi}$
$E_c = 33w_c^{1.5}\sqrt{f'_c} = 5422 \text{ ksi}$		$E_{FRP} = 6700 \text{ ksi}$
$n_s = \frac{E_s}{E_c} = 5.348$		$n_{FRP} = \frac{E_{FRP}}{E_c} = 1.236$

Geometrical Dimensions

<u>SWP</u>	<u>Corbel</u>
$t_{wyo} = t_{wyi} = t_{ins} = 3 \text{ in}$	$h_c = 14 \text{ in}$
$t_{SWP} = t_{wyo} + t_{wyi} + t_{ins} = 9 \text{ in}$	$d = 12 \text{ in}$
$b = 6 \text{ ft}$	$b_c = 10 \text{ in}$
$h = 8 \text{ ft}$	$l_p = 8 \text{ in}$
$d_{hout} = 7.5 \text{ in}$	$h_{cf} = 10 \text{ in}$
$d_{hin} = 1.5 \text{ in}$	$c_c = 1.5 \text{ in}$
$I_{gSWP} = \frac{bt_{SWP}^3}{12} - \frac{bt_{ins}^3}{12}$	$I_{gc} = \frac{b_c h_c^3}{12} = \frac{10 \text{ in}(14 \text{ in})^3}{12} = 2287 \text{ in}^4$
$= \frac{72 \text{ in}(9 \text{ in})^3}{12} - \frac{72 \text{ in}(3 \text{ in})^3}{12} = 4212 \text{ in}^4$	

$$l_{no} = d_{hout} + a_v + (1 \text{ in}) \tan \theta_R$$

$$= 7.5 \text{ in} + 5 \text{ in} + (1 \text{ in}) \tan(11.31^\circ) = 12.7 \text{ in}$$

$$\theta_{nop} = \text{atan}\left(\frac{d}{l_{no} - (d_{hout} - d_{hin})}\right)$$

$$= \text{atan}\left(\frac{12 \text{ in}}{12.7 \text{ in} - (7.5 \text{ in} - 1.5 \text{ in})}\right) = 60.82^\circ$$

$$l_{mn} = d = 12 \text{ in}$$

$$l_{mp} = d_{hout} - d_{hin} = 7.5 \text{ in} - 1.5 \text{ in} = 6 \text{ in}$$

$$\theta_{pno} = \text{atan}\left(\frac{d}{l_{mp}}\right) = \text{atan}\left(\frac{12}{6}\right) = 63.44^\circ$$

$$\theta_{npo} = 180^\circ - \theta_{pno} - \theta_{nop}$$

$$= 180^\circ - 63.44^\circ - 60.82^\circ$$

$$= 55.74^\circ$$

$$\theta_{mpn} = \theta_{pno} = 63.44^\circ$$

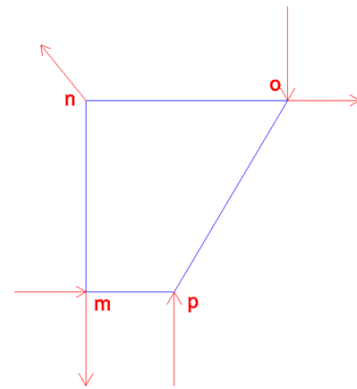
Determine Forces in Truss Components

$$\Sigma M_m = V_u l_{no} + N_{uc} l_{mn} - R_{py} l_{mp} - R_{nx} l_{mn} = 0$$

$$R_{py} = \frac{V_u l_{no} + N_{uc} l_{mn}}{l_{mp}} - R_{nx} \frac{l_{mn}}{l_{mp}}$$

$$\Sigma F_y = R_{py} + R_{ny} - R_{my} - V_u = 0$$

$$\Sigma F_x = N_{uc} - R_{mx} - R_{nx} = 0$$

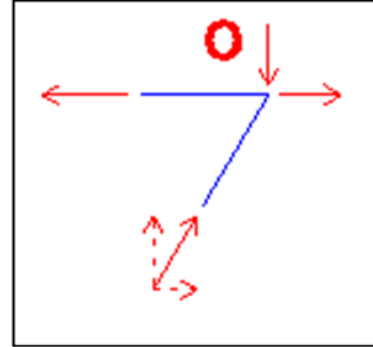


$$N_{opy} = V_u = 30.5 \text{ kip}$$

$$N_{opx} = \frac{N_{opy}}{\tan(\theta_{nop})} = \frac{30.5 \text{ kip}}{\tan(60.82^\circ)} = 17.0 \text{ kip}$$

$$\begin{aligned} N_{op} &= \sqrt{N_{opx}^2 + N_{opy}^2} \\ &= \sqrt{(17.0 \text{ kip})^2 + (30.5 \text{ kip})^2} \\ &= 34.9 \text{ kip (C)} \end{aligned}$$

$$\begin{aligned} N_{no} &= N_{opx} + N_{uc} = 17.0 \text{ kip} + 6.1 \text{ kip} \\ &= 23.1 \text{ kip (T)} \end{aligned}$$



$$R_{nx} = N_{no} = 23.1 \text{ kip}$$

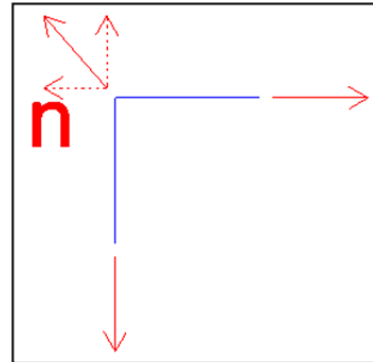
$$R_n = \sqrt{R_{nx}^2 + R_{ny}^2} = \sqrt{2(23.1 \text{ kip})^2} = 32.69 \text{ kip}$$

$$\Sigma F_x = N_{uc} + R_{mx} - R_{nx} = 0$$

$$R_{mx} = R_{nx} - N_{uc} = 17.02 \text{ kip (T)}$$

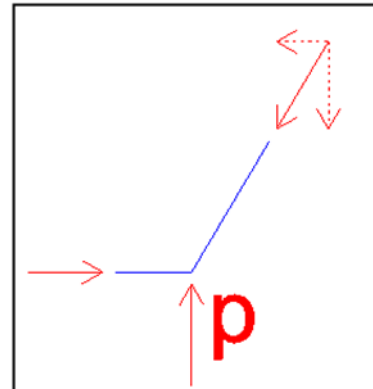
Assume bend acts similar to a pulley

$$N_{mn} = R_{nx} = 23.1 \text{ kip (T)}$$

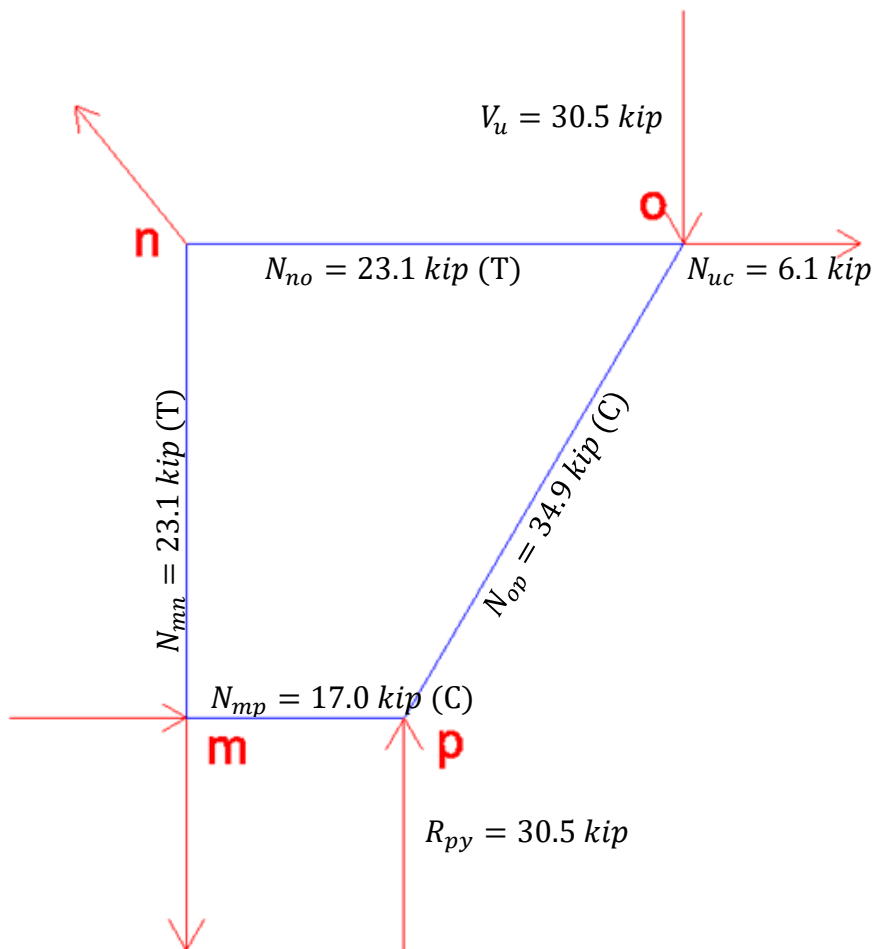
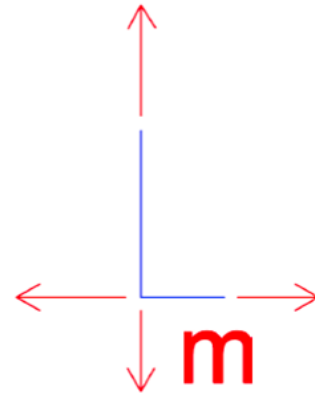


$$N_{mp} = N_{opx} = 17.02 \text{ kip (C)}$$

$$\begin{aligned} R_{py} &= \frac{V_u l_{no} + N_{uc} l_{mn}}{l_{mp}} - R_{nx} \frac{l_{mn}}{l_{mp}} \\ &= \frac{30.5 \text{ kip}(12.7 \text{ in}) + (6.1 \text{ kip})(12 \text{ in})}{6 \text{ in}} - (23.1 \text{ kip}) \frac{12}{6} \\ &= 30.5 \text{ kip} \end{aligned}$$



$$N_{mp} - R_{mx} = 17.0 \text{ kip} - 17.0 \text{ kip} = 0 \therefore OK$$



Select Strut, Tie, and Nodal Zone Dimensions

The most conservative β value for any relevant component will govern.

Nodes	Struts	
$\beta_{Nm} = 0.60$ (C-T-T)	$\beta_{s_{py}} = 1.0$	A bottle-shaped strut could develop in the concrete, so 0.75 will be used if reinforced properly. Otherwise, 0.6 must be used. Will assume inadequate reinforcement ($\beta=0.6$).
$\beta_{Nm} = 0.60$ (C-T-T)	$\beta_{s_{np}} = 0.6$	
$\beta_{Nm} = 0.80$ (C-C-T)	$\beta_{s_{op}} = 0.6$	
$\beta_{Nm} = 0.80$ (C-C-T)		

Because all components are affected by an element with a limiting value of 0.6, design must use $\beta = 0.6$ for all members.

$$\beta_s = 0.6$$

$$f_{ce} = 0.85\beta_s f'_c = 0.85(0.6)(8.0 \text{ ksi}) = 4.08 \text{ ksi}$$

$$\Phi f_{ce} = 0.75(4.08 \text{ ksi}) = 3.06 \text{ ksi}$$

Design Tension Ties

Member mn

$$w_{mn} = \frac{N_{mn}}{\Phi f_{ce} b_c} = \frac{23.1 \text{ kip}}{0.75(3.06 \text{ ksi})(10 \text{ in})} = 0.76 \text{ in} < \text{wythe thickness, } \therefore \text{OK}$$

$$A_{sreq,mn} = \frac{N_{mn}}{\Phi f_y} = \frac{23.1 \text{ kip}}{0.75(60 \text{ ksi})} = 0.51 \text{ in}^2 \quad \text{Therefore use (4) \#4 at 2.5" o.c.}$$

$$A_{smn} = 4(0.2 \text{ in}^2) = 0.8 \text{ in}^2$$

$$N_{nmn} = \Phi A_{smn} f_y = 0.75(0.8 \text{ in}^2)(60 \text{ ksi}) = 36 \text{ kip} \geq N_{mn} = 23.1 \text{ kip} \therefore \text{OK}$$

Anchorage Requirements

$$l_{dmp} = \left(\frac{3}{40} * \frac{f_y}{\lambda \sqrt{f'_c}} * \frac{\Psi_t \Psi_e \Psi_s}{\frac{(c_b + K_{tr})}{d_b}} \right) d_b \quad (\text{ACI 318-14 §25.4.2.3})$$

If clear cover of $1.0d_b$ and a minimum clear spacing of $2d_b$ exists, the simplified version may be used:

$$l_{dmp} = \left(\frac{f_y \Psi_t \Psi_e}{25 \lambda \sqrt{f'_c}} \right) d_b \quad (\text{ACI 318-14 §25.4.2.2})$$

$$\Psi_t = 1 \quad (\text{because not horizontal reinforcement})$$

$$\Psi_e = 1 \quad (\text{because using uncoated, regular rebar})$$

$$\lambda = 1 \quad (\text{because normalweight concrete})$$

$$d_b = 0.5 \text{ in}$$

$$l_{dmp} = \left(\frac{(60 \text{ ksi})(1)(1)}{25(1)\sqrt{8000 \text{ psi}} \left(1 \frac{\text{ksi}}{1000 \text{ psi}}\right)} \right) (0.5 \text{ in}) = 13.4 \text{ in}$$

Therefore 16 inches of rebar must be extended on each side of the corbel for a total of 46 inches.

Member n_o

$$w_{no} = \frac{N_{no}}{\Phi f_{ce} b_c} = \frac{23.1 \text{ kip}}{0.75(3.06 \text{ ksi})(10 \text{ in})} = 0.76 \text{ in}$$

$$A_{sreq, no} = \frac{N_{no}}{\Phi f_{yFRP3}} = \frac{23.1 \text{ kip}}{0.75(120 \text{ ksi})} = 0.26 \text{ in}^2 \quad \text{Therefore (3) GFRP \#3 bars}$$

Creep rupture typically controls with GFRP, however. This requires an area of:

$$A_{creepreq3} = \frac{N_{no} \left(\frac{V_{sus}}{V_u} \right)}{\Phi_v f_{FRP3sus}} = \frac{23.1 \text{ kip} \left(\frac{16.46}{30.5} \right)}{0.75(24 \text{ ksi})} = 0.69 \text{ in}^2$$

Therefore use (7) GFRP #3 bars at 1.375" o.c.

$$A_{sno} = 7(0.11 \text{ in}^2) = 0.77 \text{ in}^2$$

$$N_{nno} = \Phi A_{sno} f_y = 0.75(0.77 \text{ in}^2)(120 \text{ ksi}) = 69.3 \text{ kip} \geq N_{mn} = 23.1 \text{ kip} \therefore OK$$

Anchorage Length Requirements

$$l_{bhf} = 12d_b = 12(0.375 \text{ in}) = 4.5 \text{ in} \quad (\text{ACI 440.1R-15 §8.3})$$

$$l_{bhf,out} = l_{bhf} + d_{s3} + 3d_{s3} = 6 \text{ in}$$

Therefore specify legs out-to-out of 8 inches.

Anchorage Concrete Breakout Strength

By treating the GFRP reinforcement as an anchor, the transverse reinforcement may be considered to transfer the load vertically and horizontally to the outside wythe. According to ACI D4.4, this allows the panel to meet the requirements of Condition A (using supplementary reinforcement) and being governed by concrete breakout, blowout, pullout, etc.

$$N_{cb} = \frac{A_{Nc}}{A_{Nco}} \Psi_{ecN} \Psi_{edN} \Psi_{cN} \Psi_{cpN} N_b \quad (\text{ACI 440.1R-15 Eq D-5})$$

$$\begin{aligned} h_{ef} &= t_{wyo} - 1 \text{ in} - d_b \\ &= 3 \text{ in} - 1 \text{ in} - 0.375 \text{ in} = 1.625 \text{ in} \end{aligned}$$

$$A_{Nco} = 9h_{ef}^2 = 9(1.625 \text{ in})^2 = 23.77 \text{ in}^2 \quad (\text{ACI 440.1R-15 Eq D-6})$$

$$\begin{aligned} A_{Nc} &= [2(1.5h_{ef})][2(1.5h_{ef}) + s_c(N_{FRP} - 1)] \\ &= [3(1.625 \text{ in})][3(1.625 \text{ in}) + (1.375 \text{ in})(7 - 1)] \\ &= 64.0 \text{ in}^2 \end{aligned}$$

$$N_b = k_c \lambda \sqrt{f'_c} h_{ef}^{1.5} \quad (\text{ACI 440.1R-15 Eq D-7})$$

$k_c = 24$ for cast-in-place anchors

$$N_b = 24(1)\sqrt{8000 \text{ psi}}(1.375 \text{ in})^{1.5} = 4.45 \text{ kip}$$

$$\Psi_{ecN} = \frac{1}{1 + \frac{2e'_N}{3h_{ef}}} = \frac{1}{1 + \frac{2(0)}{3h_{ef}}} = 1 \text{ because symmetric}$$

$$\Psi_{edN} = 1 \text{ since edges further away than } 1.5h_{ef}$$

$$\Psi_{cN} = 1 \text{ to be conservative}$$

$$\Psi_{cpN} = 1 \text{ since edge cover is greater than } 4h_{ef}$$

$$N_{cb} = 12.0 \text{ kip} < 23.1 \text{ kip}, \therefore \text{No Good}$$

However, provisions from ACI D.5.2.9 state that if development is obtained on both sides of the breakout, “the design strength of the anchor reinforcement shall be permitted to be used instead of the concrete breakout strength.” Therefore OK.

Shear Strength of Rebar in Shear (estimated to be about $0.6f_u$)

$$R_{\text{rebarShear}} = 0.6f_u A_{gv} = R_n$$

$$A_{gv} = \frac{R_n}{\Phi_v(0.6f_u)} = \frac{32.7 \text{ kip}}{0.75(0.6(75 \text{ ksi}))} = 0.97 \text{ in}^2 \quad \begin{array}{l} \text{Therefore use (5)\#4 @ 1.5"} \\ \text{o.c.} \end{array}$$

Adequate development is required on both sides of the corbel, so we will need a bar 42” long.

Design Compression Struts

Member op

$$w_{op} = \frac{N_{op}}{\Phi f_{ce} b_c} = \frac{34.9 \text{ kip}}{0.75(3.06 \text{ ksi})(10 \text{ in})} = 1.14 \text{ in}$$

Member mp

$$w_{mp} = \frac{N_{mp}}{\Phi f_{ce} b_c} = \frac{17.0 \text{ kip}}{0.75(3.06 \text{ ksi})(10 \text{ in})} = 0.56 \text{ in}$$

Since the foam is not able to withstand this force over such a small area, the compressive material used in this instance must have a height of at least 0.6 in. Wood typically has a low thermal conductivity, is very cheap, and is readily available on the job site. Because the compressive strength is difficult to find published, the strength of Douglas Fir Larch will be used as a conservative design value ($f_{HDO} = f_{DFL} = 1.36 \text{ ksi}$). Simply for feasibility, if a prism of HDO board is used that is 3 inches thick, 3.5 inches tall, and 10 inches long, the area required to resist the compressive force of member mp is

$$A_{HDOreq} = \frac{N_{mp}}{\Phi_v f_{HDO}} = \frac{17.0 \text{ kip}}{0.75(1.36 \text{ ksi})} = 16.68 \text{ in}^2$$

$$b_{HDOreq} = \frac{A_{HDOreq}}{h_{HDO}} = \frac{16.68 \text{ in}^2}{3.5 \text{ in}} = 4.77 \text{ in}$$

We will be safe by using a 10 in long compressive segment, equal to the width of the corbel.

$$\Phi_v f_{HDO} h_{HDO} b_{HDO} = 0.75(1.36 \text{ ksi})(3.5 \text{ in})(10 \text{ in}) = 35.7 \text{ kip} \geq N_{mp} = 17.0 \text{ kip}$$

$\therefore OK$

Member Rp

$$w_{py} = \frac{R_{py}}{\Phi f_{ce} b_c} = \frac{30.5 \text{ kip}}{0.75(3.06 \text{ ksi})(10 \text{ in})} = 1.0 \text{ in} < \text{wythe thickness therefore OK}$$

Shear at Corbel/SWP Interface

The shear to be resisted at this interface will be equal to the applied load. The friction from the interface shall be ignored conservatively. Stirrups shall be used to resist the shear.

$$R_{rebarShear} = 0.6f_u A_{gv}$$

$$A_{gv} = \frac{V_u}{\Phi_v 0.6f_u} = \frac{30.5 \text{ kip}}{0.75(0.6)(75 \text{ ksi})} = 0.9 \text{ in}^2 \quad \therefore \text{use (3)\#4 stirrups @ 3" o.c.}$$

$$A_{gv} = 3(2 * 0.2 \text{ in}^2) = 1.2 \text{ in}^2$$

Vertical/Longitudinal Reinforcement, A_{sl}

$$\rho = \frac{A_{sl,min}}{A_{gc}} = 0.0012 \quad (\text{ACI 381-14 §14.3.2})$$

$$\begin{aligned} A_{gcl} &= b * (t_{wy0} + t_{wyi}) = 72 \text{ in} * 6 \text{ in} \\ &= 432 \text{ in}^2 \end{aligned}$$

$$A_{sl,min} = \rho A_{gcl} = 0.0012(432 \text{ in}^2) = 0.52 \text{ in}^2$$

$$s_{max} = \min\left(\frac{3t}{18 \text{ in}}\right) = \max\left(\frac{27 \text{ in}}{18 \text{ in}}\right) = 18 \text{ in}$$

$$\begin{aligned} N_{sl} &= \frac{b - 2(0.75 \text{ in})}{s_{max}} = \frac{72 \text{ in} - 2(0.75 \text{ in})}{18 \text{ in}} \\ &= 3.92 \text{ bars} \end{aligned}$$

$$A_{slbarmin} = \frac{A_{sl,min}}{N_{sl}} = \frac{0.52 \text{ in}^2}{4} = 0.13 \text{ in}^2 \quad \therefore \text{use (4)\#4 bars @ 18" o.c.}$$

Therefore use (4) #4 bars spaced 18" o.c. Place second layer of rebar on compression side for any reversed loading.

Horizontal/Transverse Reinforcement, A_{st}

$$\rho = \frac{A_{st,min}}{A_{gc}} = 0.0020 \quad (\text{ACI 381-14 §14.3.3})$$

$$\begin{aligned} A_{gct} &= h * (t_{wy0} + t_{wyi}) = 96 \text{ in} * 6 \text{ in} \\ &= 576 \text{ in}^2 \end{aligned}$$

$$A_{st,min} = \rho A_{gcl} = 0.002(576 \text{ in}^2) = 1.15 \text{ in}^2$$

$$s_{max} = \min \left(\frac{3t}{18 \text{ in}} \right) = \max \left(\frac{27 \text{ in}}{18 \text{ in}} \right) = 18 \text{ in}$$

$$\begin{aligned} N_{st} &= \frac{h - 2(0.75 \text{ in})}{s_{max}} = \frac{96 \text{ in} - 2(0.75 \text{ in})}{18 \text{ in}} \\ &= 5.25 \text{ bars} \end{aligned}$$

$$A_{stbarmin} = \frac{A_{st,min}}{N_{st}} = \frac{1.15 \text{ in}^2}{6} = 0.19 \text{ in}^2 \quad \therefore \text{use (6)\#4 bars @ 18" o.c.}$$

Therefore use (6) #4 bars spaced 18" o.c. Place second layer of rebar on opposite side for symmetry.

Lifting

$$x_{lift} = 18 \text{ in} = 1.5 \text{ ft} \quad (\text{anchor to edge distance})$$

$$x_{midL} = h - 2x_{anchor} = 8 \text{ ft} - 3 \text{ ft} = 5 \text{ ft}$$

$$x_{midR} = b - 2x_{anchor} = 6 \text{ ft} - 3 \text{ ft} = 3 \text{ ft}$$

Longitudinal Direction

$$w_{sw} = w_c b t = (150 \text{ pcf})(6 \text{ ft})(0.5 \text{ ft}) = 450 \frac{\text{lb}}{\text{ft}}$$

$$R_A = \frac{w_{sw} h}{2} = \frac{\left(0.45 \frac{\text{kip}}{\text{ft}}\right)(8 \text{ ft})}{2} = 1.8 \text{ kip}$$

$$V_{lift,left} = w_{sw}x_{lift} = \left(0.45 \frac{kip}{ft}\right)(1.5 ft)$$

$$= -0.675 kip$$

$$V_{lift,right} = w_{sw}x_{lift} + R_A = -0.675 kip + 1.8 kip$$

$$= 1.125 kip$$

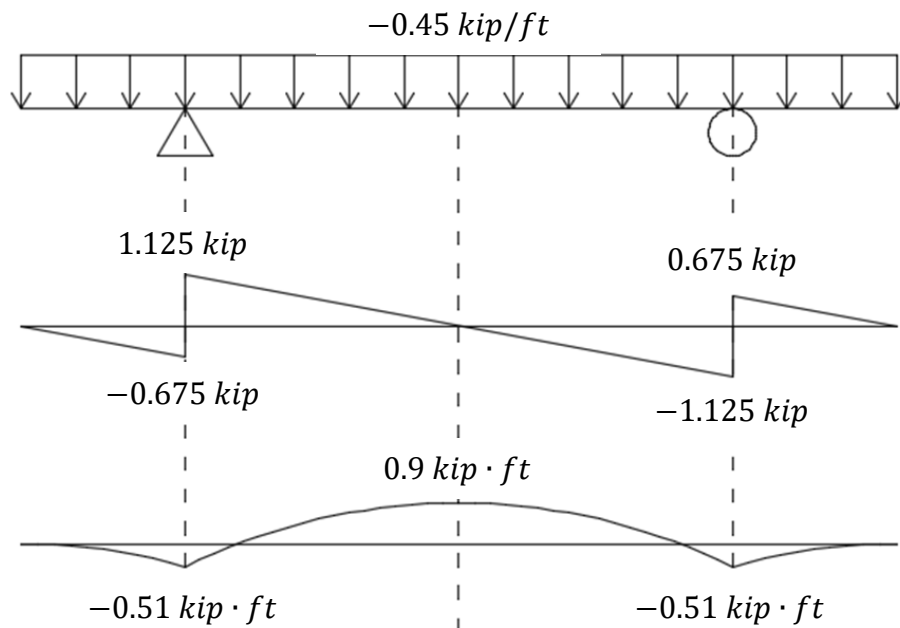
$$M_{lift} = \frac{V_{lift,left}x_{lift}}{2} = \frac{(-0.675 kip)(1.5 ft)}{2}$$

$$= -0.506 kip \cdot ft$$

$$M_{mid} = M_{lift} + \frac{V_{lift,right}(0.5x_{midL})}{2}$$

$$= -0.51 kip \cdot ft + \frac{0.675 kip(0.5 \cdot 5 ft)}{2} = 0.9 kip \cdot$$

ft



Cracking moment is equal to

$$M_{cr} = \frac{7.5\sqrt{f'_c}I_g}{0.5t}$$

$$f'_{c,req} = \left(\frac{0.5(t_{wy0} + t_{wyi})M_{mid}}{7.5I_g} \right)^2$$

$$= \left(\frac{0.5(6 \text{ in}) \left(0.9 \text{ kip} \cdot \text{ft} * \frac{12 \text{ in}}{\text{ft}} \right)}{7.5(4212 \text{ in}^4)} \right)^2 = 0.0024 \text{ ksi}$$

Therefore we need to attain at least 0.0024 ksi before lifting.

Transverse Direction

$$w_{sw} = w_c ht = (150 \text{ pcf})(8 \text{ ft})(0.5 \text{ ft}) = 600 \frac{\text{lb}}{\text{ft}}$$

$$R_A = \frac{w_{sw}b}{2} = \frac{\left(0.6 \frac{\text{kip}}{\text{ft}}\right)(6 \text{ ft})}{2} = 1.8 \text{ kip}$$

$$V_{lift,left} = w_{sw}x_{lift} = \left(0.6 \frac{\text{kip}}{\text{ft}}\right)(1.5 \text{ ft})$$

$$= -0.9 \text{ kip}$$

$$V_{lift,right} = w_{sw}x_{lift} + R_A = -0.9 \text{ kip} + 1.8 \text{ kip}$$

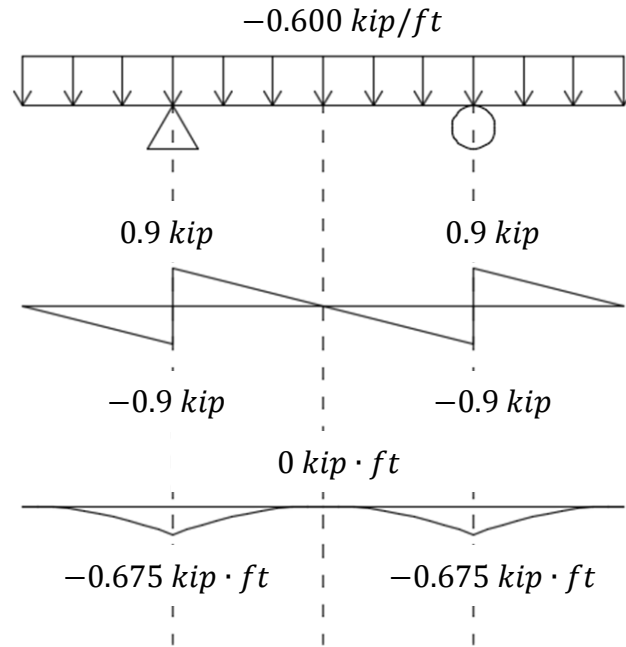
$$= 0.9 \text{ kip}$$

$$M_{lift} = \frac{V_{lift,left}x_{lift}}{2} = \frac{(-0.9 \text{ kip})(1.5 \text{ ft})}{2}$$

$$= -0.675 \text{ kip} \cdot \text{ft}$$

$$M_{mid} = M_{lift} + \frac{V_{lift,right}(0.5x_{midT})}{2}$$

$$= -0.675 \text{ kip} \cdot \text{ft} + \frac{0.9 \text{ kip}(0.5*3 \text{ ft})}{2} = 0 \text{ kip} \cdot \text{ft}$$



Cracking moment is equal to

$$M_{cr} = \frac{7.5\sqrt{f'_c}I_g}{0.5t}$$

$$f'_{c,req} = \left(\frac{0.5(t_{wy0} + t_{wyi})M_{lift}}{7.5I_{gSWP}} \right)^2$$

$$= \left(\frac{0.5(6 \text{ in}) \left(0.675 \text{ kip} \cdot \text{ft} * \frac{12 \text{ in}}{\text{ft}} \right)}{7.5(4212 \text{ in}^4)} \right)^2 = 0.0013 \text{ ksi}$$

Therefore we need to attain at least 0.0013 ksi before lifting to avoid cracking the panel.

Since the concrete lifting anchor strengths are based on a concrete strength of 3.5 ksi,

however, the panels may not be lifted until $f'_c = 3.5 \text{ ksi}$.

$$f'_{c,req} = \max \begin{pmatrix} f'_{c,reqL} \\ f'_{c,reqT} \\ f'_{c,reqA} \end{pmatrix} = \max \begin{pmatrix} 0.0024 \text{ ksi} \\ 0.0013 \text{ ksi} \\ 3.5 \text{ ksi} \end{pmatrix} = 3.5 \text{ ksi}$$

GFRP2 Calculations

The GFRP2 specimen used the Strut-and-Tie method for design.

Material Properties

<u>Concrete</u>	<u>Steel</u>	<u>FRP</u>
$f'_c = 8.0 \text{ ksi}$	$f_y = 60 \text{ ksi}$	$f_{yFRP2} = 130 \text{ ksi}$
$f_r = 7.5\sqrt{f'_c} = 0.671 \text{ ksi}$	$f_u = 75 \text{ ksi}$	$f_{FRP2SUS} = 0.2f_{yFRP2}$
$w_c = 150 \text{ lb/ft}$	$E_s = 29000 \text{ ksi}$	$= 0.2(130 \text{ ksi}) = 26 \text{ ksi}$
$E_c = 33w_c^{1.5}\sqrt{f'_c} = 5422 \text{ ksi}$		$E_{FRP} = 6700 \text{ ksi}$
$n_s = \frac{E_s}{E_c} = 5.348$		$n_{FRP} = \frac{E_{FRP}}{E_c} = 1.236$

Geometrical Dimensions

<u>SWP</u>	<u>Corbel</u>
$t_{wy0} = t_{wyi} = t_{ins} = 3 \text{ in}$	$h_c = 14 \text{ in}$
$t_{SWP} = t_{wy0} + t_{wyi} + t_{ins} = 9 \text{ in}$	$d = 12 \text{ in}$
$b = 6 \text{ ft}$	$b_c = 10 \text{ in}$
$h = 8 \text{ ft}$	$l_p = 8 \text{ in}$
$d_{hout} = 7.5 \text{ in}$	$h_{cf} = 10 \text{ in}$
$d_{hin} = 1.5 \text{ in}$	$c_c = 1.5 \text{ in}$
$I_{gSWP} = \frac{bt_{SWP}^3}{12} - \frac{bt_{ins}^3}{12}$	$I_{gc} = \frac{b_ch_c^3}{12} = \frac{10 \text{ in}(14 \text{ in})^3}{12} = 2287 \text{ in}^4$
$= \frac{72 \text{ in}(9 \text{ in})^3}{12} - \frac{72 \text{ in}(3 \text{ in})^3}{12} = 4212 \text{ in}^4$	

Plate Size

$$V_u = \Phi P_{nb} = \Phi 0.85 f'_c A_1 \quad (\text{ACI 318-14 } \S 22.8.3.2)$$

$$\Phi_{\text{bear}} = 0.65 \quad (\text{ACI 318-14 } \S 21.2.1)$$

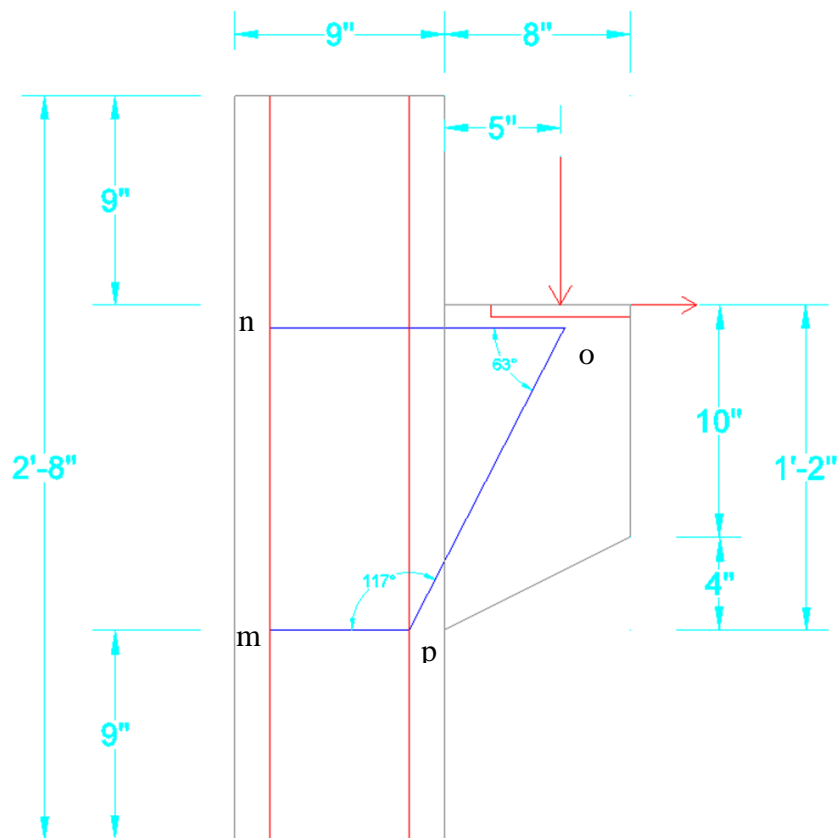
$$A_1 = \frac{V_u}{\Phi_{\text{bear}} 0.85 f'_c} = \frac{30.5 \text{ kip}}{0.65(0.85)(8 \text{ ksi})} = 6.9 \text{ in}^2$$

$$L_{\text{bear}, \min} = \frac{A_1}{b_c} = 0.69 \text{ in}$$

Therefore use at least 1 in \times 10 in plate.

Shear Span, a_v

Assume $a_v = 5 \text{ in}$.

Determine Truss Geometry

$$l_{no} = d_{hout} + a_v + (1 \text{ in}) \tan \theta_R$$

$$= 7.5 \text{ in} + 5 \text{ in} + (1 \text{ in}) \tan(11.31^\circ) = 12.7 \text{ in}$$

$$\theta_{nop} = \text{atan}\left(\frac{d}{l_{no} - (d_{hout} - d_{hin})}\right)$$

$$= \text{atan}\left(\frac{12 \text{ in}}{12.7 \text{ in} - (7.5 \text{ in} - 1.5 \text{ in})}\right) = 60.82^\circ$$

$$l_{mn} = d = 12 \text{ in}$$

$$l_{mp} = d_{hout} - d_{hin} = 7.5 \text{ in} - 1.5 \text{ in} = 6 \text{ in}$$

$$\theta_{pno} = \text{atan}\left(\frac{d}{l_{mp}}\right) = \text{atan}\left(\frac{12}{6}\right) = 63.44^\circ$$

$$\theta_{npo} = 180^\circ - \theta_{pno} - \theta_{nop} = 180^\circ - 63.44^\circ - 60.82^\circ$$

$$= 55.74^\circ$$

$$\theta_{mpn} = \theta_{pno} = 63.44^\circ$$

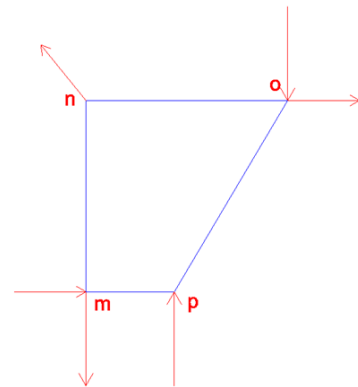
Determine Forces in Truss Components

$$\Sigma M_m = V_u l_{no} + N_{uc} l_{mn} - R_{py} l_{mp} - R_{nx} l_{mn} = 0$$

$$R_{py} = \frac{V_u l_{no} + N_{uc} l_{mn}}{l_{mp}} - R_{nx} \frac{l_{mn}}{l_{mp}}$$

$$\Sigma F_y = R_{py} + R_{ny} - R_{my} - V_u = 0$$

$$\Sigma F_x = N_{uc} - R_{mx} - R_{nx} = 0$$

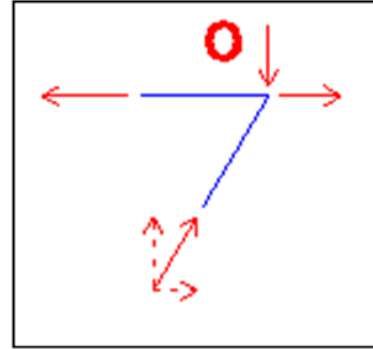


$$N_{opy} = V_u = 30.5 \text{ kip}$$

$$N_{opx} = \frac{N_{opy}}{\tan(\theta_{nop})} = \frac{30.5 \text{ kip}}{\tan(60.82^\circ)} = 17.0 \text{ kip}$$

$$\begin{aligned} N_{op} &= \sqrt{N_{opx}^2 + N_{opy}^2} \\ &= \sqrt{(17.0 \text{ kip})^2 + (30.5 \text{ kip})^2} \\ &= 34.9 \text{ kip (C)} \end{aligned}$$

$$\begin{aligned} N_{no} &= N_{opx} + N_{uc} = 17.0 \text{ kip} + 6.1 \text{ kip} \\ &= 23.1 \text{ kip (T)} \end{aligned}$$



$$R_{nx} = N_{no} = 23.1 \text{ kip}$$

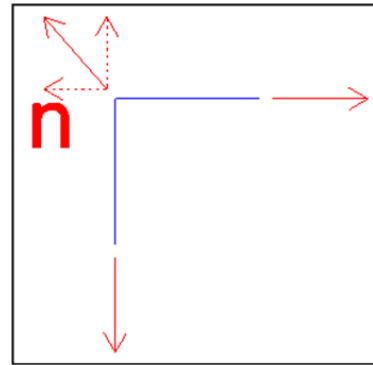
$$R_n = \sqrt{R_{nx}^2 + R_{ny}^2} = \sqrt{2(23.1 \text{ kip})^2} = 32.69 \text{ kip}$$

$$\Sigma F_x = N_{uc} + R_{mx} - R_{nx} = 0$$

$$R_{mx} = R_{nx} - N_{uc} = 17.02 \text{ kip (T)}$$

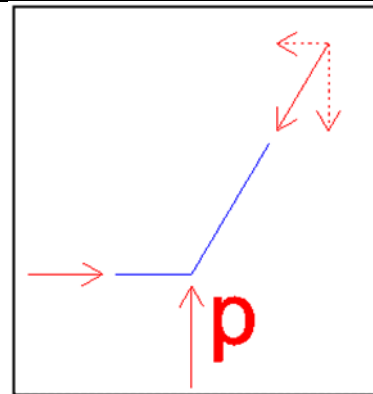
Assume bend acts similar to a pulley

$$N_{mn} = R_{nx} = 23.1 \text{ kip (T)}$$

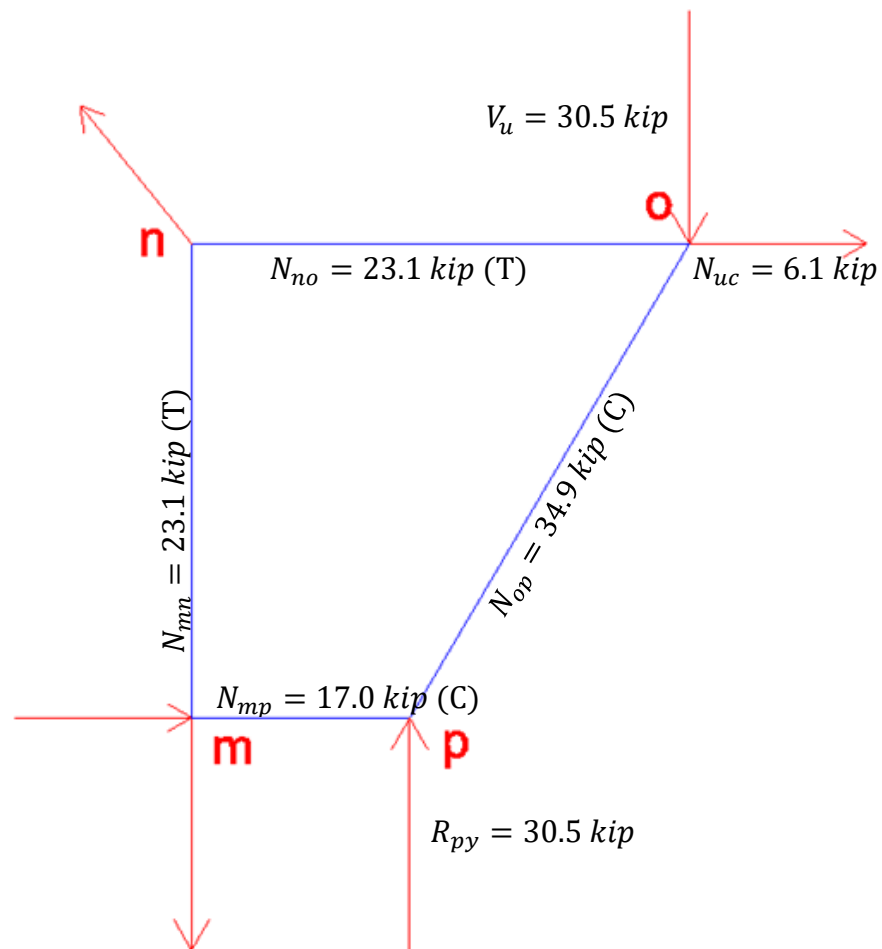
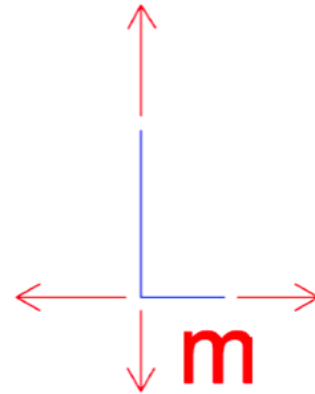


$$N_{mp} = N_{opx} = 17.02 \text{ kip (C)}$$

$$\begin{aligned} R_{py} &= \frac{V_u l_{no} + N_{uc} l_{mn}}{l_{mp}} - R_{nx} \frac{l_{mn}}{l_{mp}} \\ &= \frac{30.5 \text{ kip}(12.7 \text{ in}) + (6.1 \text{ kip})(12 \text{ in})}{6 \text{ in}} - (23.1 \text{ kip}) \frac{12}{6} \\ &= 30.5 \text{ kip} \end{aligned}$$



$$N_{mp} - R_{mx} = 17.0 \text{ kip} - 17.0 \text{ kip} = 0 \therefore OK$$



Select Strut, Tie, and Nodal Zone Dimensions

The most conservative β value for any relevant component will govern.

Nodes	Struts	
$\beta_{Nm} = 0.60$ (C-T-T)	$\beta_{s_{py}} = 1.0$	A bottle-shaped strut could develop in the concrete, so 0.75 will be used if reinforced properly. Otherwise, 0.6 must be used. Will assume inadequate reinforcement ($\beta=0.6$).
$\beta_{Nm} = 0.60$ (C-T-T)	$\beta_{s_{np}} = 0.6$	
$\beta_{Nm} = 0.80$ (C-C-T)	$\beta_{s_{op}} = 0.6$	
$\beta_{Nm} = 0.80$ (C-C-T)		

Because all components are affected by an element with a limiting value of 0.6, design must use $\beta = 0.6$ for all members.

$$\beta_s = 0.6$$

$$f_{ce} = 0.85\beta_s f'_c = 0.85(0.6)(8.0 \text{ ksi}) = 4.08 \text{ ksi}$$

$$\Phi f_{ce} = 0.75(4.08 \text{ ksi}) = 3.06 \text{ ksi}$$

Design Tension Ties

Member mn

$$w_{mn} = \frac{N_{mn}}{\Phi f_{ce} b_c} = \frac{23.1 \text{ kip}}{0.75(3.06 \text{ ksi})(10 \text{ in})} = 0.76 \text{ in} < \text{wythe thickness, } \therefore \text{OK}$$

$$A_{sreq,mn} = \frac{N_{mn}}{\Phi f_y} = \frac{23.1 \text{ kip}}{0.75(60 \text{ ksi})} = 0.51 \text{ in}^2 \quad \text{Therefore use (4) \#4 at 2.5" o.c.}$$

$$A_{smn} = 4(0.2 \text{ in}^2) = 0.8 \text{ in}^2$$

$$N_{nmn} = \Phi A_{smn} f_y = 0.75(0.8 \text{ in}^2)(60 \text{ ksi}) = 36 \text{ kip} \geq N_{mn} = 23.1 \text{ kip} \therefore \text{OK}$$

Anchorage Requirements

$$l_{dmp} = \left(\frac{3}{40} * \frac{f_y}{\lambda \sqrt{f'_c}} * \frac{\Psi_t \Psi_e \Psi_s}{\frac{(c_b + K_{tr})}{d_b}} \right) d_b \quad (\text{ACI 318-14 §25.4.2.3})$$

If clear cover of $1.0d_b$ and a minimum clear spacing of $2d_b$ exists, the simplified version may be used:

$$l_{dmp} = \left(\frac{f_y \Psi_t \Psi_e}{25 \lambda \sqrt{f'_c}} \right) d_b \quad (\text{ACI 318-14 §25.4.2.2})$$

$$\Psi_t = 1 \quad (\text{because not horizontal reinforcement})$$

$$\Psi_e = 1 \quad (\text{because using uncoated, regular rebar})$$

$$\lambda = 1 \quad (\text{because normalweight concrete})$$

$$d_b = 0.5 \text{ in}$$

$$l_{dmp} = \left(\frac{(60 \text{ ksi})(1)(1)}{25(1)\sqrt{8000 \text{ psi}} \left(1 \frac{\text{ksi}}{1000 \text{ psi}} \right)} \right) (0.5 \text{ in}) = 13.4 \text{ in}$$

Therefore 16 inches of rebar must be extended on each side of the corbel for a total of 46 inches.

Member no

$$w_{no} = \frac{N_{no}}{\Phi f_{ce} b_c} = \frac{23.1 \text{ kip}}{0.75(3.06 \text{ ksi})(10 \text{ in})} = 0.76 \text{ in}$$

$$A_{sreq,no} = \frac{N_{no}}{\Phi f_{yFRP2}} = \frac{23.1 \text{ kip}}{0.75(130 \text{ ksi})} = 0.24 \text{ in}^2 \quad \text{Therefore (5) GFRP \#2 bars}$$

Creep rupture typically controls with GFRP, however. This requires an area of:

$$A_{creepreq2} = \frac{N_{no} \left(\frac{V_{sus}}{V_u} \right)}{\Phi_v f_{FRP2sus}} = \frac{23.1 \text{ kip} \left(\frac{16.46}{30.5} \right)}{0.75(26 \text{ ksi})} = 0.64 \text{ in}^2$$

Therefore use two rows of (7) GFRP #2 bars at 1.375" o.c. for a total of (14) bars

$$A_{sno} = 14(0.049 \text{ in}^2) = 0.69 \text{ in}^2$$

$$N_{nno} = \Phi A_{sno} f_y = 0.75(0.69 \text{ in}^2)(130 \text{ ksi}) = 66.9 \text{ kip} \geq N_{mn} = 23.1 \text{ kip} \therefore OK$$

Anchorage Length Requirements

$$l_{bhf} = 12d_b = 12(0.25 \text{ in}) = 3 \text{ in} \quad (\text{ACI 440.1R-15 §8.3})$$

$$l_{bhf,out} = l_{bhf} + d_{s3} + 3d_{s3} = 4 \text{ in}$$

Therefore specify legs out-to-out of 6 inches.

Anchorage Concrete Breakout Strength

By treating the GFRP reinforcement as an anchor, the transverse reinforcement may be considered to transfer the load vertically and horizontally to the outside wythe. According to ACI D4.4, this allows the panel to meet the requirements of Condition A (using supplementary reinforcement) and being governed by concrete breakout, blowout, pullout, etc.

$$N_{cb} = \frac{A_{Nc}}{A_{Nco}} \Psi_{ecN} \Psi_{edN} \Psi_{cN} \Psi_{cpN} N_b \quad (\text{ACI 440.1R-15 Eq D-5})$$

$$\begin{aligned} h_{ef} &= t_{wyo} - 1 \text{ in} - d_b \\ &= 3 \text{ in} - 1 \text{ in} - 0.375 \text{ in} = 1.625 \text{ in} \end{aligned}$$

$$A_{Nco} = 9h_{ef}^2 = 9(1.625 \text{ in})^2 = 23.77 \text{ in}^2 \quad (\text{ACI 440.1R-15 Eq D-6})$$

$$\begin{aligned} A_{Nc} &= [2(1.5h_{ef})][2(1.5h_{ef}) + s_c(N_{FRP} - 1)] \\ &= [3(1.625 \text{ in})][3(1.625 \text{ in}) + (1.375 \text{ in})(7 - 1)] \\ &= 64.0 \text{ in}^2 \end{aligned}$$

$$N_b = k_c \lambda \sqrt{f'_c} h_{ef}^{1.5} \quad (\text{ACI 440.1R-15 Eq D-7})$$

$k_c = 24$ for cast-in-place anchors

$$N_b = 24(1)\sqrt{8000 \text{ psi}}(1.375 \text{ in})^{1.5} = 4.45 \text{ kip}$$

$$\Psi_{ecN} = \frac{1}{1 + \frac{2e'_N}{3h_{ef}}} = \frac{1}{1 + \frac{2(0)}{3h_{ef}}} = 1 \text{ because symmetric}$$

$$\Psi_{edN} = 1 \text{ since edges further away than } 1.5h_{ef}$$

$$\Psi_{cN} = 1 \text{ to be conservative}$$

$$\Psi_{cpN} = 1 \text{ since edge cover is greater than } 4h_{ef}$$

$$N_{cb} = 12.0 \text{ kip} < 23.1 \text{ kip}, \therefore \text{No Good}$$

However, provisions from ACI D.5.2.9 state that if development is obtained on both sides of the breakout, “the design strength of the anchor reinforcement shall be permitted to be used instead of the concrete breakout strength.” Therefore OK.

Shear Strength of Rebar in Shear (estimated to be about $0.6f_u$)

$$R_{rebarShear} = 0.6f_u A_{gv} = R_n$$

$$A_{gv} = \frac{R_n}{\Phi_v(0.6f_u)} = \frac{32.7 \text{ kip}}{0.75(0.6(75 \text{ ksi}))} = 0.97 \text{ in}^2 \quad \text{Therefore use (5)\#4 @ 1.5" o.c.}$$

Adequate development is required on both sides of the corbel, so we will need a bar 42" long.

Design Compression Struts

Member op

$$w_{op} = \frac{N_{op}}{\Phi f_{ce} b_c} = \frac{34.9 \text{ kip}}{0.75(3.06 \text{ ksi})(10 \text{ in})} = 1.14 \text{ in}$$

Member mp

$$w_{mp} = \frac{N_{mp}}{\Phi f_{ce} b_c} = \frac{17.0 \text{ kip}}{0.75(3.06 \text{ ksi})(10 \text{ in})} = 0.56 \text{ in}$$

Since the foam is not able to withstand this force over such a small area, the compressive material used in this instance must have a height of at least 0.6 in. Wood typically has a low thermal conductivity, is very cheap, and is readily available on the job site. Because the compressive strength is difficult to find published, the strength of Douglas Fir Larch will be used as a conservative design value ($f_{HDO} = f_{DFL} = 1.36 \text{ ksi}$). Simply for feasibility, if a prism of HDO board is used that is 3 inches thick, 3.5 inches tall, and 10 inches long, the area required to resist the compressive force of member mp is

$$A_{HDOreq} = \frac{N_{mp}}{\Phi_v f_{HDO}} = \frac{17.0 \text{ kip}}{0.75(1.36 \text{ ksi})} = 16.68 \text{ in}^2$$

$$b_{HDOreq} = \frac{A_{HDOreq}}{h_{HDO}} = \frac{16.68 \text{ in}^2}{3.5 \text{ in}} = 4.77 \text{ in}$$

We will be safe by using a 10 in long compressive segment, equal to the width of the corbel.

$$\Phi_v f_{HDO} h_{HDO} b_{HDO} = 0.75(1.36 \text{ ksi})(3.5 \text{ in})(10 \text{ in}) = 35.7 \text{ kip} \geq N_{mp} = 17.0 \text{ kip}$$

$\therefore OK$

Member Rp

$$w_{py} = \frac{R_{py}}{\Phi f_{ce} b_c} = \frac{30.5 \text{ kip}}{0.75(3.06 \text{ ksi})(10 \text{ in})} = 1.0 \text{ in} < \text{wythe thickness therefore OK}$$

Shear at Corbel/SWP Interface

The shear to be resisted at this interface will be equal to the applied load. The friction from the interface shall be ignored conservatively. Stirrups shall be used to resist the shear.

$$R_{rebarShear} = 0.6f_u A_{gv}$$

$$A_{gv} = \frac{V_u}{\Phi_v 0.6f_u} = \frac{30.5 \text{ kip}}{0.75(0.6)(75 \text{ ksi})} = 0.9 \text{ in}^2 \quad \therefore \text{use (3)\#4 stirrups @ 3" o.c.}$$

$$A_{gv} = 3(2 * 0.2 \text{ in}^2) = 1.2 \text{ in}^2$$

Vertical/Longitudinal Reinforcement, A_{sl}

$$\rho = \frac{A_{sl,min}}{A_{gc}} = 0.0012 \quad (\text{ACI 381-14 §14.3.2})$$

$$\begin{aligned} A_{gcl} &= b * (t_{wy0} + t_{wyi}) = 72 \text{ in} * 6 \text{ in} \\ &= 432 \text{ in}^2 \end{aligned}$$

$$A_{sl,min} = \rho A_{gcl} = 0.0012(432 \text{ in}^2) = 0.52 \text{ in}^2$$

$$s_{max} = \min\left(\frac{3t}{18 \text{ in}}\right) = \max\left(\frac{27 \text{ in}}{18 \text{ in}}\right) = 18 \text{ in}$$

$$\begin{aligned} N_{sl} &= \frac{b - 2(0.75 \text{ in})}{s_{max}} = \frac{72 \text{ in} - 2(0.75 \text{ in})}{18 \text{ in}} \\ &= 3.92 \text{ bars} \end{aligned}$$

$$A_{slbarmin} = \frac{A_{sl,min}}{N_{sl}} = \frac{0.52 \text{ in}^2}{4} = 0.13 \text{ in}^2 \quad \therefore \text{use (4)\#4 bars @ 18" o.c.}$$

Therefore use (4) #4 bars spaced 18" o.c. Place second layer of rebar on compression side for any reversed loading.

Horizontal/Transverse Reinforcement, A_{st}

$$\rho = \frac{A_{st,min}}{A_{gc}} = 0.0020 \quad (\text{ACI 381-14 §14.3.3})$$

$$A_{gct} = h * (t_{wy0} + t_{wyi}) = 96 \text{ in} * 6 \text{ in} = 576 \text{ in}^2$$

$$A_{st,min} = \rho A_{gcl} = 0.002(576 \text{ in}^2) = 1.15 \text{ in}^2$$

$$s_{max} = \min \left(\frac{3t}{18 \text{ in}} \right) = \max \left(\frac{27 \text{ in}}{18 \text{ in}} \right) = 18 \text{ in}$$

$$N_{st} = \frac{h - 2(0.75 \text{ in})}{s_{max}} = \frac{96 \text{ in} - 2(0.75 \text{ in})}{18 \text{ in}}$$

$$= 5.25 \text{ bars}$$

$$A_{stbarmin} = \frac{A_{st,min}}{N_{st}} = \frac{1.15 \text{ in}^2}{6} = 0.19 \text{ in}^2 \quad \therefore \text{use (6)\#4 bars @ 18" o. c.}$$

Therefore use (6) #4 bars spaced 18" o.c. Place second layer of rebar on opposite side for symmetry.

Lifting

$$x_{lift} = 18 \text{ in} = 1.5 \text{ ft} \quad (\text{anchor to edge distance})$$

$$x_{midL} = h - 2x_{anchor} = 8 \text{ ft} - 3 \text{ ft} = 5 \text{ ft}$$

$$x_{midT} = b - 2x_{anchor} = 6 \text{ ft} - 3 \text{ ft} = 3 \text{ ft}$$

Longitudinal Direction

$$w_{sw} = w_c b t = (150 \text{ pcf})(6 \text{ ft})(0.5 \text{ ft}) = 450 \frac{\text{lb}}{\text{ft}}$$

$$R_A = \frac{w_{sw} h}{2} = \frac{\left(0.45 \frac{\text{kip}}{\text{ft}}\right)(8 \text{ ft})}{2} = 1.8 \text{ kip}$$

$$V_{lift,left} = w_{sw}x_{lift} = \left(0.45 \frac{kip}{ft}\right)(1.5 ft)$$

$$= -0.675 kip$$

$$V_{lift,right} = w_{sw}x_{lift} + R_A = -0.675 kip + 1.8 kip$$

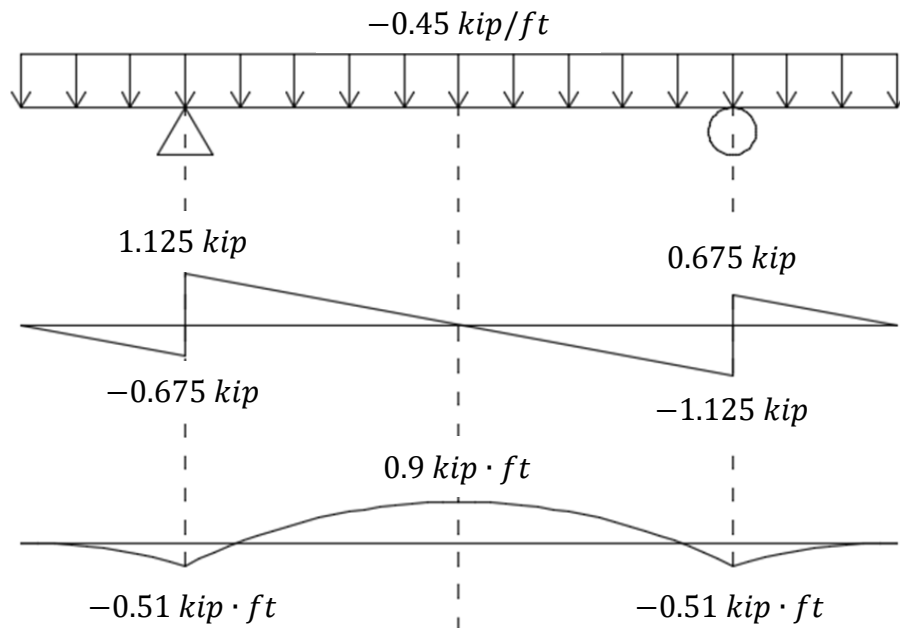
$$= 1.125 kip$$

$$M_{lift} = \frac{V_{lift,left}x_{lift}}{2} = \frac{(-0.675 kip)(1.5 ft)}{2}$$

$$= -0.506 kip \cdot ft$$

$$M_{mid} = M_{lift} + \frac{V_{lift,right}(0.5x_{midL})}{2}$$

$$= -0.51 kip \cdot ft + \frac{0.675 kip(0.5 \cdot 5 ft)}{2} = 0.9 kip \cdot ft$$



Cracking moment is equal to

$$M_{cr} = \frac{7.5\sqrt{f'_c}I_g}{0.5t}$$

$$f'_{c,req} = \left(\frac{0.5(t_{wy0} + t_{wyi})M_{mid}}{7.5I_g} \right)^2$$

$$= \left(\frac{0.5(6 \text{ in}) \left(0.9 \text{ kip} \cdot \text{ft} * \frac{12 \text{ in}}{\text{ft}} \right)}{7.5(4212 \text{ in}^4)} \right)^2 = 0.0024 \text{ ksi}$$

Therefore we need to attain at least 0.0024 ksi before lifting.

Transverse Direction

$$w_{sw} = w_c ht = (150 \text{ pcf})(8 \text{ ft})(0.5 \text{ ft}) = 600 \frac{\text{lb}}{\text{ft}}$$

$$R_A = \frac{w_{sw}b}{2} = \frac{\left(0.6 \frac{\text{kip}}{\text{ft}}\right)(6 \text{ ft})}{2} = 1.8 \text{ kip}$$

$$V_{lift,left} = w_{sw}x_{lift} = \left(0.6 \frac{\text{kip}}{\text{ft}}\right)(1.5 \text{ ft})$$

$$= -0.9 \text{ kip}$$

$$V_{lift,right} = w_{sw}x_{lift} + R_A = -0.9 \text{ kip} + 1.8 \text{ kip}$$

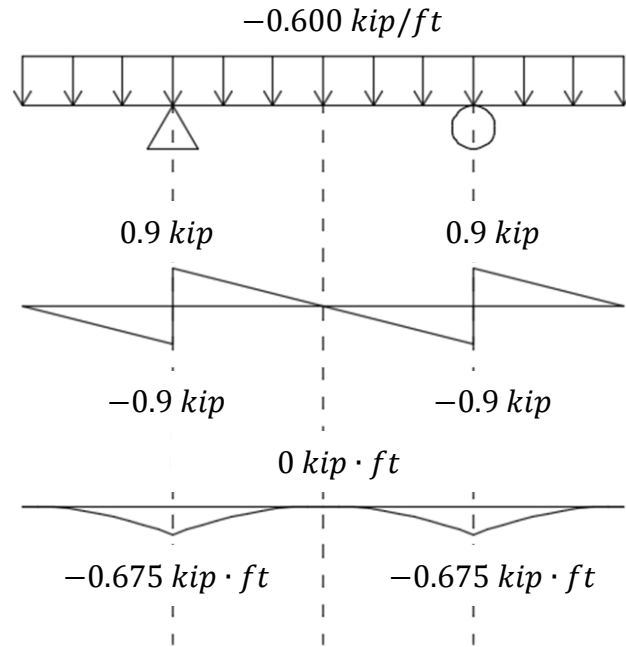
$$= 0.9 \text{ kip}$$

$$M_{lift} = \frac{V_{lift,left}x_{lift}}{2} = \frac{(-0.9 \text{ kip})(1.5 \text{ ft})}{2}$$

$$= -0.675 \text{ kip} \cdot \text{ft}$$

$$M_{mid} = M_{lift} + \frac{V_{lift,right}(0.5x_{midT})}{2}$$

$$= -0.675 \text{ kip} \cdot \text{ft} + \frac{0.9 \text{ kip}(0.5*3 \text{ ft})}{2} = 0 \text{ kip} \cdot \text{ft}$$



Cracking moment is equal to

$$M_{cr} = \frac{7.5\sqrt{f'_c}I_g}{0.5t}$$

$$f'_{c,req} = \left(\frac{0.5(t_{wyo} + t_{wyi})M_{lift}}{7.5I_{gSWP}} \right)^2$$

$$= \left(\frac{0.5(6 \text{ in}) \left(0.675 \text{ kip} \cdot \text{ft} * \frac{12 \text{ in}}{\text{ft}} \right)}{7.5(4212 \text{ in}^4)} \right)^2 = 0.0013 \text{ ksi}$$

Therefore we need to attain at least 0.0013 ksi before lifting to avoid cracking the panel.

Since the concrete lifting anchor strengths are based on a concrete strength of 3.5 ksi,

however, the panels may not be lifted until $f'_c = 3.5 \text{ ksi}$.

$$f'_{c,req} = \max \begin{pmatrix} f'_{c,reqL} \\ f'_{c,reqT} \\ f'_{c,reqA} \end{pmatrix} = \max \begin{pmatrix} 0.0024 \text{ ksi} \\ 0.0013 \text{ ksi} \\ 3.5 \text{ ksi} \end{pmatrix} = 3.5 \text{ ksi}$$

HKHor and HKVer Calculations

The HK specimens were both based off of the same design calculations, with only the detailing differing. The HK specimens used the Strut-and-Tie method for design.

Material Properties

<u>Concrete</u>	<u>Steel</u>	<u>FRP</u>
$f'_c = 8.0 \text{ ksi}$	$f_y = 60 \text{ ksi}$	$f_{yHK} = 33 \text{ ksi}$
$f_r = 7.5\sqrt{f'_c} = 0.671 \text{ ksi}$	$f_u = 75 \text{ ksi}$	$f_{HKsus} = 0.2f_{yHK}$
$w_c = 150 \text{ lb}/\text{ft}$	$E_s = 29000 \text{ ksi}$	$= 0.2(33 \text{ ksi}) = 6.6 \text{ ksi}$
$E_c = 33w_c^{1.5}\sqrt{f'_c} = 5422 \text{ ksi}$		$A_{HK} = 0.82 \text{ in}^2$
$n_s = \frac{E_s}{E_c} = 5.348$		$b_{HK} = 3 \text{ in}$
		$h_{HK} = 6 \text{ in}$

Geometrical Dimensions

<u>SWP</u>	<u>Corbel</u>
$t_{wy0} = t_{wyi} = t_{ins} = 3 \text{ in}$	$h_c = 14 \text{ in}$
$t_{SWP} = t_{wy0} + t_{wyi} + t_{ins} = 9 \text{ in}$	$d = 12 \text{ in}$
$b = 68 \text{ in} = 5.67 \text{ ft}$	$b_c = 10 \text{ in}$
$h = 102 \text{ in} = 8.5 \text{ ft}$	$l_p = 8 \text{ in}$
$d_{hout} = 7.5 \text{ in}$	$h_{cf} = 10 \text{ in}$
$d_{hin} = 1.5 \text{ in}$	$c_c = 1.5 \text{ in}$
$I_{gSWP} = \frac{bt_{SWP}^3}{12} - \frac{bt_{ins}^3}{12}$	$I_{gc} = \frac{b_ch_c^3}{12} = \frac{10 \text{ in}(14 \text{ in})^3}{12} = 2287 \text{ in}^4$
$= \frac{68 \text{ in}(9 \text{ in})^3}{12} - \frac{68 \text{ in}(3 \text{ in})^3}{12} = 3978 \text{ in}^4$	$z_c = 42 \text{ in}$ (from top SWP to corbel)

Plate Size

$$V_u = \Phi P_{nb} = \Phi 0.85 f'_c A_1 \quad (\text{ACI 318-14 §22.8.3.2})$$

$$\Phi_{\text{bear}} = 0.65 \quad (\text{ACI 318-14 §21.2.1})$$

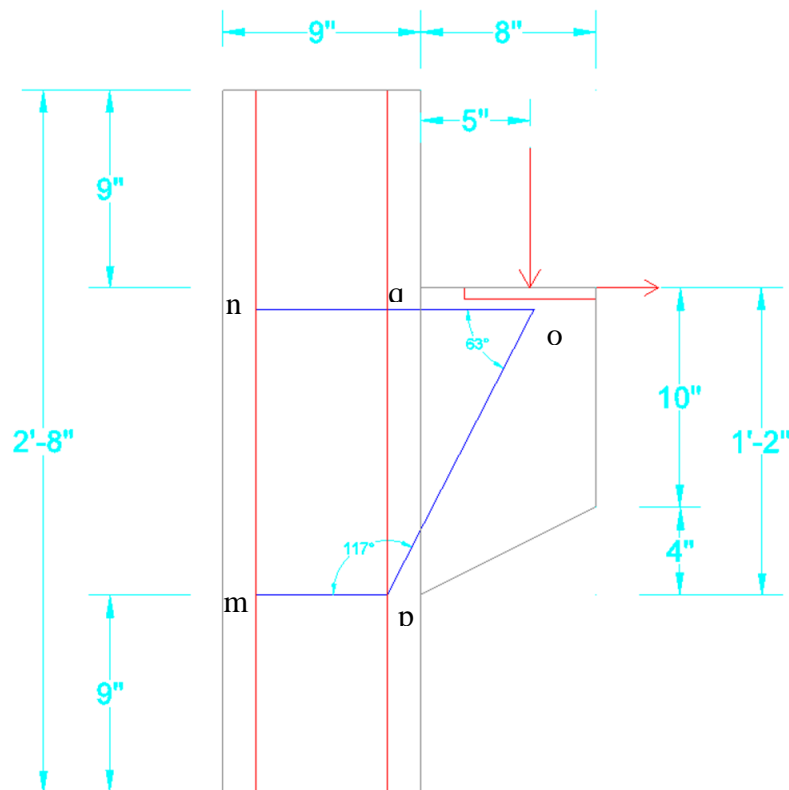
$$A_1 = \frac{V_u}{\Phi_{\text{bear}} 0.85 f'_c} = \frac{30.5 \text{ kip}}{0.65(0.85)(8 \text{ ksi})} = 6.9 \text{ in}^2$$

$$L_{\text{bear}, \text{min}} = \frac{A_1}{b_c} = 0.69 \text{ in}$$

Therefore use at least 1 in \times 10 in plate.

Shear Span, a_v

Assume $a_v = 5 \text{ in}$.

Determine Truss Geometry

$$l_{no} = d_{hout} + a_v + (1 \text{ in}) \tan \theta_R$$

$$= 7.5 \text{ in} + 5 \text{ in} + (1 \text{ in}) \tan(11.31^\circ) = 12.7 \text{ in}$$

$$\theta_{nop} = \text{atan}\left(\frac{d}{l_{no} - (d_{hout} - d_{hin})}\right)$$

$$= \text{atan}\left(\frac{12 \text{ in}}{12.7 \text{ in} - (7.5 \text{ in} - 1.5 \text{ in})}\right) = 60.82^\circ$$

$$l_{mn} = d = 12 \text{ in}$$

$$l_{mp} = d_{hout} - d_{hin} = 7.5 \text{ in} - 1.5 \text{ in} = 6 \text{ in}$$

$$\theta_{pno} = \text{atan}\left(\frac{d}{l_{mp}}\right) = \text{atan}\left(\frac{12}{6}\right) = 63.44^\circ$$

$$\theta_{npo} = 180^\circ - \theta_{pno} - \theta_{nop} = 180^\circ - 63.44^\circ - 60.82^\circ$$

$$= 55.74^\circ$$

$$\theta_{mpn} = \theta_{pno} = 63.44^\circ$$

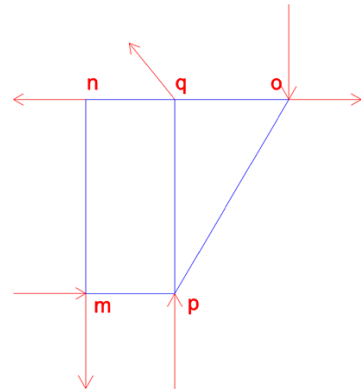
Determine Forces in Truss Components

$$\Sigma M_m = V_u l_{no} + N_{uc} l_{mn} - R_{py} l_{mp} - R_{nx} l_{mn} = 0$$

$$R_{py} = \frac{V_u l_{no} + N_{uc} l_{mn}}{l_{mp}} - R_{nx} \frac{l_{mn}}{l_{mp}}$$

$$\Sigma F_y = R_{py} + R_{ny} - R_{my} - V_u = 0$$

$$\Sigma F_x = N_{uc} - R_{mx} - R_{nx} = 0$$



$$N_{opy} = V_u = 30.5 \text{ kip}$$

$$N_{opx} = \frac{N_{opy}}{\tan(\theta_{nop})} = \frac{30.5 \text{ kip}}{\tan(60.82^\circ)} = 17.0 \text{ kip}$$

$$N_{op} = \sqrt{N_{opx}^2 + N_{opy}^2}$$

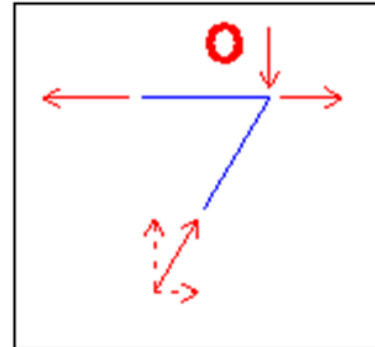
$$= \sqrt{(17.0 \text{ kip})^2 + (30.5 \text{ kip})^2}$$

$$= 34.9 \text{ kip (C)}$$

$$N_{oq} = N_{opx} + N_{uc} = 17.0 \text{ kip} + 6.1 \text{ kip}$$

$$= 23.1 \text{ kip (T)}$$

$$N_{nq} = N_{oq} = 23.1 \text{ kip (T)}$$



$$R_{nx} = N_{oq} = 23.1 \text{ kip}$$

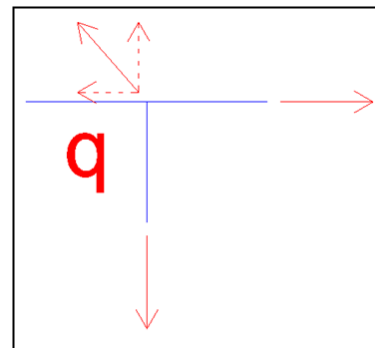
$$\Sigma F_x = N_{uc} + R_{mx} - R_{nx} = 0$$

$$R_{mx} = R_{nx} - N_{uc} = 17.02 \text{ kip (T)}$$

Assume bend acts similar to a pulley

$$N_{pq} = N_{oq} = 23.1 \text{ kip (T)}$$

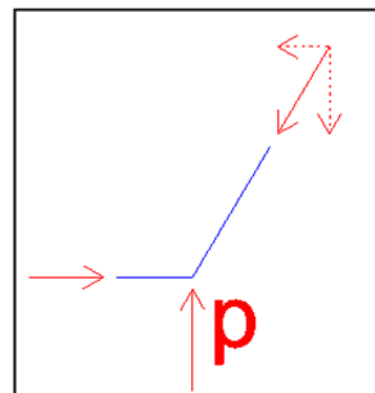
$$R_q = \sqrt{2 * N_{oq}^2} = \sqrt{2 * (23.1 \text{ kip})^2} = 32.7 \text{ kip}$$



$$N_{mp} = N_{opx} = 17.02 \text{ kip (C)}$$

$$\begin{aligned} R_{py} &= \frac{V_u l_{no} + N_{uc} l_{mn}}{l_{mp}} - R_{nx} \frac{l_{mn}}{l_{mp}} \\ &= \frac{30.5 \text{ kip}(12.7 \text{ in}) + (6.1 \text{ kip})(12 \text{ in})}{6 \text{ in}} - (23.1 \text{ kip}) \frac{12}{6} \\ &= 30.5 \text{ kip} \end{aligned}$$

$$N_{mp} - R_{mx} = 17.0 \text{ kip} - 17.0 \text{ kip} = 0 \therefore \text{OK}$$



$$\begin{aligned}
 M_{applied} &= V_u(a_v + \frac{t_{SWP}}{2}) + N_{uc}(h_c - d) \\
 &= (30.5 \text{ kip}) \left(5 \text{ in} + \frac{9 \text{ in}}{2} \right) + (6.1 \text{ kip})(14 \text{ in} - 12 \text{ in}) \\
 &= 25.146 \text{ kip} \cdot \text{ft}
 \end{aligned}$$

$$\begin{aligned}
 M_{uAbove} &= \frac{M_{applied}}{h} \left(z_c + \frac{h_c}{2} \right) \\
 &= \frac{25.15 \text{ kip} \cdot \text{ft}}{8.5 \text{ ft}} \left(42 \text{ in} + \frac{14 \text{ in}}{2} \right) = 12.1 \text{ kip} \cdot \text{ft}
 \end{aligned}$$

$$\begin{aligned}
 M_{uBelow} &= M_{applied} - M_{uAbove} \\
 &= 25.15 \text{ kip} \cdot \text{ft} - 12.1 \text{ kip} \cdot \text{ft} = 13.1 \text{ kip} \cdot \text{ft}
 \end{aligned}$$

$$M_u = C(d_{hout} - d_{hin})$$

Compression will be greatest below corbel in the inside wythe. To simplify design, both wythes are to be detailed symmetrically. Therefore, let $C = P_{wyin}$.

$$M_u = \max(M_{uAbove}, M_{uBelow}) = 13.1 \text{ kip} \cdot \text{ft}$$

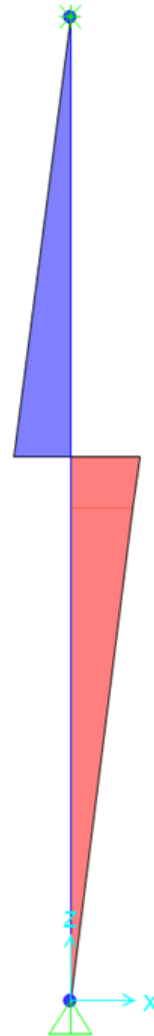
$$P_{wyin} = \frac{M_u}{d_{hout} - d_{hin}} = \frac{13.1 \text{ kip} \cdot \text{ft}}{7.5 \text{ in} - 1.5 \text{ in}} = 26.1 \text{ kip (C)}$$

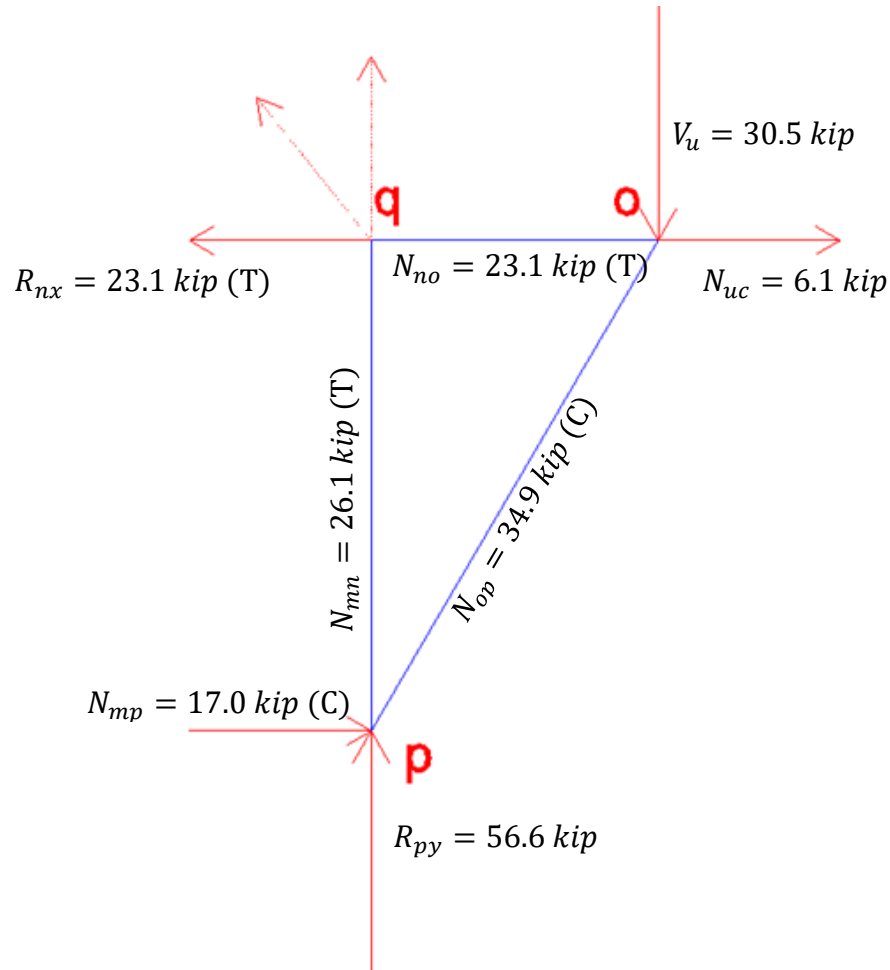
$$P_{wyout} = P_{wyin} = 26.1 \text{ kip (T)}$$

$$N_{pq} = P_{wyin} = 26.1 \text{ kip}$$

$$N_{mn} = P_{wyout} = 26.1 \text{ kip}$$

$$N_{py} = R_{py} + N_{pq} = 56.6 \text{ kip}$$





Select Strut, Tie, and Nodal Zone Dimensions

The most conservative β value for any relevant component will govern.

Nodes		Struts	
$\beta_{Nm} = 0.60$	(C-T-T)	$\beta_{Spy} = 1.0$	A bottle-shaped strut could develop in the concrete, so 0.75 will be used if reinforced properly. Otherwise, 0.6 must be used. Will assume inadequate reinforcement ($\beta=0.6$).
$\beta_{Nm} = 0.60$	(C-T-T)	$\beta_{Snp} = 0.6$	
$\beta_{Nm} = 0.80$	(C-C-T)	$\beta_{Sop} = 0.6$	
$\beta_{Nm} = 0.80$	(C-C-T)		

Because all components are affected by an element with a limiting value of 0.6, design must use $\beta = 0.6$ for all members.

$$\beta_s = 0.6$$

$$f_{ce} = 0.85\beta_s f'_c = 0.85(0.6)(8.0 \text{ ksi}) = 4.08 \text{ ksi}$$

$$\Phi f_{ce} = 0.75(4.08 \text{ ksi}) = 3.06 \text{ ksi}$$

Design Tension Ties

Member mn

$$w_{mn} = \frac{N_{mn}}{\Phi f_{ce} b_c} = \frac{26.1 \text{ kip}}{0.75(3.06 \text{ ksi})(10 \text{ in})} = 0.85 \text{ in} < \text{wythe thickness, } \therefore \text{OK}$$

$$A_{sreq,mn} = \frac{N_{mn}}{\Phi f_y} = \frac{26.1 \text{ kip}}{0.75(60 \text{ ksi})} = 0.58 \text{ in}^2 \quad \text{Therefore use (3) \#4 at 3" o.c.}$$

$$A_{smn} = 3(0.2 \text{ in}^2) = 0.6 \text{ in}^2$$

$$N_{nmn} = \Phi A_{smn} f_y = 0.75(0.6 \text{ in}^2)(60 \text{ ksi}) = 27 \text{ kip} \geq N_{mn} = 26.1 \text{ kip} \therefore \text{OK}$$

Anchorage Requirements

$$l_{dmp} = \left(\frac{3}{40} * \frac{f_y}{\lambda \sqrt{f'_c}} * \frac{\Psi_t \Psi_e \Psi_s}{\frac{(c_b + K_{tr})}{d_b}} \right) d_b \quad (\text{ACI 318-14 §25.4.2.3})$$

If clear cover of $1.0d_b$ and a minimum clear spacing of $2d_b$ exists, the simplified version may be used:

$$l_{dmp} = \left(\frac{f_y \Psi_t \Psi_e}{25 \lambda \sqrt{f'_c}} \right) d_b \quad (\text{ACI 318-14 §25.4.2.2})$$

$$\Psi_t = 1 \quad (\text{because not horizontal reinforcement})$$

$$\Psi_e = 1 \quad (\text{because using uncoated, regular rebar})$$

$$\lambda = 1 \quad (\text{because normalweight concrete})$$

$$d_b = 0.5 \text{ in}$$

$$l_{dmp} = \left(\frac{(60 \text{ ksi})(1)(1)}{25(1)\sqrt{8000 \text{ psi}} \left(1 \frac{\text{ksi}}{1000 \text{ psi}} \right)} \right) (0.5 \text{ in}) = 13.4 \text{ in}$$

Therefore 16 inches of rebar must be extended on each side of the corbel for a total of 46 inches.

Member oq

$$w_{oq} = \frac{N_{oq}}{\Phi f_{ce} b_c} = \frac{23.1 \text{ kip}}{0.75(3.06 \text{ ksi})(10 \text{ in})} = 0.76 \text{ in}$$

$$A_{sreq,oq} = \frac{N_{oq}}{\Phi f_y} = \frac{23.1 \text{ kip}}{0.75(60 \text{ ksi})} = 0.52 \text{ in}^2 \quad \text{Therefore use (3) \#4 at 3" o.c.}$$

$$A_{soq} = 3(0.2 \text{ in}^2) = 0.8 \text{ in}^2$$

$$N_{noq} = \Phi A_{soq} f_y = 0.75(0.8 \text{ in}^2)(60 \text{ ksi}) = 27 \text{ kip} \geq N_{oq} = 23.1 \text{ kip} \therefore OK$$

Anchorage Requirements

$$l_{dmp} = \left(\frac{f_y \Psi_e \Psi_c \Psi_r}{50 \lambda \sqrt{f'_c}} \right) d_b \quad (\text{ACI 318-14 §25.4.3.1})$$

$$\Psi_e = 1 \quad (\text{because using uncoated, regular rebar})$$

$$\psi_c = 1 \quad (\text{because cover not } \geq 2.5 \text{ in})$$

$$\psi_r = 1 \quad (\text{because not enclosed})$$

$$\lambda = 1 \quad (\text{because normalweight concrete})$$

$$d_b = 0.5 \text{ in}$$

$$l_{dh} = \left(\frac{1(1)(1)(60 \text{ ksi})}{50 \lambda \sqrt{8000 \text{ psi}} \left(1 \frac{\text{ksi}}{1000 \text{ psi}} \right)} \right) (0.5 \text{ in}) = 6.7 \text{ in}$$

$$l_{dh} = \max \left(\frac{l_{dh}}{8 d_b}, \frac{l_{dh}}{6 \text{ in}} \right) = 6.7 \text{ in}$$

Therefore need 7 inches of rebar beyond bend for principle reinforcement:

$$l_{out} = l_{dh} + (3d_b + d_b) = 8.7 \text{ in} \quad (\text{ACI 318-11 §12.5.1})$$

Will specify principle reinforcement to extend 12 inches from top of the bend. Anchor bar shall be welded to the end of the principle reinforcement to attain development on corbel tip.

Member nq

No need to check tie width because this member will penetrate insulation (i.e. no concrete). According to HK testing performed previously, concrete breakout strength is

$$\Phi P_{nHKBreak} = 4.58 \text{ kip}$$

$$N_{HKreq} = \frac{N_{nq}}{\Phi P_{nHKBreak}} = \frac{23.1 \text{ kip}}{4.58 \text{ kip}} = 5.043$$

\therefore must use 6 HK connectors to transfer load

Creep rupture must be considered with GFRP, however. This requires

$$N_{HKcreep} = \frac{N_{nq} \left(\frac{V_{sus}}{V_u} \right)}{\Phi_v f_{HKsus} A_{HK}} = \frac{23.1 \text{ kip} \left(\frac{16.46}{30.5} \right)}{0.75(6.6 \text{ ksi})(0.82 \text{ in}^2)} = 3.07$$

\therefore must use 3 HK connectors

Therefore concrete breakout governs. Use (6) HK ties. The recommended spacing for HK ties is 16" o.c. Because the ties will be used for localized force transfer, and because concrete breakout governs, the spacing will be based upon concrete breakout cone with an assumed breakout plane of 35° and an assumed embedment depth.

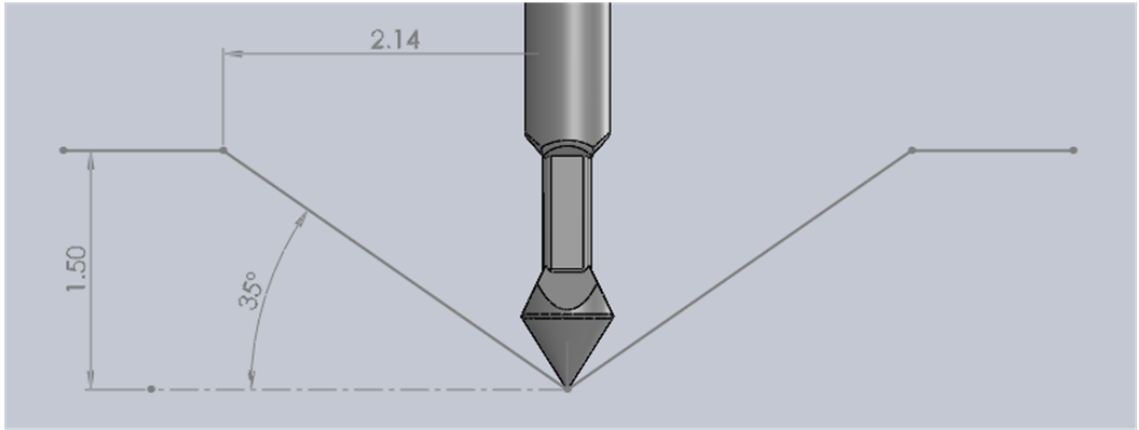


Figure A-17 Determination of HK connector spacing

$$d_{embed} = 0.5(h_{HK} - t_{ins}) = 0.5(6 \text{ in} - 3 \text{ in}) = 1.5 \text{ in}$$

$$s_{HKlat} = 2 \left(\frac{d_{embed}}{\tan(35^\circ)} \right) + t_{HK} = 2 \left(\frac{1.5 \text{ in}}{\tan(35^\circ)} \right) + 0 = 4.3 \text{ in}$$

Where thickness, t_{HK} , is thickness at the embedment tip, which is 0 because it is a point.

$$s_{HKver} = 2 \left(\frac{d_{embed}}{\tan(35^\circ)} \right) + b_{HK} = 2 \left(\frac{1.5 \text{ in}}{\tan(35^\circ)} \right) + 3 \text{ in} = 7.3 \text{ in}$$

This indicates that when placed in parallel, they can be spaced at 4.3 in apart, and when they are placed collinearly, they must be spaced at a minimum of 7.3 inches o.c. Two different configurations shall be tested, as shown in the details of Appendix B

$$N_{nnq} = N_{HKreq} \Phi P_{nHKBreak} = 6(4.58 \text{ kip}) = 27.5 \text{ kip} \geq N_{mn} = 23.1 \text{ kip} \therefore OK$$

Design Compression Struts

Member op

$$w_{op} = \frac{N_{op}}{\Phi f_{ce} b_c} = \frac{34.9 \text{ kip}}{0.75(3.06 \text{ ksi})(10 \text{ in})} = 1.14 \text{ in}$$

Member mp

$$w_{mp} = \frac{N_{mp}}{\Phi f_{ce} b_c} = \frac{17.0 \text{ kip}}{0.75(3.06 \text{ ksi})(10 \text{ in})} = 0.56 \text{ in}$$

Since the foam is not able to withstand this force over such a small area, the compressive material used in this instance must have a height of at least 0.6 in. A high-density polyethylene prism would exhibit low thermal conductivity, is cheap, and does not require any special provisions for concerns regarding absorption and expansions when exposed to moisture like wood does. The compressive strength of HDPE 2" × 4" boards (also known as plastic lumber) is ($f_{HDPE} = 1.287 \text{ ksi}$). Because these are manufactured to typical 2" × 4" specifications, the prisms used will be 3 inches thick, 3.5 inches tall, and 10 inches long. The compressive strength of the prism will therefore be

$$\begin{aligned} \Phi_V f_{HDPE} h_{HDPE} b_{HDPE} &= 0.75(1.28 \text{ ksi})(3.5 \text{ in})(10 \text{ in}) = 33.8 \text{ kip} \geq N_{mp} \\ &= 17.0 \text{ kip} \therefore OK \end{aligned}$$

Member Rp

$$w_{py} = \frac{N_{py}}{\Phi f_{ce} b_c} = \frac{56.6 \text{ kip}}{0.75(3.06 \text{ ksi})(10 \text{ in})} = 1.9 \text{ in} < \text{wythe thickness therefore OK}$$

Shear at Corbel/SWP Interface

The shear to be resisted at this interface will be equal to the applied load. The friction from the interface shall be ignored conservatively. Stirrups shall be used to resist the shear.

$$R_{rebarShear} = 0.6f_u A_{gv}$$

$$A_{gv,req} = \frac{V_u}{\Phi_v 0.6f_u} = \frac{30.5 \text{ kip}}{0.75(0.6)(75 \text{ ksi})} = 0.9 \text{ in}^2$$

$$A_{gv,more} = A_{gv,req} - A_{soq} = 0.9 \text{ in}^2 - 0.6 \text{ in}^2$$

$$= 0.3 \text{ in}^2$$

\therefore use (1)#4 stirrup @ 4" o.c.

$$A_{gv} = 2(0.2 \text{ in}^2) + 0.6 \text{ in}^2 = 1.0 \text{ in}^2 \geq A_{gv,req} \therefore OK$$

Vertical/Longitudinal Reinforcement, A_{sl}

$$\rho = \frac{A_{sl,min}}{A_{gc}} = 0.0012 \quad (\text{ACI 381-14 §14.3.2})$$

$$A_{gcl} = b * (t_{wy0} + t_{wyi}) = 68 \text{ in} * 6 \text{ in} = 408 \text{ in}^2$$

$$A_{sl,min} = \rho A_{gcl} = 0.0012(408 \text{ in}^2) = 0.49 \text{ in}^2$$

$$s_{max} = \min\left(\frac{3t_{SWP}}{18 \text{ in}}\right) = \max\left(\frac{27 \text{ in}}{18 \text{ in}}\right) = 18 \text{ in}$$

$$N_{sl} = \frac{b - 2(0.75 \text{ in})}{s_{max}} = \frac{68 \text{ in} - 2(0.75 \text{ in})}{18 \text{ in}}$$

$$= 3.69 \text{ bars}$$

$$A_{slbarmin} = \frac{A_{sl,min}}{N_{sl}} = \frac{0.49 \text{ in}^2}{4} = 0.12 \text{ in}^2$$

\therefore use (4)#4 bars @ 18" o. c.

Therefore use (4) #4 bars spaced 18" o.c. Place second layer of rebar on compression side for any reversed loading.

Horizontal/Transverse Reinforcement, A_{st}

$$\rho = \frac{A_{st,min}}{A_{gc}} = 0.0020 \quad (\text{ACI 381-14 §14.3.3})$$

$$A_{gct} = h * (t_{wy0} + t_{wyi}) = 102 \text{ in} * 6 \text{ in} = 612 \text{ in}^2$$

$$A_{st,min} = \rho A_{gcl} = 0.002(612 \text{ in}^2) = 1.23 \text{ in}^2$$

$$s_{max} = \min\left(\frac{3t_{SWP}}{18 \text{ in}}\right) = \max\left(\frac{27 \text{ in}}{18 \text{ in}}\right) = 18 \text{ in}$$

$$N_{st} = \frac{h - 2(0.75 \text{ in})}{s_{max}} = \frac{102 \text{ in} - 2(0.75 \text{ in})}{18 \text{ in}} = 5.6 \text{ bars}$$

$$A_{stbarmin} = \frac{A_{st,min}}{N_{st}} = \frac{1.2 \text{ in}^2}{6} = 0.2 \text{ in}^2 \quad \therefore \text{use (6) \#4 bars @ 18" o.c.}$$

Therefore use (6) #4 bars spaced 18" o.c. Place second layer of rebar on opposite side for symmetry.

Lifting

$$x_{lift} = 18 \text{ in} = 1.5 \text{ ft} \quad (\text{anchor to edge distance})$$

$$x_{midL} = h - 2x_{anchor} = 8.5 \text{ ft} - 3 \text{ ft} = 5.5 \text{ ft}$$

$$x_{midT} = b - 2x_{anchor} = 5.67 \text{ ft} - 3 \text{ ft} = 2.67 \text{ ft}$$

Longitudinal Direction

$$w_{sw} = w_c b t = (150 \text{ pcf})(5.67 \text{ ft})(0.5 \text{ ft}) = 425 \frac{\text{lb}}{\text{ft}}$$

$$R_A = \frac{w_{sw} h}{2} = \frac{\left(0.425 \frac{\text{kip}}{\text{ft}}\right)(8.5 \text{ ft})}{2} = 1.8 \text{ kip}$$

$$V_{lift,left} = w_{sw}x_{lift} = \left(0.425 \frac{kip}{ft}\right)(1.5 ft)$$

$$= -0.6375 kip$$

$$V_{lift,right} = w_{sw}x_{lift} + R_A = -0.64 kip + 1.8 kip$$

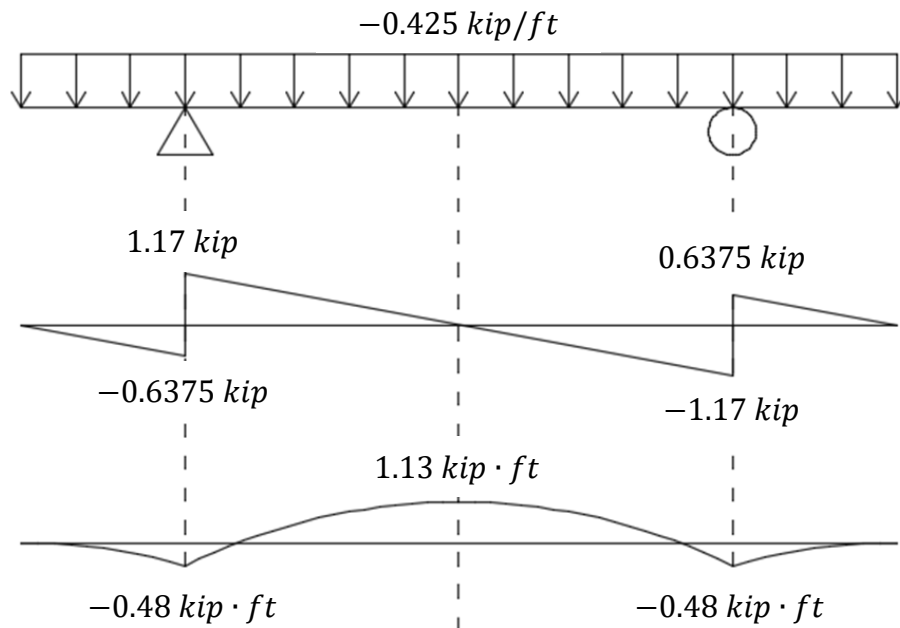
$$= 1.17 kip$$

$$M_{lift} = \frac{V_{lift,left}x_{lift}}{2} = \frac{(-0.64 kip)(1.5 ft)}{2}$$

$$= -0.48 kip \cdot ft$$

$$M_{mid} = M_{lift} + \frac{V_{lift,right}(0.5x_{midL})}{2}$$

$$= -0.48 kip \cdot ft + \frac{0.64 kip(0.5 \cdot 5.5 ft)}{2} = 1.13 kip \cdot ft$$



Cracking moment is equal to

$$M_{cr} = \frac{7.5\sqrt{f'_c}I_g}{0.5t}$$

$$f'_{c,req} = \left(\frac{0.5(t_{wy0} + t_{wyi})M_{mid}}{7.5I_g} \right)^2$$

$$= \left(\frac{0.5(6 \text{ in}) \left(1.13 \text{ kip} \cdot \text{ft} * \frac{12 \text{ in}}{\text{ft}} \right)}{7.5(3978 \text{ in}^4)} \right)^2 = 0.0042 \text{ ksi}$$

Therefore we need to attain at least 0.0042 ksi before lifting.

Transverse Direction

$$w_{sw} = w_c ht = (150 \text{ pcf})(8.5 \text{ ft})(0.5 \text{ ft}) = 638 \frac{\text{lb}}{\text{ft}}$$

$$R_A = \frac{w_{sw}b}{2} = \frac{\left(0.64 \frac{\text{kip}}{\text{ft}} \right) (5.67 \text{ ft})}{2} = 1.8 \text{ kip}$$

$$V_{lift,left} = w_{sw}x_{lift} = \left(0.64 \frac{\text{kip}}{\text{ft}} \right) (1.5 \text{ ft})$$

$$= -0.96 \text{ kip}$$

$$V_{lift,right} = w_{sw}x_{lift} + R_A = -0.96 \text{ kip} + 1.8 \text{ kip}$$

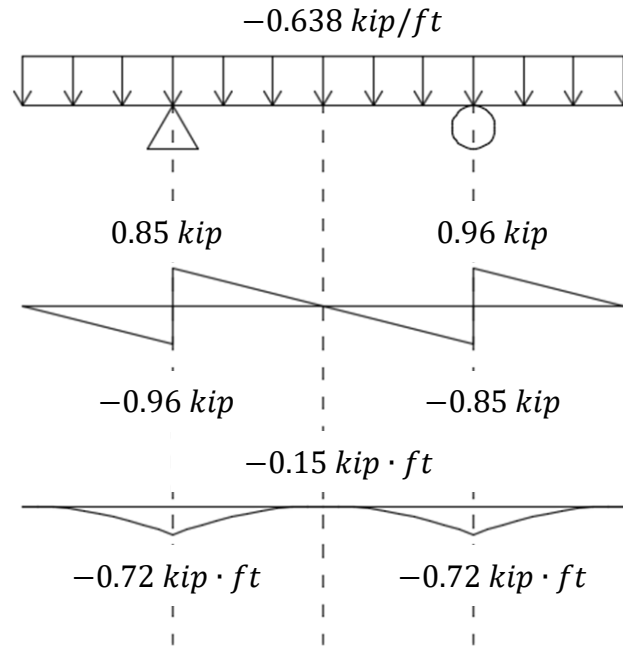
$$= 0.85 \text{ kip}$$

$$M_{lift} = \frac{V_{lift,left}x_{lift}}{2} = \frac{(-0.96 \text{ kip})(1.5 \text{ ft})}{2}$$

$$= -0.72 \text{ kip} \cdot \text{ft}$$

$$M_{mid} = M_{lift} + \frac{V_{lift,right}(0.5x_{midT})}{2}$$

$$= -0.72 \text{ kip} \cdot \text{ft} + \frac{0.85 \text{ kip}(0.5*2.67 \text{ ft})}{2} = -0.15 \text{ kip} \cdot \text{ft}$$



Cracking moment is equal to

$$M_{cr} = \frac{7.5\sqrt{f'_c}I_g}{0.5t}$$

$$f'_{c,req} = \left(\frac{0.5(t_{wyo} + t_{wyi})M_{lift}}{7.5I_{gSWP}} \right)^2$$

$$= \left(\frac{0.5(6 \text{ in}) \left(0.72 \text{ kip} \cdot \text{ft} * \frac{12 \text{ in}}{\text{ft}} \right)}{7.5(3978 \text{ in}^4)} \right)^2 = 0.0017 \text{ ksi}$$

Therefore we need to attain at least 0.0017 ksi before lifting to avoid cracking the panel.

Since the concrete lifting anchor strengths are based on a concrete strength of 3.5 ksi,

however, the panels may not be lifted until $f'_c = 3.5 \text{ ksi}$.

$$f'_{c,req} = \max \begin{pmatrix} f'_{c,reqL} \\ f'_{c,reqT} \\ f'_{c,reqA} \end{pmatrix} = \max \begin{pmatrix} 0.0042 \text{ ksi} \\ 0.0017 \text{ ksi} \\ 3.5 \text{ ksi} \end{pmatrix} = 3.5 \text{ ksi}$$

IconGFRP Calculations

The IconG specimen used the Strut-and-Tie method for design.

Material Properties

<u>Concrete</u>	<u>Steel</u>	<u>FRP</u>
$f'_c = 8.0 \text{ ksi}$	$f_y = 60 \text{ ksi}$	$t_{Icon} = 0.5 \text{ in}$
$f_r = 7.5\sqrt{f'_c} = 0.671 \text{ ksi}$	$f_u = 75 \text{ ksi}$	$b_{Icon} = 7 \text{ in}$
$w_c = 150 \text{ lb/ft}$	$E_s = 29000 \text{ ksi}$	$h_{Icon} = 8 \text{ in}$
$E_c = 33w_c^{1.5}\sqrt{f'_c} = 5422 \text{ ksi}$		
$n_s = \frac{E_s}{E_c} = 5.348$		

Geometrical Dimensions

<u>SWP</u>	<u>Corbel</u>
$t_{wyo} = t_{wyi} = t_{ins} = 3 \text{ in}$	$h_c = 14 \text{ in}$
$t_{SWP} = t_{wyo} + t_{wyi} + t_{ins} = 9 \text{ in}$	$d = 12 \text{ in}$
$b = 68 \text{ in} = 5.67 \text{ ft}$	$b_c = 10 \text{ in}$
$h = 102 \text{ in} = 8.5 \text{ ft}$	$l_p = 8 \text{ in}$
$d_{hout} = 7.5 \text{ in}$	$h_{cf} = 10 \text{ in}$
$d_{hin} = 1.5 \text{ in}$	$c_c = 1.5 \text{ in}$
$I_{gSWP} = \frac{bt_{SWP}^3}{12} - \frac{bt_{ins}^3}{12}$	$I_{gc} = \frac{b_ch_c^3}{12} = \frac{10 \text{ in}(14 \text{ in})^3}{12} = 2287 \text{ in}^4$
$= \frac{68 \text{ in}(9 \text{ in})^3}{12} - \frac{68 \text{ in}(3 \text{ in})^3}{12} = 3978 \text{ in}^4$	$z_c = 42 \text{ in}$ (from top SWP to corbel)

Plate Size

$$V_u = \Phi P_{nb} = \Phi 0.85 f'_c A_1 \quad (\text{ACI 318-14 §22.8.3.2})$$

$$\Phi_{\text{bear}} = 0.65 \quad (\text{ACI 318-14 §21.2.1})$$

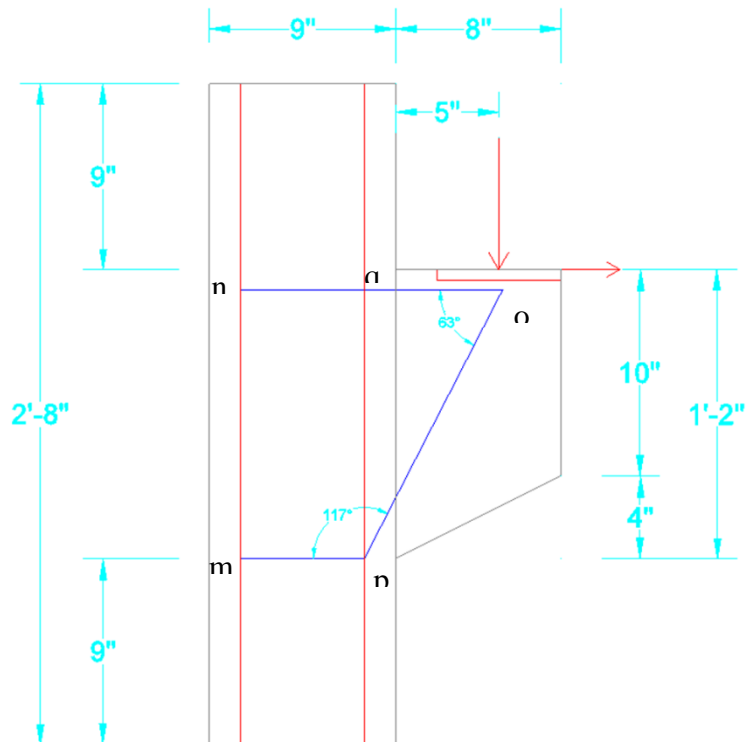
$$A_1 = \frac{V_u}{\Phi_{\text{bear}} 0.85 f'_c} = \frac{30.5 \text{ kip}}{0.65(0.85)(8 \text{ ksi})} = 6.9 \text{ in}^2$$

$$L_{\text{bear}, \text{min}} = \frac{A_1}{b_c} = 0.69 \text{ in}$$

Therefore use at least 1 in \times 10 in plate.

Shear Span, a_v

Assume $a_v = 5 \text{ in}$.

Determine Truss Geometry

$$l_{no} = d_{hout} + a_v + (1 \text{ in}) \tan \theta_R$$

$$= 7.5 \text{ in} + 5 \text{ in} + (1 \text{ in}) \tan(11.31^\circ) = 12.7 \text{ in}$$

$$\theta_{nop} = \text{atan}\left(\frac{d}{l_{no} - (d_{hout} - d_{hin})}\right)$$

$$= \text{atan}\left(\frac{12 \text{ in}}{12.7 \text{ in} - (7.5 \text{ in} - 1.5 \text{ in})}\right) = 60.82^\circ$$

$$l_{mn} = d = 12 \text{ in}$$

$$l_{mp} = d_{hout} - d_{hin} = 7.5 \text{ in} - 1.5 \text{ in} = 6 \text{ in}$$

$$\theta_{pno} = \text{atan}\left(\frac{d}{l_{mp}}\right) = \text{atan}\left(\frac{12}{6}\right) = 63.44^\circ$$

$$\theta_{npo} = 180^\circ - \theta_{pno} - \theta_{nop}$$

$$= 180^\circ - 63.44^\circ - 60.82^\circ$$

$$= 55.74^\circ$$

$$\theta_{mpn} = \theta_{pno} = 63.44^\circ$$

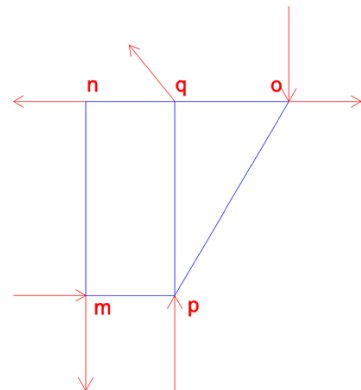
Determine Forces in Truss Components

$$\Sigma M_m = V_u l_{no} + N_{uc} l_{mn} - R_{py} l_{mp} - R_{nx} l_{mn} = 0$$

$$R_{py} = \frac{V_u l_{no} + N_{uc} l_{mn}}{l_{mp}} - R_{nx} \frac{l_{mn}}{l_{mp}}$$

$$\Sigma F_y = R_{py} + R_{ny} - R_{my} - V_u = 0$$

$$\Sigma F_x = N_{uc} - R_{mx} - R_{nx} = 0$$



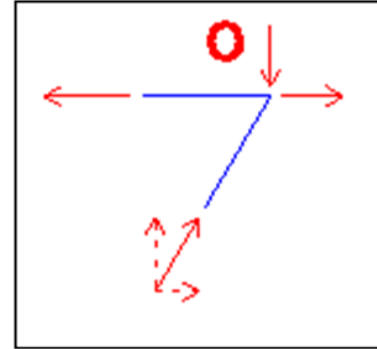
$$N_{opy} = V_u = 30.5 \text{ kip}$$

$$N_{opx} = \frac{N_{opy}}{\tan(\theta_{nop})} = \frac{30.5 \text{ kip}}{\tan(60.82^\circ)} = 17.0 \text{ kip}$$

$$\begin{aligned} N_{op} &= \sqrt{N_{opx}^2 + N_{opy}^2} \\ &= \sqrt{(17.0 \text{ kip})^2 + (30.5 \text{ kip})^2} \\ &= 34.9 \text{ kip (C)} \end{aligned}$$

$$\begin{aligned} N_{oq} &= N_{opx} + N_{uc} = 17.0 \text{ kip} + 6.1 \text{ kip} \\ &= 23.1 \text{ kip (T)} \end{aligned}$$

$$N_{nq} = N_{oq} = 23.1 \text{ kip (T)}$$



$$R_{nx} = N_{oq} = 23.1 \text{ kip}$$

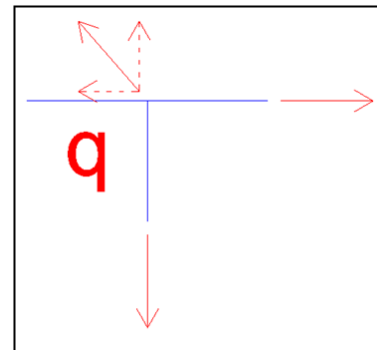
$$\Sigma F_x = N_{uc} + R_{mx} - R_{nx} = 0$$

$$R_{mx} = R_{nx} - N_{uc} = 17.02 \text{ kip (T)}$$

Assume bend acts similar to a pulley

$$N_{pq} = N_{oq} = 23.1 \text{ kip (T)}$$

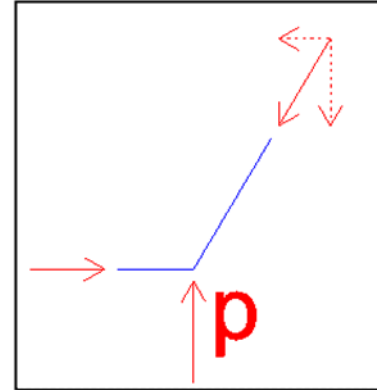
$$R_q = \sqrt{2 * N_{oq}^2} = \sqrt{2 * (23.1 \text{ kip})^2} = 32.7 \text{ kip}$$



$$N_{mp} = N_{opx} = 17.02 \text{ kip (C)}$$

$$\begin{aligned} R_{py} &= \frac{V_u l_{no} + N_{uc} l_{mn}}{l_{mp}} - R_{nx} \frac{l_{mn}}{l_{mp}} \\ &= \frac{30.5 \text{ kip}(12.7 \text{ in}) + (6.1 \text{ kip})(12 \text{ in})}{6 \text{ in}} - (23.1 \text{ kip}) \frac{12}{6} \\ &= 30.5 \text{ kip} \end{aligned}$$

$$N_{mp} - R_{mx} = 17.0 \text{ kip} - 17.0 \text{ kip} = 0 \therefore OK$$



$$M_{applied} = V_u(a_v + \frac{t_{SWP}}{2}) + N_{uc}(h_c - d)$$

$$= (30.5 \text{ kip}) \left(5 \text{ in} + \frac{9 \text{ in}}{2} \right) + (6.1 \text{ kip})(14 \text{ in} - 12 \text{ in})$$

$$= 25.146 \text{ kip} \cdot \text{ft}$$

$$M_{uAbove} = \frac{M_{applied}}{h} \left(z_c + \frac{h_c}{2} \right)$$

$$= \frac{25.15 \text{ kip} \cdot \text{ft}}{8.5 \text{ ft}} \left(42 \text{ in} + \frac{14 \text{ in}}{2} \right) = 12.1 \text{ kip} \cdot \text{ft}$$

$$M_{uBelow} = M_{applied} - M_{uAbove}$$

$$= 25.15 \text{ kip} \cdot \text{ft} - 12.1 \text{ kip} \cdot \text{ft} = 13.1 \text{ kip} \cdot \text{ft}$$

$$M_u = C(d_{hout} - d_{hin})$$

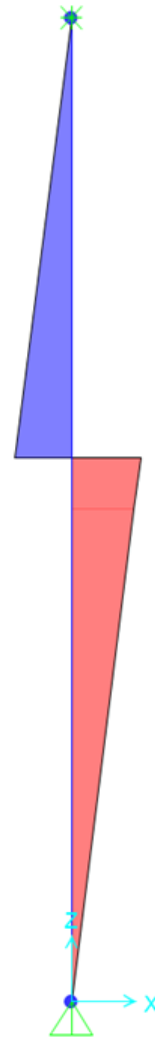
Compression will be greatest below corbel in the inside wythe. To simplify design, both wythes are to be detailed symmetrically. Therefore, let $C = P_{wyin}$.

$$M_u = \max \left(\begin{matrix} M_{uAbove} \\ M_{uBelow} \end{matrix} \right) = 13.1 \text{ kip} \cdot \text{ft}$$

$$P_{wyin} = \frac{M_u}{d_{hout} - d_{hin}} = \frac{13.1 \text{ kip} \cdot \text{ft}}{7.5 \text{ in} - 1.5 \text{ in}} = 26.1 \text{ kip (C)}$$

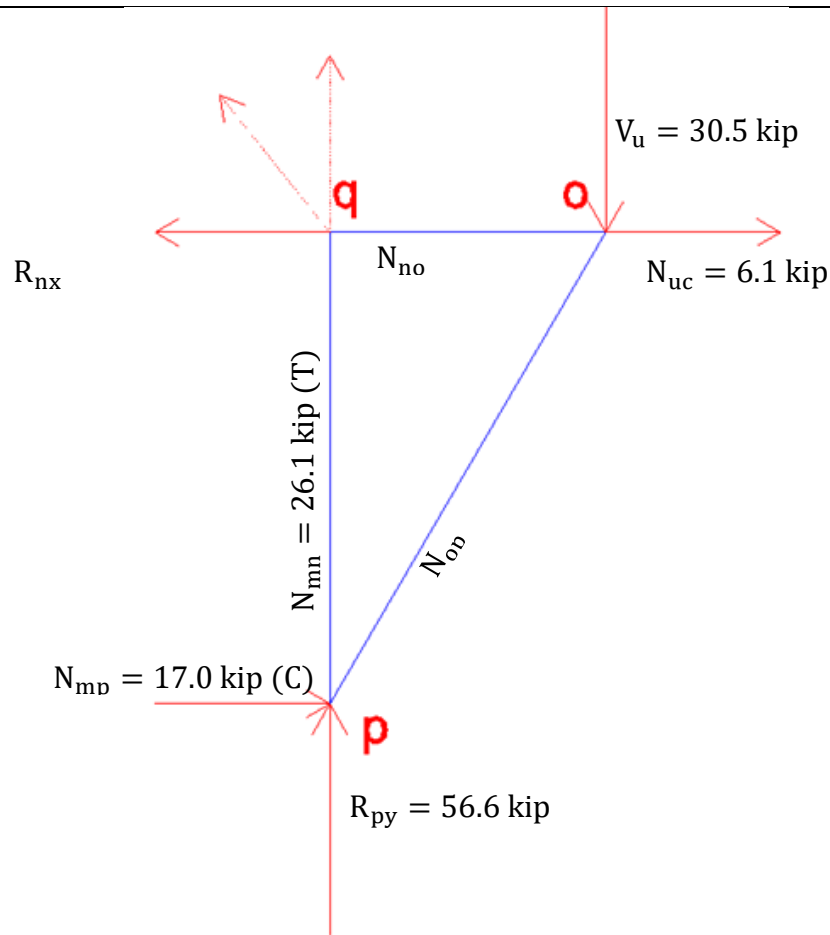
$$P_{wyout} = P_{wyin} = 26.1 \text{ kip (T)}$$

$$N_{pq} = P_{wyin} = 26.1 \text{ kip}$$



$$N_{mn} = P_{wyout} = 26.1 \text{ kip}$$

$$N_{py} = R_{py} + N_{pq} = 56.6 \text{ kip}$$



Select Strut, Tie, and Nodal Zone Dimensions

The most conservative β value for any relevant component will govern.

Nodes

Struts

$$\beta_{Nm} = 0.60 \quad (\text{C-T-T})$$

$$\beta_{S_{py}} = 1.0$$

$$\beta_{Nm} = 0.60 \quad (\text{C-T-T})$$

$$\beta_{S_{np}} = 0.6$$

$$\beta_{Nm} = 0.80 \quad (\text{C-C-T})$$

$$\beta_{S_{op}} = 0.6$$

$$\beta_{Nm} = 0.80 \quad (\text{C-C-T})$$

A bottle-shaped strut could develop in the concrete, so 0.75 will be used if reinforced properly. Otherwise, 0.6 must be used. Will assume inadequate reinforcement ($\beta=0.6$).

Because all components are affected by an element with a limiting value of 0.6, design must use $\beta = 0.6$ for all members.

$$\beta_s = 0.6$$

$$f_{ce} = 0.85\beta_s f'_c = 0.85(0.6)(8.0 \text{ ksi}) = 4.08 \text{ ksi}$$

$$\Phi f_{ce} = 0.75(4.08 \text{ ksi}) = 3.06 \text{ ksi}$$

Design Tension Ties

Member *mn*

$$w_{mn} = \frac{N_{mn}}{\Phi f_{ce} b_c} = \frac{26.1 \text{ kip}}{0.75(3.06 \text{ ksi})(10 \text{ in})} = 0.85 \text{ in} < \text{wythe thickness, } \therefore \text{OK}$$

$$A_{sreq,mn} = \frac{N_{mn}}{\Phi f_y} = \frac{26.1 \text{ kip}}{0.75(60 \text{ ksi})} = 0.58 \text{ in}^2 \quad \text{Therefore use (3) \#4 at 3" o.c.}$$

$$A_{smn} = 3(0.2 \text{ in}^2) = 0.6 \text{ in}^2$$

$$N_{nmn} = \Phi A_{smn} f_y = 0.75(0.6 \text{ in}^2)(60 \text{ ksi}) = 27 \text{ kip} \geq N_{mn} = 26.1 \text{ kip} \therefore \text{OK}$$

Anchorage Requirements

$$l_{dmp} = \left(\frac{3}{40} * \frac{f_y}{\lambda \sqrt{f'_c}} * \frac{\Psi_t \Psi_e \Psi_s}{\frac{(c_b + K_{tr})}{d_b}} \right) d_b \quad (\text{ACI 318-14 §25.4.2.3})$$

If clear cover of $1.0d_b$ and a minimum clear spacing of $2d_b$ exists, the simplified version may be used:

$$l_{dmp} = \left(\frac{f_y \Psi_t \Psi_e}{25 \lambda \sqrt{f'_c}} \right) d_b \quad (\text{ACI 318-14 §25.4.2.2})$$

$$\Psi_t = 1 \quad (\text{because not horizontal reinforcement})$$

$$\Psi_e = 1 \quad (\text{because using uncoated, regular rebar})$$

$$\lambda = 1 \quad (\text{because normalweight concrete})$$

$$d_b = 0.5 \text{ in}$$

$$l_{dmp} = \left(\frac{(60 \text{ ksi})(1)(1)}{25(1)\sqrt{8000 \text{ psi}} \left(1 \frac{\text{ksi}}{1000 \text{ psi}}\right)} \right) (0.5 \text{ in}) = 13.4 \text{ in}$$

Therefore 16 in. of rebar must be extended on each side of the corbel for a total of 46 in.

Member oq

$$w_{oq} = \frac{N_{oq}}{\Phi f_{ce} b_c} = \frac{23.1 \text{ kip}}{0.75(3.06 \text{ ksi})(10 \text{ in})} = 0.76 \text{ in}$$

$$A_{sreq,oq} = \frac{N_{oq}}{\Phi f_y} = \frac{23.1 \text{ kip}}{0.75(60 \text{ ksi})} = 0.52 \text{ in}^2 \quad \text{Therefore use (3) \#4 at 3" o.c.}$$

$$A_{soq} = 3(0.2 \text{ in}^2) = 0.8 \text{ in}^2$$

$$N_{noq} = \Phi A_{soq} f_y = 0.75(0.6 \text{ in}^2)(60 \text{ ksi}) = 27 \text{ kip} \geq N_{oq} = 23.1 \text{ kip} \therefore OK$$

Anchorage Requirements

$$l_{dmp} = \left(\frac{f_y \Psi_e \Psi_c \Psi_r}{50 \lambda \sqrt{f'_c}} \right) d_b \quad (\text{ACI 318-14 §25.4.3.1})$$

$$\Psi_e = 1 \quad (\text{because using uncoated, regular rebar})$$

$$\psi_c = 1 \quad (\text{because cover not } \geq 2.5 \text{ in})$$

$$\psi_r = 1 \quad (\text{because not enclosed})$$

$$\lambda = 1 \quad (\text{because normalweight concrete})$$

$$d_b = 0.5 \text{ in}$$

$$l_{dh} = \left(\frac{1(1)(1)(60 \text{ ksi})}{50 \lambda \sqrt{8000 \text{ psi}} \left(1 \frac{\text{ksi}}{1000 \text{ psi}}\right)} \right) (0.5 \text{ in}) = 6.7 \text{ in}$$

$$l_{dh} = \max \left(\frac{l_{dh}}{8d_b}, \frac{l_{dh}}{6 \text{ in}} \right) = 6.7 \text{ in}$$

Therefore need 7 inches of rebar beyond bend for principle reinforcement:

$$l_{out} = l_{dh} + (3d_b + d_b) = 8.7 \text{ in} \quad (\text{ACI 318-11 §12.5.1})$$

Will specify principle reinforcement to extend 12 inches from top of the bend. Anchor bar shall be welded to the end of the principle reinforcement to attain development on corbel tip.

Member nq

No need to check tie width because this member will penetrate insulation (i.e. no concrete). According to IconX shear testing performed previously, the Icon connectors typically failed in the connector itself, so there was no data regarding concrete breakout as it does not govern failure of the connector. There is no data regarding the tensile capacity of the IconX connectors currently. It was assumed that the tension capacity would be similar to the shear capacity however, due to the “X” shape of the connector.

$$\Phi P_{nIconGTens} = 8.85 \text{ kip}$$

$$\Phi P_{nIconGSus} = 0.2 \Phi P_{nIconGTens} = 0.2(8.85 \text{ kip}) = 1.77 \text{ kip}$$

Therefore creep will govern.

$$N_{IconGreq} = \frac{N_{nq} \left(\frac{V_{sus}}{V_u} \right)}{\Phi P_{nIconGSus}} = \frac{23.1 \text{ kip} \left(\frac{16.46}{30.5} \right)}{1.77 \text{ kip}} = 7.04$$

\therefore must use 8 IconX GFRP connectors

Because the ties will be used for localized force transfer, and because concrete breakout governs. The spacing will be based upon concrete breakout cone with an assumed breakout plane of 35° and an assumed embedment depth.

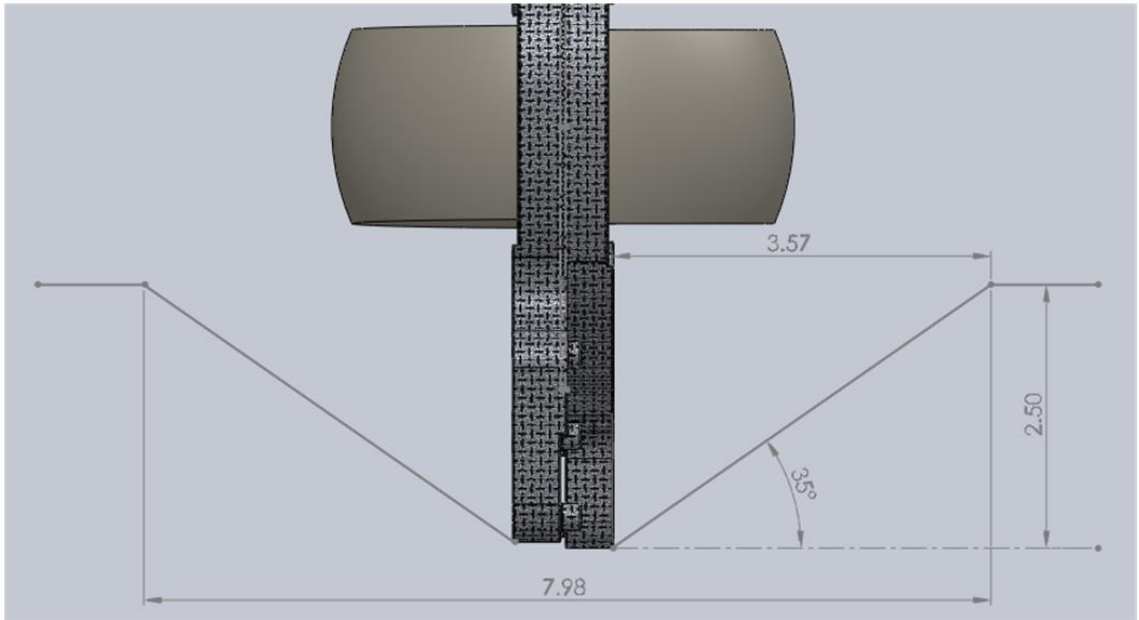


Figure A-18 Determination of IconX connector spacing

$$d_{embed} = 0.5(h_{Icon} - t_{ins}) = 0.5(8 \text{ in} - 3 \text{ in}) = 2.5 \text{ in}$$

$$s_{Iconlat} = 2 \left(\frac{d_{embed}}{\tan(35^\circ)} \right) + t_{Icon} = 2 \left(\frac{2.5 \text{ in}}{\tan(35^\circ)} \right) + 0.5 \text{ in} = 7.6 \text{ in}$$

$$s_{Iconver} = 2 \left(\frac{d_{embed}}{\tan(35^\circ)} \right) + b_{Icon} = 2 \left(\frac{2.5 \text{ in}}{\tan(35^\circ)} \right) + 7 \text{ in} = 14.1 \text{ in}$$

This indicates that when placed in parallel, they can be spaced at 8-in apart, and when they are placed collinearly, they must be spaced at a minimum of 14.5-in o.c. Eight IconX GFRP connectors spaced at 8" o.c. in two rows spaced 14.5" o.c. shall be used.

$$N_{nnq} = N_{IconGreq} \Phi P_{nIconGTens} = 8(8.85 \text{ kip}) = 70.8 \text{ kip} \geq N_{mn} = 23.1 \text{ kip} \therefore OK$$

Design Compression Struts

Member op

$$w_{op} = \frac{N_{op}}{\Phi f_{ce} b_c} = \frac{34.9 \text{ kip}}{0.75(3.06 \text{ ksi})(10 \text{ in})} = 1.14 \text{ in}$$

Member mp

$$w_{mp} = \frac{N_{mp}}{\Phi f_{ce} b_c} = \frac{17.0 \text{ kip}}{0.75(3.06 \text{ ksi})(10 \text{ in})} = 0.56 \text{ in}$$

Since the foam is not able to withstand this force over such a small area, the compressive material used in this instance must have a height of at least 0.6 in. A high-density polyethylene prism would exhibit low thermal conductivity, is cheap, and does not require any special provisions for concerns regarding absorption and expansions when exposed to moisture like wood does. The compressive strength of HDPE 2" × 4" boards (also known as plastic lumber) is ($f_{HDPE} = 1.287 \text{ ksi}$). Because these are manufactured to typical 2" × 4" specifications, the prisms used will be 3 inches thick, 3.5 inches tall, and 10 inches long. The compressive strength of the prism will therefore be

$$\begin{aligned} \Phi_V f_{HDPE} h_{HDPE} b_{HDPE} &= 0.75(1.28 \text{ ksi})(3.5 \text{ in})(10 \text{ in}) = 33.8 \text{ kip} \geq N_{mp} \\ &= 17.0 \text{ kip} \therefore OK \end{aligned}$$

Member Rp

$$w_{py} = \frac{N_{py}}{\Phi f_{ce} b_c} = \frac{56.6 \text{ kip}}{0.75(3.06 \text{ ksi})(10 \text{ in})} = 1.9 \text{ in} < \text{wythe thickness therefore OK}$$

Shear at Corbel/SWP Interface

The shear to be resisted at this interface will be equal to the applied load. The friction from the interface shall be ignored conservatively. Stirrups shall be used to resist the shear.

$$R_{rebarShear} = 0.6f_u A_{gv}$$

$$A_{gv,req} = \frac{V_u}{\Phi_v 0.6f_u} = \frac{30.5 \text{ kip}}{0.75(0.6)(75 \text{ ksi})} = 0.9 \text{ in}^2$$

$$A_{gv,more} = A_{gv,req} - A_{soq} = 0.9 \text{ in}^2 - 0.6 \text{ in}^2 = 0.3 \text{ in}^2 \quad \therefore \text{use (1)\#4 stirrup@4" o.c.}$$

$$A_{gv} = 2(0.2 \text{ in}^2) + 0.6 \text{ in}^2 = 1.0 \text{ in}^2 \geq A_{gv,req} \therefore OK$$

Vertical/Longitudinal Reinforcement, A_{sl}

$$\rho = \frac{A_{sl,min}}{A_{gc}} = 0.0012 \quad (\text{ACI 381-14 §14.3.2})$$

$$A_{gcl} = b * (t_{wyo} + t_{wyi}) = 68 \text{ in} * 6 \text{ in} = 408 \text{ in}^2$$

$$A_{sl,min} = \rho A_{gcl} = 0.0012(408 \text{ in}^2) = 0.49 \text{ in}^2$$

$$s_{max} = \min \left(\frac{3t_{SWP}}{18 \text{ in}} \right) = \max \left(\frac{27 \text{ in}}{18 \text{ in}} \right) = 18 \text{ in}$$

$$N_{sl} = \frac{b - 2(0.75 \text{ in})}{s_{max}} = \frac{68 \text{ in} - 2(0.75 \text{ in})}{18 \text{ in}} = 3.69 \text{ bars}$$

$$A_{slbarmin} = \frac{A_{sl,min}}{N_{sl}} = \frac{0.49 \text{ in}^2}{4} = 0.12 \text{ in}^2 \quad \therefore \text{use (4)\#4 bars @ 18" o.c.}$$

Therefore use (4) #4 bars spaced 18" o.c. Place second layer of rebar on compression side for any reversed loading.

Horizontal/Transverse Reinforcement, A_{st}

$$\rho = \frac{A_{st,min}}{A_{gc}} = 0.0020 \quad (\text{ACI 381-14 §14.3.3})$$

$$A_{gct} = h * (t_{wy0} + t_{wyi}) = 102 \text{ in} * 6 \text{ in} = 612 \text{ in}^2$$

$$A_{st,min} = \rho A_{gcl} = 0.002(612 \text{ in}^2) = 1.23 \text{ in}^2$$

$$s_{max} = \min \left(\frac{3t_{SWP}}{18 \text{ in}} \right) = \max \left(\frac{27 \text{ in}}{18 \text{ in}} \right) = 18 \text{ in}$$

$$N_{st} = \frac{h - 2(0.75 \text{ in})}{s_{max}} = \frac{102 \text{ in} - 2(0.75 \text{ in})}{18 \text{ in}} = 5.6 \text{ bars}$$

$$A_{stbarmin} = \frac{A_{st,min}}{N_{st}} = \frac{1.2 \text{ in}^2}{6} = 0.2 \text{ in}^2 \quad \therefore \text{use (6)\#4 bars @ 18" o.c.}$$

Therefore use (6) #4 bars spaced 18" o.c. Place second layer of rebar on opposite side for symmetry.

Lifting

$$x_{lift} = 18 \text{ in} = 1.5 \text{ ft} \quad (\text{anchor to edge distance})$$

$$x_{midL} = h - 2x_{anchor} = 8.5 \text{ ft} - 3 \text{ ft} = 5.5 \text{ ft}$$

$$x_{midT} = b - 2x_{anchor} = 5.67 \text{ ft} - 3 \text{ ft} = 2.67 \text{ ft}$$

Longitudinal Direction

$$w_{sw} = w_c b t = (150 \text{ pcf})(5.67 \text{ ft})(0.5 \text{ ft}) = 425 \frac{\text{lb}}{\text{ft}}$$

$$R_A = \frac{w_{sw} h}{2} = \frac{\left(0.425 \frac{\text{kip}}{\text{ft}}\right)(8.5 \text{ ft})}{2} = 1.8 \text{ kip}$$

$$V_{lift,left} = w_{sw} x_{lift} = \left(0.425 \frac{\text{kip}}{\text{ft}}\right)(1.5 \text{ ft})$$

$$= -0.6375 \text{ kip}$$

$$V_{lift,right} = w_{sw}x_{lift} + R_A = -0.64 \text{ kip} + 1.8 \text{ kip}$$

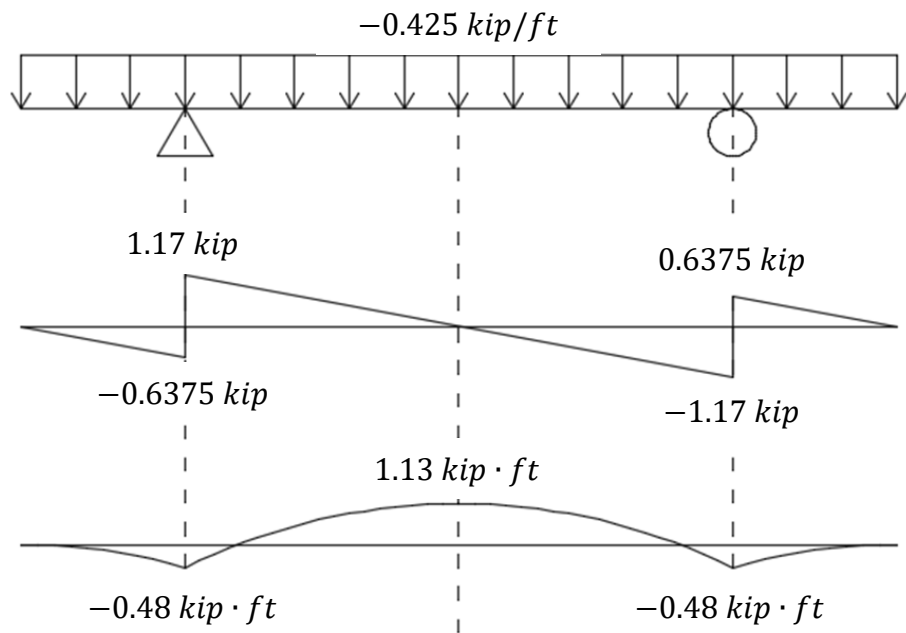
$$= 1.17 \text{ kip}$$

$$M_{lift} = \frac{V_{lift,left}x_{lift}}{2} = \frac{(-0.64 \text{ kip})(1.5 \text{ ft})}{2}$$

$$= -0.48 \text{ kip} \cdot \text{ft}$$

$$M_{mid} = M_{lift} + \frac{V_{lift,right}(0.5x_{midL})}{2}$$

$$= -0.48 \text{ kip} \cdot \text{ft} + \frac{0.64 \text{ kip}(0.5 \cdot 5.5 \text{ ft})}{2} = 1.13 \text{ kip} \cdot \text{ft}$$



Cracking moment is equal to

$$M_{cr} = \frac{7.5\sqrt{f'_c}I_g}{0.5t}$$

$$f'_{c,req} = \left(\frac{0.5(t_{wy0} + t_{wyi})M_{mid}}{7.5I_g} \right)^2$$

$$= \left(\frac{0.5(6 \text{ in}) \left(1.13 \text{ kip} \cdot \text{ft} * \frac{12 \text{ in}}{\text{ft}} \right)}{7.5(3978 \text{ in}^4)} \right)^2 = 0.0042 \text{ ksi}$$

Therefore we need to attain at least 0.0042 ksi before lifting.

Transverse Direction

$$w_{sw} = w_c h t = (150 \text{ pcf})(8.5 \text{ ft})(0.5 \text{ ft}) = 638 \frac{\text{lb}}{\text{ft}}$$

$$R_A = \frac{w_{sw}b}{2} = \frac{\left(0.64 \frac{\text{kip}}{\text{ft}}\right)(5.67 \text{ ft})}{2} = 1.8 \text{ kip}$$

$$V_{lift,left} = w_{sw}x_{lift} = \left(0.64 \frac{\text{kip}}{\text{ft}}\right)(1.5 \text{ ft})$$

$$= -0.96 \text{ kip}$$

$$V_{lift,right} = w_{sw}x_{lift} + R_A = -0.96 \text{ kip} + 1.8 \text{ kip}$$

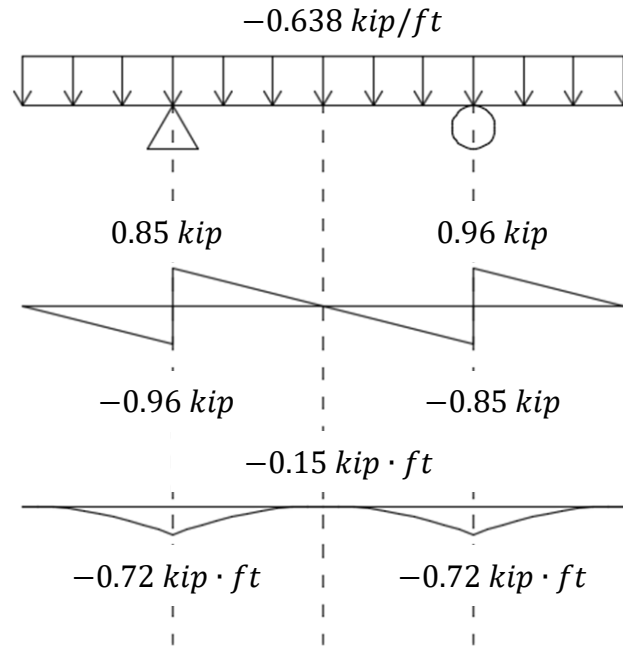
$$= 0.85 \text{ kip}$$

$$M_{lift} = \frac{V_{lift,left}x_{lift}}{2} = \frac{(-0.96 \text{ kip})(1.5 \text{ ft})}{2}$$

$$= -0.72 \text{ kip} \cdot \text{ft}$$

$$M_{mid} = M_{lift} + \frac{V_{lift,right}(0.5x_{midT})}{2}$$

$$= -0.72 \text{ kip} \cdot \text{ft} + \frac{0.85 \text{ kip}(0.5*2.67 \text{ ft})}{2} = -0.15 \text{ kip} \cdot \text{ft}$$



Cracking moment is equal to

$$M_{cr} = \frac{7.5\sqrt{f'_c}I_g}{0.5t}$$

$$f'_{c,req} = \left(\frac{0.5(t_{wy0} + t_{wyi})M_{lift}}{7.5I_{gSWP}} \right)^2$$

$$= \left(\frac{0.5(6 \text{ in}) \left(0.72 \text{ kip} \cdot \text{ft} * \frac{12 \text{ in}}{\text{ft}} \right)}{7.5(3978 \text{ in}^4)} \right)^2 = 0.0017 \text{ ksi}$$

Therefore we need to attain at least 0.0017 ksi before lifting to avoid cracking the panel.

Since the concrete lifting anchor strengths are based on a concrete strength of 3.5 ksi,

however, the panels may not be lifted until $f'_c = 3.5 \text{ ksi}$.

$$f'_{c,req} = \max \begin{pmatrix} f'_{c,reqL} \\ f'_{c,reqT} \\ f'_{c,reqA} \end{pmatrix} = \max \begin{pmatrix} 0.0042 \text{ ksi} \\ 0.0017 \text{ ksi} \\ 3.5 \text{ ksi} \end{pmatrix} = 3.5 \text{ ksi}$$

IconC and IconCHat Calculations

The IconC and IconCHat specimens used the same design calculations, with the difference between the two specimens being the detailing and bending of the rebar reinforcement in the corbel. Both used the Strut-and-Tie method for design.

Material Properties

<u>Concrete</u>	<u>Steel</u>	<u>FRP</u>
$f'_c = 8.0 \text{ ksi}$	$f_y = 60 \text{ ksi}$	$t_{Icon} = 0.5 \text{ in}$
$f_r = 7.5\sqrt{f'_c} = 0.671 \text{ ksi}$	$f_u = 75 \text{ ksi}$	$b_{Icon} = 7 \text{ in}$
$w_c = 150 \text{ lbf/ft}$	$E_s = 29000 \text{ ksi}$	$h_{Icon} = 8 \text{ in}$
$E_c = 33w_c^{1.5}\sqrt{f'_c} = 5422 \text{ ksi}$		
$n_s = \frac{E_s}{E_c} = 5.348$		

Geometrical Dimensions

<u>SWP</u>	<u>Corbel</u>
$t_{wy0} = t_{wyi} = t_{ins} = 3 \text{ in}$	$h_c = 14 \text{ in}$
$t_{SWP} = t_{wy0} + t_{wyi} + t_{ins} = 9 \text{ in}$	$d = 12 \text{ in}$
$b = 68 \text{ in} = 5.67 \text{ ft}$	$b_c = 10 \text{ in}$
$h = 102 \text{ in} = 8.5 \text{ ft}$	$l_p = 8 \text{ in}$
$d_{hout} = 7.5 \text{ in}$	$h_{cf} = 10 \text{ in}$
$d_{hin} = 1.5 \text{ in}$	$c_c = 1.5 \text{ in}$
$I_{gSWP} = \frac{bt_{SWP}^3}{12} - \frac{bt_{ins}^3}{12}$	$I_{gc} = \frac{b_c h_c^3}{12} = \frac{10 \text{ in}(14 \text{ in})^3}{12} = 2287 \text{ in}^4$
$= \frac{68 \text{ in}(9 \text{ in})^3}{12} - \frac{68 \text{ in}(3 \text{ in})^3}{12} = 3978 \text{ in}^4$	$z_c = 42 \text{ in}$ (from top SWP to corbel)

$$l_{no} = d_{hout} + a_v + (1 \text{ in}) \tan \theta_R$$

$$= 7.5 \text{ in} + 5 \text{ in} + (1 \text{ in}) \tan(11.31^\circ) = 12.7 \text{ in}$$

$$\theta_{nop} = \text{atan}\left(\frac{d}{l_{no} - (d_{hout} - d_{hin})}\right)$$

$$= \text{atan}\left(\frac{12 \text{ in}}{12.7 \text{ in} - (7.5 \text{ in} - 1.5 \text{ in})}\right) = 60.82^\circ$$

$$l_{mn} = d = 12 \text{ in}$$

$$l_{mp} = d_{hout} - d_{hin} = 7.5 \text{ in} - 1.5 \text{ in} = 6 \text{ in}$$

$$\theta_{pno} = \text{atan}\left(\frac{d}{l_{mp}}\right) = \text{atan}\left(\frac{12}{6}\right) = 63.44^\circ$$

$$\theta_{npo} = 180^\circ - \theta_{pno} - \theta_{nop} = 180^\circ - 63.44^\circ - 60.82^\circ$$

$$= 55.74^\circ$$

$$\theta_{mpn} = \theta_{pno} = 63.44^\circ$$

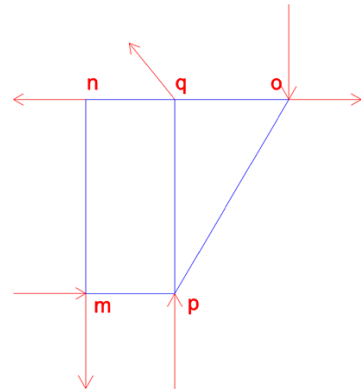
Determine Forces in Truss Components

$$\Sigma M_m = V_u l_{no} + N_{uc} l_{mn} - R_{py} l_{mp} - R_{nx} l_{mn} = 0$$

$$R_{py} = \frac{V_u l_{no} + N_{uc} l_{mn}}{l_{mp}} - R_{nx} \frac{l_{mn}}{l_{mp}}$$

$$\Sigma F_y = R_{py} + R_{ny} - R_{my} - V_u = 0$$

$$\Sigma F_x = N_{uc} - R_{mx} - R_{nx} = 0$$



$$N_{opy} = V_u = 30.5 \text{ kip}$$

$$N_{opx} = \frac{N_{opy}}{\tan(\theta_{nop})} = \frac{30.5 \text{ kip}}{\tan(60.82^\circ)} = 17.0 \text{ kip}$$

$$N_{op} = \sqrt{N_{opx}^2 + N_{opy}^2}$$

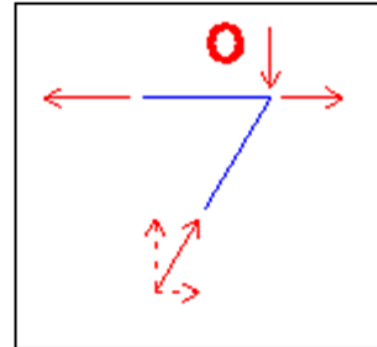
$$= \sqrt{(17.0 \text{ kip})^2 + (30.5 \text{ kip})^2}$$

$$= 34.9 \text{ kip (C)}$$

$$N_{oq} = N_{opx} + N_{uc} = 17.0 \text{ kip} + 6.1 \text{ kip}$$

$$= 23.1 \text{ kip (T)}$$

$$N_{nq} = N_{oq} = 23.1 \text{ kip (T)}$$



$$R_{nx} = N_{oq} = 23.1 \text{ kip}$$

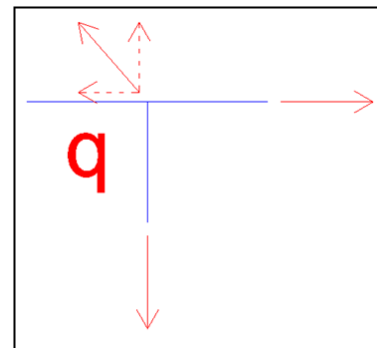
$$\Sigma F_x = N_{uc} + R_{mx} - R_{nx} = 0$$

$$R_{mx} = R_{nx} - N_{uc} = 17.02 \text{ kip (T)}$$

Assume bend acts similar to a pulley

$$N_{pq} = N_{oq} = 23.1 \text{ kip (T)}$$

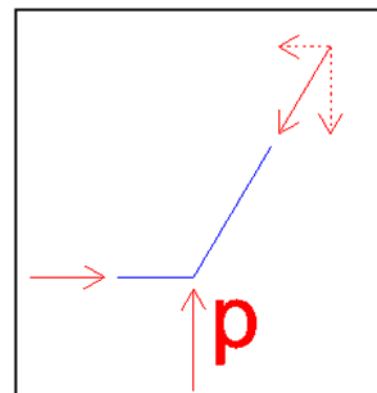
$$R_q = \sqrt{2 * N_{oq}^2} = \sqrt{2 * (23.1 \text{ kip})^2} = 32.7 \text{ kip}$$



$$N_{mp} = N_{opx} = 17.02 \text{ kip (C)}$$

$$\begin{aligned} R_{py} &= \frac{V_u l_{no} + N_{uc} l_{mn}}{l_{mp}} - R_{nx} \frac{l_{mn}}{l_{mp}} \\ &= \frac{30.5 \text{ kip}(12.7 \text{ in}) + (6.1 \text{ kip})(12 \text{ in})}{6 \text{ in}} - (23.1 \text{ kip}) \frac{12}{6} \\ &= 30.5 \text{ kip} \end{aligned}$$

$$N_{mp} - R_{mx} = 17.0 \text{ kip} - 17.0 \text{ kip} = 0 \therefore \text{OK}$$



$$\begin{aligned}
 M_{applied} &= V_u(a_v + \frac{t_{SWP}}{2}) + N_{uc}(h_c - d) \\
 &= (30.5 \text{ kip}) \left(5 \text{ in} + \frac{9 \text{ in}}{2} \right) + (6.1 \text{ kip})(14 \text{ in} - 12 \text{ in}) \\
 &= 25.146 \text{ kip} \cdot \text{ft}
 \end{aligned}$$

$$\begin{aligned}
 M_{uAbove} &= \frac{M_{applied}}{h} \left(z_c + \frac{h_c}{2} \right) \\
 &= \frac{25.15 \text{ kip} \cdot \text{ft}}{8.5 \text{ ft}} \left(42 \text{ in} + \frac{14 \text{ in}}{2} \right) = 12.1 \text{ kip} \cdot \text{ft}
 \end{aligned}$$

$$\begin{aligned}
 M_{uBelow} &= M_{applied} - M_{uAbove} \\
 &= 25.15 \text{ kip} \cdot \text{ft} - 12.1 \text{ kip} \cdot \text{ft} = 13.1 \text{ kip} \cdot \text{ft}
 \end{aligned}$$

$$M_u = C(d_{hout} - d_{hin})$$

Compression will be greatest below corbel in the inside wythe. To simplify design, both wythes are to be detailed symmetrically. Therefore, let $C = P_{wyin}$.

$$M_u = \max(M_{uAbove}, M_{uBelow}) = 13.1 \text{ kip} \cdot \text{ft}$$

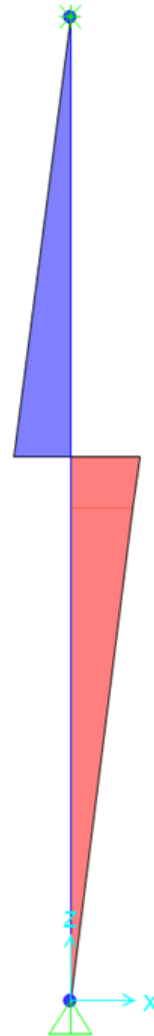
$$P_{wyin} = \frac{M_u}{d_{hout} - d_{hin}} = \frac{13.1 \text{ kip} \cdot \text{ft}}{7.5 \text{ in} - 1.5 \text{ in}} = 26.1 \text{ kip (C)}$$

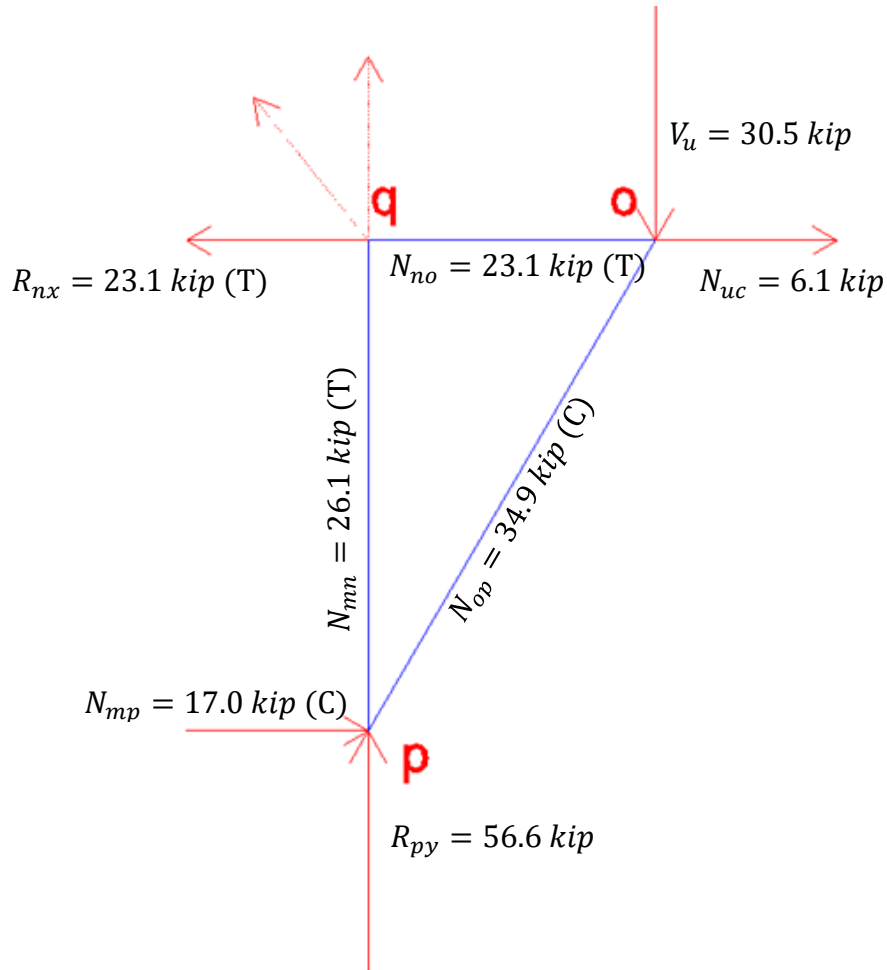
$$P_{wyout} = P_{wyin} = 26.1 \text{ kip (T)}$$

$$N_{pq} = P_{wyin} = 26.1 \text{ kip}$$

$$N_{mn} = P_{wyout} = 26.1 \text{ kip}$$

$$N_{py} = R_{py} + N_{pq} = 56.6 \text{ kip}$$





Select Strut, Tie, and Nodal Zone Dimensions

The most conservative β value for any relevant component will govern.

Nodes		Struts	
$\beta_{Nm} = 0.60$	(C-T-T)	$\beta_{S_{py}} = 1.0$	A bottle-shaped strut could develop in the concrete, so 0.75 will be used if reinforced properly. Otherwise, 0.6 must be used. Will assume inadequate reinforcement ($\beta=0.6$).
$\beta_{Nm} = 0.60$	(C-T-T)	$\beta_{S_{np}} = 0.6$	
$\beta_{Nm} = 0.80$	(C-C-T)	$\beta_{S_{op}} = 0.6$	
$\beta_{Nm} = 0.80$	(C-C-T)		

Because all components are affected by an element with a limiting value of 0.6, design must use $\beta = 0.6$ for all members.

$$\beta_s = 0.6$$

$$f_{ce} = 0.85\beta_s f'_c = 0.85(0.6)(8.0 \text{ ksi}) = 4.08 \text{ ksi}$$

$$\Phi f_{ce} = 0.75(4.08 \text{ ksi}) = 3.06 \text{ ksi}$$

Design Tension Ties

Member mn

$$w_{mn} = \frac{N_{mn}}{\Phi f_{ce} b_c} = \frac{26.1 \text{ kip}}{0.75(3.06 \text{ ksi})(10 \text{ in})} = 0.85 \text{ in} < \text{wythe thickness, } \therefore \text{OK}$$

$$A_{sreq,mn} = \frac{N_{mn}}{\Phi f_y} = \frac{26.1 \text{ kip}}{0.75(60 \text{ ksi})} = 0.58 \text{ in}^2 \quad \text{Therefore use (3) \#4 at 3" o.c.}$$

$$A_{smn} = 3(0.2 \text{ in}^2) = 0.6 \text{ in}^2$$

$$N_{nmn} = \Phi A_{smn} f_y = 0.75(0.6 \text{ in}^2)(60 \text{ ksi}) = 27 \text{ kip} \geq N_{mn} = 26.1 \text{ kip} \therefore \text{OK}$$

Anchorage Requirements

$$l_{dmp} = \left(\frac{3}{40} * \frac{f_y}{\lambda \sqrt{f'_c}} * \frac{\Psi_t \Psi_e \Psi_s}{\frac{(c_b + K_{tr})}{d_b}} \right) d_b \quad (\text{ACI 318-14 §25.4.2.3})$$

If clear cover of $1.0d_b$ and a minimum clear spacing of $2d_b$ exists, the simplified version may be used:

$$l_{dmp} = \left(\frac{f_y \Psi_t \Psi_e}{25 \lambda \sqrt{f'_c}} \right) d_b \quad (\text{ACI 318-14 §25.4.2.2})$$

$$\Psi_t = 1 \quad (\text{because not horizontal reinforcement})$$

$$\Psi_e = 1 \quad (\text{because using uncoated, regular rebar})$$

$$\lambda = 1 \quad (\text{because normalweight concrete})$$

$$d_b = 0.5 \text{ in}$$

$$l_{dmp} = \left(\frac{(60 \text{ ksi})(1)(1)}{25(1)\sqrt{8000 \text{ psi}} \left(1 \frac{\text{ksi}}{1000 \text{ psi}}\right)} \right) (0.5 \text{ in}) = 13.4 \text{ in}$$

Therefore 16 in. of rebar must be extended on each side of the corbel for a total of 46 in.

Member oq

$$w_{oq} = \frac{N_{oq}}{\Phi f_{ce} b_c} = \frac{23.1 \text{ kip}}{0.75(3.06 \text{ ksi})(10 \text{ in})} = 0.76 \text{ in}$$

$$A_{sreq,oq} = \frac{N_{oq}}{\Phi f_y} = \frac{23.1 \text{ kip}}{0.75(60 \text{ ksi})} = 0.52 \text{ in}^2 \quad \text{Therefore use (3) \#4 at 3" o.c.}$$

$$A_{soq} = 3(0.2 \text{ in}^2) = 0.8 \text{ in}^2$$

$$N_{noq} = \Phi A_{soq} f_y = 0.75(0.6 \text{ in}^2)(60 \text{ ksi}) = 27 \text{ kip} \geq N_{oq} = 23.1 \text{ kip} \therefore OK$$

Anchorage Requirements

$$l_{dmp} = \left(\frac{f_y \Psi_e \Psi_c \Psi_r}{50 \lambda \sqrt{f'_c}} \right) d_b \quad (\text{ACI 318-14 §25.4.3.1})$$

$$\Psi_e = 1 \quad (\text{because using uncoated, regular rebar})$$

$$\psi_c = 1 \quad (\text{because cover not } \geq 2.5 \text{ in})$$

$$\psi_r = 1 \quad (\text{because not enclosed})$$

$$\lambda = 1 \quad (\text{because normalweight concrete})$$

$$d_b = 0.5 \text{ in}$$

$$l_{dh} = \left(\frac{1(1)(1)(60 \text{ ksi})}{50 \lambda \sqrt{8000 \text{ psi}} \left(1 \frac{\text{ksi}}{1000 \text{ psi}}\right)} \right) (0.5 \text{ in}) = 6.7 \text{ in}$$

$$l_{dh} = \max \left(\frac{l_{dh}}{8 d_b}, 6 \text{ in} \right) = 6.7 \text{ in}$$

Therefore need 7 inches of rebar beyond bend for principle reinforcement:

$$l_{out} = l_{dh} + (3d_b + d_b) = 8.7 \text{ in} \quad (\text{ACI 318-11 §12.5.1})$$

Will specify principle reinforcement to extend 12 inches from top of the bend. Anchor bar shall be welded to the end of the principle reinforcement to attain development on corbel tip.

Member nq

No need to check tie width because this member will penetrate insulation (i.e. no concrete). According to IconX shear testing performed previously, the Icon connectors typically failed in the connector itself, so there was no data regarding concrete breakout as it does not govern failure of the connector. There is no data regarding the tensile capacity of the IconX connectors currently. It was assumed that the tension capacity would be similar to the shear capacity however, due to the “X” shape of the connector.

$$\Phi P_{nIconCTens} = 11.24 \text{ kip}$$

$$\Phi P_{nIconCSus} = 0.2\Phi P_{nIconCTens} = 0.55(11.24 \text{ kip}) = 6.182 \text{ kip}$$

Therefore creep will govern.

$$N_{IconCreep} = \frac{N_{nq} \left(\frac{V_{sus}}{V_u} \right)}{\Phi P_{nIconCSus}} = \frac{23.1 \text{ kip} \left(\frac{16.46}{30.5} \right)}{6.18 \text{ kip}} = 2.02$$

\therefore must use 3 IconX CFRP connectors

Because the ties will be used for localized force transfer, and because concrete breakout governs. The spacing will be based upon concrete breakout cone with an assumed breakout plane of 35° and an assumed embedment depth.

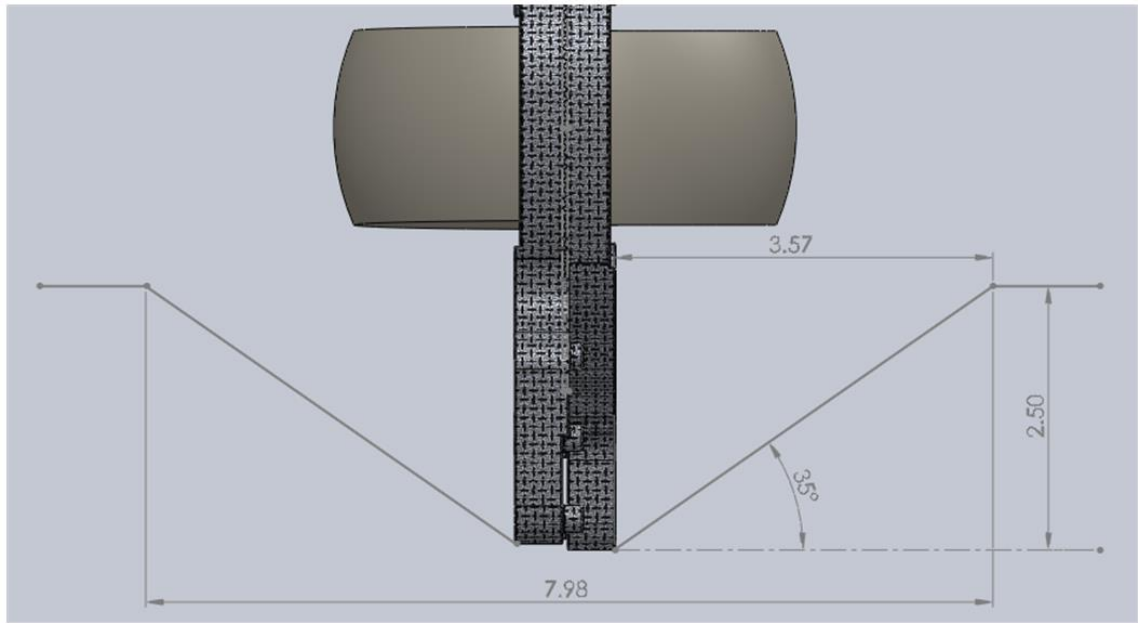


Figure A-19 Determination of IconX connector spacing

$$d_{embed} = 0.5(h_{Icon} - t_{ins}) = 0.5(8 \text{ in} - 3 \text{ in}) = 2.5 \text{ in}$$

$$s_{Iconlat} = 2 \left(\frac{d_{embed}}{\tan(35^\circ)} \right) + t_{Icon} = 2 \left(\frac{2.5 \text{ in}}{\tan(35^\circ)} \right) + 0.5 \text{ in} = 7.6 \text{ in}$$

Therefore use three IconX CFRP connectors at 8" o.c.

$$N_{nnq} = N_{IconCreq} \Phi P_{nlIconCTens} = 3(11.24 \text{ kip}) = 33.7 \text{ kip} \geq N_{mn} = 23.1 \text{ kip} \therefore OK$$

Design Compression Struts

Member mp

$$w_{mp} = \frac{N_{mp}}{\Phi f_{ce} b_c} = \frac{17.0 \text{ kip}}{0.75(3.06 \text{ ksi})(10 \text{ in})} = 0.56 \text{ in}$$

Since the foam is not able to withstand this force over such a small area, the compressive material used in this instance must have a height of at least 0.6 in. A high-density polyethylene prism would exhibit low thermal conductivity, is cheap, and does not require any special provisions for concerns regarding absorption and expansions when exposed to moisture like wood does. The compressive strength of HDPE 2" × 4" boards (also known as plastic lumber) is ($f_{HDPE} = 1.287 \text{ ksi}$). Because these are manufactured to typical 2" × 4" specifications, the prisms used will be 3 inches thick, 3.5 inches tall, and 10 inches long. The compressive strength of the prism will therefore be

$$\begin{aligned} \Phi_V f_{HDPE} h_{HDPE} b_{HDPE} &= 0.75(1.28 \text{ ksi})(3.5 \text{ in})(10 \text{ in}) = 33.8 \text{ kip} \geq N_{mp} \\ &= 17.0 \text{ kip} \therefore OK \end{aligned}$$

Member Rp

$$w_{py} = \frac{N_{py}}{\Phi f_{ce} b_c} = \frac{56.6 \text{ kip}}{0.75(3.06 \text{ ksi})(10 \text{ in})} = 1.9 \text{ in} < \text{wythe thickness therefore OK}$$

Shear at Corbel/SWP Interface

The shear to be resisted at this interface will be equal to the applied load. The friction from the interface shall be ignored conservatively. Stirrups shall be used to resist the shear.

$$R_{rebarShear} = 0.6 f_u A_{gv}$$

$$A_{gv,req} = \frac{V_u}{\Phi_v 0.6 f_u} = \frac{30.5 \text{ kip}}{0.75(0.6)(75 \text{ ksi})} = 0.9 \text{ in}^2$$

$$A_{gv,more} = A_{gv,req} - A_{soq} = 0.9 \text{ in}^2 - 0.6 \text{ in}^2 = 0.3 \text{ in}^2 \quad \therefore \text{use (1)\#4 stirrup@ 4"}$$

$$A_{gv} = 2(0.2 \text{ in}^2) + 0.6 \text{ in}^2 = 1.0 \text{ in}^2 \geq A_{gv,req} \therefore OK$$

Vertical/Longitudinal Reinforcement, A_{sl}

$$\rho = \frac{A_{sl,min}}{A_{gc}} = 0.0012 \quad (\text{ACI 381-14 §14.3.2})$$

$$A_{gcl} = b * (t_{wy0} + t_{wyi}) = 68 \text{ in} * 6 \text{ in} = 408 \text{ in}^2$$

$$A_{sl,min} = \rho A_{gcl} = 0.0012(408 \text{ in}^2) = 0.49 \text{ in}^2$$

$$s_{max} = \min \left(\frac{3t_{SWP}}{18 \text{ in}} \right) = \max \left(\frac{27 \text{ in}}{18 \text{ in}} \right) = 18 \text{ in}$$

$$N_{sl} = \frac{b - 2(0.75 \text{ in})}{s_{max}} = \frac{68 \text{ in} - 2(0.75 \text{ in})}{18 \text{ in}} = 3.69 \text{ bars}$$

$$A_{slbarmin} = \frac{A_{sl,min}}{N_{sl}} = \frac{0.49 \text{ in}^2}{4} = 0.12 \text{ in}^2 \quad \therefore \text{use (4)\#4 bars @ 18" o.c.}$$

Therefore use (4) #4 bars spaced 18" o.c. Place second layer of rebar on compression side for any reversed loading.

Horizontal/Transverse Reinforcement, A_{st}

$$\rho = \frac{A_{st,min}}{A_{gc}} = 0.0020 \quad (\text{ACI 381-14 §14.3.3})$$

$$A_{gct} = h * (t_{wy0} + t_{wyi}) = 102 \text{ in} * 6 \text{ in} = 612 \text{ in}^2$$

$$A_{st,min} = \rho A_{gcl} = 0.002(612 \text{ in}^2) = 1.23 \text{ in}^2$$

$$s_{max} = \min \left(\frac{3t_{SWP}}{18 \text{ in}} \right) = \max \left(\frac{27 \text{ in}}{18 \text{ in}} \right) = 18 \text{ in}$$

$$N_{st} = \frac{h - 2(0.75 \text{ in})}{s_{max}} = \frac{102 \text{ in} - 2(0.75 \text{ in})}{18 \text{ in}} = 5.6 \text{ bars}$$

$$A_{stbarmin} = \frac{A_{st,min}}{N_{st}} = \frac{1.2 \text{ in}^2}{6} = 0.2 \text{ in}^2 \quad \therefore \text{use (6)\#4 bars @ 18" o.c.}$$

Therefore use (6) #4 bars spaced 18" o.c. Place second layer of rebar on opposite side for symmetry.

Lifting

$$x_{lift} = 18 \text{ in} = 1.5 \text{ ft} \quad (\text{anchor to edge distance})$$

$$x_{midL} = h - 2x_{anchor} = 8.5 \text{ ft} - 3 \text{ ft} = 5.5 \text{ ft}$$

$$x_{midR} = b - 2x_{anchor} = 5.67 \text{ ft} - 3 \text{ ft} = 2.67 \text{ ft}$$

Longitudinal Direction

$$w_{sw} = w_c bt = (150 \text{ pcf})(5.67 \text{ ft})(0.5 \text{ ft}) = 425 \frac{\text{lb}}{\text{ft}}$$

$$R_A = \frac{w_{sw}h}{2} = \frac{\left(0.425 \frac{\text{kip}}{\text{ft}}\right)(8.5 \text{ ft})}{2} = 1.8 \text{ kip}$$

$$\begin{aligned} V_{lift,left} &= w_{sw}x_{lift} = \left(0.425 \frac{\text{kip}}{\text{ft}}\right)(1.5 \text{ ft}) \\ &= -0.6375 \text{ kip} \end{aligned}$$

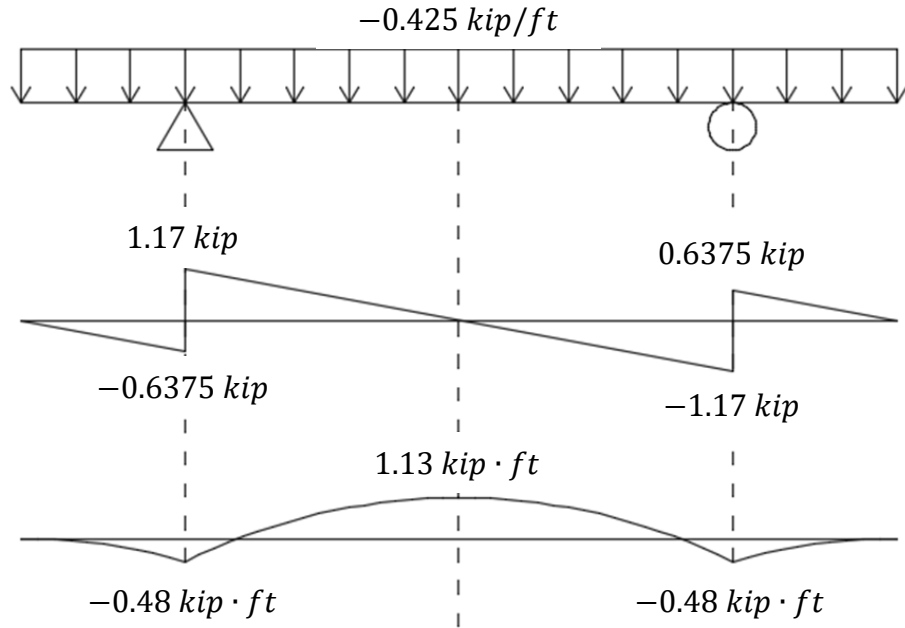
$$\begin{aligned} V_{lift,right} &= w_{sw}x_{lift} + R_A = -0.64 \text{ kip} + 1.8 \text{ kip} \\ &= 1.17 \text{ kip} \end{aligned}$$

$$M_{lift} = \frac{V_{lift,left}x_{lift}}{2} = \frac{(-0.64 \text{ kip})(1.5 \text{ ft})}{2}$$

$$= -0.48 \text{ kip} \cdot \text{ft}$$

$$M_{mid} = M_{lift} + \frac{V_{lift,right}(0.5x_{midL})}{2}$$

$$= -0.48 \text{ kip} \cdot \text{ft} + \frac{0.64 \text{ kip}(0.5 \cdot 5.5 \text{ ft})}{2} = 1.13 \text{ kip} \cdot \text{ft}$$



Cracking moment is equal to

$$M_{cr} = \frac{7.5\sqrt{f'_c}I_g}{0.5t}$$

$$f'_{c,req} = \left(\frac{0.5(t_{wy0} + t_{wyi})M_{mid}}{7.5I_g} \right)^2$$

$$= \left(\frac{0.5(6 \text{ in}) \left(1.13 \text{ kip} \cdot \text{ft} \cdot \frac{12 \text{ in}}{\text{ft}} \right)}{7.5(3978 \text{ in}^4)} \right)^2 = 0.0042 \text{ ksi}$$

Therefore we need to attain at least 0.0042 ksi before lifting.

Transverse Direction

$$w_{sw} = w_c h t = (150 \text{ pcf})(8.5 \text{ ft})(0.5 \text{ ft}) = 638 \frac{\text{lb}}{\text{ft}}$$

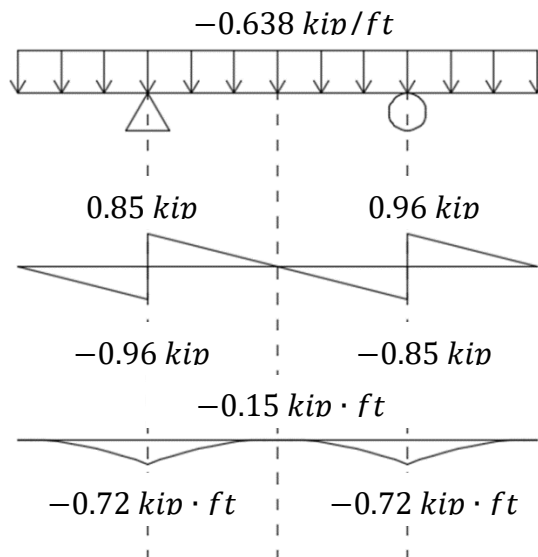
$$R_A = \frac{w_{sw} b}{2} = \frac{\left(0.64 \frac{\text{kip}}{\text{ft}}\right)(5.67 \text{ ft})}{2} = 1.8 \text{ kip}$$

$$\begin{aligned} V_{\text{lift, left}} &= w_{sw} x_{\text{lift}} = \left(0.64 \frac{\text{kip}}{\text{ft}}\right)(1.5 \text{ ft}) \\ &= -0.96 \text{ kip} \end{aligned}$$

$$\begin{aligned} V_{\text{lift, right}} &= w_{sw} x_{\text{lift}} + R_A = -0.96 \text{ kip} + 1.8 \text{ kip} \\ &= 0.85 \text{ kip} \end{aligned}$$

$$\begin{aligned} M_{\text{lift}} &= \frac{V_{\text{lift, left}} x_{\text{lift}}}{2} = \frac{(-0.96 \text{ kip})(1.5 \text{ ft})}{2} \\ &= -0.72 \text{ kip} \cdot \text{ft} \end{aligned}$$

$$\begin{aligned} M_{\text{mid}} &= M_{\text{lift}} + \frac{V_{\text{lift, right}}(0.5 x_{\text{mid}T})}{2} \\ &= -0.72 \text{ kip} \cdot \text{ft} + \frac{0.85 \text{ kip}(0.5 \cdot 2.67 \text{ ft})}{2} = -0.15 \text{ kip} \cdot \text{ft} \end{aligned}$$



Cracking moment is equal to

$$M_{cr} = \frac{7.5\sqrt{f'_c}I_g}{0.5t}$$

$$f'_{c,req} = \left(\frac{0.5(t_{wy0} + t_{wyi})M_{lift}}{7.5I_{gSWP}} \right)^2$$

$$= \left(\frac{0.5(6 \text{ in}) \left(0.72 \text{ kip} \cdot \text{ft} * \frac{12 \text{ in}}{\text{ft}} \right)}{7.5(3978 \text{ in}^4)} \right)^2 = 0.0017 \text{ ksi}$$

Therefore we need to attain at least 0.0017 ksi before lifting to avoid cracking the panel.

Since the concrete lifting anchor strengths are based on a concrete strength of 3.5 ksi,

however, the panels may not be lifted until $f'_c = 3.5 \text{ ksi}$.

$$f'_{c,req} = \max \begin{pmatrix} f'_{c,reqL} \\ f'_{c,reqT} \\ f'_{c,reqA} \end{pmatrix} = \max \begin{pmatrix} 0.0042 \text{ ksi} \\ 0.0017 \text{ ksi} \\ 3.5 \text{ ksi} \end{pmatrix} = 3.5 \text{ ksi}$$

RedIns Calculations

The RedIns specimen used the Deep Beam method for design.

Material Properties

Concrete

$$f'_c = 8.0 \text{ ksi}$$

$$f_r = 7.5\sqrt{f'_c} = 0.671 \text{ ksi}$$

$$w_c = 150 \text{ lbf/ft}$$

$$E_c = 33w_c^{1.5}\sqrt{f'_c} = 5422 \text{ ksi}$$

$$n = \frac{E_s}{E_c} = 5.348$$

Steel

$$f_y = 60 \text{ ksi}$$

$$E_s = 29000 \text{ ksi}$$

Geometrical Dimensions

SWP

$$t_{wyo} = t_{wyi} = t_{ins} = 3 \text{ in}$$

$$t_{SWP} = t_{wyo} + t_{wyi} + t_{ins} = 9 \text{ in}$$

$$b = 68 \text{ in} = 5.67 \text{ ft}$$

$$h = 102 \text{ in} = 8.5 \text{ ft}$$

$$d_{hout} = 7.5 \text{ in}$$

$$d_{hin} = 1.5 \text{ in}$$

$$I_{gSWP} = \frac{bt_{SWP}^3}{12} - \frac{bt_{ins}^3}{12}$$

$$= \frac{68 \text{ in}(9 \text{ in})^3}{12} - \frac{68 \text{ in}(3 \text{ in})^3}{12} = 3978 \text{ in}^4$$

Corbel

$$h_c = 14 \text{ in}$$

$$d = 12 \text{ in}$$

$$b_c = 10 \text{ in}$$

$$l_p = 8 \text{ in}$$

$$h_{cf} = 10 \text{ in}$$

$$c_c = 1.5 \text{ in}$$

$$I_{gc} = \frac{b_ch_c^3}{12} = \frac{10 \text{ in}(14 \text{ in})^3}{12} = 2287 \text{ in}^4$$

$$z_c = 42 \text{ in} \text{ (from top SWP to corbel)}$$

Reduced Section Properties

$$t_{wy0} = 3 \text{ in}, t_{insRed} = 1 \text{ in}, t_{wyiRed} = 5 \text{ in}$$

Plate Size

$$V_u = \Phi P_{nb} = \Phi 0.85 f'_c A_1 \quad (\text{ACI 318-14 §22.8.3.2})$$

$$\Phi_{bear} = 0.65 \quad (\text{ACI 318-14 §21.2.1})$$

$$A_1 = \frac{V_u}{\Phi_{bear} 0.85 f'_c} = \frac{30.5 \text{ kip}}{0.65(0.85)(8 \text{ ksi})} = 6.9 \text{ in}^2$$

$$L_{bear,min} = \frac{A_1}{b_c} = 0.69 \text{ in}$$

Therefore use at least 1 in \times 10 in plate.

Shear Span, a_v

Assume $a_v = 5 \text{ in}$.

Determine Corbel Depth by Limiting Shear Transfer Strength, V_n

$$V_{nmax} = \min \left[\begin{array}{c} 0.2 f'_c b_c d \\ (480 + 0.8 f'_c) b_c d \\ 1600 b_c d \end{array} \right] \quad (\text{ACI 318-14 §11.8.3.2.1})$$

$$= \min \left[\begin{array}{c} 0.2(8 \text{ ksi})(10 \text{ in})(12 \text{ in}) \\ (0.48 + 0.8(8 \text{ ksi}))(10 \text{ in})(12 \text{ in}) \\ 1600(10 \text{ in})(12 \text{ in}) \end{array} \right]$$

$$= \min \left[\begin{array}{c} 192 \text{ kip} \\ 134.4 \text{ kip} \\ 192 \text{ kip} \end{array} \right]$$

$$= 134.4 \text{ kip} \geq V_u = 30.5 \text{ kip} \therefore OK$$

$$d_{min} = \frac{V_u}{\left(\frac{\Phi V_{nmax}}{d}\right)} = \frac{30.5 \text{ kip}}{\left(\frac{0.75(134.4 \text{ kip})}{12 \text{ in}}\right)}$$

$$= 3.63 \text{ in} \leq 12 \text{ in} \therefore \text{OK, current } h \text{ will suffice}$$

$$\frac{a_v}{d} = \frac{5 \text{ in}}{12 \text{ in}} = 0.42 < 1 \therefore \text{OK} \quad (\text{ACI 318-14 §11.8.1a})$$

Determine Shear-Friction Reinforcement, A_{vf}

$$\mu = 1 \quad (\text{ACI 318-14 §11.6.4.3})$$

$$A_{vf,min} = \frac{V_u}{\Phi f_y \mu} = \frac{30.5 \text{ kip}}{0.75(60 \text{ ksi})(1)} = 0.68 \text{ in}^2$$

(ACI 318-14 §11.8.3.2)
(ACI 318-14 §11.6.4.1)

Determine Direct Tension Reinforcement, A_n

$$A_{n,min} = \frac{N_{uc}}{\Phi f_y} = \frac{6.1 \text{ kip}}{0.75(60 \text{ ksi})} = 0.14 \text{ in}^2 \quad (\text{ACI 318-14 §11.8.3.4})$$

Determine Flexural Reinforcement, A_f

$$M_u = V_u \left(a_v + \frac{t_{wyiRed}}{2} \right) + N_{uc} \left(\frac{h_c}{2} \right)$$

$$= (30.5 \text{ kip}) \left(5 \text{ in} + \frac{5 \text{ in}}{2} \right) + (6.1 \text{ kip}) \left(\frac{14 \text{ in}}{2} \right)$$

$$= 271.3 \text{ kip} \cdot \text{in}$$

$$A_{f,min} = \frac{M_u}{\Phi f_y d} = \frac{271.3 \text{ kip} \cdot \text{in}}{0.75(60 \text{ ksi})(12 \text{ in})} = 0.50 \text{ in}^2 \quad (\text{ACI 318-14 §11.8.3.3})$$

Determine Primary Tension Reinforcement, A_{sc}

$$A_{sc,min} = \max \left[\begin{array}{l} \frac{2}{3} A_{vf,min} + A_{n,min} \\ A_{f,min} + A_{n,min} \\ 0.04 \frac{f'_c}{f_y} b_c d \end{array} \right] \quad (\text{ACI 318-14 §11.8.3.4})$$

$$\begin{aligned}
&= \max \left[\begin{array}{l} \frac{2}{3} (0.68 \text{ in}^2) + (0.14 \text{ in}^2) \\ (0.5 \text{ in}^2) + (0.14 \text{ in}^2) \\ 0.04 \left(\frac{8 \text{ ksi}}{60 \text{ ksi}} \right) (10 \text{ in})(12 \text{ in}) \end{array} \right] \\
&= \max \left[\begin{array}{l} 0.59 \text{ in}^2 \\ 0.64 \text{ in}^2 \\ 0.64 \text{ in}^2 \end{array} \right] = 0.64 \text{ in}^2
\end{aligned}$$

Try (4) #4 bars, $A_{sc} = 0.8 \text{ in}^2$

$$s_{sc,max} = \frac{10 \text{ in} - 2(0.75 \text{ in})}{4 - 1} = 2.83 \text{ in}$$

Therefore use (4) #4 bars at 2" o.c.

Anchorage Requirements

$$l_{dh} = \left(\frac{f_y \psi_e \psi_c \psi_r}{50 \lambda \sqrt{f'_c}} \right) d_b \quad (\text{ACI 318-14 §25.4.3.1})$$

$$\psi_e = 1 \quad (\text{because using uncoated, regular rebar})$$

$$\psi_c = 1 \quad (\text{because cover not } \geq 2.5 \text{ in})$$

$$\psi_r = 1 \quad (\text{because not enclosed})$$

$$\lambda = 1 \quad (\text{because normalweight concrete})$$

$$d_b = 0.5 \text{ in}$$

$$l_{dh} = \left(\frac{(1)(1)(1)(60 \text{ ksi})}{50(1)\sqrt{8000 \text{ psi}} \left(\frac{1 \text{ ksi}}{1000 \text{ psi}} \right)} \right) d_b = 6.71 \text{ in}$$

$$l_{dh} = \max \left[\begin{array}{l} l_{dh} \\ 8d_{b4} \\ 6 \text{ in} \end{array} \right] = \max \left[\begin{array}{l} 6.71 \text{ in} \\ 4 \text{ in} \\ 6 \text{ in} \end{array} \right] = 6.71 \text{ in} \quad (\text{ACI 318-11 §12.5.1})$$

Therefore need 7 inches of rebar beyond bend for principle reinforcement:

$$l_{out} = l_{dh} + (3d_b + d_b) = 8.71 \text{ in} \quad (\text{ACI 318-11 §12.5.1})$$

Principle reinforcement shall extend 12 inches from top of the bend.

Determine Shear Reinforcement, A_h

$$A_{h,min} = 0.5(A_{sc,min} - A_{n,min}) \quad (\text{ACI 318-14 §11.8.4})$$

$$= 0.5(0.64 \text{ in}^2 - 0.14 \text{ in}^2) = 0.25 \text{ in}^2$$

Therefore use (1) #4 stirrup, $A_h = 0.4 \text{ in}^2$, placed at 4" o.c. below A_{sc} .

Vertical/Longitudinal Reinforcement, A_{sl}

$$\Phi_{flex} = 0.9$$

$$\begin{aligned} M_u &= V_u \left(a_v + \frac{t_{wyiRed}}{2} \right) + N_{uc} \left(\frac{h_c}{2} \right) \\ &= (30.5 \text{ kip}) \left(5 \text{ in} + \frac{5 \text{ in}}{2} \right) + (6.1 \text{ kip}) \left(\frac{14 \text{ in}}{2} \right) \\ &= 271.3 \text{ kip} \cdot \text{in} \end{aligned}$$

$$A_{sl} = \frac{M_u}{\Phi f_y d_{reinf}} = \frac{271.3 \text{ kip} \cdot \text{in}}{0.9(60 \text{ ksi})(6 \text{ in})} = 1.39 \text{ in}^2$$

$$\rho = \frac{A_{sl,min}}{A_{gc}} = 0.0012 \quad (\text{ACI 318-14 §14.3.2})$$

$$A_{gcl} = b * t = 68 \text{ in} * 8 \text{ in} = 544 \text{ in}^2$$

$$A_{sl,min} = \rho A_{gcl} = 0.0012(544 \text{ in}^2) = 0.65 \text{ in}^2 < A_{sl} \quad \text{Therefore OK}$$

Design is restricted to using #4 bars because of limitations on bend radius, therefore

$$N_l = \frac{A_{sl}}{A_{\#4}} = \frac{1.39 \text{ in}^2}{0.2 \text{ in}^2} = 6.95 \quad \therefore \text{use (7) \#4 bars at 2" o.c.}$$

$$s_{max} = \min \left(\frac{3t}{18 \text{ in}} \right) = \max \left(\frac{27 \text{ in}}{18 \text{ in}} \right) = 18 \text{ in} > s \quad \text{Therefore OK}$$

Therefore use (7) #4 bars spaced 2" o.c. to resist flexure. Place second layer of rebar on compression side for any reversed loading. The minimum reinforcement required will be used for the rest of the panel.

$$\rho = \frac{A_{sl,min}}{A_{gc}} = 0.0012 \quad (\text{ACI 381-14 §14.3.2})$$

$$A_{gcl} = b * t = 68 \text{ in} * 6 \text{ in} = 408 \text{ in}^2$$

$$A_{sl,min} = \rho A_{gcl} = 0.0012(408 \text{ in}^2) = 0.49 \text{ in}^2$$

$$s_{max} = \min\left(\frac{3t}{18 \text{ in}}\right) = \max\left(\frac{27 \text{ in}}{18 \text{ in}}\right) = 18 \text{ in}$$

$$N_{sl} = \frac{b_{SWP} - 2(0.75 \text{ in})}{s_{max}} = \frac{68 \text{ in} - 2(0.75 \text{ in})}{18 \text{ in}} = 3.7 \quad \therefore (4)\#4 \text{ bars @ } 18" \text{ o.c.}$$

Horizontal/Transverse Reinforcement, A_{st}

$$\rho = \frac{A_{st,min}}{A_{gc}} = 0.0020 \quad (\text{ACI 381-14 §14.3.3})$$

$$A_{gct} = h * t = 102 \text{ in} * 6 \text{ in} = 612 \text{ in}^2$$

$$A_{st,min} = \rho A_{gcl} = 0.002(612 \text{ in}^2) = 1.2 \text{ in}^2$$

$$s_{max} = \min\left(\frac{3t}{18 \text{ in}}\right) = \max\left(\frac{27 \text{ in}}{18 \text{ in}}\right) = 18 \text{ in}$$

$$N_t = \frac{A_{st,min}}{A_{\#4}} = \frac{1.2 \text{ in}^2}{0.2 \text{ in}^2} = 6 \quad \therefore (6) \#4 \text{ bars @ } 18" \text{ o.c.}$$

Therefore use (6) #5 bars spaced 15" o.c. per code minimum requirements. Place second layer of rebar on opposite side for symmetry.

Lifting

$$x_{lift} = 18 \text{ in} = 1.5 \text{ ft} \quad (\text{anchor to edge distance})$$

$$x_{midL} = h - 2x_{anchor} = 8.5 \text{ ft} - 3 \text{ ft} = 5.5 \text{ ft}$$

$$x_{midT} = b - 2x_{anchor} = 5.67 \text{ ft} - 3 \text{ ft} = 2.67 \text{ ft}$$

Longitudinal Direction

$$w_{sw} = w_c b t = (150 \text{ pcf})(5.67 \text{ ft})(0.5 \text{ ft}) = 425 \frac{\text{lb}}{\text{ft}}$$

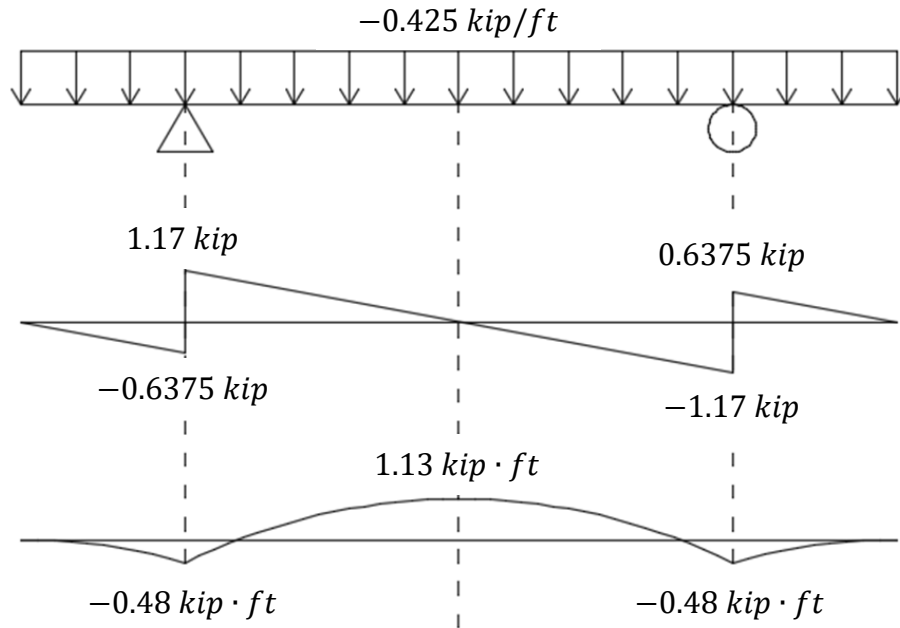
$$R_A = \frac{w_{sw} h}{2} = \frac{\left(0.425 \frac{\text{kip}}{\text{ft}}\right)(8.5 \text{ ft})}{2} = 1.8 \text{ kip}$$

$$\begin{aligned} V_{lift, left} &= w_{sw} x_{lift} = \left(0.425 \frac{\text{kip}}{\text{ft}}\right)(1.5 \text{ ft}) \\ &= -0.6375 \text{ kip} \end{aligned}$$

$$\begin{aligned} V_{lift, right} &= w_{sw} x_{lift} + R_A = -0.64 \text{ kip} + 1.8 \text{ kip} \\ &= 1.17 \text{ kip} \end{aligned}$$

$$\begin{aligned} M_{lift} &= \frac{V_{lift, left} x_{lift}}{2} = \frac{(-0.64 \text{ kip})(1.5 \text{ ft})}{2} \\ &= -0.48 \text{ kip} \cdot \text{ft} \end{aligned}$$

$$\begin{aligned} M_{mid} &= M_{lift} + \frac{V_{lift, right}(0.5x_{midL})}{2} \\ &= -0.48 \text{ kip} \cdot \text{ft} + \frac{0.64 \text{ kip}(0.5 \cdot 5.5 \text{ ft})}{2} = 1.13 \text{ kip} \cdot \text{ft} \end{aligned}$$



Cracking moment is equal to

$$M_{cr} = \frac{7.5\sqrt{f'_c}I_g}{0.5t}$$

$$f'_{c,req} = \left(\frac{0.5(t_{wyo} + t_{wyi})M_{mid}}{7.5I_g} \right)^2$$

$$= \left(\frac{0.5(6 \text{ in}) \left(1.13 \text{ kip} \cdot \text{ft} * \frac{12 \text{ in}}{\text{ft}} \right)}{7.5(3978 \text{ in}^4)} \right)^2 = 0.0042 \text{ ksi}$$

Therefore we need to attain at least 0.0042 ksi before lifting.

Transverse Direction

$$w_{sw} = w_c h t = (150 \text{ pcf})(8.5 \text{ ft})(0.5 \text{ ft}) = 638 \frac{\text{lb}}{\text{ft}}$$

$$R_A = \frac{w_{sw} b}{2} = \frac{\left(0.64 \frac{\text{kip}}{\text{ft}} \right) (5.67 \text{ ft})}{2} = 1.8 \text{ kip}$$

$$V_{lift,left} = w_{sw}x_{lift} = \left(0.64 \frac{kip}{ft}\right)(1.5 ft)$$

$$= -0.96 kip$$

$$V_{lift,right} = w_{sw}x_{lift} + R_A = -0.96 kip + 1.8 kip$$

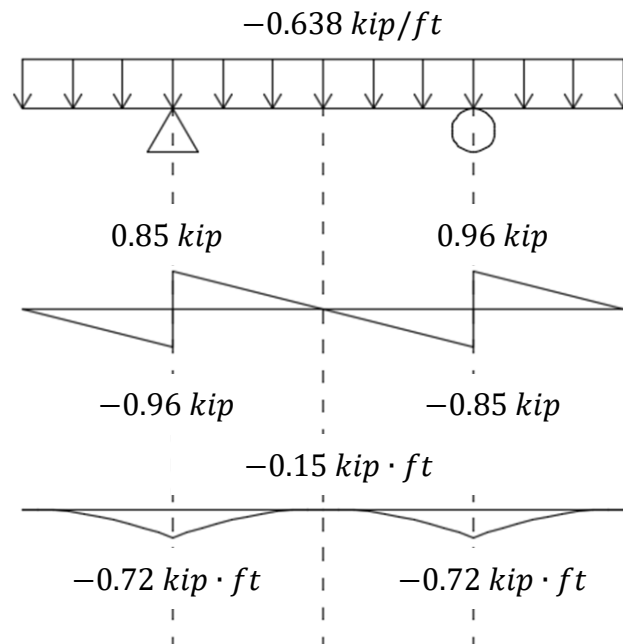
$$= 0.85 kip$$

$$M_{lift} = \frac{V_{lift,left}x_{lift}}{2} = \frac{(-0.96 kip)(1.5 ft)}{2}$$

$$= -0.72 kip \cdot ft$$

$$M_{mid} = M_{lift} + \frac{V_{lift,right}(0.5x_{midr})}{2}$$

$$= -0.72 kip \cdot ft + \frac{0.85 kip(0.5 \cdot 2.67 ft)}{2} = -0.15 kip \cdot ft$$



Cracking moment is equal to

$$M_{cr} = \frac{7.5\sqrt{f'_c}I_g}{0.5t}$$

$$f'_{c,req} = \left(\frac{0.5(t_{wy0} + t_{wyi})M_{lift}}{7.5I_{gSWP}} \right)^2$$

$$= \left(\frac{0.5(6 \text{ in}) \left(0.72 \text{ kip} \cdot \text{ft} * \frac{12 \text{ in}}{\text{ft}} \right)}{7.5(3978 \text{ in}^4)} \right)^2 = 0.0017 \text{ ksi}$$

Therefore we need to attain at least 0.0017 ksi before lifting to avoid cracking the panel.

Since the concrete lifting anchor strengths are based on a concrete strength of 3.5 ksi,

however, the panels may not be lifted until $f'_c = 3.5 \text{ ksi}$.

$$f'_{c,req} = \max \begin{pmatrix} f'_{c,reqL} \\ f'_{c,reqT} \\ f'_{c,reqA} \end{pmatrix} = \max \begin{pmatrix} 0.0042 \text{ ksi} \\ 0.0017 \text{ ksi} \\ 3.5 \text{ ksi} \end{pmatrix} = 3.5 \text{ ksi}$$

GridHor Calculations

The GridHor specimen used the Strut-and-Tie method for design.

Material Properties

Concrete

$$f'_c = 8.0 \text{ ksi}$$

$$f_r = 7.5\sqrt{f'_c} = 0.671 \text{ ksi}$$

$$w_c = 150 \text{ lbf/ft}$$

$$E_c = 33w_c^{1.5}\sqrt{f'_c} = 5422 \text{ ksi}$$

$$n_s = \frac{E_s}{E_c} = 5.348$$

Steel

$$f_y = 60 \text{ ksi}$$

$$f_u = 75 \text{ ksi}$$

$$E_s = 29000 \text{ ksi}$$

FRP

$$f_{Grid} = 47.63 \text{ ksi}$$

$$f_{Gridsus} = 0.2f_{yGrid}$$

$$= 0.2(47.6 \text{ ksi}) = 9.5 \text{ ksi}$$

$$f_{GridShear} = 7.70 \text{ ksi}$$

$$s_{Gridbar} = t_{Grid} = 1.5 \text{ in}$$

$$A_{Grid} = 2.85 \text{ in}^2$$

$$A_{Bar} = \frac{2.85 \text{ in}^2}{8} = 0.36 \text{ in}^2$$

Geometrical Dimensions

SWP

$$t_{wy0} = t_{wyi} = t_{ins} = 3 \text{ in}$$

$$t_{SWP} = t_{wy0} + t_{wyi} + t_{ins} = 9 \text{ in}$$

$$b = 68 \text{ in} = 5.67 \text{ ft}$$

$$h = 102 \text{ in} = 8.5 \text{ ft}$$

$$d_{hout} = 7.5 \text{ in}$$

$$d_{hin} = 1.5 \text{ in}$$

$$I_{gSWP} = \frac{bt_{SWP}^3}{12} - \frac{bt_{ins}^3}{12}$$

$$= \frac{68 \text{ in}(9 \text{ in})^3}{12} - \frac{68 \text{ in}(3 \text{ in})^3}{12} = 3978 \text{ in}^4$$

Corbel

$$h_c = 14 \text{ in}$$

$$d = 12 \text{ in}$$

$$b_c = 10 \text{ in}$$

$$l_p = 8 \text{ in}$$

$$h_{cf} = 10 \text{ in}$$

$$c_c = 1.5 \text{ in}$$

$$I_{gc} = \frac{b_c h_c^3}{12} = \frac{10 \text{ in}(14 \text{ in})^3}{12} = 2287 \text{ in}^4$$

$$z_c = 42 \text{ in} \text{ (from top SWP to corbel)}$$

Plate Size

$$V_u = \Phi P_{nb} = \Phi 0.85 f'_c A_1 \quad (\text{ACI 318-14 §22.8.3.2})$$

$$\Phi_{\text{bear}} = 0.65 \quad (\text{ACI 318-14 §21.2.1})$$

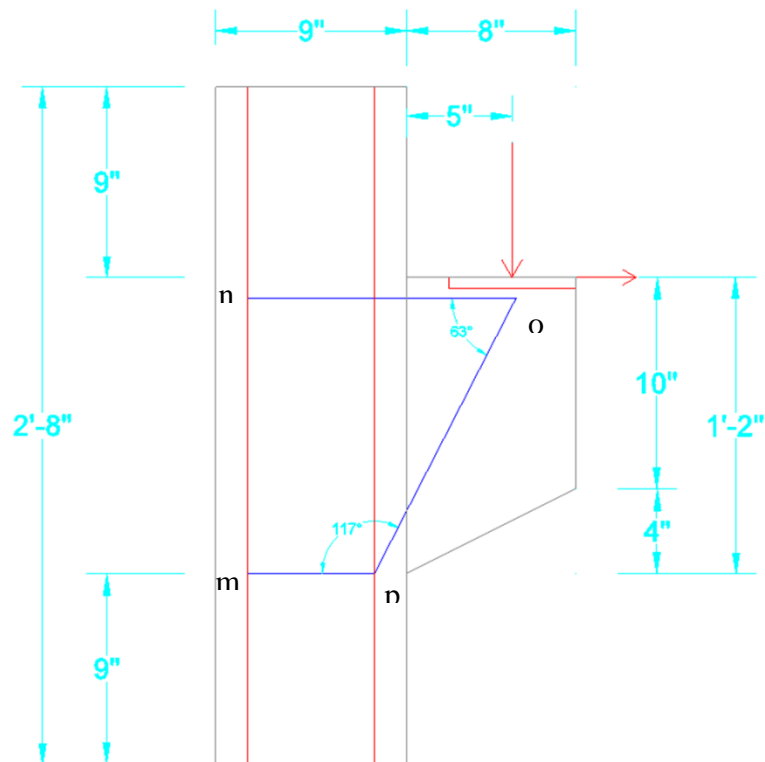
$$A_1 = \frac{V_u}{\Phi_{\text{bear}} 0.85 f'_c} = \frac{30.5 \text{ kip}}{0.65(0.85)(8 \text{ ksi})} = 6.9 \text{ in}^2$$

$$L_{\text{bear}, \min} = \frac{A_1}{b_c} = 0.69 \text{ in}$$

Therefore use at least 1 in \times 10 in plate.

Shear Span, a_v

Assume $a_v = 5 \text{ in}$.

Determine Truss Geometry

$$\begin{aligned}
 l_{no} &= d_{hout} + a_v + (1 \text{ in}) \tan \theta_R \\
 &= 7.5 \text{ in} + 5 \text{ in} + (1 \text{ in}) \tan(11.31^\circ) = 12.7 \text{ in}
 \end{aligned}$$

$$\begin{aligned}
 \theta_{nop} &= \text{atan}\left(\frac{d}{l_{no} - (d_{hout} - d_{hin})}\right) \\
 &= \text{atan}\left(\frac{12 \text{ in}}{12.7 \text{ in} - (7.5 \text{ in} - 1.5 \text{ in})}\right) = 60.82^\circ
 \end{aligned}$$

$$l_{mn} = d = 12 \text{ in}$$

$$l_{mp} = d_{hout} - d_{hin} = 7.5 \text{ in} - 1.5 \text{ in} = 6 \text{ in}$$

$$\theta_{pno} = \text{atan}\left(\frac{d}{l_{mp}}\right) = \text{atan}\left(\frac{12}{6}\right) = 63.44^\circ$$

$$\begin{aligned}
 \theta_{npo} &= 180^\circ - \theta_{pno} - \theta_{nop} = 180^\circ - 63.44^\circ - 60.82^\circ \\
 &= 55.74^\circ
 \end{aligned}$$

$$\theta_{mpn} = \theta_{pno} = 63.44^\circ$$

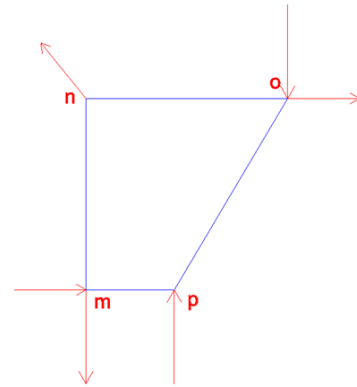
Determine Forces in Truss Components

$$\Sigma M_m = V_u l_{no} + N_{uc} l_{mn} - R_{py} l_{mp} - R_{nx} l_{mn} = 0$$

$$R_{py} = \frac{V_u l_{no} + N_{uc} l_{mn}}{l_{mp}} - R_{nx} \frac{l_{mn}}{l_{mp}}$$

$$\Sigma F_y = R_{py} + R_{ny} - R_{my} - V_u = 0$$

$$\Sigma F_x = N_{uc} - R_{mx} - R_{nx} = 0$$



$$N_{opy} = V_u = 30.5 \text{ kip}$$

$$N_{opx} = \frac{N_{opy}}{\tan(\theta_{nop})} = \frac{30.5 \text{ kip}}{\tan(60.82^\circ)} = 17.0 \text{ kip}$$

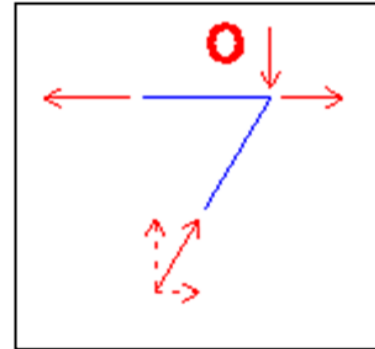
$$N_{op} = \sqrt{N_{opx}^2 + N_{opy}^2}$$

$$= \sqrt{(17.0 \text{ kip})^2 + (30.5 \text{ kip})^2}$$

$$= 34.9 \text{ kip (C)}$$

$$N_{no} = N_{opx} + N_{uc} = 17.0 \text{ kip} + 6.1 \text{ kip}$$

$$= 23.1 \text{ kip (T)}$$



$$R_{nx} = N_{no} = 23.1 \text{ kip}$$

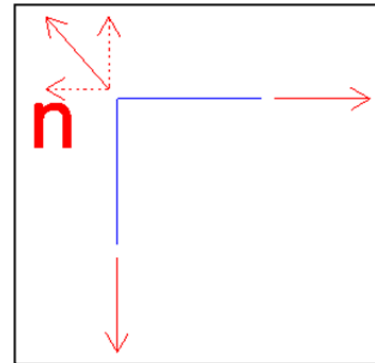
$$R_n = \sqrt{R_{nx}^2 + R_{ny}^2} = \sqrt{2(23.1 \text{ kip})^2} = 32.69 \text{ kip}$$

$$\Sigma F_x = N_{uc} + R_{mx} - R_{nx} = 0$$

$$R_{mx} = R_{nx} - N_{uc} = 17.02 \text{ kip (T)}$$

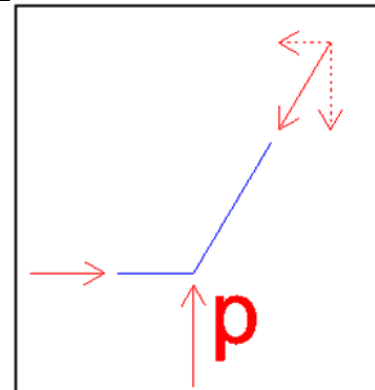
Assume bend acts similar to a pulley

$$N_{mn} = R_{nx} = 23.1 \text{ kip (T)}$$

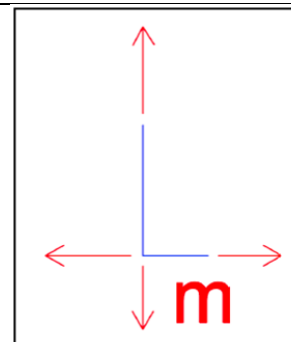


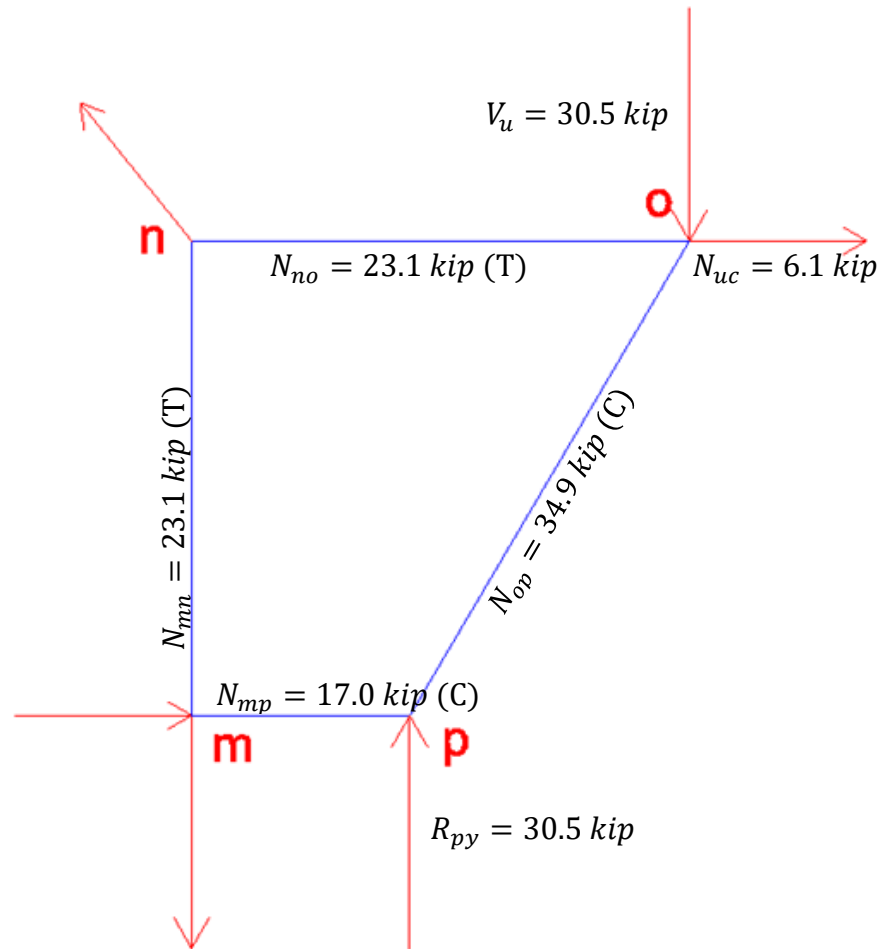
$$N_{mp} = N_{opx} = 17.02 \text{ kip (C)}$$

$$\begin{aligned} R_{py} &= \frac{V_u l_{no} + N_{uc} l_{mn}}{l_{mp}} - R_{nx} \frac{l_{mn}}{l_{mp}} \\ &= \frac{30.5 \text{ kip}(12.7 \text{ in}) + (6.1 \text{ kip})(12 \text{ in})}{6 \text{ in}} - (23.1 \text{ kip}) \frac{12}{6} \\ &= 30.5 \text{ kip} \end{aligned}$$



$$N_{mp} - R_{mx} = 17.0 \text{ kip} - 17.0 \text{ kip} = 0 \therefore OK$$





Select Strut, Tie, and Nodal Zone Dimensions

The most conservative β value for any relevant component will govern.

Nodes		Struts	
$\beta_{Nm} = 0.60$	(C-T-T)	$\beta_{S_{py}} = 1.0$	A bottle-shaped strut could develop in the concrete, so 0.75 will be used if reinforced properly. Otherwise, 0.6 must be used. Will assume inadequate reinforcement ($\beta=0.6$).
$\beta_{Nm} = 0.60$	(C-T-T)	$\beta_{S_{np}} = 0.6$	
$\beta_{Nm} = 0.80$	(C-C-T)	$\beta_{S_{op}} = 0.6$	
$\beta_{Nm} = 0.80$	(C-C-T)		

Because all components are affected by an element with a limiting value of 0.6, design must use $\beta = 0.6$ for all members.

$$\beta_s = 0.6$$

$$f_{ce} = 0.85\beta_s f'_c = 0.85(0.6)(8.0 \text{ ksi}) = 4.08 \text{ ksi}$$

$$\Phi f_{ce} = 0.75(4.08 \text{ ksi}) = 3.06 \text{ ksi}$$

Design Tension Ties

Member *mn*

$$w_{mn} = \frac{N_{mn}}{\Phi f_{ce} b_c} = \frac{23.1 \text{ kip}}{0.75(3.06 \text{ ksi})(10 \text{ in})} = 0.76 \text{ in} < \text{wythe thickness, } \therefore \text{OK}$$

$$A_{sreq,mn} = \frac{N_{mn}}{\Phi f_y} = \frac{23.1 \text{ kip}}{0.75(60 \text{ ksi})} = 0.51 \text{ in}^2 \quad \text{Therefore use (4) \#4 at 2.5" o.c.}$$

$$A_{smn} = 4(0.2 \text{ in}^2) = 0.8 \text{ in}^2$$

$$N_{nmn} = \Phi A_{smn} f_y = 0.75(0.8 \text{ in}^2)(60 \text{ ksi}) = 36 \text{ kip} \geq N_{mn} = 23.1 \text{ kip} \therefore \text{OK}$$

Anchorage Requirements

$$l_{dmp} = \left(\frac{3}{40} * \frac{f_y}{\lambda \sqrt{f'_c}} * \frac{\Psi_t \Psi_e \Psi_s}{\frac{(c_b + K_{tr})}{d_b}} \right) d_b \quad (\text{ACI 318-14 §25.4.2.3})$$

If clear cover of $1.0d_b$ and a minimum clear spacing of $2d_b$ exists, the simplified version may be used:

$$l_{dmp} = \left(\frac{f_y \Psi_t \Psi_e}{25 \lambda \sqrt{f'_c}} \right) d_b \quad (\text{ACI 318-14 §25.4.2.2})$$

$$\Psi_t = 1 \quad (\text{because not horizontal reinforcement})$$

$$\Psi_e = 1 \quad (\text{because using uncoated, regular rebar})$$

$$\lambda = 1 \quad (\text{because normalweight concrete})$$

$$d_b = 0.5 \text{ in}$$

$$l_{dmp} = \left(\frac{(60 \text{ ksi})(1)(1)}{25(1)\sqrt{8000 \text{ psi}} \left(1 \frac{\text{ksi}}{1000 \text{ psi}}\right)} \right) (0.5 \text{ in}) = 13.4 \text{ in}$$

Therefore 16 inches of rebar must be extended on each side of the corbel for a total of 46 inches.

Member no

No need to check tie width because this member will penetrate insulation (i.e. no concrete).

For ultimate strength, the area required will be

$$A_{Gridreq} = \frac{N_{no}}{\Phi_v f_{Grid}} = \frac{23.1 \text{ kip}}{0.75(47.6 \text{ ksi})} = 0.65 \text{ in}^2 < A_{Grid} = 2.49 \text{ in}^2 \therefore OK$$

Creep rupture typically controls with GFRP, however. This requires an area of:

$$A_{creepreq} = \frac{N_{no} \left(\frac{V_{sus}}{V_u} \right)}{\Phi_v f_{Gridsus}} = \frac{23.1 \text{ kip} \left(\frac{16.46}{30.5} \right)}{0.75(9.5 \text{ ksi})} = 1.75 \text{ in}^2 < A_{Grid} = 2.49 \text{ in}^2 \therefore OK$$

$$N_{nno} = \Phi A_{Grid} f_{Grid} = 0.75(2.49 \text{ in}^2)(47.6 \text{ ksi}) = 89.1 \text{ kip} \geq N_{mn} = 23.1 \text{ kip}$$

$\therefore OK$

Design Compression Struts

Member op

$$w_{op} = \frac{N_{op}}{\Phi f_{ce} b_c} = \frac{34.9 \text{ kip}}{0.75(3.06 \text{ ksi})(10 \text{ in})} = 1.14 \text{ in}$$

Member mp

$$w_{mp} = \frac{N_{mp}}{\Phi f_{ce} b_c} = \frac{17.0 \text{ kip}}{0.75(3.06 \text{ ksi})(10 \text{ in})} = 0.56 \text{ in}$$

Since the foam is not able to withstand this force over such a small area, the compressive material used in this instance must have a height of at least 0.6 in. A high-density polyethylene prism would exhibit low thermal conductivity, is cheap, and does not require any special provisions for concerns regarding absorption and expansions when exposed to moisture like wood does. The compressive strength of HDPE 2" × 4" boards (also known as plastic lumber) is ($f_{HDPE} = 1.287 \text{ ksi}$). Because these are manufactured to typical 2" × 4" specifications, the prisms used will be 3 inches thick, 3.5 inches tall, and 10 inches long. The compressive strength of the prism will therefore be

$$\begin{aligned}\Phi_V f_{HDPE} h_{HDPE} b_{HDPE} &= 0.75(1.28 \text{ ksi})(3.5 \text{ in})(10 \text{ in}) = 33.8 \text{ kip} \geq N_{mp} \\ &= 17.0 \text{ kip} \therefore OK\end{aligned}$$

Member Rp

$$w_{py} = \frac{N_{py}}{\Phi f_{ce} b_c} = \frac{30.48 \text{ kip}}{0.75(3.06 \text{ ksi})(10 \text{ in})} = 1.0 \text{ in} < \text{wythe thickness therefore OK}$$

Shear at Corbel/SWP Interface

The shear to be resisted at this interface will be equal to the applied load. The friction from the interface shall be ignored conservatively. The shear strength of the grid is

$$\Phi R_{n\text{Shear}} = \Phi_v A_{Grid} f_{Grid} + \Phi_v A_{gv} f_y$$

$$\begin{aligned}A_{gv,req} &= \frac{V_u - \Phi_v A_{grid} f_{Grid}}{\Phi_v 0.6 f_u} \\ &= \frac{30.5 \text{ kip} - 0.75(2.49 \text{ in}^2)(7.7 \text{ ksi})}{0.75(0.6)(75 \text{ ksi})} = 0.48 \text{ in}^2 \quad \therefore \text{use (2)\#4 stirrups @ 3" o.c.}\end{aligned}$$

$$A_{gv} = 2(0.4 \text{ in}^2) = 0.8 \text{ in}^2 > 0.48 \text{ in}^2 \therefore OK$$

Vertical/Longitudinal Reinforcement, A_{sl}

$$\rho = \frac{A_{sl,min}}{A_{gc}} = 0.0012 \quad (\text{ACI 381-14 §14.3.2})$$

$$A_{gcl} = b * (t_{wy0} + t_{wyi}) = 68 \text{ in} * 6 \text{ in} = 408 \text{ in}^2$$

$$A_{sl,min} = \rho A_{gcl} = 0.0012(408 \text{ in}^2) = 0.49 \text{ in}^2$$

$$s_{max} = \min \left(\frac{3t_{SWP}}{18 \text{ in}} \right) = \max \left(\frac{27 \text{ in}}{18 \text{ in}} \right) = 18 \text{ in}$$

$$N_{sl} = \frac{b - 2(0.75 \text{ in})}{s_{max}} = \frac{68 \text{ in} - 2(0.75 \text{ in})}{18 \text{ in}} = 3.69 \text{ bars}$$

$$A_{slbarmin} = \frac{A_{sl,min}}{N_{sl}} = \frac{0.49 \text{ in}^2}{4} = 0.12 \text{ in}^2 \quad \therefore \text{use (4)\#4 bars @ 18" o.c.}$$

Therefore use (4) #4 bars spaced 18" o.c. Place second layer of rebar on compression side for any reversed loading.

Horizontal/Transverse Reinforcement, A_{st}

$$\rho = \frac{A_{st,min}}{A_{gc}} = 0.0020 \quad (\text{ACI 381-14 §14.3.3})$$

$$A_{gct} = h * (t_{wy0} + t_{wyi}) = 102 \text{ in} * 6 \text{ in} = 612 \text{ in}^2$$

$$A_{st,min} = \rho A_{gcl} = 0.002(612 \text{ in}^2) = 1.23 \text{ in}^2$$

$$s_{max} = \min \left(\frac{3t_{SWP}}{18 \text{ in}} \right) = \max \left(\frac{27 \text{ in}}{18 \text{ in}} \right) = 18 \text{ in}$$

$$N_{st} = \frac{h - 2(0.75 \text{ in})}{s_{max}} = \frac{102 \text{ in} - 2(0.75 \text{ in})}{18 \text{ in}} = 5.6 \text{ bars}$$

$$A_{stbarmin} = \frac{A_{st,min}}{N_{st}} = \frac{1.2 \text{ in}^2}{6} = 0.2 \text{ in}^2 \quad \therefore \text{use (6)\#4 bars @ 18" o.c.}$$

Therefore use (6) #4 bars spaced 18" o.c. Place second layer of rebar on opposite side for symmetry.

Lifting

$$x_{lift} = 18 \text{ in} = 1.5 \text{ ft} \quad (\text{anchor to edge distance})$$

$$x_{midL} = h - 2x_{anchor} = 8.5 \text{ ft} - 3 \text{ ft} = 5.5 \text{ ft}$$

$$x_{midT} = b - 2x_{anchor} = 5.67 \text{ ft} - 3 \text{ ft} = 2.67 \text{ ft}$$

Longitudinal Direction

$$w_{sw} = w_c b t = (150 \text{ pcf})(5.67 \text{ ft})(0.5 \text{ ft}) = 425 \frac{\text{lb}}{\text{ft}}$$

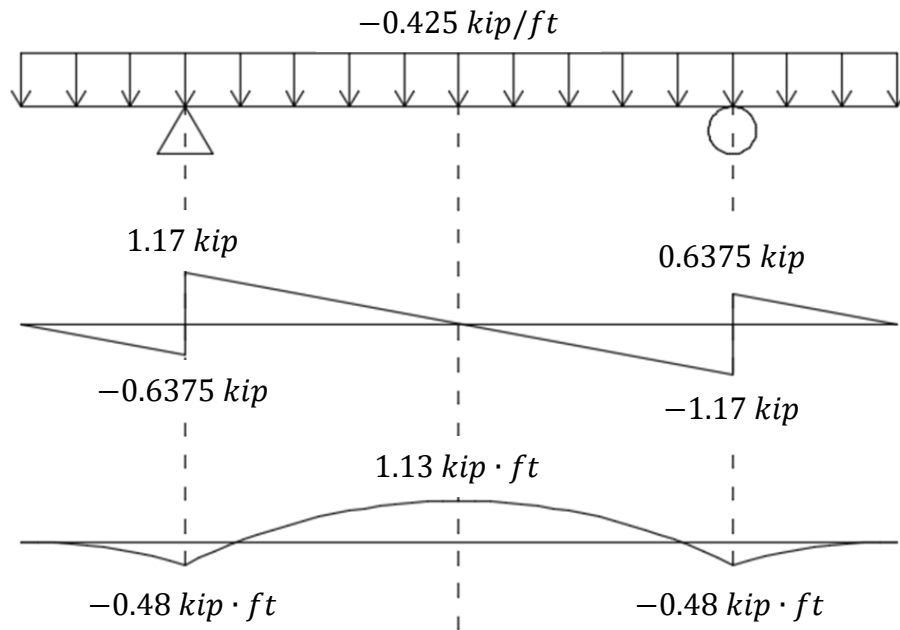
$$R_A = \frac{w_{sw} h}{2} = \frac{\left(0.425 \frac{\text{kip}}{\text{ft}}\right)(8.5 \text{ ft})}{2} = 1.8 \text{ kip}$$

$$\begin{aligned} V_{lift, left} &= w_{sw} x_{lift} = \left(0.425 \frac{\text{kip}}{\text{ft}}\right)(1.5 \text{ ft}) \\ &= -0.6375 \text{ kip} \end{aligned}$$

$$\begin{aligned} V_{lift, right} &= w_{sw} x_{lift} + R_A = -0.64 \text{ kip} + 1.8 \text{ kip} \\ &= 1.17 \text{ kip} \end{aligned}$$

$$\begin{aligned} M_{lift} &= \frac{V_{lift, left} x_{lift}}{2} = \frac{(-0.64 \text{ kip})(1.5 \text{ ft})}{2} \\ &= -0.48 \text{ kip} \cdot \text{ft} \end{aligned}$$

$$\begin{aligned} M_{mid} &= M_{lift} + \frac{V_{lift, right}(0.5x_{midL})}{2} \\ &= -0.48 \text{ kip} \cdot \text{ft} + \frac{0.64 \text{ kip}(0.5 \cdot 5.5 \text{ ft})}{2} = 1.13 \text{ kip} \cdot \text{ft} \end{aligned}$$



Cracking moment is equal to

$$M_{cr} = \frac{7.5\sqrt{f'_c}I_g}{0.5t}$$

$$f'_{c,req} = \left(\frac{0.5(t_{wyo} + t_{wyi})M_{mid}}{7.5I_g} \right)^2$$

$$= \left(\frac{0.5(6 \text{ in}) \left(1.13 \text{ kip} \cdot \text{ft} * \frac{12 \text{ in}}{\text{ft}} \right)}{7.5(3978 \text{ in}^4)} \right)^2 = 0.0042 \text{ ksi}$$

Therefore we need to attain at least 0.0042 ksi before lifting.

Transverse Direction

$$w_{sw} = w_c h t = (150 \text{ pcf})(8.5 \text{ ft})(0.5 \text{ ft}) = 638 \frac{\text{lb}}{\text{ft}}$$

$$R_A = \frac{w_{sw}b}{2} = \frac{\left(0.64 \frac{\text{kip}}{\text{ft}}\right)(5.67 \text{ ft})}{2} = 1.8 \text{ kip}$$

$$V_{lift,left} = w_{sw}x_{lift} = \left(0.64 \frac{\text{kip}}{\text{ft}}\right)(1.5 \text{ ft})$$

$$= -0.96 \text{ kip}$$

$$V_{lift,right} = w_{sw}x_{lift} + R_A = -0.96 \text{ kip} + 1.8 \text{ kip}$$

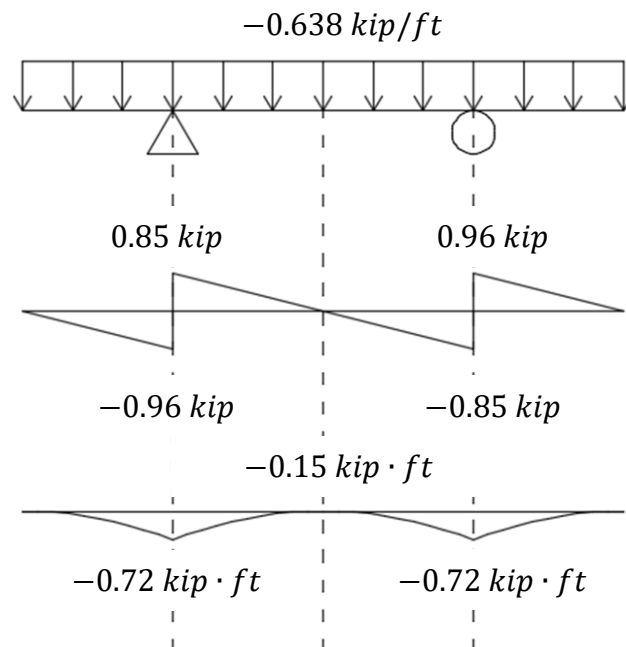
$$= 0.85 \text{ kip}$$

$$M_{lift} = \frac{V_{lift,left}x_{lift}}{2} = \frac{(-0.96 \text{ kip})(1.5 \text{ ft})}{2}$$

$$= -0.72 \text{ kip} \cdot \text{ft}$$

$$M_{mid} = M_{lift} + \frac{V_{lift,right}(0.5x_{midT})}{2}$$

$$= -0.72 \text{ kip} \cdot \text{ft} + \frac{0.85 \text{ kip}(0.5 \cdot 2.67 \text{ ft})}{2} = -0.15 \text{ kip} \cdot \text{ft}$$



Cracking moment is equal to

$$M_{cr} = \frac{7.5\sqrt{f'_c}I_g}{0.5t}$$

$$f'_{c,req} = \left(\frac{0.5(t_{wy0} + t_{wyi})M_{lift}}{7.5I_{gSWP}} \right)^2$$

$$= \left(\frac{0.5(6 \text{ in}) \left(0.72 \text{ kip} \cdot \text{ft} * \frac{12 \text{ in}}{\text{ft}} \right)}{7.5(3978 \text{ in}^4)} \right)^2 = 0.0017 \text{ ksi}$$

Therefore we need to attain at least 0.0017 ksi before lifting to avoid cracking the panel.

Since the concrete lifting anchor strengths are based on a concrete strength of 3.5 ksi,

however, the panels may not be lifted until $f'_c = 3.5 \text{ ksi}$.

$$f'_{c,req} = \max \begin{pmatrix} f'_{c,reqL} \\ f'_{c,reqT} \\ f'_{c,reqA} \end{pmatrix} = \max \begin{pmatrix} 0.0042 \text{ ksi} \\ 0.0017 \text{ ksi} \\ 3.5 \text{ ksi} \end{pmatrix} = 3.5 \text{ ksi}$$

GridVer Calculations

The GridVer specimen used the Strut-and-Tie method for design.

Material Properties

<u>Concrete</u>	<u>Steel</u>	<u>FRP</u>
$f'_c = 8.0 \text{ ksi}$	$f_y = 60 \text{ ksi}$	$f_{Grid} = 47.63 \text{ ksi}$
$f_r = 7.5\sqrt{f'_c} = 0.671 \text{ ksi}$	$f_u = 75 \text{ ksi}$	$f_{Gridsus} = 0.2f_{yGrid}$
$w_c = 150 \text{ lb/ft}$	$E_s = 29000 \text{ ksi}$	$= 0.2(47.6 \text{ ksi}) = 9.5 \text{ ksi}$
$E_c = 33w_c^{1.5}\sqrt{f'_c} = 5422 \text{ ksi}$		$f_{GridShear} = 7.70 \text{ ksi}$
$n_s = \frac{E_s}{E_c} = 5.348$		$s_{Gridbar} = t_{Grid} = 1.5 \text{ in}$
		$A_{Grid} = 2.85 \text{ in}^2$
		$A_{Bar} = \frac{2.85 \text{ in}^2}{8} = 0.36 \text{ in}^2$

Geometrical Dimensions

<u>SWP</u>	<u>Corbel</u>
$t_{wyo} = t_{wyi} = t_{ins} = 3 \text{ in}$	$h_c = 14 \text{ in}$
$t_{SWP} = t_{wyo} + t_{wyi} + t_{ins} = 9 \text{ in}$	$d = 12 \text{ in}$
$b = 68 \text{ in} = 5.67 \text{ ft}$	$b_c = 10 \text{ in}$
$h = 102 \text{ in} = 8.5 \text{ ft}$	$l_p = 8 \text{ in}$
$d_{hout} = 7.5 \text{ in}$	$h_{cf} = 10 \text{ in}$
$d_{hin} = 1.5 \text{ in}$	$c_c = 1.5 \text{ in}$
$I_{gSWP} = \frac{bt_{SWP}^3}{12} - \frac{bt_{ins}^3}{12}$	$I_{gc} = \frac{b_c h_c^3}{12} = \frac{10 \text{ in}(14 \text{ in})^3}{12} = 2287 \text{ in}^4$
$= \frac{68 \text{ in}(9 \text{ in})^3}{12} - \frac{68 \text{ in}(3 \text{ in})^3}{12} = 3978 \text{ in}^4$	$z_c = 42 \text{ in}$ (from top SWP to corbel)

Plate Size

$$V_u = \Phi P_{nb} = \Phi 0.85 f'_c A_1 \quad (\text{ACI 318-14 } \S 22.8.3.2)$$

$$\Phi_{\text{bear}} = 0.65 \quad (\text{ACI 318-14 } \S 21.2.1)$$

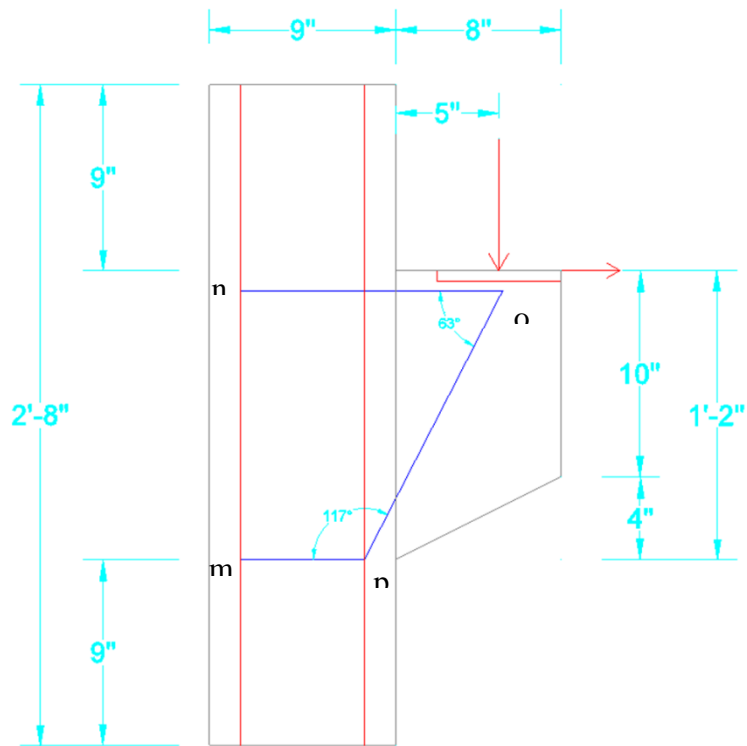
$$A_1 = \frac{V_u}{\Phi_{\text{bear}} 0.85 f'_c} = \frac{30.5 \text{ kip}}{0.65(0.85)(8 \text{ ksi})} = 6.9 \text{ in}^2$$

$$L_{\text{bear}, \text{min}} = \frac{A_1}{b_c} = 0.69 \text{ in}$$

Therefore use at least 1 in \times 10 in plate.

Shear Span, a_v

Assume $a_v = 5 \text{ in}$.

Determine Truss Geometry

$$\begin{aligned}
 l_{no} &= d_{hout} + a_v + (1 \text{ in}) \tan \theta_R \\
 &= 7.5 \text{ in} + 5 \text{ in} + (1 \text{ in}) \tan(11.31^\circ) = 12.7 \text{ in}
 \end{aligned}$$

$$\begin{aligned}
 \theta_{nop} &= \text{atan}\left(\frac{d}{l_{no} - (d_{hout} - d_{hin})}\right) \\
 &= \text{atan}\left(\frac{12 \text{ in}}{12.7 \text{ in} - (7.5 \text{ in} - 1.5 \text{ in})}\right) = 60.82^\circ
 \end{aligned}$$

$$l_{mn} = d = 12 \text{ in}$$

$$l_{mp} = d_{hout} - d_{hin} = 7.5 \text{ in} - 1.5 \text{ in} = 6 \text{ in}$$

$$\theta_{pno} = \text{atan}\left(\frac{d}{l_{mp}}\right) = \text{atan}\left(\frac{12}{6}\right) = 63.44^\circ$$

$$\begin{aligned}
 \theta_{npo} &= 180^\circ - \theta_{pno} - \theta_{nop} = 180^\circ - 63.44^\circ - 60.82^\circ \\
 &= 55.74^\circ
 \end{aligned}$$

$$\theta_{mpn} = \theta_{pno} = 63.44^\circ$$

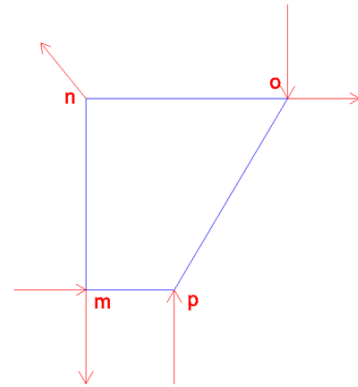
Determine Forces in Truss Components

$$\Sigma M_m = V_u l_{no} + N_{uc} l_{mn} - R_{py} l_{mp} - R_{nx} l_{mn} = 0$$

$$R_{py} = \frac{V_u l_{no} + N_{uc} l_{mn}}{l_{mp}} - R_{nx} \frac{l_{mn}}{l_{mp}}$$

$$\Sigma F_y = R_{py} + R_{ny} - R_{my} - V_u = 0$$

$$\Sigma F_x = N_{uc} - R_{mx} - R_{nx} = 0$$



$$N_{opy} = V_u = 30.5 \text{ kip}$$

$$N_{opx} = \frac{N_{opy}}{\tan(\theta_{nop})} = \frac{30.5 \text{ kip}}{\tan(60.82^\circ)} = 17.0 \text{ kip}$$

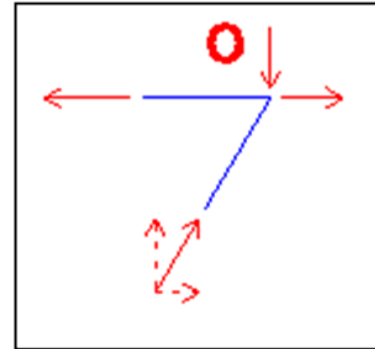
$$N_{op} = \sqrt{N_{opx}^2 + N_{opy}^2}$$

$$= \sqrt{(17.0 \text{ kip})^2 + (30.5 \text{ kip})^2}$$

$$= 34.9 \text{ kip (C)}$$

$$N_{no} = N_{opx} + N_{uc} = 17.0 \text{ kip} + 6.1 \text{ kip}$$

$$= 23.1 \text{ kip (T)}$$



$$R_{nx} = N_{no} = 23.1 \text{ kip}$$

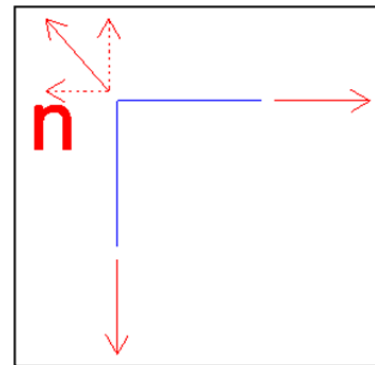
$$R_n = \sqrt{R_{nx}^2 + R_{ny}^2} = \sqrt{2(23.1 \text{ kip})^2} = 32.69 \text{ kip}$$

$$\Sigma F_x = N_{uc} + R_{mx} - R_{nx} = 0$$

$$R_{mx} = R_{nx} - N_{uc} = 17.02 \text{ kip (T)}$$

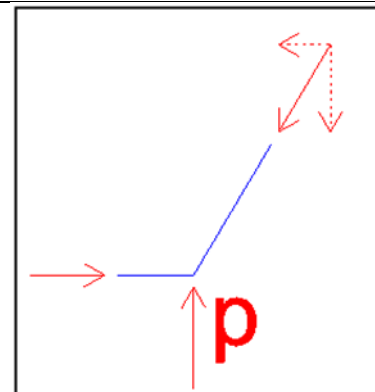
Assume bend acts similar to a pulley

$$N_{mn} = R_{nx} = 23.1 \text{ kip (T)}$$

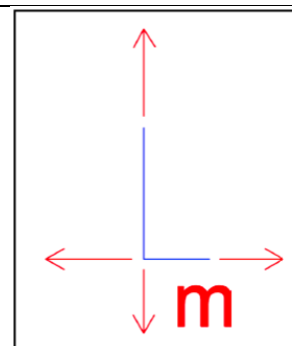


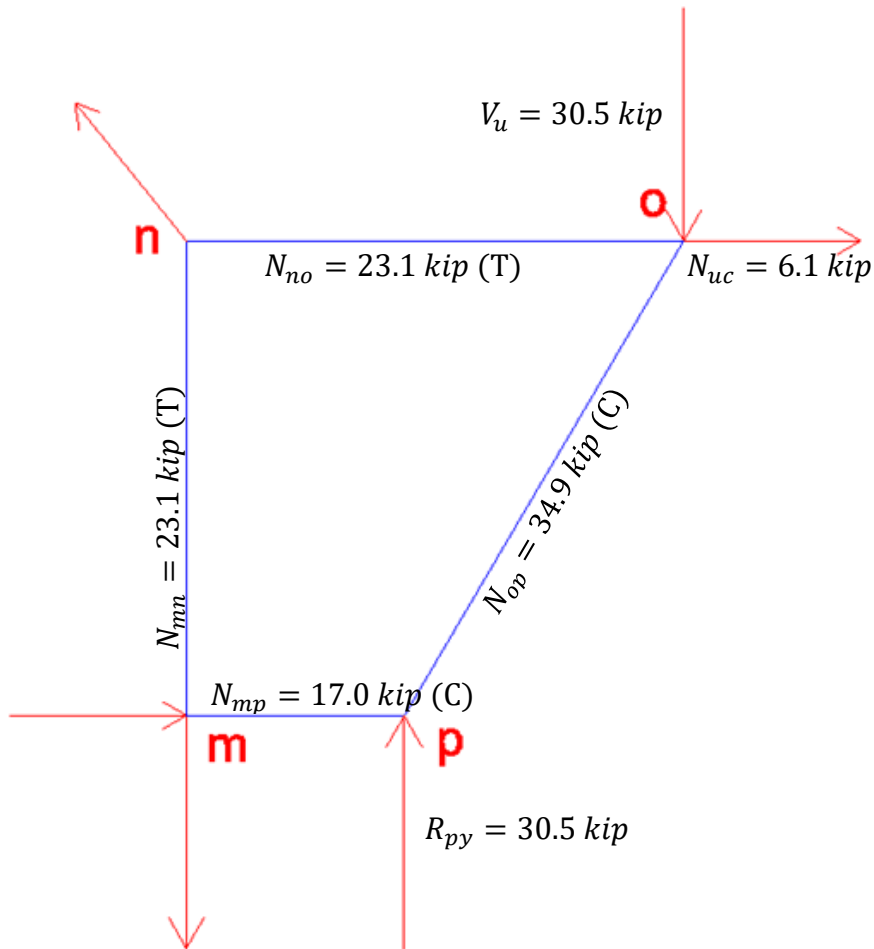
$$N_{mp} = N_{opx} = 17.02 \text{ kip (C)}$$

$$\begin{aligned} R_{py} &= \frac{V_u l_{no} + N_{uc} l_{mn}}{l_{mp}} - R_{nx} \frac{l_{mn}}{l_{mp}} \\ &= \frac{30.5 \text{ kip}(12.7 \text{ in}) + (6.1 \text{ kip})(12 \text{ in})}{6 \text{ in}} - (23.1 \text{ kip}) \frac{12}{6} \\ &= 30.5 \text{ kip} \end{aligned}$$



$$N_{mp} - R_{mx} = 17.0 \text{ kip} - 17.0 \text{ kip} = 0 \therefore OK$$





Select Strut, Tie, and Nodal Zone Dimensions

The most conservative β value for any relevant component will govern.

Nodes		Struts	
$\beta_{Nm} = 0.60$	(C-T-T)	$\beta_{S_{py}} = 1.0$	A bottle-shaped strut could develop in the concrete, so 0.75 will be used if reinforced properly. Otherwise, 0.6 must be used. Will assume inadequate reinforcement ($\beta=0.6$).
$\beta_{Nm} = 0.60$	(C-T-T)	$\beta_{S_{np}} = 0.6$	
$\beta_{Nm} = 0.80$	(C-C-T)	$\beta_{S_{op}} = 0.6$	
$\beta_{Nm} = 0.80$	(C-C-T)		

Because all components are affected by an element with a limiting value of 0.6, design must use $\beta = 0.6$ for all members.

$$\beta_s = 0.6$$

$$f_{ce} = 0.85\beta_s f'_c = 0.85(0.6)(8.0 \text{ ksi}) = 4.08 \text{ ksi}$$

$$\Phi f_{ce} = 0.75(4.08 \text{ ksi}) = 3.06 \text{ ksi}$$

Design Tension Ties

Member *mn*

$$w_{mn} = \frac{N_{mn}}{\Phi f_{ce} b_c} = \frac{23.1 \text{ kip}}{0.75(3.06 \text{ ksi})(10 \text{ in})} = 0.76 \text{ in} < \text{wythe thickness, } \therefore \text{OK}$$

$$A_{sreq,mn} = \frac{N_{mn}}{\Phi f_y} = \frac{23.1 \text{ kip}}{0.75(60 \text{ ksi})} = 0.51 \text{ in}^2 \quad \text{Therefore use (3) \#4 at 2.5" o.c.}$$

$$A_{smn} = 3(0.2 \text{ in}^2) = 0.6 \text{ in}^2$$

$$N_{nmn} = \Phi A_{smn} f_y = 0.75(0.6 \text{ in}^2)(60 \text{ ksi}) = 27 \text{ kip} \geq N_{mn} = 23.1 \text{ kip} \therefore \text{OK}$$

Anchorage Requirements

$$l_{dmp} = \left(\frac{3}{40} * \frac{f_y}{\lambda \sqrt{f'_c}} * \frac{\Psi_t \Psi_e \Psi_s}{\frac{(c_b + K_{tr})}{d_b}} \right) d_b \quad (\text{ACI 318-14 §25.4.2.3})$$

If clear cover of $1.0d_b$ and a minimum clear spacing of $2d_b$ exists, the simplified version may be used:

$$l_{dmp} = \left(\frac{f_y \Psi_t \Psi_e}{25 \lambda \sqrt{f'_c}} \right) d_b \quad (\text{ACI 318-14 §25.4.2.2})$$

$$\Psi_t = 1 \quad (\text{because not horizontal reinforcement})$$

$$\Psi_e = 1 \quad (\text{because using uncoated, regular rebar})$$

$$\lambda = 1 \quad (\text{because normalweight concrete})$$

$$d_b = 0.5 \text{ in}$$

$$l_{dmp} = \left(\frac{(60 \text{ ksi})(1)(1)}{25(1)\sqrt{8000 \text{ psi}} \left(1 \frac{\text{ksi}}{1000 \text{ psi}}\right)} \right) (0.5 \text{ in}) = 13.4 \text{ in}$$

Therefore 16 inches of rebar must be extended on each side of the corbel for a total of 46 inches.

Member no

No need to check tie width because this member will penetrate insulation (i.e. no concrete).

It will be assumed that only the top 3 rows will resist the tension force. For ultimate strength, the area required will be

$$A_{Gridreq} = \frac{N_{no}}{\Phi_v f_{Grid}} = \frac{23.1 \text{ kip}}{0.75(47.6 \text{ ksi})} = 0.65 \text{ in}^2$$

$$N_{Grid} = \frac{A_{Gridreq}}{3A_{Bar}} = \frac{0.65 \text{ in}^2}{3(0.356 \text{ in}^2)} = 0.6 \therefore \text{only 1 grid required}$$

Creep rupture typically controls with GFRP, however. This requires an area of:

$$A_{creepreq} = \frac{N_{no} \left(\frac{V_{sus}}{V_u} \right)}{\Phi_v f_{Gridsus}} = \frac{23.1 \text{ kip} \left(\frac{16.46}{30.5} \right)}{0.75(9.5 \text{ ksi})} = 1.75 \text{ in}^2$$

$$N_{Grid} = \frac{A_{creepreq}}{3A_{Bar}} = \frac{1.75 \text{ in}^2}{3(0.356 \text{ in}^2)} = 1.64 \therefore 2 \text{ grates required to resist the load}$$

$$A_{no} = 2(3A_{bar}) = 6(0.356 \text{ in}^2) = 2.14 \text{ in}^2$$

$$N_{no} = \Phi A_{no} f_{Grid} = 0.75(2.14 \text{ in}^2)(47.6 \text{ ksi}) = 76.4 \text{ kip} \geq N_{mn} = 23.1 \text{ kip} \therefore OK$$

There is not adequate data regarding embedment of the grate in concrete, so 3 transverse rebar will be included to improve the mechanical bond of the grate to the outside and

inside wythes. The same development length as those required to reinforce member mn will be used here to make the total length of these reinforcing rebars 46 inches.

Design Compression Struts

Member op

$$w_{op} = \frac{N_{op}}{\Phi f_{ce} b_c} = \frac{34.9 \text{ kip}}{0.75(3.06 \text{ ksi})(10 \text{ in})} = 1.14 \text{ in}$$

Member mp

The tensile and compressive stress of GFRP is equal. Since the grate area crossing the insulation is evenly distributed, only the bottom 3 rows will be assumed to resist the compressive force, meaning the same reinforcement area as tie NO is required for member MP. Since the force to be resisted in Strut MP is less than Tie NO, and the reinforcement of Tie NO was adequate, we can therefore conclude by observation that the reinforcement of Strut MP is sufficient to resist the load of 17.018 kips.

$$A_{mp} = 2(3A_{bar}) = 2.14 \text{ in}^2$$

$$\Phi N_{nmp} = \Phi_v A_{mp} f_{Grid} = 0.75(2.14 \text{ in}^2)(47.6 \text{ ksi}) = 76.4 \text{ kip} \geq N_{mp} = 17.0 \text{ kip}$$

$\therefore OK$

Member Rp

$$w_{py} = \frac{N_{py}}{\Phi f_{ce} b_c} = \frac{30.48 \text{ kip}}{0.75(3.06 \text{ ksi})(10 \text{ in})} = 1.0 \text{ in} < \text{wythe thickness therefore OK}$$

Shear at Corbel/SWP Interface

The shear to be resisted at this interface will be equal to the applied load. The friction from the interface shall be ignored conservatively. The shear strength of the grid is

$$\Phi R_{nShear} = \Phi_v A_{GridShear} f_{GridShear} \quad N_{BarSear} = 9$$

$$\Phi V_n = 0.75[2(9(0.356 \text{ in}^2))](7.7 \text{ ksi}) = 37.0 \text{ kip} > V_u \quad \therefore OK$$

Vertical/Longitudinal Reinforcement, A_{sl}

$$\rho = \frac{A_{sl,min}}{A_{gc}} = 0.0012 \quad (\text{ACI 381-14 §14.3.2})$$

$$A_{gcl} = b * (t_{wy0} + t_{wyi}) = 68 \text{ in} * 6 \text{ in} = 408 \text{ in}^2$$

$$A_{sl,min} = \rho A_{gcl} = 0.0012(408 \text{ in}^2) = 0.49 \text{ in}^2$$

$$s_{max} = \min\left(\frac{3t_{SWP}}{18 \text{ in}}\right) = \max\left(\frac{27 \text{ in}}{18 \text{ in}}\right) = 18 \text{ in}$$

$$N_{sl} = \frac{b - 2(0.75 \text{ in})}{s_{max}} = \frac{68 \text{ in} - 2(0.75 \text{ in})}{18 \text{ in}} = 3.69 \text{ bars}$$

$$A_{slbarmin} = \frac{A_{sl,min}}{N_{sl}} = \frac{0.49 \text{ in}^2}{4} = 0.12 \text{ in}^2 \quad \therefore \text{use (4)\#4 bars @18"}$$

Therefore use (4) #4 bars spaced 18" o.c. Place second layer of rebar on compression side for any reversed loading.

Horizontal/Transverse Reinforcement, A_{st}

$$\rho = \frac{A_{st,min}}{A_{gc}} = 0.0020 \quad (\text{ACI 381-14 §14.3.3})$$

$$A_{gct} = h * (t_{wy0} + t_{wyi}) = 102 \text{ in} * 6 \text{ in} = 612 \text{ in}^2$$

$$A_{st,min} = \rho A_{gcl} = 0.002(612 \text{ in}^2) = 1.23 \text{ in}^2$$

$$s_{max} = \min\left(\frac{3t_{SWP}}{18 \text{ in}}\right) = \max\left(\frac{27 \text{ in}}{18 \text{ in}}\right) = 18 \text{ in}$$

$$N_{st} = \frac{h - 2(0.75 \text{ in})}{s_{max}} = \frac{102 \text{ in} - 2(0.75 \text{ in})}{18 \text{ in}} = 5.6 \text{ bars}$$

$$A_{stbarmin} = \frac{A_{st,min}}{N_{st}} = \frac{1.2 \text{ in}^2}{6} = 0.2 \text{ in}^2 \quad \therefore \text{use (6)\#4 bars @ 18"}$$

Therefore use (6) #4 bars spaced 18" o.c. Place second layer of rebar on opposite side for symmetry.

Lifting

$$x_{lift} = 18 \text{ in} = 1.5 \text{ ft} \quad (\text{anchor to edge distance})$$

$$x_{midL} = h - 2x_{anchor} = 8.5 \text{ ft} - 3 \text{ ft} = 5.5 \text{ ft}$$

$$x_{midT} = b - 2x_{anchor} = 5.67 \text{ ft} - 3 \text{ ft} = 2.67 \text{ ft}$$

Longitudinal Direction

$$w_{sw} = w_c b t = (150 \text{ pcf})(5.67 \text{ ft})(0.5 \text{ ft}) = 425 \frac{\text{lb}}{\text{ft}}$$

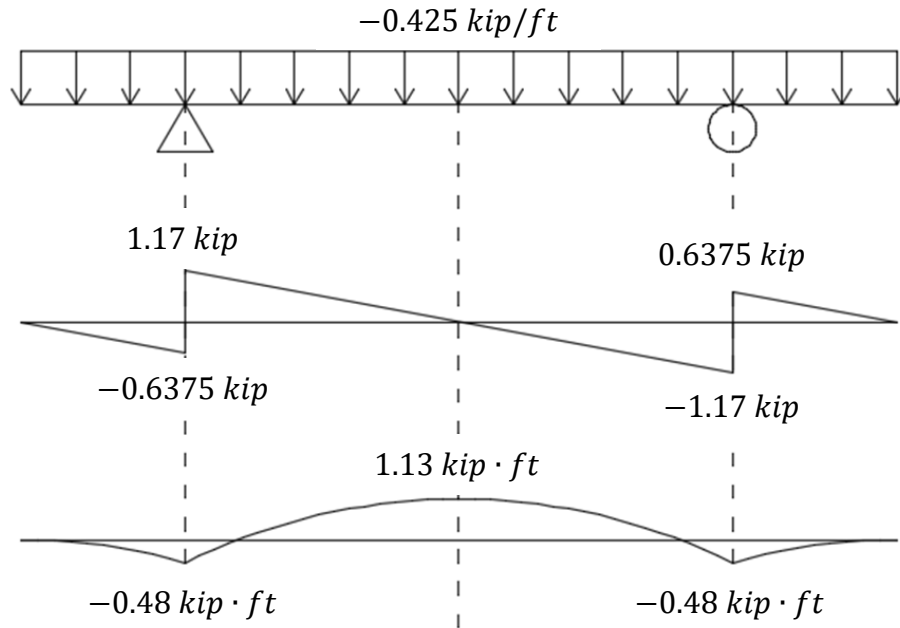
$$R_A = \frac{w_{sw} h}{2} = \frac{\left(0.425 \frac{\text{kip}}{\text{ft}}\right)(8.5 \text{ ft})}{2} = 1.8 \text{ kip}$$

$$\begin{aligned} V_{lift,left} &= w_{sw} x_{lift} = \left(0.425 \frac{\text{kip}}{\text{ft}}\right)(1.5 \text{ ft}) \\ &= -0.6375 \text{ kip} \end{aligned}$$

$$\begin{aligned} V_{lift,right} &= w_{sw} x_{lift} + R_A = -0.64 \text{ kip} + 1.8 \text{ kip} \\ &= 1.17 \text{ kip} \end{aligned}$$

$$\begin{aligned} M_{lift} &= \frac{V_{lift,left} x_{lift}}{2} = \frac{(-0.64 \text{ kip})(1.5 \text{ ft})}{2} \\ &= -0.48 \text{ kip} \cdot \text{ft} \end{aligned}$$

$$\begin{aligned} M_{mid} &= M_{lift} + \frac{V_{lift,right}(0.5x_{midL})}{2} \\ &= -0.48 \text{ kip} \cdot \text{ft} + \frac{0.64 \text{ kip}(0.5 \cdot 5.5 \text{ ft})}{2} = 1.13 \text{ kip} \cdot \text{ft} \end{aligned}$$



Cracking moment is equal to

$$M_{cr} = \frac{7.5\sqrt{f'_c}I_g}{0.5t}$$

$$f'_{c,req} = \left(\frac{0.5(t_{wyo} + t_{wyi})M_{mid}}{7.5I_g} \right)^2$$

$$= \left(\frac{0.5(6 \text{ in}) \left(1.13 \text{ kip} \cdot \text{ft} * \frac{12 \text{ in}}{\text{ft}} \right)}{7.5(3978 \text{ in}^4)} \right)^2 = 0.0042 \text{ ksi}$$

Therefore we need to attain at least 0.0042 ksi before lifting.

Transverse Direction

$$w_{sw} = w_c h t = (150 \text{ pcf})(8.5 \text{ ft})(0.5 \text{ ft}) = 638 \frac{\text{lb}}{\text{ft}}$$

$$R_A = \frac{w_{sw}b}{2} = \frac{\left(0.64 \frac{\text{kip}}{\text{ft}}\right)(5.67 \text{ ft})}{2} = 1.8 \text{ kip}$$

$$V_{lift,left} = w_{sw}x_{lift} = \left(0.64 \frac{\text{kip}}{\text{ft}}\right)(1.5 \text{ ft})$$

$$= -0.96 \text{ kip}$$

$$V_{lift,right} = w_{sw}x_{lift} + R_A = -0.96 \text{ kip} + 1.8 \text{ kip}$$

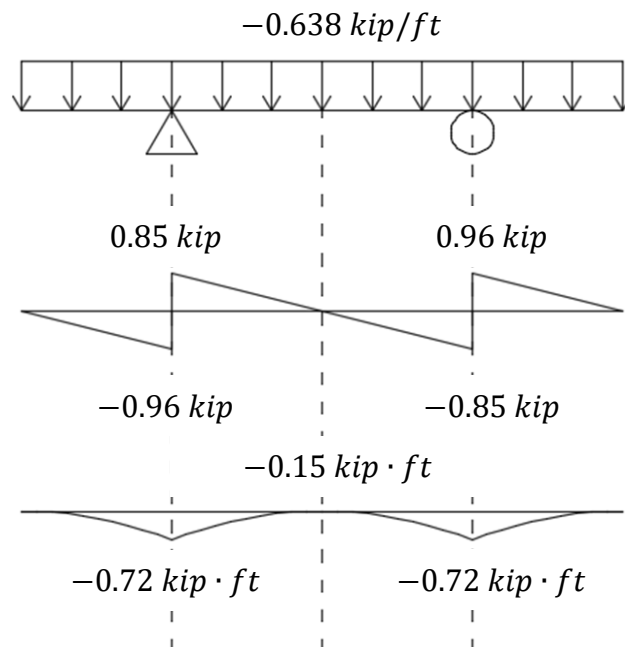
$$= 0.85 \text{ kip}$$

$$M_{lift} = \frac{V_{lift,left}x_{lift}}{2} = \frac{(-0.96 \text{ kip})(1.5 \text{ ft})}{2}$$

$$= -0.72 \text{ kip} \cdot \text{ft}$$

$$M_{mid} = M_{lift} + \frac{V_{lift,right}(0.5x_{midT})}{2}$$

$$= -0.72 \text{ kip} \cdot \text{ft} + \frac{0.85 \text{ kip}(0.5 \cdot 2.67 \text{ ft})}{2} = -0.15 \text{ kip} \cdot \text{ft}$$



Cracking moment is equal to

$$M_{cr} = \frac{7.5\sqrt{f'_c}I_g}{0.5t}$$

$$f'_{c,req} = \left(\frac{0.5(t_{wy0} + t_{wyi})M_{lift}}{7.5I_{gSWP}} \right)^2$$

$$= \left(\frac{0.5(6 \text{ in}) \left(0.72 \text{ kip} \cdot \text{ft} * \frac{12 \text{ in}}{\text{ft}} \right)}{7.5(3978 \text{ in}^4)} \right)^2 = 0.0017 \text{ ksi}$$

Therefore we need to attain at least 0.0017 ksi before lifting to avoid cracking the panel.

Since the concrete lifting anchor strengths are based on a concrete strength of 3.5 ksi,

however, the panels may not be lifted until $f'_c = 3.5 \text{ ksi}$.

$$f'_{c,req} = \max \begin{pmatrix} f'_{c,reqL} \\ f'_{c,reqT} \\ f'_{c,reqA} \end{pmatrix} = \max \begin{pmatrix} 0.0042 \text{ ksi} \\ 0.0017 \text{ ksi} \\ 3.5 \text{ ksi} \end{pmatrix} = 3.5 \text{ ksi}$$

APPENDIX C. CORBEL FABRICATION DRAWINGS

Solid Wall

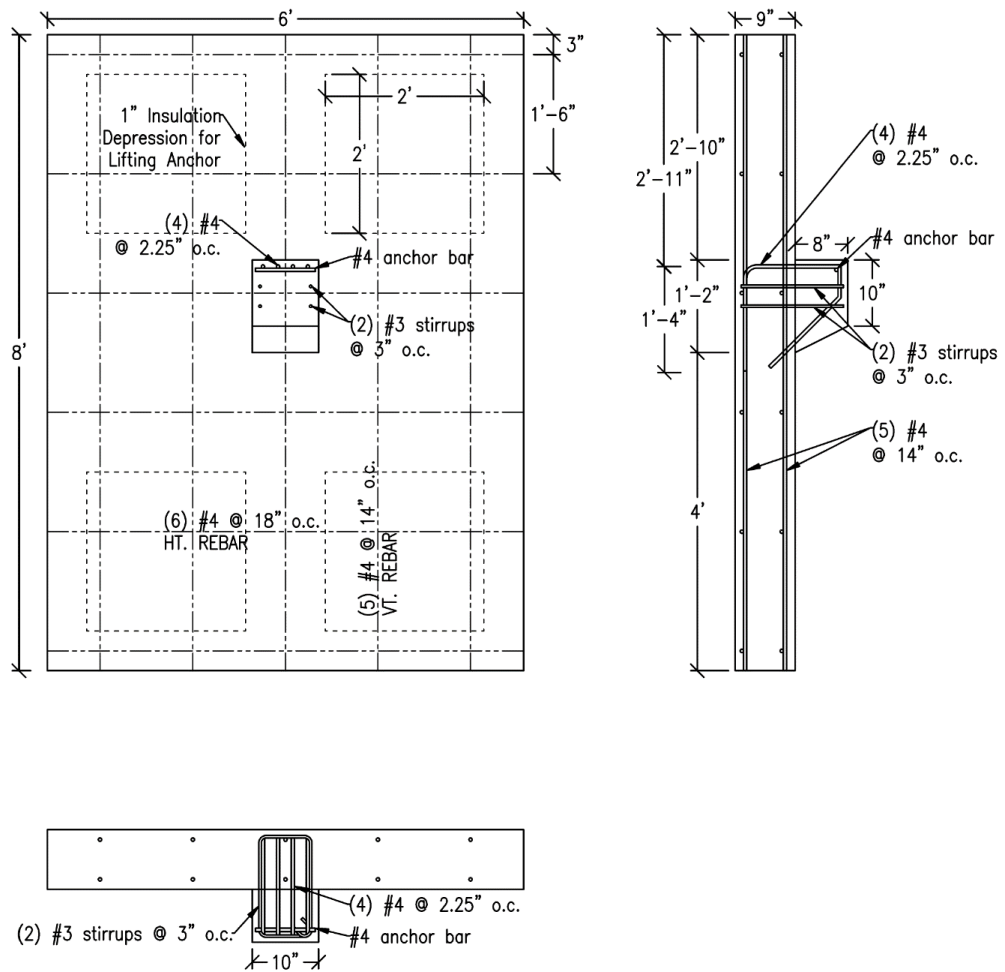


Figure C-1 SolidWall specimen details

Solid-section

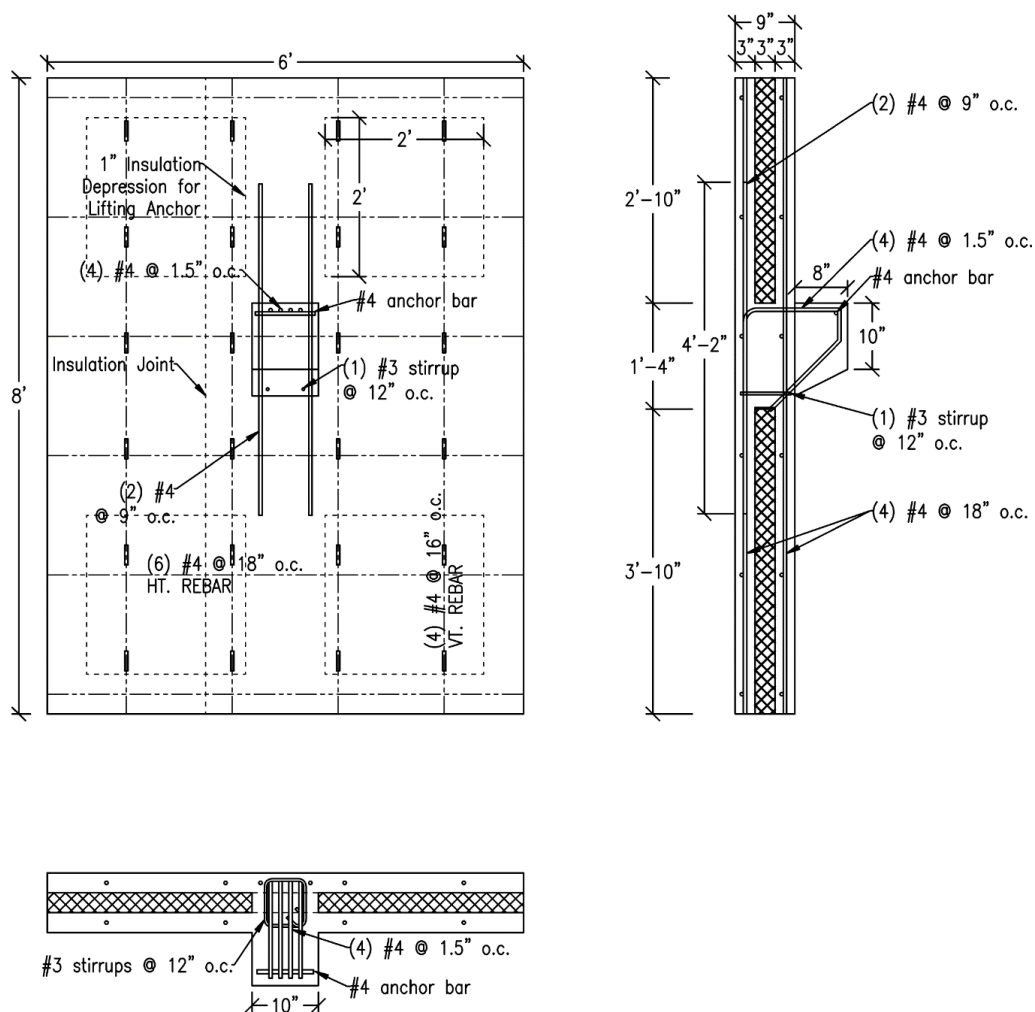


Figure C-2 SolidSec specimen details

GFRP #3s

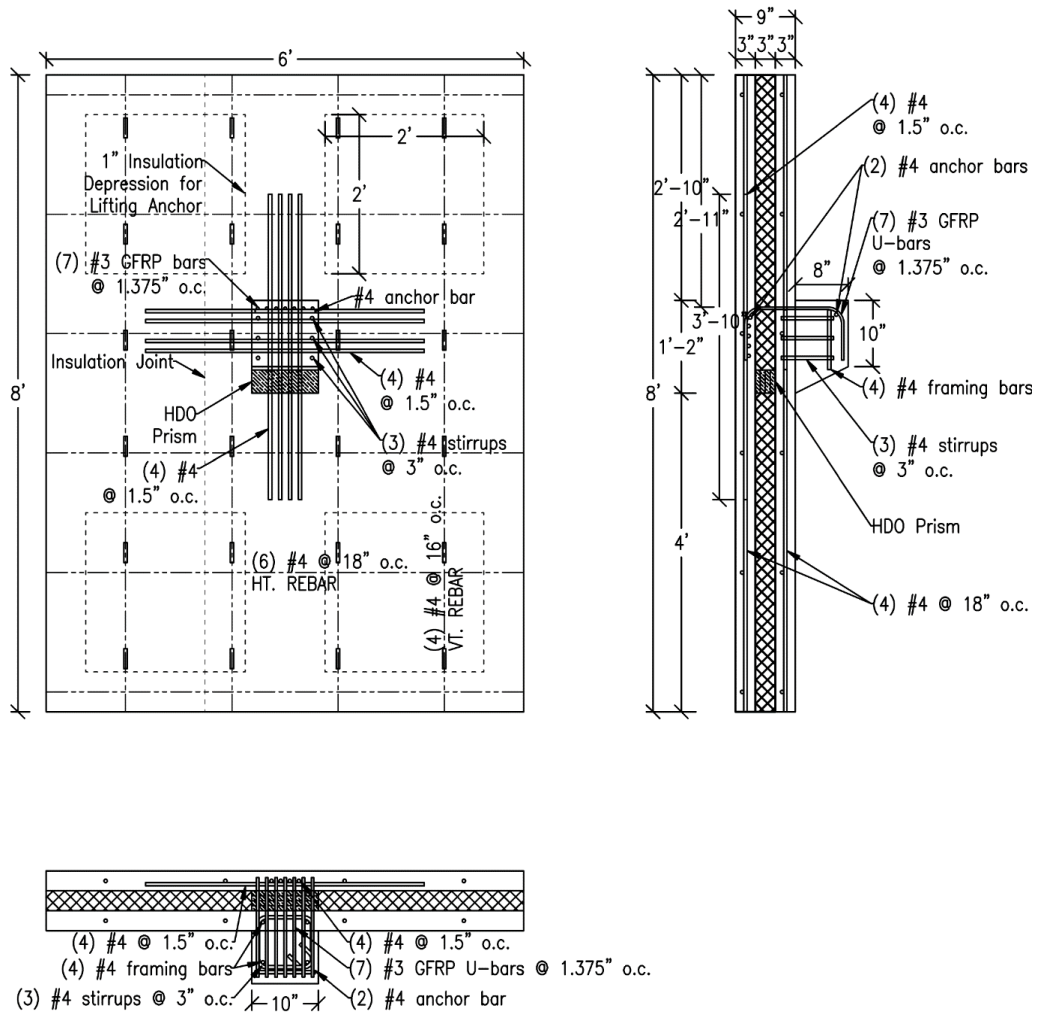


Figure C-3 GFRP3 specimen details

GFRP #2s

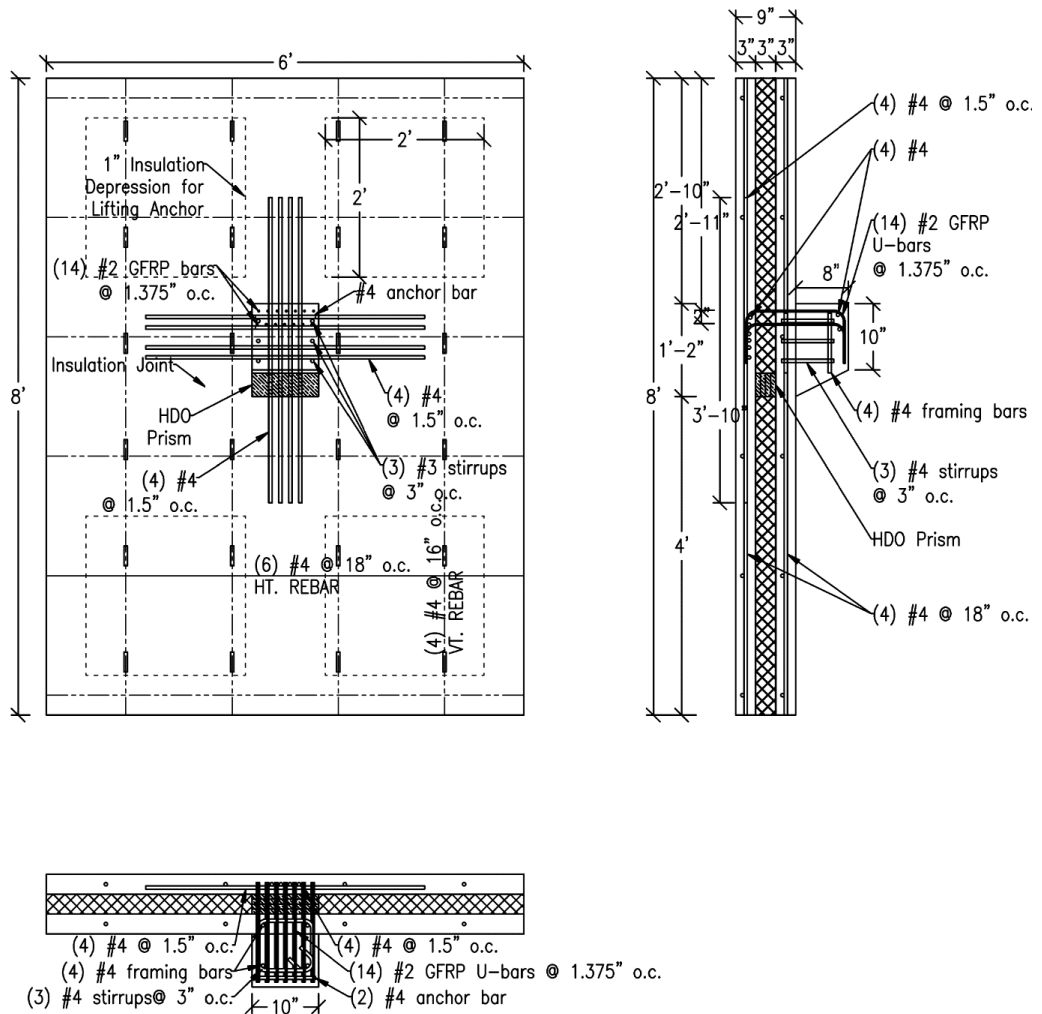


Figure C-4 GFRP2 specimen details

HK Hor

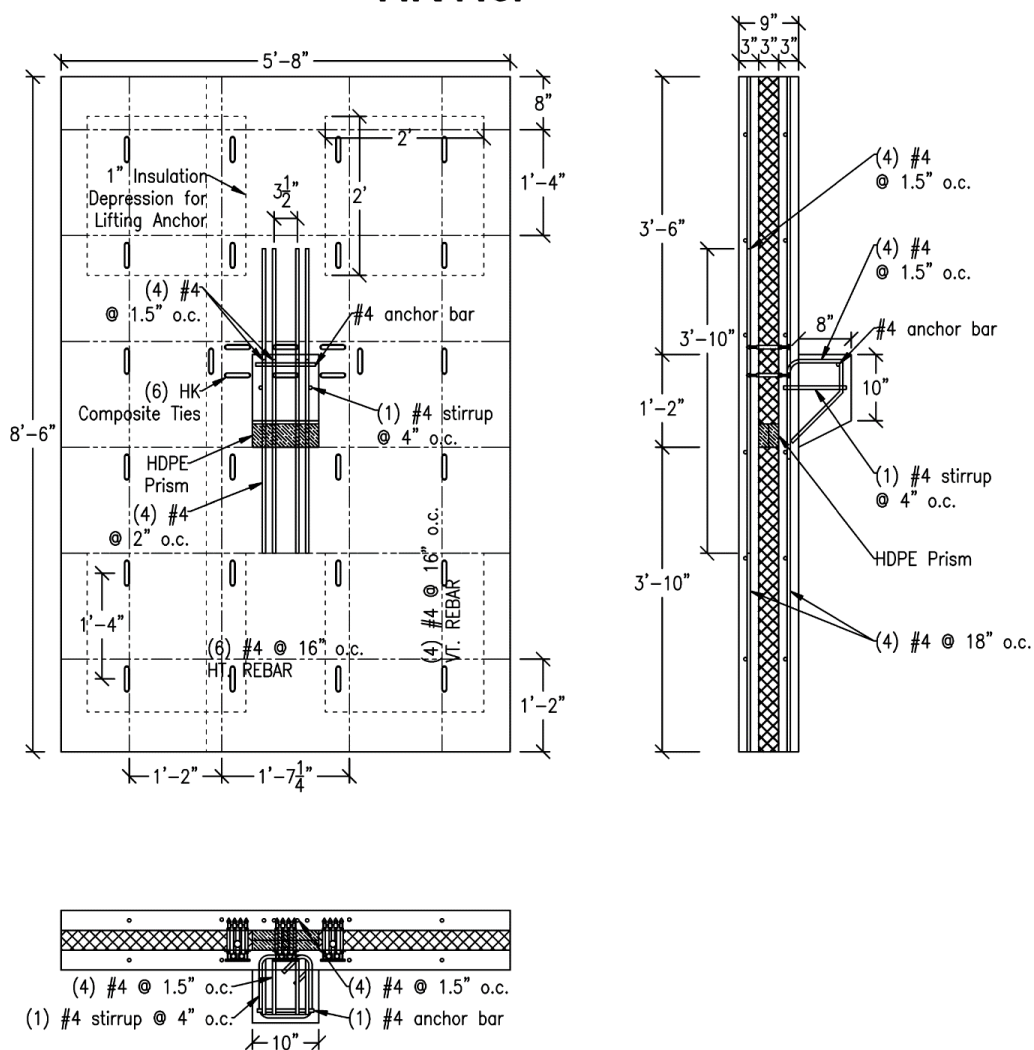


Figure C-5 HKHor specimen details

HK Vert

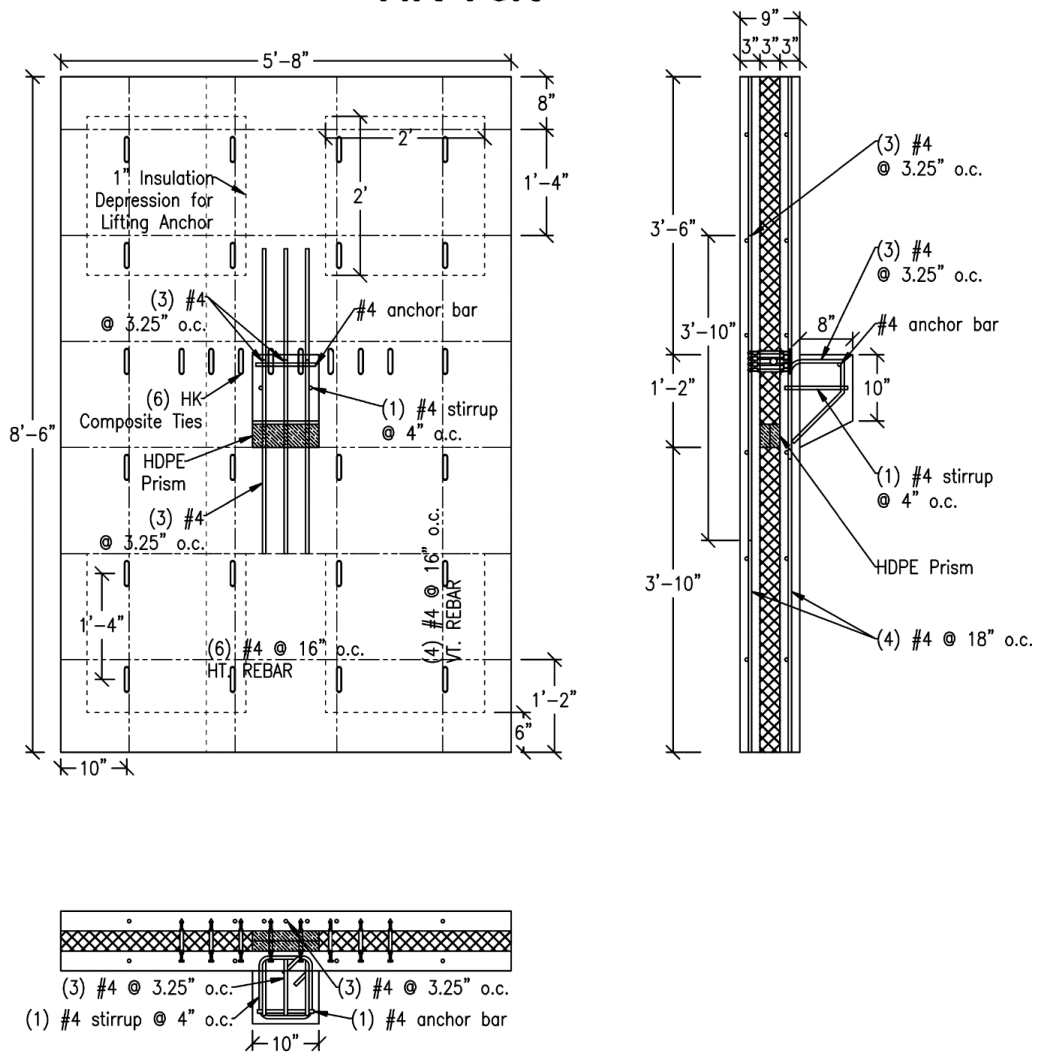


Figure C-6 HKVer specimen details

IconX-GFRP

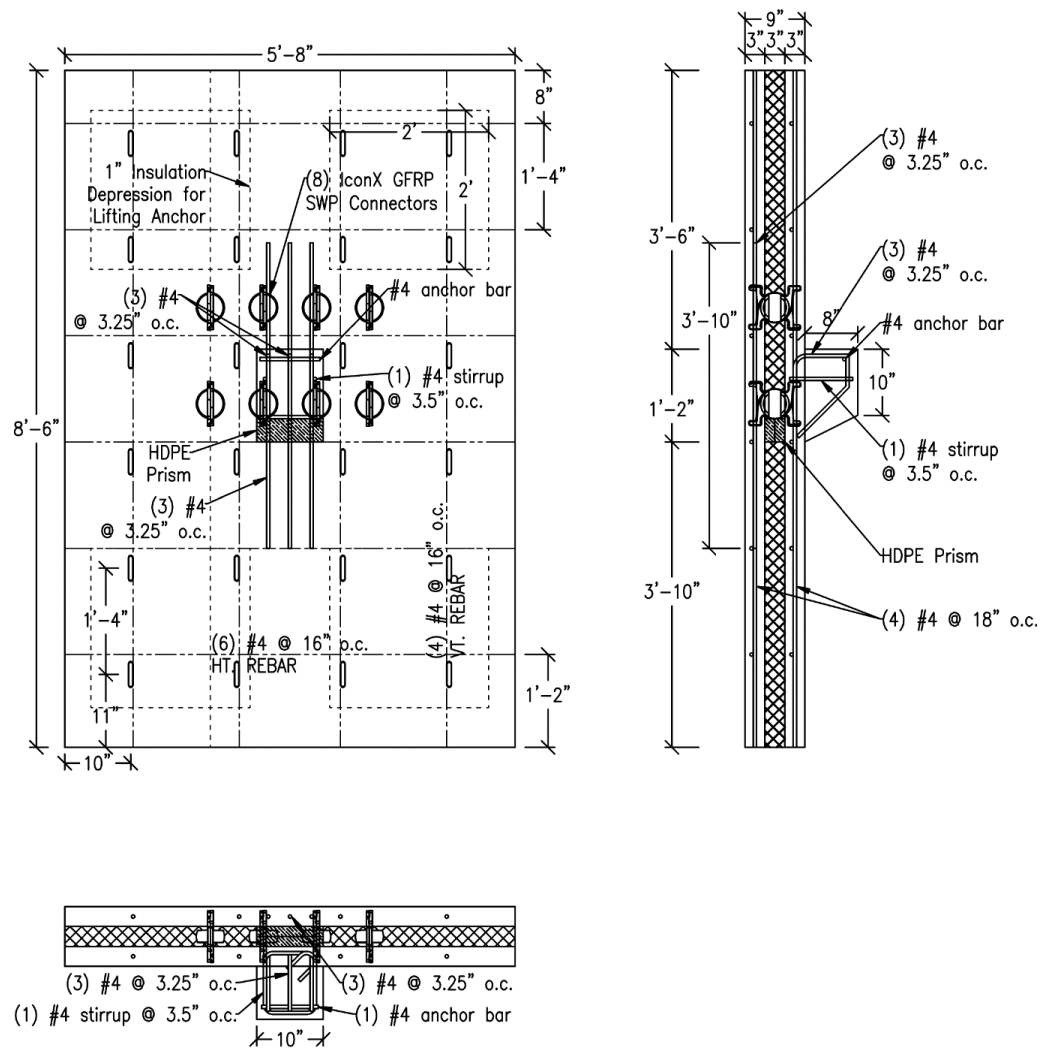


Figure C-7 IconG specimen details

IconX-CFRP

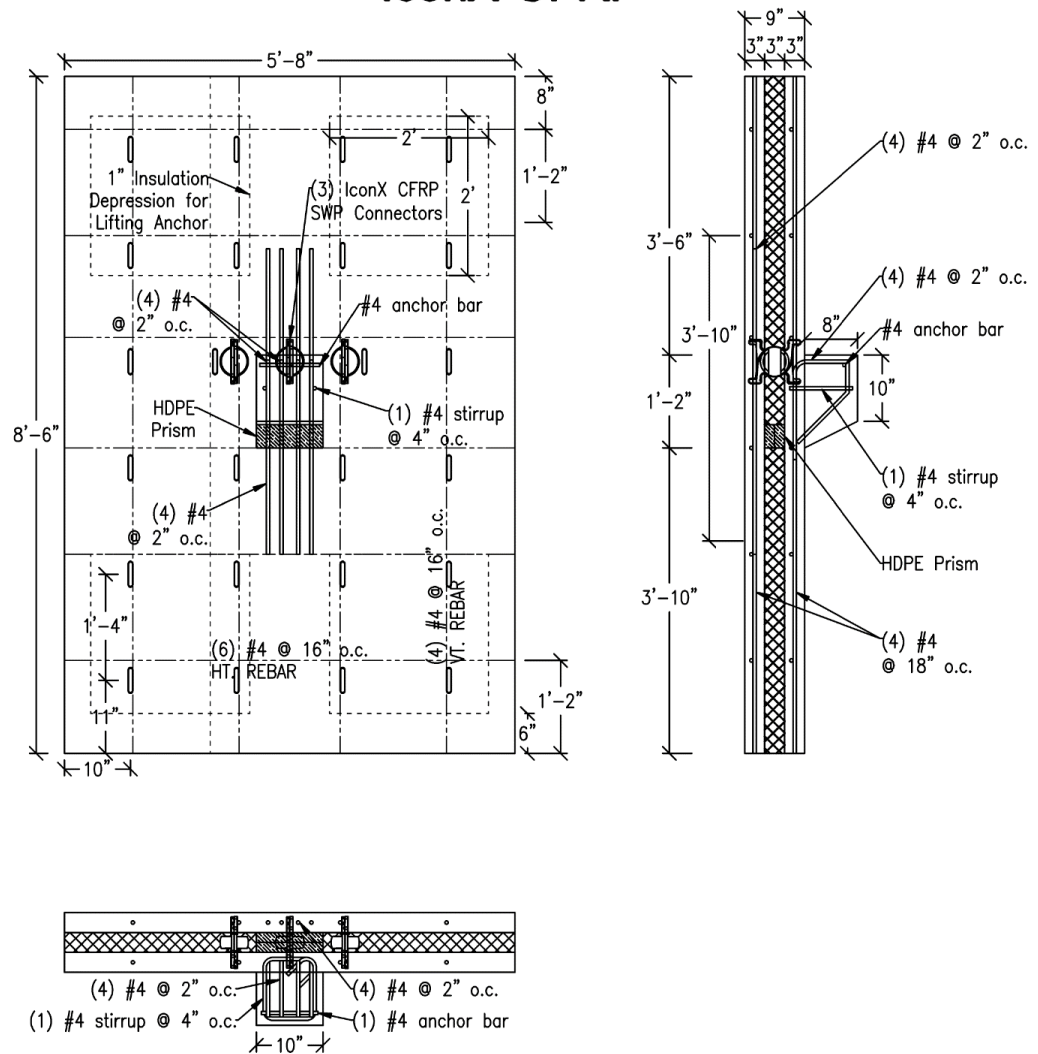


Figure C-8 IconC specimen details

HatBar IconX-CFRP

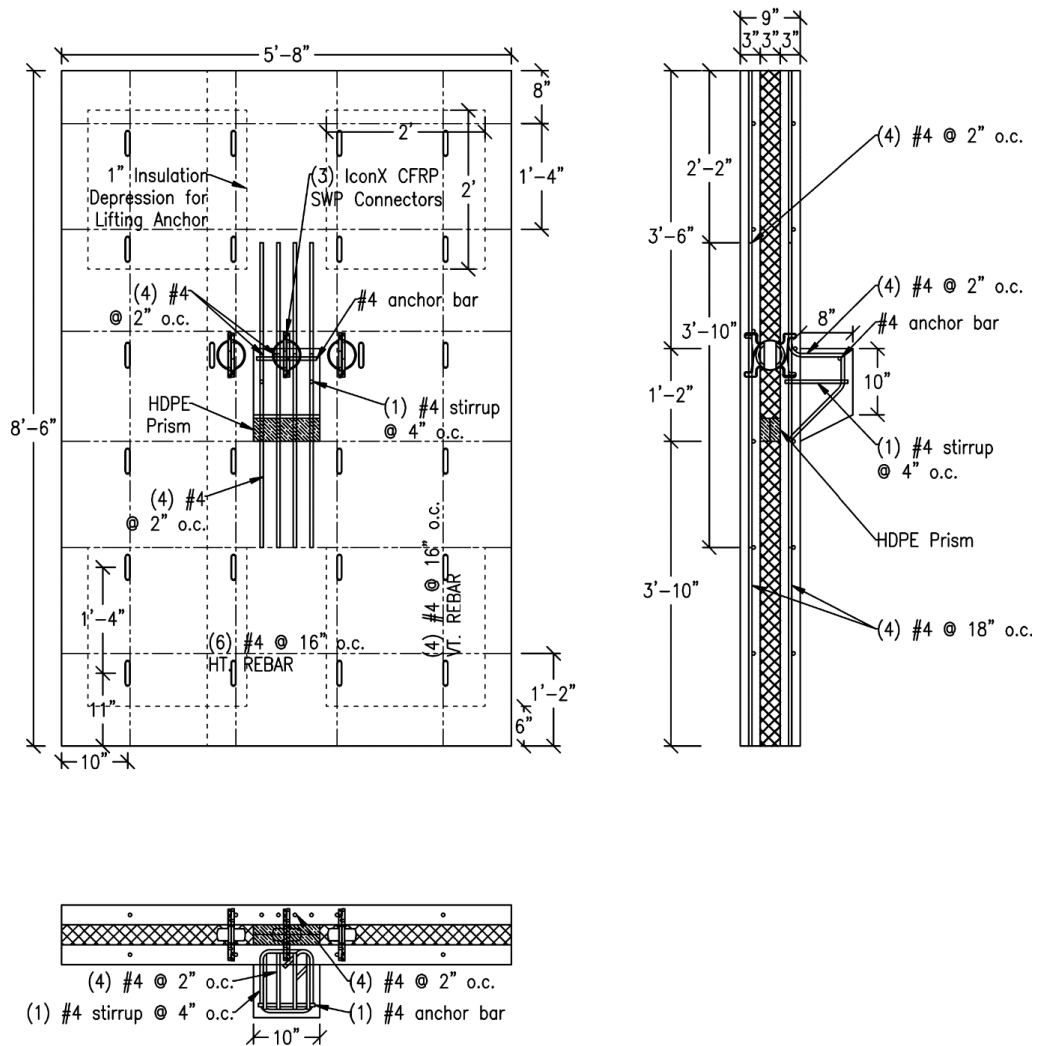


Figure C-9 IconCHat specimen details

Reduced Insulation

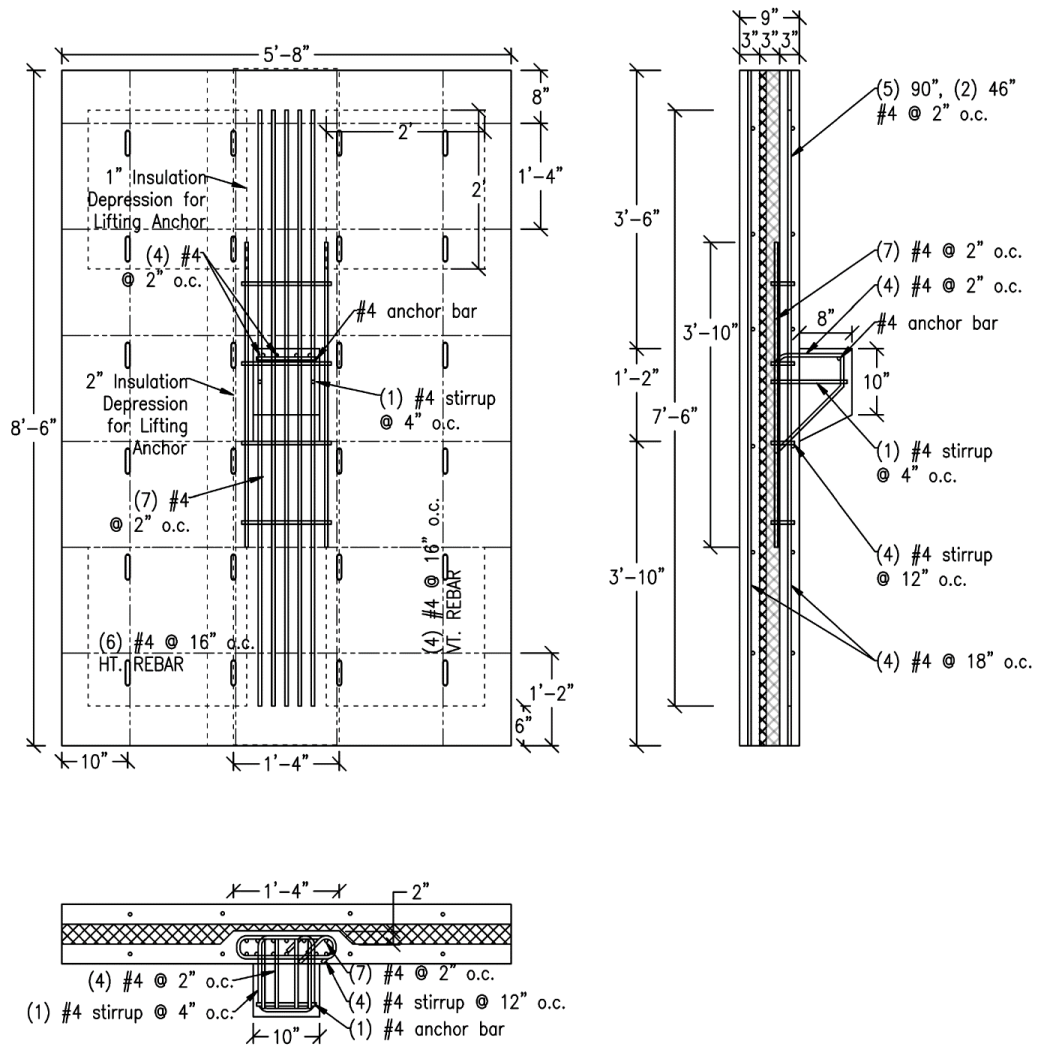


Figure C-10 RedIns specimen details

GFRP Grid (Vert)

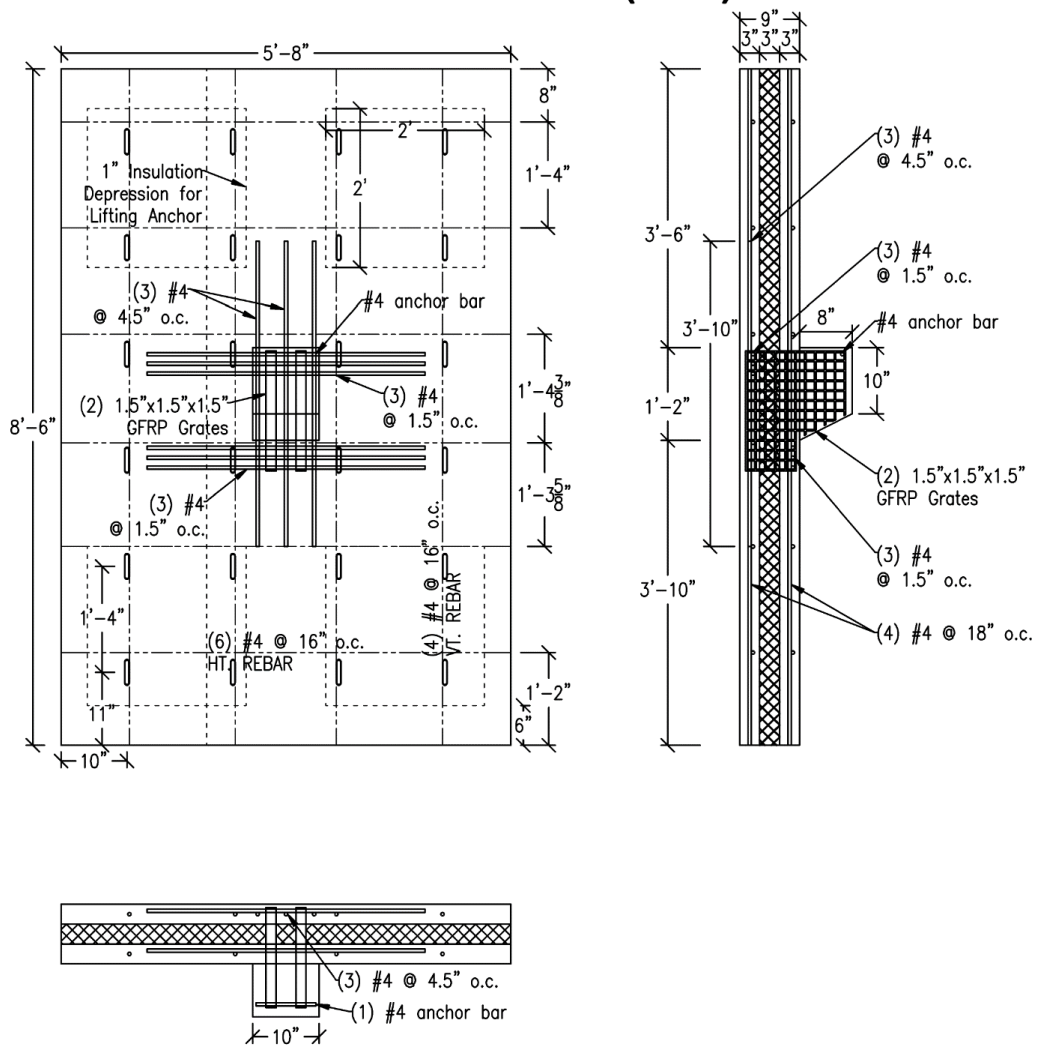


Figure C-11 GridVer specimen details

GFRP Grid (Hor)

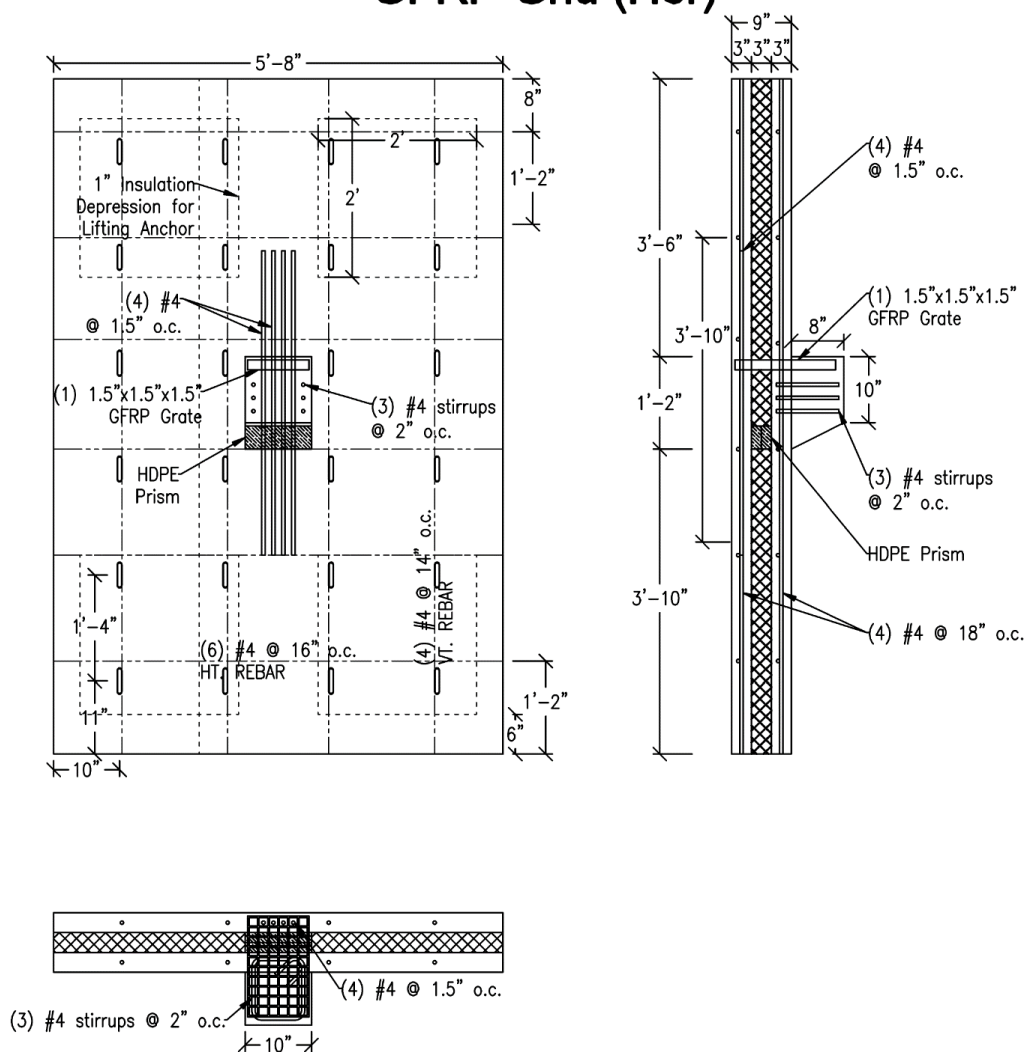


Figure C-12 GridHor specimen details

APPENDIX D. BEAM-SPRING MODEL SPRING STIFFNESSES

Boundary conditions were simulated in the Beam-Spring Model with a vertical, transverse, and rotational spring at the top and bottom of the inside wythe. The stiffnesses used in the model are displayed below in Table D-1.

Table D-1 Boundary condition spring input values (in kips/in)

	Bottom Spring			Top Spring		
	Long	Trans	Rot	Long	Trans	Rot
SolidWall	-	-	-	-	-	-
SolidSec	1.00E+00	1.00E+01	1.00E+05	1.00E+02	1.00E+02	7.50E+03
GFRP3	1.00E+00	1.00E+01	1.00E+05	1.00E+02	1.00E+02	1.50E+03
GFRP2	1.00E+00	1.00E+01	1.00E+05	1.00E+02	1.00E+02	7.50E+03
HKHor	1.00E+01	1.00E+01	1.00E+06	1.00E+02	1.00E+02	7.50E+03
HKVer	1.00E+01	1.00E+01	1.00E+05	1.00E+02	1.00E+02	1.75E+04
IconG	1.00E+00	1.00E+01	1.00E+05	1.00E+02	1.00E+02	7.50E+03
IconC	1.00E+00	1.00E+01	5.00E+04	1.00E+02	1.00E+02	1.00E+03
IconCHat	1.00E+00	1.00E+01	1.00E+06	1.00E+02	1.00E+02	1.00E+03
RedIns	1.00E+02	1.00E+01	1.00E+06	1.00E+02	1.00E+02	1.00E+05
GridHor	1.00E+00	1.00E+01	1.00E+05	1.00E+02	1.00E+02	7.50E+03
GridVer	1.00E+00	1.00E+01	1.00E+05	1.00E+02	1.00E+02	7.50E+03

APPENDIX E. PCI SECOND-ORDER ANALYSIS EXAMPLE

This appendix presents an example of the calculations performed to calculate the predicted stress and deflections of a SWP under axial and flexural loading using the PCI Second-Order Analysis method for a 3-3-3 SWP with 8 ksi concrete and a uniform connector distribution. This example emulates the steps included on pages 5-107 thru 5-109 of the PCI Handbook (2010) with slight modifications due to the difference between modeling a solid concrete wall panel and a concrete sandwich wall panel. The wall panel is assumed to carry a 30 kip axial dead load with an eccentricity of 9.5 inches in addition to a 35 psf wind suction load.

$L_{SWP} = 36 \text{ ft}$	$f'_c = 8000 \text{ psi}$	$D = 30 \text{ kip}$
$b_{SWP} = 12 \text{ ft}$	$E_c = 5422 \text{ ksi}$	$L = 12 \text{ kip}$
$t_{wyi} = t_{wyo} = 3 \text{ in}$	$\rho_c = 150 \text{ pcf}$	$w_w = 35 \text{ psf}$
$t_{ins} = 3 \text{ in}$	$K = 100 \text{ k/in}$	$e = 9.5 \text{ in}$

The first step is to calculate basic section properties that will be used in the calculations.

The centroid of the section is calculated as

$$y_c = \frac{\sum yA}{\sum A} = \frac{(bt_{wyi})(0.5t_{wyi}) + (bt_{wyo})(0.5t_{wyo} + t_{ins} + t_{wyi})}{b(t_{wyi} + t_{wyo})}$$

$$= \frac{\left(\frac{3 \text{ in}}{2}\right)^2 + (3 \text{ in})\left(\frac{3 \text{ in}}{2} + 3 \text{ in} + 3 \text{ in}\right)}{(3 \text{ in} + 3 \text{ in})} = 4.5 \text{ in}$$

The area of the wythes and total cross-sectional area of the SWP is

$$A_{wyo} = A_{wyi} = t_{wy} * b_{SWP} = 3 \text{ in} * 144 \text{ in} = 432 \text{ in}^2$$

$$A_{SWP} = A_{wyi} + A_{wyo} = 2(432 \text{ in}^2) = 864 \text{ in}^2$$

The PCI Second-Order analysis relies on an accurate prediction of the modulus of elasticity and section modulus of the panel. The degree of composite action (DCA) can be used to determine these values by interpolation between the perfectly non-composite and fully-composite scenarios. Each of these calculations will use the moment of inertia of each wythe

$$I_{wyo} = I_{wyi} = \frac{1}{12} b_{SWP} t_{wy}^3 = \frac{1}{12} (144 \text{ in}) (3 \text{ in})^3 = 324 \text{ in}^4$$

The moment of inertia if the panel is non-composite will simply be the sum of each wythe:

$$I_{NC} = I_{wyi} + I_{wyo} = 2(324 \text{ in}^4) = 648 \text{ in}^4$$

The fully-composite moment of inertia, however, would be

$$\begin{aligned} I_{FC} &= I_{wyi} + A_{wyi} d_{wyi}^2 + I_{wyo} + A_{wyo} d_{wyo}^2 \\ &= I_{wyi} + A_{wyi} \left(y_c - \frac{t_{wyi}}{2} \right)^2 + I_{wyo} + A_{wyo} \left(y_c - \frac{t_{wyo}}{2} \right)^2 \\ &= 324 \text{ in}^4 + 432 \text{ in}^2 \left(4.5 \text{ in} - \frac{3 \text{ in}}{2} \right)^2 + 324 \text{ in}^4 + 432 \text{ in}^2 \left(4.5 \text{ in} - \frac{3 \text{ in}}{2} \right)^2 \\ &= 8424 \text{ in}^4 \end{aligned}$$

A finite element model (such as the BSM) is commonly used by connector manufacturers to determine DCA. Because the moment of inertia is proportional to the deflection, and because section modulus is proportional to stress, deflection and stress can be used to calculate the DCA. Therefore a BSM was created with only a uniformly distributed unit load to determine deflection and stress. The DCA is heavily influenced by connector spacing, connector stiffness, and length of the panel, so it was calculated for every individual panel modeled. The resultant midspan deflection and stress of the outside

wythe for the BSM of this example was $\delta = 0.4311 \text{ in}$ and $\sigma_{wy0} = 0.223 \text{ ksi}$. The deflection assuming fully-composite and non-composite action is

$$\delta_{NC} = \frac{5wL^4}{384EI} = \frac{5 \left(100 \frac{\text{lb}}{\text{ft}} * \frac{\text{ft}}{12 \text{ in}} * \frac{\text{k}}{1000 \text{ lb}} \right) (432 \text{ in})^4}{384(5422 \text{ ksi})(648 \text{ in}^4)} = 1.0755 \text{ in}$$

$$\delta_{FC} = \frac{5wL^4}{384EI} = \frac{5 \left(100 \frac{\text{lb}}{\text{ft}} * \frac{\text{ft}}{12 \text{ in}} * \frac{\text{k}}{1000 \text{ lb}} \right) (432 \text{ in})^4}{384(5422 \text{ ksi})(8424 \text{ in}^4)} = 0.0827 \text{ in}$$

The effective section modulus can actually be calculated directly from the BSM as

$$S_{eff} = \frac{M}{\sigma} = \frac{\left(\frac{\left(\frac{100 \text{ k}}{12000 \text{ in}} \right) (432 \text{ in})^2}{8} \right)}{0.223 \text{ ksi}} = 873.4 \text{ in}^3$$

For the sake of comparison, a DCA can be calculated with this value as well. The section modulus for the fully-composite and non-composite sections are

$$S_{NC} = \frac{I}{y} = \frac{I_{NC}}{0.5t_{wy}} = \frac{648 \text{ in}^4}{0.5(3 \text{ in})} = 432 \text{ in}^3$$

$$S_{FC} = \frac{I}{y} = \frac{I_{FC}}{0.5t_{SWP}} = \frac{8424 \text{ in}^4}{0.5(3 \text{ in} + 3 \text{ in} + 3 \text{ in})} = 1872 \text{ in}^3$$

The degree composite action based off of deflection and stress was therefore:

$$DCA_{I_{eff}} = \frac{\delta_{BSM} - \delta_{FC}}{\delta_{NC} - \delta_{FC}} = 1 - \frac{\delta_{BSM} - \delta_{FC}}{\delta_{NC} - \delta_{FC}} = 1 - \frac{0.4311 \text{ in} - 0.0827 \text{ in}}{1.0755 \text{ in} - 0.0827 \text{ in}} = 0.649$$

$$DCA_{S_{eff}} = \frac{S_{eff} - S_{FC}}{S_{NC} - S_{FC}} = \frac{873.4 \text{ in}^3 - 432 \text{ in}^3}{1.0755 \text{ ksi} - 0.0827 \text{ ksi}} = 0.307$$

Using the DCA values, the effective moment of inertia was calculated as

$$I_{eff} = 648 \text{ in}^4 + 0.649(8424 \text{ in}^4 - 648 \text{ in}^4) = 1861.5 \text{ in}^4$$

Now applied loads can be calculated. Using the load case of $1.2D + 0.5L_r + 1.0W$, the load at the top of panel is calculated as

$$P_{u,top} = 1.2D + 0.5L_r = 1.2(30 \text{ kip}) + 0.5(12) = 42 \text{ kip}$$

The midspan will carry half of the self-weight, therefore

$$\begin{aligned} P_{sw,mid} &= \rho_c b_{SWP} (t_{wyi} + t_{wyo}) (0.5 h_{SWP}) \\ &= 1.2 \left(\frac{150}{12^3 * 1000} \frac{k}{in^3} \right) (144 \text{ in}) (3 \text{ in} + 3 \text{ in}) \frac{(432 \text{ in})}{2} = 19.44 \text{ kip} \end{aligned}$$

The total load at midheight, assuming normalweight concrete (150 pcf), will be

$$P_{u,mid} = P_{u,top} + P_{sw,mid} = 42 \text{ kip} + 19.4 \text{ kip} = 61.4 \text{ kip}$$

The PCI Second-Order Analysis requires a moment magnification factor

$$\beta = \frac{P_{sw,mid} + 1.2D_{top}}{P_{u,mid}} = \frac{19.44 \text{ k} + 1.2(30 \text{ kip})}{61.4 \text{ kip}} = 0.90$$

With a stiffness-reduction factor assumed to be at least 0.85 due to strict accuracy found in precasting plants, EI can be calculated as

$$EI = \frac{\phi_k E_c I_{eff}}{1 + \beta_d} = \frac{0.85(5422 \text{ ksi})(1861.5 \text{ in}^4)}{1 + 0.9} = 4510211 \text{ k} \cdot \text{in}^2$$

Deflection at midheight due to the applied load at the top of the corbel can be calculated by using the eccentricity:

$$\delta_{top} = \frac{P_{u,top} e_p h_{SWP}^2}{16EI} = \frac{(42 \text{ kip})(9.5 \text{ in})(432 \text{ in})^2}{16(4510211 \text{ k} \cdot \text{in}^2)} = 1.032 \text{ in}$$

The deflection due to the applied wind load will have a $\beta = 0$, therefore EI will be:

$$EI_w = \frac{\phi_k E_c I_{eff}}{1 + \beta_{dw}} = \frac{0.85(5422 \text{ ksi})(1861.5 \text{ in}^4)}{1} = 8579972 \text{ k} \cdot \text{in}^2$$

The deflection due to the wind load is therefore:

$$\delta_{wind} = \frac{5wL^4}{384EI_w} = \frac{5 \left(0.035 \frac{k}{in}\right) (432 in)^4}{384(8579972 k \cdot in^2)} = 1.85 in$$

The total initial midheight deflection will be the sum of initial deflections,

$$\delta_0 = \delta_{top} + \delta_{wind} = 1.032 in + 1.85 in = 2.882 in$$

Deflection due to second-order effects can then be calculated and iterated until convergence is achieved, or can be solved for directly by using a geometric series.

The total deflection at midheight is equal to

$$\delta_{mid} = \delta_0 + \delta$$

The deflection due to P- δ at midheight can be calculated as

$$\delta = \frac{P_{u,mid}\delta_{mid}h_{SWP}^2}{8EI} = \frac{61.4 kip (432 in)^2 \delta_{mid}}{8(4510211 k \cdot in^2)} = \Delta e * \delta_{mid} = 0.318\delta_{mid}$$

By substituting δ into the equation for δ_0 ,

$$\delta_{mid} = \delta_0 + \Delta e \delta_{mid}$$

This can then be rearranged to isolate δ_{mid} , allowing the total midspan deflection to be solved for directly:

$$\delta_{mid} = \frac{\delta_0}{1 - \Delta e}$$

The total midspan deflection is therefore predicted to be

$$\delta_{mid} = \frac{2.882 in}{1 - 0.318} = 4.224 in$$

Predicted moment will be

$$M_{mid} = \frac{P_{u,top} * e}{2} + P_u * \delta_{mid} + \frac{w_W * h_{SWP}^2}{8}$$

$$\begin{aligned}
&= \frac{42 \text{ kip}(9.5 \text{ in})}{2} + (42 \text{ kip})(4.224 \text{ in}) + \frac{\left(0.035 \frac{k}{in}\right) * (432 \text{ in})^2}{8} \\
&= 1193.4 \text{ k} \cdot \text{in}
\end{aligned}$$

The stress can then be calculated as

$$\sigma_{mid} = -\frac{P_{u,mid}}{0.5(A_{wyo})} + \frac{M_{mid}}{S_{eff}} = -\frac{61.4 \text{ kip}}{0.5(432 \text{ in}^2)} + \frac{1193.4 \text{ k} \cdot \text{in}}{873.4 \text{ in}^3} = 1.224 \text{ ksi}$$

CURRICULUM VITAE

TAYLOR SORENSEN

EDUCATION

<i>Doctor of Philosophy</i>	<u>Civil and Environmental Engineering (Structural Engineering and Mechanics)</u> Utah State University , Logan, UT (2015 - 2019) Advisor: Marc Maguire Dissertation: " <i>Reducing Thermal Bridging and Understanding Second-Order Effects in Concrete Sandwich Wall Panels</i> "
<i>Certificate</i>	<u>Certificate of Engineering Education</u> Utah State University , Logan, UT (2019)
<i>Certificate</i>	<u>Responsible Conduct of Research</u> Utah State University , Logan, UT (2016)
<i>Master of Science</i>	<u>Civil and Environmental Engineering (Structural Engineering and Mechanics)</u> Utah State University , Logan, UT (2014 - 2016) Advisor: Marc Maguire Thesis: " <i>Quantifying the Lateral Bracing Provided by Standing Seam Roof Systems</i> " (Confidential, Abstract Published Online)
<i>Bachelor of Science</i>	<u>Civil Engineering (Structural Emphasis)</u> Utah State University , Logan, UT (2008 - 2014) Honors: <i>cum laude</i> Minor: Portuguese

TEACHING EXPERIENCE

<i>Courses Taught</i>	CEE 6930- Precast/Prestressed Concrete Design (100%) Teaching Reviews: 4.4/5	Fall 2018
	CEE 3165- Civil Engineering Materials Laboratory (80%)	Fall 2018
	CEE 6930- Precast/Prestressed Concrete Design (50%)	Fall 2017
<i>Education Courses Taken</i>	EED 6090- Developing an Online Education Curriculum	Spring 2019
	EED 6150- Teaching, Learning, and Assessment in EED	Fall 2017
	EED 7230- Foundations of Engineering Education Course	Fall 2016

<i>Guest Lecturer</i>	CEE 3080- Reinforced Concrete Design	Spring 2019
	CEE 3020- Structural Analysis	Spring 2018
	CEE 5070- Steel Design I	Fall 2016
	CEE 3160- Civil Engineering Materials	Fall 2016
<i>Lead Writing Fellow</i>	Utah State University, Logan, UT ▪ Tutoring, editing, and teaching writing and English	2012-2014
<i>Professor Workshops</i>	Portland Cement Association Professor Workshop. Invited	July 2016

RESEARCH AND ENGINEERING EXPERIENCE

<i>Quality Manager</i>	USU Systems, Materials and Structural Health Laboratory, 2018 - 2019 Logan, UT
<i>Technical Manager</i>	USU Systems, Materials and Structural Health Laboratory, 2016 - 2019 Logan, UT
<i>Research Assistant</i>	Utah State University, 2014 - 2019 Logan, UT
<i>Surveyor</i>	Cache Landmark Engineering, 2013 Logan, UT
<i>Internship</i>	US Dept. of Health and Human Service- Indian Health Services, 2013 Crow Agency, MT
<i>Internship</i>	Utah Department of Transportation, 2009 Salt Lake City, UT

PUBLICATIONS AND PRESENTATIONS

<i>Journal Articles</i>	Al-Rubaye, S., Sorensen, T. , Maguire, M. (2019). "Elastic Hand Method for Partially Composite Concrete Sandwich Wall Panels." <i>Engineering Structures</i> . (In Preparation)
	Sorensen, T. , Goodridge, W., Maguire, M. (2019). "Bridging the Gap Between Engineering Education and the Practice of Educating Engineers." <i>ASCE Journal of Professional Issues in Engineering Education and Practice</i> . (In Preparation)

Al-Rubaye, S., **Sorensen, T.**, Thomas, R., Maguire, M. (2019). "Generalized Beam–Spring Model for Partially Composite Concrete Sandwich Wall Panels." *Engineering Structures*. ([Published Online](#))

Sorensen, T., Thomas, R., Maguire, M. (2018). "Thermal Bridging in Concrete Sandwich Walls." *Concrete International*. ([Published Online](#))

Al-Rubaye, S., **Sorensen, T.**, Olsen, J., Maguire, M. (2018). "Evaluating Elastic Behavior for Partially Composite Precast Concrete Sandwich Wall Panels." *PCI Journal*. ([Published Online](#))

*Refereed
Conference Papers*

Sorensen, T., Maguire, M. (2019). "Structural Evaluation of Common Corbel Connections in Composite Concrete Sandwich Wall Panels." *Proceedings of the PCI Convention and National Bridge Conference*. Denver, CO. (Abstract Accepted)

Al-Rubaye, S., **Sorensen, T.**, Dorafshan, S., Maguire, M. (2018). "Matrix Model Accuracy of Partially Composite Concrete Sandwich Panels." *Proceedings of the PCI Convention and National Bridge Conference*. Denver, CO. ([Published Online](#))

Sorensen, T., Dorafshan, S., Maguire, M. (2017). "Thermal Evaluation of Common Locations of heat Loss in Sandwich Wall Panels." *ASCE Congress on Technical Advancement*. Duluth, MN. ([Published Online](#))

Al-Rubaye, S., **Sorensen, T.**, Maguire, M. (2017). "Investigating Composite Action at Ultimate for Commercial Sandwich Panel Composite Connectors." *Proceedings of the PCI Convention and National Bridge Conference*. Cleveland, OH. ([Published Online](#))

Shwani, M., **Sorensen, T.**, Maguire, M. (2017). "Enhancing Ductility of WWR Slabs." *Proceedings of the PCI Convention and National Bridge Conference*. Cleveland, OH. ([Published Online](#))

Presentations

Sorensen, T., Maguire M. (2018). "Reducing Heat Loss in Sandwich Wall Panel Corbel Connections." *USU SRS Symposium*. Logan, UT. ([Published Online](#))

Sorensen, T., Maguire M. (2018). "Development of Thermally and Structurally Efficient Corbel Floor Connections in Concrete Sandwich Wall Panels." *ACI Convention*. Salt Lake City, UT. **Received Award.**

Sorensen, T., Maguire, M. (2017). "Reducing the Holes in the Bucket." *Governor's Utah Energy Development Summit*. Salt Lake City, UT. **Invited**

Sorensen, T., Al-Rubaye, S., Maguire, M. (2017). “Investigation of Composite Action at Ultimate for Sandwich Wall Panel Composite Connectors.” *USU SRS Symposium*. Logan, UT. ([Published Online](#))

Sorensen, T., Olsen, J., Maguire, M. (2016). “Shear Testing of Precast Concrete Sandwich Wall Panel Composite Shear Connectors.” *USU SRS Symposium*. Logan, UT. ([Published Online](#))

Standards IAPMO EC031-2017. (2017). “Modified Base Test Method for Open-Web Steel Joists Supporting a Standing Seam Roof System.” *International Association of Plumbing and Mechanical Officials*. Ontario, CA. ([Published Online](#))

Final Reports **Sorensen, T.**, Maguire, M. (2018). “Phase 2: Energy-Efficient Corbel Design for Concrete Sandwich Wall Panels.” A Report Submitted to PCA.

Sorensen, T., Maguire, M. (2017). “Phase 1: Identification of Energy-Efficient Detailing for Concrete Sandwich Wall Panels.” A Report Submitted to PCA.

Olsen, J., Al-Rubaye, S., **Sorensen, T.**, Maguire, M. (2017). “Developing a General Methodology for Evaluating Composite Action in Insulated Wall Panels.” A Report Submitted to PCI. ([Published Online](#))

Sorensen, T., Maguire, M. (2016). “Modified Base Test Report.” A Report Submitted to Nucor.

HONORS AND AWARDS

USUSA Graduate Enhancement Award	2019
USU CEE Outstanding Graduate Researcher	2018
SEAU Academic Scholarship	2018
ACI Convention Outstanding Poster Award (3 rd Place)	2018
Utah State University Presidential Doctoral Research Fellowship	2015-2019
PCA Education Foundation J. P. Gleason Fellowship Award	2016
SEAU Academic Scholarship	2016
ACI Intermountain Chapter Scholarship	2015

WRI Education Foundation Academic Scholarship	2014
BYU Management Society Scholarship	2008
Utah State University Presidential Scholarship	2008-2014
Eagle Scout	2007


SERVICE

<i>Outreach</i>	State Science Olympiad Competition, Event Coordinator (2019)
	Engineering State, Event Assistant (2019, 2017)
	State Science Olympiad Competition, Event Assistant (2012, 2009)
<i>Membership</i>	American Society of Civil Engineers (ASCE)
	American Society for Engineering Education (ASEE)
	Portland Cement Association (PCA)
	Precast Concrete Institute (PCI)
	Structural Engineers Association of Utah (SEAU)
	Structural Engineers Institute (SEI)
	Wire Reinforcement Institute (WRI)

PROFESSIONAL LICENSING

<i>Engineer in Training (Utah)</i>	2013
<i>Commercial Driver's License (CDL)</i>	2012

CERTIFICATION

<i>Certified SolidWorks Professional (CSWP)</i>	2018	
<i>Certified SolidWorks Associate (CSWA)</i>	2017	